Ollscoil Chathair
Bhaile Átha Cliath
Dublin City University

Modelling and forecasting changes in rivers and lakes for improved water resource management

A thesis presented to the School of Health and Science, Dundalk Institute of Technology in fulfilment of the degree of

Doctor of Philosophy

Ricardo Leonel Marroquín Paíz

Academic supervisors: Dr. Eleanor Jennings[1]

Dr. Don C. Pierson[2]

Dr. Valerie McCarthy[3]

Dr. Suzanne Linnane[1]

---

[1]Centre for Freshwater and Environmental Studies, Dundalk Institute of Technology, A91 K584 Dundalk, Ireland

[2]Department of Ecology and Genetics – Limnology, Uppsala University, 75236 Uppsala, Sweden

[3]School of History and Geography, Dublin City University, D09 YT18, Dublin 9, Ireland

August 2025

Declaration

We, the undersigned declare that this thesis entitled Modelling and forecasting changes in rivers and lakes for improved water resource management is entirely the author's own work and has not been taken from the work of others, except as cited and acknowledged within the text.

The thesis has been prepared according to the regulations of Dundalk Institute of Technology and has not been submitted in whole or in part for an award in this or any other institution.

Author Name: Ricardo Leonel Marroquín Paíz

Author Signature: 

Date: 12/ 08 / 2025

Supervisor Name: Suzanne Linnane

Supervisor Signature: 

Date: 14 / 08 / 2025

Funding

This work has been funded by the inventWater Innovative Training Network (ITN) (Inventive forecasting tools for adapting water quality management to a new climate) through the European Union's Horizon 2020 research and innovation programme, under the Marie Sklodowska-Curie grant agreement no. 956623.

The work undertaken in Chapter 5 and Chapter 6 of this thesis was also funded by the United States National Science Foundation (DBI-1933016, OAC-2209866).

This thesis is dedicated to my parents,

Alba Dolores Paiz Recinos and

Hugo Leonel Marroquín Hernández

and to my brothers,

Hugo Roberto Marroquín Paiz and

Carlos Adolfo Marroquín Paiz

Acknowledgements

The writing of these acknowledgements concludes the journey of my PhD. I am grateful for everything I have learned during this part of my education and my life, and I am looking forward to continuing my professional career. I consider this thesis to be the most fitting conclusion to my time and research at different institutions, especially at DkIT.

First, I would like to express my gratitude to Eleanor Jennings. I feel extremely privileged to have been mentored and supervised by you. You have had a positive impact not only on how I approach research but also beyond. I admire your practice and see you as a role model. On a personal level, I have learned a lot from you – to be more patient, to remain calm, and to view challenges with a more open and rational perspective. Thanks for involving yourself in my project the way you did, with active contributions to the modelling and genuine curiosity in the research. I feel lucky I was able to work with you and observe your way of doing science. Your professional mark will always remain with me, and I hope that a little piece of your wisdom as well. Thank you, Eleanor.

I would also like to express my gratitude to Don C. Pierson. Thank you for your guidance and supervision throughout my project. I enjoyed working with you and learning from you, especially during the model development phases. Your expertise and calm have taught me a lot. Thank you for being an excellent host during my visits to Sweden in both Uppsala and Erken – I had a good time at Limnology with Ana, Jorrit and you.

Many thanks go out to Cayelan Carey and Quinn Thomas. There was definitely a before and after in my career when I visited Blacksburg. Cayelan, thanks for allowing me to carry out such a secondment at Virginia Tech and for providing me with good support. Thank you very much for sharing your pasta when I arrived, it meant and means a lot. Quinn, thanks for being always available and checking on me during my visit. A lot of my concepts in short-term forecasting come from my time in Steger Hall and from chats

with you that ranged from informal to in-depth technical conversations, which I enjoyed big time. I feel privileged that I was able to experience Virginia Tech, and although it is a huge institution, for me, Virginia Tech is the Carey Lab. Many thanks to Austin Delany for training me on FLARE, Docker and GitHub. Thanks to Adrian for taking me on a good day of fieldwork and teaching me water quality monitoring at Falling Creek. Special thanks to Abby and Heather, I share many nice memories with you two.

One million thanks to Elvira de Eyto. Thanks for your flexibility and availability not only when I dropped you all those data requests but overall. Thanks for having that nice human touch in your interactions and for showing me around the Burrishoole catchment and the Marine Institute. Thank you for fostering the growth of many students, researchers and individuals.

I am also thankful to Ian Jones. Thanks for hosting me at the University of Stirling. Our discussions on methods were always interesting, and I appreciate you putting my feet on the ground several times with arguments full of common sense. Thanks for sharing some facts about Scotland and for that lovely dinner on my last night in Stirling.

Many thanks go out to the people within inventWater who made all this possible. I am proud to have been part of such a project, which allowed me to expand my professional network and scientific vision. I am grateful for the opportunity to meet supervisors who are at the forefront of water research. To my colleagues, it was a pleasure. Our annual meetings were fun and left nice memories.

Thanks to the DkIT office people, old and new. I was privileged to experience both great senior and junior colleagues, with whom long-lasting relationships arose. Ryan Smazal, Steven, Emma, Sofía and Clodagh – thanks for leading the way, for the chats and the company in and outside the office. To my juniors, Ryan Callan, Trisha and Roger, thanks for the sparks and chats during my final phase at my desk.

Por último, expreso mis más profundos agradecimientos a mi núcleo familiar. Padres, gracias por todo. Esto no lo hice solo, ustedes estuvieron conmigo desde muy lejos, de muchas maneras, pero especialmente como mi fuerza interior. Los llevo conmigo siempre, y celebro con ustedes este logro, que es nuestro. Carlos y Hugo, gracias por llenarme de inspiración y valentía para mantenerme a flote en mis buenos y no tan buenos momentos. En estos últimos años me di cuenta de que puedo contar con ustedes más que nunca.



Ricardo Leonel Marroquín Paíz

113 Muirhevna, Dublin Road, Dundalk, Co. Louth, Ireland

Table of Contents

Declaration I

Funding II

Acknowledgements IV

List of Figures XIII

List of Tables XXI

List of Abbreviations XXIV

Abstract XXVIII

Chapter 1. Introduction 1

1.1 Background 1

1.2 Aim and objectives 5

1.3 Thesis outline 6

1.4 Contributions to knowledge 8

Chapter 2. Literature Review 10

2.1 Ecological forecasting 10

2.1.1 Forecasting water quality 12

2.1.2 Forecasting biodiversity dynamics 14

2.2 Ecological forecasting for improved management 16

2.2.1 Dissolved organic carbon (DOC) 18

2.2.3 Diadromous fish migrations and water temperature 25

2.3 Modelling approaches 29

2.3.1 Catchment-scale models 30

2.3.2 Lake-scale models 37

2.4 Model performance, sensitivity and uncertainty 42

2.4.1 Performance metrics 42

2.4.2 Sensitivity and uncertainty analyses 44

2.5 Forecasting frameworks 47

2.5.1 Short-term frameworks 48

2.5.2 Long-term frameworks 51

2.6 Forecast performance 55

2.7 Forecast uncertainty 56

2.7.1 Uncertainty propagation 57

2.8 Conclusions 58

Chapter 3. Modelling Tools 60

3.1 Catchment model 60

3.1.1 Hydrology module 62

3.1.2 DOC module 66

3.2 Lake model 71

3.2.1 Layer structure 73

3.2.2 Water balance 74

3.2.3 Surface energy budget 75

3.2.4 Stratification and vertical mixing 76

3.2.5 Inflows and outflows 76

3.2.6 Sediment heating 77

3.2.7 Bottom stress 77

3.3 Conclusions 78

Chapter 4. Accounting for model parameter uncertainty provides more robust projections of dissolved organic carbon dynamics to aid drinking water management 79

4.1 Abstract 80

4.2 Introduction 81

4.3 Materials and methods 84

4.3.1 Study sites 84

4.3.2 Model development 87

4.3.3 Model calibration 93

4.3.4 Model uncertainty and sensitivity 96

4.3.5 Future projections 97

4.4. Results 99

4.4.1 Model performance and uncertainty 99

4.4.2 Future climate impacts 114

4.4.3 Future change in discharge 117

4.4.4 Future change in DOC concentrations and flux 118

4.4.5 Uncertainty partitioning 122

4.5 Discussion 129

4.5.1 DOC dynamics in the context of hydrology 131

4.5.2 Implications for water management 133

4.6. Conclusions 135

Chapter 5. Short-term lake water temperature forecasts can be used to anticipate the dynamics of freshwater species 136

5.1 Abstract 137

5.2 Introduction 138

5.3 Materials and methods 141

5.3.1 Study site 141

5.3.2 Water temperature forecasting 144

5.3.3 Historical analysis: fish migrations and water temperature 149

5.3.4 Probabilistic forecasting of fish migrations 151

5.4 Results 153

5.4.1 Water temperature observations 153

5.4.2 Water temperature forecasts 154

5.4.3 Fish migration dynamics 158

5.4.4 Water temperature conditions for fish migrations 159

5.4.5 Probabilistic predictions of fish migrations 161

5.5 Discussion 171

5.5.1 Uncertainty in the predictions 173

5.5.2 Scalability and further development 175

5.6 Conclusions 177

Chapter 6. Insights on short-term process-based forecasting of dissolved organic carbon concentration in a temperate river across seasons 178

6.1 Abstract 179

6.2 Introduction 180

6.3 Materials and methods 183

6.3.1 Study site 183

6.3.2 The model 183

6.3.3 Data availability 186

6.3.4 Model long-term calibration 187

6.3.5 Workflows for forecast generation 188

6.3.6. Forecast input data assessment 189

6.3.7 Model parameters and initial conditions 190

6.3.8 Forecast evaluation 191

6.4 Results 192

6.4.1 Model long-term calibration performance 192

6.4.2 Magnitude and variability of forecast input data 195

6.4.3 DOC concentration forecasts 200

6.5 Discussion 210

6.5.1 Implications for water management 214

6.6 Conclusions 215

Chapter 7. Synthesis 216

7.1 Forecasting frameworks 217

7.2 Future research 218

7.3 Personal development 222

7.4 Concluding statements 223

References 224

Appendix A 1

Appendix B 14

Appendix C 16

Appendix D 21

List of Figures

Figure 1.1 Thesis structure outline. 7

Figure 2.1 Conceptual diagram of an ecological forecasting framework (Lewis et al., 2022a). 11

Figure 2.2 Representation of the decision-making process by stakeholders with and without the use of ecological forecasting (Dietze et al., 2024). 12

Figure 2.3 Differences in water colour between freshwaters due to differences in the concentration of organic matter (Kritzberg et al., 2020). 19

Figure 2.4 Irish catchment maps with peat presence (a), slope < 5.25% and annual average rainfall > 1400 mm year^{-1} with corresponding THM concentrations overlain (b) (O'Driscoll et al., 2018). 23

Figure 2.5 Location of the Burrishoole catchment in western Ireland, including main water bodies and topographic elevation. The monitoring sites for diadromous fish are indicated green dots. 28

Figure 2.6 CMIP6 Scenarios – Shared Socioeconomic Pathways with corresponding 2100 radiative forcing levels. Source: German Climate Computing Center (Deutsches Klimarechenzentrum, DKRZ). 53

Figure 2.7 CMIP6 Scenarios – Shared Socioeconomic Pathways with corresponding anthropogenic Radiative Forcing. Source: German Climate Computing Center (Deutsches Klimarechenzentrum, DKRZ). 54

Figure 2.8 CMIP6 Scenarios – Shared Socioeconomic Pathways with corresponding global CO_2 emissions. Source: German Climate Computing Center (Deutsches Klimarechenzentrum, DKRZ). 54

Figure 3.1 Catchment hydrology as conceptualised in GWLF (Schneiderman et al., 2010). 63

Figure 3.2 Simplified diagram of the hydrology module of GWLF, based on the original model schematics within VENSIM software (Ventana Systems Inc.). Model parameters are indicated in brackets. 65

Figure 3.3 Two-phase process of production and washout represented in GWLF-DOC (Naden et al., 2010). 66

Figure 3.4 Simplified diagram of the DOC module of GWLF-DOC, based on the original model schematics within VENSIM software (Ventana Systems Inc.). Model parameters are indicated in brackets. 70

Figure 3.5 GLM simulation domain, input information and key simulated processes (Hipsey et al., 2014). 74

Figure 3.6 Schematic of the surface heat fluxes impacting the surface mixed layer as conceptualised in the General Lake Model (GLM) (Hipsey et al., 2014). 75

Figure 4.1 Location of the study catchments including river network and topographic elevation. 85

Figure 4.2 Conceptual diagram depicting change 1 in the model structure of the Generalised Watershed Loading Functions Model (GWLF). 89

Figure 4.3 Conceptual diagram depicting change 2 in the model structure of the Generalised Watershed Loading Functions Model with an integrated DOC module (GWLF-DOC). 90

Figure 4.4 Observed and simulated monthly river discharge for Vattholma (a) and Glenamong (b) catchments during model calibration and validation. NSE and r² values are indicated for the calibrated parameter set (best optimised simulation). The grey area denotes the 5% - 95% range GLUE uncertainty bounds for river discharge based on the 100 best-performing parameter sets. 100

Figure 4.5 Observed and simulated daily river discharge for Vattholma (a) and Glenamong (b) catchments during model calibration and validation. NSE and r² values are indicated for the calibrated parameter set (best optimised simulation). The grey area denotes the 5% - 95% range GLUE uncertainty bounds for river discharge based on the 100 best-performing parameter sets..... 101

Figure 4.6 Observed and simulated daily DOC flux and DOC concentrations for Vattholma (a and c) and Glenamong (b and d) catchments during model calibration. NSE and r² values are indicated for the calibrated parameter set (best optimised simulation). The grey area denotes the 5% - 95% range GLUE uncertainty bounds for DOC flux and DOC concentrations based on the 100 best-performing parameter sets. 102

Figure 4.7 Simulated calendar month average DOC flux, simulated calendar month average discharge, and measured average calendar month discharge for Vattholma (a, c and e) and Glenamong (b, d and f), respectively. A red dashed line indicates the mean calendar month value for each panel. The stacked areas in panels a – b display baseflow and runoff carbon export contributions to total river discharge carbon export. The average contribution ratio between baseflow and runoff to total DOC export for each catchment is indicated as a percentage ratio (baseflow:runoff). The stacked areas in panels c – f display baseflow and runoff contributions to total discharge contributions. Measured runoff and baseflow obtained as per the Arnold et al. (1995) hydrograph separation method; see Schneiderman et al. 2010. 103

Figure 4.8 Scatter diagrams (sensitivity plots according to the GLUE methodology) applied to hydrological model parameters against NSE model performance (likelihood measure) at Vattholma. The threshold for behavioural parameter sets was 0.60 NSE (simulated vs measured river discharge) and is used for the horizontal axis value in the lower panels of each model parameter. Each dot represents one run of the model from a Monte Carlo experiment with randomly chosen model parameter values. The 100 best behavioural parameter sets are highlighted in red. 106

Figure 4.9 Scatter diagrams (sensitivity plots according to the GLUE methodology) applied to hydrological model parameters against NSE model performance (likelihood measure) at Glenamong. The threshold for behavioural parameter sets was 0.60 NSE (simulated vs measured river discharge) and is used for the horizontal axis value in the lower panels of each model parameter. Each dot represents one run of the model from a Monte Carlo experiment with randomly chosen model parameter values. The 100 best behavioural parameter sets are highlighted in red. 107

Figure 4.10 Scatter diagrams (sensitivity plots according to the GLUE methodology) applied to DOC model parameters against NSE model performance (likelihood measure) at Vattholma. The threshold for behavioural parameter sets was 0.30 NSE (simulated vs measured DOC concentrations) and is used for the horizontal axis value in the lower panels of each model parameter. Each dot represents one run of the model from a Monte Carlo experiment with randomly chosen model parameter values. The 100 best behavioural parameter sets are highlighted in red. 108

Figure 4.11 Scatter diagrams (sensitivity plots according to the GLUE methodology) applied to DOC model parameters against NSE model performance (likelihood measure) at Glenamong. The threshold for behavioural parameter sets was 0.30 NSE (simulated vs measured DOC concentrations) and is used for the horizontal axis value in the lower panels of each model parameter. Each dot represents one run of the model from a Monte Carlo experiment with randomly chosen model parameter values. The 100 best behavioural parameter sets are highlighted in red. 109

Figure 4.12 Correlation matrix for the 100 best behavioural hydrological parameter sets for the Vattholma catchment. The correlation coefficient for each relationship corresponds to the Pearson correlation coefficient. Note that the names of the model parameters were abbreviated. 110

Figure 4.13 Correlation matrix for the 100 best behavioural hydrological parameter sets for the Glenamong catchment. The correlation coefficient for each relationship corresponds to the Pearson correlation coefficient. Note that the names of the model parameters were abbreviated. 111

Figure 4.14 Correlation matrix for the 100 best behavioural DOC model parameter sets for the Vattholma catchment. The correlation coefficient for each relationship corresponds to the Pearson correlation coefficient. Note that the names of the model parameters were abbreviated. 112

Figure 4.15 Correlation matrix for the 100 best behavioural DOC model parameter sets for the Glenamong catchment. The correlation coefficient for each relationship corresponds to the Pearson correlation coefficient. Note that the names of the model parameters were abbreviated. 113

Figure 4.16 ISIMIP3b GCM-ensemble average monthly precipitation (a and b), ISIMIP3b GCM-ensemble mean air temperature (c and d), average modelled monthly actual evapotranspiration (e and f), average

modelled unsaturated zone deficit (g and h) and average modelled soil temperature (i and j) for the baseline period and for the SSP126, SS370 and SSP585 scenarios during P1 and P2. Note the different scaling in panels a and b. Vattholma: a, c, e, g, i; Glenamong: b, d, f, h, j. 116

Figure 4.17 Average calendar month discharge (a and d); boxplot distributions of average daily discharge for the baseline period, and for the SSP126, SS370 and SSP585 scenarios during P1 and P2 (b and e); annual anomalies for discharge under SSP126, SS370 and SSP585 scenarios from 2030 to 2100 (c and f). Uncertainty in the discharge anomaly panels is indicated by the standard deviation (±SD). Vattholma: a, b, c; Glenamong: d, e, f. 119

Figure 4.18 Average calendar month DOC concentration (a and d); boxplot distributions of average daily DOC concentrations for the baseline period, and for the SSP126, SS370 and SSP585 scenarios during P1 and P2 (b and e); annual anomalies for DOC concentration under SSP126, SS370 and SSP585 scenarios from 2030 to 2100 (c and f). Uncertainty in the DOC concentration anomaly panels is indicated by the standard deviation (±SD). Vattholma: a, b, c; Glenamong: d, e, f. 121

Figure 4.19 Tercile plots displaying the probability of exceeding the 95th percentile baseline DOC concentration (mg L^{-1}) for each typical meteorological season in the future (every 5 years) under SSP126, SSP370 and SSP585 scenarios for Vattholma (a) and Glenamong (b). The shading of each square represents the probability of exceedance based on the categorised colour bar legend. The ensemble size was comprised of 500 members for each scenario. 123

Figure 4.20 Tercile plots displaying the probability of exceeding the 95th percentile baseline flux (kg C km^{-2} day^{-1}) for each typical meteorological season in the future (every 5 years) under SSP126, SSP370 and SSP585 scenarios for Vattholma (a) and Glenamong (b). The shading of each square represents the probability of exceedance based on the categorised colour bar legend. The ensemble size was comprised of 500 members for each scenario. 124

Figure 4.21 Relative contribution of (1) future climate input data and (2) model parametrisation as individual sources of uncertainty to the total uncertainty in future projections of discharge under SSP126, SSP370 and SSP585 scenarios for Vattholma. 125

Figure 4.22 Relative contribution of (1) future climate input data and (2) model parametrisation as individual sources of uncertainty to the total uncertainty in future projections of discharge under SSP126, SSP370 and SSP585 scenarios for Glenamong..... 126

Figure 4.23 Relative contribution of (1) future climate input data and (2) model parameterisation as individual sources of uncertainty to the total uncertainty in future projections of DOC concentration under SSP126, SSP370 and SSP585 scenarios for Vattholma. 127

Figure 4.24 Relative contribution of (1) future climate input data and (2) model parameterisation as individual sources of uncertainty to the total uncertainty in future projections of DOC concentration under SSP126, SSP370 and SSP585 scenarios for Glenamong. 128

Figure 5.1 Flow diagram of the forecasting framework structure. The framework contains three main phases indicated by dashed lines in the legend. The automated components of the framework are indicated by five iterative steps denoted in bold fonts alongside a continuous solid yellow arrow..... 141

Figure 5.2 Location of Lough Feeagh and the Burrishoole catchment in western Ireland, including main water bodies and topographic elevation. The monitoring sites for water temperature and fish are indicated by red and green dots, respectively. 144

Figure 5.3 Illustrative example of a daily output of the forecasting framework containing (a) an average lake water temperature forecast, (b) an average cumulative lake water temperature forecast, and (c) probabilistic predictions of the P66 and P95 regimes for the Atlantic Salmon downstream migration. The red and blue bands in (a) and (b) indicate the lake water temperature conditions necessary for the P66 and P95 regimes to occur, respectively. The two black dots in (a) represent measured water temperature observations used for data assimilation. The continuous grey lines around the ensemble mean (dotted black line) in (a) and (b) denote the 95% confidence interval uncertainty of the temperature forecasts. 152

Figure 5.4 Measured average water temperature observations in Lough Feeagh and daily fish counts of Atlantic salmon downstream, Atlantic salmon upstream, and European eel downstream migrations in the Burrishoole catchment. The observed data within the forecasting period (black dashed box) in the upper panel (a) is highlighted in greater detail in the lower panel (b). 154

Figure 5.5 Measured water temperature observations for all 13 monitoring depths in Lough Feeagh from 2004 to 2020 (historical period of this study). 155

Figure *5*.6 Root mean square error (RMSE) of the (a) surface lake water temperature (0.9 m) and (b) average lake water temperature forecasts produced over the entire forecasting period. FLARE (S) and FLARE (M) indicate FLARE RMSE values for forecasts produced during stratified and mixed lake conditions only, respectively. Climatology and Persistence indicate RMSE performance for forecasts produced following their forecasting approach, respectively..... 156

Figure 5.7 Reliability diagram for all lake water temperature forecasts produced by FLARE over the entire forecasting period. The percentage of lake water temperature observations within different forecast confidence intervals is indicated for different forecast horizons. The continuous black dotted line represents ideal forecast confidence calibration (i.e., a forecasting system that perfectly characterises uncertainty; 1:1 relationship between forecast confidence interval and the percentage of observations within it). 157

Figure 5.8 P95 and P66 metrics for fish run counts of the (a) Atlantic salmon downstream migration, (b) Atlantic salmon upstream migration, and (c) European eel downstream migration from 2004 to 2020 (historical period of this study). 160

Figure 5.9 Daily probabilistic predictions of Atlantic salmon downstream migration for different forecast horizons (1-, 7-, 14-, 21-, and 28-days ahead) against observed fish run counts during 2021. Panel (a) displays the P66 regime predictions and panel (b) displays the P95 regime predictions. The observed fish run counts equal to or above the historical P66 and P95 fish run counts are highlighted in blue and red in their respective panels. 162

Figure 5.10 P66 regime daily probabilistic predictions for the Atlantic salmon downstream migration for different forecast horizons (1-, 7-, 14-, 21-, and 28-days ahead) against observed fish run counts during (a) 2022 and (b) 2023. The observed fish run counts equal to or above the historical P66 historical fish run are highlighted in blue. 163

Figure 5.11 P95 regime daily probabilistic predictions for the Atlantic salmon downstream migration for different forecast horizons (1-, 7-, 14-, 21-, and 28-days ahead) against observed fish run counts during (a) 2022 and (b) 2023. The observed fish run counts equal to or above the historical P95 historical fish run are highlighted in red. 164

Figure 5.12 P66 regime daily probabilistic predictions for the Atlantic salmon upstream migration for different forecast horizons (1-, 7-, 14-, 21-, and 28-days ahead) against observed fish run counts during (a) 2021, (b) 2022 and (c) 2023. The observed fish run counts equal to or above the historical P66 historical fish run are highlighted in blue. 165

Figure 5.13 P95 regime daily probabilistic predictions for the Atlantic salmon upstream migration for different forecast horizons (1-, 7-, 14-, 21-, and 28-days ahead) against observed fish run counts during (a) 2021, (b) 2022 and (c) 2023. The observed fish run counts equal to or above the historical P95 historical fish run are highlighted in red. 166

Figure 5.14 P66 regime daily probabilistic predictions for the European eel downstream migration for different forecast horizons (1-, 7-, 14-, 21-, and 28-days ahead) against observed fish run counts during (a) 2021, (b) 2022 and (c) 2023. The observed fish run counts equal to or above the historical P66 historical fish run are highlighted in blue. 167

Figure 5.15 P95 regime daily probabilistic predictions for the European eel downstream migration for different forecast horizons (1-, 7-, 14-, 21-, and 28-days ahead) against observed fish run counts during (a) 2021, (b) 2022 and (c) 2023. The observed fish run counts equal to or above the historical P95 historical fish run are highlighted in red. 168

Figure 5.16 Average probabilistic predictions for each forecast horizon of (a) Atlantic salmon downstream, (c) Atlantic salmon upstream and (3) European eel downstream migrations during the entire forecasting period..... 169

Figure 5.17 Continuous ranked probability score (CRPS) of the P66 (a) and P95 (b) probabilistic predictions of Atlantic salmon downstream, Atlantic salmon upstream, and European eel downstream migrations produced over the entire forecasting period. 170

Figure 6.1 Location of the study catchment including river network and topographic elevation, overview of the GWLF-DOC model long-term calibration, and main components of the workflows A and B for forecasting DOC concentration. 184

Figure 6.2 Observed and simulated daily river discharge during the model calibration and validation of the hydrology module of GWLF-DOC (a), and observed and simulated daily DOC concentration during the model calibration of the DOC module of GWLF-DOC (b) for the Glenamong catchment. 187

Figure 6.3 Observed and simulated daily river discharge during the long-term model calibration and validation of the hydrology module of GWLF-DOC (a), and observed and simulated daily DOC concentration during the long-term model calibration of the DOC module of GWLF-DOC (b) for the Glenamong catchment. 193

Figure 6.4 Boxplot distributions of the weather forecast product input data for GWLF-DOC (i.e., daily forecasted catchment precipitation and mean air temperature; n = 774 690 respectively) (a and b), modelled daily catchment discharge (n = 774 690) (c) and DOC observations used for data assimilation (n = 716) (d) over the meteorological seasons in the forecasting period (1st March 2021 – 1st March 2023). 196

Figure 6.5 RMSE, NSE and r^2 values between the ensemble mean of the weather forecast product (NOAA GEFS) grid-cell for the Glenamong catchment and climate observations from a local meteorological station along the forecast horizon in the entire forecasting period (n = 24 990). 198

Figure 6.6 DOC concentration forecasts for the two process-based workflows (Workflow A and Workflow B) and for Site Persistence for 1- and 2-days ahead (forecast horizon) throughout the entire forecasting period plotted against the observed DOC concentrations used for evaluation. 200

Figure 6.7 DOC concentration forecasts for the two process-based workflows (Workflow A and Workflow B) and for Site Persistence for 3-, 7- and 14-days ahead (forecast horizon) throughout the entire forecasting period plotted against the observed DOC concentrations used for evaluation. 201

Figure 6.8 DOC concentration forecasts for the two process-based workflows (Workflow A and Workflow B) and for Site Persistence for 3-, 7- and 14-days ahead (forecast horizon) throughout the entire forecasting period plotted against the observed DOC concentrations used for evaluation. 202

Figure 6.9 Average calibrated values for the initial conditions (i.e., carbon pools) (a) and DOC model parameters (b) of GWLF-DOC for DOC concentration forecasts using Workflow A and Workflow B (1st March 2021 – 1st March 2023) (n = 731 respectively). To facilitate comparison, ranges have been normalised (0.00 – 1.00). Carbon pools (a): deep saturated zone (DeepSat), saturated zone (Sat), unsaturated zone (Unsat), DOC producing surface areas excluding wetlands (SS) and wetlands (SSwetlands). DOC model parameters (b): activation energy (Ea), aerobic decomp. rate (b), anaerobic decomp. rate (a), anaerobic decomp. rate wetlands (aw), surface carbon loss coeff. (Rcl), surface flow cap (Sf cap), baseflow ratio (Br), fast groundwater carbon loss coeff. (fgw) and slow groundwater carbon loss coeff. (sgw). 204

Figure 6.10 Root mean squared error (RMSE) and Nash-Sutcliffe coefficient (NSE) performance of Workflow A, Workflow B and Site Persistence for DOC concentration forecasts along the forecast horizon across seasons in the forecasting period..... 206

Figure 6.11 Coefficient of determination (r^2) performance and quantified forecast uncertainty (standard deviation) of Workflow A, Workflow B and Site Persistence for DOC concentration forecasts along the forecast horizon across seasons in the forecasting period. 208

Figure 6.12 DOC concentration forecast skill visualization by means of tercile plots for each method (Workflow A, Workflow B and Site Persistence) along different forecast horizons and across seasons. Forecast skill is indicated based on the r^2 performance scale (0.00 – 1.00). 209

List of Tables

Table 2.1 Commonly employed catchment-scale hydrological and water quality models 31

Table 2.2 Commonly employed lake-scale 1-D hydrodynamic models 39

Table 3.1 Model parameters for the hydrology module of the Generalised Watershed Loading Functions Model (GWLF). 63

Table 3.2 Model parameters for the DOC module of the Generalised Watershed Loading Functions Model with an integrated DOC module (GWLF-DOC). 69

Table 4.1 Main characteristics of the study catchments. Units for altitude are meters above sea level. ... 86

Table 4.2 Description of the model parameters of the hydrology module in the Generalised Watershed Loading Functions Model (GWLF) with an incorporated model parameter for the current study (the river channel flow coefficient). 88

Table 4.3 Description of the model parameters of the DOC module related to DOC production in the Generalised Watershed Loading Functions Model (GWLF-DOC) with an incorporated model parameter for the current study (anaerobic decomposition rate for wetlands). 90

Table 4.4 Description of the new model parameters for DOC washout of the DOC module in the Generalised Watershed Loading Functions Model with an integrated DOC module (GWLF-DOC). 92

Table 4.5 Model calibration ranges used for each of the model parameters of the hydrology module and DOC module in GWLF-DOC. 94

Table 4.6 Description of the model calibration script used for the hydrology module of GWLF-DOC..... 95

Table 4.7 Description of the model calibration script used for the DOC module of GWLF-DOC. 96

Table 4.8 Set of calibrated GWLF-DOC model parameters for Vattholma and Glenamong..... 104

Table 4.9 ISIMIP3b GCM ensemble-mean future annual precipitation and mean air temperature values for the historical period (baseline) and for the SSP126, SSP370 and SSP585 scenarios during P1 (2050 – 2060) and P2 (2090 – 2100), for each study catchment. The standard deviation is indicated in parentheses. 115

Table 5.1 Average, median, maximum, P66, and P95 regime fish run counts for the Atlantic salmon downstream, Atlantic salmon upstream, and European eel downstream migrations in the Burrishoole catchment during the historical period of this study. The P66 and P95 time frames indicate the earliest and latest months in a year when the P66 and P95 fish runs have been counted, respectively. 159

Table 5.2 Lake water temperature conditions established for the different regimes (P95 and P66) of the Atlantic salmon downstream, Atlantic salmon upstream, and European eel downstream migrations in Lough Feeagh, Burrishoole catchment. 161

Table 6.1 Model parameters with their calibration ranges used for each of the model parameters of the hydrology module and DOC module in GWLF-DOC..... 185

Table 6.2 Model long-term calibration results for the hydrology module and DOC module of GWLF-DOC. 194

Table 6.3 Magnitude and variability across seasons of all driver data used to generate DOC concentration forecasts using both Workflow A and Workflow B..... 197

Table 6.4 Magnitude and variability across seasons of all driver data used to generate DOC concentration forecasts using both Workflow A and Workflow B..... 209

Table A.1 Vattholma - annual precipitation values for each ISIMIP3b ensemble member during the baseline period (1985 – 2014). 2

Table A.2 Vattholma – annual mean air temperature values for each ISIMIP3b ensemble member during the baseline period (1985 – 2014). 3

Table A.3 Vattholma – SSP126, SSP370 and SSP585 scenarios. Future annual precipitation values for each ISIMIP3b ensemble member during P1 (2050 – 2060). 4

Table A.4 Vattholma – SSP126, SSP370 and SSP585 scenarios. Future annual mean air temperature values for each ISIMIP3b ensemble member during P1 (2050 – 2060)..... 5

Table A.5 Vattholma – SSP126, SSP370 and SSP585 scenarios. Future annual precipitation values for each ISIMIP3b ensemble member during P2 (2090 – 2100). 6

Table A.6 Vattholma – SSP126, SSP370 and SSP585 scenarios. Future annual mean air temperature values for each ISIMIP3b ensemble member during P2 (2090 – 2100)..... 7

Table A.7 Glenamong - annual precipitation values for each ISIMIP3b ensemble member during the baseline period (1985 – 2014). 8

Table A.8 Glenamong – annual mean air temperature values for each ISIMIP3b ensemble member during the baseline period (1985 – 2014). 9

Table A.9 Glenamong – SSP126, SSP370 and SSP585 scenarios. Future annual precipitation values for each ISIMIP3b ensemble member during P1 (2050 – 2060). 10

Table A.10 Glenamong – SSP126, SSP370 and SSP585 scenarios. Future annual mean air temperature values for each ISIMIP3b ensemble member during P1 (2050 – 2060)..... 11

Table A.11 Glenamong– SSP126, SSP370 and SSP585 scenarios. Future annual precipitation values for each ISIMIP3b ensemble member during P2 (2090 – 2100). 12

Table A.12 Glenamong– SSP126, SSP370 and SSP585 scenarios. Future annual mean air temperature values for each ISIMIP3b ensemble member during P2 (2090 – 2100)..... 13

Table C.1 Forecast skill along the forecast horizon and across seasons for the DOC concentration forecasts of Workflow A, Workflow B and Site Persistence indicated by the root mean squared error (RMSE)..... 17

Table C.2 Forecast skill along the forecast horizon and across seasons for the DOC concentration forecasts of Workflow A, Workflow B and Site Persistence indicated by the by the Nash-Sutcliffe coefficient (NSE). 18

Table C.3 Forecast skill along the forecast horizon and across seasons for the DOC concentration forecasts of Workflow A, Workflow B and Site Persistence indicated by the coefficient of determination (r^2). 19

Table C.4 Estimated forecast uncertainty (quantified using the standard deviation of the forecast ensemble) along the forecast horizon and across seasons for the DOC concentration forecasts of Workflow A and Workflow B. 20

List of Abbreviations

Abbreviation	Full Description
1-D	One Dimension
2-D	Two Dimensions
3-D	Three Dimensions
AET	Actual Evapotranspiration
AWQMS	Automatic Water Quality Monitoring Station
C	Carbon
CDOM	Chromophoric Dissolved Organic Matter
CLIME	Climate and Lake Impacts in Europe
CMIP	Coupled Model Intercomparison Project
CN	Curve Number
CO2	Carbon Dioxide
CORINE	Coordination of Information on the Environment
CRPS	Continuous Ranked Probability Score
DA	Data Assimilation
DBP	Disinfection By-product
DkIT	Dundalk Institute of Technology
DOC	Dissolved Organic Carbon

DOM	Dissolved Organic Matter
DYRESM	Dynamic Reservoir Simulation Model
ECA&D	The European Climate Assessment & Dataset Project
EnKF	Ensemble Kalman Filter
EPA	Environmental Protection Agency
ET	Evapotranspiration
EU	European Union
FAO	Food and Agriculture Organization of the United Nations
FLARE	Forecasting Lake and Reservoir Ecosystems
GCM	Global Climate Model
GHG	Greenhouse Gas
GLEON	Global Lake Ecological Observatory Network
GLM	General Lake Model
GLUE	The Generalised Likelihood Uncertainty Estimation Method
GWLF	The Generalised Watershed Loading Functions Model
GWLF-DOC	The Generalised Watershed Loading Functions Model with an Integrated DOC Module
HAA	Haloacetic Acids
HFM	High Frequency Monitoring
INCA	The Integrated Catchment Model

INCA-C	The Integrated Catchment Model with an DOC Module
INCA-P	The Integrated Catchment Model with a Phosphorus Module
IPCC	Intergovernmental Panel on Climate Change
ISIMIP	Inter-Sectoral Impact Model Intercomparison Project
ITN	Innovative Training Network
KF	Kalman Filter
NOAA	National Oceanic and Atmosphere Administration
NOAA GEFS	The National Oceanic and Atmospheric Administration Global Ensemble Forecasting System
NSE	Nash-Sutcliffe Efficiency
NYC DEP	New York City Department of Environmental Protection
OC	Organic Carbon
PET	Potential Evapotranspiration
QA	Quality Assurance
QC	Quality Control
QUALs	Enhanced Stream Water Quality Models
r^2	Coefficient of Determination
RCP	Representative Concentration Pathway
RMSE	Root Mean Square Error
SA	Sensitivity Analysis

SGU	The Swedish Geological Survey
SLU	The Swedish Agricultural University
SMHI	The Swedish Meteorological and Hydrological Institute
SPARROW	The Spatially Referenced Regression Model on Watershed Attributes
SSP	Shared Socioeconomic Pathway
SWAT	Soil and Water Assessment Tool
THMs	Trihalomethanes
TOC	Total Organic Carbon
UK	United Kingdom
USA	United States of America
USGS	The United States Geological Survey
UWA	University of Western Australia
WASP	The Water Quality Analysis Simulation Program
WFD	Water Framework Directive
WHO	World Health Organisation

Abstract

Water, a key element for life and societal development, is increasingly subjected to pressures due to climate dynamics and human activities. Management is required to anticipate change related to these pressures in both the short- and long-term for improved environmental intervention, more efficient water use and a safer supply. Emerging forecasting techniques and software modelling tools provide a set of powerful methods for predicting change in environmental and water systems. Here, three case studies are presented, in which different model-based forecasting framework approaches were implemented for predicting specific water variables in either river or lake systems. In each case, the forecasting addressed a present-day water management issue. In the first study, long-term changes in river discharge and dissolved organic carbon (DOC) dynamics were projected under climate change scenarios for two catchments: one in Ireland (Glenamong, Co. Mayo) and one in Sweden (Vattholma, Uppsala). Projections for discharge differed between the two sites in magnitude, variability and direction of change depending on the future scenario and temporal scale. However, DOC was always projected to show increases in concentration throughout the annual cycle and over time, a change that would have important implications for drinking water supply. In the second study, short-term water temperature forecasting was used to generate predictions for lake water temperature, and based on those, on the timing of migrations of Atlantic salmon *(Salmo salar)* and European eel *(Anguilla anguilla)* between a freshwater lake (Lough Feeagh, Co. Mayo, Ireland) and the Atlantic Ocean. The short-term forecasts for water temperature performed exceptionally well, while the predictions of fish movements performed well for migration regimes that were not extreme, especially for the Atlantic salmon. The approach highlighted the value of coupling ecological forecasting, lake modelling and statistics to assist short-term management decision-making in settings where species can face risk. In the third study, DOC concentrations for the Glenamong River were forecasted in the short-term using

two different workflows, as a novel proof-of-concept to advance near real-time prediction for water quality variables. The results indicated that the variability and accuracy in DOC predictions were largely influenced by the forcing data, the forecasting strategy and river hydrology, especially when using a DOC model that is driven by hydrological modelling as a forecasting tool. However, with reasonable performance for predictions four days ahead, this approach offered useful information not only for the development of near-term ecological forecasts but also for DOC-related water treatment applications. The findings of these studies represent a step forward in both modelling and predicting change in water systems, especially in the context of an increasingly uncertain world where more tools for improved adaptative capacity are needed. The development and application of the forecasting frameworks in this work are a novel contribution to ecological forecasting research and add to efforts bridging the gap between model outputs and decision-making to support water resource management.

Chapter 1

Introduction

1.1 Background

Rivers and lakes are being subjected to increasing human and climatic pressures, resulting in changes affecting ecosystem services and freshwater ecology (Malhi et al., 2020; Weiskopf et al., 2020; Priya et al., 2023). Such changes represent a challenge for resource allocation because they are often unforeseen and therefore appropriate mitigation or conservation measures cannot always be applied (Abbass et al., 2022; IPCC et al., 2023). It is becoming apparent that we cannot rely on the envelope of historic variation as the basis for future management, conservation, and sustainability (Dietze et al., 2018). An approach to address these challenges is through the application of ecological forecasting frameworks i.e., by providing predictions of future environmental conditions with quantified uncertainty (Lewis et al., 2022a; Dietze et al., 2024). Decisions are made every day that impact the interactions between water resources and human systems, and improved decision-making requires making science more useful and relevant beyond the scientific community (Dietze et al., 2018; Bodner et al., 2021). Therefore, it is critical to develop methods that go beyond measuring and monitoring to using data to anticipate change, make predictions, and inform management actions (Dietze and Lynch, 2019; Bradford et al., 2020b).

In an era of rapid technological advancements, new software modelling tools and forecasting techniques are emerging which enable the development of methods for anticipating ecological changes (Dietze et al., 2018; Lewis et al., 2022a; Lofton et al., 2023). There has been a massive increase in the availability and accumulation of data, as well as advances in statistics, models, and cyberinfrastructure that facilitate the ability to create forecasting frameworks at the scale and speed needed by society (Dietze et al., 2018; Bradford et al., 2020a). For instance, at the long-term scale, forecasting frameworks can provide scenario-based projections to be used in planning, mitigation protocols and policymaking (Nissan et al., 2019). In contrast, a short-term forecasting framework can assist managers in anticipating change in more operational timeframes (Cuddington et al., 2013; Bodner et al., 2021). The use of any forecast temporal scale, however, needs to be assessed and designed based on the site-specific context and management needs (Dietze, 2017a; Bradford et al., 2020a; Bodner et al., 2021) taking into consideration relevant limitations and boundary conditions related to the modelling approach adopted (Beven, 2009; Beven and Binley, 2014; Cuddington et al., 2013).

In terms of societal demand, ecological forecasting applications are also growing considerably and have been proven useful in areas such as flood risk management, wildfire, agriculture and human disease (Brown et al., 2018; Dietze et al., 2018; Bradford et al., 2020b; Dietze et al., 2024). An increase in ecological forecasting applications can also benefit intervention in other two key priority areas such as (1) drinking water supply and (2) the conservation of freshwater biodiversity (Carey et al., 2022; King et al., 2023; Lofton et al., 2023). While these two areas are wide, they have specific components for which anticipating both short- and long-term changes in the dynamics of river and lake water systems requires new and innovative methods (Rousso et al., 2020; Teichert et al., 2020b; Bodner et al., 2021).

An important management challenge for drinking water suppliers is to adapt to the increasing levels of dissolved organic matter (DOM) in source waters (Anderson et al.,

2023). Increasing DOM concentrations (quantified using dissolved organic carbon (DOC)) lead to water browning (Kritzberg et al., 2020), a condition that affects ecosystem function (Evans et al., 2005) and drinking water quality (Riyadh and Peleato, 2024). Treating raw water with elevated DOC concentrations can be more difficult (Köhler et al., 2016) and can lead to the formation of disinfection-by products (DBPs) (Srivastav et al., 2020; Franklin et al., 2021a; Valenti-Quiroga et al., 2024), which are toxic compounds that affect human health (Diana et al., 2019). This issue represents a concern in many regions including northern Europe (Villanueva et al., 2023), as many drinking water sources are within catchments that are rich in organic carbon (e.g., catchments dominated by peatland and other high organic soils) (J. Xu et al., 2020; Fenner et al., 2021). Ireland and Sweden, in particular, have been experiencing persisting and elevated levels of DBPs in some of their water supplies which have been associated with increasing levels of DOC in source waters (Gonsior et al., 2014; O'Driscoll et al., 2018b; Klante et al., 2022). This represents an opportunity for the application of ecological forecasting frameworks, to assist in anticipating DOC raw water quality for improved decision-making along the drinking water cycle.

Forecasting DOC concentrations in drinking source waters in both the short- and long-term could lead to better water treatment and supply (J. Xu et al., 2020; DeMont et al., 2021; Anderson et al., 2023; Xiao et al., 2024). By anticipating DOC dynamics including DOC concentration levels, policymakers can develop better mitigation protocols and strategies at the catchment scale to protect source waters, and water managers could enhance treatment processes in order to improve the removal of DOM and reduce the formation of DBPs (J. Xu et al., 2020; Franklin et al., 2021b; Siddique et al., 2022a; Anderson et al., 2023; Daraei et al., 2023).

Another important management challenge is related to the conservation of migratory fish species in freshwater ecosystems (Tamario et al., 2019; Teichert et al., 2020b). Fish migrating from freshwaters to the sea and vice versa (i.e., diadromous fish) have

important life cycle components (e.g., spawning, reaching adult maturity) in freshwater bodies such as lakes (de Eyto et al., 2022; Ouellet et al., 2022). Some lake habitats have been modified by humans in order to expand productive systems (e.g., hydropower plants, dam construction, navigation, fishing) and for recreational purposes (e.g., tourism, water sports). This, along with climate-induced pressures, can put at risk the life cycle of many diadromous fish species including potential population decreases (Lowerre-Barbieri et al., 2019; Legrand et al., 2021; Dambrine et al., 2023; Rinaldo et al., 2024).

In general, diadromous fish migrations are driven by a combination of environmental factors including temperature, flow conditions, photoperiod, and moonlight exposure (Valiente et al., 2011; Lin, 2017; Sparks et al., 2019). Water temperature, in particular, has been highlighted as a key controller for diadromous fish migrations (Sykes et al., 2009; Riley et al., 2012; Zydlewski et al., 2014; Sparks et al., 2019). Moreover, water temperature is a variable that is being widely monitored across a large number of lakes and reservoirs globally (Piccolroaz et al., 2024), including sites that are important for diadromous fish (Tickner et al., 2020; Ouellet et al., 2022). Therefore, there is huge potential for developing and applying an ecological forecasting framework for diadromous fish migrations based on modelling and quantifying changes in lake water temperature conditions. Anticipating such ecological dynamics, especially in the short-term, could be useful for many management operations (e.g., dam release, fishing timings, pumping and turbine shutdowns) (Barbarossa et al., 2020; Trancart et al., 2020; Harringmeyer et al., 2021; Carter et al., 2023).

Recent studies have used modelling tools, often statistical- or process-based, to simulate DOC dynamics or fish migrations either in river or lake systems in specific sites and under specific conditions (e.g., Futter et al., 2011; Riley et al., 2012; Ledesma et al., 2012; O'Driscoll et al., 2018a; Zydlewski et al., 2014). Nevertheless, most of these studies focused on simulating historical observations and not on the value of generating

future predictions. This gap could be filled by adding methods for the prediction of such water quality and ecological dynamics (Bradford et al., 2020a; Lofton et al., 2023). However, it is important to acknowledge that the use of a specific modelling approach would have advantages, limitations and intrinsic sources of uncertainty (Beven, 2009; Hattermann et al., 2018; Her et al., 2019a). In the case of a process-based modelling approach, for example, it provides insights into modelled system dynamics beyond model outputs, information that could be useful for management as well (Beven, 2009; Cuddington et al., 2013). However, other factors such as the forcing data characteristics, the number of model state variables and governing equations (i.e., the model parameterisation), model equifinality (i.e., different calibration sets of model parameters producing equally good results) and uncertainty propagation should be considered when using such models in forecasting frameworks (Beven, 2009; Beven and Binley, 2014; Bodner et al., 2021; Pianosi et al., 2016). The consideration of such aspects is critical for a proper interpretation of model outputs and future predictions (Beven and Freer, 2001; Anderson et al., 2014) and for the communication of results to managers (Dietze, 2017a; Carey et al., 2022; Lofton et al., 2023).

1.2 Aim and objectives

The main aim of this research was to expand the range of available methods for modelling and forecasting short- and long-term changes in water systems to assist decision-making in water resource management applications. To achieve this, three case studies were conducted, each involving the development of a specific model-driven forecasting framework. Each forecasting framework was tailored to address a present-day water management issue by means of providing predictions about context-relevant water variables and/or ecological dynamics to support drinking water supply or the protection of freshwater biodiversity. In line with this, the main objectives of this thesis are to:

1. Design innovative forecasting frameworks for water quality and ecological dynamics that build on previous research efforts and benefit from emerging modelling tools, techniques and methods that can be integrated based on science.
2. Test the forecasting frameworks in settings where their application and future predictions are relevant and can serve as an example for supporting water resource allocation in either the drinking water supply sector or freshwater biodiversity conservation.
3. Evaluate the application of each forecast framework based on model performance, predictive skill, uncertainty estimation, scalability and its usefulness in real-world management applications.

1.3 Thesis outline

This thesis is divided into seven chapters which are represented in Fig. 1. This introductory chapter is followed by a literature review (Chapter 2) on ecological forecasting, modelling approaches for environmental and water systems, and related complementary methods and techniques relevant for the development of forecasting frameworks. Chapter 2 also provides an overview of the two main water management issues addressed in this work, which are related to drinking water quality and the conservation of freshwater biodiversity. Chapter 3 describes the main modelling tools used to drive the forecasting applications in this thesis. The first case study is presented in Chapter 4, in which long-term changes in river discharge and DOC dynamics were projected under different climate change scenarios to assist management in preserving drinking water quality and supply. Differently, in Chapter 5, a short-term forecasting approach was adopted. This time to develop a framework that uses lake water temperature forecasting as a tool to predict the migrations of diadromous fish, which are globally important freshwater species. Building on components of both Chapter 4 and Chapter 5, Chapter 6 tests workflows for short-term forecasting of DOC concentration in

river water, expanding the set of methods that can support drinking water treatment in operational timeframes. Lastly, Chapter 7 provides a synthesis of this thesis, summarising the structure of the frameworks and outlining actions for future modelling and forecasting efforts.



Figure 1.1 Thesis structure outline.

1.4 Contributions to knowledge

The work in Chapter 4 showed that model parameterisation can be an important source of uncertainty in future projections of river discharge and DOC concentration, especially in scenarios of high climatic variability such as the SSP585 scenario. The study showed that accounting for model parameter uncertainty in climate change impact assessments produces more robust outputs, by producing a more accurate range of variability for the modelled variables. This adds to the growing efforts of the modelling community in providing more accurate future predictions of water quality at the catchment scale. The work also showed how DOC concentrations are likely to increase in the future for the study sites, especially by the end of the century and under scenarios with low adaptation efforts and higher global warming. Moreover, the likelihood of extreme events for DOC flux and DOC concentration in the future was to projected increase as well. The results of this study could be indicative of future levels of change and the occurrence of extreme events that could be expected in similar settings, which is valuable information for catchment-scale management and water treatment protocols. Moreover, a key aspect of this study was model development. Changes to the model structure were made to improve the representation of hydrological processes in basins of large size (through the incorporation of a river channel water storage mechanism), and of DOC dynamics in high-organic soils, accounting for a better traceability of carbon washout via hydrological pathways, especially from peatlands.

The work in Chapter 5 showed that GLM and FLARE can be applied to successfully forecast water temperature in a deep (46.8 m) and large (≈ 3.95 km^2) lake system such as Lough Feeagh. This is an important aspect to highlight, as it was the first application of short-term water temperature forecasting using FLARE for a water body of such size and depth. Importantly, the predictions of fish migrations that were generated performed well for regimes that were not extreme, especially for the migrations of Atlantic salmon. This is an achievement in forecasting, especially because the framework was based on

the use of a single variable (water temperature) as a controller of the predicted ecological dynamic. This work expands the available pool of ecological forecasting tools for predicting fish migrations in the short term (daily scale). In line with this, the scalability of the framework was highlighted as an important component, as many settings around the world could benefit from exploring, applying and tailoring such an approach. This was supported by how the infrastructure of the framework was designed, with cloud-based repositories and automated online actions that require relatively little operation once the system is set up. This aspect also enables research to be more easily reproduced, archived, and used in the future to facilitate collaboration among stakeholders.

The work in Chapter 6 showed that it is possible to produce forecasts of DOC concentration in the short term using two different workflows. While there was large variability in the results for forecast performance, the work showed that by applying an specific approach it is possible to anticipate DOC concentration in river water in short forecast horizons (e.g., 3-days ahead), particularly during periods of high variability that could challenge water treatment applications. This study also highlighted the importance of assessing forecast forcing data, model parameterisation and calibration strategies and their impacts on forecast accuracy and uncertainty. Therefore, it has the potential to guide modellers to better integrate the different components (e.g., high-frequency monitoring, data assimilation techniques, modelling approach, forecast input data) into forecasting frameworks for, but not limited to, DOC. These insights represent an initial step to better understand the use of process-based models in short-term forecasting applications. It was critical to assess how potential forecasting configurations including their forcing data could influence future predictions, especially of DOC concentration, a relatively complex water quality variable to simulate and which has many implications for the environment and human health.

Chapter 2

Literature Review

2.1 Ecological forecasting

Ecological forecasting involves the combination of ecological theory with data availability and modelling tools to test specific, quantitative hypotheses about future ecosystem states (Dietze, 2017a; Lewis et al., 2022a). As a field, ecological forecasting has grown immensely along with new technology, cyberinfrastructure, software development and more efficient ways of collecting and transferring data (Beven, 2009; Dietze et al., 2024). There are now more ways of producing and gathering environmental data than ever (Dietze and Lynch, 2019; Wickberg et al., 2024). For instance, sensor technologies, satellites and genomics provide access to unprecedented volumes of environmental information that are born-digital and available in multiple time scales (Dietze et al., 2024). Similarly, software modelling tools have become more accessible and arguably more accurate in representing specific processes for which they are designed (Beven, 2009; Holman et al., 2019; Wagener et al., 2022). This has been accompanied by an increase in the development of complementary methods used within, before or after the modelling workflows, such as advanced statistics, data assimilation techniques, uncertainty estimation and sensitivity analyses (Beven and Freer, 2001; Beven, 2009; Beven and Binley, 2014; Pianosi et al., 2016; Dietze, 2017a). As a result, the rate of

forecast publication has increased, and ecological forecasts have now been produced for terrestrial, freshwater and marine ecosystems all around the world (Lewis et al., 2022a, 2022b; Payne et al., 2017).

Theoretically, the core of any ecological forecasting framework starts with a hypothesis of a natural process that would be represented in a model which can fall anywhere on the spectrum from empirical to fully process-based (Bodner et al., 2021; Lewis et al., 2022a) (Fig. 2.1). Then, a prediction is made about the future based upon that hypothesis, preferably including quantified uncertainty. Lastly, the forecast can be tested with measured data, allowing an evaluation of the model and refinement of the proposed hypothesis. This process can be iterative and carried out in a forecasting framework as new data are collected (Lofton et al., 2023; Thomas et al., 2023a). The forecasting outputs will then provide an insight into what is to come regarding the problem of interest and therefore, support decision-making regarding its solution.

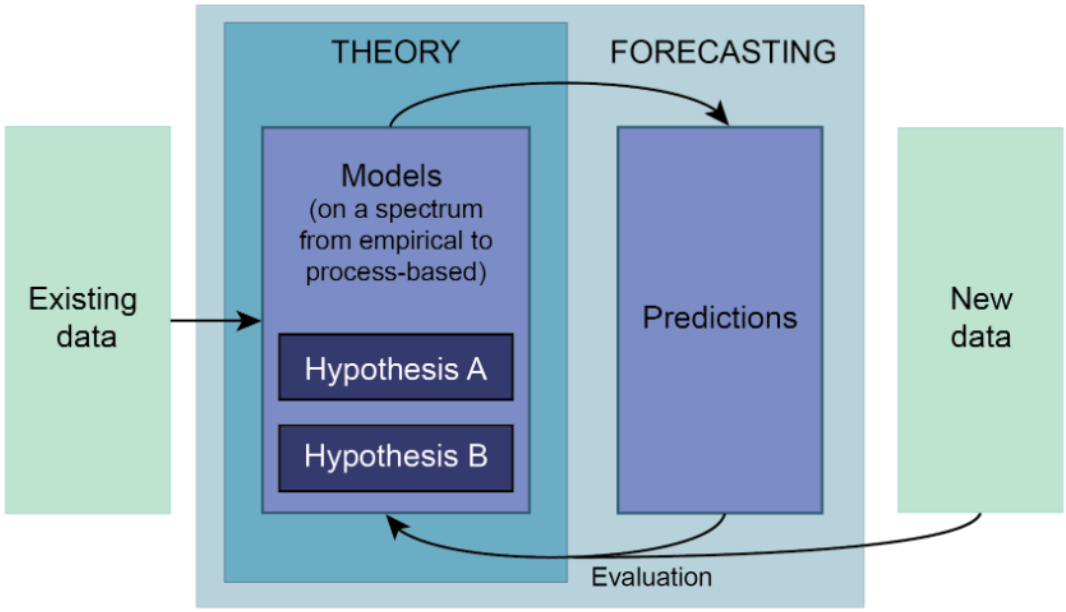


Figure 2.1 Conceptual diagram of an ecological forecasting framework (Lewis et al., 2022a).

By providing the capacity to quantify and anticipate change, forecasting frameworks are contributing to advancing fundamental ecological research (Payne et al., 2017;

Lewis et al., 2022a) and are transforming decision-making for numerous applied ecological problems (Bradford et al., 2020b; Bodner et al., 2021). Forecasts are useful to decision makers when they are decision-relevant. Relevance arises from understanding the current and future environmental priorities of stakeholders and by knowing the potential strategies being considered to manage an environmental issue (Bodner et al., 2021). For instance, different management scenarios could be evaluated by having quantitative predictions of changes in relevant environmental conditions that will have impacts of societal interest thus leading to improved decision-making (Fig. 2.2)

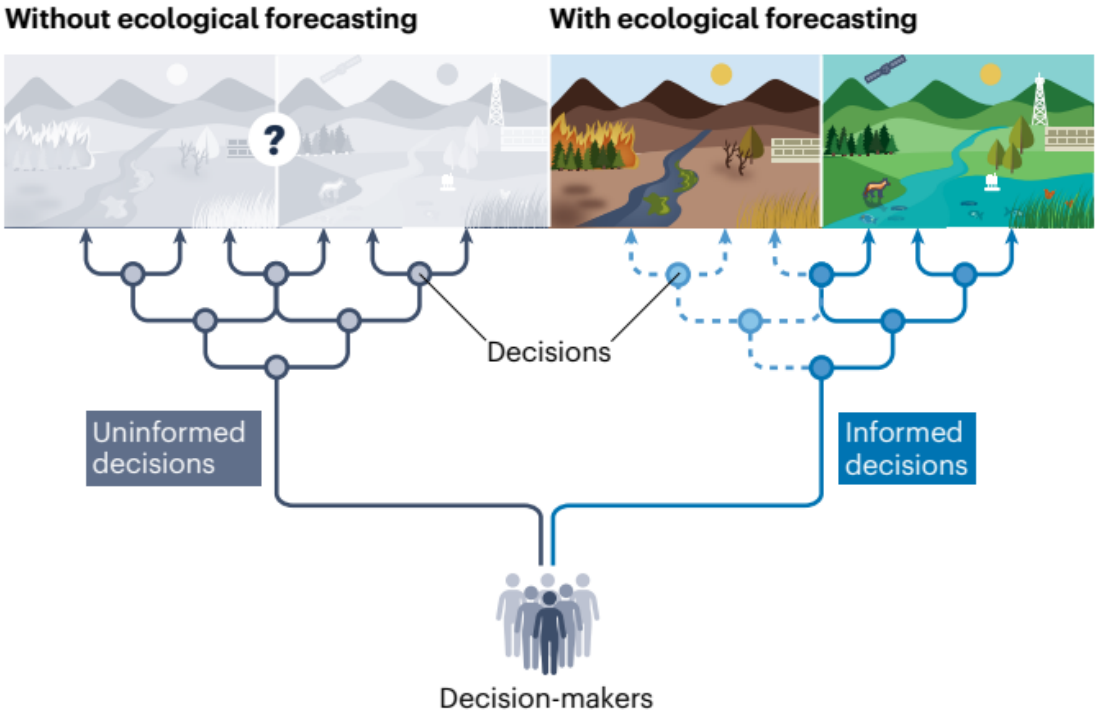


Figure 2.2 Representation of the decision-making process by stakeholders with and without the use of ecological forecasting (Dietze et al., 2024).

2.1.1 Forecasting water quality

When it comes to quantifying and forecasting changes in lakes and rivers, there is a large range of available methods for generating future predictions that are related to water quantity (e.g., runoff, discharge, water level, water demand, water volume change in lakes and reservoirs) (Lofton et al., 2023). Progress in water quantity forecasting has

been motivated by the risk to human health and property posed by the occurrence of flooding and droughts, which have both become more acute under global change (Jain et al., 2018; Troin et al., 2021; Kikon and Deka, 2022). This has prompted the creation of agencies around the globe that have developed forecasting frameworks to support water quantity forecasting at local, regional, national, and international scales (Jain et al., 2018). However, when it comes to water quality, there are less available tools and methods for predicting changes in water systems (Loos et al., 2020a; Lofton et al., 2023). Water quality forecasting has received less attention overall as water quality deterioration in rivers and lakes and its impacts on society have been relatively underestimated when compared to those of water quantity (van Vliet et al., 2017, 2023). In addition, hydrological modellers have tended to be engineers while water quality modellers come more often from a biology or environmental science background. Consequently, water quality forecasting has been less explored in environmental software-based research and water engineering (Lofton et al., 2023). However, there is a growing community of practice around ecological forecasting focusing on advancing water quality (Dietze and Lynch, 2019) although more applications are needed to supply societal demand (Bradford et al., 2020b), especially under an increasingly variable climate (Dietze et al., 2024).

Water quality forecasting can build on from existing meteorological and water quantity forecasting for projecting both short- and long-term changes in water systems. Meteorological forecasting, in particular, has progressed immensely over the last decades demonstrating that it is possible to generate reliable predictions for complex natural systems (Bauer et al., 2015; Dietze et al., 2024). Changes in water quality, similarly, often result from complex interactions in the environment that involve multiple factors including water quantity dynamics (van Vliet et al., 2023). Meteorology also illustrates the potential for both short-term forecasting in the provisioning of public goods (e.g., early warning systems) and private-sector innovation (e.g., weather apps), and

long-term forecasting by providing future projections through global climate models (GMCs) for a variety of purposes (e.g., climate change impact assessments) (Boretti and Rosa, 2019; Dietze et al., 2024). All these predictions are more than just the outputs from numerical models; they often involve different types of analytical adjustments and techniques along the forecasting workflow (Beven, 2009; Pianosi et al., 2016; Dietze, 2017a). In the case of meteorological weather forecasts, for example, climate models are iteratively updated with new data, sometimes multiple times a day, from a globally connected network of satellite and ground sensors, and new predictions are generated from the updated models (Hutton, 2019). These numerical predictions are then interpreted and adjusted by human forecasters and algorithms to produce the forecasts society depends on (Bodner et al., 2021; Dietze et al., 2024). Water quality forecasting should build on these frameworks and benefit from recent advancements including more and better data to provide decision-makers with the best available scientific insight, accelerate scientific discovery and improve understanding of ecological predictability more broadly (Loos et al., 2020b; Lewis et al., 2022a, 2022b).

2.1.2 Forecasting biodiversity dynamics

Over the last decades, there has been increasing recognition that ecological predictions for biodiversity must be advanced with clear statements of their uncertainty. How best to choose the model or models for predicting population and community dynamics, and how best to then define and present the uncertainties in these predictions, have been active and contentious topics in statistical and ecological research (Doak et al., 2008; Lewis et al., 2022a). Increased ecosystem variability experienced in habitats under global change precludes the use of historical baselines to inform our expectation of their future conditions (IPCC et al., 2023). Much of this variability occurs on different time scales (sub-daily to decades) and is often manifested across physical, chemical, and biological freshwater variables (Dietze, 2017a; Sánchez-Pinillos et al., 2024). For example, intense droughts and floods due to climate change are altering water quantity

in lakes, rivers, and wetlands, leading to changes in phenology and behaviour (Weiskopf et al., 2020; Staudinger et al., 2021). Similarly, dissolved oxygen concentrations, a key control on freshwater quality, are declining in temperate lakes worldwide as water temperatures warm and peak summertime algal bloom intensity increases (Carey et al., 2022; Lofton et al., 2023), which might affect the life cycle of freshwater species. These examples are a few of the many physical and chemical changes that may lead managers to seek skilful forecasts providing actionable, decision-relevant information about future habitat conditions that have impacts on the protection of biodiversity.

Compared with other forecasting fields, however, predicting ecological dynamics of biodiversity presents unique challenges. Unlike weather models, which rely on a predetermined number of state variables governed by relatively uniform physical equations (Dietze et al., 2024), ecological systems encompass millions of species, each exhibiting variability in key drivers of their dynamics and responses to environmental change (Doak et al., 2008). Organisms are heterogeneous across space and time in how they respond to changes induced by humans and climate, and those responses are continually adapting and evolving across a cascade of different timescales (Staudinger et al., 2021; Priya et al., 2023). Even if there is only interest in forecasting a specific ecological dynamic, biodiversity itself causes the parameters in the equations, and sometimes the equations themselves, to continuously change across space and time (Singer et al., 2016; Åkesson et al., 2021). However, this variability is not unconstrained, nor wholly unpredictable (Beven, 2009; Dietze et al., 2024). Beyond being important to theory, sharing information on the different forecasting frameworks being developed across the scientific community could lower the amount of data necessary to make predictions, allowing the scope of forecasting ecological dynamics to be extended (Bodner et al., 2021; Lewis et al., 2022b, 2022a).

The inherent complexity of biodiversity also introduces further challenges in ecological forecasting related to both monitoring requirements and the infrastructure for producing

forecasts (Fer et al., 2021; Recknagel, 2023). Forecasts for biodiversity dynamics can vary widely in scale (from global to local), approach (process-based, statistical, machine learning), system (terrestrial, freshwater, marine), and biological level (physiological, organismal, population, community, phenological) (Tulloch et al., 2020). This diversity generally requires a larger amount of data processing and forecasting workflows, often requiring significant resources and expertise to develop and maintain (Fer et al., 2021; Recknagel, 2023). However, these challenges also create opportunities to refine monitoring programs, advance sensor technologies, and improve the integration of data and forecasting infrastructure (Lewis et al., 2022a; Lofton et al., 2023). These advancements not only have the potential to enhance predictions for the dynamics of biodiversity but also to increase confidence in ecological forecasting overall (Dietze, 2017a; Tulloch et al., 2020).

2.2 Ecological forecasting for improved management

All decisions, whether individual or collective, are fundamentally about what decision-makers think will happen in the future, given what they know now, and the alternatives being considered (Beven, 2009; Dietze et al., 2024). In other words, they require forecasts. Many human activities that rely on the use of water need relevant, quantitative and evidence-based forecasts. It is of note, however, that no forecast is perfect, so it is critical to quantify uncertainties and provide either deterministic or probabilistic assessments that clearly articulate (rather than merely minimise) the uncertainties involved (Beven and Freer, 2001; Dietze and Lynch, 2019). Forecasts, therefore, should not only be aimed to be practically useful but to provide a mechanism for adapting ecological services to the rapidly changing environmental conditions (Bodner et al., 2021; Carey et al., 2022).

For a forecast to be used effectively, it should be prepared before decisions are made and should provide an adequate time window to be considered in the planning (Beven, 2009). Moreover, not only the expected outcome, but also other likely outcomes (such

as the worst, best outcomes and “do nothing” scenarios) should, if possible, be included in the forecast. If the worst outcome poses significant risk, forecast scenarios should be made for alternative interventions (Bodner et al., 2021). Forecast uncertainty should be communicated to the stakeholders as well and addressed properly in the planning stage (Lofton et al., 2023). Useful forecasts not only allow an estimation of future conditions but can inform on new, challenging existing expectations (Armstrong and Trevarthen, 1999; Bodner et al., 2021). This way, ecological forecasts can support many human applications and their interactions with the natural environment and contribute to adaptation efforts against climate change (Dietze et al., 2024).

Recent work on ecological forecasting aimed to support management has focused on a range of different variables of either water quantity, water quality or biodiversity dynamics at multiple temporal scales. For instance, seasonal forecasts are being used to predict the climate extremes (e.g., droughts) to assist ecological restoration efforts in freshwater and terrestrial ecosystems (Bradford et al., 2018, 2020a; Mercado-Bettín et al., 2021). In marine systems, predictions about the impacts of climate variability on species populations are assisting fisheries, aquaculture and navigation (Hobday et al., 2016; Roberts et al., 2023). Similarly, the dynamics of some bird species are being predicted to assist offshore renewable energies (Bradarić et al., 2024). Seasonal forecasts on crop yield are being used in agriculture (Brown et al., 2018; Zachow et al., 2023). Ecological forecasts are also started to be used by freshwater managers. Near real-time forecasts of water quality variables such as water temperature, dissolved oxygen, chlorophyll a, phosphorus and turbidity across diverse water systems (e.g., rivers, lakes, reservoirs and distribution networks) are assisting management in different sectors (e.g., water supply, hydropower, fisheries and agriculture) (Carey et al., 2022; Y. Liu et al., 2023; Lofton et al., 2023; Kiani and Ylivainio, 2024).

Moreover, long-term simulations of a diverse range of environmental dynamics have been produced, often to evaluate the impact of climate change scenarios in such

projections. For instance, projections on future evaporation levels on lakes, the occurrence of droughts, nutrient exports from rivers (e.g., phosphorus, nitrogen and carbon) and aspects of fish physiology offer long-term scale information to multiple sectors to assist policymaking, environmental intervention and resource allocation (Bell et al., 2021; Ayala et al., 2023; IPCC et al., 2023; La Fuente et al., 2024; Rinaldo et al., 2024). It is of note that a distinctive feature of long-term ecological forecasting is that it is generally more employed for regional and global extents (Boulange et al., 2023; IPCC et al., 2023; van Vliet et al., 2023), in addition to local case studies .

Ecological forecasts can also support management in other two key priority areas such as (1) drinking water supply and (2) the conservation of freshwater biodiversity (Carey et al., 2022; King et al., 2023; Lofton et al., 2023). Drinking water suppliers are facing challenges in adapting to increasing and more variable levels of dissolved organic carbon (DOC) in source waters (Anderson et al., 2023) while conservation efforts for protecting migratory fish species are struggling to cope with human and climatic pressures (Tamario et al., 2019; Teichert et al., 2020b).

2.2.1 Dissolved organic carbon (DOC)

Increases in dissolved organic matter (DOM) in source waters can represent an issue for drinking water supply, as these are associated with water browning (Kritzberg et al., 2020) a condition that affects raw water quality and its treatability (Gonsior et al., 2014; Köhler et al., 2016). Water browning refers to a considerable increase in water colour (Fig. 2.3) mainly attributed to rising concentrations of terrestrially derived dissolved organic matter (DOM) that are quantified using dissolved organic carbon (DOC) (Kritzberg et al., 2020; Anderson et al., 2023).

Concentrations of DOC must be reduced during drinking water treatment prior to any chlorination (Köhler et al., 2016; Piai et al., 2024), as DOM is a precursor to the formation of disinfection by-products (DBPs) (Srivastav et al., 2020; Franklin et al., 2021a). DBPs are toxic compounds formed via chemical reactions with chlorine-based disinfectants

(Sohn and Kim, 2002) and they are recognised to have negative implications on human health (Benson et al., 2017; Gilca et al., 2020). Some DBPs are known to be carcinogenic and cytotoxic when users are exposed to long-term drinking water consumption (WHO, 2011; Wang et al., 2019). Some of the most common (and most regulated) DBPs are the trihalomethanes (THMs), bromate and haloacetic acids (HAAs). For instance, in the European Union, THMs are one of the few DBPs that are currently regulated (Valenti-Quiroga et al., 2024). The concentrations of THMs in drinking water should be under the parametric value of 100 µg/L to be considered safe. This value was established in the European Communities (Drinking Water) (No. 2) Regulations 2007 (S.I. No. 278 of 2007) which enacted the Drinking Water Directive (Directive 98/83/EC).



Figure 2.3 Differences in water colour between freshwaters due to differences in the concentration of organic matter (Kritzberg et al., 2020).

The formation of DBPs has raised concern in many regions (Villanueva et al., 2023), including northern Europe where there are many drinking water sources located in settings in which DOC drains from terrestrial soil stores that are rich in organic carbon (e.g., from catchments dominated by peatlands and other organic soils) (Jennings et al., 2010a; J. Xu et al., 2020; Fenner et al., 2021). For instance, many lakes and rivers in Sweden, Ireland, Scotland and England have been reported to be affected by brownification, leading to issues in drinking water treatment and supply (Jennings et al., 2010a; Kritzberg et al., 2020; Meyer-Jacob et al., 2019). In fact, long-term DOC increases have been observed in recent decades across the northern hemisphere, and have been attributed to a combination of environmental factors and landscape

conditions with differing levels of importance depending on the specific site under analysis (Evans et al., 2005; de Wit et al., 2007; Oulehle and Hruška, 2009; SanClements et al., 2012; Anderson et al., 2023).

The export of DOC from terrestrial environments to freshwaters is linked to two processes: DOC production and DOC transport. Both production and transport result from complex interactions between landscape, land use and climate, including atmospheric deposition factors (Jennings et al., 2010a; Adler et al., 2021). On one side, DOC production is driven by physicochemical and biological mechanisms that regulate soil decomposition (e.g., microbial populations that break down soil organic matter). These mechanisms are largely regulated by temperature levels, water availability and acid deposition conditions (e.g., sulphur deposition) in the soil matrix. Temperature-dependent decomposition, in general, increases as temperature levels rise (see Davidson and Janssens, 2006; Mitchell and McDonald, 1992; Naden et al., 2010). However, differences in the quality and availability of substrate, constraints on the access of microbial enzymes to substrate molecules and fluctuations in microbial populations contribute to a wide variability in reported temperature sensitivities (Davidson and Janssens, 2006; Jennings et al., 2010a). Moisture-dependent decomposition dynamics in the soil matrix are complex, especially during waterlogged conditions or after drought-rewetting cycles (Jennings et al., 2010a). However, moisture-dependent decomposition tends to increase as the soil water decreases until it reaches a certain point, where decomposition will decrease as soil water continues to decrease (see Silvola et al., 1996; Naden et al., 2010). Acid deposition conditions will regulate decomposition by modifying pH levels, acid neutralization capacity or alkalinity (Anderson et al., 2023). However, acid deposition levels are gradually levelling off globally (Garmo et al., 2014; Wit et al., 2021) which makes this factor relatively less relevant in driving future DOC production at the catchment scale (Clark et al., 2010; Anderson et al., 2023; Wu and Yao, 2024).

In terms of DOC transport, catchment hydrological processes control DOC dynamics (Evans et al., 2006; Clark et al., 2009; Wit et al., 2021). DOC is transported primarily through surface and subsurface hydrological pathways, with the relative contributions of these pathways varying depending on precipitation patterns, soil properties, and topographical gradients (Clark et al., 2010; Blaurock et al., 2021). During high-flow conditions, such as storm events or snowmelt periods, overland flow (i.e., surface runoff) and shallow subsurface flow tend to transport DOC rapidly from the upper soil layers into receptor waters (Clark et al., 2010; Jennings et al., 2010a; Naden et al., 2010). Both important pulses and dilutions in DOC export can occur during high-rainfall periods and floods (Jennings et al., 2020). During low-flow periods, baseflow typically drives DOC transport with governing contributions from deep soil layers, where DOC experiences longer water residence times and potential sorption or degradation processes (Wu et al., 2023a, 2023b). Soil pore connectivity plays a crucial role in regulating DOC export, especially in riparian, wetland or peatland areas, that often represent key sources for DOC export to freshwater systems (Clark et al., 2009; Winterdahl et al., 2011; Arsenault et al., 2024). Season and event-driven hydrological shifts such as prolonged dry conditions, drought-rewetting cycles, lower water tables, and flooding, all impact DOC transport dynamics as well (Blaurock et al., 2021; Dong et al., 2021; Wu and Yao, 2024).

Importantly, an increase of DOC levels in rivers and lakes can lead to environmental degradation, independent of water use. Increasing DOC concentrations can affect the physical and biological cycles of freshwaters, ultimately affecting ecosystem biodiversity (Horppila et al., 2022). An increase in water colour can also reduce the penetration of sunlight radiation to deeper layers in lakes and reservoirs, modifying biological cycles (Arvola et al., 2010). High-coloured waters can also pose a risk to nutrient availability (George et al., 2010; Pettersson et al., 2010), especially when this availability is linked to seasonal patterns as in lakes, resulting in strong stratification in spring after the winter ice-melt (Arvola et al., 2010; Graneli, 2012).

2.2.1.1 Irish context

Irish drinking water supplies are predominantly sourced from surface waters i.e. rivers and lakes. In 2021, around 80% of the population was supplied from surface water sources (Rolston and Linnane, 2020). Generally, surface water bodies are more likely to be affected by brownification due to direct contributions of DOC loading from overland flows that tend to transport higher amounts of DOC relative to subsurface flows (Clark et al., 2010). Many Irish drinking water sources are located in areas where DOC drains from high-organic terrestrial stores such as peatland-dominated landscapes, resulting in elevated DOC loading to receptor waters (Doyle et al., 2019, 2021a; Jennings et al., 2010b, 2020).

In line with EU legislation, the parametric value for THMs in drinking water supplies in Ireland is 100 µg L^{-1}. However, there has been an on-going issue with breaches of this value especially since 2008, when it was reduced from 150 µg L^{-1}. Recently, Ireland has been found to be non-compliant regarding the concentrations of THMs in some of its drinking water supply zones over several years. In 2018, The European Commission sent a letter of formal notice to Ireland for failures regarding THMs in drinking water (MEMO-18-4486). A reasoned opinion followed in May 2020 (INF/20/859). The reasoned opinion concerned 44 water supply zones across the whole country. In November 2021, 30 drinking water supply zones serving a population of more than 200 000 citizens continued to exceed the parametric value for THMs. Because of this, the European Commission decided to refer Ireland to the European Court of Justice for failure to comply with the requirements of the Drinking Water Directive (IP/21/5356). Consequently, Ireland has been ruled against by the Court of Justice of the European Union (25 January 2024; Case C-481/22) for failure to fulfil obligations on the quality of water intended for human consumption.

The high levels of THMs in Ireland have been spatially related to catchment characteristics from where water is abstracted for drinking water. Land-use

characteristics, topographical gradient, local and regional climate have a strong influence on increasing DOM loading (Doyle et al., 2019, 2021), and hence on THMs formation (O'Driscoll et al., 2018c). For instance, peat land cover has been indicated as an important driver for DOC in Irish catchments (Doyle et al., 2019) and has been found to be a positive determinant of THMs formation. Areas with annual rainfall above the country's average (1400 mm year^{-1}) were also found to correlate with THMs formation (O'Driscoll et al., 2018). Moreover, relatively shallow slopes (< 5%) also can play a role in THM formation in Irish drinking water supplies. The distribution of these characteristics in Ireland is shown in Figure 2.4, highlighting the most affected regions in the country with respect to THMs concentrations (O'Driscoll et al. 2018). The regions that have had more problems related to breaches of THMs exceedances are located along the west coast of Ireland, running from south to north of the island.

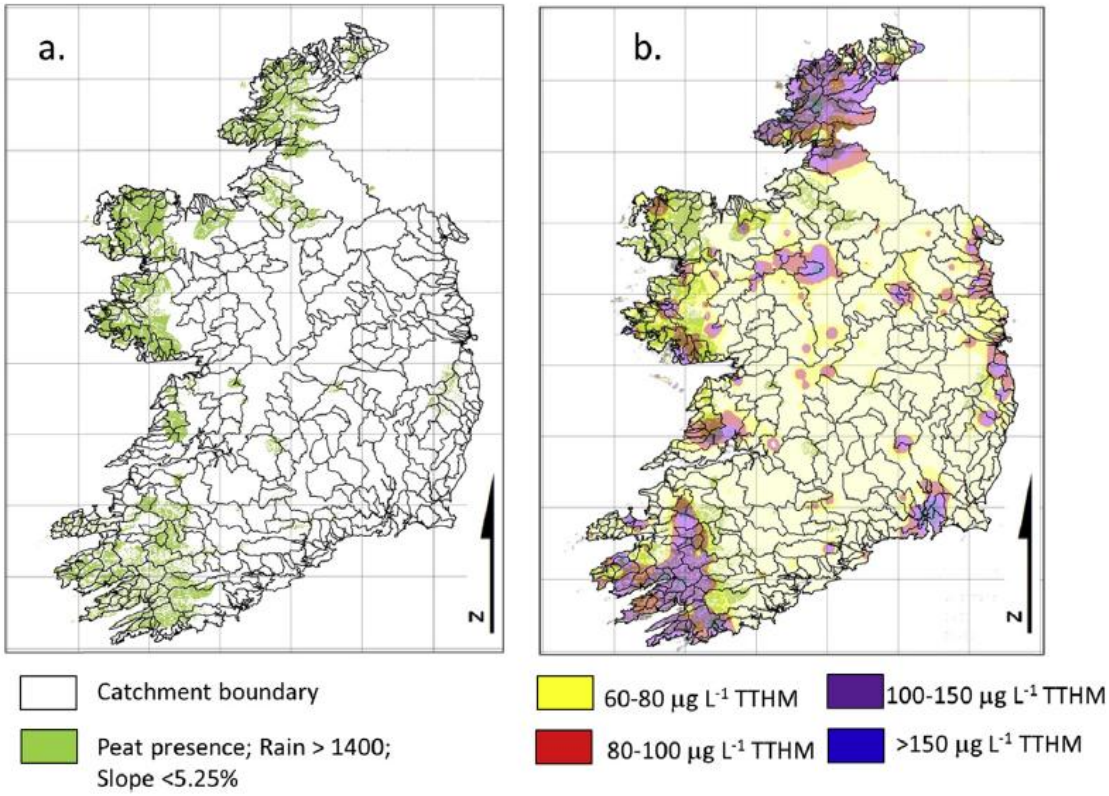


Figure 2.4 Irish catchment maps with peat presence (a), slope < 5.25% and annual average rainfall > 1400 mm year^{-1} with corresponding THM concentrations overlain (b) (O'Driscoll et al., 2018).

A range of both small- and large-scale mitigation measures are currently being required to be implemented in the country to address THM breaches (see EPA, 2013). The aim of these mitigation measures is focused mainly on the protection of sources, raw water quality and water treatment improvement. The importance, therefore, of determining raw water quality, including the concentration of DOC prior to treatment, is increasingly relevant. By informing managers about potential DOC levels at the source, action could be taken not only for source protection but for water treatment as well, ultimately leading to a potential reduction in THM levels (Li and Mitch, 2018; Absalan et al., 2024).

2.2.2.2 Swedish context

Browning of surface waters has been observed in Sweden for some decades already (Winterdahl et al., 2011; Kritzberg et al., 2020; Klante et al., 2021). Increasing DOC levels in Swedish freshwaters affect local aquatic ecology (Creed et al., 2018), contribute to higher CO_2 emissions (Lapierre et al., 2013) and complicate drinking water production (Lavonen et al., 2015; Lundqvist et al., 2019). The increases in DOC have been mainly attributed to an increased export of organic matter from terrestrial environments, especially those with high-organic soils and covered by forests (Kritzberg et al., 2020). Similar to Ireland, many drinking water supplies in Sweden are sourced from rivers and lakes located in such high-organic soil landscapes. This has affected drinking water quality with persisting breaches of THMs in some water supplies in addition to the formation of other DBPs (Gonsior et al., 2014; Lundqvist et al., 2019). These issues affect, for instance, Lake Mälaren, which is the third largest lake in Sweden and an important drinking water source (Ledesma et al., 2012). It supplies over two million people in Stockholm and provides of water to additional cities around the area.

Moreover, climate change is expected to intensify DOC loading into Swedish freshwaters and further complicate water treatment (Meyer-Jacob et al., 2019; Klante et al., 2021). For instance, a warmer climate could increase soil organic matter decomposition and thus DOM loading, especially in warmer periods which are estimated

that will be more prolonged in regions such as Scandinavia (Naden et al., 2010; Finstad et al., 2016). Mitigation measures addressing drinking water source protection and improved water treatment strategies have been identified in the country (Lundqvist et al., 2019; Kritzberg et al., 2020; Klante et al., 2022). All these measures could be enhanced by anticipating DOC dynamics in drinking water sources, especially in the context of an increasingly variable climate that could continue the browning of Swedish freshwaters and impose even further challenges for water supply.

2.2.3 Diadromous fish migrations and water temperature

Diadromous fish are species that migrate between freshwater and marine environments during their life cycle. This group includes the Atlantic salmon (*Salmo salar*), which migrates from freshwater to the ocean and returns to spawn, and the European eel (*Anguilla anguilla*), which follows the opposite pattern by growing in freshwater and migrating to the sea to reproduce (de Eyto et al., 2022; Ouellet et al., 2022). These migrations are essential for their survival, allowing them to complete key life stages such as growth and reproduction (Sparks et al., 2019; Long et al., 2023; Rinaldo et al., 2024). In addition, these fish species have direct implications on aquatic food webs (Dias et al., 2019; de Eyto et al., 2022; Ouellet et al., 2022) and nutrient cycling (Weaver et al., 2018; Oke and Hendry, 2019). However, because they rely on both freshwater and marine habitats, diadromous fish are especially vulnerable to changes in their environment and human activities (Piper et al., 2013; Lowerre-Barbieri et al., 2019; Legrand et al., 2021; Rinaldo et al., 2024).

The timing of diadromous fish migrations, known as their phenology, is influenced by environmental conditions. Factors such as water temperature, river flow, day length, photoperiod and moonlight exposure play a major role in regulating when fish begin their migrations (Valiente et al., 2011; Lin, 2017; Sparks et al., 2019). Water temperature, in particular, influences the metabolism and other physiological processes of fish directly (Seebacher and Post, 2015), resulting in pronounced effects on the timing and extent of

migrations (Riley et al., 2012; Zydlewski et al., 2014). It, therefore, has potential as an explanatory variable on which to associate the migration dynamics of diadromous fish, especially in the face of an increasingly variable climate, which can induce shifts in fish phenology (Lowerre-Barbieri et al., 2019; Legrand et al., 2021; Rinaldo et al., 2024). Disruptions to water temperature and other environmental drivers can affect migration timing and reduce the chances of successful reproduction (Lowerre-Barbieri et al., 2019; Legrand et al., 2021; Long et al., 2023). In addition, a more climate change can put additional pressures on their natural habitats with, for example, water quality degradation (e.g., occurrence of algal blooms in lakes) and the occurrence of extreme events (e.g., prolonged dry periods and decreased water availability) (Battin et al., 2007; de Eyto et al., 2016; Reed et al., 2017; Ouellet et al., 2022; Rinaldo et al., 2024).

Human activities can also put pressure on diadromous fish populations. For instance, hydropower dams and other barriers can block migration routes, preventing fish from reaching their spawning or feeding grounds (Barbarossa et al., 2020; Carter et al., 2023; Knott et al., 2023). Land-use changes, pollution, and overfishing can also harm these species by degrading habitats and reducing population sizes (Teichert et al., 2020a; Roberts et al., 2023). To protect diadromous fish like Atlantic salmon and European eels, it is essential to maintain migration pathways, manage fisheries sustainably, and restore damaged habitats (Battin et al., 2007; Reed et al., 2017).

Many diadromous fish populations can be found in temperate and subarctic regions of the world, where rivers and coastal waters optimal environmental conditions for different stages of their life cycle (Bolstad et al., 2021; Sparks et al., 2019; de Eyto et al., 2022). In Europe, many rivers and estuaries support populations of species like Atlantic salmon and European eel, with long-term monitoring programs providing valuable data on their movements and population trends (Teichert et al., 2020b; Legrand et al., 2021; de Eyto et al., 2022). These programs track migration patterns, growth rates, and environmental conditions, offering insights into how these species respond to changing ecosystems

(e.g., de Eyto et al., 2020; Legrand et al., 2021; de Eyto et al., 2022). These aspects are key to developing new approaches for management (Bradford et al., 2018; Bodner et al., 2021), including ways of anticipating changes in the ecological dynamics of diadromous fish (Teichert et al., 2020b; King et al., 2023), that could lead to improved adaptation efforts to protect these species.

2.2.3.1 Irish context

Ireland is home to important populations of diadromous fish. The Burrishoole catchment (Co. Mayo, western Ireland) hosts both Atlantic salmon (*Salmo salar*) and European eel (*Anguilla anguilla*) which are endemic to this location and represent key constituents of its aquatic food web (de Eyto et al., 2020). Long-term monitoring at the Burrishoole, conducted by the Marine Institute (http://marine.ie), has produced detailed records of fish movements, including the timing of upstream and downstream migrations. Water temperature has also been monitored long-term at different points within the catchment, allowing the opportunity to explore the relationship between this variable and diadromous fish phenology.

All fish moving into and out of the catchment are counted at two sites, the Salmon Leap and the Mill Race, the two water channels connecting freshwater Feeagh with the downstream brackish lagoon, Lough Furnace (Fig. 2.5). Consequently, the migrations of these species to and from Burrishoole freshwaters and the ocean are well documented (e.g., Byrne et al. 2003, Reed et al. 2017, Sandlund et al. 2017, Poole et al. 2018, and de Eyto et al. 2022).

In brief, salmon spawn in the Burrishoole catchment in winter, and juveniles spend a little over two years in freshwater (de Eyto et al., 2022). They migrate to the Atlantic Ocean as smolts in late spring, and after spending one winter at sea, return to freshwater in the summer as mature adults to spawn. Current evidence supports the view that European eel spawn as a single spawning stock in the Atlantic Ocean, in the area of the Sargasso Sea (de Eyto et al., 2022). Juveniles arrive off the Irish coast in autumn and

enter estuaries from November to February. As temperatures rise during the year, many commence active migration into freshwaters as elvers. Once in freshwater, elvers grow into yellow eel which is the life stage in which they spend most of their life (7–58 years in the west of Ireland). Eels mature only once when they undergo a process known as silvering before returning to the Atlantic Ocean to spawn (de Eyto et al., 2022). These information records are crucial for understanding how environmental changes, such as rising water temperatures and altered flow patterns, affect fish populations (Byrne et al., 2003; Rinaldo et al., 2024) and offer an opportunity to explore new approaches to improve the interactions between humans and these fish species.

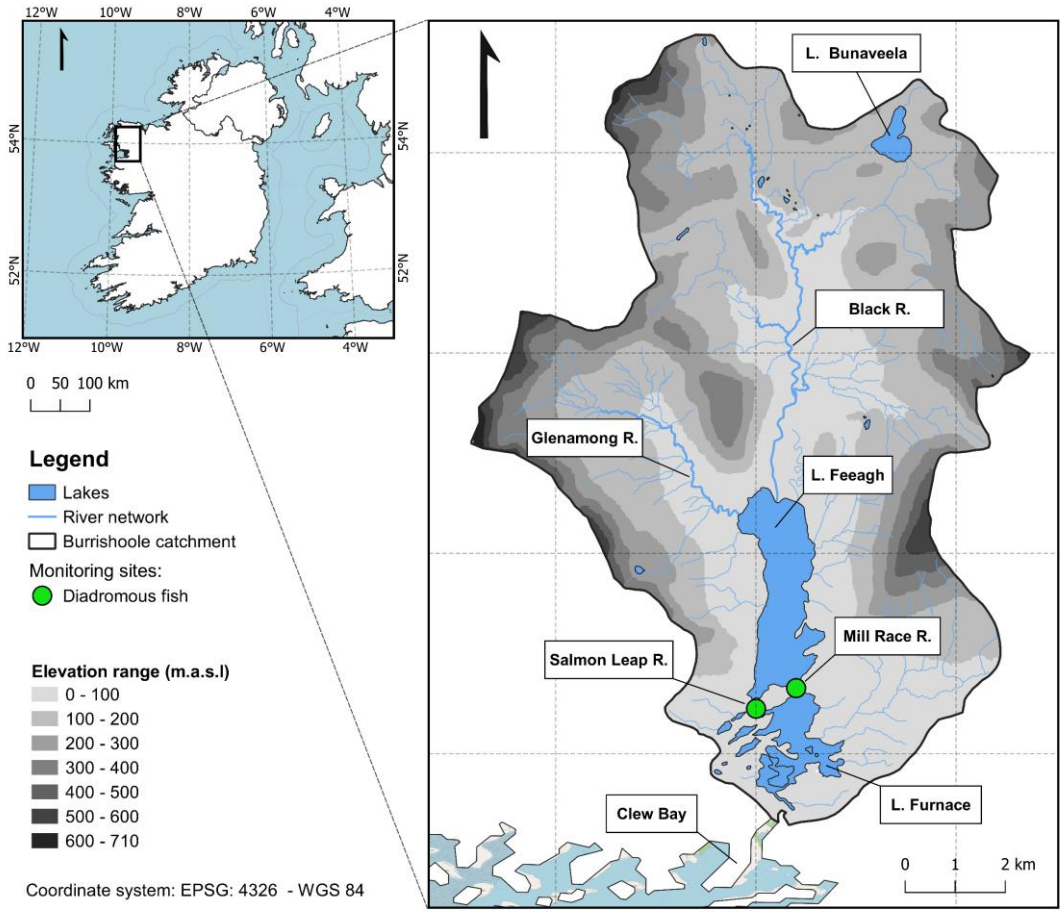


Figure 2.5 Location of the Burrishoole catchment in western Ireland, including main water bodies and topographic elevation. The monitoring sites for diadromous fish are indicated green dots.

2.3 Modelling approaches

The choice of a modelling approach in a forecasting framework depends on multiple factors, including the forecasting scope, the availability and quality of data, computational resources, and how well the model represents the processes of interest (Beven, 2009; Dietze, 2017a, 2017b). Different modelling approaches such as process-based, machine learning (ML), statistical, and hybrid can drive forecasting applications (Dietze et al., 2024) and offer distinct advantages and limitations (Beven, 2009; Cuddington et al., 2013). Process-based models, for example, offer insights into system dynamics by simulating variables that influence model outputs (Cuddington et al., 2013; Chen et al., 2021). However, depending on the model, data requirements can be extensive, and the number of model parameters could be large (Beven, 2009; Cuddington et al., 2013). In contrast, ML models rely on whatever data is available to feed data-intensive algorithms, offering flexibility and reasonable predictive power even when process knowledge is limited, though they may lack interpretability (Feigl et al., 2021; Mohammed et al., 2022). Hybrid models, which integrate multiple approaches, aim to combine the strengths of each method but also retain their respective limitations (Brentan et al., 2017; Deng et al., 2022). The balance between model complexity and predictive accuracy is critical when selecting a model, as more complex models may better capture system dynamics but also introduce greater uncertainty along the forecasting workflow (Beven and Binley, 2014; Pianosi et al., 2016; Dietze, 2017b).

To quantify and simulate changes in rivers and lakes, catchment-scale and lake-scale models are particularly useful. These models are often designed using a process-based approach, allowing researchers to analyse system dynamics of interest depending on the research scope (Beven and Freer, 2001; Schneiderman et al., 2010; Cuddington et al., 2013; Gao and Li, 2014; Paniconi and Putti, 2015; Tan et al., 2020; Mesman et al., 2020; Moore et al., 2021). For example, catchment models can simulate how changes in precipitation, temperature, and other factors influence river water quality over time

(Nasr et al., 2007; Jennings et al., 2009; Pierson et al., 2010; Jackson-Blake et al., 2016; Son et al., 2019). Similarly, lake models can quantify changes in aquatic habitats by representing key processes such as thermal stratification and oxygen levels (Hipsey et al., 2019; Mercado-Bettín et al., 2021; Mesman et al., 2020; Moore et al., 2021; Ayala et al., 2023). Together, catchment and lake models represent useful tools for understanding and forecasting the impacts of environmental variability and human activities on freshwater ecosystems.

2.3.1 Catchment-scale models

Catchment-scale water quality modelling has become an important instrument for simulating environmental processes that are relevant for societal interest worldwide (Fu et al., 2019). Many models exist, built generally around simplifying assumptions of natural hydrological systems (Beven, 2012). While catchment models are widely used in scientific research, they have also proven valuable for water management and industrial applications (Daniel, 2011; Yuan et al., 2020). However, different models have different advantages and limitations under specific conditions (Gao and Li, 2014). The selection of a catchment model or a set of models is mainly dependent on the output variable to be modelled, applicability, processes of interest to be simulated and input and output data (Costa et al., 2021).

In a spatial context, catchment-scale models can be categorized as lumped, semi-distributed or distributed (Gao and Li, 2014; Maskey, 2022). The lumped models represent the catchment by a single hydrological response unit i.e., assume homogeneity across the entire catchment. Meanwhile distributed models, which are more complex, consider spatial variability of the catchment's physical properties. This is generally done by subdividing the catchment area into smaller hydrological response units that simulate spatially-specific hydrological processes. Semi-distributed models on the other hand can fall anywhere within the spectrum from lumped to distributed and are aimed to be optimised to benefit from the strengths of each (Okiria et al., 2022).

Similarly, different models can simulate hydrological processes at different dimensions (i.e., 1-D, 2-D and 3-D) (Glock et al., 2019). Some of the most commonly used catchment models that simulate hydrology and water quality include (1) SWAT, (2) INCA, (3) SPARROW, (4) WASP, (5) QUALs, and (6) GWLF (see Table 2.1 for abbreviations) (Costa et al., 2021; Fu et al., 2020, 2019; Gao and Li, 2014). Each of these models is briefly described in the following subsections with a focus on simulating hydrological and DOC dynamics.

Table 2.1 Commonly employed catchment-scale hydrological and water quality models

Catchment-scale model	Abbreviation	Main reference
Soil and Water Assessment Tool	SWAT	Gassman et al. (2007)
The Integrated Catchment Model	INCA	Whitehead et al. (1998)
The Spatially Referenced Regression Model on Watershed Attributes	SPARROW	Smith et al. (1997)
The Water Quality Analysis Simulation Program	WASP	Wool et al. (2020)
Enhanced Stream Water Quality Models	QUALs	US EPA (1987)
Generalised Watershed Loadings Function Model	GWLF	Haith and Shoemaker (1987)

2.3.1.1 SWAT

The Soil and Water Assessment Tool (SWAT) is a semi-distributed hydrological and water quality model developed by the USDA Agricultural Research Service (USDA-ARS) and Texas A&M AgriLife Research, part of The Texas A&M University System (Gassman et al., 2007). SWAT includes multiple components for simulating hydrological processes, crop growth and yield, erosion processes, sediment transport, pollutant cycling and transport, and the effects of land management practices.

Spatially, SWAT operates at the sub-basin scale, subdividing each catchment into smaller hydrologic response units (HRUs) based on physical characteristics such as

topography, flow routing, land use, and soil properties (Tan et al., 2020). The model can simulate processes on a daily, monthly, or annual timescales and has been widely applied over the past two decades (Tan et al., 2020). SWAT has been employed to simulate hydrology and water quality across various regions, including northern Europe (Bärlund et al., 2007; Exbrayat et al., 2010; Abbaspour et al., 2015; Basu et al., 2022; Carstensen et al., 2023). However, its limitations are often linked to specific site conditions and data availability. For example, Qi et al. (2016) and Nafees Ahmad et al. (2011) reported issues in simulating baseflow discharge, soil temperature, and nutrient loadings (e.g., sediment, phosphorus, and nitrate) in areas with substantial winter snow cover. Similarly, Yang and Zhang (2016) showed that the model does not simulate forest dynamics very accurately.

However, SWAT has been successfully applied to simulate river discharge in a range of different study sites to assist water management in areas such as agriculture, and hydropower (Francesconi et al., 2016; Chen et al., 2019; Busico et al., 2020; Musyoka et al., 2021; Kouadio et al., 2022). Regarding water quality, SWAT has been mainly used to simulate nitrogen and phosphorus concentrations (Hollaway et al., 2018; Qi et al., 2020; Carstensen et al., 2023). Other water quality variables such as DOC are not supported by the main model. Nevertheless, there has been some work related to DOC simulations using SWAT by integrating specific DOC processes in the model. For instance, Du et al. (2019) integrated DOC production in soils and aquatic transport processes into SWAT which resulted a satisfactory applications for a specific catchment located in the USA.

2.3.1.2 INCA

The Integrated Catchment (INCA) model is a semi-distributed hydrological and water quality model developed by Paul Whitehead and Dan Butterfield around 1990 (Whitehead et al., 1998). The first version of the model was developed to simulate inorganic nitrogen for rivers in the United Kingdom. Since then, versions of the model

have been developed for phosphorus, carbon, sediments and organic micropollutants (Futter et al., 2011; Jackson-Blake et al., 2016; Whitehead et al., 2021)

The flow and water quality mechanisms in the model include plant and soil system dynamics and in-stream biogeochemical and hydrological processes. Similar to the SWAT model, the INCA model can operate at a daily time step through HRUs, tracking the stores and fluxes of water, sediments, and of the water quality parameter of interest. For instance, for phosphorus simulations (for which the model would be usually called INCA-P), the dissolved and particulate phosphorus in both the land and in-stream phases would be represented in each functional unit of the model. Jackson-Blake et al. (2016) described in detail the INCA model with an emphasis on phosphorus simulations.

The INCA model has been applied to a large number of study sites varying in catchment size and geographical distribution. Applications of INCA are mainly for simulating sediment loads, and phosphorus and carbon dynamics (Rankinen et al., 2010; Futter et al., 2011; Jackson-Blake et al., 2016; O'Driscoll et al., 2018a); but has been also used to simulate other parameters in waters such as metals, pathogens and microplastics (Whitehead et al., 2016, 2021). Nevertheless, the model has some limitations with respect to the representation of specific hydrological and hydrochemical processes. For instance, the predictive ability of the model to predict in-stream DOC could be improved. Futter et al. (2007) indicated that the effects on droughts on flow paths within the soil may not be adequately modelled and could underestimate DOC concentrations in the modelled system. However, the INCA model has been demonstrated to provide useful information of hydrological and water quality processes; and support assessing the impacts of climate change in sectors such as agriculture and drinking water supply (e.g., Farkas et al., 2023; Ledesma et al., 2012; Ervinia et al., 2020; J. Xu et al., 2020).

2.3.1.3 SPARROW

The Spatially Referenced Regression Model on Watershed Attributes (SPARROW) is a mechanistic/statistical catchment model developed by the United States Geological

Survey (USGS) (Smith et al., 1997). It was developed for simulating contaminant transport processes by relating the water quality data of monitoring stations within the catchment system. The model consists of nonlinear regression equations describing the non-conservative transport of contaminants from point and non-point (or diffuse) sources on land to rivers and through the river network (Schwarz et al., 2006).

SPARROW can operate at a daily time step and requires the integration of geospatial data for use as explanatory variables which are considered as either constituent sources or delivery factors (Schwarz et al., 2006; Preston et al., 2011). The model identifies the relative importance of contaminant sources to streams and estimates the importance of landscape factors in the delivery of those contaminants to streams (Schwarz et al., 2006; Preston et al., 2011). It also imposes mass balance constraints on all estimates of contaminant loading. In general, the SPARROW model simulations of nutrient sources and loads reflect long-term nutrient conditions in streams.

There are, however, limitations mainly related to scale when using the model for water-quality management (Schwarz et al., 2006). These include: (1) increased uncertainty at locations and scales that differ from those of the existing monitoring data used for model calibration and (2) the possibility of differing model results for models developed at different scales (Schwarz et al., 2010). Other limitations are that SPARROW model calibration runs for different but overlapping spatial areas may not provide identical predictions of mean conditions for a given catchment. In addition, one important factor for uncertainty in the model is the limitation in the number of monitoring sites available for calibration (Smith et al., 1997; Schwarz et al., 2010).

Nevertheless, the SPARROW model has become popular and increasingly employed, especially in the USA. Applications of the SPARROW model are mainly to assess stream sediment and nutrient loads into water bodies and ecosystems (Dai et al., 2021; Duan et al., 2015). It is of note that SPARROW does not support simulations of DOC loads but it does simulate total organic carbon (TOC) loads (Schwarz et al., 2010).

2.3.1.4 WASP

The Water Quality Analysis Simulation Program (WASP) is a surface water quality model developed by the US Environmental Protection Agency (EPA) (Wool et al., 2020). A hydrodynamic module is needed to be incorporated within the model for hydrological routing which would be generally driven by meteorological inputs (Obin et al., 2021). WASP is aimed to help users to interpret and predict water quality to natural and human-induced pollution, and includes the representation of management decisions. WASP operates at a daily time step and allows simulations to be done in one (1-D), two (2-D), and three (3-D) dimensions. The processes of advection, dispersion, point and diffuse mass loading and boundary exchange are represented in the model and tracked over model time steps (Wool et al., 2020).

WASP supports simulations of DOC loads but is mainly applied for simulating eutrophication, phosphorus loading and metal pollution in rivers and estuaries (Jian et al., 2016; Zafer Defne et al., 2017). The model has been employed mainly in the USA, for assisting management practices and long-term environmental interventions (Wang et al., 2018; Mamani Larico and Zúñiga Medina, 2019; Wool et al., 2020; Obin et al., 2021). Nevertheless, the model present some limitations with respect to the representation of some of the in-stream processes that some pollutants undergo (Kannel et al., 2011). For instance, solving advection in flow current is not supported by the model and is usually addressed by coupling hydrodynamic models to WASP. The coupling of hydrodynamic models to WASP would be a general practice and often used to improve the capabilities of the water quality simulations related to the parameter of interest (Jian et al., 2016; Zafer Defne et al., 2017).

2.3.1.5 QUALs

The US Environmental Protection Agency (EPA) released a series of QUAL models that include QUAL2E, QUAL2K AND QUAL2KW (US EPA, 1987; Fang et al., 2008; Raeisi et al., 2022). These models allow the simulation of various water quality parameters

(e.g. dissolved oxygen, biological oxygen demand, temperature, and phosphorus) at a daily time step. QUALs use a one-dimensional steady state structure for non-uniform steady flow in streams and rivers (Raeisi et al., 2022) and can be coupled with additional modules to integrate components relevant for the scope of the study. For instance, CE-QUAL-W2 results from model integrations that allow two-dimensional, longitudinal/vertical hydrodynamics to simulate catchment water quality with a distributed configuration. This was developed by the US Army Corps of Engineers to best suit the model for relatively long and narrow rivers exhibiting longitudinal and vertical water quality gradients.

Different versions of QUALs have been applied to a number of rivers, lakes and reservoirs and combinations thereof, mainly in North America (Lindenschmidt et al., 2019; Shabani et al., 2021; Bornstein et al., 2022). The current versions of QUALs models do not support DOC simulations. They are mainly used to simulate other nutrients (e.g., phosphorus and nitrogen), algae, and temperature (Noori et al., 2015; Zhu et al., 2017; Khodabandeh et al., 2021). There exist important limitations for these QUALs models (see Raeisi et al., 2022). For instance, with respect to CE-QUAL-W2, the governing hydrodynamics and transport equations are laterally averaged; thus, variations in temperatures, velocities and constituents can be negligible. This might result in not-so-appropriate outputs for catchments and waterbodies with relevant variations in water quality (Noori et al., 2015; Lindenschmidt et al., 2019).

2.3.1.6 GWLF

The Generalised Watershed Loadings Function (GWLF) model is a lumped to semi-distributed hydrological and water quality model first introduced by Haith and Shoemaker (1987). The model simulates water balance and partitions water among the different pathways of the hydrological cycle. The catchment is viewed as a system of different land areas and concentrations of dissolved and suspended substances (e.g.,

nutrients and sediment) in streamflow are estimated at the outlet by loading functions that relate the hydrological components to catchment specific characteristics.

Different versions of the model that follow the base structure of GWLF have been used for simulating streamflow, sediment loads and nutrient loads (e.g., nitrogen, phosphorus and DOC) in different countries including Finland, Ireland, Sweden, USA, and China (Moore, 2007; Jennings et al., 2009; Einola, 2013; Niraula et al., 2013; Qi et al., 2017). It has also been used to assess the impact of climate change for a set of catchments across Europe with satisfactory results for hydrology (Schneiderman et al., 2010; Matonse et al., 2013) and a set of nutrients (Climate and Lake Impacts in Europe, 2003-2005) (Jennings et al., 2009; Pierson et al., 2010) including DOC (Naden et al., 2010).

The benefits of using GWLF include a relatively easy set-up, fewer data requirements, and less software computing time than most of the more distributed models, while at the same time, it can provide outputs at a daily time step. However, in general, the structure of the model is simpler than the alternatives and might not represent some specific processes well depending on the study catchment (Qi et al., 2017). Despite not being as complex as some more commonly used models (e.g. SWAT and INCA) GWLF has been found to perform well under specific conditions compared to such models in hydrological simulations (Niraula et al., 2013; Qi et al., 2017). A more detailed description of GWLF is provided in Chapter 3.

2.3.2 Lake-scale models

Lake models are tools frequently used to simulate and quantify lake hydrodynamics. These models enable improved understanding on how shifts in climate, land use, and nutrient inputs affect lake structures, thermal stratification, oxygen dynamics, and water quality (Bruce et al., 2018; Hipsey et al., 2019; Moore et al., 2021; Piccolroaz et al., 2024). Depending on spatial resolution, lake models are classified into one-dimensional (1-D), two-dimensional (2-D) and three-dimensional (3-D) models. While 2-D and 3-D models provide detailed spatial representation, they require substantial computational

resources and extensive data inputs. In contrast, 1-D models, which simulate processes along the vertical axis while assuming horizontal homogeneity, are more computationally efficient and are therefore the most widely employed for simulating lake dynamics (Bruce et al., 2018; Moore et al., 2021).

The assumption of complete horizontal mixing in 1-D lake models is verified across a range of lake studies that have highlighted the dominant role of seasonal changes across the vertical axis (Gal et al., 2009; Bruce et al., 2018; Hipsey et al., 2019). A range of different 1-D models have been applied to many lakes around the world to simulate key physical processes (e.g., vertical mixing, heat fluxes, and inflow dynamics) which are critical for understanding seasonal thermal stratification and its influence on other ecological dynamics (Bruce et al., 2018; Hipsey et al., 2019; Moore et al., 2021; Ayala et al., 2023).

The structure of 1D lake models typically follows either a Lagrangian or Eulerian framework. Lagrangian models represent the lake as horizontal layers with uniform properties that can expand, contract, or merge based on the parameterization of mixing processes (Hipsey et al., 2014; Moore et al., 2021). Examples of Lagrangian models include the General Lake Model (GLM) and the Dynamic Reservoir Simulation Model (DYRESM). In contrast, Eulerian models use a fixed grid structure where fluxes occur between discrete layers. Examples of Eulerian models include the General Ocean Turbulence Model (GOTM), Simstrat, and the multi-year lake simulation model (MyLake) (Moore et al., 2021). Each of these commonly employed 1-D lake models (Flake, Simstrat, MyLake, GOTM and GLM; Table 2.2) is briefly described in the following subsections. Note that each of these lake models has different data requirements, model set-up configuration, computational demands and model outputs display (see Moore et al. (2021) for more details).

Table 2.2 Commonly employed lake-scale 1-D hydrodynamic models

Lake-scale 1-D hydrodynamic model	Abbreviation	Main reference
Freshwater Lake Model	FLake	Mironov (2005)
Simstrat	Simstrat	Goudsmit et al. (2002)
Multi-layer Lake Simulation Model	MyLake	Saloranta and Andersen (2007)
The General Ocean Turbulence Model	GOTM	Burchard et al. (1999)
The General Lake Model	GLM	Hipsey et al. (2019)

2.3.2.1 FLake

The Freshwater Lake Model (FLake) is a bulk model designed for efficient coupling between lake systems and the atmosphere, particularly in numerical weather prediction models (Mironov, 2005; Moore, 2020). It employs a two-layer parametric approach focused on the heat budget of the lake. The upper layer is considered thermally homogeneous and well-mixed, while the lower, stably stratified layer is represented by a self-similar temperature profile (Mironov, 2005). This approach is also applied to simulate ice and sediment temperatures. FLake is relatively computationally efficient, which makes it widely used for both global and local lake studies, particularly when rapid simulations of thermal dynamics are required (Thiery et al., 2014b, 2014a; Woolway et al., 2014; Moore et al., 2021).

The model simulates vertical temperature dynamics up to the mean lake depth, assuming a rectangular basin shape, and does not account for the lake's specific hypsography. Consequently, FLake is often applied in shallow water bodies, where the mean depth offers a reasonable approximation of vertical temperature profiles (Moore, 2020; Moore et al., 2021). To run FLake, input data typically includes meteorological variables such as air temperature, radiation, wind speed, humidity, and precipitation, alongside lake-specific information such as inflows, depth, and surface area (Mironov et al., 2010; Moore et al., 2021).

2.3.2.2 Simstrat

Simstrat is a 1-D vertical hydrodynamic lake model that combines a buoyancy-extended k-epsilon turbulence model with seiche parameterization to simulate lake dynamics (see Goudsmit et al., 2002). Simstrat simulates surface energy fluxes, vertical profiles of turbulent diffusivity, and water temperature dynamics, while offering flexibility in external forcing (Gaudard et al., 2019; Moore et al., 2021). The model includes variable wind drag coefficients, inflow settings, and the ability to simulate ice and snow formation. Simstrat has been successfully applied to many lakes and reservoirs across the world for various purposes, including for evaluating the impacts of global warming (Stepanenko et al., 2013; Thiery et al., 2014a, 2014b; Kobler and Schmid, 2019; Moore et al., 2021). The model requires input data such as meteorological variables, inflow temperatures, and wind drag coefficients (see Gaudard et al., (2019) and Moore et al., (2021) for more details).

2.3.2.3 MyLake

The Multi-year Lake Simulation Model (MyLake) is a vertical 1-D lake model developed and maintained by the Norwegian Institute for Water Research (NIVA), the University of Helsinki (Finland), and Université Laval (Canada). It simulated water temperature profiles, seasonal ice and snow cover, sediment-water interactions, density stratification, and phosphorus-phytoplankton dynamics in a daily time step (Saloranta and Andersen, 2007; Moore, 2020). MyLake has been employed to simulate lake dynamics mainly in lakes located in the northern hemisphere (e.g., Saloranta and Andersen, 2007; Couture et al., 2018). MyLake requires meteorological data as inputs (shortwave radiation, air temperature, air humidity, wind speed, cloud cover and longwave radiation) in addition to lake characterization parameters (see Moore et al., 2021).

2.3.2.4 GOTM

The General Ocean Turbulence Model (GOTM) is a vertical 1D hydrodynamic model designed to simulate key hydrodynamic and thermodynamic processes related to vertical mixing in natural waters. Initially developed for ocean turbulence, GOTM has since been adapted for use in lakes (Burchard et al., 1999, 2006). The model has been employed for multiple purposes including assessing the impact of extreme events in aquatic systems, evaluating the role of macrophytes in water quality, and projecting the thermal structure of lakes under both past and future climate conditions (Sachse et al., 2014; Moras et al., 2019; Ayala et al., 2020; Mesman et al., 2020; Ayala et al., 2023).

GOTM features a modular structure, allowing users to select different turbulence closure schemes, providing flexibility in simulating vertical mixing processes (Burchard et al., 2006). Using an Eulerian framework with a fixed vertical grid, the model resolves fluxes between layers to capture thermal stratification and mixing dynamics (Burchard et al., 2006). Detailed input data is required, including meteorological forcing (e.g., air temperature, wind speed, humidity, and radiation), bathymetric information, and inflow characteristics (Umlauf et al., 2005; Burchard et al., 2006; Moore et al., 2021).

2.3.2.5 GLM

The General Lake Model (GLM) is a 1-D hydrodynamic lake model developed mainly by the University of Western Australia. It employs a flexible Lagrangian structure where layers split or merge based on their density, allowing for a dynamic representation of mixing processes (Hipsey et al., 2013, 2014). Surface mixing is calculated using an energy balance approach, comparing available kinetic energy to the potential energy of the water column (Hipsey et al., 2019). GLM has been widely used to simulate seasonal temperature and ice cover dynamics, evaluate the effects of water management strategies on lake ecosystems, and assess the impacts of extreme events (Hipsey et al., 2017; Bruce et al., 2018; Mesman et al., 2020; Moore, 2020; Piccolroaz et al., 2024). A detailed description of GLM is provided in Chapter 3.

2.4 Model performance, sensitivity and uncertainty

When employing a model to quantify changes in water systems (here rivers and lakes), it is essential to evaluate its performance. Model performance can be assessed using various goodness-of-fit metrics, which generally measure how well the simulations replicate the observed behaviour of the target variable during a specific period or multiple timeframes (Krause et al., 2005). Common performance metrics used in software-driven environmental modeling include root mean squared error (RMSE), the Nash-Sutcliffe coefficient (NSE) and the coefficient of determination (r^2) (Krause et al., 2005; Beven, 2009). These metrics all quantify the alignment between simulated values and the observed values of the variable of interest. Each metric considers different aspects of how well the data fit (see Krause et al., 2005).

When evaluating model performance, it is also crucial to perform a sensitivity analysis (SA) and assess uncertainties as thoroughly as possible (Beven and Freer, 2001; Pianosi et al., 2016). SA examines how variations in the output of a numerical model can be attributed to changes in its input factors. This process helps identify which inputs have the most influence on model behaviour (Pianosi et al., 2016). Following sensitivity analysis, an uncertainty analysis should be performed to estimate the degree of uncertainty in the model's predictions (Beven, 2009; Beven and Binley, 2014; Pianosi et al., 2016). An uncertainty analysis evaluates the potential variability in the model results by considering relevant sources of uncertainty (e.g., input data, model structure and model parameterization), providing a more comprehensive understanding of how reliable is the model (Pianosi et al., 2016).

2.4.1 Performance metrics

2.4.1.1 Root mean squared error (RMSE)

The root mean squared error (RMSE) quantifies the average magnitude of the errors between predicted and observed values. The RMSE is calculated by taking the square

root of the mean of the squared differences between predicted and observed values. A lower RMSE indicates a better agreement between predicted and observed values.

$$RMSE = \sqrt{\frac{1}{n}\sum_{i=1}^{n}(y_i - \hat{y}_i)^2} \quad (2.1)$$

where n is the number of observations, y_i represents the observed values, and $\hat{y}_i$ represents the predicted values. Its analytical expression is similar to the standard deviation in the sense that RMSE refers to n data points instead of $n-1$.

2.4.1.2 Nash-Sutcliffe coefficient (NSE)

The Nash-Sutcliffe Efficiency (NSE) measures how well the predicted values replicate the observed data, by comparing the error variance to the observed data variance. It ranges from -∞ to 1, with 1 representing a perfect fit, 0 indicating that the model performs no better than the mean of the observed values, and negative values suggesting worse performance than simply using the mean (Krause et al., 2005).

$$NSE = 1 - \frac{\sum_{i=1}^{n}(y_i - \hat{y}_i)^2}{\sum_{i=1}^{n}(y_i - \bar{y}_i)^2} \quad (2.2)$$

where n is the number of observations, y_i represents the observed values, $\bar{y}_i$ is the mean of the observed data, and $\hat{y}_i$ represents the predicted values.

2.4.1.3 Coefficient of determination (r^2)

The coefficient of determination (r^2) estimates the combined dispersion against the single dispersion of the observed and predicted series. The range of r^2 lies between 0 and 1 which describes how much of the observed dispersion is explained by the prediction. A value of zero means no correlation at all whereas a value of 1 means that the dispersion of the prediction is equal to that of the observation (Artusi et al., 2002; Krause et al., 2005).

$$r^2 = \left(\frac{\sum_{i=1}^{n}(y_i - \bar{y}_i)\ (z_i - \bar{z}_i)}{\sqrt{\sum_{i=1}^{n}(y_i - \bar{y}_i)^2}\ \sqrt{\sum_{i=1}^{n}(z_i - \bar{z}_i)^2}} \right)^2 \quad (2.3)$$

where n is the number of observations, y_i represents the observed values, $\bar{y}_i$ is the mean of the observed data, z_i represents the predicted values and $\bar{z}_i$ is the mean of the predicted values.

2.4.2 Sensitivity and uncertainty analyses

There are several methods for conducting sensitivity analysis (SA) in environmental modelling that broadly fall into two categories: local sensitivity analysis and global sensitivity analysis (Pianosi et al., 2016). Local SA typically examines how variations in model parameters influence model performance by assessing changes relative to an optimal or reference parameter set. Partial derivatives or finite difference techniques are often used to generate sensitivity indices in local SA (Pianosi et al., 2016). Other methods such as adjoint methods or algebraic techniques can also be used in local SA to track spatiotemporal variations (Vautard et al., 2000). In contrast, global SA may consider model parameters but also other input factors of the simulation procedure such as forcing data or its spatial resolution (Pianosi et al., 2016). Several indices can be used in global SA, ranging from correlation measures between inputs and outputs to statistical descriptors like output variance. However, since the analytical computation of these indices is hard in practice for most models, sensitivity indices are typically estimated using input-output samples (Beven, 2009). Global SA is used for multiple purposes, including model calibration and validation, model structure optimisation and simplification, uncertainty reduction, system control analysis, and supporting decision-making processes (Beven, 2009; Anderson et al., 2014; Pianosi et al., 2016).

A common distinction in sensitivity analysis is between “One-[factor]-At-a-Time” (OAT) methods and “All-[factors]-At-a-Time” (AAT) methods, which differ in their sampling strategies for estimating sensitivity indices (Pianosi et al., 2016). Sensitivity indices based on input-output relationships are typically approximated using numerical

sampling. OAT methods vary one input factor at a time while holding others constant, whereas AAT methods vary all input factors simultaneously, capturing both the direct effect of each factor and the combined effects due to interactions (Beven and Freer, 2001; Beven, 2009; Pianosi et al., 2016). While local SA generally employs OAT sampling, global SA can use either approach. AAT methods, however, offer a more comprehensive evaluation of model interactions, including higher-order combinations of factors, but require larger sample sizes and increased computational effort (Beven, 2009).

The application of SA to numerical models, in particular of global SA, is closely linked to uncertainty analysis. While the uncertainty analysis focuses on quantifying the overall uncertainty in model outputs, global SA aims to attribute this uncertainty to specific input factors (Beven and Binley, 2014; Pianosi et al., 2016). Both global SA and uncertainty analysis rely on the use of relatively complex mathematical sampling techniques. For example, Monte Carlo simulations and its variations (e.g., Markov Chain Monte Carlo simulations) are commonly used in uncertainty analysis to propagate uncertainty. In fact, Monte Carlo simulations form the basis for many global SA and uncertainty analysis (Beven and Binley, 2014). Some methodologies, such as the Generalised Likelihood Uncertainty Estimation (GLUE) method (Beven and Binley, 1992, 2014) originated from concepts in sensitivity analysis. GLUE is a method to explore parameter uncertainty by sampling from the parameter space and evaluating model performance against observed data.

2.4.2.1 The Generalised Likelihood Uncertainty Estimation (GLUE) method

GLUE is a well-stablished method for uncertainty analysis (GLUE is also referred as a regional sensitivity analysis) (Beven and Binley, 1992; Beven and Freer, 2001). GLUE is generally driven by Monte Carlo simulations to identify regions within the input space associated with specific output values, facilitating both mapping and the analysis of dominant controls (Beven and Binley, 2014). GLUE typically divides input samples, such

as model parameters, into two groups: behavioural and non-behavioural. This classification depends on whether the corresponding model simulations meet a defined pattern of state variable response. Alternatively, inputs can be separated based on whether the output exceeds a given threshold, that could be based on model performance (Beven, 2009). Comparing these groups (behavioural and non-behavioural) using, for example, empirical cumulative distribution functions (CDFs) provides insight into model uncertainty and highlights differences in the input distributions even with small sample sizes (Beven and Freer, 2001; Pianosi et al., 2016). This is advantageous when working with models that have a large number of parameters, as the behavioural parameter space could be limited despite a large number of simulations (Beven and Binley, 2014). This also leads to the exploration of model equifinality (i.e., how sensitive the model is to different parameter sets that produce acceptable simulations of observed behaviour). More broadly, model equifinality refers to the phenomenon where multiple, different parameter sets or model structures can produce similar outputs or equally acceptable model performance. This concept recognises that there may not be a single "best" parameter set but rather a range of parameter combinations that fit the observed data within acceptable limits.

Equifinality arises due to the complexity and uncertainty in environmental and hydrological systems (Beven and Freer, 2001), where multiple pathways or processes can lead to the same observed outcome. This is particularly common in highly parameterised models, where many parameters interact non-linearly, allowing different configurations to reproduce similar results (Anderson et al., 2014; Her et al., 2019a). In GLUE, equifinality is reflected in the presence of multiple behavioural parameter sets that meet the performance threshold, suggesting that no unique solution exists. As a result, GLUE and similar methods often aim to identify regions of acceptable parameters rather than isolating a single optimal value (that is why they are often called regional sensitivity analyses). In GLUE, these regions are often named as GLUE uncertainty

bounds which are generally based on a ranked percentile-based distribution of the behavioural parameter sets (Beven and Binley, 2014).

2.5 Forecasting frameworks

The selection of the modelling approach for the forecasting framework (and how many components to include) directly depends on factors such as the scope of the forecast, management objectives, available data and resources, and its relevance for real-world decision-making (Armstrong and Trevarthen, 1999; Beven, 2009; Bradford et al., 2020a). However, another key factor to define in forecasting is the temporal scale for future projections. In fact, this aspect is to be defined along with the modelling approach based on all criteria aforementioned (Dietze, 2017b). Broadly, forecasting frameworks can be classified into two groups based on the temporal scale of future predictions: short-term forecasting frameworks (providing sub-daily to decadal predictions) and long-term forecasting frameworks (providing decadal or longer projections) (Carey et al., 2022; Lewis et al., 2022b).

A short-term forecasting framework is generally iterative, designed for operational timeframes and typically incorporates the most recent observed data into its modelling workflow (Dietze et al., 2018). Excellent examples of short-term forecasting are weather forecast products (Hutton, 2019; Dietze et al., 2024). In contrast, a long-term forecasting framework is typically used to project changes over the coming decades (e.g., climate change impact assessments from 2025 to 2100) (e.g., Hattermann et al., 2018; Ayala et al., 2020; J. Xu et al., 2020). These predictions are usually performed to support long-term environmental interventions, adaptation strategies, and policymaking (Bradford et al., 2020a). Although both forecasting approaches are primarily driven by a model or a set of models (Dietze, 2017a), they can be enhanced by complementary methods and techniques, which often vary with the temporal scale of the predictions (Lewis et al., 2022b). Below, some of the most commonly employed methods and techniques for each approach are briefly described in the context of forecasting changes in water systems.

Note that forecasting refers to making predictions about future conditions with quantified uncertainty over specific timeframes; simulation refers to using models to explore how systems behave under certain conditions; and a scenario refers to a potential future trajectory under which the dynamic of interest might respond, such as changes in climate or land use.

2.5.1 Short-term frameworks

Short-term forecasting frameworks are a relatively new approach to predicting changes in rivers and lakes (Carey et al., 2022; Lofton et al., 2023). Short-term frameworks are generally performed iteratively, set up using cyberinfrastructure and typically incorporate new relevant environmental observations as they become available into the workflow (Lofton et al., 2023). Environmental observations are now being collected through a variety of new methods (e.g., remote measurements, satellite imagery) including high-frequency technologies (Dietze and Lynch, 2019; Seifert-Dähnn et al., 2021). Short-term forecasting for water quality can integrate new environmental data by applying a range of different data assimilation techniques, methods that are becoming increasingly efficient (Loos et al., 2020a; Zwart et al., 2023). Additionally, other already-designed systems can be employed to apply short-term forecasting frameworks. An example of such a system is FLARE (Forecasting Lake and Reservoir Ecosystems System) (Thomas et al., 2020), a near-term iterative forecasting system that uses GLM for simulating and predicting lake hydrodynamics. Importantly, most short-term forecasting frameworks for environmental and water systems are driven by, or in large part by, weather forecasts, data available near real-time that are key environmental factors influencing the dynamics of freshwater systems (Lofton et al., 2023; Dietze et al., 2024).

2.5.1.1 High-frequency monitoring

Monitoring programmes for freshwater and environmental systems used to rely primarily on sample collection and laboratory analysis (Jennings et al., 2022). However, advances in technology have introduced new methods for monitoring water resources.

Environmental data are now collected through a variety of methods, especially for near real-time monitoring (Dietze et al., 2024). Emerging methods (e.g., remote measurements, satellite imagery) along with high-frequency technologies, enable forecasters now to use that data as these are collected (Dietze and Lynch, 2019; Wickberg et al., 2024). High-frequency monitoring provides measurements at sub-daily and often sub-hourly intervals, capturing both short-term variability and, with long-term deployments, broader trends (Seifert-Dähnn et al., 2021; Jennings et al., 2022). This allows researchers to explore innovative approaches for integrating these data into short-term forecasting frameworks and improving predictive accuracy (Dietze et al., 2018).

2.5.1.2 Data assimilation

Data assimilation refers to the process of incorporating new observational data into a model to update its states aiming to improve model prediction accuracy (Beven and Freer, 2001). By adjusting model predictions based on observed values, data assimilation methods help reduce uncertainties as well and enhance the reliability of short-term forecasts (Dietze, 2017a). Data assimilation methods range from statistical techniques to more advanced ensemble-based approaches (Loos et al., 2020b). Among these, the Kalman filter (KF) is one of the most employed methods especially in the context of water quality forecasting (Loos et al., 2020b). The KF is designed to manage non-linear processes and dynamically update model states (Evensen, 2009) when incorporating new observations. It is an iterative algorithm that combines model predictions with observational data to estimate the true state of a system while accounting for uncertainties (Evensen, 2009). In general, the KF operates through a two-step process: prediction (where the model forecasts future states) and update, (where the same forecasts are corrected using new observations). Variations of the KF such as the Dud-EnKF and EnKF-GS have been explored to improve computational efficiency and initial condition estimates in water quality applications (Loos et al., 2020b).

2.5.1.3 Weather forecast products

Weather forecast products provide critical inputs for short-term forecasting applications, particularly in environmental and water systems modelling (Fer et al., 2021; Dietze et al., 2024). Weather forecasts are comprised of an ensemble of future trajectories which is an important feature related to uncertainty in future weather predictions (Hutton, 2019). Weather products are generally globally gridded and include forecasts for air temperature, precipitation, wind speed and solar radiation, among others. All these variables are key drivers of environmental dynamics and therefore important forcing data in forecasting applications for predicting the behaviour of freshwater ecosystems (Hutton, 2019; Moore, 2020; Dietze et al., 2024). Although there are some weather forecast ensemble products available, one of the most commonly employed in short-term forecasting applications is the National Oceanic and Atmospheric Administration Global Ensemble Forecasting System (0.5° NOAA GEFS) (ncei.noaa.gov) (Hamill et al., 2022). This product comprises 31 ensemble members and provides predictions out to 35 days lead time.

2.5.1.4 FLARE

The Forecasting Lake and Reservoir Ecosystems system (FLARE) is an open-source system for lake and reservoir water quality forecasting aimed at supporting management (Thomas et al., 2020; Carey et al., 2022). By integrating real-time monitoring, hydrodynamic modelling with data assimilation, and an ensemble-based forecasting algorithm, FLARE provides daily water quality forecasts for multiple lake/reservoir depths with a forecast horizon of up to 35 days with quantified uncertainty (Thomas et al., 2020, 2023b; Wander et al., 2023). FLARE uses as input data the weather forecasts from the NOAA GEFS weather ensemble product (Hamill et al., 2022). FLARE requires real-time monitoring data to be streamed from field lake instrumentation to a local data server which then is downloaded for use within the forecasting system. These data allow FLARE to perform data assimilation on hydrodynamic modelling, updating initial

conditions and calibrating model parameters. FLARE uses the General Lake Model (GLM) (Hipsey et al., 2019), as the process model to generate predictions for each ensemble member.

FLARE-based forecasting systems have been deployed to provide predictions of different water quality variables e.g., water temperature, dissolved oxygen, and chlorophyll a (Thomas et al., 2020; Carey et al., 2022; Woelmer et al., 2022; Thomas et al., 2023b; Wander et al., 2023). Most of this research describes the predictability engine of FLARE by way of forecasting experiments to support local management in different applications e.g., drinking water (where forecasts can be used to determine withdrawal depths for water treatment), dam operations (where forecasts can be used to schedule outlet flows), and environmental remediation (where forecasts can allow managers to initiate interventions). FLARE has also been applied to anticipate ecological dynamics associated with a particular forecasted variable. For instance, water temperature forecasts have been used to anticipate the onset of turnover of a reservoir in Virginia (USA), where this dynamic was identified 14 and 4 days in advance in 2018 and 2019, respectively (Thomas et al., 2020). Similarly, chlorophyll-a forecasts have been used as an indicative metric of phytoplankton biomass in two reservoirs in Virginia (USA), leading to an improvement in the capacity of local managers to anticipate these algae blooms (Woelmer et al., 2022).

2.5.2 Long-term frameworks

Long-term forecasting frameworks are designed to project system dynamics over extended periods, typically spanning decades to centuries. These frameworks are often employed to assess the impacts of long-term trends such as climate change, land use changes, or other large-scale environmental shifts (e.g., Jennings et al., 2009; Naden et al., 2010; Pierson et al., 2010; Schneiderman et al., 2010; Chen et al., 2019; Ayala et al., 2020; Chawanda et al., 2024; La Fuente et al., 2024). Unlike short-term frameworks, long-term frameworks employ input data that follow specific scenario configurations

rather than near real-time data and typically incorporate broader socio-economic, environmental, and policy assumptions (Lange and Büchner, 2021; Wu et al., 2022; IPCC et al., 2023; De Hertog et al., 2025).

2.5.2.1 Climate change scenarios

Global climate models (GCMs) can reproduce past climate characteristics and project future climate evolution, and they are currently one of the most effective tools for climate change research (Hattermann et al., 2018; Wu et al., 2022). As part of the phase 6 of the Coupled Model Intercomparison Project (CMIP6) developed by World Climate Research Programme (WCRP), numerous GCMs have been employed to provide future climate projections. These results serve as a basis for the assessment reports of the Intergovernmental Panel on Climate Change (IPCC). The most recent set of future scenarios are the Shared Socioeconomic Pathways (SSPs) which incorporate different futures of greenhouse gas (GHG) emission levels, societal development, and adaptation to climate change (IPCC, 2023) (Fig. 2.6 – Fig. 2.8). It is of note that each SSP scenario is linked to a specific Representative Concentration Pathways (RCPs) adopted by IPCC. The RCPs include scenario-specific time series emissions and concentrations of the full range of GHGs, as well as land use and land cover (Moss et al., 2008).

Many studies have employed long-term forecasting frameworks using different SSP future climate trajectories to perform climate change impact assessments on water resources (He et al., 2023; IPCC et al., 2023; Murphy et al., 2023; Siabi et al., 2023; Jin et al., 2024). For example, SSP126, SSP245, SSP370 and SPP585 project different future conditions within the overall range of SSP scenarios, as follows:

- SSP126 scenario: This scenario with 2.6 W m^{-2} by the year 2100 is a remake of the optimistic scenario RCP2.6. The SSP126 scenario was designed with the aim of simulating a development that is compatible with the 2°C target. This scenario reflects rapid efforts to mitigate GHG emissions while promoting environmental and economic sustainability.

- SSP245: With above 4.0 W m^{-2} by the year 2100, this scenario represents a middle pathway between sustainability-focused and fossil-fuel-driven futures. It is an update of the RCP4.5 scenario, balancing moderate greenhouse gas mitigation with continued reliance on fossil fuels.
- SSP370 scenario: With 7 W m^{-2} by the year 2100, this scenario is in the upper-middle part of the full range of scenarios. It was newly introduced after the RCP scenarios, closing the gap between RCP6.0 and RCP8.5. This scenario adopts intermediate efforts for both adaptation and mitigation.
- SSP585 scenario: With an additional radiative forcing of 8.5 W m^{-2} by the year 2100, this scenario represents the upper boundary of the range of scenarios. It can be understood as an update of the CMIP5 scenario RCP8.5, now combined with socioeconomic reasons. SSP585 assumes increasing trends in fossil-fuelled development i.e., a high level of human-induced global warming.

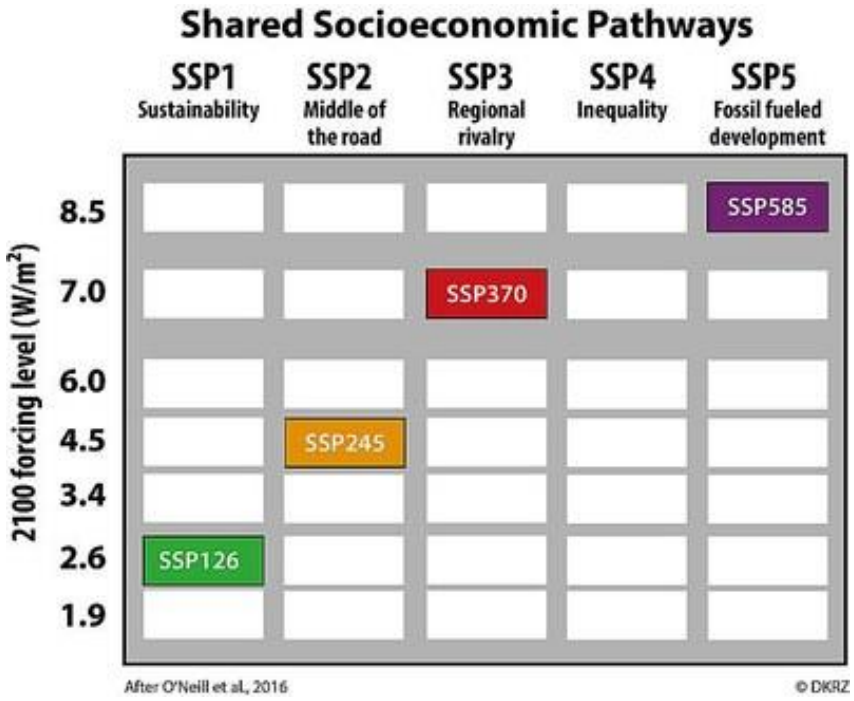


Figure 2.6 CMIP6 Scenarios – Shared Socioeconomic Pathways with corresponding 2100 radiative forcing levels. Source: German Climate Computing Center (Deutsches Klimarechenzentrum, DKRZ).

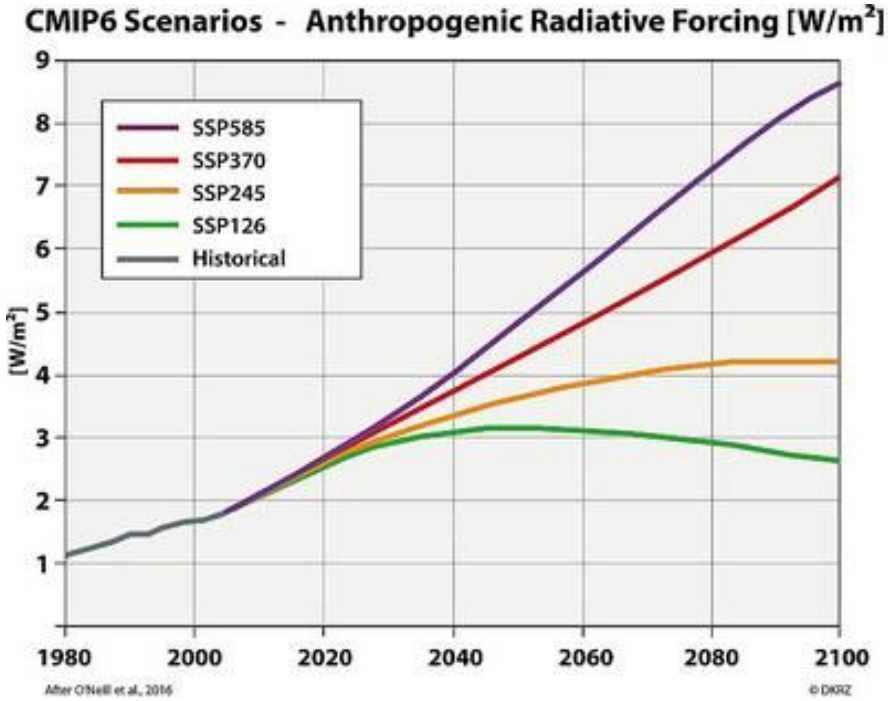


Figure 2.7 CMIP6 Scenarios – Shared Socioeconomic Pathways with corresponding anthropogenic Radiative Forcing. Source: German Climate Computing Center (Deutsches Klimarechenzentrum, DKRZ).

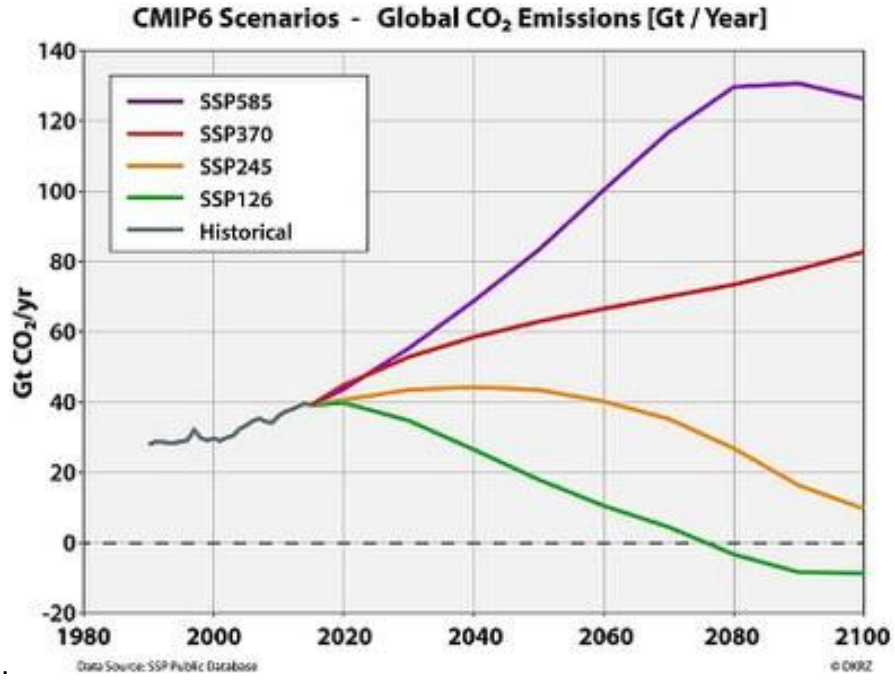


Figure 2.8 CMIP6 Scenarios – Shared Socioeconomic Pathways with corresponding global CO_2 emissions. Source: German Climate Computing Center (Deutsches Klimarechenzentrum, DKRZ).

2.6 Forecast performance

There are many ways in which forecast performance can be assessed (Lofton et al., 2023; Zwart et al., 2023). Predictive skill can be quantified, for instance, based on the various goodness-of-fit metrics described in Section 2.4 (Krause et al., 2005). However, if the forecasts generated are ensemble-based (which is generally the norm), to account for ensemble variability the use of such deterministic metrics (RMSE, NSE and r^2) would require computing a summary statistic (e.g., mean or median values) for the output variable and using that value as a prediction or computing a summary statistic of the metric itself (e.g., Thomas et al., 2020; Woelmer et al., 2022). There are other metrics that account for this variability with a probabilistic approach, designed to capture better the performance of ensemble-based forecasts. The continuous ranked probability score (CRPS) is one of the forecast performance metrics most commonly used in environmental modelling and water engineering (Bröcker, 2012; Lofton et al., 2023), especially in short-term forecast applications (e.g., Thomas et al., 2020; Taillardat et al., 2023; Zwart et al., 2023; Wander et al., 2024).

CRPS is a metric used to evaluate probabilistic forecast accuracy and precision (Bröcker, 2012). It assesses the discrepancy between the observations and the cumulative distribution function (CDF) of the forecast. The CRPS is calculated by integrating the squared difference between the forecast CDF and the Heaviside step function. Similar to RMSE, units for CRPS will be based on the units of the variable under analysis. Lower CRPS values indicate a better performance.

$$CRPS(F, y) = \int_{-\infty}^{\infty} (F(x) - H(x))^2 dx \tag{2.4}$$

where $F(x)$ is the cumulative distribution function (CDF) of the ensemble-based forecast distribution, y is the observed value, and $H(x)$ is the Heaviside function equal to 0 if $x < y$ and 1 otherwise. A lower CRPS indicates a smaller error margin, encompassing both underestimation and overestimation relative to the true observation of the variable of

interest. Bröcker (2012) provides an extensive description of the CRPS metric and its use in forecasting applications.

In addition to evaluating forecasts against observations, predictive skill can be compared to other simpler approaches such as null models or static predictions based on past conditions (Lofton et al., 2023). This has been identified as good practice to contextualise new forecasting systems (Perretti et al., 2013; Thomas et al., 2020; Zwart et al., 2023). For instance, a model can assume that future conditions will be the same as the recent past (a site persistence forecast) (Wilks, 2019) or that they will be the same as historical day-of-year conditions from previous observations if sufficient data are available (e.g., a historical mean forecast, or a climatology forecast) (Murphy, 1992; Yang, 2019; Bento et al., 2022). Furthermore, a newly developed forecasting framework can also be compared with the previously best-performing forecasting method for a specific target variable (Jin et al., 2019; Lofton et al., 2023).

2.7 Forecast uncertainty

A key aspect of a successful forecasting workflow is incorporating, quantifying, propagating, and reporting the uncertainty associated with estimates of future ecosystem states (Carey et al., 2022; Dietze, 2017a, 2017b). Total forecast uncertainty can be quantified using various methods that analyse the spread of the prediction ensemble, such as calculating confidence intervals, standard deviation, variance and other percentile-based ranges (Beven, 2009; Bodner et al., 2021). Total uncertainty in each forecast, however, is a result of many contributing factors. In freshwater forecasting applications, uncertainty can arise from a variety of sources, including model structure, model parameterisation, estimates of initial conditions and forcing data (Beven, 2009; Pianosi et al., 2016; Dietze, 2017a; Hattermann et al., 2018). When a forecast is produced, these uncertainties propagate resulting in increased uncertainty as the forecast progresses farther into the future (Lofton et al., 2022, 2023).

Assessing uncertainties requires identifying both their location in the model (e.g., initial conditions, covariates, parameters, structure) and their qualities (e.g., degree, type) (Dietze, 2017b). Some uncertainties result from gaps in knowledge (epistemic uncertainty) and can potentially be reduced, while others are due to natural variability (aleatory uncertainty) and cannot be reduced (Beven, 2009; Bodner et al., 2021). Sensitivity and uncertainty analyses are useful for identifying which sources of uncertainty have largest effect on a forecast (Beven and Binley, 2014; Pianosi et al., 2016). By identifying and focusing on the most influential uncertainties, researchers can provide clearer insights to decision-makers and highlight areas where reducing uncertainty could improve forecast reliability (Dietze, 2017a; Carey et al., 2022). Various methods can be used to estimate relative uncertainty contributions, including techniques based on statistical metrics such as the variance (Thomas et al., 2020; Lofton et al., 2022; Wu et al., 2022). Although it is impossible to account for every source of uncertainty, prioritising the most important and addressable sources can contribute in producing more reliable and actionable forecasts (Beven, 2009; Dietze et al., 2018, 2024).

2.7.1 Uncertainty propagation

Once uncertainties have been identified and characterised, a key step is to acknowledge and, whenever possible, quantify how these propagate through the forecasting system and assess their influence on model outputs (Beven and Freer, 2001). In hydrological and water quality forecasting, this involves simulating the combined effect of model inputs, model processes, parameters, and initial conditions on predicted variables such as river discharge or DOC concentrations. Uncertainty propagation allows for the representation of forecast outputs as a distribution of possible future states, rather than as a single deterministic trajectory. This is particularly important in environmental systems with strong nonlinearities, where small variations in inputs can lead to large

differences in outcomes, especially when forecasts are extended further into the future (Beven and Binley, 2014; Dietze, 2017a).

In this context, an ensemble-based approach is typically used to propagate uncertainty, whereby multiple simulations are performed using different combinations of uncertain inputs or parameters. For instance, ensembles can be generated by sampling from posterior parameter distributions, using multiple climate or weather scenarios, or applying a range of different initial conditions. These simulations produce a spread of possible outcomes that reflect the underlying uncertainty, which can then be summarised through statistical measures such as prediction intervals or confidence bounds. In catchment and lake systems, such propagation is critical for understanding the range of relevant hydrological responses or DOC dynamics under both the near-term and long-term.

Importantly, propagating uncertainty not only supports better communication of forecast confidence, but also helps diagnose model behaviour under varying conditions and assess robustness across different management or decision-making scenarios (Carey et al., 2022; Lofton et al., 2022). It also provides a foundation for future efforts aimed at improving forecast skill by identifying which sources of uncertainty are most impactful and may therefore warrant targeted model development, improved data collection, or better parameter estimation (Thomas et al., 2020; Wander et al., 2024).

2.8 Conclusions

In this chapter, the main concepts and developments relevant to ecological forecasting were reviewed, with emphasis on water quality and biodiversity dynamics. The role of modelling and predicting DOC and water temperature-driven fish migrations was discussed as key indicators of environmental change, with relevance for adaptive water resource management. Modelling approaches at both the catchment and lake scale were presented, highlighting their structure, data requirements, and suitability for different applications. Model and forecasting performance evaluation, and sensitivity

analyses were discussed as essential components to support model reliability. Finally, forecast performance and uncertainty were addressed for both short- and long-term contexts, highlighting the importance of quantifying and propagating uncertainty to ensure forecasts are robust, transparent, and as informative as possible for users and managers.

Chapter 3

Modelling Tools

Two software modelling tools were used in this thesis to predict changes in water systems at different scales: (1) a catchment-scale model for river systems and (2) a lake-scale model for lake systems. These models are sourced in code and have been previously employed to simulate hydrology and water quality in different settings worldwide (see Section 2.4). The catchment model was used in a long-term forecasting workflow in Chapter 4 and in a short-term forecasting workflow in Chapter 6. The lake model was used in a short-term forecasting workflow in Chapter 5. Although the forecasting workflows in each case study of this thesis comprised multiple components, these models represent the main element of their respective frameworks.

3.1 Catchment model

The catchment model used was the Generalised Watershed Loading Functions Model (GWLF), a lumped parameter process-based hydrological and water quality model introduced by Haith and Shoemaker (1987). GWLF simulates water balance, water partition among the different flow pathways, sediment loading and nutrient export in a daily time step. The model input requirements include daily time series of precipitation and air temperature as well as land cover, land use, and soil characterisation. The benefits of a model such as GWLF include a relatively easy set-up, fewer data

requirements, and less software computing time than most of the more distributed catchment models.

Different versions of the model, in addition to the original Haith and Shoemaker model, have been developed and used for a variety of applications (e.g., Schneiderman et al., 2002; Smedberg et al., 2006; Jennings et al., 2009; Moore et al., 2010; Pierson et al., 2010; Schneiderman et al., 2010). Each of these versions has undergone different modifications, but all follow the same conceptual structure of GWLF. In this thesis, the GWLF version used was initially developed by the New York City Department of Environmental Protection (NYC DEP) (Schneiderman et al., 2002), a version that was further enhanced by Schneiderman et al. (2010) and Naden et al. (2010) to include a process-based module for DOC (GWLF-DOC). This development occurred during the EU-funded CLIME project (Climate and Lake Impacts in Europe, 2003-2005) (George et al., 2010), and was focused on simulating a set of nutrients including DOC in high-organic soil catchments. This model structure has been employed to assess the impact of climate change for a set of study sites across Europe including quantifying future changes in DOC dynamics (Naden et al., 2010; Schneiderman et al., 2010; Lindqvist, 2022).

Within this context, GWLF-DOC was selected as a suitable tool for modelling DOC in the river study sites of this thesis, as these have catchments dominated by high organic soils in Ireland (Chapter 4 and Chapter 6) and Sweden (Chapter 4). In addition, the model has demonstrated good performance in previous studies conducted in similar settings. Its structure, which has undergone several modifications over time, provides opportunities for further model development. However, it is of note that GWLF-DOC does not simulate detailed hydrochemical processes such as pH responses, microbial activity in soils, or in-stream biogeochemical transformations. It also does not capture other hydrological processes such as hysteresis or recession limb dynamics. Nevertheless, the model effectively represents the fundamental processes related to

temperature and water availability variations in the soil that drive DOC dynamics at the catchment scale.

The main structure of GWLF-DOC is composed of two modules: a hydrology module (to simulate catchment hydrology, water balance and water distribution among the different hydrological pathways) and a DOC module (to simulate catchment DOC production and DOC washout). The hydrology module is dynamically coupled with the DOC module.

3.1.1 Hydrology module

GWLF simulates river discharge from both surface runoff and from subsurface baseflow based on interactions between climate and the catchment land cover characteristics. Surface runoff is calculated using the USDA SCS curve number method (Boughton, 1989), as a non-linear function of precipitation, snowmelt and the catchment water retention capacity (see Schneiderman et al., 2010). Catchment water retention capacity varies as a function of land uses and soil characteristics, including modelled soil moisture conditions. Modelled soil moisture is based on average 5-day antecedent catchment water availability (Schneiderman et al., 2010). Rain and snowmelt that do not translate into surface runoff are either lost through evapotranspiration or infiltrate into the subsurface to become baseflow (see Fig. 3.1).

Baseflow is calculated as a lumped contribution from the entire watershed as both slow- and fast-moving groundwater flows (Schneiderman et al., 2010) from three subsurface lumped reservoirs (i.e., averaged over the whole catchment): (1) the unsaturated zone (subjected to evapotranspiration), (2) a saturated zone (not subjected to evapotranspiration), and (3) a deep saturated zone with sustained low flow discharge. Evapotranspiration is calculated using the Hamon temperature index equation as default (Hamon, 1961), employing an approximation of the saturated vapor pressure developed by Bosen (1960). Evapotranspiration can also be calculated using the Penman-Monteith method or Priestley-Taylor method (Lhomme, 1997; Allen, 2005), but these would require additional data inputs such as solar radiation, relative humidity and wind speed.

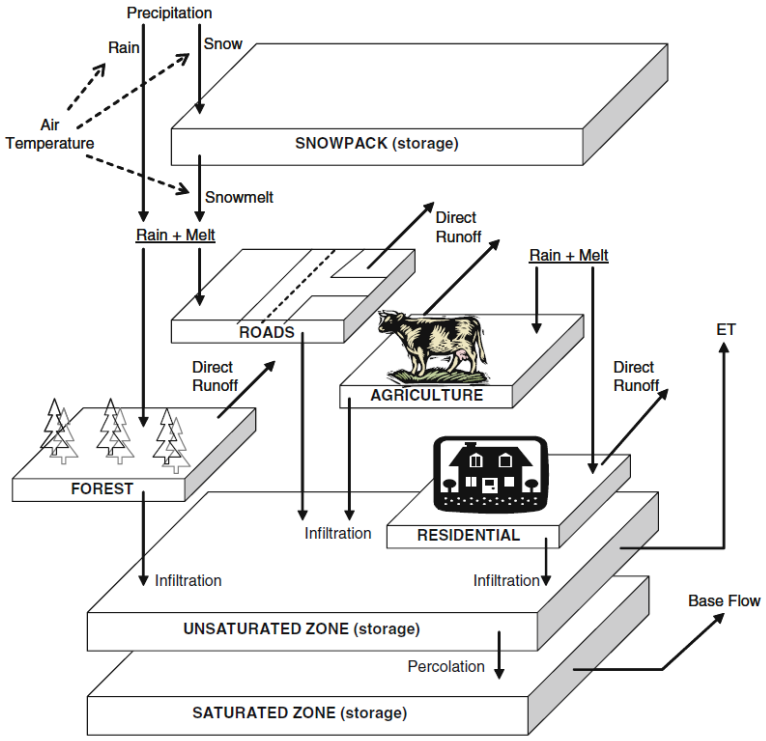


Figure 3.1 Catchment hydrology as conceptualised in GWLF (Schneiderman et al., 2010).

The hydrology module includes seven adjustable parameters to regulate the different hydrological states: (1) *precipitation correction factor*, (2) *melt coefficient*, (3) *runoff curve number adjustment*, (4) *soil water capacity*, (5) *recess coefficient*, (6) *slow recess coefficient* and (7) *baseflow capacity* (Schneiderman et al., 2010). Each model parameters of the hydrology module of GWLF including their respective units are presented in Table 3.1.

Table 3.1 Model parameters for the hydrology module of the Generalised Watershed Loading Functions Model (GWLF).

Model parameters - hydrology module (GWLF)	
Parameter	**Units**
Precipitation correction factor	factor day^{-1}
Melt coefficient	cm $°C^{-1}$ day^{-1}
Runoff curve number adjustment	-
Soil water capacity	cm
Recess coefficient	coeff. day^{-1}
Slow recess coefficient	coeff. day^{-1}
Baseflow capacity	cm

The precipitation correction factor adjusts precipitation inputs to account for potential measurement bias. The melt coefficient controls the rate of snowmelt based on temperature conditions. The runoff curve number adjustment indirectly regulates surface runoff (through the USDA SCS curve number method; see Schneiderman et al. 2010) based on land cover and soil type characteristics. The soil water capacity represents the maximum water-holding capacity of the soil in the unsaturated zone of the catchment. The recess coefficient controls the rate at which fast-groundwater flow is output from the saturated zone. Similarly, the slow recess coefficient controls the rate at which slow-groundwater flow is output from the deep saturated zone. Baseflow capacity limits the amount of deep percolation (baseflow output from the saturated zone to the deep saturated zone).

All contributions of both surface runoff and baseflow to streamflow are summed up in each time step to calculate river discharge at the catchment outlet. The default output units for river discharge in GWLF are normalised to the watershed area (e.g., cm day^{-1}). However, these units can be transformed into other more commonly employed units such as m^3 s^{-1}. A simplified diagram of the hydrology module of GWLF is displayed in Fig. 3.2, based on the original model schematics within VENSIM software (Ventana Systems Inc.). VENSIM software has been commonly used as a development platform for GWLF, as it features a graphical interface in addition to a programming language interface.

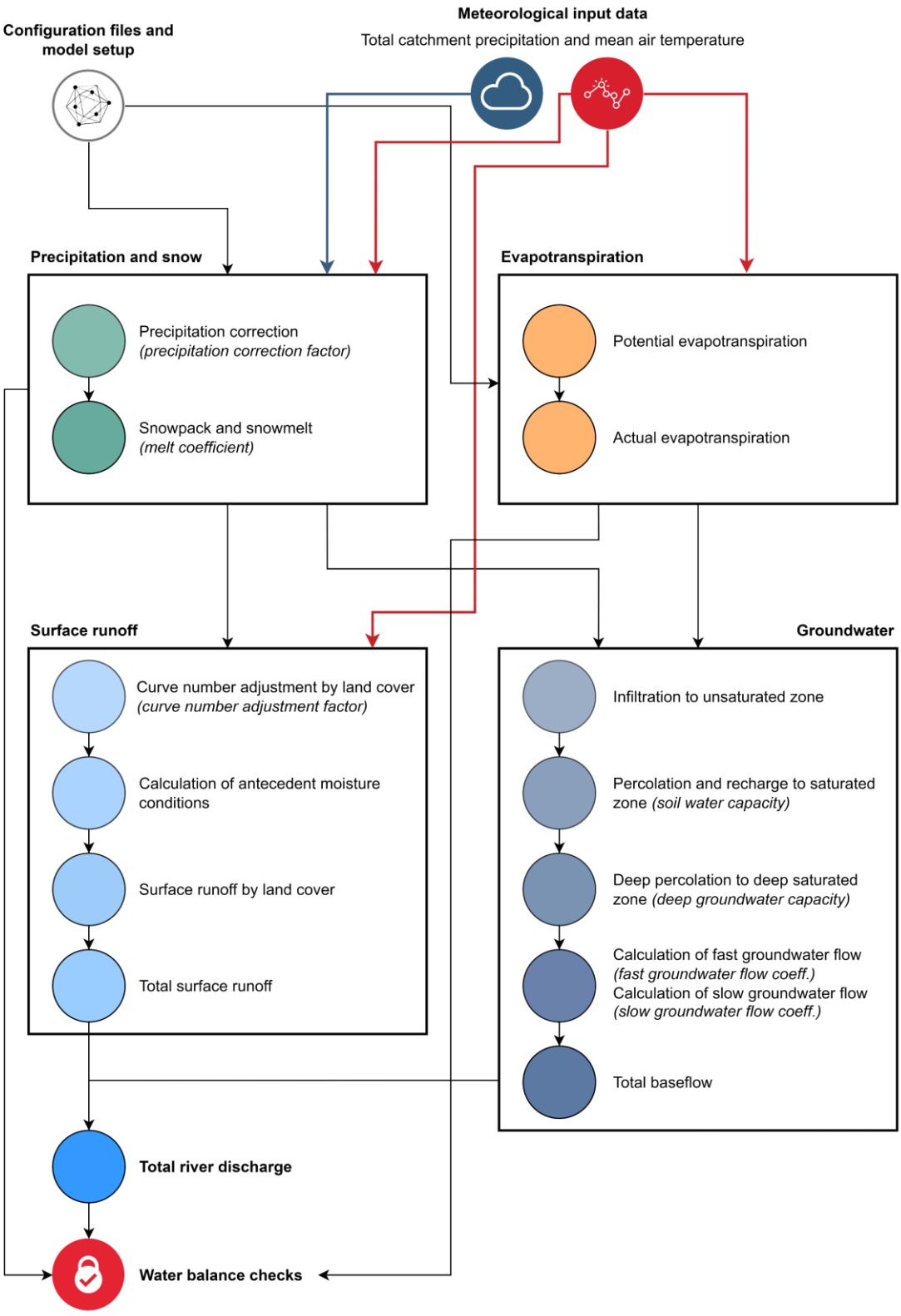


Figure 3.2 Simplified diagram of the hydrology module of GWLF, based on the original model schematics within VENSIM software (Ventana Systems Inc.). Model parameters are indicated in brackets.

3.1.2 DOC module

GWLF-DOC follows a two-phase process for simulating DOC flux and concentrations at the catchment outlet: (1) DOC production and (2) DOC washout. In general, simulated DOC is represented in GWLF-DOC by lateral transport mechanisms through the various hydrological pathways and is a function of available DOC stored in the soil matrix. The soil matrix store is defined by a single catchment-scale carbon pool in which decomposition processes lead to DOC production and hence, available DOC for washout downstream (see Fig. 3.3).

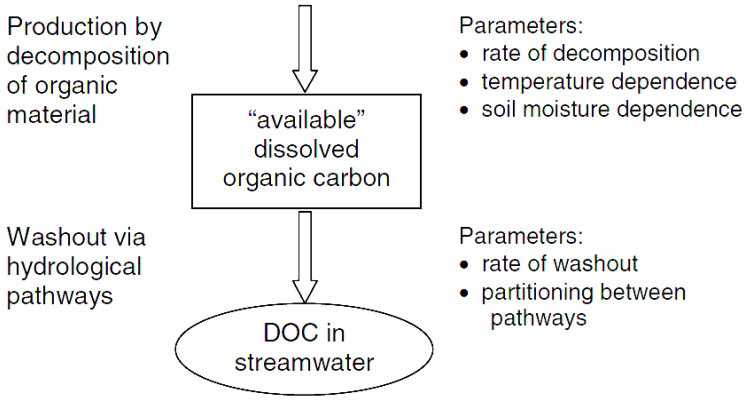


Figure 3.3 Two-phase process of production and washout represented in GWLF-DOC (Naden et al., 2010).

DOC production in GWLF-DOC is regulated by two processes: temperature-dependent decomposition (D_T) and moisture-dependent decomposition (D_S) of soil organic matter. In the model, three adjustable parameters control production: (1) *activation energy* (E_a) and (2) *anaerobic decomposition rate* (a) control D_T, while (3) the *aerobic decomposition rate* (b) controls D_S. Temperature-dependent decomposition is based on the Arrhenius equation (Worrall et al., 2004; Naden et al., 2010), given by:

$$D_T = a \left\{ exp\left(\frac{E_a}{R} \left[\frac{1}{T_{ref}} - \frac{1}{T} \right] \right) \right\} \quad (3.1)$$

where D_T is DOC production rate (g C m^{-2} day^{-1}) at soil temperature T (K). E_a is activation energy and (a) is the anaerobic decomposition rate. T_{ref} is the reference soil

temperature, which is set to 10℃ (283 K). R corresponds to the universal gas constant (6.928×10^{-4} kJ K^{-1} g C^{-1}). Soil temperature is estimated using a 10-day moving average of the air temperature above zero (Naden et al., 2010). A higher activation energy (E_a) leads to higher temperature sensitivity and a higher DOC production in the soil matrix (Davidson and Janssens, 2006). Similarly, the anaerobic decomposition rate (a) will dictate the estimated rate at which bacteria would break down organic matter in the soil matrix for the catchment.

Moisture-dependent decomposition of soil organic matter in the model is based on experimental research of Mitchell and McDonald (1992) (Naden et al., 2010), given by:

$$D_S = \ exp\left(-b\left[\left(\frac{(S_{max} - S)}{1.6S_{max}} - 0.35\right)^2 - 0.1225\right]\right) \quad (3.2)$$

where D_S is DOC production rate (g C m^{-2} day^{-1}) at soil moisture S. b is the aerobic decomposition rate. Soil moisture is given by a relationship between the soil water capacity S_{max} (cm) and the soil water content S (cm) of the unsaturated zone of the catchment. Regarding the soil moisture dependence (determined by the aerobic decomposition rate (b)), decomposition will increase as the soil water decreases until it reaches a certain point, where decomposition will decrease as soil water continues to decrease (Silvola et al., 1996).

The DOC produced is stored in the catchment carbon pool and made available for washout. DOC can be washed out via three different hydrological pathways dependent on the current water balance of the system. These three pathways are surface runoff, percolation and deep percolation. DOC loss will only occur from DOC-producing land covers which are assigned by the user, and which are generally based on a specific land cover classification. DOC washout is regulated by three parameters: (1) *fast rate of washout* (k_{fast}), (2) *slow rate of washout* (k_{slow}), and (3) mineral adjustment factor (M).

DOC washout through runoff (W_{runoff}, gC m^{-2} day^{-1}) is defined for each land cover and is diluted during high rainfall or snowmelt events (Naden et al., 2010). This is given by:

$$W_{runoff} = k_{fast} C \times \min\left(R_{luDOC}, R_0\right) \frac{S}{S_{max}} \quad (3.3)$$

where k_{fast} is the fast rate of washout, given as a fraction cm^{-1}, C is the available DOC, R_{luDOC} is the runoff from DOC producing land covers, R_0 is the threshold that determines when dilution occurs, and the soil moisture dependence term adjusts for the control of pore space connectivity on DOC (Naden et al., 2010).

DOC washout through subsurface flow (W_{ssf}, gC m^{-2} day^{-1}) is given by:

$$W_{ssf} = k_{slow} C \times P \quad (3.4)$$

where k_{slow} is the slow rate of washout, given as a fraction cm^{-1}, C is the available DOC and P is percolation (cm day^{-1}). Depending on catchment soil characteristics, the organic layer can be underlain by mineral soil. This will affect the slow subsurface washout as DOC concentrations in this layer will be different, and DOC may adsorb to mineral grains (Naden et al., 2010). To account for this, the mineral adjustment factor (M) adjusts the washout of DOC from slow subsurface flow ($W_{slowssf}$, gC m^{-2} day^{-1}), given by:

$$W_{ssf} = k_{slow} C P_{deep} \left(\frac{M A_{min} + A_{organic}}{A_{luDOC}}\right) \quad (3.5)$$

where M is the mineral adjustment factor, A_{min} is the area of soils with a mineral soil horizon, $A_{organic}$ is the area of deep organic soils and A_{luDOC} is the area of DOC producing land covers.

Fast rate of washout (k_{fast}), is computed by multiplying the slow rate of washout (k_{slow}) with a washout ratio coefficient. Therefore, to define a value for the fast rate of washout (k_{fast}), an estimation of the washout ratio coefficient needs to be provided by the user otherwise it should be included in the calibration together with the DOC model

parameters k_{slow} and M. Each model parameter of the DOC module of GWLF-DOC including their respective units are presented in Table 3.2.

Table 3.2 Model parameters for the DOC module of the Generalised Watershed Loading Functions Model with an integrated DOC module (GWLF-DOC).

Model parameters - DOC module (GWLF-DOC)	
Parameters for production	**Units**
Activation energy *(Ea)*	kJ gC^{-1}
Aerobic decomposition rate (b)	-
Anaerobic decomposition rate (a)	gC m^{-2} day^{-1}
Parameters for washout	**Units**
Slow rate of washout	fraction cm^{-1}
Fast rate of washout	fraction cm^{-1}
Washout ratio coefficient	fraction
Mineral adjustment factor	-

In each model simulation time step, the available DOC stored in the catchment carbon pool is updated based on production and loss. DOC fluxes and concentrations at the catchment outlet are calculated from the sum of all DOC washed out (kg C day^{-1}) and using the total discharge (m^3 day^{-1}) (Naden et al., 2010). The DOC module schematics within VENSIM software (Ventana Systems Inc.) are displayed in Fig. 3.4.

It is of note that GWLF-DOC does not replicate some other factors that may influence DOC dynamics such as those related to biochemistry in soils (e.g., pH response, sorption-desorption, mineralisation in soils and microbial populations) or in-stream processes. Nevertheless, the model is considered to capture the fundamental processes related to temperature and water availability variations in the soil that drive DOC dynamics at the catchment scale (Naden et al., 2010).

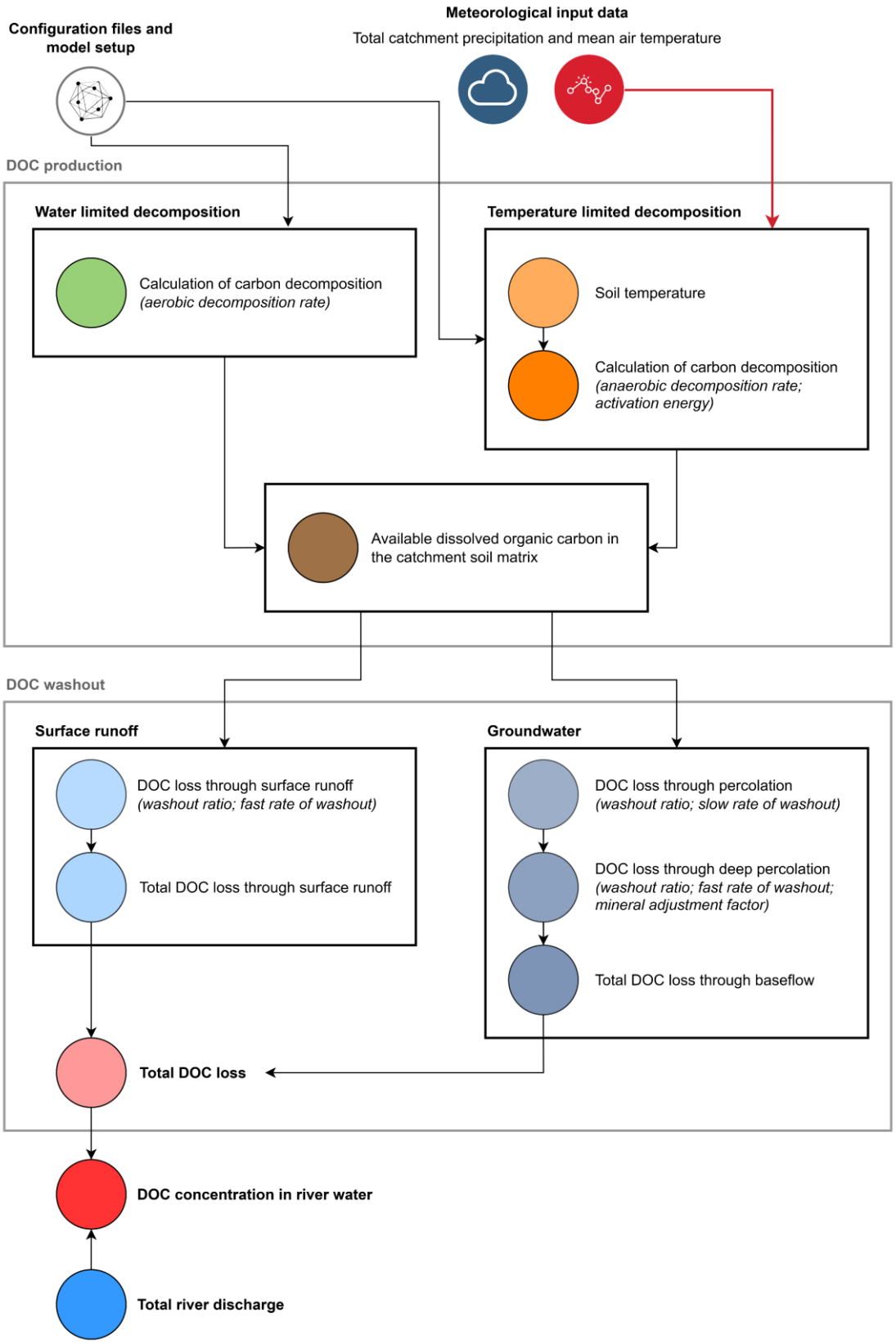


Figure 3.4 Simplified diagram of the DOC module of GWLF-DOC, based on the original model schematics within VENSIM software (Ventana Systems Inc.). Model parameters are indicated in brackets.

3.2 Lake model

The lake model used was the General Lake Model (GLM), a one-dimensional (1-D) process-based hydrodynamic model for simulating the water balance and vertical stratification of lakes and other standing water bodies (Hipsey et al., 2019). GLM is open-access, sourced in code, and was developed by the Aquatic EcoDynamics Research Group team at the University of Western Australia (UWA) in collaboration with the Lake Ecosystem Restoration research group at the University of Waikato to support the science needs of the Global Lake Ecological Observatory Network (GLEON). GLEON is a network of researchers aiming for an improved understanding of lake functioning and how lakes around the globe respond to external pressures (e.g., human activities, climate and land use changes).

GLM simulates lake vertical profiles of temperature, salinity and density by accounting for the effect of inflows and outflows on the water balance, in addition to surface heating and cooling, and vertical mixing. The model also includes the effects of ice cover formation and subsequent melting on the heating and mixing processes within the water system. Being a 1-D model, GLM assumes no horizontal variability within the water system domain. However, its modelling structure is verified across a range of lake studies that have highlighted the dominant role of seasonal changes across the vertical axis (Gal et al., 2009; Bruce et al., 2018; Hipsey et al., 2019). GLM is generally more computationally efficient than more complex alternatives such as 2-D or 3-D lake models (Moore, 2020). GLM was selected for use in Chapter 5 as it had been previously applied to the study site, building on earlier lake modelling insights, offers relatively low computational demands, and has been the focus of recent research exploring its integration with forecasting frameworks globally.

GLM was originally designed to be employed in long-term investigations ranging from months to decades, however, it can also be applied in short-term modelling applications (e.g., Thomas et al., 2020; Carey et al., 2022; Thomas et al., 2023). Besides simulating

hydrodynamics, GLM can be used to simulate water quality variables when coupled with other modelling tools such as the Aquatic EcoDynamics (AED) set of modules (Hipsey et al., 2013, 2014, 2019). GLM and GLM-AED have been applied to many lakes around the world, particularly to simulate and predict changes in water temperature (Bruce et al., 2018; Hipsey et al., 2019; Moore, 2020; Mesman et al., 2020) but also in water quality variables such as dissolved oxygen, dissolved organic carbon, nitrogen, phosphorus, zooplankton and phytoplankton (e.g., Hipsey et al., 2019; Carey et al., 2022; Woelmer et al., 2022, 2024).

GLM requires time series of a set of meteorological variables (shortwave radiation, longwave radiation, cloud cover, air temperature, relative humidity, wind spend, precipitation and snowfall) as inputs (Hipsey et al., 2019). These time series can be discretised in different temporal scales (e.g., sub-daily, daily, weekly, monthly or annual). Lake inflow and outflow data can also be input, although not mandatory. If these data are not input, it is assumed that the lake has inflow-outflow equilibrium i.e., the same amount of water coming into the lake goes out from the lake within the same period. Modelled depths need to be specified by the user as well as the time step for simulation and output controls. These, along other settings, are defined in a set of GLM configuration files (see Hipsey et al. (2014) for more details).

GLM is a model with a relatively high quantity of model parameters (i.e., a relatively highly parameterised model) (Hipsey et al., 2014). It contains a range of different model parameters, some of which are scaling factors for the input variables and some of which regulate modelled processes such as lake heat transfer, energy balance and mixing (see Hipsey et al. (2014) for more details). Generally, however, depending on the scope of the study, some parameters are set to default values and calibration strategies focus only on parameters estimated more relevant for the specific research scope (Hipsey et al., 2017). Below, key features of GLM hydrodynamic modelling are described, with an emphasis on simulating lake temperature profiling, as this was the purpose of employing

GLM for the lake case study in Chapter 5, which enabled the forecasting of fish migration dynamics. An extensive description of the scientific basis and numerical implementation algorithms of GLM is provided by Hipsey et al. (2014, 2019).

3.2.1 Layer structure

GLM adopts a one-dimension solution processes of vertical mixing by incorporating a series of vertical layers that are used to describe the variation in water column properties (Hipsey et al., 2014). The model adopts a flexible Lagrangian structure, which was originally introduced for the model Dynamic Reservoir Simulation Model (DYRESM) by Imberger and Patterson (1981).

The Lagrangian structure assumes each layer represents a control volume that can change thickness by contracting and expanding in response to inflows, outflows, mixing with adjacent layers, and surface mass fluxes (Hipsey et al., 2014). Each modelled layer has a unique density computed based on the local temperature and salinity. When sufficient energy becomes available to overcome density differences between adjacent layers, layers will merge thus accounting for the process of mixing. For deeper lake systems, a stable vertical density gradient will form in response to periods of high solar radiation creating warm, less-dense conditions near the surface with cooler conditions deeper in the water separated by a thermocline region (metalimnion) (Hipsey et al., 2014). Layer thicknesses are adjusted throughout the water column within the model to resolve the vertical density gradient with fine resolution occurring in the thermocline and thicker cells where mixing is occurring (see Fig. 1) (Hipsey et al., 2014).

More specifically, the water column in GLM is represented by a series of dynamic layers from the lake bottom to the surface. The number of layers adjusts throughout the simulation to ensure each layer remains internally homogeneous. Initially, layers are of equal thickness, determined by user-specified minimum and maximum layer thickness constraints and the total lake depth. Over time, vertical mixing, heating, and hydrology will cause layers to expand or contract, with built-in processes maintaining the optimal

thickness needed to resolve stratification algorithm (Hipsey et al., 2014). Layer volumes are interpolated from a user-defined hypsographic curve that relates lake depth to lake catchment area. The model can either use prescribed layer volumes or compute them via interpolation, assuming a conical shape for the bottom layer and applying a recursive formula for upper layers (Hipsey et al., 2014). A refined depth-area-volume relationship is generated using fine depth increments (e.g., 0.1 m) to improve resolution. Density in each layer is computed from the local temperature and salinity of each layer at any given time step.

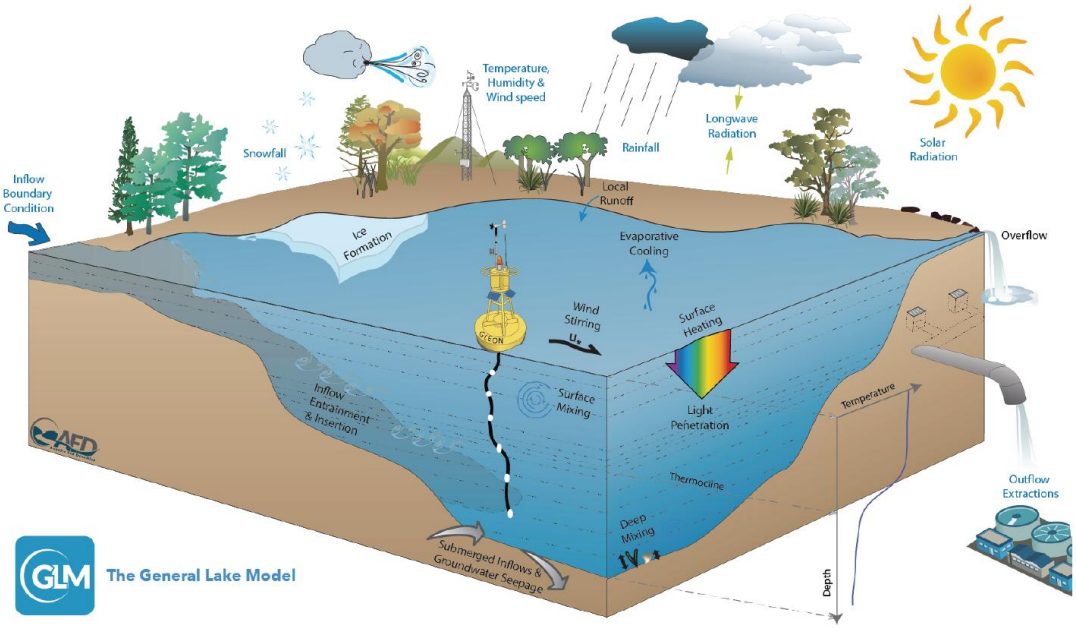


Figure 3.5 GLM simulation domain, input information and key simulated processes (Hipsey et al., 2014).

3.2.2 Water balance

GLM simulates lake water balance by accounting for user-configurable fluxes. The main water balance components include mass fluxes (evaporation, rainfall, and snowfall), inflows (surface and deep inflows, as well as catchment runoff), and outflows (withdrawals, overflow, and seepage) (Hipsey et al., 2014). Water exchange occurs through all modelled layers, but evaporation and precipitation affect only the top layer, and seepage occurs only at the lake bottom. Inflows and outflows are computed on a daily time step, while surface mass fluxes can be resolved hourly or daily, depending on

the meteorological forcing data. All modelled layers within the lake system are subject to mass conservation and can be impacted by inflowing and outflowing water (Hipsey et al., 2014).

3.2.3 Surface energy budget

GLM simulates the lake surface energy budget by balancing shortwave radiation, longwave radiation, sensible and evaporative fluxes. The general heat budget equation in GLM used to determine the net cooling and heating for the lake system is given by:

$$\left[\frac{c_p}{A_s z_{sml}}\right]\frac{dT_s}{dt} = \emptyset_{SW_s} - \emptyset_E + \emptyset_H + \emptyset_{LWin} - \emptyset_{LWout} \quad (3.6)$$

where c_p is the specific heat capacity of air, A_s is the surface area of the lake, z_{sml} is the depth of the surface mixed layer, T_s is the surface temperature of the surface mixed layer, $\emptyset_{SW_s}$ is the shortwave radiation penetration into the lake, $\emptyset_E$ is the latent heat, $\emptyset_H$ is the sensible heat , $\emptyset_{LWin}$ is the incoming longwave radiation and $\emptyset_{LWout}$ is the outgoing longwave radiation. Each of the components that impact the lake general heat budget in GLM are described in detail by Hipsey et al., (2014).

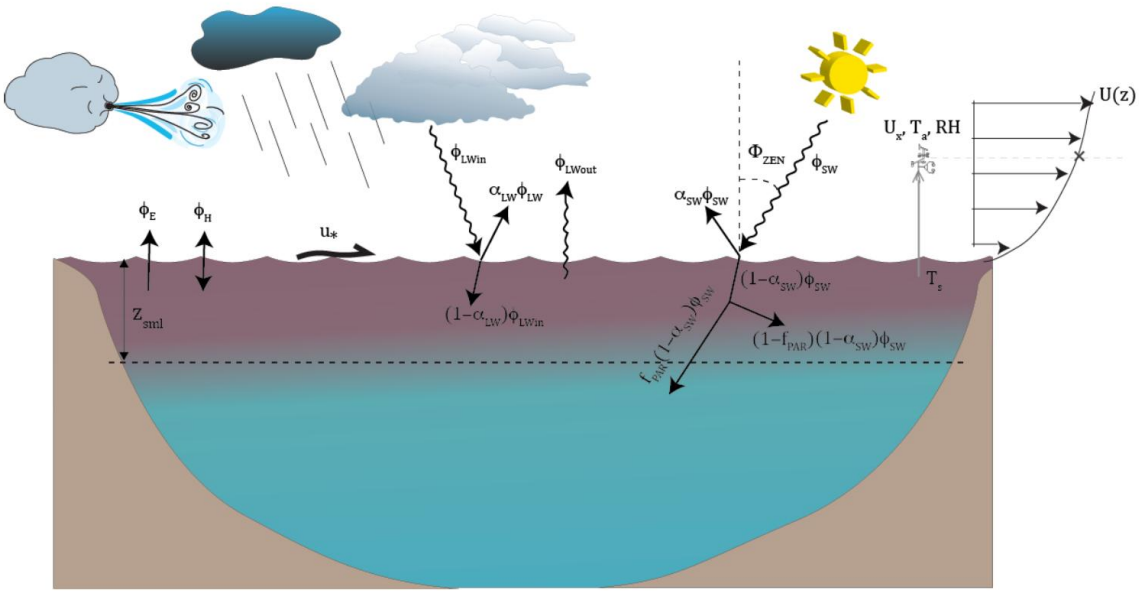


Figure 3.6 Schematic of the surface heat fluxes impacting the surface mixed layer as conceptualised in the General Lake Model (GLM) (Hipsey et al., 2014).

3.2.4 Stratification and vertical mixing

Mixing dynamics in GLM are simulated based on an energy balance approach established for DYRESM by Imberger and Patterson (1981) (see Hipsey et al., 2014). This approach focuses on estimating the amount of turbulent energy available, which is separately computed for the surface mixed layer (surface mixing) and for mixing below the thermocline (deep mixing). The available kinetic energy that drives the lake mixing dynamics is calculated due to contributions from wind stirring, shear production between layers, convective overturn and billowing (Hipsey et al., 2014, 2019).

3.2.5 Inflows and outflows

Lake inflows in GLM can be specified as surface runoff from the lake catchment, rivers entering at the surface of the lake or submerged inflows. Lake outflows can be specified as groundwater seepage, outflow from a specified depth or as lake overflow. Any number of inflows and outflows to/from the lake body can be configured in GLM.

For river inflows, depending on the density of the river water, the inflow will form a positive or negatively buoyant intrusion (Hipsey et al., 2014, 2019). As the inflow crosses lake layers it will entrain water out of them, until it reaches a level of neutral buoyancy and undergoes insertion (see Hipsey et al. (2014) for more details). Therefore, when the inflowing water reaches neutral buoyancy a new layer of thickness dependent on the inflow volume at that time is created. Following insertion, the inflow layer may then amalgamate with adjacent layers depending on the algorithm within the model for combining or splitting layers. Submerged inflows in GLM are inserted at a specified depth. The submerged inflow layer is then mixed with adjacent layers above or below depending on the density difference until neutral buoyancy is reached.

Lake outflows can be specified at any depth over the water column. Outflows will remove water from the adjacent layer, layers above or below depending on the magnitude of the discharge and stability of the water column (Hipsey et al., 2014, 2019). The amount of

outflowing water leaving the lake system is calculated by the volume of water in excess of maximum storage once rainfall, evaporation and all inflows and outflows have been accounted for (Hipsey et al., 2014, 2019). This calculation applies to all three types of outflows in GLM (i.e., seepage, withdraw and overflow).

3.2.6 Sediment heating

Different sediment zones can be defined in GLM for the lake system. These zones represent different levels of thermal interaction between water layers and the soil sediment bottom. By defining different sediment zones, the model balances the thermal budget of the lake accounting for a different heat exchange of shallow waters compared to deeper waters (see Hipsey et al., 2014, 2019 for more details). For each layer in the lake system, the rate of temperature change depends on the temperature gradient and the relative area of the layer volume in contact with the bottom sediment.

3.2.7 Bottom stress

Resuspension in the lake bed sediments can occur as a result of waves and wind-induced oscillatory currents taking place on the lake water surface. While GLM does not predict resuspension and sediment concentration directly, it computes the lake bottom shear stress. With this, GLM identifies the areal extent and potential for bed-sediment resuspension by computing the area of the lake over which the bed shear stress exceeds some critical value required for resuspension to occur. To compute the stress at the lake bottom, GLM estimates the surface wave conditions using a simple, fetch-based, steady state wave model (see Hipsey et al., 2014, 2019 for more details). The wave geometry (wave period, wave height and wave length), is predicted based on the windspeed and fetch over the lake system surface.

3.3 Conclusions

This chapter described the two process-based modelling tools used in this thesis to simulate and forecast water quantity, quality and ecosystem dynamics in river and lake systems. The GWLF-DOC catchment model was outlined for its capacity to simulate DOC dynamics in rivers, particularly in high-organic soil catchments, offering a balance between simplicity, flexibility, and performance. The GLM lake model was described as a computationally efficient and widely applied tool for simulating lake thermal structure and supporting short-term temperature forecasting. Both models have been used in a range of different applications in environmental modelling worldwide, are available as open-source code, and were integrated into the forecasting frameworks developed in the following chapters. These two modelling tools provide the mechanistic foundation in this thesis required for simulating system responses under changing conditions across different temporal scales.

Chapter 4

Accounting for model parameter uncertainty provides more robust projections of dissolved organic carbon dynamics to aid drinking water management

---

Ricardo Paíz[a], Donald C. Pierson[b], Klara Lindqvist[c,d], Pamela S. Naden[e], Elvira de Eyto[f], Mary Dillane[f], Valerie McCarthy[g], Suzanne Linnane[a], Eleanor Jennings[a]

[a]Centre for Freshwater and Environmental Studies, Dundalk Institute of Technology, A91 K584, Co. Louth, Ireland

[b]Department of Ecology and Genetics – Limnology, Uppsala University, 752 36 Uppsala, Sweden

[c]Department of Earth Sciences, Uppsala University, 752 36 Uppsala, Sweden

[d]Swedish Meteorological and Hydrological Institute, 601 76 Norrköping, Sweden

[e]UK Centre for Ecology and Hydrology, Crowmarsh Gifford, Wallingford, Oxfordshire, OX10 8BB, UK

[f]Fisheries & Ecosystem Advisory Services, Marine Institute, F28 PF65 Newport, Co. Mayo, Ireland

[g]School of History and Geography, Dublin City University, D09 YT18, Dublin 9, Ireland

---

This chapter led to the publication of the following research paper: Paíz, R., Pierson, D.C., Lindqvist, K., Naden, P.S., de Eyto, E., Dillane, M., McCarthy, V., Linnane, S., Jennings, E., 2025. *Accounting for model parameter uncertainty provides more robust projections of dissolved organic carbon dynamics to aid drinking water management*. Water Res. 123238. https://doi.org/10.1016/j.watres.2025.123238 (see Appendix D).

4.1 Abstract

Changes in climate and human behaviour impact catchment hydrology and the export of nutrients including dissolved organic carbon (DOC), with consequences for drinking water supply. In this study, we projected future river discharge and DOC dynamics under three Shared Socioeconomic Pathways (i.e., different futures of climatic conditions, socio-economic development and adaptation to climate change) and quantified change relative to a baseline for two contrasting catchments: one in Sweden and one in Ireland. For this, we used the Generalised Watershed Loading Functions Model (GWLF) with an integrated DOC module (GWLF-DOC) and drove it with data from an ensemble of global climate models, taking into account variability derived from multiple model parameter sets. We assessed the relative contribution of each of these two factors (climate input data and model parameterisation) to the total uncertainty in predictions. Projections for river discharge differed between the two sites in magnitude, variability and direction of change depending on the future scenario and time period. In contrast, DOC was always projected to show increases in concentration throughout the annual cycle and over time, with the highest levels by the end of the century, for scenarios with greater warming and low mitigation efforts. Future climate data provided the dominant source of uncertainty in all of our projections. However, the DOC model parameters, which respond to temperature and soil moisture conditions, became more influential in scenarios of higher climatic variability. Our approach highlights the benefits of incorporating often ignored parameter uncertainty in climate change impact assessments for both interpreting outputs and communicating results to water managers.

Keywords: Hydrological modelling; Water quality modelling; DOC; Climate change; Uncertainty analysis; GWLF

4.2 Introduction

Terrestrially sourced dissolved organic matter (DOM) entering freshwaters has many impacts on aquatic ecology (Rodríguez-Cardona et al., 2022) and on water use and supply (Johnes et al., 2023). High concentrations are associated with water browning (Kritzberg et al., 2020), a condition that affects both ecosystem function (Evans et al., 2005) and drinking water quality (Riyadh and Peleato, 2024). Concentrations of DOM (operationally quantified using dissolved organic carbon (DOC)) must be reduced during drinking water treatment prior to any chlorination (Köhler et al., 2016; Piai et al., 2024), as it is a precursor to the formation of disinfection by-products (DBPs) (Srivastav et al., 2020; Franklin et al., 2021a). The presence of DBPs in drinking water, although unintended, remains a critical safety issue due to the adverse effects of DBPs such as trihalomethanes (THMs) on human health (Diana et al., 2019; Kumari and Gupta, 2022). The formation of these contaminants has raised concern in many regions (Villanueva et al., 2023), especially those where DOC drains from terrestrial soil stores that are rich in organic carbon (e.g., from peatlands and other organic soils) (J. Xu et al., 2020; Fenner et al., 2021).

The production and transport of DOC in catchments result from interactions between landscape, land use and climate, including atmospheric deposition factors (Jennings et al., 2010a; Adler et al., 2021). Temperature, water availability and acid deposition (e.g., sulphur deposition) influence physicochemical and biological mechanisms that regulate soil decomposition and hence DOC production, while hydrological processes control its transport (Evans et al., 2006; Clark et al., 2009; Wit et al., 2021). All of these factors have been reported as drivers of long-term DOC increases in recent decades across the northern hemisphere, although the importance of any factor can vary from site to site (Evans et al., 2005; de Wit et al., 2007; Oulehle and Hruška, 2009; SanClements et al., 2012; Anderson et al., 2023). However, with acid deposition gradually levelling off (Garmo et al., 2014; Wit et al., 2021), the interactions between the other climatic factors

and catchment hydrology will likely be more relevant in future DOC dynamics (Clark et al., 2010; Anderson et al., 2023; Wu and Yao, 2024).

Increasingly variable temperature and precipitation patterns, including those related to global warming (Wang et al., 2017; van der Wiel and Bintanja, 2021), can induce important changes in the magnitude and seasonality of DOC export. For instance, dry periods (e.g., hotter, drier summers), wet periods (e.g., wetter winters), prolonged dry conditions, drought-rewetting cycles, lower water tables, and flooding, can all lead to higher variability in catchment DOC concentrations and fluxes (Blaurock et al., 2021; Dong et al., 2021; Wu and Yao, 2022; Wu et al., 2023a, 2023b) that can, in turn, result in higher DBP levels following treatment (Warner and Saros, 2019; Fenner et al., 2021). Increased variability in source water DOC levels can also make water treatment more difficult to manage (Köhler et al., 2016; Piai et al., 2024). It is important, therefore, to quantify the response of both catchment hydrology and DOC dynamics to future climatic conditions. By determining this, drinking water managers may better anticipate future DOC levels, assess risk for supplies, and prepare basin and/or treatment scale mitigation actions accordingly (Ritson et al., 2014; J. Xu et al., 2020; Klante et al., 2022).

Catchment modelling exercises allow us to quantify change between past and future water quantity and quality, including DOC concentrations and flux. However, all modelling is associated with differing degrees of uncertainty, that are related to a range of sources (Hattermann et al., 2018; Her et al., 2019a). While uncertainty related to projecting future climate (by using ensembles of global climate models [GCMs]) and to human behaviour (by use of multiple scenarios for population behaviour) are now generally incorporated into climate change impact assessments (Kundzewicz et al., 2018; Schürz et al., 2019a), other sources are generally not. These include variability related to climate bias correction methods, model structure and model parameterisation i.e., the model state variables, governing equations and parameter selection. Model parameterisation, in particular, can be a complex source of uncertainty since differing

sets of parameters can produce equally good simulations of key model variables during calibration (i.e., model parameter equifinality) (Beven and Binley, 1992, 2014), but produce differing results in future scenarios. This uncertainty has been quantified in some studies of changes in DOC dynamics (e.g., O'Driscoll et al. 2018a; Xu et al. 2020), but to date, has not been incorporated into climate change impact simulations. Moreover, the relative contribution of both GCM uncertainty and parameter uncertainty to these future projections has not been explored. Accounting for such uncertainty in future projections will produce more robust outputs (Her et al., 2019a; Marshall et al., 2021), and therefore provide more appropriate information to assist decision making at a catchment management level (Teweldebrhan et al., 2018; Cui et al., 2021).

In this study, we used a previously described DOC model (Naden et al., 2010) that is coupled with the Generalised Watershed Loading Functions Model (GWLF) (Schneiderman et al., 2010) to calibrate and simulate future discharge, DOC concentration and DOC flux under climate change scenarios in one Irish and one Swedish catchment. These sites were selected as they are contrasting in size, climate and hydrology, with high organic soils, and represent systems in countries where drinking water is affected by increases in DOC (O'Driscoll et al., 2018b; Kritzberg et al., 2020), leading to issues in treatment and supply. After years of continuous THM exceedances in several supplies, Ireland has recently been ruled against by the Court of Justice of the European Union (25 January 2024; Case C-481/22) for failure to fulfil obligations on the quality of water intended for human consumption. Similarly, the formation of DBPs has been a persistent problem in Sweden, affecting many drinking water schemes (Kritzberg et al., 2020) including the supply to its capital Stockholm (Köhler et al., 2016).

Within this context, we aimed to: (1) quantify the future change in catchment discharge, DOC concentration and DOC flux between a historical baseline and three future scenarios; (2) determine the periods in the annual cycle when any future changes will

be most relevant; and (3) quantify the relative contribution from future climate conditions and model parametrisation to the total uncertainty in these predictions. We capture and summarise the modelling outputs in a way that would be usable by catchment and source water managers. Lastly, we discuss how these results could assist the drinking water sector.

4.3 Materials and methods

4.3.1 Study sites

The Glenamong and Vattholma catchments are located in western Ireland (53° 57' N, 9° 35' W) and southeastern Sweden (60° 10' N, 17° 50' E), respectively (Fig. 1). Both catchments export relatively large quantities of carbon from terrestrial stores to downstream lakes (Ryder et al., 2014; Doyle et al., 2021a; Lindqvist, 2022), reflecting their peatland and forest dominated land covers (Coordination of Information on the Environment – CORINE – classification) (Büttner et al., 2017) (Table 1). The Glenamong River is one of the two main inflows to Lough Feeagh and Vattholma flows into Lake Mälaren, the drinking water source for two million people, including the city of Stockholm. While the Glenamong and Feeagh are not used as a source of potable water, they are intensively monitored sites that are representative of similar rivers and small lakes used as drinking water supplies in the region.

The study sites have contrasting characteristics. The Glenamong is small (18 km²) and unpopulated, characterised by a relatively high variability in daily river discharge due to high precipitation levels and a steep landscape (Doyle et al., 2019; Jennings et al., 2020). Vattholma, in contrast, hosts several communities in a much larger area (261 km²) and features more gradual variations in daily discharge reflecting a much flatter terrain, longer river network, lower precipitation levels and cooler air temperatures. Vattholma is also drier than Glenamong, only registering measurable rainfall on 37% of days within a calendar year versus 84% at the Irish site. While the average DOC concentration recorded at Vattholma is over twice that of the Glenamong,

the annual DOC flux on an areal basis is four times lower for the Swedish site due to its much larger basin area (Fig. 1; Table 1).

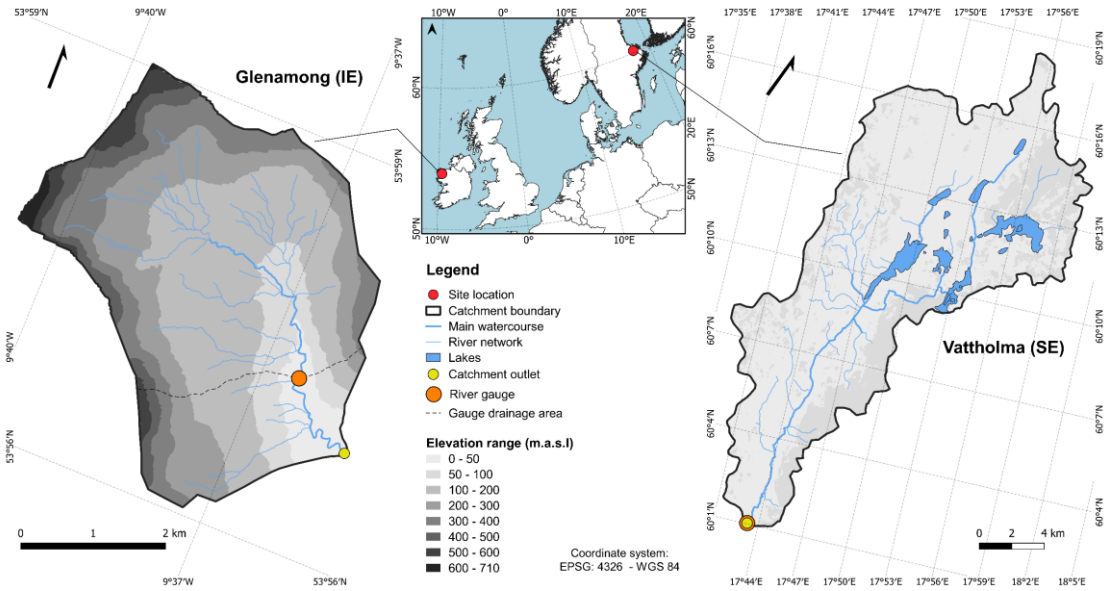


Figure 4.1 Location of the study catchments including river network and topographic elevation.

4.3.1.1 Data availability

Observed climate data for Vattholma were obtained from the European Climate Assessment & Dataset E-OBS repository (0.1°grid, www.ecad.eu). Daily discharge data at the river outlet (1980 - 2022) were obtained from the Swedish Meteorological and Hydrological Institute monitoring services (www.smhi.se). Monthly total organic carbon (TOC) (mg TOC L^{-1}) concentrations at the outlet (1991 - 2022) were obtained from the Swedish Agricultural University monitoring services (www.slu.se) and were used as a direct proxy for DOC (mg DOC L^{-1}) in line with previous studies for this and other Swedish catchments (e.g., Ledesma et al. 2012; Lindqvist 2022); TOC = 0.95 DOC + 1.4, r^2 = 0.93, n = 47. In Glenamong, climate observations from in situ meteorological stations and daily river discharge data (2013 to 2023) were obtained from the Marine Institute monitoring services (https://www.marine.ie). Weekly water colour measurements (expressed as mg PtCo L^{-1}) were also available (2016 – 2023), based on absorption measurements performed with a HACH Dr 2000 spectrophotometer at

455 nm (wavelength accuracy of ±2 nm) on water filtered through Whatman GF/C filters (1.2 µm pore size). These were used as a proxy for DOC (Doyle et al., 2019), converted via a linear regression relationship with DOC laboratory measurements (samples filtered through 0.45 µm pore size); DOC = 0.067 water colour + 2.69, $r^2 = 0.88$, n = 551. Observed daily DOC fluxes (kg C km^{-2} day^{-1}) for both sites were computed as the product of DOC concentrations and mean daily measured discharge.

Table 4.1 Main characteristics of the study catchments. Units for altitude are meters above sea level.

Catchment	**Glenamong (IE)**	**Vattholma (SE)**
Area (km^2)	18	261
Altitude range (m.a.s.l.)	8 – 710	5 – 83
Main soil type	Blanket peat	Silty clay
Land cover		
Peatland	69%	5%
Agriculture	0%	17%
Grassland	4%	15%
Urban	0%	2%
Forest	26%	58%
Watercourse	1%	3%
Climate and hydrology	*2013 - 2023*	*1980 - 2022*
Mean air temperature (°C)	10.8	6.0
Annual precipitation range (mm yr^{-1})	1660 – 2570	460 – 875
Mean annual precipitation (mm yr^{-1})	2050	610
Main watercourse length (km)	4.8	39.1
Median river discharge (m^3 s^{-1})	0.4	1.1
Mean river discharge (m^3 s^{-1})	0.8	1.7
Q5 river discharge (m^3 s^{-1})	2.8	5.3
DOC	*2016 - 2023*	*1992 - 2022*
DOC concentration range (mg L^{-1})	2.8 – 18.0	8.2 – 36.9
Mean DOC concentration (mg L^{-1})	8.7	19.6
Mean annual DOC flux (tC km^{-2} yr^{-1})	16.2	4.0
Mean monthly DOC flux (tC km^{-2} $month^{-1}$)	1.4	0.3

4.3.2 Model development

In this study, we used the Generalised Watershed Loading Functions Model (GWLF) to simulate river discharge, DOC flux and DOC concentration. More specifically, we used the version developed by the New York City Department of Environmental Protection (NYC DEP) (Schneiderman et al., 2002) that was further developed by Schneiderman et al. (2010) and Naden et al. (2010) and which includes a process-based module for DOC (GWLF-DOC). This model has been previously applied to several catchments to quantify changes in DOC export, including in the Lough Feeagh and Mälaren catchments (Naden et al., 2010; Lindqvist, 2022). Importantly, three changes were made to the model configuration in the current study, with the aim of improving DOC simulation capacity and better reflect DOC dynamics. These changes do not represent large increases in model complexity and do not require additional input data. Below, we describe key features of the base model and the changes we have implemented.

4.3.2.1 Hydrology module

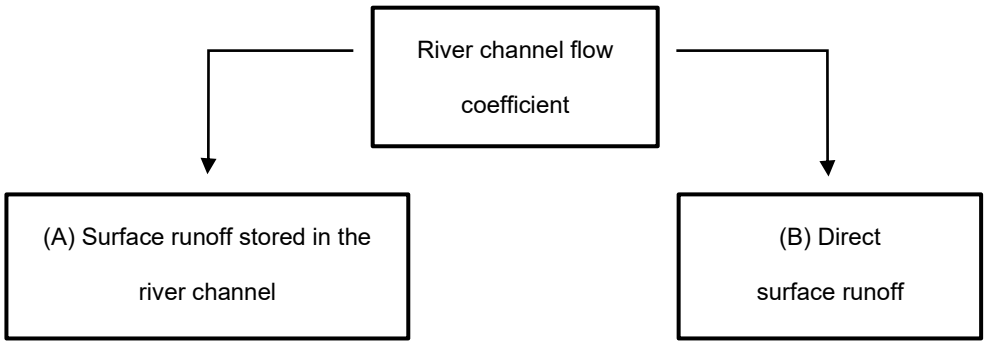
GWLF simulates discharge from both surface runoff and from subsurface baseflow based on interactions between climate and a set of catchment land cover areas (see Chapter 3 for more details). Surface runoff is calculated using the USDA SCS curve number method (Boughton, 1989), and varies as a function of land uses and soil characteristics. In the current study, curve numbers associated with watershed CORINE land use areas were extracted from the GCN 250 dataset (Jaafar et al., 2019) and a value was calculated for each land cover area based as an area-weighted mean. Baseflow is calculated as a lumped contribution from the entire watershed as both slow- and fast-moving groundwater flows (see Schneiderman et al., 2010) from three subsurface lumped reservoirs (i.e., averaged over the whole catchment): (1) the unsaturated zone (subjected to evapotranspiration), (2) a saturated zone (not subjected to evapotranspiration), and (3) a deep saturated zone with sustained low flow discharge. Evapotranspiration was calculated using the Hamon temperature index

equation (Hamon, 1961). The original hydrology model included seven adjustable parameters to regulate the different hydrological states (see Chapter 3). We incorporated one additional parameter: a *river channel flow coefficient* (change 1). The latter partitions surface runoff into two separate pathways: a *direct runoff* pathway and a *river channel stored discharge* pathway. With this, we aimed to represent better the timing of water flow and DOC in basins of large size and/or regulated river networks, in which water (and the DOC contained therein) is stored in the channel at times exceeding the daily time step. This stored water was subjected to evapotranspiration. A description of the model parameters for hydrology and a conceptual diagram depicting change 1 in the model structure are presented in Table 4.2 and Fig. 4.2, respectively.

Table 4.2 Description of the model parameters of the hydrology module in the Generalised Watershed Loading Functions Model (GWLF) with an incorporated model parameter for the current study (the river channel flow coefficient).

Model parameters - hydrology module (GWLF)		
Parameter	**Concept**	**Units**
Precipitation correction factor	Adjusts precipitation input to account for potential measurement bias	factor day^{-1}
Melt coefficient	Controls the rate of snowmelt based on temperature conditions	cm $°C^{-1}$ day^{-1}
Runoff curve number adjustment	Adjusts the runoff curve number to better simulate surface runoff based on land cover and soil type	-
Soil water capacity	Represents the maximum water-holding capacity of the soil in the unsaturated zone	cm
Recess coefficient	Controls the rate at which fast-groundwater flow is output from the saturated zone	coeff. day^{-1}
Slow recess coefficient	Controls the rate at which slow groundwater flow is output from the deep saturated zone	coeff. day^{-1}
Baseflow capacity	Limits the amount of deep percolation (baseflow output from the saturated zone to the deep saturated zone)	cm
River channel flow coefficient	Partitions surface runoff into direct runoff and a river channel stored discharge	coeff. day^{-1}

Figure 4.2 Conceptual diagram depicting change 1 in the model structure of the Generalised Watershed Loading Functions Model (GWLF).



(A) $Surface\ runoff * (1 - River\ channel\ flow\ coefficient)$

(B) $Surface\ runoff * River\ channel\ flow\ coefficient$

4.3.2.2 DOC module

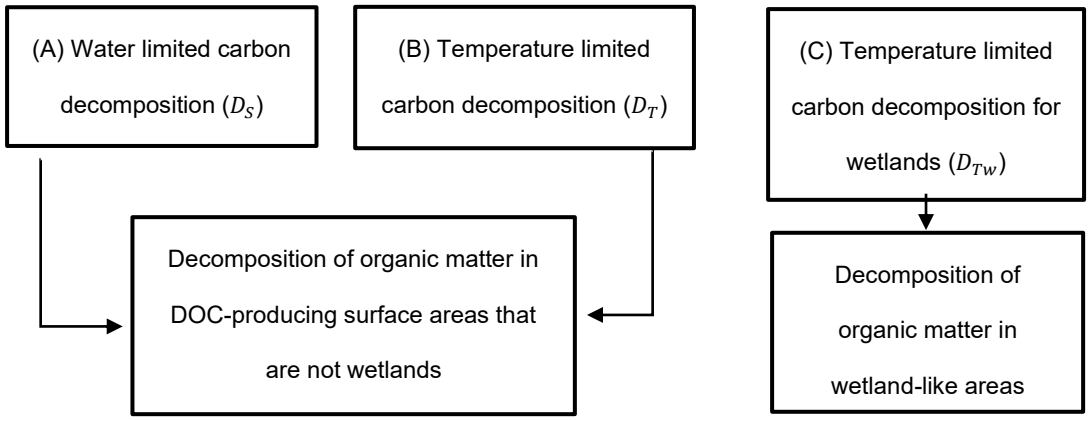
As described in Chapter 3, GWLF follows a two-phase process for simulating DOC concentrations at the catchment outlet: (1) DOC production and (2) DOC washout. DOC production is regulated by two processes: temperature-dependent decomposition (D_T) and moisture-dependent decomposition (D_S) of soil organic matter. In the model described by Naden et al. (2010), three adjustable parameters controlled production: (1) *activation energy* (E_a) and (2) *anaerobic decomposition rate* (a) controlled D_T, while (3) the *aerobic decomposition rate* (b) controlled D_S. Here, we assigned an independent D_T for surface land covers we defined as wetland areas (e.g., peatlands, inland marshes) for which a new separate (4) *anaerobic decomposition rate* (a_w) only was used (change 2). The aim was to account for the difference in DOC production between areas that would be subject to continual fluctuations in water level and areas which would remain water-logged, and therefore not be subjected to the same decomposition rates (Mozafari et al., 2023; Arsenault et al., 2024). Furthermore, the calculation of D_S is based

on simulated soil water storage which is a basin lumped variable, and which would not be representative of the conditions in water-logged areas. A description of the parameters for DOC production and a conceptual diagram depicting change 2 are presented in Table 4.3 and Fig. 4.3, respectively.

Table 4.3 Description of the model parameters of the DOC module related to DOC production in the Generalised Watershed Loading Functions Model (GWLF-DOC) with an incorporated model parameter for the current study (anaerobic decomposition rate for wetlands).

Model parameters (DOC production) - DOC module (GWLF-DOC)		
Parameter	**Concept**	**Units**
Activation energy (Ea)	Energy required to drive microbial processes that break down organic matter in the soil matrix	kJ gC^{-1}
Aerobic decomposition rate (b)	Rate at which carbon decomposition occurs in the organic soil matrix in the presence of oxygen (aerobic conditions)	-
Anaerobic decomposition rate (a)	Rate at which carbon decomposition occurs in the organic soil matrix in oxygen-limited conditions (anaerobic conditions) for surface areas that are not assigned as wetland-like areas	gC m^{-2} day^{-1}
Anaerobic decomposition rate wetlands (aw)	Rate at which carbon decomposition occurs in the organic soil matrix in oxygen-limited conditions (anaerobic conditions) for surface areas that are assigned as wetland-like areas	gC m^{-2} day^{-1}

Figure 4.3 Conceptual diagram depicting change 2 in the model structure of the Generalised Watershed Loading Functions Model with an integrated DOC module (GWLF-DOC).



(A) $D_S = exp\left(-b\left[\left(\frac{(S_{max}-S)}{1.6S_{max}} - 0.35\right)^2 - 0.1225\right]\right)$

(B) $D_T = a\left\{exp\left(\frac{E_a}{R}\left[\frac{1}{T_{ref}} - \frac{1}{T}\right]\right)\right\}$

(C) $D_{Tw} = a_w\left\{exp\left(\frac{E_a}{R}\left[\frac{1}{T_{ref}} - \frac{1}{T}\right]\right)\right\}$

where $D_{S,T}$ is DOC production rate (g C m^{-2} day^{-1}) at soil moisture S and at soil temperature T (K), respectively. *The* aerobic decomposition rate (b) controls D_S. Activation energy (E_a), anaerobic decomposition rate (a) control D_T. Activation energy (E_a), anaerobic decomposition rate for wetland-like areas (a_w) control D_{Tw}. Soil moisture is given by a relationship between the soil water capacity S_{max} (cm) and the soil water content S (cm) of the unsaturated zone of the catchment. T_{ref} is the reference soil temperature, which is set to 10℃ (283 K). R corresponds to the universal gas constant (6.928 × 10^{-4} kJ K^{-1} g C^{-1}).

The DOC produced in the original model was stored in a single carbon catchment pool and made available for washout via all runoff and groundwater flows, regulated by three parameters (Naden et al., 2010). Here, instead of using a single pool, we defined pools that mirrored the main hydrological stores (i.e., the surface soils of the catchment, the unsaturated zone, and the deeper saturated zones), and accounting for the available carbon resulting from wetlands production as well. With this change, we aimed to track more closely how the different hydrological states drive DOC production and transport in the model. Four main pools were defined as lumped carbon reservoirs (change 3): (1) DOC stored in surface wetland-like areas, (2) DOC stored in DOC-producing surface areas that are not wetlands (see Naden et al. 2010), (3) DOC stored in the catchment unsaturated zone, and (4) DOC stored in the catchment saturated zones.

Consistent with the model hydrology, DOC from surface pools 1 and 2 is available for washout via runoff flows (*direct runoff* and *channel stored discharge*), while DOC from

pools 3 and 4 is available for washout via baseflow (slow- and fast- moving groundwater flows). As a result, the number of parameters to regulate the DOC transport increased from three to five: (1) *surface carbon loss coefficient,* (2) *surface flow cap,* (3) *baseflow ratio,* (4) *fast groundwater flow carbon loss coefficient* and (5) *slow groundwater flow carbon loss coefficient*. A description of the new model parameters for DOC washout is presented in Table 4.4. Streamflow DOC concentrations and fluxes were calculated as in the original model, from the sum of all DOC contributions (kg C day^{-1}) and using the total discharge (m^3 day^{-1}) (Naden et al., 2010).

Table 4.4 Description of the new model parameters for DOC washout of the DOC module in the Generalised Watershed Loading Functions Model with an integrated DOC module (GWLF-DOC).

Model parameters (DOC washout) - DOC module (GWLF-DOC)		
Parameter	**Concept**	**Units**
Surface carbon loss coefficient	Proportion of carbon washed out via surface runoff, from both surface wetland-like areas and DOC-producing surface areas that are not wetlands	coeff. day^{-1}
Surface flow cap	Threshold value for surface runoff above which the surface runoff occurs as overland flow and will dilute DOC concentration	cm
Baseflow ratio	Ratio controlling the proportion of carbon transported by fast-moving groundwater flow from the saturated zone relative to the carbon transferred to the deep saturated zone through deep percolation	fast- to slow-groundwater ratio day^{-1}
Fast groundwater flow carbon loss coefficient	Rate at which DOC is output through fast groundwater flow from the saturated zone	coeff. day^{-1}
Slow groundwater flow carbon loss coefficient	Rate at which DOC is output through slow groundwater flow from the deep saturated zone	coeff. day^{-1}

4.3.3 Model calibration

For calibration of the hydrology, the discharge datasets were divided into two periods. The first was used for calibration and the second for validation: Vattholma (1980 – 2011, 2012 – 2022) and Glenamong (2013 –2018, 2019 – 2023). For DOC, due to lower data availability, a single period was used for calibration only: Vattholma (1992 – 2022) and Glenamong (2016 – 2023). Model performance was evaluated based on the Nash-Sutcliffe coefficient (NSE) and the coefficient of determination (r^2) (Krause et al. 2005) between daily measured and simulated discharge, DOC concentration and DOC flux.

We adopted multistep script-based calibrations to adjust the model parameters. In line with Schneiderman et al. (2010) and Naden et al. (2010), on each calibration step, target functions were defined and the Powell search-optimisation method (Zhong and Cai, 2015) within VENSIM software (Ventana Systems Inc.) was used to calibrate parameters between pre-determined ranges. The range limits were set based on previous modelling studies and relevant literature (e.g., Evans et al., 2006; Karhu et al., 2010; Naden et al., 2010; Klimek et al., 2020; Lindqvist, 2022). The calibration range used for each model parameter is displayed in Table 4.5.

The calibration target functions for hydrology included checks for daily water balance and payoffs between simulated and measured discharge, runoff and baseflow (measured runoff and baseflow based on the Arnold et al. (1995) hydrograph separation method; see Schneiderman et al. 2010). For DOC, a payoff between daily measured and simulated DOC concentration was used as the target function on each step. Model spin-up periods of four and two years were used for Vattholma and Glenamong, respectively. A summary description of the model calibration script used for hydrology and DOC are presented in Table 4.6 and Table 4.7, respectively.

Table 4.5 Model calibration ranges used for each of the model parameters of the hydrology module and DOC module in GWLF-DOC.

Hydrological parameters				
	Precipitation correction factor	**River channel flow coeff.**	**Melt coeff.**	**Curve adj. number**
Units	*factor / day*	*coeff. / day*	*cm / °C / day*	*-*
Calibration range	*0.50 - 1.50*	*0.01 - 1.00*	*0.05 - 0.60*	*-10.0 to 10.0*

	Soil water capacity	**Baseflow capacity**	**Slow recess coeff.**	**Recess coeff.**
Units	*cm*	*cm*	*coeff. / day*	*coeff. / day*
Calibration range	*12.00 - 20.00*	*2.50 - 8.00*	*0.001 - 0.100*	*0.005 - 0.030*

DOC parameters				
DOC production				
	Activation energy (E_a)	**Aerobic decomp. rate** (b)	**Anaerobic decomp. rate** (a)	**Anaerobic decomp. rate (wetlands)** (a_w)
Units	*kJ / gC*	*-*	*gC / m² / day*	*gC / m² / day*
Calibration range	*3.0 - 7.0*	*1.0 - 7.5*	*0.005 - 0.15*	*0.005 - 0.15*

DOC washout - runoff		
	Surface carbon loss coeff.	**Surface flow cap**
Units	*coeff. / day*	*cm*
Calibration range	*0.01 - 1.00*	*0.01 - 6.00*

DOC washout - baseflow			
	Baseflow ratio	**Fast groundwater carbon loss coeff.**	**Slow groundwater carbon loss coeff.**
Units	*fast- to slow- groundwater ratio / day*	*coeff. / day*	*coeff. / day*
Calibration range	*0.01 - 1.00*	*0.001 - 1.000*	*0.001 - 1.000*

Table 4.6 Description of the model calibration script used for the hydrology module of GWLF-DOC.

Calibration script for the hydrology module (GLWF-DOC)		
Step No.	**Optimisation control on:**	**Optimisation target function (payoff)**
Step 1	Precipitation correction factor	Optimise the precipitation correction factor to a catchment water balance
Step2	Curve adj. number	Optimise the curve adjustment number by comparing total cummulative simulated and measured runoff (based on hydrograph separation)
Step 3	Melt coeff.	Optimise the melt coefficient factor by comparing simulated and measured river discharge
Step 4	Soil water capacity and recess coeff.	Optimise soil water capacity and recess coefficient by comparing simulated baseflow discharge with measured baseflow discharge (based on hydrograph separation)
Step 5	Baseflow capacity + slow recess coeff.	Optimise slow recess coefficient and baseflow capacity against slow-moving groundwater flow (20th percentile of baseflow)
Step 6	River channel flow coeff.	Optimise the river channel flow coefficient by comparing simulated and measured surface runoff (based on hydrograph separation)
Step 7	Precipitation correction factor	Optimise the precipitation correction factor to a catchment water balance
Step 8	Curve adj. number	Optimise the curve number adjustment factor by comparing total cummulative simulated and measured runoff (based on hydrograph separation)
Step 9	Melt coeff.	Optimise the melt coefficient factor by comparing simulated and measured river discharge
Step 10	Soil water capacity and recess coeff.	Optimise soil water capacity and recess coefficient by comparing simulated baseflow discharge with measured baseflow discharge (based on hydrograph separation)
Step 11	Baseflow capacity + slow recess coeff.	Optimise slow recess coefficient and baseflow capacity against slow-moving groundwater flow (20th percentile of baseflow)
Step 12	River channel flow coeff.	Optimise the river channel flow coefficient by comparing simulated and measured surface runoff (based on hydrograph separation)
Step 13	Recess coeff. and slow recess coeff.	Optimise both the recess coefficient and slow recess coefficient by minimising the mean square error between simulated and measured baseflow (based on hydrograph separation)
Step 14	Precipitation correction factor	Optimise the precipitation correction factor to a catchment water balance

Table 4.7 Description of the model calibration script used for the DOC module of GWLF-DOC.

Calibration script for the DOC module (GLWF-DOC)		
Step No.	**Optimisation control on:**	**Optimisation target function (payoff)**
Step 1	Initial conditions	Optimise initial conditions by comparing simulated DOC concentration and measured DOC concentration
Step2	Activation energy + aerobic decomp. rate + anaerobic decomp. rate + anaerobic decomp. rate (wetlands) + surface carbon loss coeff. + surface flow cap	Optimise model parameters by comparing simulated DOC concentration and measured DOC concentration
Step 3	Baseflow ratio + fast groundwater carbon loss coeff.	Optimise model parameters by comparing simulated DOC concentration and measured DOC concentration
Step 4	Soil water capacity and recess coeff.	Optimise model parameters by comparing simulated DOC concentration and measured DOC concentration
Step 5	Initial conditions	Optimise initial conditions by comparing simulated DOC concentration and measured DOC concentration
Step 6	Activation energy + aerobic decomp. rate + anaerobic decomp. rate + anaerobic decomp. rate (wetlands) + surface carbon loss coeff. + surface flow cap	Optimise model parameters by comparing simulated DOC concentration and measured DOC concentration
Step 7	Baseflow ratio + fast groundwater carbon loss coeff.	Optimise model parameters by comparing simulated DOC concentration and measured DOC concentration
Step 8	Aerobic decomp. rate + slow groundwater carbon loss coeff. + surface carbon loss coeff.	Optimise model parameters by comparing simulated DOC concentration and measured DOC concentration

4.3.4 Model uncertainty and sensitivity

We employed the Generalised Likelihood Uncertainty Estimation (GLUE) method (Beven and Binley, 1992, 2014) to quantify model parameter uncertainty. GLUE allows the exploration of parameter uncertainty by sampling from the parameter space and evaluating model performance against observed data. First, a Monte Carlo simulation round (30,000 model runs) was performed for each catchment, varying the parameters within calibration ranges. Second, an NSE threshold of 0.60 was defined for hydrology (simulated vs measured discharge) and of 0.30 for DOC (simulated vs measured DOC concentration) respectively, as a likelihood measure to constrain parameter variability

space (i.e., to further constrain the parameter ranges so that more simulations with an acceptable NSE value above the selected thresholds are output) (Pianosi et al., 2016). A second simulation round (30,000 runs) was then performed using these constrained ranges. From all parameter sets above the likelihood measure thresholds (i.e., behavioural parameter sets), the 100 best-performing sets were used to compute 5% to 95% range GLUE uncertainty bounds (Beven, 2009). Model equifinality (i.e., how sensitive the model is to different parameter sets that produce acceptable simulations of observed behaviour) (Beven and Freer, 2001) was assessed individually for hydrology and DOC, relative to the selected likelihood measure (i.e., the NSE metric) and using all behavioural parameter sets.

4.3.5 Future projections

Future climate projections for the meteorological input variables were derived from the 5-member GCM ensemble comprising GFDL-ESM4, IPSL-CM6A-LR, MPI-ESM1-2-HR, MRI-ESM2-0 and UKESM1-0-LL, provided by the open-access Inter-Sectoral Impact Model Intercomparison Project (0.5° ISIMIP 3b simulation round; data.isimip.org) (Lange and Büchner, 2021).

Grid-cell daily bias-corrected values of future precipitation and mean air temperature from 2021 to 2100 were extracted for each study catchment for three Shared Socioeconomic Pathways (SSP): SSP126, SSP370 and SSP585. These represent three different futures of greenhouse gas (GHG) emission levels, societal development, and adaptation to climate change (IPCC, 2023). Ranging from a more to a less optimistic scenario, SSP126 reflects rapid efforts to mitigate GHG emissions while promoting environmental and economic sustainability, SSP370 adopts intermediate efforts for both adaptation and mitigation, and SSP585 assumes increasing trends in fossil-fuelled development i.e., a high level of human-induced global warming. In addition, a 30-year baseline period from 1985 to 2014 was defined, for which daily input data for each catchment were extracted from the historical period of the same ISIMIP3b GCMs. In

total therefore, we used 15 future GCM scenarios and five historical scenarios to make comparisons between the historical and future conditions simulated by the five GCM models.

All ISIMIP3b data have been subject to robust statistical downscaling and bias adjustment as part of the ISIMIP quality control/quality assurance (QC/QA) protocols, before making it available for use in modelling. The observational reference dataset used for bias adjustment and statistical downscaling in ISIMIP3b is version 2.0 of WFDE5 over land, merged with ERA5 over the ocean (W5E5; Lange and Büchner, 2021). Details on the downscaling and bias correction for these data can be found on the official ISIMIP3b method fact sheets (see Lange and Büchner, 2021).

4.3.5.1 Data processing and analysis

For each scenario simulation (baseline, SSP126, SSP370 and SSP585), one meteorological dataset for each GCM was used to drive GWLF-DOC for each of the 100 top behavioural parameter sets (see Section 4.3.4) so that the uncertainty associated with the different GCMs and that associated with model parameters were estimated. A daily, monthly, and annual ensemble mean of the resulting 500 simulations for each scenario (5 GCMs x 100 behavioural parameter sets) was calculated for each SSP scenario. The model outputs for the SSPs were collated for two decadal periods: 2050 – 2059 (P1) and 2090 – 2099 (P2), which were used to compare against outputs for the baseline period. Furthermore, we computed future anomalies at the annual scale (Du and Deng, 2022) from 2030 to 2100 for discharge and DOC concentration between each future scenario and the baseline. The uncertainty in the predictions was calculated as the standard deviation of the ensemble. We also displayed the likelihood that each scenario would exceed 95th percentile baseline levels for DOC concentration and flux (as metrics of current extreme conditions) in future meteorological seasons. Seasonal analyses were based on the typical three-month periods relevant for management: spring (March to May), summer (June to August), autumn (September to November)

and winter (December to February). Lastly, the relative contribution of (1) future climate input data and (2) model parameterisation to the total uncertainty in predictions was assessed based on a variance partitioning procedure (Watling et al., 2015; Lofton et al., 2022). For this, the model was run with all five GCMs but using only the calibrated set of model parameters (see Section 4.3.3). Then, it was run using all 100 best-performing model parameter sets with each GCM dataset. A normalised difference of the variances in the simulation results was then computed to estimate individual relative uncertainty contributions (Lofton et al., 2022). The same calculations were followed for each of the two catchments.

4.4. Results

4.4.1 Model performance and uncertainty

The results from the optimisation procedure for catchment hydrology indicated a good fit at both sites. The NSE values for average monthly and daily discharge based on the best optimised simulation ranged from 0.73 to 0.79 for Vattholma, and from 0.60 to 0.78 for Glenamong (Fig. 4.4; Fig. 4.5). Similarly, r^2 values ranged from 0.76 to 0.80 for Vattholma, and from 0.60 to 0.78 for Glenamong (Fig. 4.4; Fig. 4.5). For DOC, the metrics for the best optimised simulation were higher for DOC fluxes than for DOC concentrations at both sites. For Vattholma, the NSE and r^2 values for the daily DOC flux were 0.73 and 0.74 respectively, while those for daily DOC concentration were 0.39 and 0.39 (Fig. 4.6a and b). For Glenamong, the NSE and r^2 values for daily DOC flux were 0.60 and 0.62, while those for daily DOC concentration were 0.45 and 0.47 respectively (Fig. 4.6c and d).

Simulated DOC flux for each study site reflected site-specific dynamics and intra-annual variations (Fig. 4.7a - b). Baseflow was a major contributor to both discharge (Fig. 4.7c - f) and carbon export in Vattholma, while there was a more balanced ratio between baseflow and surface runoff for Glenamong.

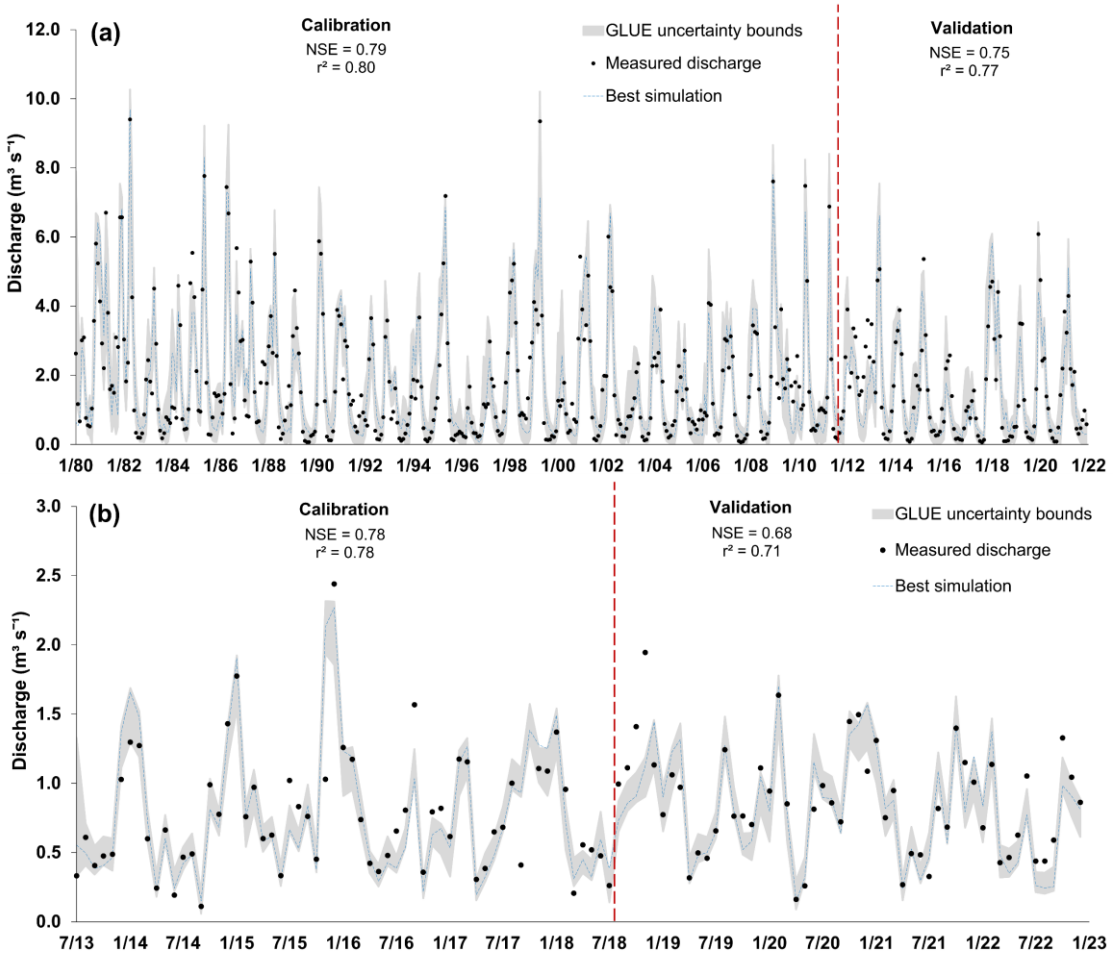


Figure 4.4 Observed and simulated monthly river discharge for Vattholma (a) and Glenamong (b) catchments during model calibration and validation. NSE and r² values are indicated for the calibrated parameter set (best optimised simulation). The grey area denotes the 5% - 95% range GLUE uncertainty bounds for river discharge based on the 100 best-performing parameter sets.

The set of calibrated model parameters obtained for the best optimisation run reflected the differences between the study sites (Table 4.8). Except for the precipitation correction factor and soil water capacity, the optimised values for the hydrological parameters were generally higher for Glenamong than for Vattholma, particularly the river channel flow coefficient. For DOC production, the optimisation resulted in a higher activation energy (E_a = 6.4) and aerobic decomposition rate (b = 7.4) for Vattholma, indicating a greater sensitivity to changes in soil temperature and moisture levels at this site than for Glenamong (E_a = 3.0 and b = 1.0). In contrast, the values for both anaerobic

decomposition rates were an order of magnitude greater at the Glenamong, reflecting the importance of saturation of the deep Irish peat soils.

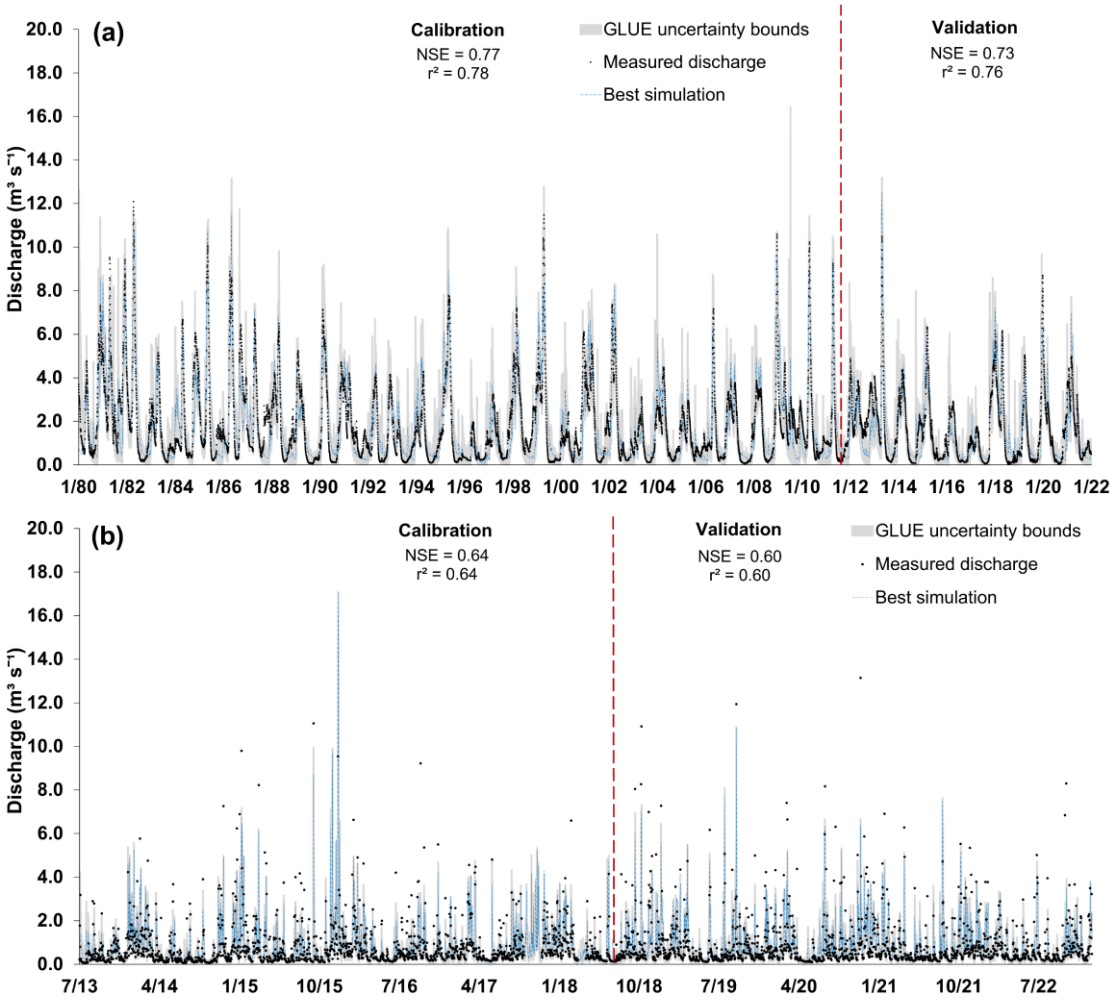


Figure 4.5 Observed and simulated daily river discharge for Vattholma (a) and Glenamong (b) catchments during model calibration and validation. NSE and r² values are indicated for the calibrated parameter set (best optimised simulation). The grey area denotes the 5% - 95% range GLUE uncertainty bounds for river discharge based on the 100 best-performing parameter sets

In terms of DOC transport, the optimised values for the Glenamong reflected a larger contribution of surface runoff at that site, with higher values for the runoff carbon loss coefficient and surface flow cap than for Vattholma. Subsurface carbon transport through fast groundwater flow was favoured over slow groundwater flow at both sites, with both optimisations also indicating relatively low groundwater carbon loss coefficients.

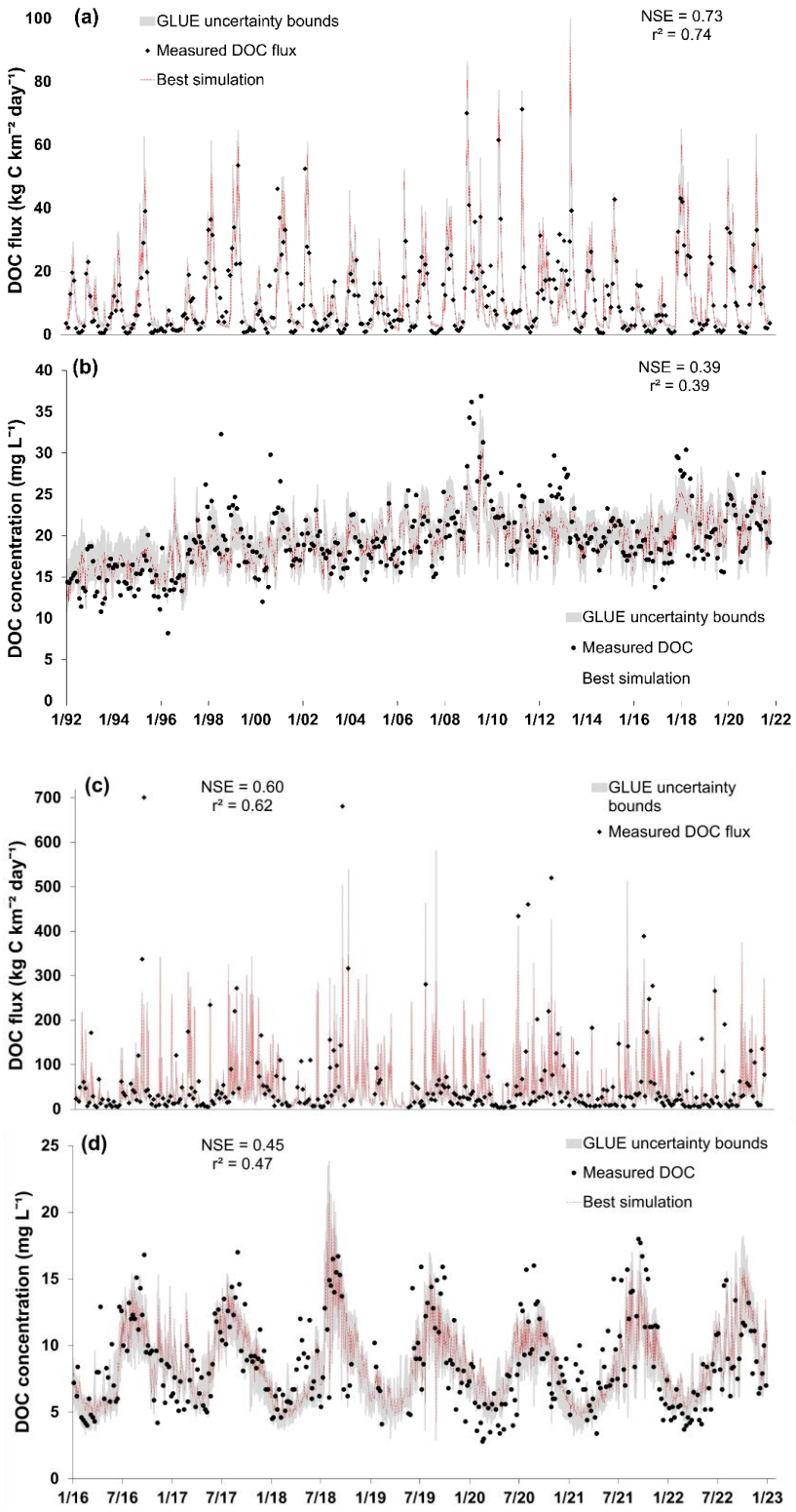


Figure 4.6 Observed and simulated daily DOC flux and DOC concentrations for Vattholma (a and c) and Glenamong (b and d) catchments during model calibration. NSE and r² values are indicated for the calibrated parameter set (best optimised simulation). The grey area denotes the 5% - 95% range GLUE uncertainty bounds for DOC flux and DOC concentrations based on the 100 best-performing parameter sets.

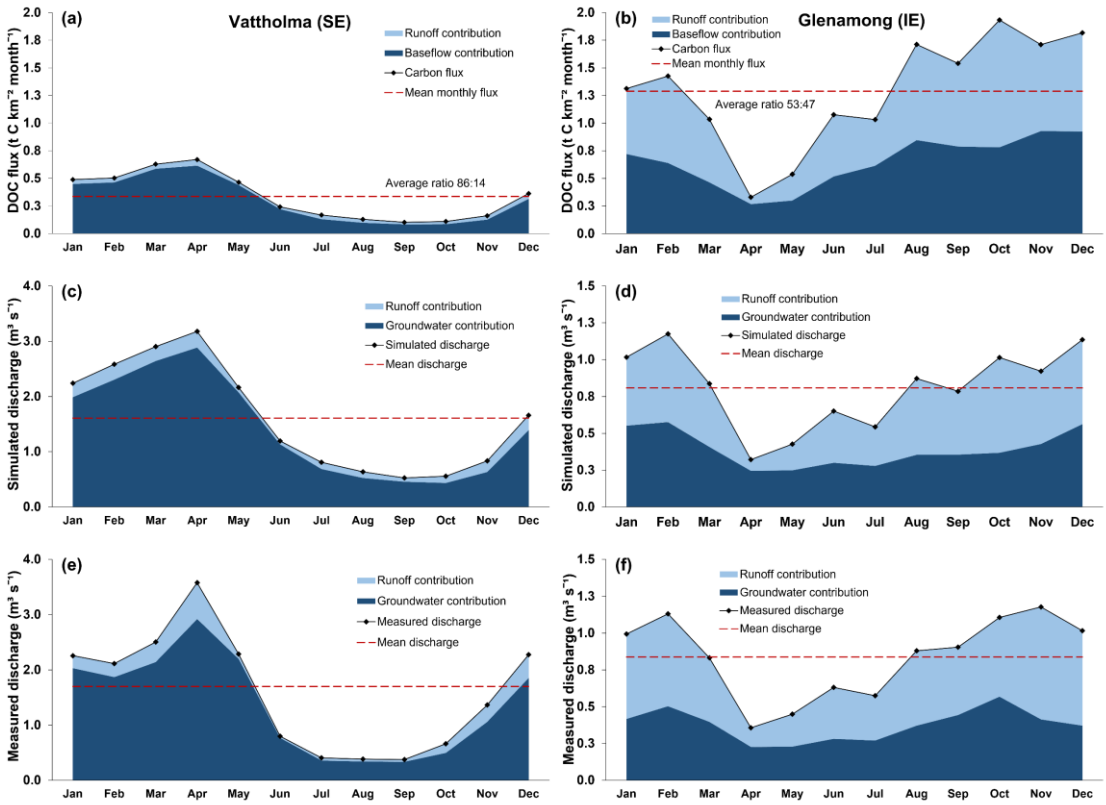


Figure 4.7 Simulated calendar month average DOC flux, simulated calendar month average discharge, and measured average calendar month discharge for Vattholma (a, c and e) and Glenamong (b, d and f), respectively. A red dashed line indicates the mean calendar month value for each panel. The stacked areas in panels a – b display baseflow and runoff carbon export contributions to total river discharge carbon export. The average contribution ratio between baseflow and runoff to total DOC export for each catchment is indicated as a percentage ratio (baseflow:runoff). The stacked areas in panels c – f display baseflow and runoff contributions to total discharge contributions. Measured runoff and baseflow obtained as per the Arnold et al. (1995) hydrograph separation method; see Schneiderman et al. 2010.

The GLUE uncertainty bounds captured a similar level of variation in measured discharge and DOC concentration to that captured by the optimisation process, but allowed for a range of parameter values rather than a single optimised set (Table 4.8). For discharge, 73% and 60% of the measured monthly observations and 65% and 50% of the daily observations were captured by the uncertainty bounds for Vattholma (Fig. 4.4a; Fig. 4.5a) and Glenamong (Fig. 4.5b; Fig. 4.5b) respectively, while the values for DOC concentration were 45% and 38% (Fig. 4.6b and d).

Table 4.8 Set of calibrated GWLF-DOC model parameters for Vattholma and Glenamong.

Hydrological parameters				
	Precipitation correction factor	**River channel flow coeff.**	**Melt coeff.**	**Curve adj. number**
Units	*factor / day*	*coeff. / day*	*cm / °C / day*	-
Calibration range	*0.50 - 1.50*	*0.01 - 1.00*	*0.05 - 0.60*	*-10.0 to 10.0*
Vattholma				
Calibrated value	1.09	0.05	0.20	2.7
Behavioural range	*0.85 - 1.23*	*0.01 - 1.00*	*0.06 - 0.59*	*-10.0 to 10.0*
Glenamong				
Calibrated value	1.08	0.91	0.05	5.5
Behavioural range	*0.89 - 1.30*	*0.66 - 1.00*	*0.05 - 0.60*	*-2.6 to 10.0*

	Soil water capacity	**Baseflow capacity**	**Slow recess coeff.**	**Recess coeff.**
Units	*cm*	*cm*	*coeff. / day*	*coeff. / day*
Calibration range	*12.00 - 20.00*	*2.50 - 8.00*	*0.001 - 0.100*	*0.005 - 0.030*
Vattholma				
Calibrated value	19.46	2.93	0.006	0.024
Behavioural range	*12.00 - 20.00*	*2.50 - 8.00*	*0.001 - 0.060*	*0.010 - 0.060*
Glenamong				
Calibrated value	13.27	5.11	0.010	0.159
Behavioural range	*12.00 - 20.00*	*2.50 - 8.00*	*0.001 - 0.100*	*0.006 - 0.030*

DOC parameters				
DOC production				
	Activation energy (E_a)	**Aerobic decomp. rate** (b)	**Anaerobic decomp. rate** (a)	**Anaerobic decomp. rate (wetlands)** (a_w)
Units	*kJ / gC*	-	*gC / m² / day*	*gC / m² / day*
Calibration range	*3.0 - 7.0*	*1.0 - 7.5*	*0.005 - 0.15*	*0.005 - 0.15*
Vattholma				
Calibrated value	6.4	7.4	0.007	0.008
Behavioural range	*3.4 - 6.9*	*5.7 - 7.5*	*0.007 - 0.01*	*0.005 - 0.01*
Glenamong				
Calibrated value	3.0	1.0	0.096	0.014
Behavioural range	*3.0 - 4.7*	*1.0 - 7.5*	*0.04 - 0.10*	*0.005 - 0.04*

DOC washout - runoff

	Surface carbon loss coeff.	**Surface flow cap**
Units	*coeff. / day*	*cm*
Calibration range	*0.01 - 1.00*	*0.01 - 6.00*
Vattholma		
Calibrated value	0.06	1.98
Behavioural range	*0.03 - 0.11*	*1.86 - 6.00*
Glenamong		
Calibrated value	0.17	2.47
Behavioural range	*0.08 - 0.45*	*0.71 - 6.00*

DOC washout - baseflow

	Baseflow ratio	**Fast groundwater carbon loss coeff.**	**Slow groundwater carbon loss coeff.**
Units	*fast- to slow- groundwater ratio / day*	*coeff. / day*	*coeff. / day*
Calibration range	*0.01 - 1.00*	*0.001 - 1.000*	*0.001 - 1.000*
Vattholma			
Calibrated value	0.99	0.008	0.012
Behavioural range	*0.98 - 1.00*	*0.008 - 0.016*	*0.008 - 0.239*
Glenamong			
Calibrated value	0.87	0.168	0.002
Behavioural range	*0.46 - 1.00*	*0.097 - 0.651*	*0.001 - 0.004*

Furthermore, sensitivity plots showed that the DOC model was typically more sensitive to parameter variation than the hydrology model (Fig. 4.8 – 4.11). Discharge was sensitive to the value of the precipitation correction factor for both sites, and insensitive to the value used for baseflow capacity and soil water capacity (i.e., acceptable model

performance occurred over the entire parameter range). Parameters related to flow attenuation (recess coefficient, slow recess coefficient and melt coefficient*)* were sensitive only at Vattholma. In contrast, parameters more related to catchment surface water retention (runoff curve number adjustment and river channel flow coefficient*)* were more sensitive for Glenamong. Parameters related to DOC production were sensitive for both catchments except for activation energy at Vattholma, where a wide range of values produced an equally good fit. Similarly, parameters related to DOC transport were sensitive at both sites, although the surface flow cap displayed less sensitivity (i.e., acceptable performance over a large extent of its parameter range)

Moreover, the 100 best behavioural sets of hydrological model parameters showed weak parameter correlation at both Vattholma and Glenamong (Fig. 4.12 – Fig. 4.13). Nevertheless, the precipitation factor did show some degree of correlation with the soil water capacity at Vattholma and the channel flow coefficient at Glenamong (Pearson correlation coefficient values of 0.48 and 0.45, respectively). In terms of DOC, the 100 best behavioural sets of DOC model parameters showed more correlation than the hydrological parameters (Fig. 4.14 – Fig. 4.15). For instance, the two parameters that drive temperature-dependent decomposition of soil organic matter (activation energy and anaerobic decomposition rate) showed a negative correlation at Vattholma (-0.63) (see Fig. 4.14). The aerobic decomposition rate at that site also showed some correlation with the anaerobic decomposition rate (-0.57). In contrast, the anaerobic decomposition rate at Glenamong correlated with other parameters (see Fig. 4.15): the anaerobic decomposition wetlands (-0.82), baseflow ratio (-0.81) and the fast-groundwater carbon loss coefficient (-0.74). The baseflow ratio showed a strong correlation with related subsurface DOC transport coefficients at both Vattholma (-0.89 and 0.73 with slow- and fast-groundwater carbon loss coefficients, respectively) and Glenamong although less strong (-0.52 and 0.55 with slow- and fast-groundwater carbon loss coefficients, respectively).

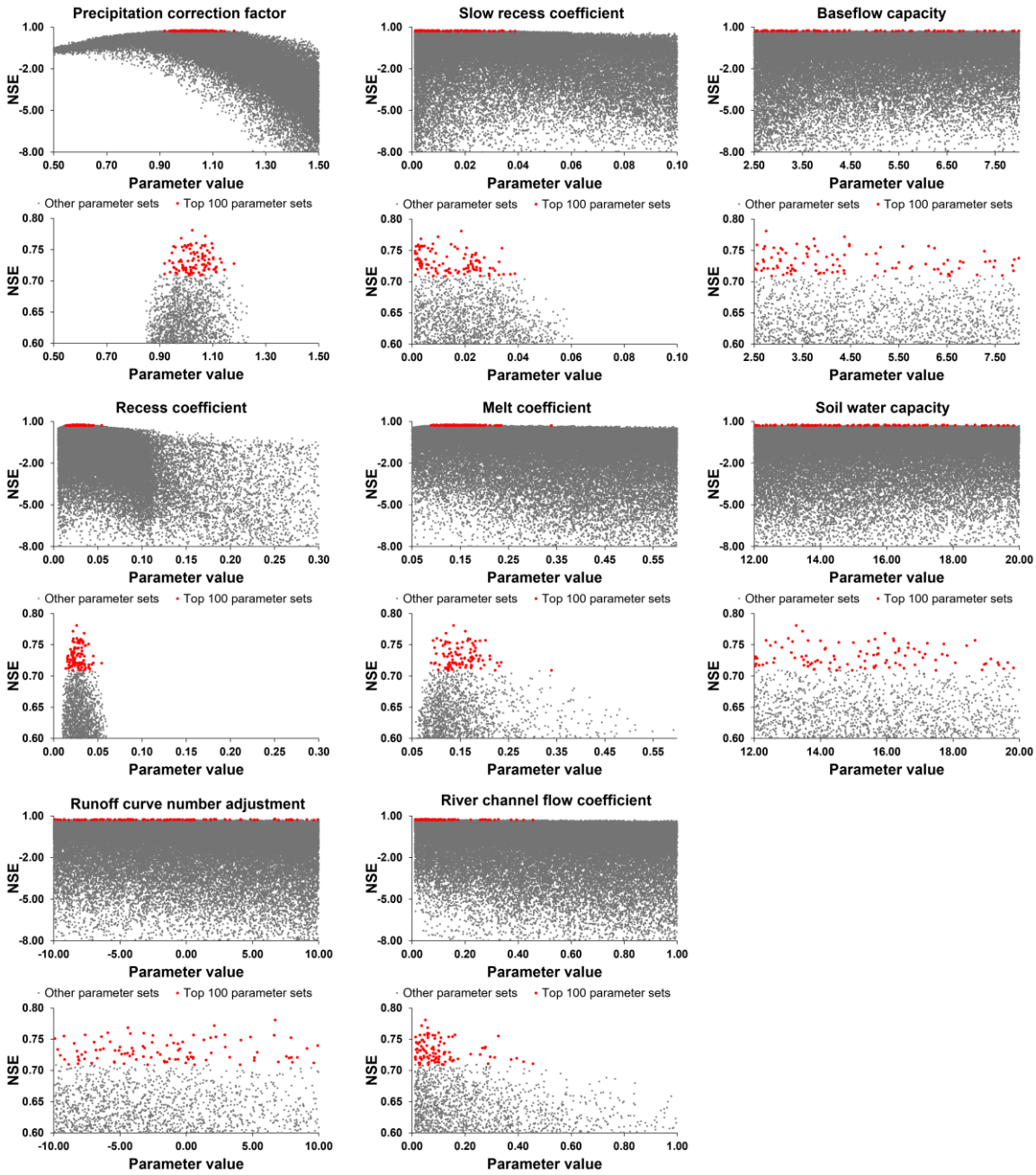


Figure 4.8 Scatter diagrams (sensitivity plots according to the GLUE methodology) applied to hydrological model parameters against NSE model performance (likelihood measure) at Vattholma. The threshold for behavioural parameter sets was 0.60 NSE (simulated vs measured river discharge) and is used for the horizontal axis value in the lower panels of each model parameter. Each dot represents one run of the model from a Monte Carlo experiment with randomly chosen model parameter values. The 100 best behavioural parameter sets are highlighted in red.

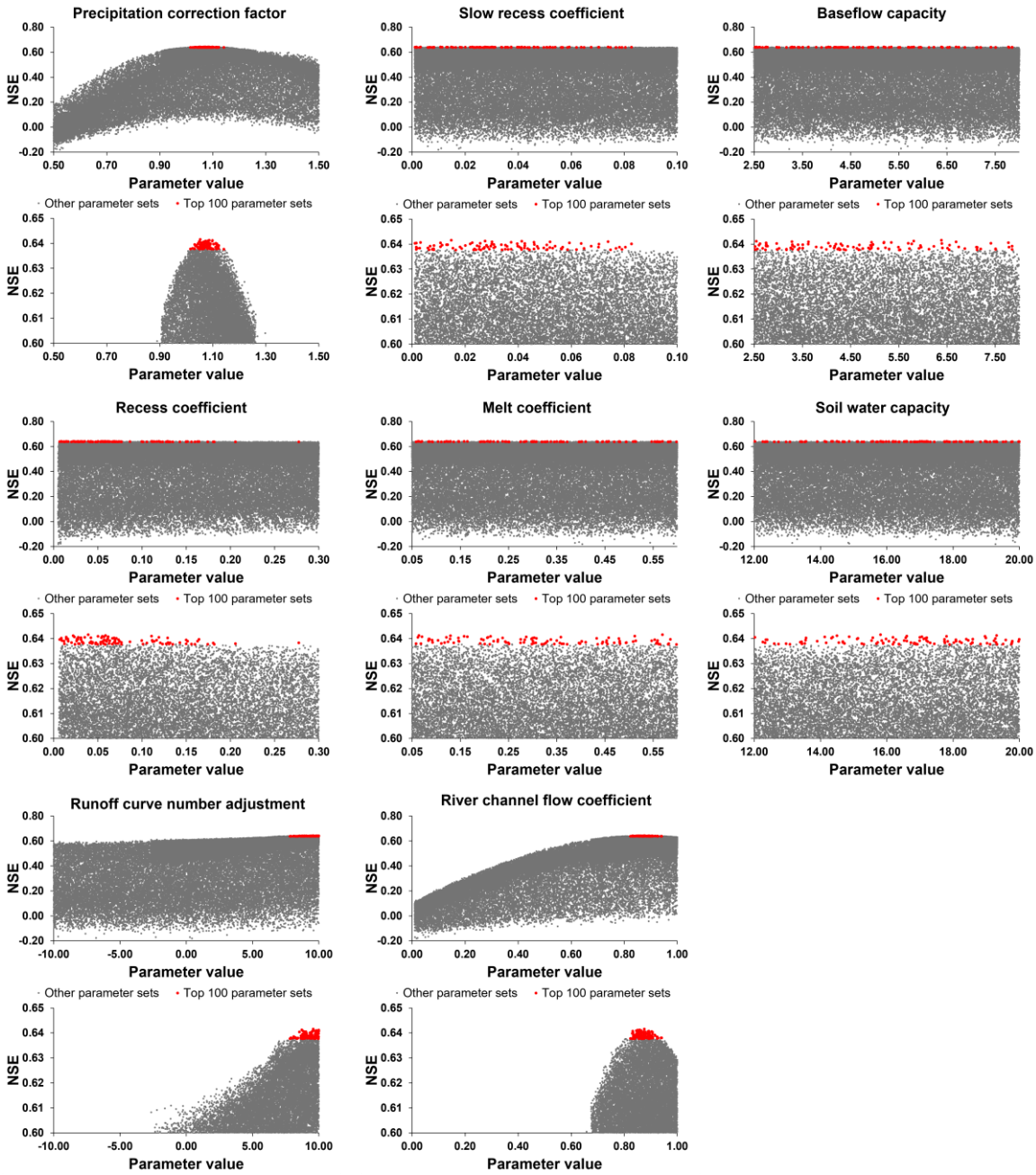


Figure 4.9 Scatter diagrams (sensitivity plots according to the GLUE methodology) applied to hydrological model parameters against NSE model performance (likelihood measure) at Glenamong. The threshold for behavioural parameter sets was 0.60 NSE (simulated vs measured river discharge) and is used for the horizontal axis value in the lower panels of each model parameter. Each dot represents one run of the model from a Monte Carlo experiment with randomly chosen model parameter values. The 100 best behavioural parameter sets are highlighted in red.

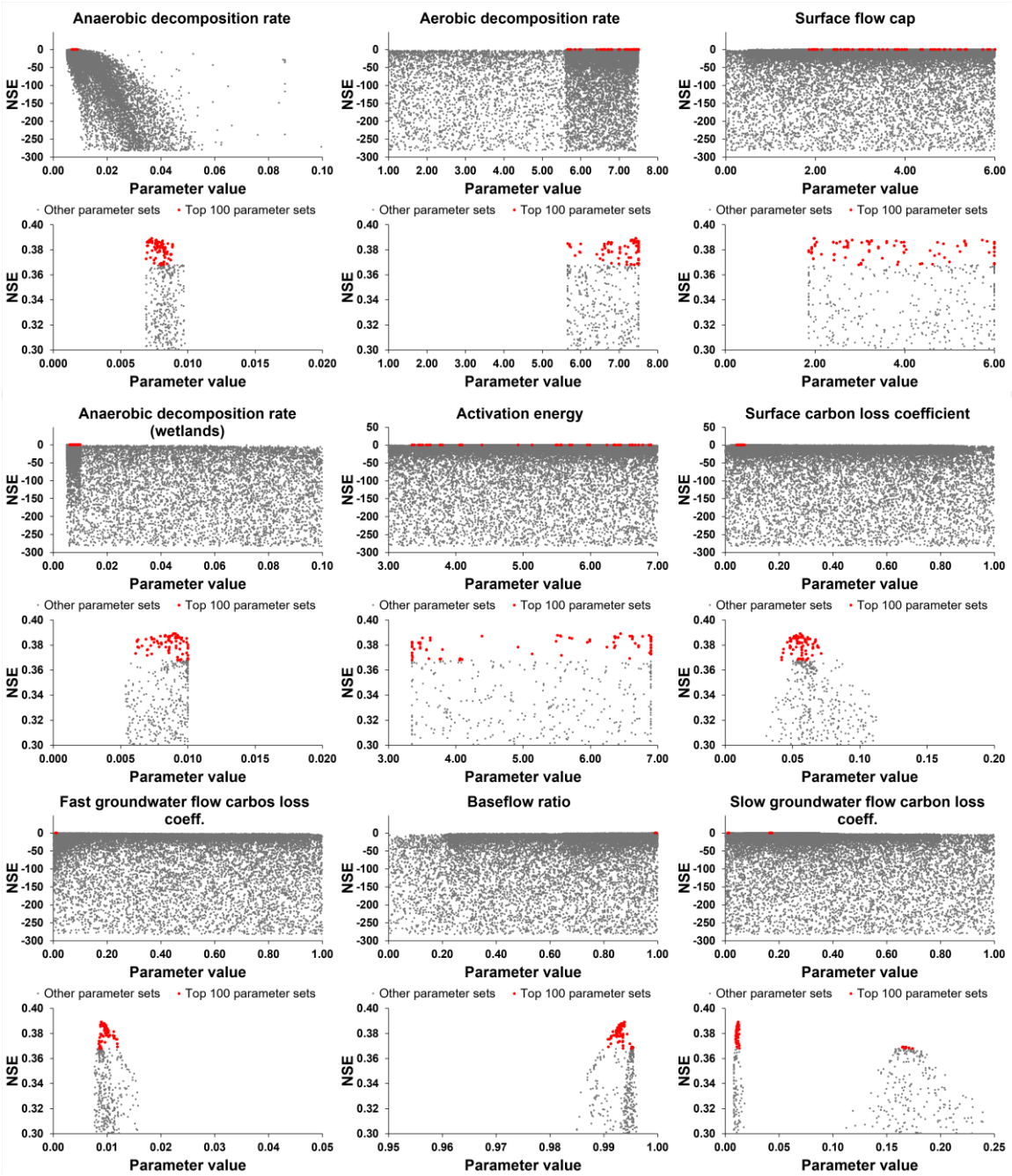


Figure 4.10 Scatter diagrams (sensitivity plots according to the GLUE methodology) applied to DOC model parameters against NSE model performance (likelihood measure) at Vattholma. The threshold for behavioural parameter sets was 0.30 NSE (simulated vs measured DOC concentrations) and is used for the horizontal axis value in the lower panels of each model parameter. Each dot represents one run of the model from a Monte Carlo experiment with randomly chosen model parameter values. The 100 best behavioural parameter sets are highlighted in red.

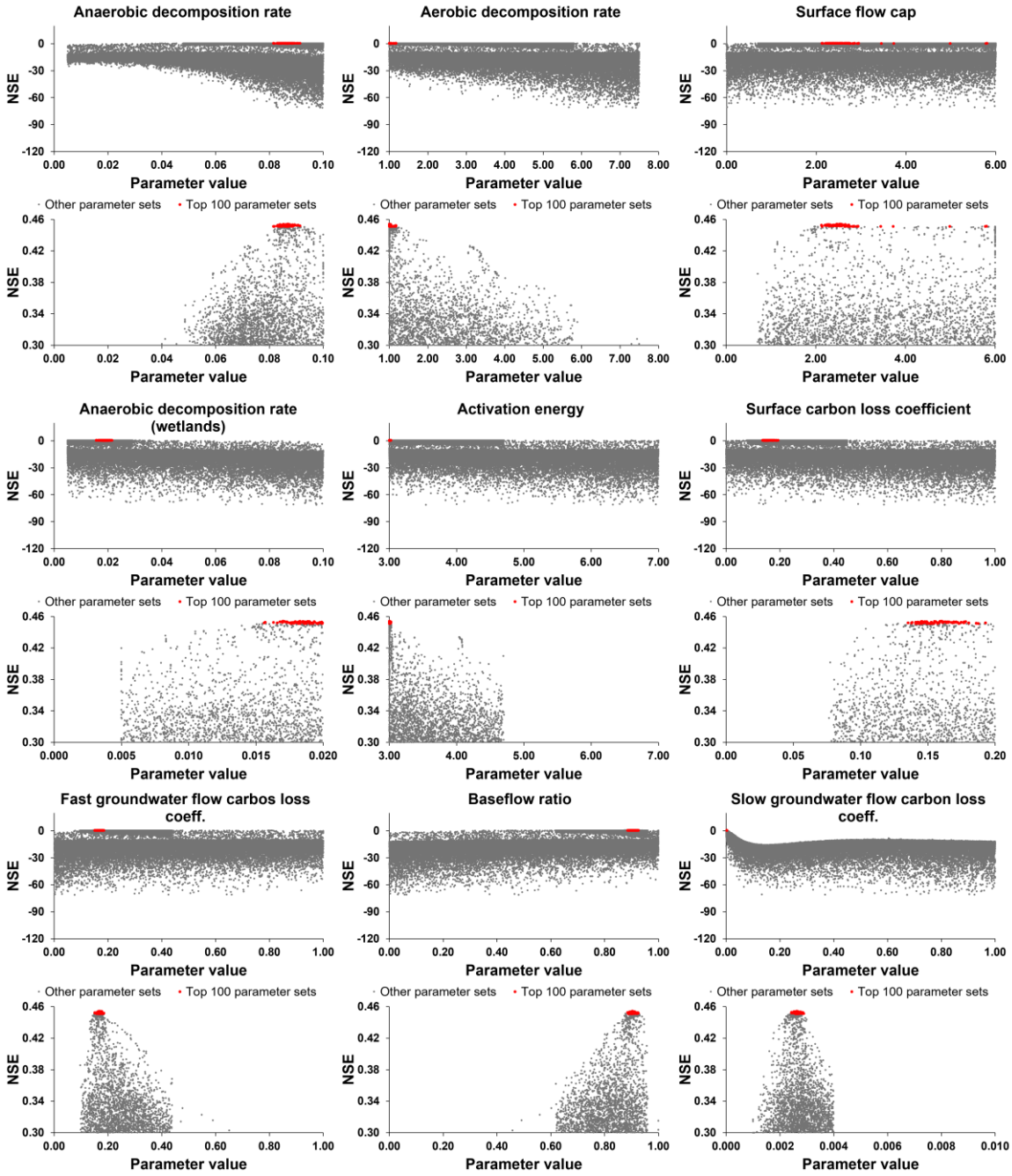


Figure 4.11 Scatter diagrams (sensitivity plots according to the GLUE methodology) applied to DOC model parameters against NSE model performance (likelihood measure) at Glenamong. The threshold for behavioural parameter sets was 0.30 NSE (simulated vs measured DOC concentrations) and is used for the horizontal axis value in the lower panels of each model parameter. Each dot represents one run of the model from a Monte Carlo experiment with randomly chosen model parameter values. The 100 best behavioural parameter sets are highlighted in red.

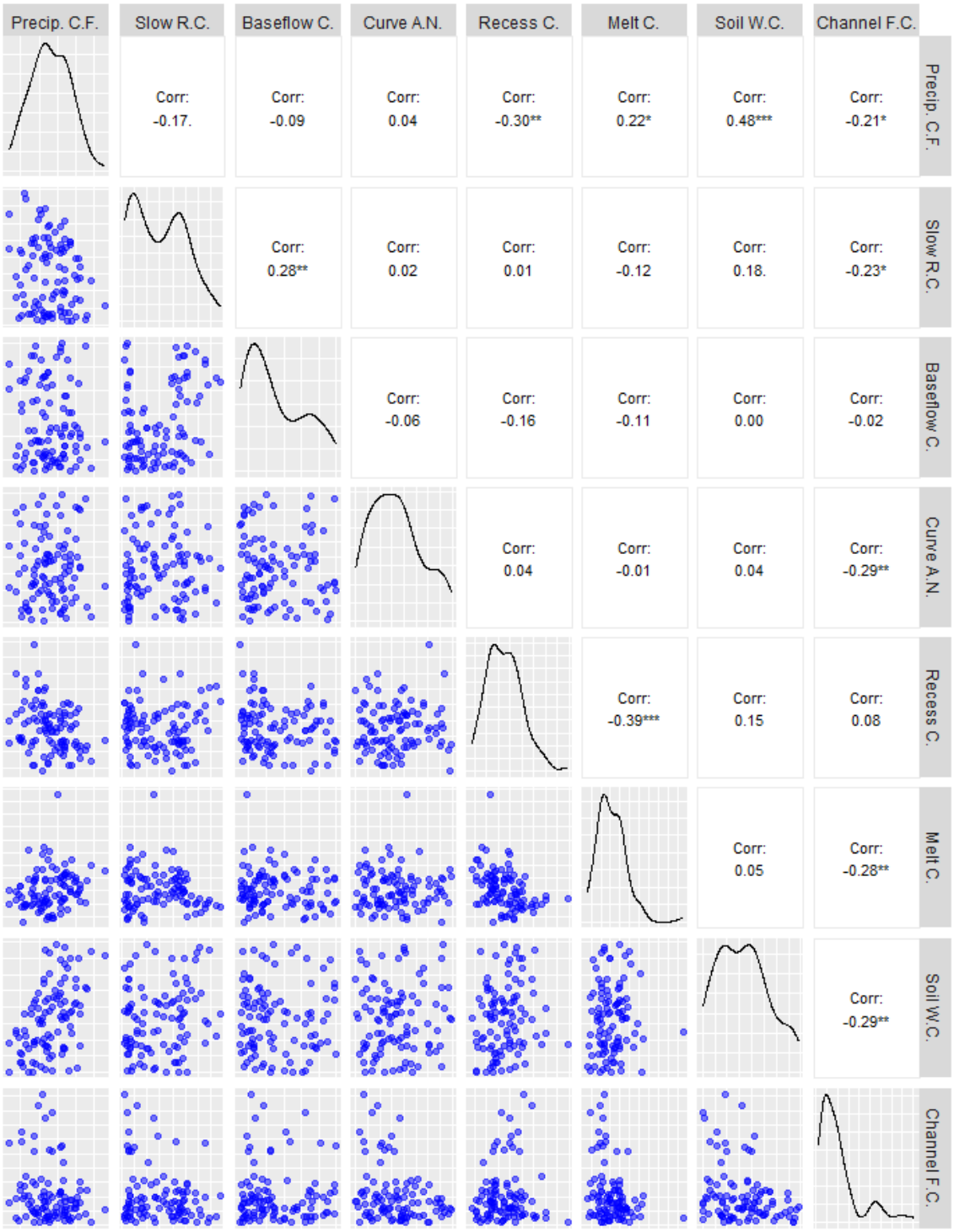


Figure 4.12 Correlation matrix for the 100 best behavioural hydrological parameter sets for the Vattholma catchment. The correlation coefficient for each relationship corresponds to the Pearson correlation coefficient. Note that the names of the model parameters were abbreviated.

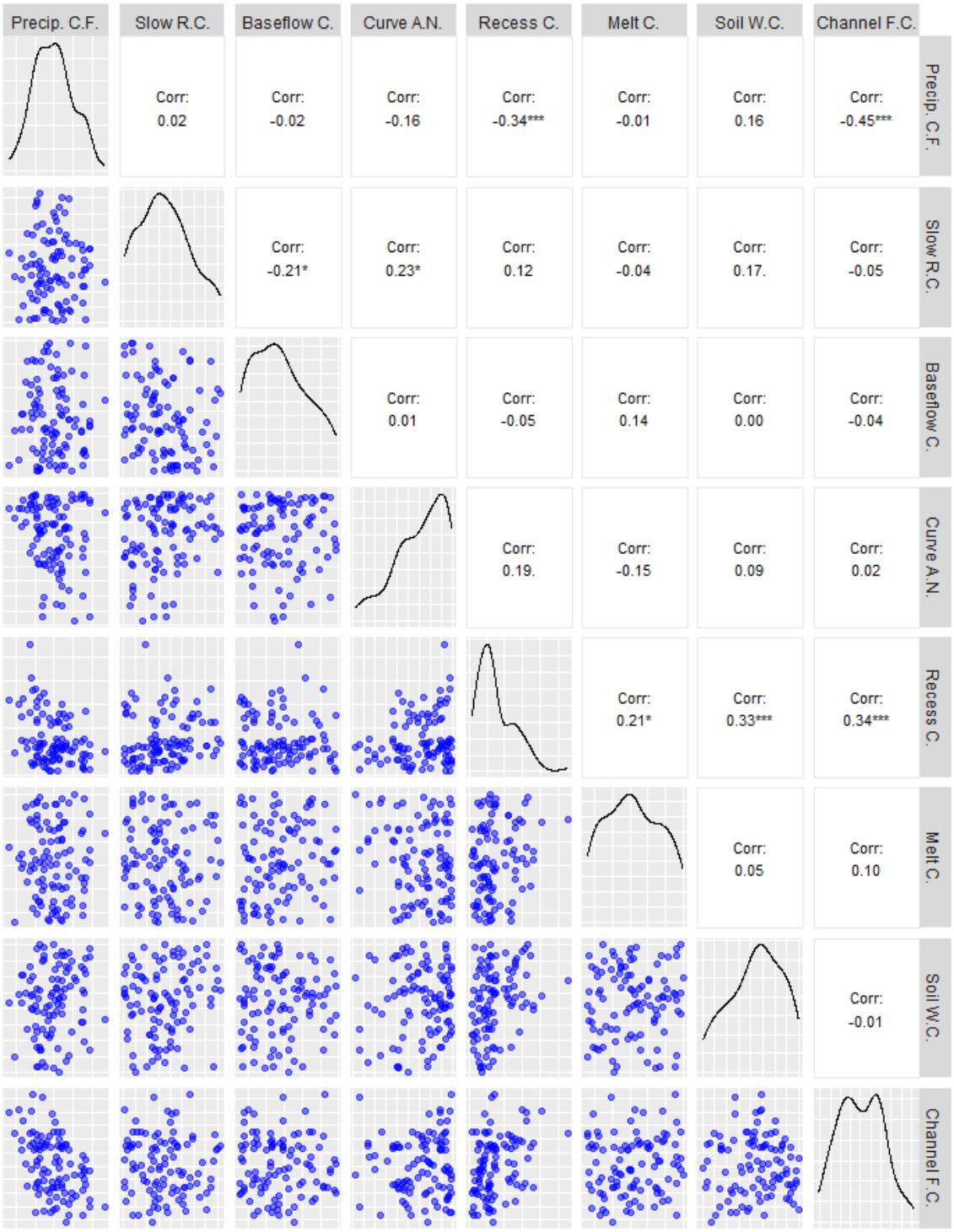


Figure 4.13 Correlation matrix for the 100 best behavioural hydrological parameter sets for the Glenamong catchment. The correlation coefficient for each relationship corresponds to the Pearson correlation coefficient. Note that the names of the model parameters were abbreviated.

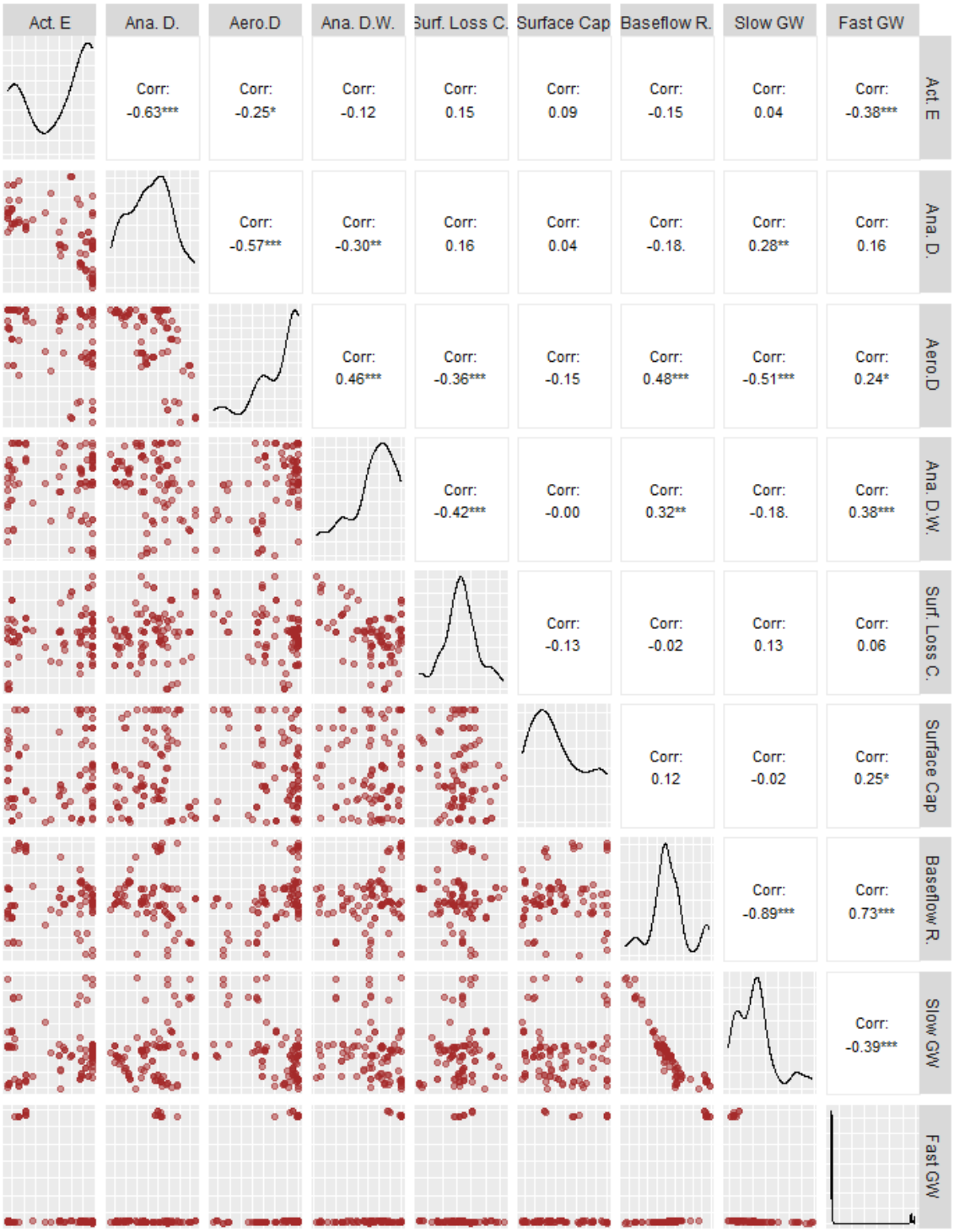


Figure 4.14 Correlation matrix for the 100 best behavioural DOC model parameter sets for the Vattholma catchment. The correlation coefficient for each relationship corresponds to the Pearson correlation coefficient. Note that the names of the model parameters were abbreviated.

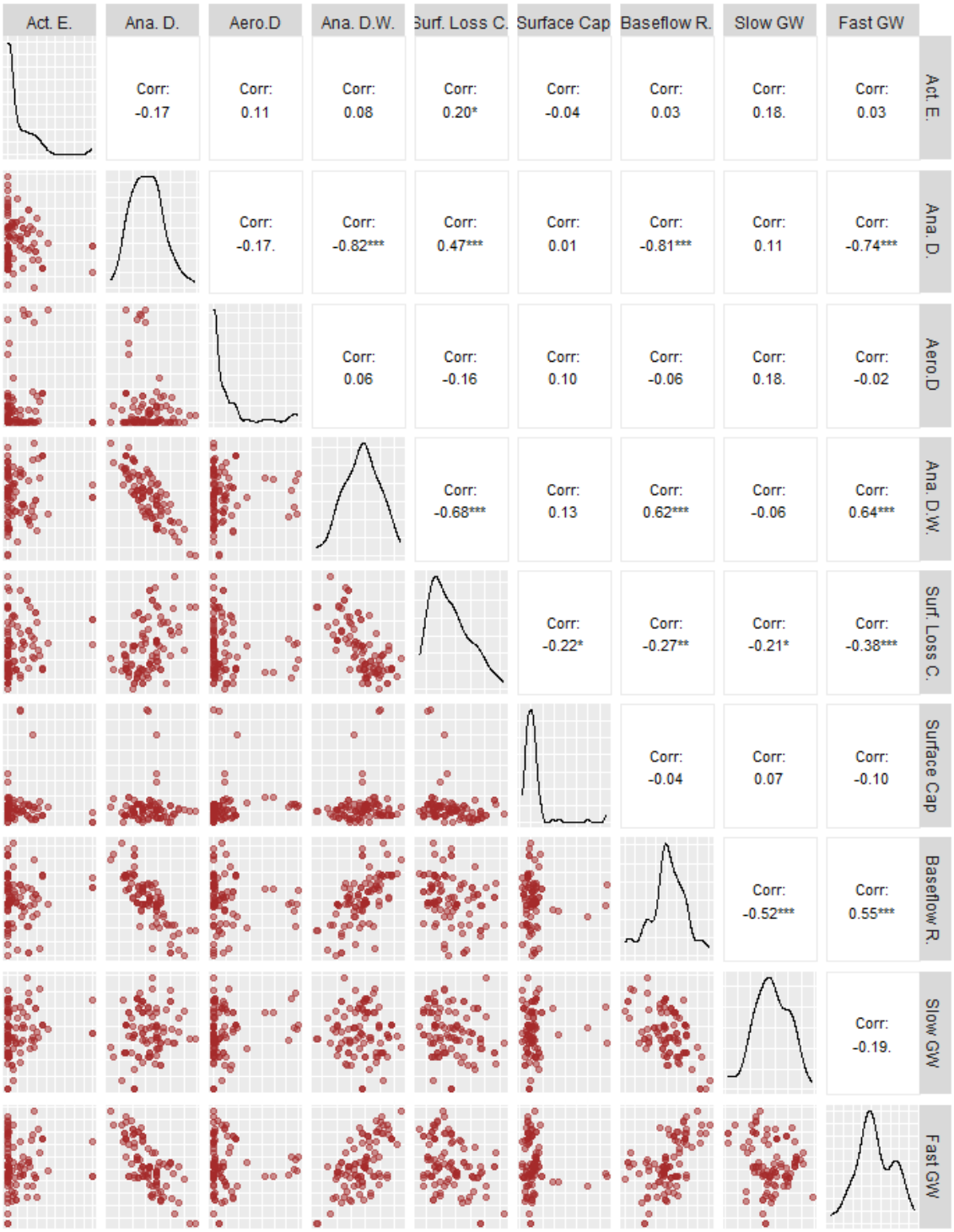


Figure 4.15 Correlation matrix for the 100 best behavioural DOC model parameter sets for the Glenamong catchment. The correlation coefficient for each relationship corresponds to the Pearson correlation coefficient. Note that the names of the model parameters were abbreviated.

4.4.2 Future climate impacts

The GCM ensemble for all three future SSP scenarios projected changes in climatic conditions for each site relative to their baseline periods (Table 4.9; Fig. 4.16a – 4.16d) (Tables A1 – A12 in Appendix A show conditions projected by each GCM ensemble member). Large air temperature increases were projected for Vattholma, ranging from +1.5 °C (+24%; SSP126) to +6.0 °C (+95%; SSP585) across the scenarios. However, SSP126, the scenario that incorporates some mitigation effects, was the only scenario for which temperature first increased in P1 (2050 – 2059) (+2.1 °C; +33%) and then decreased in P2 (2090 – 2099) (+1.5 °C; +24%). For the Glenamong, there was only a slight increase in air temperature for projections based on SSP126 in both P1 (+0.4 °C; +4%) and P2 (+0.2 °C; +2%). In contrast, the ensemble mean for SSP370 and SSP585 indicated much warmer conditions during both P1 (up to +12%) and P2 (up to +33%). Under SSP585, it was of note that, although similar annual air temperatures were projected for both sites in the final decade of the century (Vattholma: 12.3 °C; Glenamong: 12.2 °C), this represented a more extreme increase at the Swedish site (+6.0 °C; +95%) than at the Irish site (+3.0 °C; +33%). Increases in air temperature were projected for all months at both sites, exceeding baseline levels continuously throughout the year (Fig. 4.16c – 4.16d).

Annual precipitation was also projected to increase in Vattholma under all scenarios during both P1 and P2 (Table 2). However, the increases were, in relative terms, less extreme than those for temperature. They ranged by up to +10% in P1 and +15% in P2. The largest increase in that latter period was actually projected for SSP370 (+108 mm yr^{-1}). Smaller relative increases in annual precipitation were projected for Glenamong, up to +2% in P1 and +8% in P2. In fact, for Glenamong, where annual precipitation was already over twice that at Vattholma for the baseline period (1710 mm yr^{-1} versus 712 mm yr^{-1}, respectively), all projections were similar to the baseline with the exception for SSP585 in P2 (+136 mm yr^{-1}).

Table 4.9 ISIMIP3b GCM ensemble-mean future annual precipitation and mean air temperature values for the historical period (baseline) and for the SSP126, SSP370 and SSP585 scenarios during P1 (2050 – 2060) and P2 (2090 – 2100), for each study catchment. The standard deviation is indicated in parentheses.

	Vattholma (SE)		***Glenamong (IE)***	
Period	Mean air temperature (°C)	Precipitation (mm yr^{-1})	Mean air temperature (°C)	Precipitation (mm yr^{-1})
Baseline (1985- 2014)	6.3 (±1.1)	712 (±100)	9.2 (±0.5)	1710 (±171)
SSP 126				
P1 (2050 - 2059)	8.4 (±1.0)	730 (±116)	9.6 (±0.7)	1728 (±162)
P2 (2090 - 2099)	7.8 (±1.6)	764 (±142)	9.4 (±1.2)	1715 (±182)
SSP 370				
P1 (2050 - 2059)	9.1 (±1.3)	782 (±116)	10.2 (±0.7)	1749 (±204)
P2 (2090 - 2099)	11.3 (±2.2)	820 (±136)	11.4 (±1.6)	1763 (±184)
SSP 585				
P1 (2050 - 2059)	9.3 (±1.4)	764 (±109)	10.3 (±0.9)	1737 (±227)
P2 (2090 - 2099)	12.3 (±2.5)	812 (±145)	12.2 (±1.9)	1846 (±224)

There was, however, a pronounced seasonal shift in precipitation at the Irish site, with generally drier conditions than the baseline period between April and September, and wetter conditions between October and March (Fig. 4.16a – 4.16b). At Vattholma, future precipitation was clearly elevated in the autumn and winter from October to March, but the direction of change projected by the different CGMs varied in other months. The variability in future climate, indicated by the standard deviation, increased by the end of the century at both sites and was highest under SSP585 (Table 4.9).

The future changes in evapotranspiration reflected the changes in both air temperature and precipitation (Fig. 4.16e – 4.16f). In general, higher monthly actual evapotranspiration was projected from October to May at both sites, followed by decreases from June to September, although the changes were greater at Vattholma. The relative changes across the scenarios were more extreme by the end of the century, ranging from -9 to +22 mm $month^{-1}$ at Vattholma (baseline average of 34 mm $month^{-1}$), and from -7 to +5 mm $month^{-1}$ at Glenamong (baseline average of 31 mm $month^{-1}$).

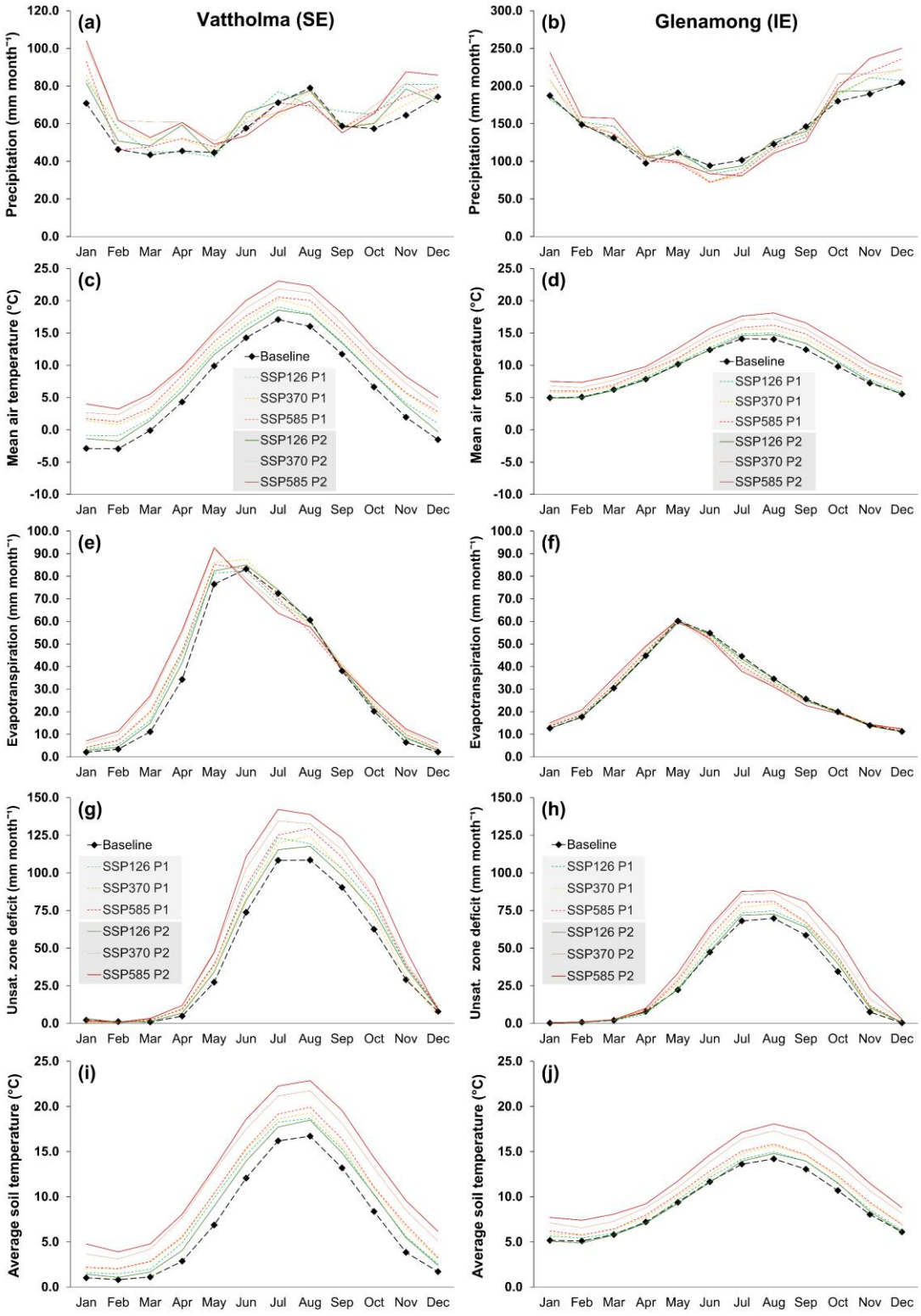


Figure 4.16 ISIMIP3b GCM-ensemble average monthly precipitation (a and b), ISIMIP3b GCM-ensemble mean air temperature (c and d), average modelled monthly actual evapotranspiration (e and f), average modelled unsaturated zone deficit (g and h) and average modelled soil temperature (i and j) for the baseline period and for the SSP126, SS370 and SSP585 scenarios during P1 and P2. Note the different scaling in panels a and b. Vattholma: a, c, e, g, i; Glenamong: b, d, f, h, j.

4.4.3 Future change in discharge

While there were some changes projected for mean monthly discharge at both Vattholma and Glenamong, the overall distribution of annual means was similar to the baseline for any scenario at either site, although discharge variability at the end of the century was greater for SSP370 at Vattholma and was highest for SSP585 at Glenamong (Fig. 4.17).

There were, however, pronounced changes in seasonal discharge patterns, especially for Vattholma during the first six calendar months (Fig. 4.17a). Most noticeable was that, except for SSP126 in P1, the peak month for discharge shifted to earlier in the year, with increased discharge from January to March particularly in P2 (+63%; SSP585). These increases were followed by decreases in discharge from April to June under all three scenarios, with the lowest levels in P2 as well (up to -38%; SSP585). There was a slight upward shift in daily discharge magnitudes for SSP126 during the last decade of the century, while values for SSP370 and SSP585 were similar to those during P1 but with more variability (Fig. 4.17b). In the Glenamong, the projections indicated that discharge would be relatively unchanged under SSP126 (Fig. 4.17d). In contrast to the Swedish site, it was projected to decrease from April to September followed by increased levels from October to March under SSP370 and SSP585. The decreases were greatest for July in P1 (up to -25%; SSP370) and the largest increases in discharge were for January in P2 (up to +30%; SSP585). There was little change in the magnitude of discharge at the daily timescale for the Glenamong in both P1 and P2 under all three scenarios, although SSP585 had a greater range of values (Fig. 4.17e).

Ensemble mean annual discharge anomalies for Vattholma sometimes contrasted between future scenarios, but were all similar in magnitude: up to ±1.1 $m^3 s^{-1}$ under SSP126, up to ±1.3 $m^3 s^{-1}$ under SSP370, and up to ±1.1 $m^3 s^{-1}$ under SSP585 relative to a baseline average of 2.4 $m^3 s^{-1}$ (Fig. 4.17c). For Glenamong, discharge anomalies were lower in magnitude than for the Swedish site but greatest for SSP585 (up to

±0.2 $m^3 s^{-1}$) than for SSP126 and SSP370 (up to ±0.1 $m^3 s^{-1}$) relative to a baseline average of 0.6 $m^3 s^{-1}$ (Fig. 4.17f). At each of the study sites, all three future projections displayed a similar uncertainty range throughout the simulation, which slightly increased towards the end of the century (Fig. 4.17c and 4.17f).

4.4.4 Future change in DOC concentrations and flux

The variables that drive carbon decomposition in the model also showed large changes in the future, with increases projected in soil temperatures (reflecting higher air temperature), and a drier soil matrix in summer (reflecting both increases in evapotranspiration and lower precipitation in summer) (Fig. 4.16g – 4.16j). Conditions that would be expected to increase decomposition and ultimately stream DOC concentration. Soil temperatures were projected to increase least in January and the most in August, particularly during P2, ranging from +0.3 °C (SSP126) to +6.5 °C (SSP585) at Vattholma (baseline average of 7.0 °C), and from +0.1 °C (SSP126) to +4.2 °C (SSP585) at Glenamong (baseline average of 9.2 °C). Soil water deficits were projected to increase throughout the calendar year except from January to March, a time during which the unsaturated zone was full at both sites. The increases in monthly deficits were greatest for July particularly at the end of the simulation period, up to +37 mm $month^{-1}$ (SSP585) at Vattholma (baseline average of 43 mm $month^{-1}$) and up to +23 mm $month^{-1}$ (SSP585) at Glenamong (baseline average of 27 mm $month^{-1}$).

The simulations indicated that DOC concentrations would increase for Vattholma throughout the calendar year under all three SSPs (Fig. 4.18a). In P1, these increases ranged from +4 mg L^{-1} (SSP370) to +6 mg L^{-1} (SSP585) (baseline average of 13.7 mg L^{-1}). In P2, even larger increases were projected, particularly for SSP370 and SSP585, exceeding baseline levels by up to +9 mg L^{-1}. However, it is of note that the increases projected for SSP126 were lower in P2 (up to +3 mg L^{-1}) than those for all scenarios in P1.

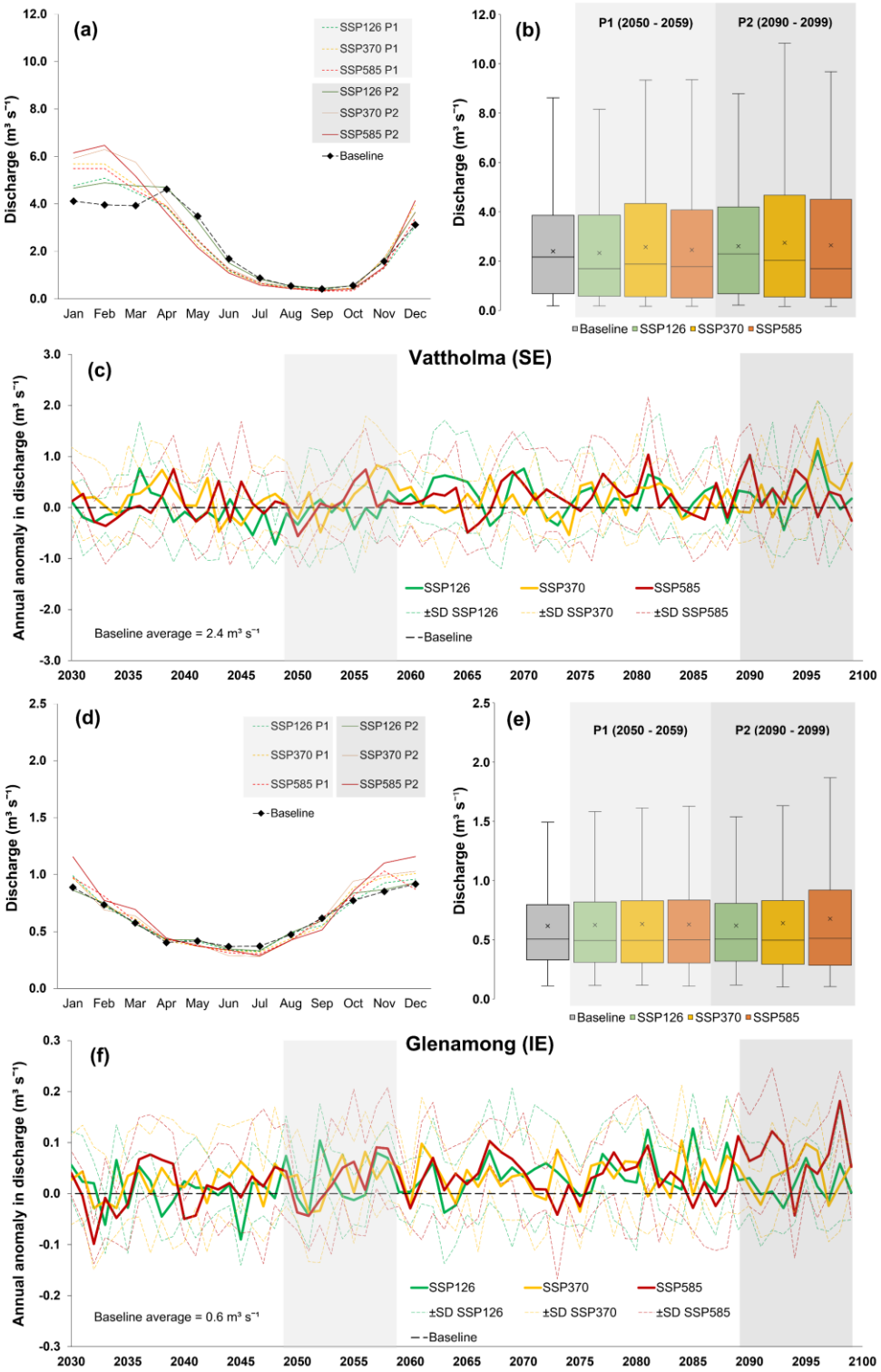


Figure 4.17 Average calendar month discharge (a and d); boxplot distributions of average daily discharge for the baseline period, and for the SSP126, SS370 and SSP585 scenarios during P1 and P2 (b and e); annual anomalies for discharge under SSP126, SS370 and SSP585 scenarios from 2030 to 2100 (c and f). Uncertainty in the discharge anomaly panels is indicated by the standard deviation (±SD). Vattholma: a, b, c; Glenamong: d, e, f.

A clear general upward shift in the magnitude and minimum DOC concentration was indicated for all three scenarios (Fig. 4.18b). Again, the levels projected using SSP126 were closer to the baseline by the end of the century. DOC variability was also projected to increase, especially in P2 under SSP370 and SSP585. Ensemble mean annual DOC concentration anomalies for Vattholma were always positive, that is they were always higher than the historical baseline, in the order of ≃ +3, +4 and +5 mg L^{-1} for SSP126, SSP370 and SSP585, respectively (Fig. 4.18c). The anomalies continued to increase until the end of the century under both SSP370 and SSP585, while those for SSP126 decreased after 2060. The output for SSP126 also had the lowest uncertainty range, while that for SSP585 was the largest, particularly during P2, projecting futures with extremely high annual DOC concentrations of up to +13 mg L^{-1} above the baseline mean.

DOC concentrations were also projected to increase for Glenamong in all months under all three SSPs (Fig. 4.18d). The lowest increases were for SSP126, and were similar in P1 and in P2 (≃ +1 mg L^{-1}) (baseline average of 9.2 mg L^{-1}). The concentrations projected under SSP370 and SSP585 were larger, particularly from July to November in P2, exceeding baseline levels by ≃ +4 mg L^{-1}. A small upward shift in the magnitudes and variability of DOC concentrations relative to the baseline was projected in P1 under all three scenarios (Fig. 4.18e). In P2, the magnitude and variability increased more under SSP370 and SSP585 but, as with Vattholma, decreased under SSP126. Ensemble mean annual DOC concentration anomalies were also consistently positive for Glenamong in the order of ≃ +0.6, +1.0 and +1.3 mg L^{-1} for SSP126, SSP370 and SSP585, respectively (Fig. 4.18f). The anomalies increased over time under SSP370 and SSP585, while SSP126 anomalies decreased after 2070. Uncertainty increased with time under all three scenarios, with SSP126 displaying the narrowest range. SSP585 projections were the most uncertain, with anomalies of up to +5 mg L^{-1} over the last decade.

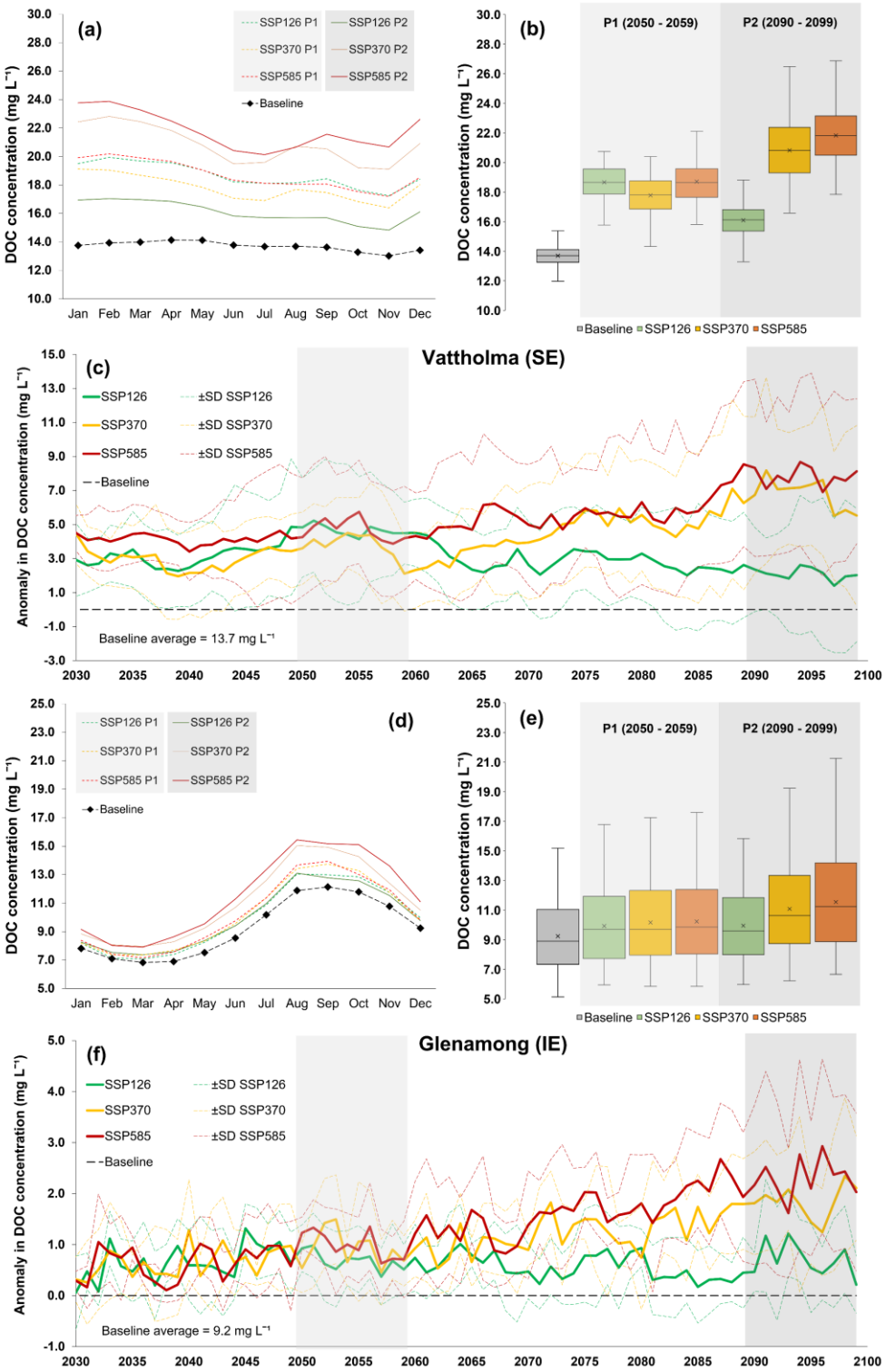


Figure 4.18 Average calendar month DOC concentration (a and d); boxplot distributions of average daily DOC concentrations for the baseline period, and for the SSP126, SS370 and SSP585 scenarios during P1 and P2 (b and e); annual anomalies for DOC concentration under SSP126, SS370 and SSP585 scenarios from 2030 to 2100 (c and f). Uncertainty in the DOC concentration anomaly panels is indicated by the standard deviation (±SD). Vattholma: a, b, c; Glenamong: d, e, f.

The probabilities of exceeding the 95th percentile baseline DOC concentration level (a metric of current extreme conditions) were much higher for Vattholma during each season than for Glenamong under all three future climate scenarios (Fig. 4.19). In line with other results, extreme DOC concentrations for Vattholma were lowest for SSP126 than for the other two scenarios, and therefore the probabilities of exceeding the historical 95th percentile threshold concentration of 15 mg L^{-1} were also lower across seasons (Fig. 4.19a). In particular, increases in the likelihood of occurrence for extreme concentrations were projected for all seasons under SSP370 and SSP585, while spring and winter were the most affected under SSP126. For Glenamong, in contrast, the probability of exceeding the baseline 95th percentile DOC concentration threshold of 13 mg L^{-1} were zero during the spring and winter under all three scenarios (Fig. 4.19b). However, there was an increased probability for exceeding this threshold in the summer and even higher probability of exceedance for the autumn under all three scenarios but higher under SSP370 and SSP585.

Furthermore, extreme DOC concentrations for Vattholma were projected to be accompanied by an increasing likeliness of extreme DOC flux in spring and winter under all three scenarios, while the summer and autumn were not affected (Fig. 4.20a). For Glenamong, the likelihood of occurrence for extreme DOC flux was virtually zero across seasons under all three SSPs (Fig. 4.20b).

4.4.5 Uncertainty partitioning

In all projections for both river discharge and DOC concentration, the total uncertainty (indicated by the standard deviation) typically increased with time and the relative contribution of the future climate driving data (i.e., for the five GCMs) to total uncertainty was generally much larger than the contribution of model parameterisation (i.e., for the 100 behavioural parameter sets) (Fig. 4.21 – Fig. 4.24). Variation between GCMs made the greatest contributions (up to 85%) to total uncertainty for all discharge simulations,

although the hydrological model parameters accounted for a greater percentage of variation in simulation for Vattholma than for Glenamong (Fig. 4.21 – Fig. 4.22).

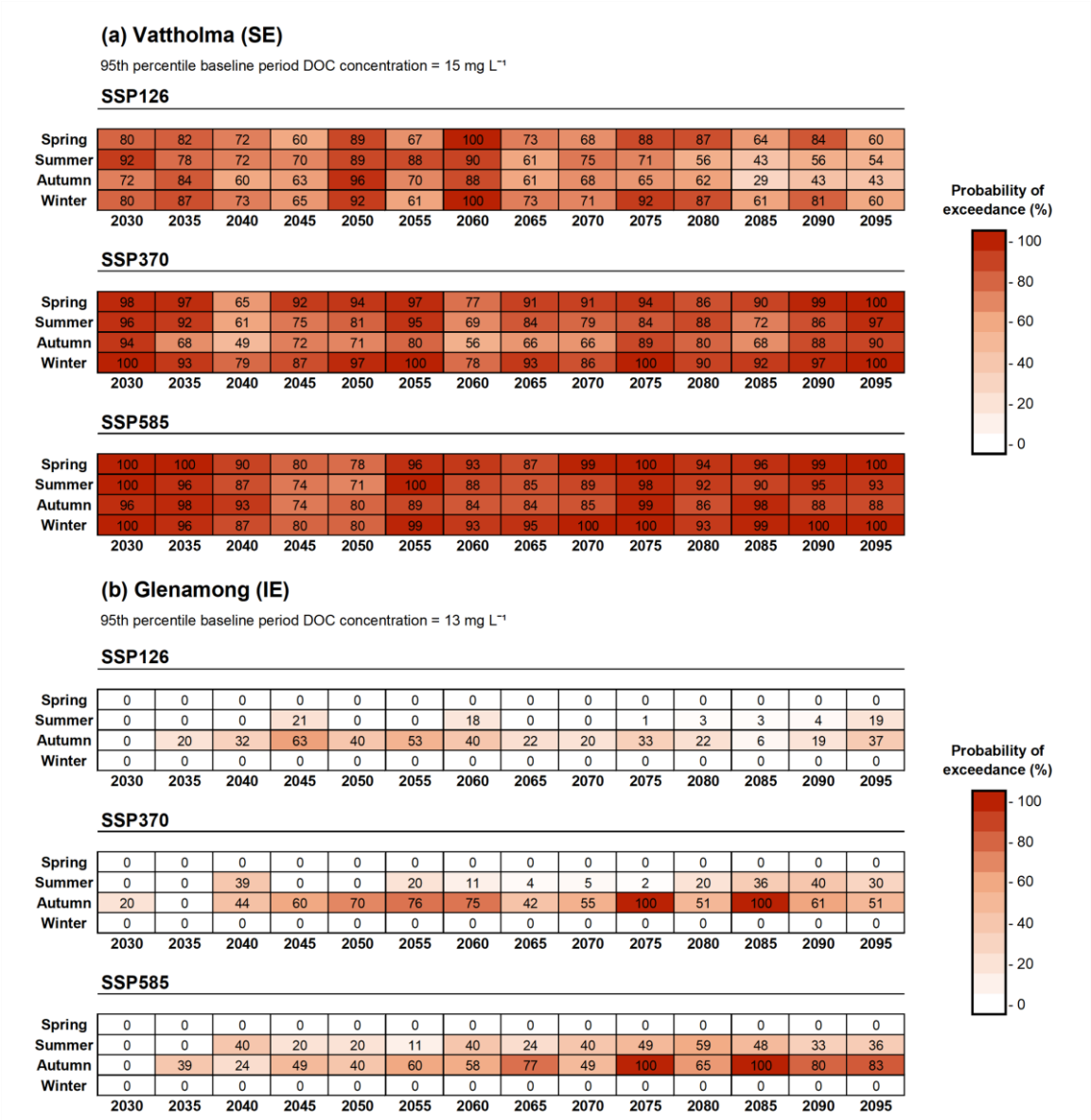


Figure 4.19 Tercile plots displaying the probability of exceeding the 95th percentile baseline DOC concentration (mg L^{-1}) for each typical meteorological season in the future (every 5 years) under SSP126, SSP370 and SSP585 scenarios for Vattholma (a) and Glenamong (b). The shading of each square represents the probability of exceedance based on the categorised colour bar legend. The ensemble size was comprised of 500 members for each scenario.

For DOC concentrations, future climate data were also the most important source of uncertainty, but of note were the higher contributions from the DOC model parameters

for the Swedish site (Fig. 4.23 – Fig. 4.24). These were relatively large, particularly under SSP370 and SSP585, and at times contributed up to 50%. In contrast, the DOC model parameters contributed much less to the uncertainty in DOC projections for the Glenamong, especially under SSP585., while the contributions for SSP370 and SSP126 were slightly higher but rarely reached 30%.

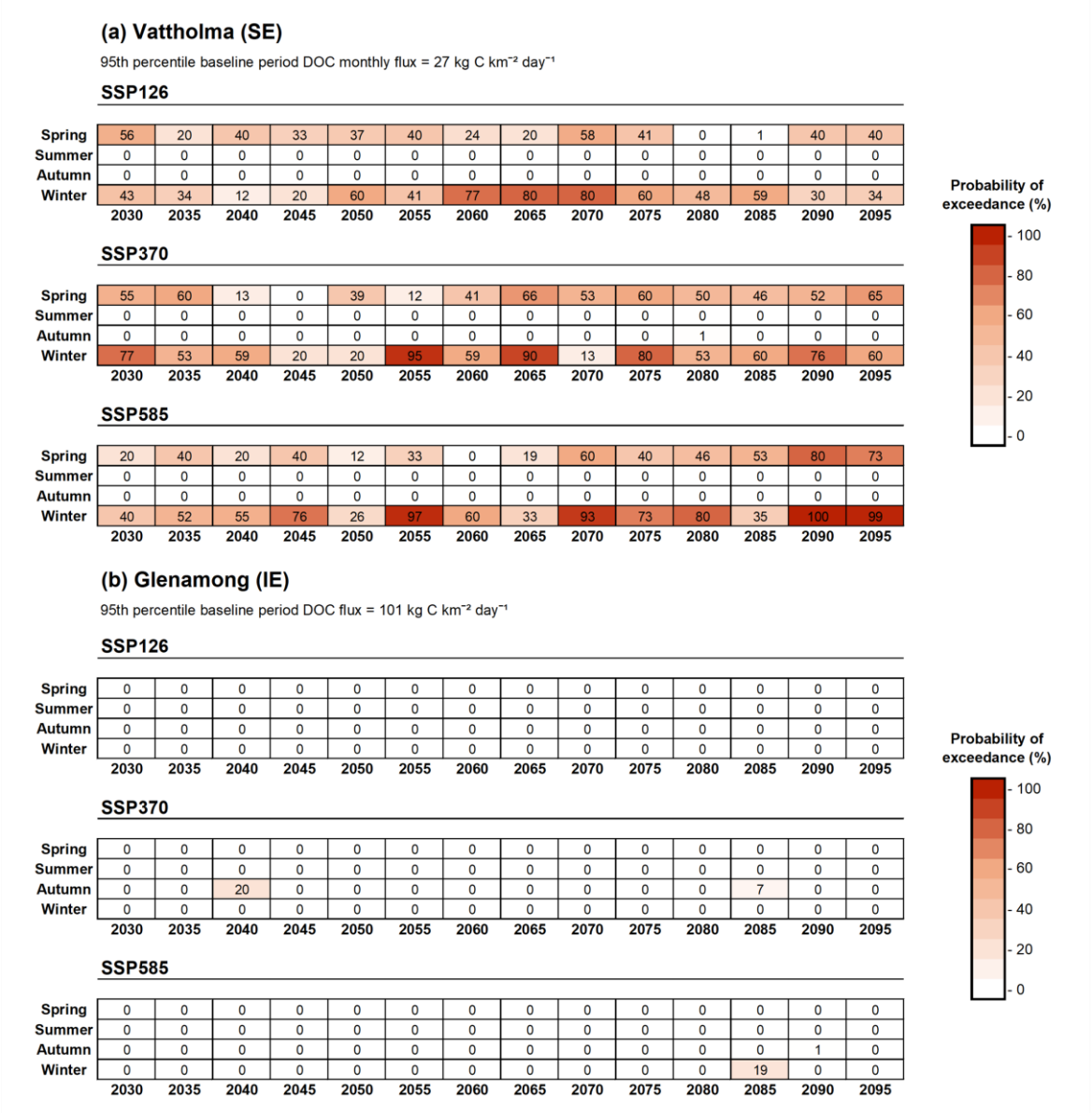


Figure 4.20 Tercile plots displaying the probability of exceeding the 95th percentile baseline flux (kg C km^{-2} day^{-1}) for each typical meteorological season in the future (every 5 years) under SSP126, SSP370 and SSP585 scenarios for Vattholma (a) and Glenamong (b). The shading of each square represents the probability of exceedance based on the categorised colour bar legend. The ensemble size was comprised of 500 members for each scenario.

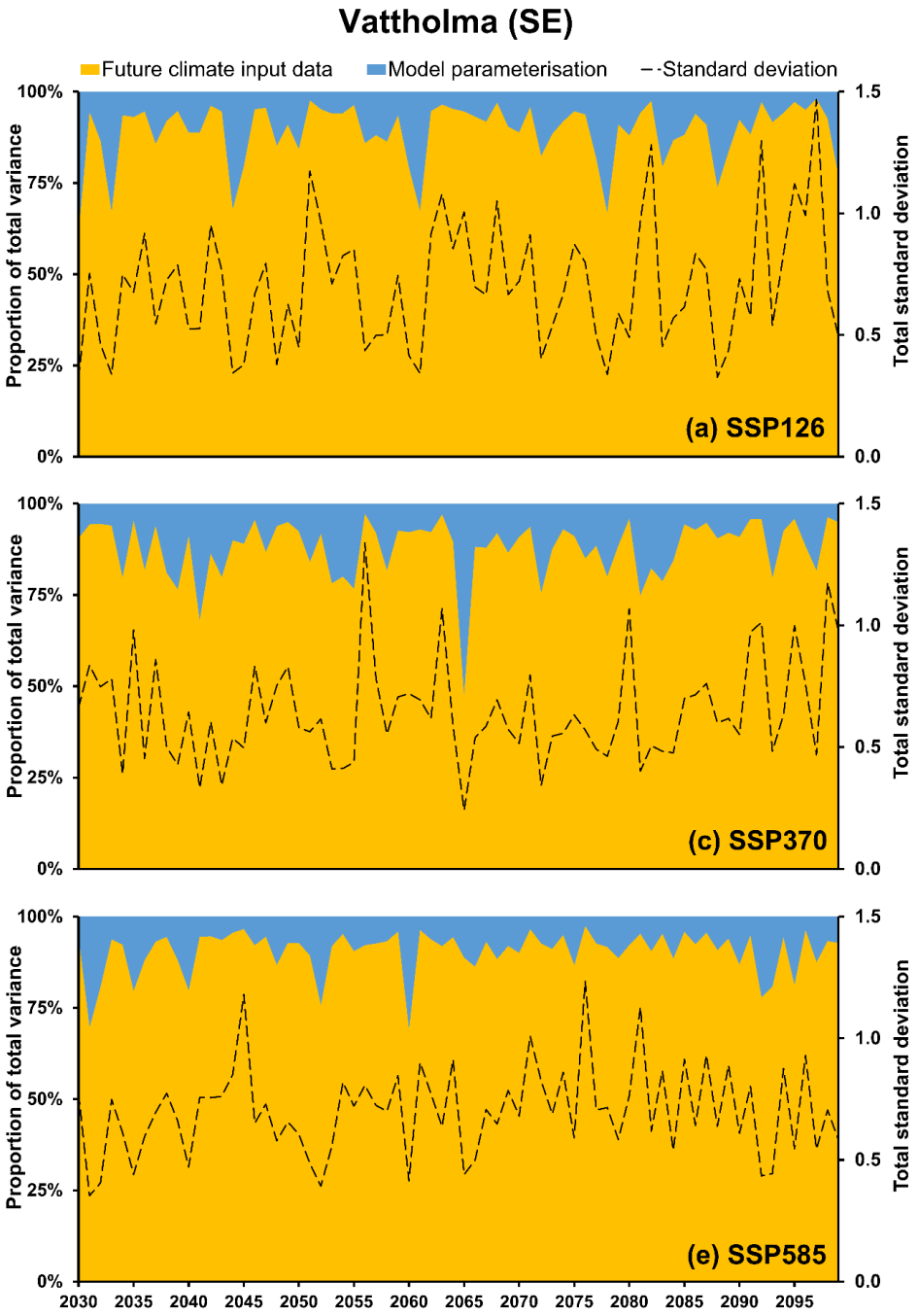


Figure 4.21 Relative contribution of (1) future climate input data and (2) model parametrisation as individual sources of uncertainty to the total uncertainty in future projections of discharge under SSP126, SSP370 and SSP585 scenarios for Vattholma.

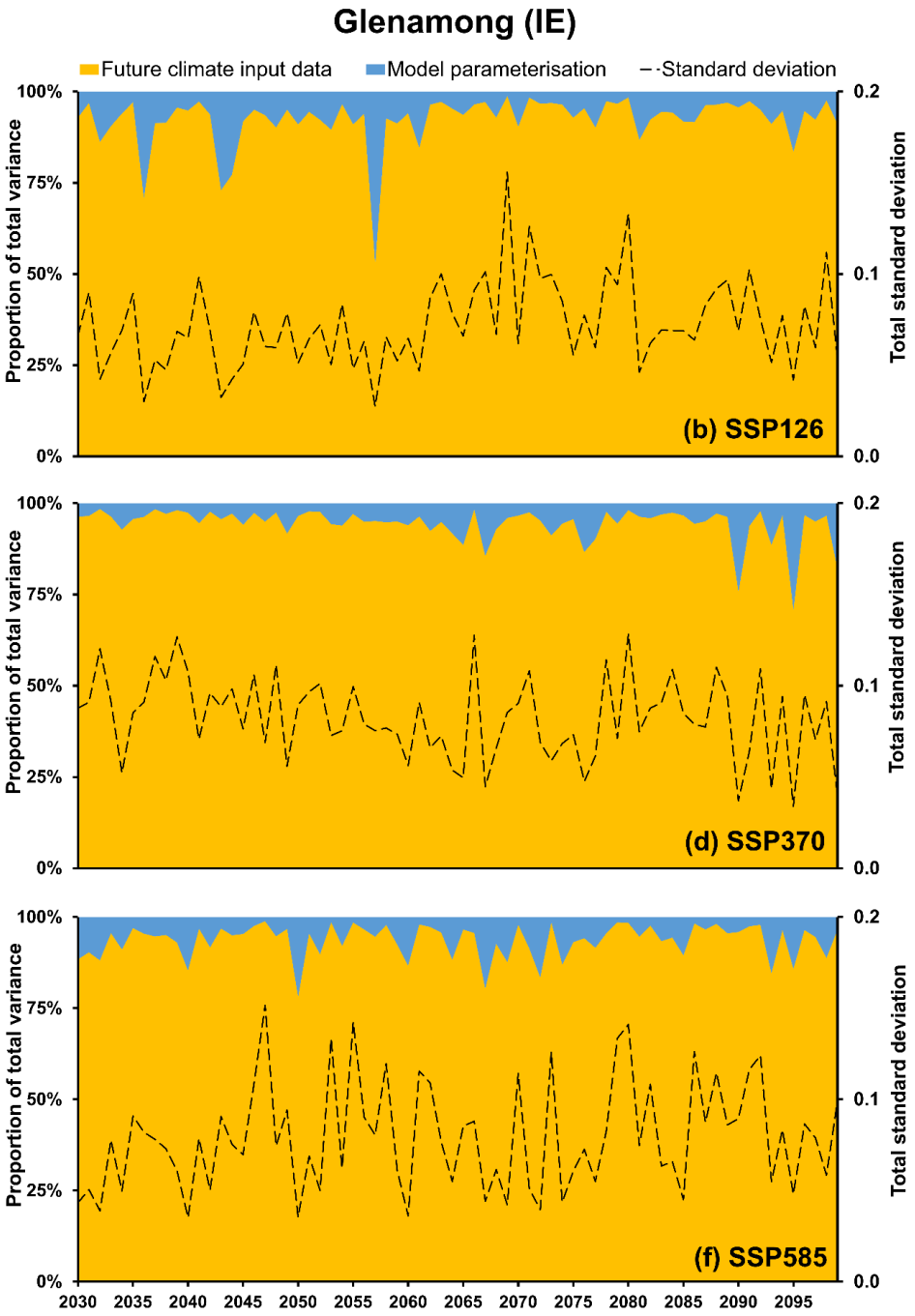


Figure 4.22 Relative contribution of (1) future climate input data and (2) model parametrisation as individual sources of uncertainty to the total uncertainty in future projections of discharge under SSP126, SSP370 and SSP585 scenarios for Glenamong.

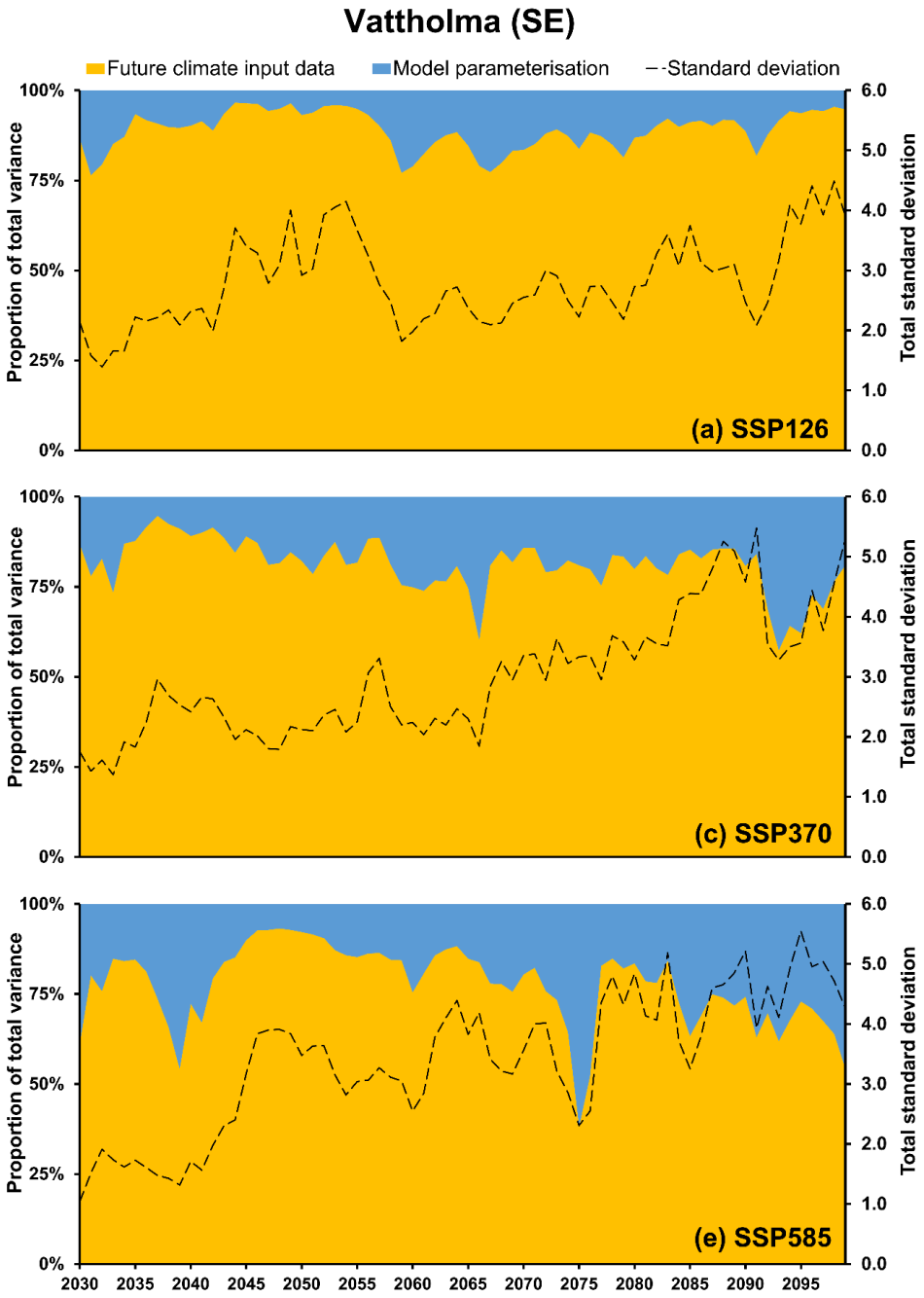


Figure 4.23 Relative contribution of (1) future climate input data and (2) model parameterisation as individual sources of uncertainty to the total uncertainty in future projections of DOC concentration under SSP126, SSP370 and SSP585 scenarios for Vattholma.

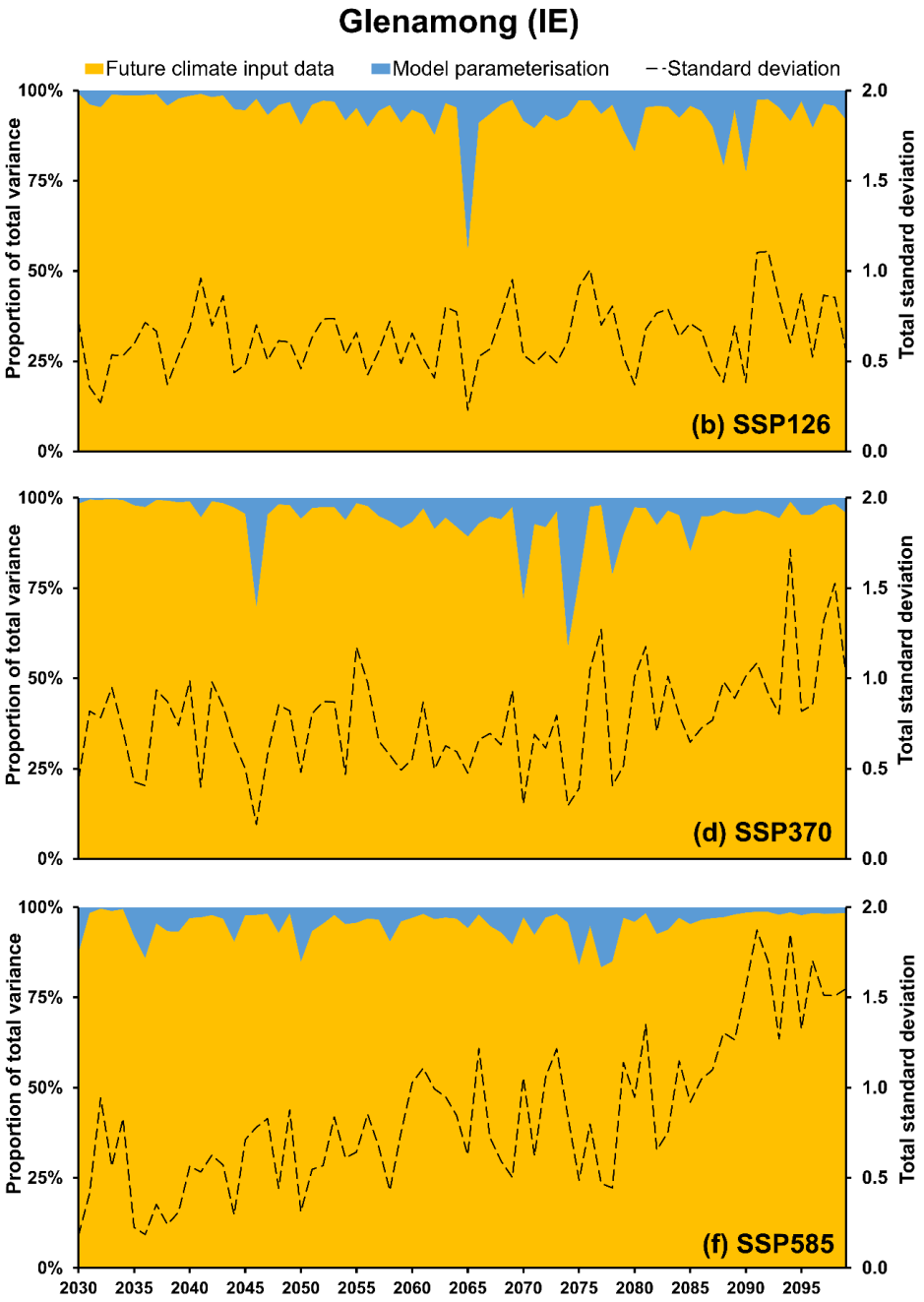


Figure 4.24 Relative contribution of (1) future climate input data and (2) model parameterisation as individual sources of uncertainty to the total uncertainty in future projections of DOC concentration under SSP126, SSP370 and SSP585 scenarios for Glenamong.

4.5 Discussion

Implementing adaptive management in response to the impacts of global warming is becoming more and more critical as records of climatic extremes continue to be exceeded (Ripple et al., 2023; Esper et al., 2024). These changes are having profound impacts on water quantity and quality (van Vliet et al., 2023), including on the DOC concentration in drinking source waters and therefore potentially on the formation of DBPs (Absalan et al., 2024). In order to respond and adapt, water managers require robust estimates of future change from the modelling community. Our projections for two contrasting catchments, in regions were DBP formation is already an issue, show that DOC concentrations are projected to show large increases, with the highest levels related to scenarios where mitigation is not addressed. They also highlight the importance of incorporating model parameter uncertainty into the future projections, a source of uncertainty that is often omitted. This is especially important for model parameters such as those related to carbon decomposition and transport in organic soils, that will respond directly to variations in temperature and water availability.

Our results relative to many recent studies (e.g., Futter et al., 2011; Son et al., 2019; J. Xu et al., 2020; Lindqvist, 2022) have a similarly good or better model performance, especially for modelling DOC concentration. The future changes quantified for river discharge and DOC concentration in this study also lie in a similar order of magnitude to those projected in other research for these sites (e.g., Naden et al., 2010; Lindqvist, 2022). That is, discharge projections indicate both decreasing and increasing levels under different scenarios depending on the time scale, season and context. In terms of DOC, the overall picture is for an increase in concentration and flux with different magnitudes depending on the study site and scenario. It is important to be aware, however, that these results should not be compared directly to the work of others without acknowledging the differences in modelling approach. These include changes in model structure, driver data type (e.g., stationary projections compared to transient GCM-

driven projections), future scenario conditions, and the examination here of effects related to model parameterisation.

Although accounting for model parameterisation can result in simulations with larger uncertainty (Schürz et al., 2019a), this is generally outweighed by producing a more accurate range of variability for the modelled variables (Her et al., 2019b; Marshall et al., 2021). Furthermore, by partitioning the total uncertainty of the predictions, we have quantified the impacts of this parameterisation on long-term projections for river discharge and DOC concentration (Fig.8; Fig. B8). While the GCM ensemble was the dominant source of uncertainty, a finding in line with many other climate change impact assessments (Hattermann et al., 2018; Kundzewicz et al., 2018), the variability in DOC model parameterisation was also important for some of our simulations. This was the case for the Vattholma catchment in Sweden under all three SSPs. An important contributing factor to this was that the behavioural ranges of key soil decomposition parameters (i.e., activation energy (E_a) and aerobic decomposition rate (b)) were higher in magnitude for this site than for the Irish site. This led to the parameters showing larger responses to increasing temperatures and changes in soil moisture levels in the Swedish catchment, and in turn to larger uncertainty contributions, particularly under SSP370 and SSP585. This also led to such large increases projected for DOC concentration at that site under these two scenarios (see Fig. 6a), as the response of these parameters likely translated to a higher amount of DOC produced in the soil matrix and, therefore, to a higher DOC export.

Determining the relative importance of model parameterisation versus future climate inputs can inform efforts to reduce total uncertainty in such projections. In GCM-driven projections for water resources, improving the quality of climate data, increasing GCM ensemble size, and better spatial and temporal input resolution are often indicated as the most effective steps (Hattermann et al., 2018; Kundzewicz et al., 2018; Her et al., 2019b). However, when model parameter uncertainty plays an important role, improving

catchment model structure and parameter representation for both hydrology and water quality should also be evaluated (Schürz et al., 2019a; Marshall et al., 2021). Using as an example the model structure of GWLF-DOC, these actions could be focused on the parameters that showed the greatest sensitivity and a degree of model parameter correlation (see Section 4.4.1).

Moreover, although other potential sources of uncertainty were not included (e.g., methods for bias correction, use of an ensemble of catchment models, land use change projections, and input data downscaling), this study represents a step forward in catchment DOC water quality modelling. By incorporating model parameter uncertainty, all of our results including those representing the likelihood of extreme DOC concentration and DOC flux account, to a large extent, for model equifinality. This key aspect is required for a better interpretation of the results (Naden et al., 2010), especially of DOC model outputs that were produced using a model structure forced by hydrology (Wei et al., 2024). It is to note, however, that GWLF-DOC does not replicate other factors that influence DOC dynamics such as those related to biochemistry in soils (e.g., pH response and microbial populations) or in-stream processes. Nevertheless, we consider it captured the fundamental processes related to temperature and water availability variations in the soil that drive DOC dynamics at the catchment scale.

4.5.1 DOC dynamics in the context of hydrology

At Vattholma (Sweden), although relatively constant DOC concentration increases were projected throughout the year, discharge dynamics were projected to change the most only during the winter and the spring, especially under SSP370 and SSP585. Both future precipitation and temperature were clearly elevated for the winter, which represents higher ice melt and rain mobility and its impact on discharge. This discharge was projected to be accompanied by a higher amount of DOC, which was in turn influenced by a higher temperature-dependent decomposition (driven by increased soil temperatures) but not by changes in moisture-dependent decomposition (driven by

relatively constant soil moisture conditions). Differently, still elevated future precipitation and temperature for the spring but this time with both a higher evapotranspiration and soil water deficit, resulted in decreases for discharge. Future spring discharge would also transport more DOC, influenced by a higher organic soil decomposition driven this time by both increased soil temperatures and unsaturated zone water deficits. Interestingly, the increases in DOC concentration for the contrasting change in discharge indicated for the spring and the winter were such that also DOC fluxes were projected to increase largely during those periods, again more under SSP370 and SSP585. In the case of the summer and autumn, future change for discharge was minimal and the increases in DOC (which were similar in magnitude to those for the winter and spring) did not translate into probabilities of exceeding baseline extreme condition DOC fluxes.

At Glenamong (Ireland), future DOC would be transported by a relatively similar discharge to that of the baseline except during the winter, where it was projected to be higher, particularly under SSP585. Elevated future precipitation and temperature but minimal change projected for catchment evapotranspiration would lead to increases in discharge for the winter and, to a lesser extent, for the spring. Although increases in DOC concentration were projected for all four seasons, the winter and the spring were the least affected. This would be a result of only a slight increase in temperature-dependent decomposition (induced by increased soil temperatures) plus a minimal change projected for moisture-dependent decomposition (induced by soil moisture), especially under SSP126. In contrast, the DOC concentrations for the summer and autumn were projected to increase much more, such that reflected in probabilities of exceeding extreme baseline levels. Summer and autumn DOC concentrations would be directly linked to peak air temperatures and lower precipitation inputs which, among others, translate into a higher organic soil decomposition driven by both a drier soil matrix and increased soil temperatures.

4.5.2 Implications for water management

Our simulations quantify the DOC concentration envelope within which water managers at similar sites may need to operate in the future. Such results could be used to evaluate scenario-based management for preserving source water quality and supply. It was clear, however, that the SSP126 scenario represented the best trajectory in terms of future change, not only for climate but also for DOC source waters. Higher and more variable concentrations, and the likelihood of extremes, were much smaller under this scenario, especially over the long term. Moreover, a process-based modelling approach such as that described can provide insights into how climate and other key catchment dynamics influence DOC concentrations at the outlet. This allows the identification of site-specific measures to reduce DOC thereby safeguard drinking water in the context of DBPs both by catchment management or improved water treatment.

Catchment-scale measures could include improved soil management, riparian buffers, land use regulations, soil treatment, drain-blocking in peatlands, and preservation of organic soils (Ritson et al., 2014; Kritzberg et al., 2020; Anderson et al., 2023). These could be implemented in a targeted way for a specific hydrological zone or land cover (Xu et al., 2018; Williamson et al., 2023). At the treatment scale, understanding the magnitude of future increases could allow planning for mitigation measures, for example, improved DOM removal during pretreatment (Anderson et al., 2023) and enhanced disinfection during treatment and post-treatment (Xiao et al., 2024). Both catchment and treatment scale measures could be applied for a particular time of the year, for a management period (e.g., 5 years), or implemented gradually over the years (Anderson et al., 2023; Williamson et al., 2023). They can also be conducted while closely monitoring key variables at the water source intake (e.g., meteorology, discharge, DOC) and intensified accordingly during periods of rising DOM, such as a particular season, flow regime, or event (e.g., a drought) (Warner and Saros, 2019; Srivastav et al., 2020; Xiao et al., 2024).

At our Swedish site Vattholma, the elevated river discharge and DOC loading projected in the winter and spring may pose additional challenges, along with increased DOC concentrations. Higher amounts of carbon export would have implications downstream for Lake Mälaren that further complicate current water treatment (Köhler et al., 2016) and DBP reduction (Andersson, 2021) during these seasons. Moreover, our results indicated that groundwater flow pathways play a critical role in DOC export for this site. This finding has also been highlighted for other Swedish sites in other modelling studies (Naden et al., 2010; Jutebring Sterte et al., 2022). Therefore, extra attention could be paid to measures that consider the saturated sub-surface zone, its impacts on baseflow and the transport of DOC in the porous media including sorption-related processes (Ploum et al., 2020).

The Glenamong (Ireland) represents catchments that face a challenge directly associated with the sensitivity of a peatland-dominated land cover to climate-induced DOC release (Jennings et al., 2010a; Mozafari et al., 2023). Here, the largest increases in DOC concentration, combined with a lower discharge, were indicated for the summer and autumn especially under warmer, drier scenarios. Both surface runoff and baseflow were equally important for DOC export in this catchment, emphasizing the role of the peaty topsoil not only for organic carbon decomposition (Arsenault et al., 2024) but also for transport (Prijac et al., 2023). Moreover, maximum DOC concentrations (indicated by increases and extreme events) would have a pronounced seasonality, peaking in the autumn (Fig. 4.19). This volatility, in particular, could represent an important challenge for water treatment (Klante et al., 2022; Riyadh and Peleato, 2024) that, along with other climate-induced impacts on catchment dynamics (Jennings et al., 2009), can further complicate Irish water supply in complying with European Union regulations, especially in the context of DPBs (O'Driscoll et al., 2018b). Management steps should, therefore, evaluate not only reducing the potential DOC increases over monthly to annual time

scales but also account for high levels of temporal variability associated with extreme events (Jennings et al., 2020).

4.6. Conclusions

Our study has highlighted the dominant impacts of future climate variability on the uncertainty in future projections of catchment discharge and DOC dynamics. However, it also showed how model parameterisation can be an important source of uncertainty in climate change impact assessments. Importantly, DOC concentrations for our study sites were projected to increase in all simulated futures, sometimes to levels that can largely exceed the historical reference. It is of note, however, that the smallest increases and variability were estimated under SSP126, especially by the end of the century. This suggests, with regard to catchment DOC export and potentially for drinking water supply, that it might be worth adopting more long-term sustainability actions aligned with that scenario (e.g., efforts for climate adaptation, infrastructure development, and a reduction in GHG emissions). We propose that the use of our site-specific findings can assist in developing mitigation protocols and strategies that can lead to a more adaptive catchment and water treatment management.

Chapter 5

Short-term lake water temperature forecasts can be used to anticipate the dynamics of freshwater species

---

Ricardo Paíz[a], R. Quinn Thomas[b,c,d], Cayelan C. Carey[b,d], Elvira de Eyto[e], Ian D. Jones[f], Austin D. Delany[b,d], Russell Poole[e], Pat Nixon[e], Mary Dillane[e], Valerie McCarthy[g], Suzanne Linnane[a], Eleanor Jennings[a]

[a]Centre for Freshwater and Environmental Studies, Dundalk Institute of Technology, A91 K584, Co. Louth, Ireland

[b]Department of Biological Sciences, Virginia Tech, Blacksburg, Virginia, USA

[c]Department of Forest Resources and Environmental Conservation, Virginia Tech, Blacksburg, Virginia, USA

[d]Center for Ecosystem Forecasting, Virginia Tech, Blacksburg, Virginia, USA

[e]Fisheries & Ecosystem Advisory Services, Marine Institute, F28 PF65 Newport, Co. Mayo, Ireland

[f]Biological and Environmental Science, University of Stirling, Stirling, UK

[g]School of History and Geography, Dublin City University, D09 YT18, Dublin 9, Ireland

---

This chapter led to the publication of the following research paper: Paíz, R., Thomas, Q., Carey, C., de Eyto, E., Delany, A.D., Poole, R., Nixon, P., Dillane, M., McCarthy, V., Linnane, S., Jennings, E., *Near-term lake water temperature forecasts can be used to anticipate the dynamics of freshwater species*. Ecosphere 16(7): e70335. https://doi.org/10.1002/ecs2.70335 (see Appendix D).

5.1 Abstract

Near-term ecological forecasting can be used to improve operational resource management in freshwater ecosystems. Here, we developed a framework that uses water temperature forecasting as a tool to predict the migrations of Atlantic salmon (Salmo salar) and European eel (Anguilla anguilla) between freshwater and the sea. We used historical observations of lake water temperature and fish migrations from an internationally important long-term monitoring site (the Burrishoole catchment, Ireland) to generate daily probabilistic predictions (0 – 100%) of when relatively large numbers of fish migrate. For this, we produced daily lake water temperature forecasts that extended up to 34 days into the future using FLARE (Forecasting Lake and Reservoir Ecosystems), an open-source ensemble-based forecasting system. We used this system to forecast lake water temperature conditions associated with percentile-based fish migrations. Two metrics, P66 and P95, were used to indicate days with migrations in excess of 66% and 95% respectively of the historical daily fish counts. The results were first validated against water temperature observations, with an overall root mean squared error (RMSE) of 0.97 °C. Our forecasts outperformed two other possible water temperature forecasting approaches, using site climatology (1.36 °C) and site persistence (1.19 °C). The predictions for fish migrations performed better for the P66 metric than for the more extreme P95 metric based on the continuous ranked probability score (CRPS), and the best results were obtained for the salmon downstream migration. This forecasting approach with quantified uncertainty levels has the potential to assist decision-making, especially in the face of increased risks for these species. We conclude by discussing the scalability of the framework to other settings as a tool aimed at supporting management practices in real time.

Keywords: Ecological forecasting; Lake modelling; Probabilistic prediction; Diadromous fish; Water management

5.2 Introduction

The biota of freshwater ecosystems is responding to an increasing range of human and climatic pressures (Priya et al., 2023), resulting in changes in behaviour and ecology (Mishra et al., 2021; Staudinger et al., 2021). Such changes represent a challenge for environmental management because they are often unforeseen and therefore appropriate mitigation or conservation measures cannot always be applied (Abbass et al., 2022; IPCC et al., 2023). Basing management actions on past conditions is becoming less reliable (Nissan et al., 2019; Diffenbaugh, 2020), especially as ecosystem dynamics become more variable, leaving managers with limited time to react (Foley et al., 2015). However, anticipating some of these alterations in ecosystem function is becoming possible through the application of short-term ecological forecasting systems (Dietze et al., 2018; Bradford et al., 2020b). Providing forecasts – i.e., predictions of future environmental conditions with quantified uncertainty (Lewis et al., 2022a) – to managers can inform their operations and assist in decision-making (Tulloch et al., 2020; Bodner et al., 2021; Lofton et al., 2023).

Recent short-term ecological forecasts to provide predictions of specific environmental variables, including water temperature, have successfully supported water management in a range of applications e.g., drinking water supply (Kim and Ahn, 2022; Georgescu et al., 2023; Zwart et al., 2023), hydropower (Fry et al., 2020; Y. Liu et al., 2023) and agriculture (Crippa et al., 2023; Saeed et al., 2024). Water temperature is a key controller of many processes in the freshwater environment (Maberly et al., 2020; Bonacina et al., 2023) and one of the most monitored parameters in lakes and reservoirs worldwide (Peñas et al., 2023; Piccolroaz et al., 2024). This makes it a useful parameter for forecasting change in aquatic systems (Gumpinger et al., 2010; St-Hilaire et al., 2021). For example, water column mixing (turnover), the occurrence of algal blooms and the sediment nutrient release in lakes/reservoirs are often associated with water temperature changes (Cai et al., 2023; H. Liu et al., 2023; Yin et al., 2023) and hence,

have been the focus of short-term forecasting in aquatic systems (e.g., Rousso et al., 2020; Thomas et al., 2020; Schaeffer et al., 2024). To date, however, there has been less focus on forecasting the dynamics of other, equally important, biological components of freshwater ecology, such as the dynamics of fish (Slingsby et al., 2023).

Fish are an important component of freshwater ecosystems globally (Tamario et al., 2019) and migratory species are of intrinsic social, cultural and economic value to many societies (Gende et al., 2002; Oke et al., 2020). The life cycle timing (phenology) of fish migrating from freshwaters to the sea and vice versa (i.e., diadromous fish) have a direct impact on aquatic food webs (Dias et al., 2019; Ouellet et al., 2022), nutrient cycling (Weaver et al., 2018; Oke and Hendry, 2019), aquaculture (Vladic and Petersson, 2016; Ouellet et al., 2022) and hydropower (Carter et al., 2023; Knott et al., 2023). In general, diadromous fish migrations are driven by a combination of environmental factors including temperature, flow conditions, photoperiod, and moonlight exposure (Valiente et al., 2011; Lin, 2017; Sparks et al., 2019). In particular, water temperature influences the metabolism and other physiological processes of fish directly (Seebacher and Post, 2015), resulting in pronounced effects on the timing and extent of migrations (Riley et al., 2012; Zydlewski et al., 2014). It, therefore, has potential as an explanatory variable on which to build a short-term migration forecast, especially in the face of an increasingly variable climate which can induce shifts in diadromous fish phenology (Lowerre-Barbieri et al., 2019; Legrand et al., 2021; Rinaldo et al., 2024).

Previous work on predicting or hindcasting diadromous fish migrations (e.g., Battin et al., 2007; Durif and Elie, 2008; Sykes et al., 2009; Hobday et al., 2016; Jacox et al., 2020; Teichert et al., 2020a) has centred on recreating catchment flow conditions in specific settings with modelling approaches (e.g., statistical, process-based), often using long-term climate projections and incorporating multiple variables besides water temperature. However, most of those predictions have been on a seasonal to annual scale, while management applications and conservation measures for these species

could benefit from short-term forecasts (Welch et al., 2019; Roberts et al., 2023), that could be deployed using a lower number of variables (Teichert et al., 2020b; King et al., 2023). Such an approach could be particularly applicable in sites (a) with limited monitoring, (b) where the timing of migrations presents day- or week-sensitive fish runs spread throughout the year, and/or (c) where migrations are impacted by human activities (e.g., dam operations) (Barbarossa et al., 2020; Carter et al., 2023).

Here, a near-real time framework that uses water temperature as a determinant of diadromous fish migrations is presented. A daily automated ensemble-based forecasting system was developed to provide probabilistic predictions of fish migrations and applied at Lough Feeagh (Burrishoole catchment, western Ireland), a site with long-term observation datasets for fish and for water temperature. Historical data were used to determine the lake temperature conditions associated with percentile-based migration regimes of two diadromous species: Atlantic salmon (*Salmo salar*) and European eel (*Anguilla anguilla*). Then, both the ensemble lake temperature forecasts and the percentile-based migration conditions were used to generate daily probabilistic predictions of future migrations. The prediction skill was evaluated against the most recent fish monitoring records.

This study aimed to address the gap in short-term forecasting of daily fish migrations by building a near-real time forecast for fish migration using a single explanatory variable that is both readily available in near-real time and relatively straightforward to model (i.e., water temperature). The approach was assessed by first evaluating the water temperature forecasting system performance at the study site, and second by quantifying forecast performance for the probabilistic predictions of the different fish migrations. The implications of the results are discussed within a freshwater resource management context, focusing on the potential benefits and limitations of the forecasting framework for real-world operational applications and how it might be a scalable tool in those settings.

5.3 Materials and methods

The framework of this study was composed of three main phases graphically presented in Fig. 5.1, which also outlines the study site monitoring arrangement.

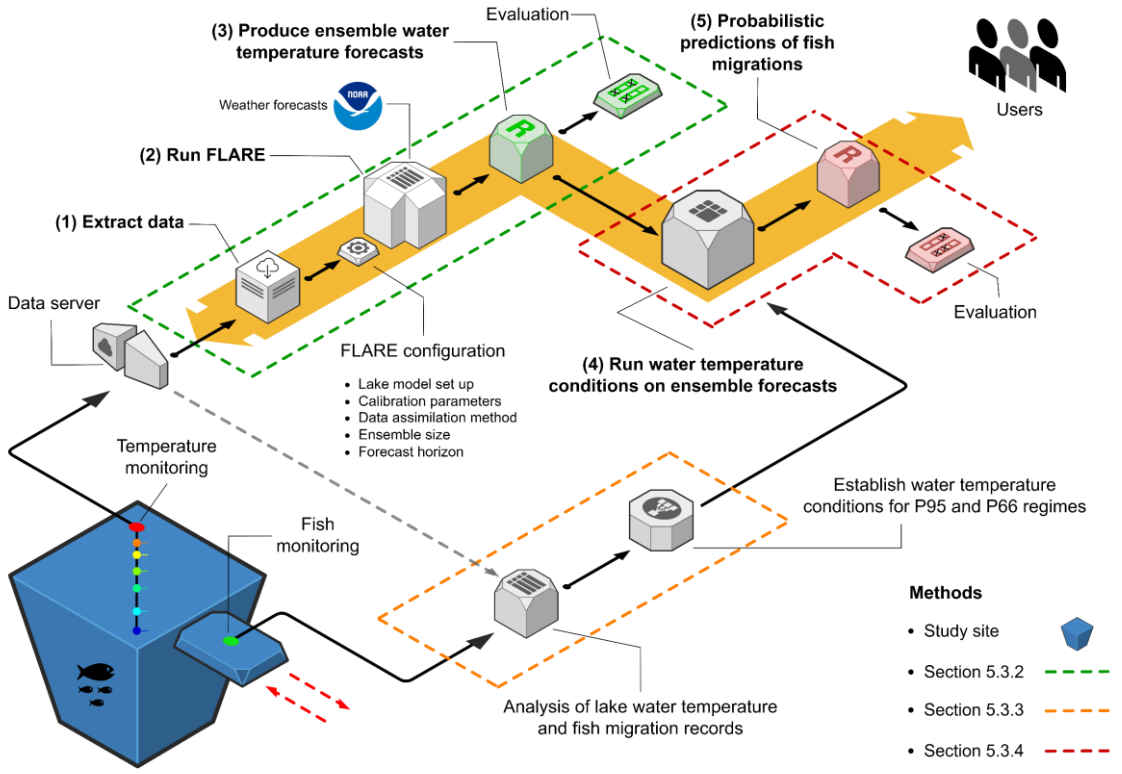


Figure 5.1 Flow diagram of the forecasting framework structure. The framework contains three main phases indicated by dashed lines in the legend. The automated components of the framework are indicated by five iterative steps denoted in bold fonts alongside a continuous solid yellow arrow.

5.3.1 Study site

Lough Feeagh is a monomictic lake located in the Burrishoole catchment in western Ireland (53° 56′ N, 9° 35′ W). It is the largest water body (≈ 3.95 km^2) in a system of lakes interconnected by river networks that discharge into the Atlantic Ocean (Fig. 5.2). It holds a volume of ≈ 6.0 x10^7 m^3, with mean and maximum depths of 14.5 and 46.8 m, respectively. The Black and the Glenamong rivers are its primary inflows. The rivers and lakes in the Burrishoole catchment are coloured (≈ 80 mgl^{-1} PtCo) and slightly acidic (pH ≈ 6.7), owing to the underlying igneous geology and overlaying blanket bogs

(Doyle et al., 2019; Jennings et al., 2020; de Eyto et al., 2022). The climate in the area is temperate oceanic, with an average annual rainfall of 1700 mm $year^{-1}$ and mean air temperature of 11 °C (2004 - 2023). Air temperature typically ranges between 4 to 20°C in a calendar year and rainfall occurs on more than 75% of days in the year (de Eyto et al., 2016).

The Burrishoole catchment provides key ecosystem services such as carbon sequestration through its sediments and buffering soils (Harenda et al., 2018; Doyle et al., 2023) and as an habitat for biodiversity including some species of diadromous fish. Atlantic salmon (*Salmo salar*) and European eel (*Anguilla anguilla*) fish species are endemic to the Burrishoole and are key constituents of its aquatic food web (de Eyto et al., 2020). The migrations of these species to and from freshwater and the ocean are well documented (e.g., Byrne et al. 2003, Reed et al. 2017, Sandlund et al. 2017, Poole et al. 2018, and de Eyto et al. 2022). In brief, salmon spawn in the Burrishoole catchment in winter, and juveniles spend a little over two years in freshwater. They migrate to the Atlantic Ocean as smolts in late spring, and after spending one winter at sea, return to freshwater in the summer as mature adults to spawn. Current evidence supports the view that European eel spawn as a single spawning stock in the Atlantic Ocean, in the area of the Sargasso Sea. Juveniles arrive off the Irish coast in autumn and enter estuaries from November to February. As temperatures rise, many commence active migration into freshwaters as elvers. Once in freshwater, elvers grow into yellow eel which is the life stage in which they spend most of their life (7–58 years in the west of Ireland). Eels mature only once when they undergo a process known as silvering before returning to the Atlantic Ocean to spawn.

5.3.1.1 Water temperature monitoring

As part of an Automatic Water Quality Monitoring System (AWQMS) deployed in Feeagh, the water temperature has been measured at 13 different depths (0.9, 2.5, 5, 8, 11, 14, 16, 18, 20, 22, 27, 32 and 42 m) at a high frequency (2 min intervals) since

2004. The surface water temperature (0.9 m) is measured via a Hach Environmental Hydrolab Data Sonde X5 with an accuracy of ± 0.1 °C (UK OTT Hydrometry Ltd; https://www.otthydromet.com) while the other 12 depths are measured via platinum resistance thermometers with an accuracy of ± 0.2 °C (UK Labfacility Ltd. PT100 1/10DIN 4 wire sensor; http://labfacility.com), enabling a complete vertical profile reading. The sensors are cleaned monthly and the multiparameter probe is calibrated once per month (de Eyto et al., 2016).

Water temperature data from the AWQMS that had undergone appropriate quality assurance/quality control (QA/QC) were obtained from the Marine Institute monitoring web services (http://marine.ie). Data from 2004 to 2023 were used in this study, together with the volumetric percentage of lake water corresponding to each depth (Marine Institute, 2017). Lake thermal stratification in Feeagh was defined as the difference of > 1°C between the surface (0.9 m) and bottom (42 m) lake temperatures (Woolway et al., 2020).

5.3.1.2 Fish monitoring

All fish moving into and out of the catchment were counted at two sites, the Salmon Leap and the Mill Race, the two water channels connecting freshwater Feeagh with the downstream brackish lagoon, Lough Furnace (Fig. 5.2). The daily counts were performed manually using permanent whole river upstream and downstream fish traps and were part of long-term records of fish migrations between the freshwater and marine domains (Poole et al., 2018; de Eyto et al., 2022; Long et al., 2023).Three fish migration datasets from 2004 to 2023 (matching the water temperature monitoring data period) were used in this study: (1) daily downstream (juvenile smolt) and (2) daily upstream movements (adults) of Atlantic salmon; and (3) daily downstream movements of maturing adult European “silver” eel.

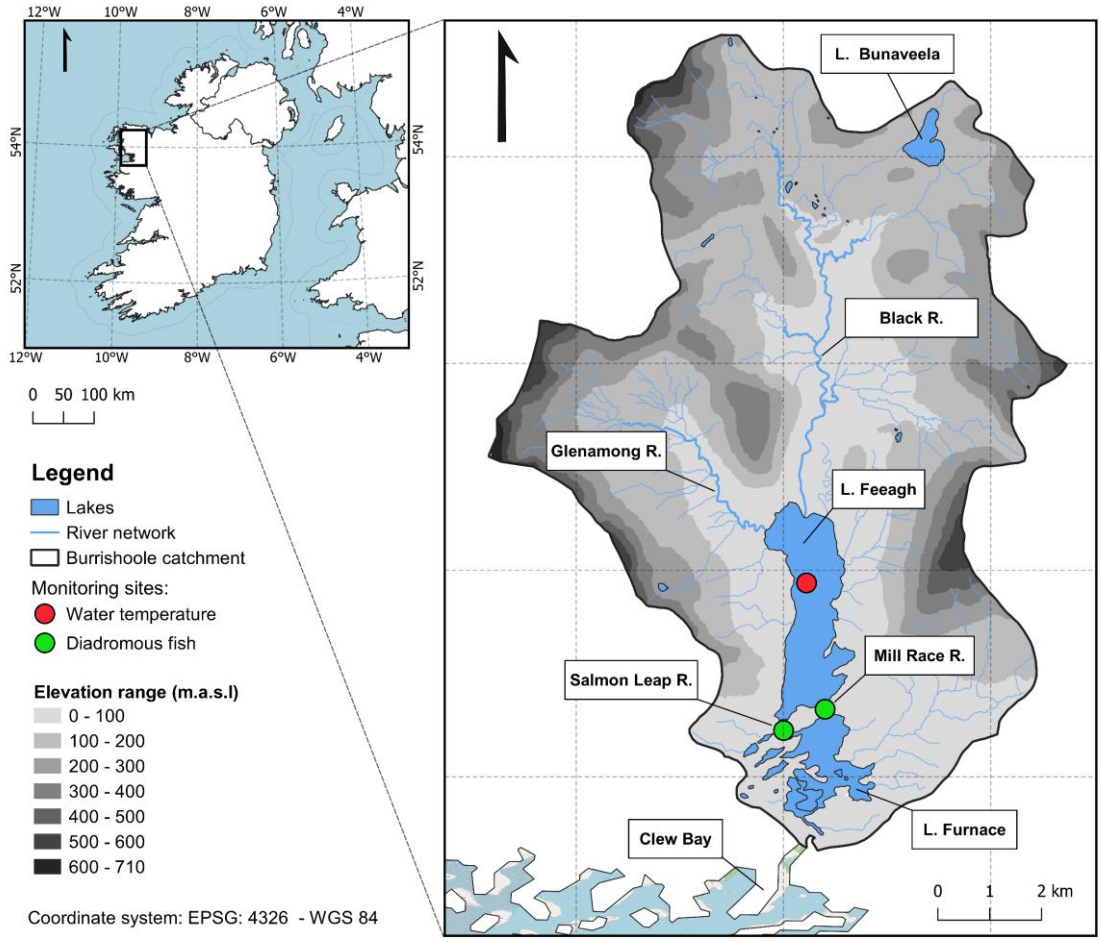


Figure 5.2 Location of Lough Feeagh and the Burrishoole catchment in western Ireland, including main water bodies and topographic elevation. The monitoring sites for water temperature and fish are indicated by red and green dots, respectively.

5.3.2 Water temperature forecasting

The system employed to generate daily water temperature forecasts in Feeagh was the Forecasting Lake and Reservoir Ecosystems system (FLARE). Water temperature forecasts in Feeagh were generated on a daily basis for three years (1st Nov 2020 – 1st Nov 2023; 1095 days). FLARE is an open-source system for lake and reservoir water quality forecasting aimed at supporting management (Thomas et al., 2020; Carey et al., 2022). By integrating real-time monitoring, hydrodynamic modelling with data assimilation, and an ensemble-based forecasting algorithm, FLARE provides daily water

quality forecasts for multiple lake/reservoir depths with a forecast horizon of up to 35 days with quantified uncertainty (Thomas et al., 2020, 2023b; Wander et al., 2024).

To date, several FLARE-based forecasting systems have been deployed to provide predictions of different water quality variables e.g., water temperature, dissolved oxygen, and chlorophyll a (Carey et al., 2022; Woelmer et al., 2022; Thomas et al., 2023b; Wander et al., 2024; Woelmer et al., 2024). Most of this research describes the predictability engine of FLARE by way of forecasting experiments to support local different management applications e.g., drinking water (where forecasts can be used to determine withdrawal depths for water treatment), dam operations (where forecasts can be used to schedule outlet flows), and environmental remediation (where forecasts can allow managers to initiate interventions). FLARE has also been applied to anticipate ecological dynamics associated with a particular forecasted variable. For instance, water temperature forecasts have been used to anticipate the onset of turnover of a reservoir in Virginia (USA), where this dynamic was identified 14 and 4 days in advance in 2018 and 2019, respectively (Thomas et al., 2020). Similarly, chlorophyll-a forecasts have been used as an indicative metric of phytoplankton biomass in two reservoirs in Virginia (USA), leading to an improvement in the capacity of local managers to anticipate these algae blooms (Woelmer et al., 2022)

The process-based lake model to generate predictions for each ensemble member in FLARE is the General Lake Model (GLM) (Hipsey et al., 2019). GLM has been previously applied to Feeagh in non-forecasting studies (Bruce et al., 2018; Mesman et al., 2020). The weather forecast ensemble used to drive the forecasting was the 31-member National Oceanic and Atmospheric Administration Global Ensemble Forecasting System (NOAA GEFS) (https://www.ncei.noaa.gov) (Hamill et al., 2022) output for the grid-cell that contains Feeagh.

FLARE quantifies uncertainty by adding random noise to each FLARE ensemble member (process uncertainty), assigning one of the 31 members of the weather forecast

ensemble to each FLARE ensemble member (driver uncertainty) and having different parameter values for each FLARE ensemble member (see Wander et al. 2024 for more details). FLARE uses data assimilation (specifically the Ensemble Kalman Filter with state augmentation) to calibrate the parameter values and set the spread of the ensemble when each forecast was initiated (day 0 of the forecast) (see Thomas et al., 2020 for more details).

5.3.2.1 Configuration

FLARE was configured based on previous applications of the system (Thomas et al., 2020, 2023b; Wander et al., 2024). First, GLM was configured for Feeagh with the bathymetry used in previous model applications at the site (Mesman et al., 2020). Second, FLARE-specific settings for water temperature forecasting were configured.

GLM parameters for Lough Feeagh were set to the default values (Hipsey et al., 2019) except for six parameters that are commonly calibrated in other FLARE applications (Thomas et al., 2023b; Wander et al., 2024). Specifically, the calibration was for the mean temperature for each of the four sediment zones (*sed_temp_mean)* located at heights of *5, 15, 30* and *47* m (bottom to top), the light extinction coefficient (*Kw*), and the longwave scaling factor (*lw_factor*). The GLM configuration files including initial conditions and calibration ranges, can be found in Appendix B.

A range of 36 depths to generate depth-specific water temperature forecasts was defined, with an increasing resolution towards the lake water surface. These depths included all 13 monitoring depths. The number of FLARE forecast ensemble members was set to 248 to avoid erroneous data correlations that can arise when using smaller ensembles (Wander et al., 2024) (so that each of the 31 weather forecast ensemble members was used 8 times to drive the lake model). The normal distribution standard deviations for each calibrating parameter were defined based on previous studies (Thomas et al., 2023b; Wander et al., 2024) (1.00 °C for the *sed_temp_mean* of all four

sediment zones and 0.02 for both the *Kw* and the *lw_factor*), for water temperature observations (0.10 °C) and for the process noise (1.35 °C).

All six parameters (*sed_temp_mean 1, 2, 3* and *4; Kw* and *lw_factor)* were initially calibrated during a GLM spin-up from 1st October to 1st November 2020, a period on which data assimilation occurred but forecasts were not produced. This allowed a spin-up of the lake model before the start of the forecasting period (1st Nov 2020). For each forecast generation, all calibrating parameters and water temperature values were continuously updated via data assimilation when observations were available. All FLARE configuration files used in this study can be found in Appendix B.

5.3.2.2 Infrastructure

To make FLARE functional in real-time, an infrastructure is required. This infrastructure runs in the cloud and interconnects the framework system with the extraction of field observations to generate forecasts (see Fig. 5.1).

For each day that a forecast is generated, first, the most recent water temperature monitoring data were extracted from a local data server using an R script (see Appendix B). This script was automatically run, in a public GitHub repository via a scheduled GitHub Action (.yml file). These data were collated into daily mean water temperature values for each monitoring sensor and stored in a single target file in the same repository. This target file was updated every time the action ran. The FLARE workflow was then run in the same repository using an R script with the “FLAREr” R package via a scheduled GitHub Action (.yml file). The target file with the new observations was acquired within the workflow before a forecast generation, allowing FLARE to perform data assimilation as specified in the configuration. The resulting water temperature forecasts were collated by several filters including depth, ensemble member, date and forecast horizon, and were allocated into columnar storage data format files (.parquet) (see Appendix B).

5.3.2.3 Evaluation

The performance of the lake water temperature forecasts was evaluated against observations based on root mean square error (RMSE). RMSE is commonly used to assess the accuracy of water temperature predictions in many forecasting applications (Feigl et al., 2021; Qiu et al., 2021), including other FLARE deployments (Thomas et al., 2023b; Wander et al., 2024). The evaluation was carried out for the volume-averaged lake water temperature calculated using the 13 monitoring depths (hereafter referred to as average lake water temperature) and for each monitored depth. RMSE values were computed for all 1-34 forecast horizon days over the entire forecasting period (excluding the time from 1st January to 9th May 2021 when no observations were available). The results were averaged for each forecast horizon day and for FLARE (overall performance calculated by aggregating all FLARE forecasts produced i.e., all average lake water temperature forecasts and all individual depth forecasts).

The performance of FLARE was compared to (1) site persistence and (2) site climatology forecasts for the average lake water temperature and the surface lake water temperature (0.9 m sensor). Predictions based on both persistence and climatology have been widely used in environmental science as they are relatively easy to generate (Murphy, 1992), and provide an important baseline that enables the performance of new forecasting systems to be contextualised (Yang, 2019; Thomas et al., 2020; Brown et al., 2018; Bento et al., 2022; Zachow et al., 2023). Persistence predictions were based on the assumption that future water temperature conditions will be the same as the recent past (Wilks, 2019), i.e., they would vary depending on the forecast horizon. For example, a persistence forecast set with a 16-day forecast horizon and produced on date d will use the observed water temperature on date $d-1$ as a prediction, extending that value over the next 16 days. Climatology predictions were based on long-term average conditions of lake water temperature so that the historical average of a specific day in a year is indicative of the water temperature for the same day in the future. A

climatology forecast produced for *18th March 2021* will, for example, be equal to the average water temperature of Feeagh on that same day (*18th March*) in the historical records (2004 to 2020).

Lastly, a reliability diagram was generated to evaluate how well the uncertainty was characterised for the water temperature forecasts (Thomas et al., 2020; Zwart et al., 2023) by quantifying proportions of observations within different confidence intervals (10th, 25th, 50th, 75th and 90th) for different forecast horizons (1-, 7-, 14-, 21-, 28- and 34-days ahead). An ideally calibrated forecasting system would have 10% observations within the 10% forecast confidence interval (the range containing the middle 10% of the ensemble distribution), 25% observations in the 25% forecast confidence interval (the range containing the middle 25% values of the ensemble distribution), etc. If the percentage of observations within its given confidence interval is higher or lower, the forecasting would be considered underconfident or overconfident, respectively (Bröcker and Smith, 2007).

5.3.3 Historical analysis: fish migrations and water temperature

To relate the fish migrations with lake water temperature, research on which water temperatures have been linked to diadromous fish migrations was consulted. This indicated that (1) ambient water temperatures and (2) cumulative water temperature values have a strong role in triggering the timing and extent of diadromous migrations (e.g., Zydlewski et al., 2005; Sykes et al., 2009; Riley et al., 2012; Zydlewski et al., 2014; Sparks et al., 2019). Therefore, both temperature metrics were used as hydrologic controllers of daily fish runs of Atlantic salmon and European eel migrations. Note that daily fish runs refer to fish migrations occurring in a day.

Cumulative lake water temperature is a function of the start date chosen. For instance, Zydlewski et al. (2005, 2014) defined the start of cumulative temperatures on 1st January. In contrast, Riley et al. (2012) defined the start using two dates, 21st December (winter solstice) and 15th February, and found a better correlation for the latter date

which was attributed to the proximity of their migrations to that time (15th March). Similarly, Sykes et al. (2009) defined the start on 9th March and found a strong correlation with salmon smolt migrations (which started in April). Here, 1st March was defined as the start of the cumulative temperatures for Feeagh, as this date indicates the beginning of spring in Ireland; the season when temperatures start to rise and when salmonids start to manifest strong migratory behaviour (de Eyto et al., 2022).

Daily observed values of average lake water temperature in °C and average lake cumulative temperature in °C-days were computed for Feeagh. These were compared with datasets for all three diadromous fish migrations, matching daily fish counts from January 2004 to November 2020. Then, two sub-datasets were created by extracting values based on two daily fish count percentiles respectively: 95th (P95) and 66th (P66). These metrics were selected to represent two different regimes for the number of fish going through the traps each day for each species. P66 and P95 therefore indicate days when daily counts are in excess of 66% and 95% respectively of the historical daily fish count records.

On each of these sub-datasets, a symmetric outlier reduction (5% trim) on the driver data was performed (i.e., the lake water temperatures and cumulative lake water temperatures) to focus on the central tendency of the migrations (Osborne and Overbay, 2004). Then, for each sub-dataset, the minimum and maximum values of the two water temperature metrics were extracted, respectively. As a result, (1) a range of daily lake water temperatures and (2) a range of daily lake cumulative water temperatures for each fish migration regime were obtained. These ranges were then used as the start and end points for the specific lake water temperature conditions necessary for the different fish migrations to occur, notwithstanding that other recognised controlling factors including photoperiod, moon phase and water flow, also operate (Byrne et al., 2003; Sandlund et al., 2017).

5.3.4 Probabilistic forecasting of fish migrations

Using both the lake water temperature forecasts produced and the lake water temperature ranges established, daily probabilistic predictions for each fish migration regime were generated (forecasting period: 1st Nov 2020 to 1st Nov 2023). For the generation of each fish migration prediction, the nowcasted lake average water temperature was used, instead of using temperature observations from individual sensors. This approach enables the framework to be robust for failure and/or maintenance of any or multiple sensors, as an average lake water temperature could still be computed in the absence of observations.

First, a daily value for forecasted lake cumulative water temperatures from the daily forecasted lake water temperatures was calculated (both collated by forecast horizon – 1 to 34 days ahead – and ensemble member – 1 to 248 –). Then, to generate the probabilistic predictions for a specific fish migration regime (e.g., P66 salmon downstream), a check on when both water temperature conditions were met was performed. For each day, the percentage of the 248 ensemble members that (1) fell within the maximum-minimum range for the lake water temperature condition and (2) also fell within the maximum-minimum range for the cumulative lake water temperature condition represented the daily probability of that fish migration regime occurring. Consequently, daily probabilistic predictions were obtained, in the order of 0% - 100%, for each forecast horizon (i.e., 1- to 34-days ahead probabilistic predictions per fish migration regime). This modelling approach, therefore, would predict fish migrations based solely on lake water temperature variation. Similar to other models (e.g., Sykes et al. 2009; Teichert et al. 2020b), this forecasting framework does not account for any fish stock number in the catchment before and after a model prediction. An illustrative example of a daily output of the forecasting framework showing an average lake water temperature forecast, an average cumulative lake water temperature forecast and

probabilistic predictions for the P66 and P95 regimes of the Atlantic Salmon downstream migration is presented in Fig. 5.3.

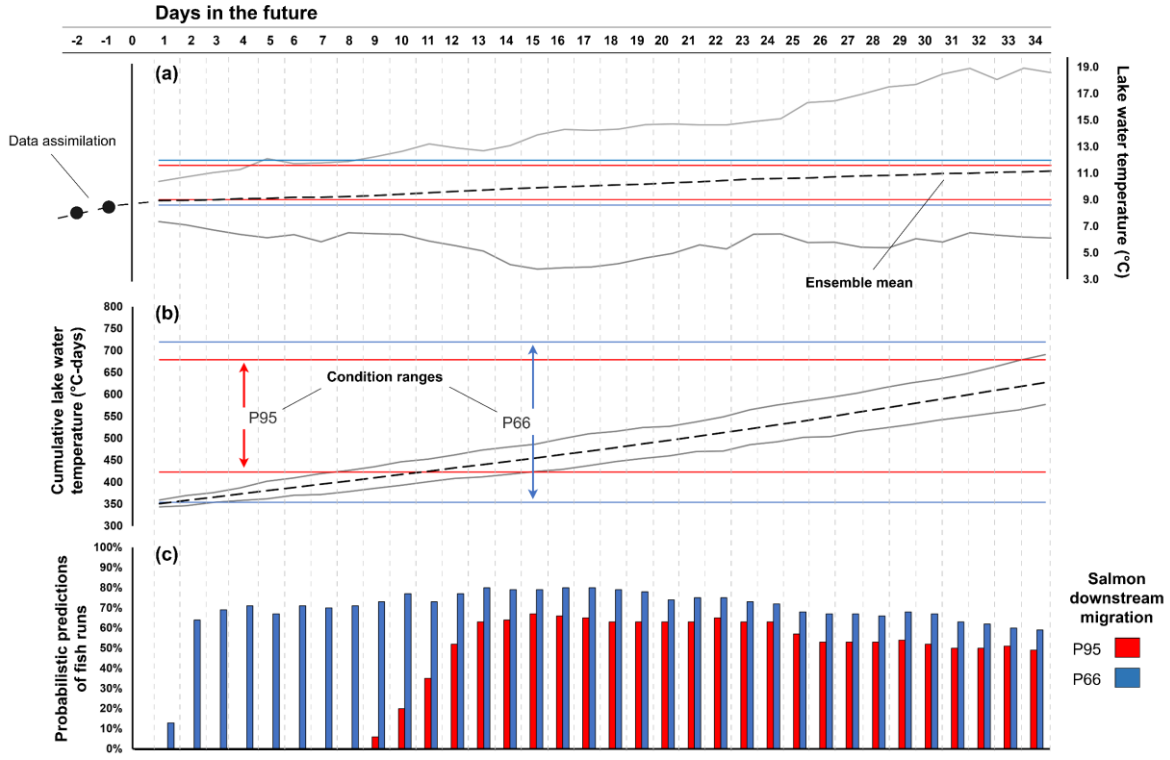


Figure 5.3 Illustrative example of a daily output of the forecasting framework containing (a) an average lake water temperature forecast, (b) an average cumulative lake water temperature forecast, and (c) probabilistic predictions of the P66 and P95 regimes for the Atlantic Salmon downstream migration. The red and blue bands in (a) and (b) indicate the lake water temperature conditions necessary for the P66 and P95 regimes to occur, respectively. The two black dots in (a) represent measured water temperature observations used for data assimilation. The continuous grey lines around the ensemble mean (dotted black line) in (a) and (b) denote the 95% confidence interval uncertainty of the temperature forecasts.

5.3.4.1 Infrastructure

In line with the FLARE infrastructure (Section 5.3.2), the generation of the different fish run probabilistic predictions was set in the cloud, using R scripts on a GitHub repository. The different lake water temperature conditions established in Section 5.3.4 are embedded in the code and the daily forecasts of lake water temperature feed the workflow after they are produced. The daily probabilistic predictions generated are

scored into a comma delimited file (.csv) and are collated by species (*Salmo salar* or *Anguilla anguilla*), movement direction (downstream or upstream), and regime (P66 or P95). These data can be allocated either in cloud storage or locally via download for subsequent analysis, and evaluation. The GitHub repository can be found in Appendix B.

5.3.4.2 Evaluation

The performance of the probabilistic predictions for the fish migrations was evaluated against the most recent fish monitoring data based on the continuous ranked probability score (CRPS). CRPS measures both the precision and accuracy of our probabilistic forecasts by comparing them to observations (Bröcker, 2012; Taillardat et al., 2023). A lower CRPS indicates a smaller error margin, encompassing both underestimation and overestimation of fish migration occurrences. The evaluation was carried out for all 1-34 forecast horizon days over the entire forecasting period (Nov 2020 – Nov 2023) and the results were averaged for each forecast horizon day. Only the observed daily fish runs equal to or exceeding historical P66 and P95 runs were used for the P66 and P95 regime CRPS evaluation, respectively, and represented percentage values of 100% against the probabilistic predictions (the rest were treated as 0%).

5.4 Results

5.4.1 Water temperature observations

The observed average lake temperatures in Feeagh exhibited relatively stable dynamics during both the historical period (Jan 2004 – Nov 2020) and forecasting period (Nov 2020 – Nov 2023) (Fig. 5.4). They ranged between 3.5 and 16.5 °C, with an average water temperature of 10.7 °C. Peak temperatures and thermal stratification were observed typically from April to September (spring and summer). Conversely, mixed lake conditions presenting the lowest water temperatures prevailed from October to March (autumn and winter) (see Fig. 5.5 for water temperature measurements at each

monitoring depth). Throughout the forecasting period, the lake exhibited thermal stratification 44% of the time (486 / 1095 days) and mixed conditions 56% of the time (609 / 1095 days).

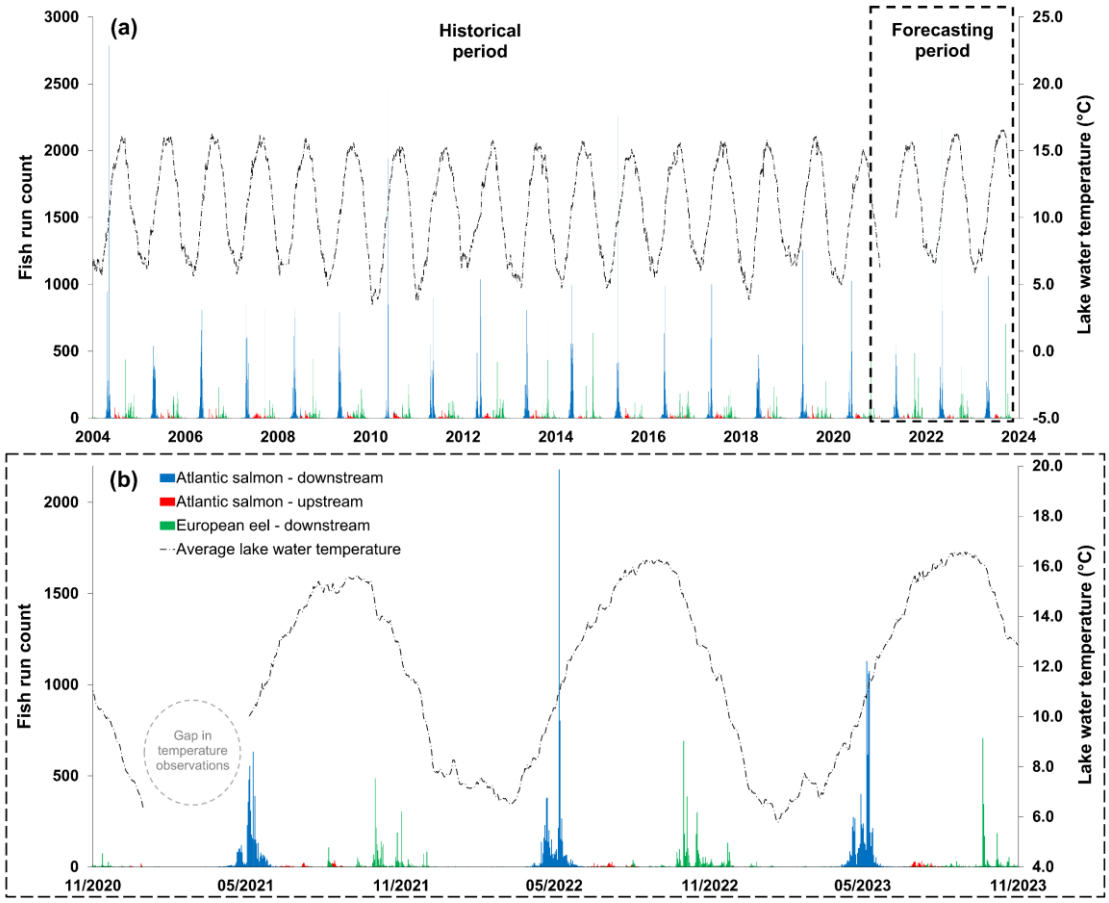


Figure 5.4 Measured average water temperature observations in Lough Feeagh and daily fish counts of Atlantic salmon downstream, Atlantic salmon upstream, and European eel downstream migrations in the Burrishoole catchment. The observed data within the forecasting period (black dashed box) in the upper panel (a) is highlighted in greater detail in the lower panel (b).

5.4.2 Water temperature forecasts

The overall RMSE performance for all forecasts produced using FLARE (for all 13 individual depths and the average lake water temperature aggregated across all 1-34 day-ahead horizons) over the three-year forecasting period was 0.94 °C. The climatology and persistence forecasts performed worse than FLARE, with overall values of 1.36 and 1.19 °C RMSE, respectively.

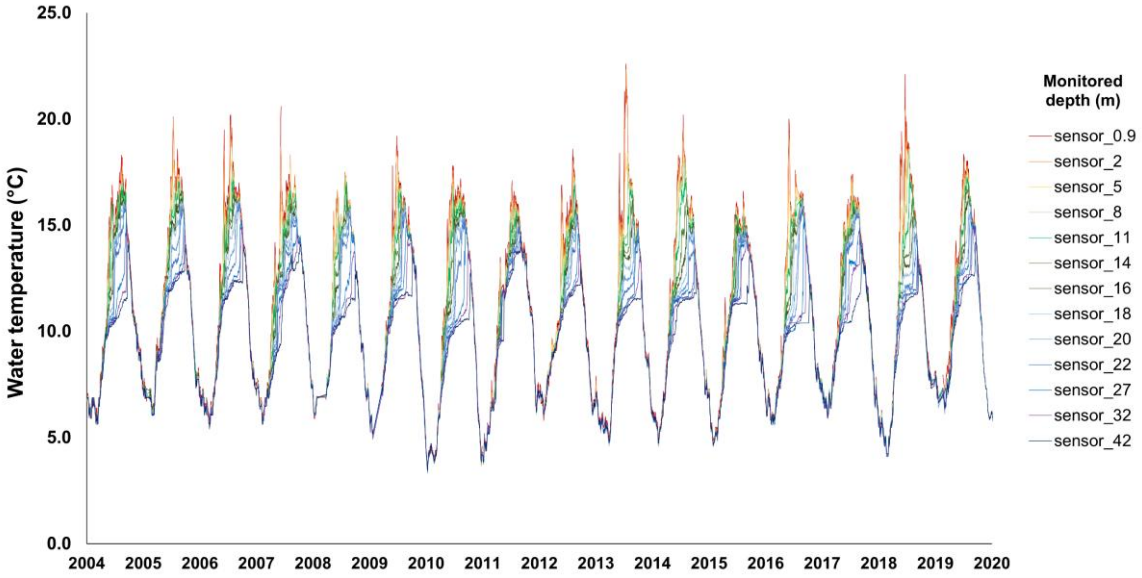


Figure 5.5 Measured water temperature observations for all 13 monitoring depths in Lough Feeagh from 2004 to 2020 (historical period of this study).

For the surface temperature only, the RMSE values of the FLARE temperature forecasts consistently increased as the forecast horizon became longer (indicating a decrease in performance), from 0.30 to 1.58 °C (Fig. 5.6a). Climatology surface temperature forecasts, with an RMSE of 1.41 °C, were outperformed by FLARE on the first 28 of 34 forecast horizon days. Persistence forecasts for the surface temperature ranged from 0.34 to 1.96 °C and were consistently outperformed by FLARE on all forecast horizon days. The average lake water temperature forecasts using FLARE performed slightly better than the surface temperature forecasts, with RMSE values ranging from 0.20 to 1.34 °C (Fig. 5.6b). Climatology average lake water temperature forecasts, with an RMSE of 1.10 °C, were outperformed by FLARE on the first 21 of 34 forecast horizon days. Persistence forecasts for the average lake water temperature ranged from 0.20 to 1.59 °C and performed similarly to FLARE on the first 21 forecast horizon days, but then were outperformed by FLARE on days 21 to 34. Typically, FLARE predictions produced during lake mixed conditions were more accurate than those produced during stratified conditions (Fig. 5.6).

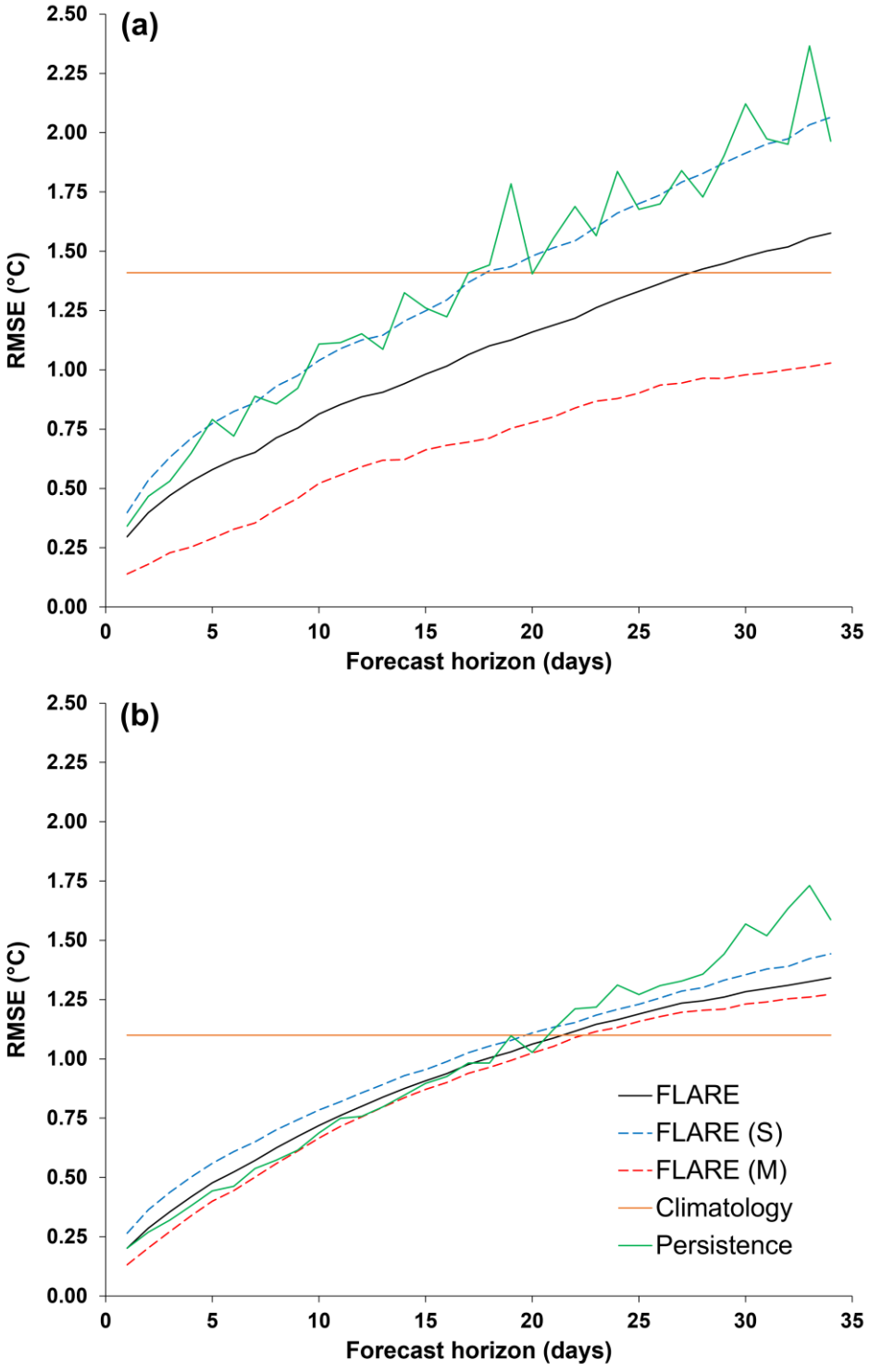


Figure 5.6 Root mean square error (RMSE) of the (a) surface lake water temperature (0.9 m) and (b) average lake water temperature forecasts produced over the entire forecasting period. FLARE (S) and FLARE (M) indicate FLARE RMSE values for forecasts produced during stratified and mixed lake conditions only, respectively. Climatology and Persistence indicate RMSE performance for forecasts produced following their forecasting approach, respectively.

Moreover, forecast uncertainty was well characterised by FLARE for all forecasts produced in Feeagh (forecasts for average lake water temperature and each monitoring depth). Relatively small variations in confidence from an ideal forecast were observed, although these varied depending on the forecast horizon length (Fig. 5.7). On short to intermediate forecast horizons (< 21 days ahead), FLARE predictions were mostly underconfident by up to 16 %. In longer forecast horizons (> 28 days ahead) the uncertainty estimates fluctuated from more confidence (up to -9 %) to less confidence (up to 6 %).

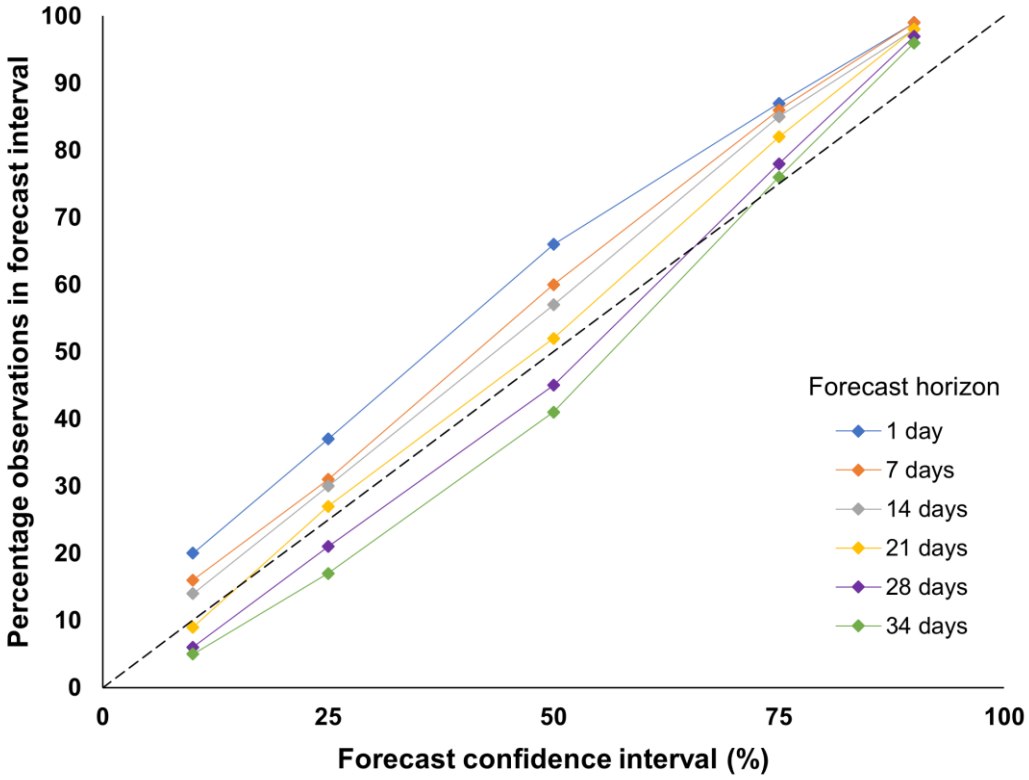


Figure 5.7 Reliability diagram for all lake water temperature forecasts produced by FLARE over the entire forecasting period. The percentage of lake water temperature observations within different forecast confidence intervals is indicated for different forecast horizons. The continuous black dotted line represents ideal forecast confidence calibration (i.e., a forecasting system that perfectly characterises uncertainty; 1:1 relationship between forecast confidence interval and the percentage of observations within it).

5.4.3 Fish migration dynamics

The fish migrations during the historical period (Jan 2004 – Nov 2020) exhibited a day-sensitive phenological behaviour with substantial differences in magnitudes and regime timings (Fig. 4; Table 1). On average, 90 juvenile smolt Atlantic salmon fish moved downstream per day during fish runs (median of 14), with a maximum count of 2733 observed in a single day (7th May 2004). The P66 and P95 numbers of salmon migrating downstream were 39 and 431 fish, respectively. Salmon began to go downstream around April, coinciding with rising lake water temperatures (Fig. 5.4). Their migratory behaviour decreased in mid-May and generally ceased after June. The maximum count of adult salmon migrating upstream was 92 individuals (18th July 2019), with an average of 7 fish (median of 3). The P66 and P95 for the daily upstream migration of salmon were 6 and 27 fish. The counts were more sporadic than daily counts of downstream migrating salmon. Salmon started to migrate upstream in June, sometimes overlapping with the end of the downstream migration movements. The fish runs of salmon going upstream decreased usually around October, but some counts extended till December.

In contrast to Atlantic salmon, the core of European eel migrations took place when there was a decreasing trend in lake water temperatures (Fig. 5.4). The daily average for the number of adult eel migrating was 18 individuals (median of 5). The maximum count was 813 (17th September 2007). The P66 and P95 daily downstream migrations were 9 and 80 eels respectively. Downstream migrations of eel were recorded all year round. However, the highest numbers (in the order of the P95) were recorded between August and November. The P66 and P95 metrics established for all three fish migrations were representative of all annual cycles of the 17 years of the historical period of this study (Fig. 5.8).

Table 5.1 Average, median, maximum, P66, and P95 regime fish run counts for the Atlantic salmon downstream, Atlantic salmon upstream, and European eel downstream migrations in the Burrishoole catchment during the historical period of this study. The P66 and P95 time frames indicate the earliest and latest months in a year when the P66 and P95 fish runs have been counted, respectively.

Data: 01/2004 - 11/2020 (n = 6150)	Atlantic salmon downstream	Atlantic salmon upstream	European eel downstream
Average fish run count	90	7	18
Median fish run count	14	3	5
Maximum fish run count in a day	2733	92	813
P66 fish run count	39	6	9
P66 time frame	April to July	June to December	January to December
P95 fish run count	431	27	80
P95 time frame	April to May	June to September	August to November

5.4.4 Water temperature conditions for fish migrations

In general, all six fish migration regimes (P66 and P95 for all three migrations) required the lake water temperatures to be temperate to warm (8.8 - 15.9 °C), with the ranges for the P95 regimes generally being narrower than those for the P66 regimes (Table 5.2). The widest ranges were for eel downstream, reflecting the longer period over which that migration occurred. The salmon upstream migration coincided with the warmest lake water temperatures. In contrast, colder temperatures were associated with the two downstream migrations, with lower range limits in the order of 9.0 °C (Table 5.2). These low temperatures aligned with the onset and end of winter, when eel migration terminated and salmon downstream migration started, respectively.

The cumulative lake water temperature conditions differed for the three different fish migrations. The salmon downstream migration occurred over small and well-constrained ranges of cumulative lake water temperatures for both regimes. In contrast, much larger and broader ranges of cumulative lake water temperatures were associated with the salmon upstream and eel downstream migrations (Table 5.2).

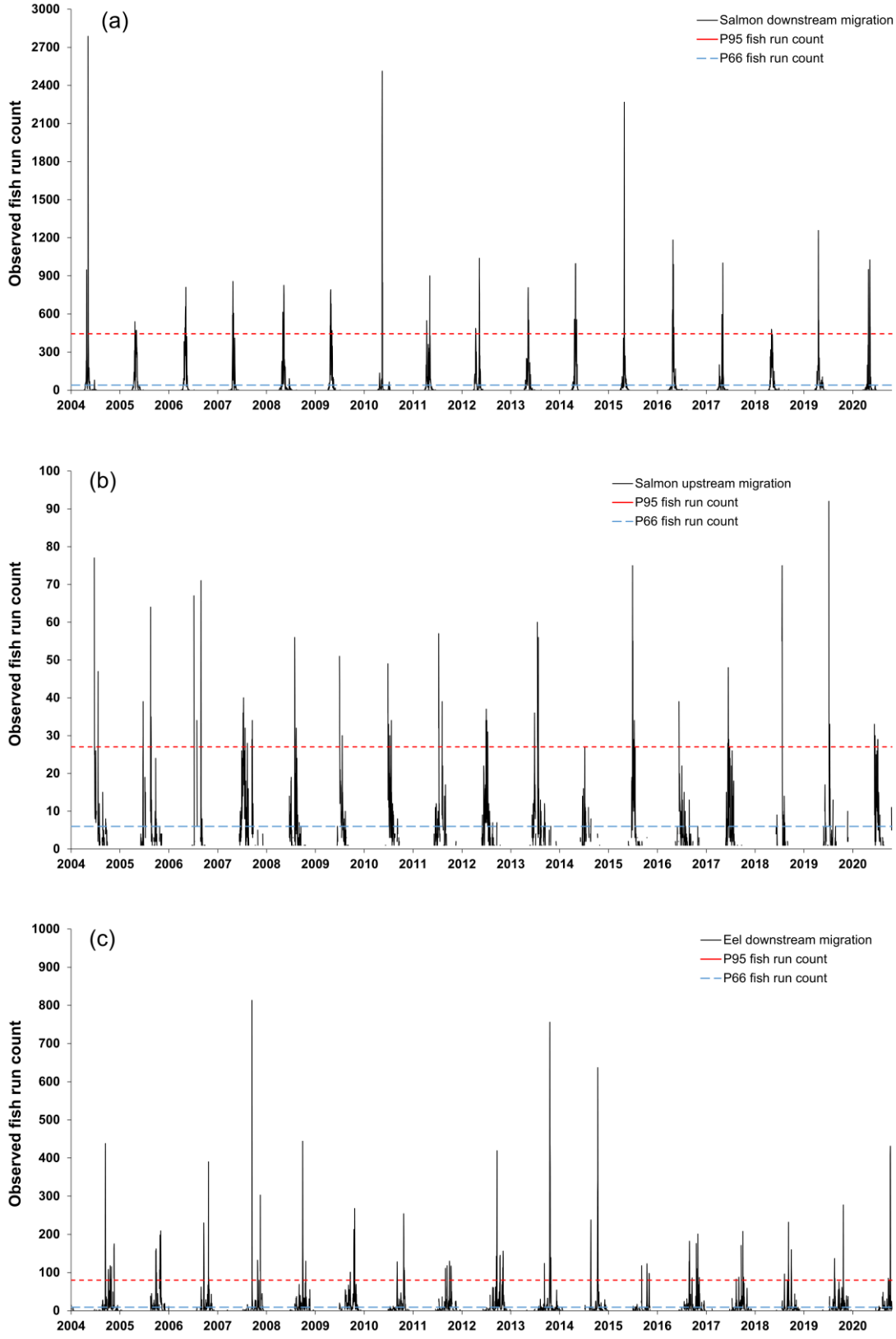


Figure 5.8 P95 and P66 metrics for fish run counts of the (a) Atlantic salmon downstream migration, (b) Atlantic salmon upstream migration, and (c) European eel downstream migration from 2004 to 2020 (historical period of this study).

Table 5.2 Lake water temperature conditions established for the different regimes (P95 and P66) of the Atlantic salmon downstream, Atlantic salmon upstream, and European eel downstream migrations in Lough Feeagh, Burrishoole catchment.

Lake water temperature condition	Atlantic salmon - downstream	
	P95	**P66**
Lake water temperature range (°C)	9.2 - 11.8	8.8 - 12.2
Cumulative lake water temperature range (°C-days)	423 - 679	354 - 720
	Atlantic salmon - upstream	
	P95	**P66**
Lake water temperature range (°C)	13.4 - 15.9	12.8 - 15.8
Cumulative lake water temperature range (°C-days)	1078 - 2122	1053 - 2475
	European eel - downstream	
	P95	**P66**
Lake water temperature range (°C)	10.0 - 15.3	8.9 - 15.6
Cumulative lake water temperature range (°C-days)	2151 - 3132	1746 - 3247

5.4.5 Probabilistic predictions of fish migrations

Using predictions of Atlantic salmon downstream migration for 2021 as an example, the P95 regime predictions generally extended before and after the observed P95 fish runs, however, the observed P66 fish runs were well captured by the forecasts (Fig. 5.9; Fig. 5.10 – Fig. 5.15 display the rest of the forecasts generated for all three fish migrations).

Predictions for shorter horizons displayed relatively large fluctuations in value before and after observed fish run counts reflecting that not only the general block of migrations could be captured but also a degree of day-to-day variations. For instance, European eel predictions for short horizons (< 8-days ahead) displayed much lower probabilities prior to observed events than during events (Fig. 5.14 – Fig. 5.15). Another clear difference among the probabilistic predictions for the different forecast horizons was the order of percentage magnitude, which decreased on average with the horizon (Fig. 5.16).

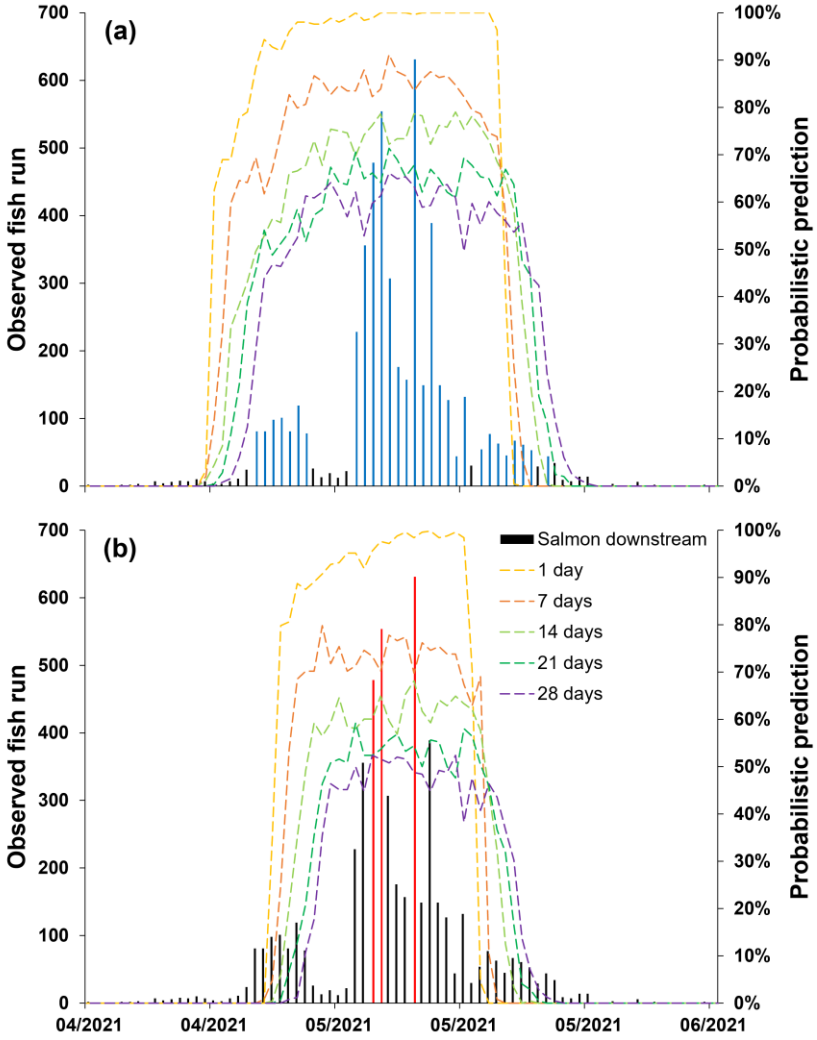


Figure 5.9 Daily probabilistic predictions of Atlantic salmon downstream migration for different forecast horizons (1-, 7-, 14-, 21-, and 28-days ahead) against observed fish run counts during 2021. Panel (a) displays the P66 regime predictions and panel (b) displays the P95 regime predictions. The observed fish run counts equal to or above the historical P66 and P95 fish run counts are highlighted in blue and red in their respective panels.

In general, the P66 regime probabilistic predictions for all three fish migrations performed better, with lower CRPS values, than those for the P95 regimes (Fig. 5.17). The predictions for the salmon downstream migration performed best, starting at a CRPS of 5% followed by a generally linear trend (Fig. 5.17a). However, the score was still under 11% at the end of the forecast. The upstream migration for salmon had the widest range of CRPS values, increasing from 9 to 18% over the forecast. The P66 predictions for eel performed more stably, with CRPS starting at 8% but then remaining

at about 12% from 5-days ahead. In contrast, the performance of the P95 regime predictions across the forecast horizon was not as good. Higher CRPS values were obtained, of up to 31% (Fig. 5.17b). The predictions for eel were the best in this regime, with a narrow CRPS range of values from 13% to 16%. The CRPS values for the two salmon migrations increased steeply in very short horizons (< 5-days ahead) and then continuously decreased.

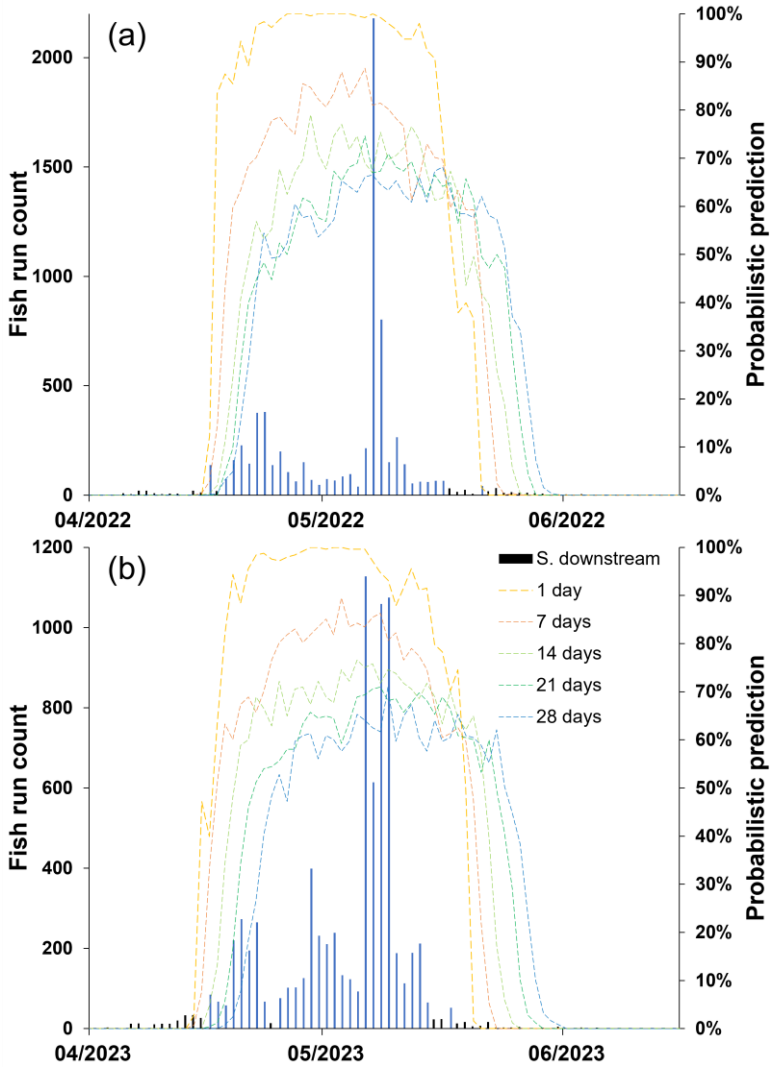


Figure 5.10 P66 regime daily probabilistic predictions for the Atlantic salmon downstream migration for different forecast horizons (1-, 7-, 14-, 21-, and 28-days ahead) against observed fish run counts during (a) 2022 and (b) 2023. The observed fish run counts equal to or above the historical P66 historical fish run are highlighted in blue.

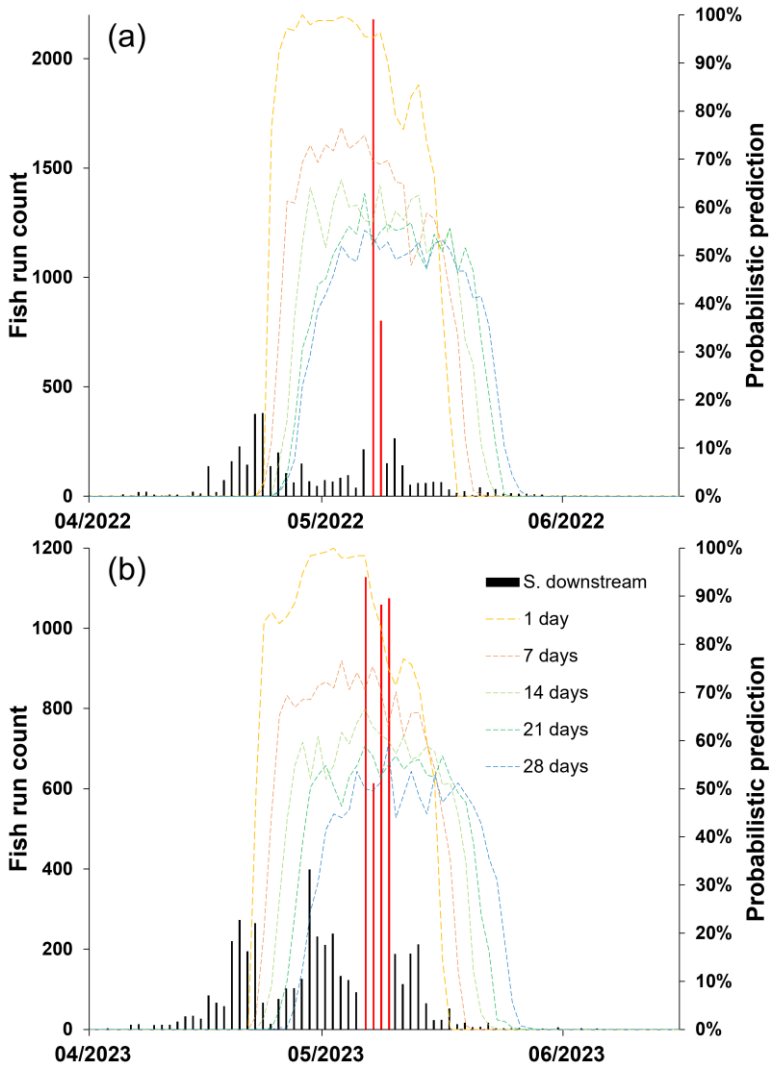


Figure 5.11 P95 regime daily probabilistic predictions for the Atlantic salmon downstream migration for different forecast horizons (1-, 7-, 14-, 21-, and 28-days ahead) against observed fish run counts during (a) 2022 and (b) 2023. The observed fish run counts equal to or above the historical P95 historical fish run are highlighted in red.

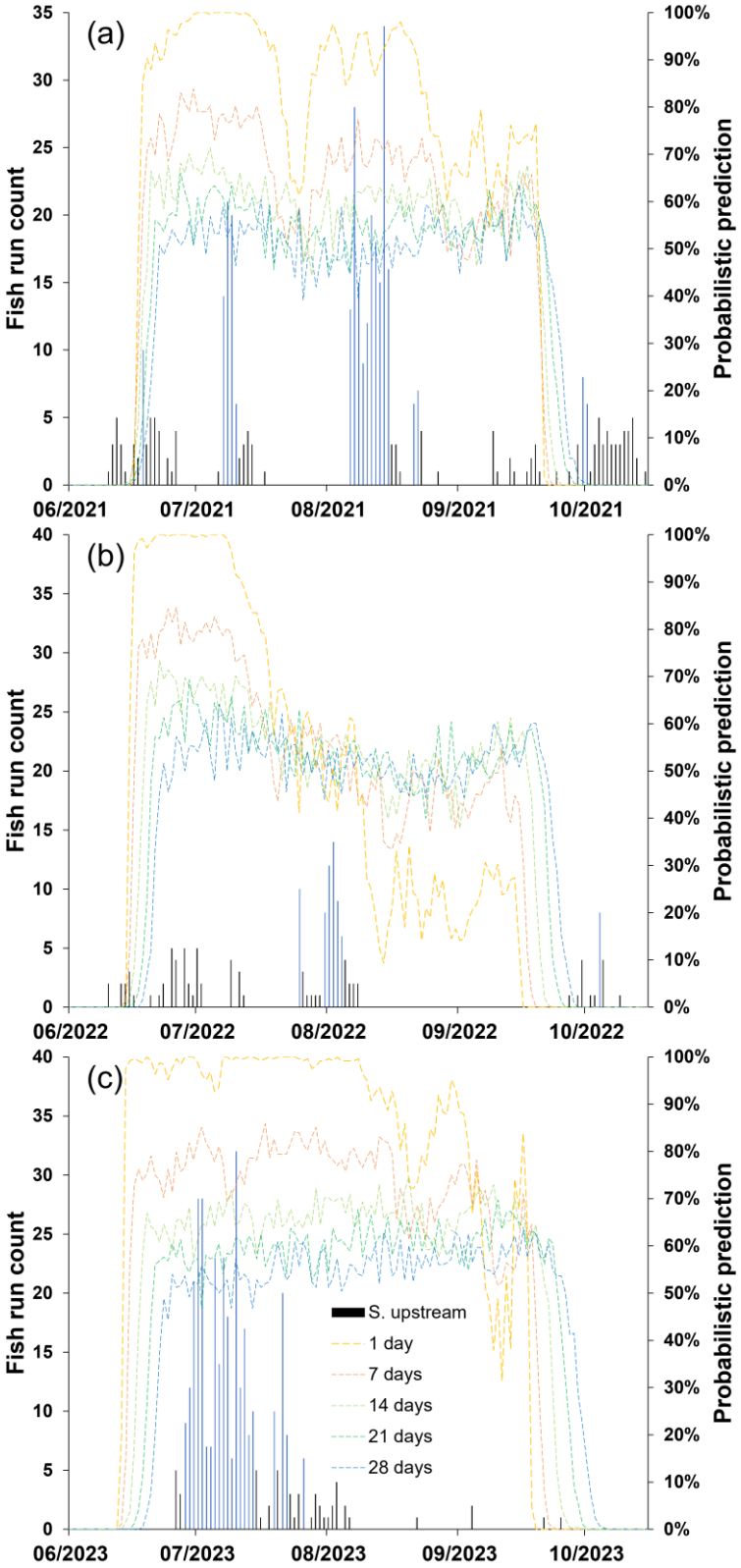


Figure 5.12 P66 regime daily probabilistic predictions for the Atlantic salmon upstream migration for different forecast horizons (1-, 7-, 14-, 21-, and 28-days ahead) against observed fish run counts during (a) 2021, (b) 2022 and (c) 2023. The observed fish run counts equal to or above the historical P66 historical fish run are highlighted in blue.

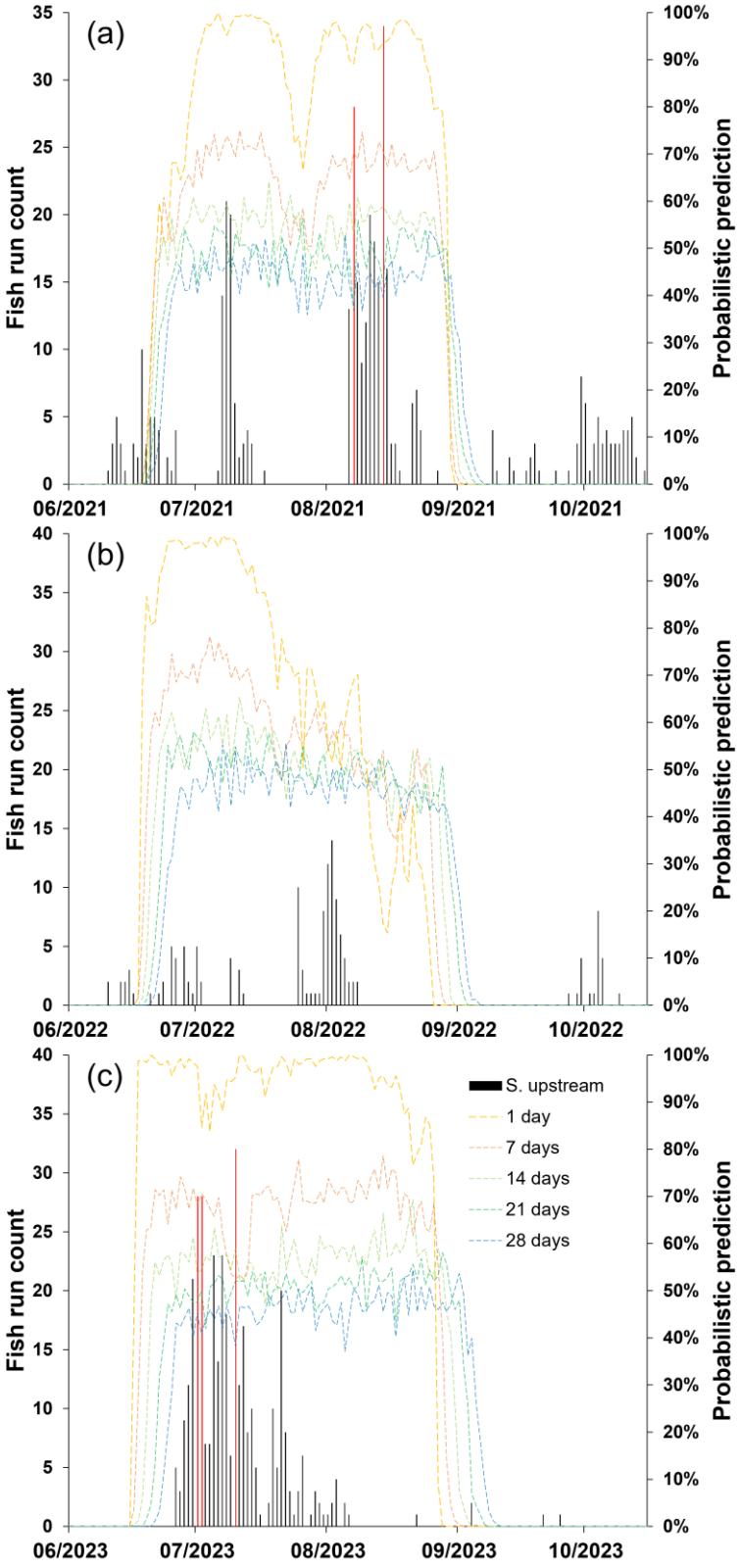


Figure 5.13 P95 regime daily probabilistic predictions for the Atlantic salmon upstream migration for different forecast horizons (1-, 7-, 14-, 21-, and 28-days ahead) against observed fish run counts during (a) 2021, (b) 2022 and (c) 2023. The observed fish run counts equal to or above the historical P95 historical fish run are highlighted in red.

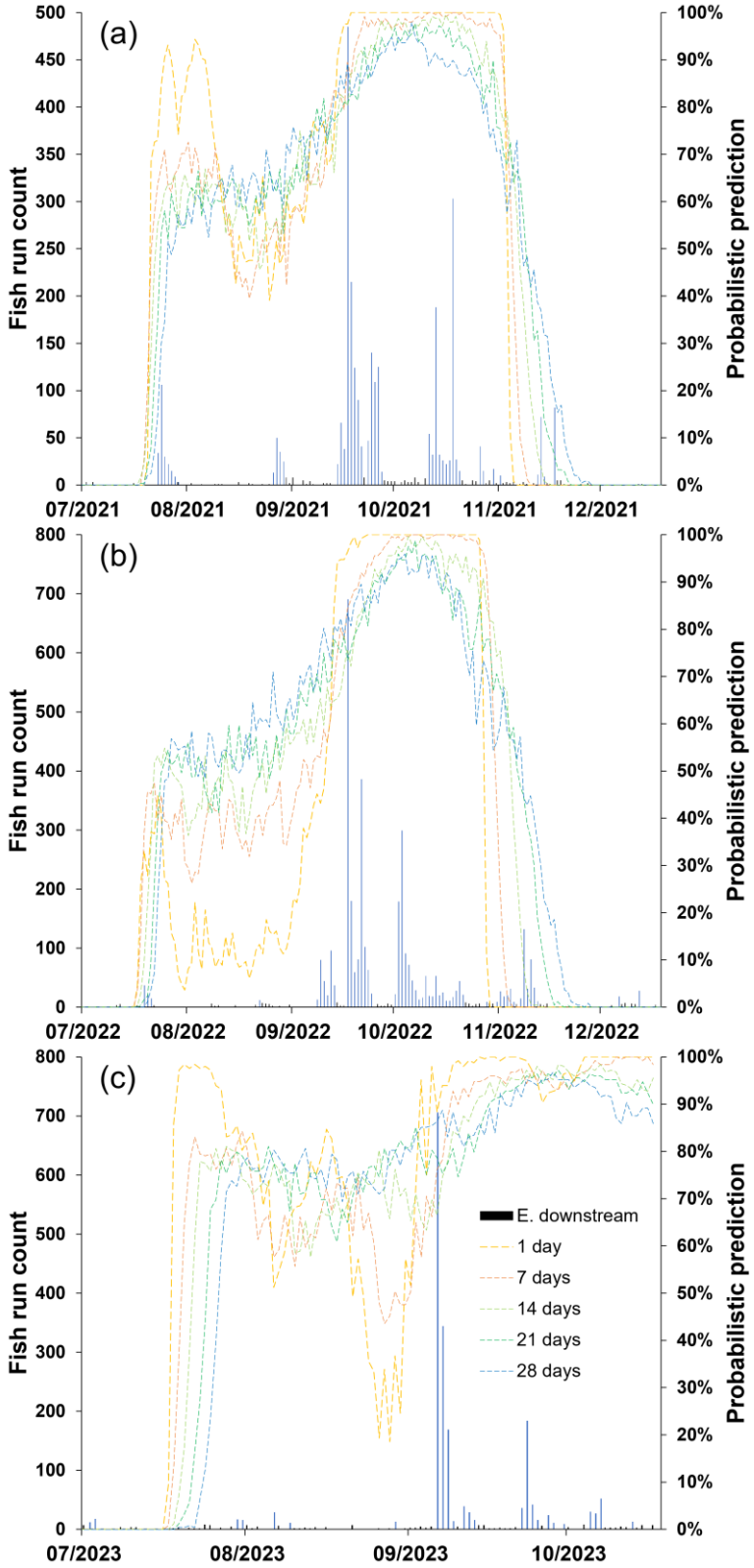


Figure 5.14 P66 regime daily probabilistic predictions for the European eel downstream migration for different forecast horizons (1-, 7-, 14-, 21-, and 28-days ahead) against observed fish run counts during (a) 2021, (b) 2022 and (c) 2023. The observed fish run counts equal to or above the historical P66 historical fish run are highlighted in blue.

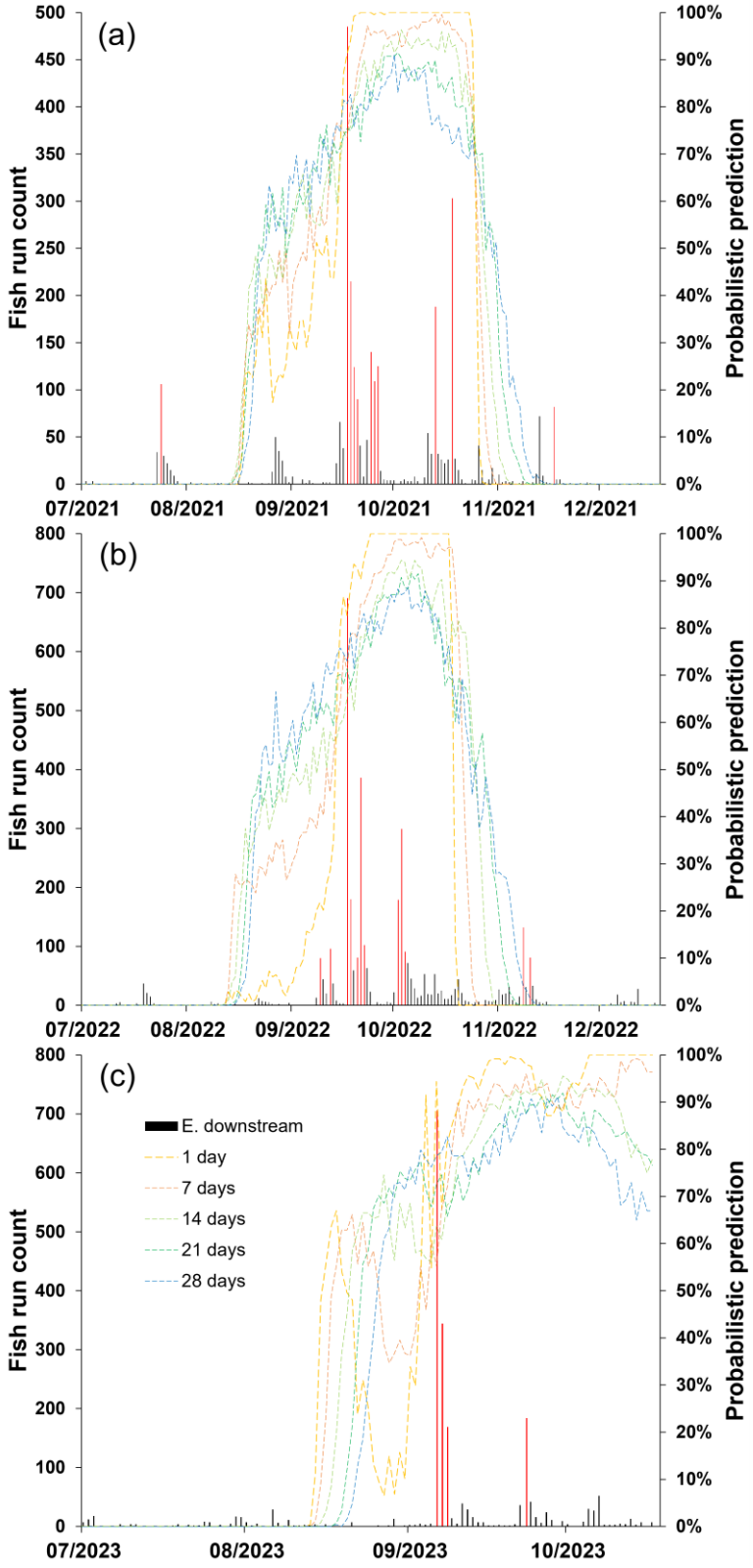


Figure 5.15 P95 regime daily probabilistic predictions for the European eel downstream migration for different forecast horizons (1-, 7-, 14-, 21-, and 28-days ahead) against observed fish run counts during (a) 2021, (b) 2022 and (c) 2023. The observed fish run counts equal to or above the historical P95 historical fish run are highlighted in red.

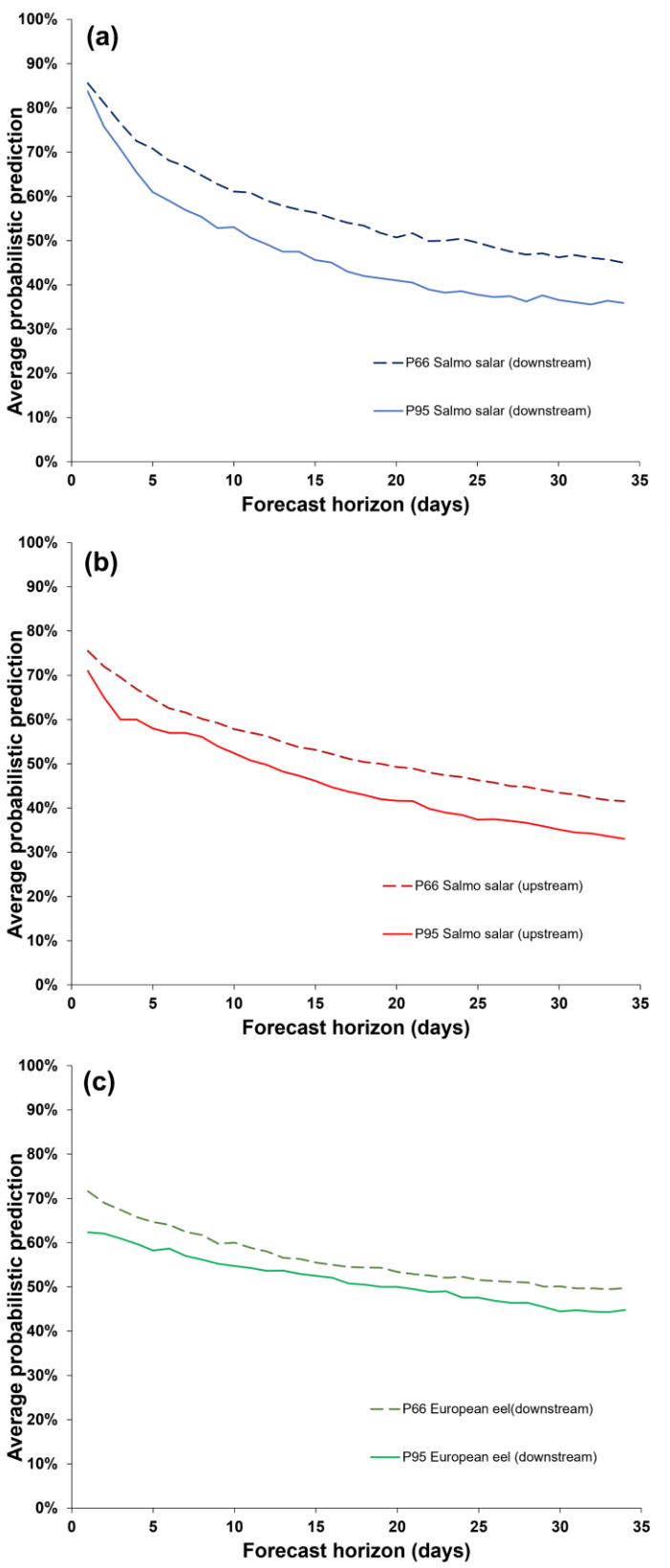


Figure 5.16 Average probabilistic predictions for each forecast horizon of (a) Atlantic salmon downstream, (c) Atlantic salmon upstream and (3) European eel downstream migrations during the entire forecasting period.

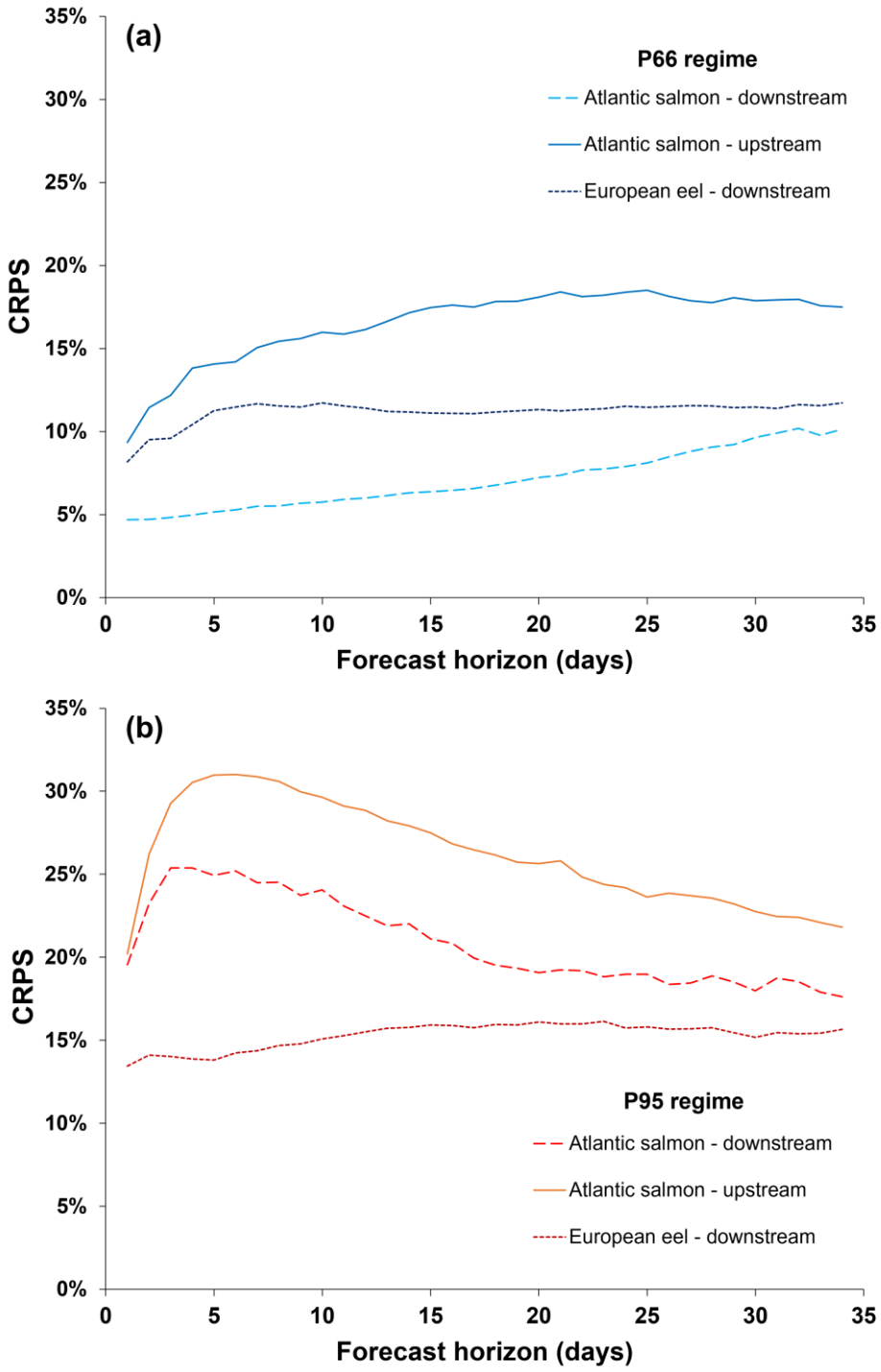


Figure 5.17 Continuous ranked probability score (CRPS) of the P66 (a) and P95 (b) probabilistic predictions of Atlantic salmon downstream, Atlantic salmon upstream, and European eel downstream migrations produced over the entire forecasting period.

5.5 Discussion

Accurate ecological forecasts and associated uncertainty have the potential to aid management in an increasingly uncertain world, including decisions on the allocation of resources for fish monitoring programmes. This study shows that the FLARE system accurately replicated lake temperature dynamics in the study lake, forecasts which were used to produce reasonable probabilistic predictions for three fish migrations up to 34 days into the future, with the best results being for the P66 regime of Atlantic salmon downstream migration (Fig. 5.9 – Fig. 5.15). Enhancing decision-making in freshwater management with such forecasts has the potential to yield not only environmental but also economic benefits as it can allow more appropriate allocation of human and economic resources (Baker et al., 2020; Z. Xu et al., 2020; Franklin et al., 2024). A forecast of fish migration with associated probability produced today for the subsequent seven to ten-day period, for example, could allow an operator to plan resource allocation in advance. This could be particularly relevant for lakes and reservoirs that have been modified for different purposes (e.g., navigation, drinking water supply, flood control, hydropower, aquaculture) where daily or sub-daily operational actions are needed to ensure the protection of diadromous fish (Harris et al., 2016; Carter et al., 2023; Norman et al., 2023).

Although this study case was for a catchment with a relatively low degree of human intervention, the approach is transferrable to catchments where daily management of fish migrations is considered crucial to their survival (Bolstad et al., 2021; Ouellet et al., 2022). With informed fish migration regime forecasts, various mitigation measures can be evaluated for improved conservation of diadromous fish. Forecasts for relatively short horizons (e.g., < 14-days ahead) could enhance daily-scale actions such as the operation of fish passage structures in drinking water reservoirs (Piper et al., 2013; Song et al., 2019), scheduling of dam releasing in flood control (Katopodis and Williams, 2012; Trancart et al., 2020), and periodic pumping and turbine shutdowns in hydropower

(Nyqvist et al., 2017; Carter et al., 2023). Forecasts for longer horizons (e.g., > 14-days ahead) could be more relevant for (but not limited to) the control of nature-like fishways (Steffensen et al., 2013), planning of fishing timings in aquaculture (Gargan et al., 2015; Harringmeyer et al., 2021), and routine operation of fish traps/racks in monitoring and research (Piper et al., 2020; Ruokonen et al., 2022).

While many studies have simulated diadromous fish migrations, there are few that have developed true forecasts with quantified uncertainty, especially on a daily time scale. By using lake water temperature as a core variable, this study expands the available pool of near-term ecological forecasting tools for predicting fish migrations (e.g., King et al. (2023) and Teichert et al. (2020b); two previous frameworks that were developed using river hydrologic connectivity data). Importantly, the forecasting framework presented is flexible. It can be adapted with site-specific information to anticipate local fish migration regimes and therefore inform decisions as to when mitigation measures should be applied. An optimal approach to implement and adapt it would be with a human-centred design to supply context-dependent management needs (Carey et al., 2022; Lofton et al., 2023).

Mitigation measures for migrating fish will differ between sites depending on many factors e.g., management concerns, ecological status, infrastructure, financial options, socio-economic conditions, and regulatory frameworks (Tamario et al., 2019). Although two specific regimes were forecasted in this study, P66 and P95, other tailored solutions could be explored as appropriate. Such a modelling framework could also allow scenario testing to be undertaken for the upcoming management period. For example, trade-offs between the requirements of different stakeholders and sectors could be evaluated, aiming to achieve sustainability in management practices and production systems (Franklin et al., 2024).

5.5.1 Uncertainty in the predictions

Including uncertainty in forecasts and communicating that uncertainty to stakeholders is a critical aspect of successful ecological forecasting (Dietze et al., 2018; Lewis et al., 2022a). The forecasts generated with the presented framework will have uncertainty related to both aspects of the workflow: water temperature and fish migration. In general, the water temperature forecasts performed very well at the lake study site (with a low RMSE), although uncertainty estimates tended to be slightly underconfident, especially in shorter horizons (Fig. 5.7). This is likely due to overfitting observations during data assimilation, a factor that is relatively common in model-based forecasting frameworks (Zwart et al., 2023; Wander et al., 2024). Water temperature forecast uncertainty also increased for longer time horizons (see Fig. 5.3), again a common feature of ecological forecasting. A partitioning of uncertainty could be used in future work to quantify the relative contribution of different sources to total uncertainty so that key areas for improvement could be identified (Wander et al., 2024). Previous studies have reported that the ability of FLARE to reproduce water temperatures (i.e., model process) and the error related to the meteorological driver data contributed most to total uncertainty, especially in longer horizons (Thomas et al., 2020). The results presented in this study performed similarly to other deployments of FLARE for surface water temperature forecasting (Thomas et al., 2020, 2023b; Wander et al., 2024), which is reassuring, as this was the first application of FLARE for forecasting volume-averaged lake water temperature and cumulative water temperature.

The uncertainty associated with the water temperature forecasts will feed into the fish migration forecasts, while additional uncertainty will be related to how well water temperature acts as a control of fish movements. Although water temperature is a key driver of diadromous fish migrations, it is of note that it is only one of a suite of variables that act together (Sandlund et al., 2017; Tamario et al., 2019; Teichert et al., 2020a). The degree to which a change in water temperatures will trigger fish run events is difficult

to quantify even under completely controlled conditions (Sparks et al., 2019) because of its intrinsic interactions with other triggering variables (Zydlewski et al., 2014). Despite these complexities, the presented framework was still able to (1) represent historical fish migrations through the use of the P66 and P95 metrics, as these accounted for events in all 17 years of migration data (see Fig. 5.8), and (2) hindcast migration extent and timing relatively well, especially for the P66 regime. It is of note that the temporal distribution of the probabilistic predictions for all three migrations was somewhat restricted by the cumulative lake water temperature condition. However, relying solely on ambient lake water temperature as a condition would have been problematic. Predictions for the salmon downstream migration, for example, would then have extended not only from April to July for this site but also included November to January, a period with no observed fish runs. The use of a combination of both lake water temperature metrics as conditions to trigger the diadromous fish migrations was therefore more prudent.

The probabilistic predictions for all three fish migrations based on P66 regimes performed best, again with a decrease in performance for longer forecast horizons. In contrast, a different pattern was observed for the more extreme P95 regimes, where the performance of the salmon migration predictions increased for longer horizons. This may appear counterintuitive, however, since the magnitudes of the predictions decreased with the horizon what these increases in CRPS performance mean is that the fish runs were overestimated less in longer horizons (representing fewer prediction fails). This occurred because the P95 daily probabilistic predictions tended to overextend around P95 fish run observations throughout the forecasting period (see Fig. 5.9 – Fig. 5.15) and higher probabilities are penalised more on days with no observed P95 fish run than lower probabilities in the CRPS metric. The absolute magnitude difference between 0% (no observed P95 fish run) and 55% (longer horizon

daily probability) is smaller than with 82% (shorter horizon daily probability), for example, favouring the CRPS metric.

There were also differences in performance across the selected migrations, with a lower performance for the salmon upstream migration, especially for the P95 regimes. This may have reflected stochasticity in fish migration dynamics (Baldursson, 1991; Lewy and Nielsen, 2003). For instance, during the forecasting period, a limited number of salmon upstream runs (five in total) fell within the range of the historical P95 runs. Consequently, there was a clear overestimation of theP95 for salmon migrating upstream. For example, P95 events were predicted from June to September 2022 when no P95 upstream runs were observed (see 5.13b) It is likely that runs with very large numbers migrating upstream are more controlled by factors other than temperature (e.g., increased water flow enabling catchment upstream accessibility) (Milner et al., 2012). Moreover, adult salmon going upstream will have experienced marine temperatures before migrating (Jonsson and Jonsson, 2009). This may induce different phenotypical responses than in fish undertaking downstream migration, which will have been regulated by temperatures in the freshwater environment.

5.5.2 Scalability and further development

The presented framework provides an initial step that can be built on, not only at this lake study site but also potentially at other sites. It has several advantages that increase its potential to be scalable to other settings.

First, a large number of lakes and reservoirs globally already monitor water temperature with a range of different methods (e.g., point measurements, profilers, thermistor chains) (Piccolroaz et al., 2024). This includes sites that are important for diadromous fish (Tickner et al., 2020; Ouellet et al., 2022) and where available data for fish runs could provide points of reference for testing the framework (Nyqvist et al., 2017; Teichert et al., 2020a, 2020b; Piper et al., 2020). Furthermore, data-poor sites could implement the necessary water temperature monitoring relatively easily, as temperature is one of the

initial and least resource-consuming parameters included in monitoring programmes (Peñas et al., 2023). A critical point in other settings would be to investigate site-specific temperature conditions for fish migration at other sites. Indeed, by undertaking a comparison with other lakes with fish migration data, it could be possible to identify general conditions so that the approach could be applied even in locations which do not monitor fish counts but have water temperature monitoring.

A second aspect that facilitates the application of the framework at other sites is its use of cyberinfrastructure. Having the framework set up in the cloud provides additional flexibility and utility, especially as more advanced modelling techniques and forecasting approaches emerge. For instance, other lake water temperature models than GLM could be tested within FLARE (Olsson et al., 2024), or weather forecast products could be used as driver data. Having the framework online also allows remote management and troubleshooting which may lead to lower maintenance efforts than on more traditional systems (Fer et al., 2021; Recknagel, 2023).

Additionally, the forecasting framework can operate iteratively and automatically. The production of forecasts does not require manually triggered actions unless wanted, rather it can work with scheduled actions in online repositories. This feature is particularly relevant because, once the system is set up and its accuracy assessed, its automation can facilitate the dissemination of both water temperature and, in this example, fish migration forecasts to operators and managers. This also enables forecasts to be easily reproduced, archived, and used in the future for research and to facilitate collaboration (Dietze et al., 2018; Carey et al., 2022; Lofton et al., 2023).

5.6 Conclusions

This study provides an investigative example of near-term (daily-scale) ecological forecasting of freshwater species (here, Atlantic salmon and European eel) using water temperature as an environmental driver. It was demonstrated that daily lake water temperature forecasts could be translated into fish migration predictions extending up to 34 days ahead. While such predictions and their associated uncertainty would need to be put in context for local users, it is proposed that a similar approach could assist ecological forecasting and management applications at other sites where understanding the dynamics of fish migration has management implications. It, therefore, has the potential to contribute to adaptation in freshwater management in a time of increasing global change.

Chapter 6

Insights on short-term process-based forecasting of dissolved organic carbon concentration in a temperate river across seasons

---

Ricardo Paíz[a], Donald C. Pierson[b], R. Quinn Thomas[c,d,e], Cayelan C. Carey[c,e], Elvira de Eyto[f], Mary Dillane[f], Valerie McCarthy[g], Suzanne Linnane[a], Eleanor Jennings[a]

[a]Centre for Freshwater and Environmental Studies, Dundalk Institute of Technology, A91 K584, Co. Louth, Ireland

[b]Department of Ecology and Genetics – Limnology, Uppsala University, 75236 Uppsala, Sweden

[c]Department of Biological Sciences, Virginia Tech, Blacksburg, Virginia, USA

[d]Department of Forest Resources and Environmental Conservation, Virginia Tech, Blacksburg, Virginia, USA

[e]Center for Ecosystem Forecasting, Virginia Tech, Blacksburg, Virginia, USA

[f]Fisheries & Ecosystem Advisory Services, Marine Institute, F28 PF65 Newport, Co. Mayo, Ireland

[g]School of History and Geography, Dublin City University, D09 YT18, Dublin 9, 9, Ireland

---

6.1 Abstract

Access to forecasts of short-term changes in water quality could provide an important tool for managing drinking water. This study explores the short-term (daily-scale) forecasting of dissolved organic carbon (DOC), a proxy for dissolved organic matter, which is a precursor of disinfection by-products in chlorine-treated water. For this, a recently available ensemble-based weather forecast product was used in conjunction with a process-based model to forecast DOC concentrations in river water for sequential 35-day periods. The Generalised Watershed Loading Functions Model and coupled DOC module (GWLF-DOC) were first calibrated for an Irish study site using long-term observational data. Then, two differing workflows for forecast generation were explored. In one, both the DOC model parameters and DOC model initial conditions were calibrated during the assimilation step for new data, while in the other, only the initial conditions were calibrated. The forecasts were evaluated using a range of metrics along the forecast horizon (1- to 35-days ahead) and on a seasonal basis (spring, summer, autumn and winter). The two workflows were also compared to a third baseline model: Site Persistence (i.e., predictions based solely on recurring conditions for day 1). The predictive skill differed throughout the annual cycle depending on the method and forecast horizon, with large differences both between the two workflows and relative to Site Persistence, especially during wetter periods (autumn and winter). The results indicated that calibrating a large number of target variables does not translate into improved accuracy and uncertainty estimation in process-based short-term forecasting of DOC, while factors such as the forcing data and the model structure may also have important implications. All these insights are discussed in the context of further development of short-term forecasting for DOC water quality and their usefulness for operational water management.

Keywords: Ecological forecasting; Water quality modelling; DOC; GWLF; Water management

6.2 Introduction

Many human activities that rely on water availability could benefit from short-term ecological forecasts (i.e., hour-to-decadal future predictions of environmental conditions with quantified uncertainty) (Carey et al., 2022; Lewis et al., 2022). While predictions of water quantity are widely employed, there is less availability of tools and approaches for predicting short-term changes in water quality (Loos et al., 2020; Lofton et al., 2023). Although water quantity and quality are intrinsically linked (van Vliet et al., 2017), forecasting water quality is generally more challenging as it often derives from water quantity modelling frameworks and results from relatively more complex interactions in the environment (Loos et al., 2020; van Vliet et al., 2023). Different water quality variables encompass unique challenges, each exhibiting variability in key drivers of their dynamics and responses to environmental change (Nallakaruppan et al., 2024). Consequently, there are fewer applications of water quality forecasts than water quantity forecasts (Lofton et al., 2023). However, advancements in technology (e.g., sensor technologies, cyberinfrastructure and software) have created new opportunities for their development, offering the potential to assist operational management (Dietze et al., 2018, 2024).

Recent work on short-term water quality forecasting has focused on variables such as water temperature, dissolved oxygen, chlorophyll a, phosphorus and turbidity across diverse water systems (e.g., rivers, lakes, reservoirs and distribution networks) for assisting management in different sectors (e.g., water supply, hydropower, fisheries and agriculture) (Carey et al., 2022; Liu et al., 2023; Lofton et al., 2023; Kiani and Ylivainio, 2024). However, other water quality variables, such as dissolved organic carbon (DOC), have received less attention despite their relevance for water management (Anderson et al., 2023; Lofton et al., 2023). Concentrations of DOC reflect levels of dissolved organic matter (DOM), a precursor to the formation of disinfection by-products (DBPs), which are toxic compounds formed during chlorination in drinking water treatment

(Köhler et al., 2016; Piai et al., 2024). DBPs such as trihalomethanes (THMs) have adverse effects on human health (Diana et al., 2019; Kumari and Gupta, 2022) and are a concern for water supplies in several countries (e.g., Australia, Brazil, Canada, Ireland, Spain, Sweden and South Africa) (Villanueva et al., 2023).

Forecasting DOC concentrations in drinking source waters could lead to better water treatment and supply (DeMont et al., 2021; Xiao et al., 2024). The dynamics of DOC in source waters can be very variable depending on the water system and site-specific conditions (Warner and Saros, 2019; Fenner et al., 2021). Riverine DOC concentrations, in particular, tend to exhibit relatively large daily and seasonal fluctuations (Jennings et al., 2020; Wu and Yao, 2022; Wu et al., 2023b) which can make the treatment of such waters difficult (Siddique et al., 2022a; Piai et al., 2024). By anticipating DOC concentrations in operational timeframes (e.g., 1-day ahead to 1-month ahead), managers could enhance a suite of water treatment processes currently used to manage DOM (e.g., coagulation, flocculation, adsorption, degradation and chlorine dosage) that would, in turn, contribute to a reduction in the formation of DBPs (Franklin et al., 2021; Anderson et al., 2023; Siddique et al., 2022a; Daraei et al., 2023). Therefore, the development of frameworks for short-term forecasting of DOC concentration would both advance the science of water quality forecasting and have implications for safe water supply.

Short-term forecasting of DOC concentration could be driven by, for example, statistical, process-based, machine learning or hybrid models. A process-based approach, however, offers the additional benefit of providing insights into system dynamics by simulating variables that influence model outputs (Cuddington et al., 2013; Chen et al., 2021). At the river scale, the use of a process-based model can capture catchment-scale DOC dynamics (Naden et al., 2010; Futter et al., 2011), which result from complex interactions induced by hydrology and site characteristics (i.e., climate, landscape and land use) (Jennings et al., 2010; Adler et al., 2021; Wit et al., 2021). Furthermore,

emerging techniques used in short-term forecasting (e.g., observed data assimilation and use of high-frequency monitoring) combined with higher availability of forecast data used to drive the models (e.g., ensemble weather forecast products) make it more feasible to apply such an approach (Chen et al., 2021; Whitehead et al., 2024). These advancements also better facilitate the quantification of uncertainty in the predictions (Dietze, 2017) and the exploration of the suitability of the model structure for forecasting (Lofton et al., 2023).

When forecasting water quality (here DOC) using a process-based approach, it is especially important to consider how the model parameterisation (i.e., the model state variables and parameter selection) responds to the forcing data (Beven, 2009; Paíz et al., 2025). Differing values for model parameters and initial conditions could yield completely different results during model simulations or, in contrast, similarly good ones (i.e., model equifinality) (Beven and Binley, 1992, 2014). These issues, which are intrinsic to process-based modelling frameworks (Cuddington et al., 2013), could affect future predictions and thus their impact on forecasting accuracy should be explored. This could allow the identification of actions for improvement in the forcing data, model calibration, data assimilation steps and/or the modelling workflow in order to generate more accurate predictions for end users.

In this study, two process-based workflows for forecasting DOC concentration were tested, compared and contextualised using a third baseline model: Site Persistence (i.e., predictions based solely on past site conditions) (Jolliffe and Stephenson, 2012). Note that the terms workflow and framework were used interchangeably in this study. The study site was characterised by high variability in discharge and DOC export and therefore represented a challenge for short-term forecasts. The predictions were evaluated against new observations across the typical meteorological seasons, as these are key periods for DOC variability in the study site (Jennings et al., 2020). The main aim of this study was to explore the short-term forecasting of DOC concentration in river

water using a process-based model and evaluate its potential for assisting management applications. Within this context, the objectives were to: (1) design two potential workflows to forecast DOC concentration in the short-term using an ensemble of meteorological forecast data, and (2) quantify forecast performance and associated uncertainty for such workflows, and compare to using Site Persistence. The results are discussed in the context of further development and their usefulness for operational water treatment.

6.3 Materials and methods

6.3.1 Study site

The Glenamong River is located in western Ireland (53° 57' N, 9° 35' W) (Fig. 6.1) and is one of the two main inflows to Lough Feeagh, an oligotrophic temperate lake (Doyle et al., 2023). The river catchment is small (18 km²), unpopulated, and in line with the regional landscape, is dominated by peatland and other high organic soils. The interactions among its land cover, climate, and a steep topographic gradient result in high variability in daily river discharge and DOC export (Doyle et al., 2019; Jennings et al., 2020). While the river is not used as a source of potable water, it is an intensively monitored site representative of similar river-sourced drinking water supplies in the region.

6.3.2 The model

The Generalised Watershed Loading Functions Model (GWLF) is a lumped parameter process-based hydrological and water quality model introduced by Haith and Shoemaker (1987). The version of GWLF with an integrated DOC module (GWLF-DOC) used in this study follows the structure described by Paíz et al. (2025). The model simulates catchment hydrology (water balance and water distribution among the different hydrological pathways) and DOC dynamics (DOC production and DOC washout) in a daily time step.

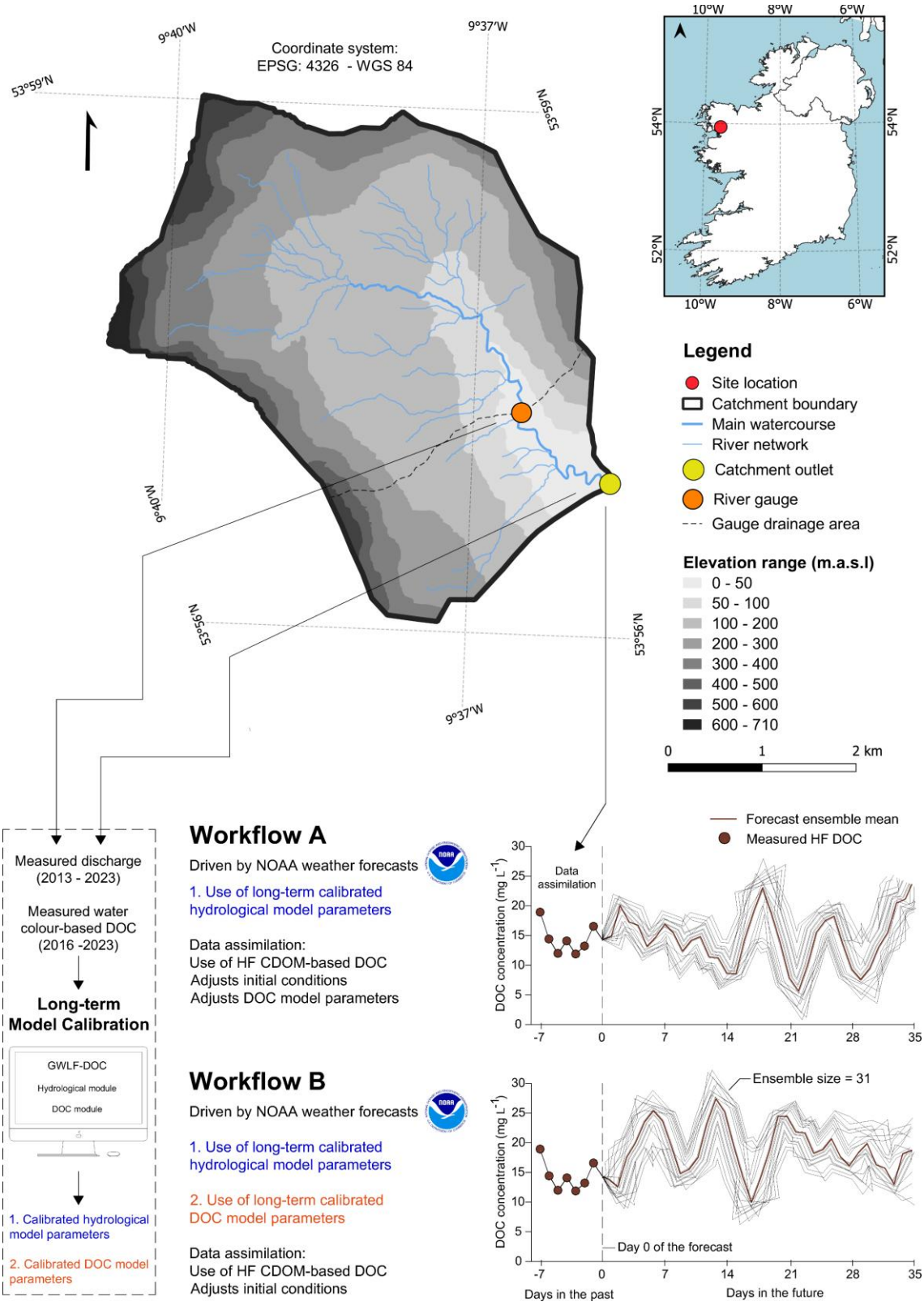


Figure 6.1 Location of the study catchment including river network and topographic elevation, overview of the GWLF-DOC model long-term calibration, and main components of the workflows A and B for forecasting DOC concentration.

Eight parameters regulate the hydrological module while nine regulate the DOC module (four for DOC production and five for DOC washout) (see Table 6.1). The DOC catchment dynamics are simulated using five different carbon pools that represent hydrologically connected reservoirs: (1) the deep saturated zone, (2) the saturated zone, (3) the unsaturated zone, (4) DOC producing surface areas excluding wetlands and (5) wetlands (see Paíz et al., 2025), for which their initial conditions are required to be specified. The hydrological module is dynamically coupled with the DOC module.

The model input requirements include daily time series of two meteorological variables: total catchment precipitation and mean air temperature, as well as land cover, land use, and soil characterisation. GWLF-DOC has been applied to multiple catchments to evaluate long-term changes in DOC dynamics (Naden et al., 2010; Lindqvist, 2022; Paíz et al., 2025). However, to date, the model has not been employed for short-term DOC forecasting.

Table 6.1 Model parameters with their calibration ranges used for each of the model parameters of the hydrology module and DOC module in GWLF-DOC.

Hydrological parameters

	Precipitation correction factor	**River channel flow coeff.**	**Melt coeff.**	**Curve adj. number**
Units	*factor / day*	*coeff. / day*	*cm / °C / day*	*-*
Calibration range	*0.50 - 1.50*	*0.01 - 1.00*	*0.05 - 0.60*	*-10.0 to 10.0*

	Soil water capacity	**Baseflow capacity**	**Slow recess coeff.**	**Recess coeff.**
Units	*cm*	*cm*	*coeff. / day*	*coeff. / day*
Calibration range	*12.00 - 20.00*	*2.50 - 8.00*	*0.001 - 0.100*	*0.005 - 0.030*

DOC parameters

DOC production

	Activation energy (E_a)	**Aerobic decomp. rate** (b)	**Anaerobic decomp. rate** (a)	**Anaerobic decomp. rate (wetlands)** (a_w)
Units	*kJ / gC*	*-*	*gC / m² / day*	*gC / m² / day*
Calibration range	*3.0 - 7.0*	*1.0 - 7.5*	*0.005 - 0.15*	*0.005 - 0.15*

DOC washout - runoff

	Surface carbon loss coeff.	**Surface flow cap**
Units	*coeff. / day*	*cm*
Calibration range	*0.01 - 1.00*	*0.01 - 6.00*

DOC washout - baseflow

	Baseflow ratio	**Fast groundwater carbon loss coeff.**	**Slow groundwater carbon loss coeff.**
Units	*fast- to slow- groundwater ratio / day*	*coeff. / day*	*coeff. / day*
Calibration range	*0.01 - 1.00*	*0.001 - 1.000*	*0.001 - 1.000*

6.3.3 Data availability

6.3.3.1 Data for the model long-term calibration

Climate observations were obtained from a local meteorological station (2013 – 2023) (station 1175, Newport; www.met.ie). Daily river discharge data (2013 to 2023) and a long-term monitoring dataset of estimated DOC concentration at the river outlet based on water colour (2016 – 2023) were obtained from the Marine Institute's long-term monitoring program at the catchment (http://burrishoole.marine.ie). Water colour-based DOC data were converted from weekly water colour measurements based on absorption and expressed as mg PtCo L^{-1}, via a linear regression relationship with DOC measured in the laboratory: DOC = 0.07 water colour + 2.7, r^2 = 0.88, n = 551 (Doyle et al., 2019). The water colour measurements were performed using a HACH Dr 2000 spectrophotometer at 455 nm (wavelength accuracy of ±2 nm) on water filtered through Whatman GF/C filters (1.2 µm pore size).

6.3.3.2 Data for the forecasting

A second estimated DOC dataset was used in the forecasting workflows of this study, this time based on higher frequency sensor-based measurements of chromophoric dissolved organic matter (CDOM) (2020 – 2023) (see Fig. 6.2). CDOM-based DOC data were converted from daily averaged high-frequency CDOM data (raw data interval: 2-minute). These were first temperature-corrected and then converted to DOC using a linear regression relationship with DOC laboratory measurements: DOC = 0.13 CDOM – 6.46, r^2 = 0.48, n = 1570 (Jennings et al., 2020). The data were collected using a Seapoint UV fluorometer sensor (Seapoint Sensors Inc., Exeter, NH, USA) and river water temperature data was measured using a TidbiT v2 Water Temperature Data Logger UTBI-001 (LiCOR). The Seapoint CDOM fluorometer used UV light emitting diodes (LEDs) as the CDOM excitation source (excitation wavelength of 370 nm CWL, 12 nm FWHM; emission wavelength of 440 nm CWL, 40 nm FWHM, where CWL is the centre wavelength and FWHM is the full width at half maximum wave height).

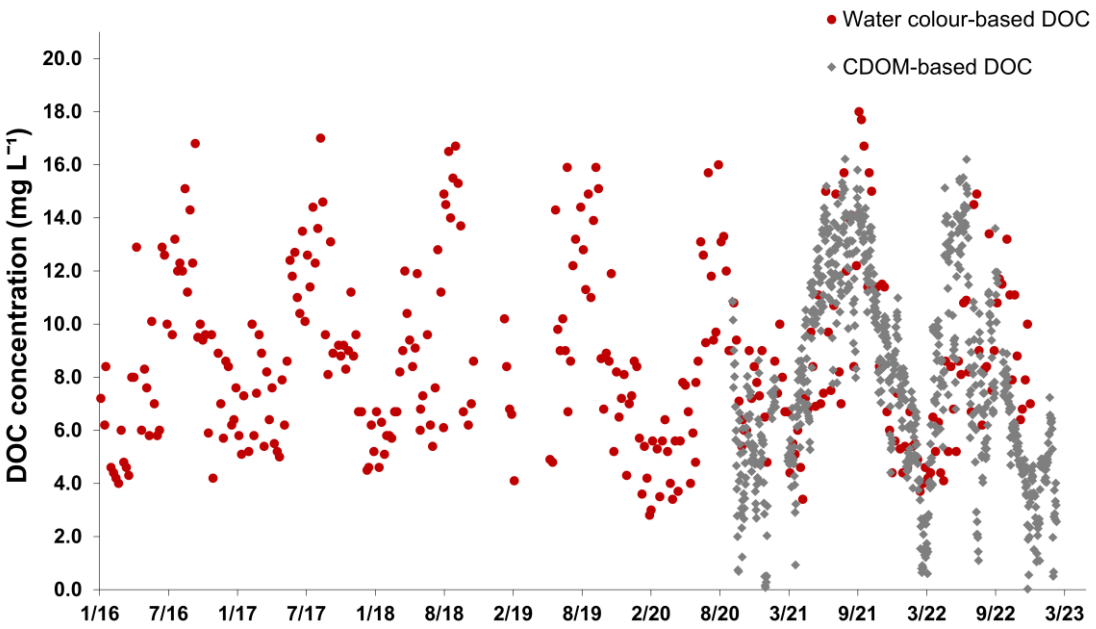


Figure 6.2 Observed and simulated daily river discharge during the model calibration and validation of the hydrology module of GWLF-DOC (a), and observed and simulated daily DOC concentration during the model calibration of the DOC module of GWLF-DOC (b) for the Glenamong catchment.

The weather forecast data product used to drive the forecasting was the open-access 31-member National Oceanic and Atmospheric Administration Global Ensemble Forecasting System (0.5° NOAA GEFS) (www.ncei.noaa.gov) (Hamill et al., 2022) output for the grid-cell that contains the Glenamong catchment. This product provided daily ensemble forecasts 1 out to 35 days lead time.

6.3.4 Model long-term calibration

Measured river discharge data were used to calibrate and validate the hydrological module (2013 –2018 and 2019 – 2023 respectively) and the longer record of estimated DOC data i.e., the water colour-based DOC data were used to calibrate the DOC module (2016 – 2023). The calibration was performed using the multistep script-based optimisation strategy employed by Paíz et al. (2025), for which daily observed meteorological inputs (total precipitation and mean air temperature) were used as forcing data. GWLF-DOC was run within VENSIM software (Ventana Systems Inc.) on a daily time step. The calibration range limits to adjust each of the eight hydrological and

nine DOC model parameters are displayed in Table 6.1, and were those defined by Paíz et al. (2025), which were based on previous modelling studies and relevant literature (e.g., Evans et al., 2006; Karhu et al., 2010; Naden et al., 2010; Klimek et al., 2020; Lindqvist, 2022). A model spin-up period of two years was used to adjust the initial conditions of the DOC module i.e., the carbon pools. Model performance was evaluated based on root mean squared error (RMSE), the Nash-Sutcliffe coefficient (NSE) and the coefficient of determination (r^2) (Krause et al. 2005) between daily observed and simulated river discharge and DOC concentration.

6.3.5 Workflows for forecast generation

Two ensemble-based short-term forecasting workflows for DOC concentration were defined, hereafter referred to as Workflow A and Workflow B respectively. Forecasts using both workflows were generated starting on every day (each forecast comprising daily values of DOC concentration 1- to 35-days ahead) during two full hydrological years (1st March 2021 – 1st March 2023; 731 days). Both were driven by the NOAA GEFS ensemble-based weather forecast product and shared some features that benefit from the long-term model calibration (Fig. 6.1).

Both workflows incorporated data assimilation for a period of 7 days before the generation of any prediction (day -7 to day 0 of the forecast) (see Fig. 6.1). This 7-day period would allow occasional maintenance work and quality control on the data that were assimilated i.e., high-frequency daily mean CDOM-based estimated DOC. These data were used for the forecasting framework as they were independent of the long-term model calibration and could be available in near real-time for incorporation into the workflow. The Kalman filtering (KF) (Evensen, 2009; Loos et al., 2020a) was the data assimilation algorithm used to combine the DOC measurements and adjust the DOC model parameter values and/or initial conditions. The KF measurement noise for the DOC observations was 3.8 mg L^{-1} (standard deviation).

In Workflow A, all five initial conditions (i.e., the carbon pools) together with the nine DOC model parameters were calibrated during the 7-day data assimilation period in each forecast simulation. In contrast, in Workflow B, only the five initial conditions were calibrated; the nine DOC model parameter values were fixed to those obtained during the long-term model calibration. The ranges used in each were those used during the long-term model calibration. In both Workflow A and Workflow B, the DOC module was forced by the same model hydrology i.e., using the same set of hydrological model parameters obtained during the long-term model calibration (see Fig. 6.1).

Each of the 31 members of the weather forecast ensemble was used to individually force GWLF-DOC. For both workflows, GWLF-DOC was initially run for 5 months (1st Oct 2020 – 28th Feb 2021), a spin-up period for the model during which data assimilation occurred but no forecasts were produced. Then, on each forecast generation (start of the forecasting period: 1st March 2021), all calibrating DOC parameters (Workflow A) and initial conditions (both Workflow A and Workflow B) were continuously adjusted during data assimilation when observed data were available. Thus, for each generated forecast starting on each day after 1st March 2021, an ensemble of 31 model output values for DOC concentration was produced for each forecast horizon day (1-day to 35-days ahead) (see Fig. 6.1).

6.3.6. Forecast input data assessment

The variability and magnitude in all data used for the forecasting i.e., the weather ensemble forecast product, the modelled hydrological forcing for the DOC module and the observed high-frequency based DOC concentrations used for data assimilation, were assessed. Variability was quantified using the standard deviation of the input variables (forecasted catchment precipitation and mean air temperature ensemble), the main modelled hydrological variable (ensemble of modelled total catchment discharge) and the observational variable (observed DOC concentrations) respectively. The magnitude of the variables was assessed using the mean, median and 95th percentile

(as an indicative metric of extreme conditions). In the case of the forcing hydrology, modelled mean daily surface runoff and baseflow contributions to total discharge were also calculated based on the Arnold et al. (1995) hydrograph separation method (Schneiderman et al., 2010).

The assessment was performed on a seasonal basis over the two full hydrological years of the forecasting period (1st March 2021 – 1st March 2023), for which the typical three-month periods were used: spring (March to May), summer (June to August), autumn (September to November) and winter (December to February). In addition, daily ensemble-mean values of the weather forecast product were compared to climate observations from local meteorological stations using RMSE, NSE and r^2 over the forecast horizon in the entire forecasting period.

6.3.7 Model parameters and initial conditions

As a result of the data assimilation for each forecast, an ensemble of 31 sets of calibrated carbon pool initial conditions (Workflow A and Workflow B) and 31 sets of calibrated DOC model parameters (Workflow A) were output in response to the 31-member weather forecast product ensemble, 31-member modelled forcing hydrology ensemble and the available DOC observations. Variability in the calibrated values for the initial conditions was compared between both workflows. In the case of the DOC model parameters, the variability in the calibrated values for Workflow A was compared to the fixed values of Workflow B (i.e., from the long-term DOC module calibration; see Section 6.3.4). For each forecast, the value of each initial condition and each DOC model parameter used for the comparison was the ensemble mean. In addition, the ensemble mean and its respective calibration range were normalised to a range of 0.00 – 1.00. This allowed comparison in relative terms of how calibrated values varied across their entire range using each method. For instance, in the case of a parameter that had a calibration range from 3.00 and 7.00 (i.e., the range for the activation energy; see Table 1), a calibrated ensemble mean value that resulted in 3.00 represented 0.00

(minimum of the normalised range value), while a value of 7.00 represented 1.00 (maximum of the normalised range value).

6.3.8 Forecast evaluation

In line with the model calibration, the forecast performance of each workflow was evaluated based on RMSE, NSE, and r² between daily measured and forecasted DOC concentration. For each forecast, the DOC concentration prediction used for the evaluation on each forecast horizon day (1-day to 35-days ahead) was the ensemble mean, and the forecast uncertainty was quantified as the standard deviation of the ensemble. The evaluation was performed on a seasonal basis accounting for all predictions generated during the full forecasting period.

Importantly, besides comparing the performance of the two process-based forecast workflows, their performance was compared to a non-process-based model: Site Persistence. Predictions based on Site Persistence have been widely used in environmental science as they are relatively easy to generate (Murphy, 1992), and provide an important baseline that enables the performance of new forecasting systems to be contextualised (Yang, 2019; Thomas et al., 2020; Bento et al., 2022).

Persistence predictions were based on the assumption that the DOC concentrations will be the same as in the recent past (Wilks, 2019), i.e., they would vary depending on the forecast horizon. For example, a persistence forecast set with a 12-day forecast horizon and produced on date d will use the observed DOC concentration on date $d-1$ as the Site Persistence value for the following 12 days. In addition, a tercile plot was generated displaying the predictive skill of each method along different forecast horizons and across seasons based on the r² performance scale (0.00 – 1.00). The range of r² describes how much of the observed dispersion is explained by the prediction; a value of zero means no correlation at all whereas a value of 1.00 means that the dispersion of the prediction is equal to that of the observation (Krause et al., 2005).

The uncertainty associated with both Workflow A and Workflow B was also compared on a seasonal basis. Moreover, the number of observations within selected forecast confidence intervals (10^{th}, 25^{th}, 50^{th}, 75^{th}, 90^{th} and 95^{th}) for different forecast horizon days (1-, 7-, 14-, 21-, 28- and 35-days ahead) was calculated following the reliability procedure employed by Thomas et al. (2020) and Zwart et al. (2023).

An ideally calibrated forecasting system would have 10% of observations within the 10% forecast confidence interval (the range containing the middle 10% of the ensemble distribution), 25% of observations in the 25% forecast confidence interval (the range containing the middle 25% values of the ensemble distribution), etc. If the percentage of observations within its given confidence interval is higher or lower, the forecasting would be considered underconfident or overconfident, respectively (Bröcker and Smith, 2007).

6.4 Results

6.4.1 Model long-term calibration performance

The results from the optimisation procedure for both the hydrological module and the DOC module of GWLF-DOC indicated a relatively good model fit at a daily time. The RMSE, NSE and r^2 values for average daily discharge were 7.44 mm day^{-1}, 0.64 and 0.64 respectively for the calibration period, and 7.36 mm day^{-1}, 0.60 and 0.60 respectively for the validation period (Fig. 6.3a). The RMSE, NSE and r^2 values for DOC concentration were 2.49 mg L^{-1}, 0.45 and 0.47 for the calibration period respectively (Fig. 6.3b). The set of calibrated hydrological model parameters and the set of calibrated DOC model parameters obtained from the optimisation procedure including calibration ranges are presented in Table 6.2.

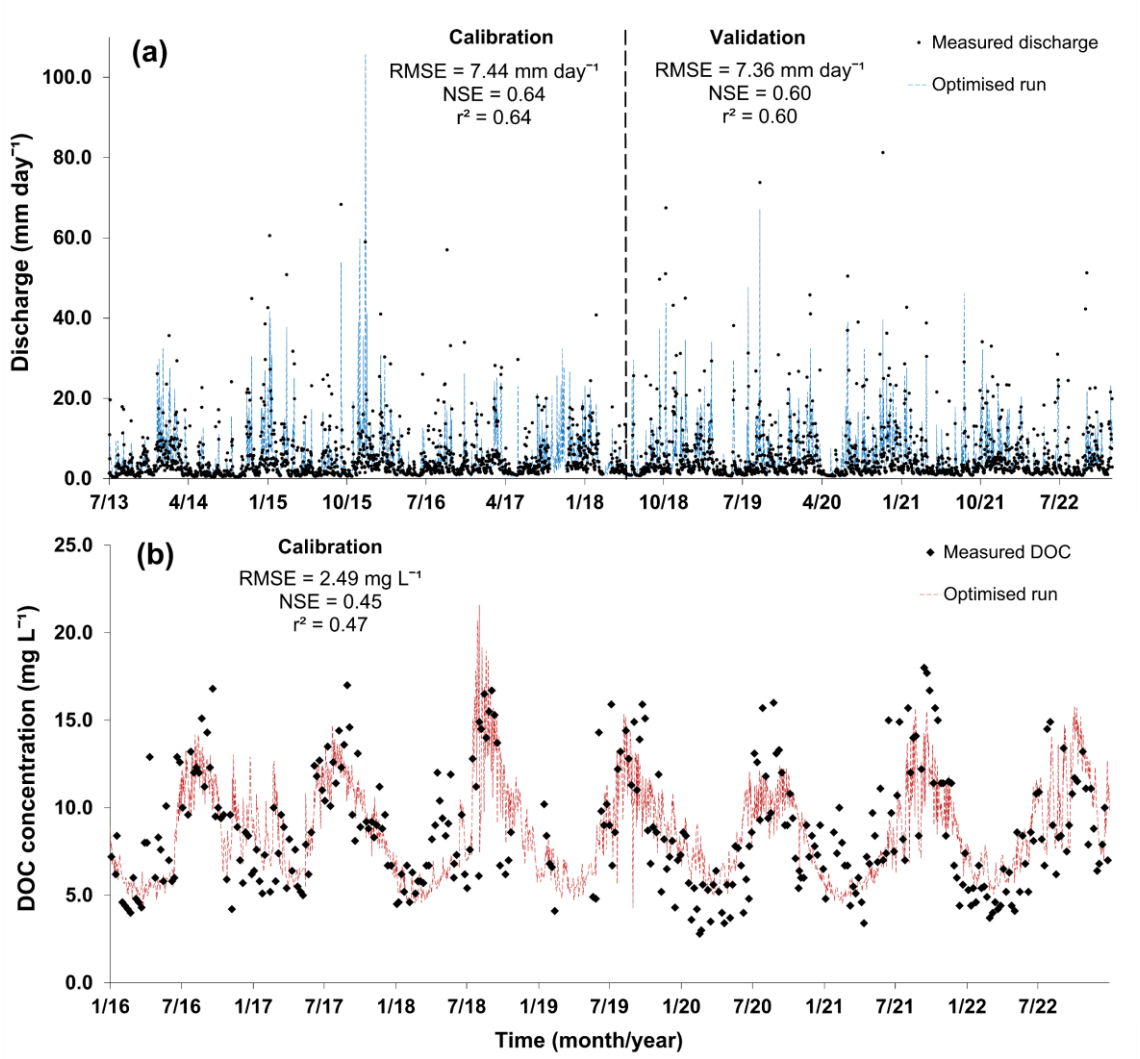


Figure 6.3 Observed and simulated daily river discharge during the long-term model calibration and validation of the hydrology module of GWLF-DOC (a), and observed and simulated daily DOC concentration during the long-term model calibration of the DOC module of GWLF-DOC (b) for the Glenamong catchment.

Table 6.2 Model long-term calibration results for the hydrology module and DOC module of GWLF-DOC.

Model long-term calibration results

Hydrology Module			
Model parameter	**Units**	**Calibration range**	**Calibrated value**
Precipitation correction factor	*factor day⁻¹*	*0.50 - 1.50*	1.08
River channel flow coeff.	*coeff. day⁻¹*	*0.01 - 1.00*	0.91
Melt coeff.	*cm °C⁻¹ day⁻¹*	*0.05 - 0.60*	0.05
Curve adj. number	-	*10.0 to 10.0*	5.50
Soil water capacity	*cm*	*12.00 - 20.00*	13.27
Baseflow capacity	*cm*	*2.50 - 8.00*	5.11
Slow recess coeff.	*coeff. day⁻¹*	*0.001 - 0.100*	0.010
Recess coeff.	*coeff. day⁻¹*	*0.005 - 0.030*	0.159
DOC Module			
Model parameter (DOC production)			
Activation energy (Ea)	*kJ gC⁻¹*	*3.0 - 7.0*	3.0
Aerobic decomp. rate (b)	-	*1.0 - 7.5*	1.0
Anaerobic decomp. rate (a)	*gC m⁻² day⁻¹*	*0.005 - 0.15*	0.096
Anaerobic decomp. rate wetlands (aw)	*gC m⁻² day⁻¹*	*0.005 - 0.15*	0.014
Model parameter (DOC washout - runoff)			
Surface carbon loss coeff. (Rcl)	*coeff. day⁻¹*	*0.01 - 1.00*	0.17
Surface flow cap (Sf cap)	*cm*	*0.01 - 6.00*	2.47
Model parameter (DOC washout - baseflow)			
Baseflow ratio (Br)	*fast- to slow-groundwater ratio day⁻¹*	*0.01 - 1.00*	0.87
Fast groundwater carbon loss coeff. (fgw)	*coeff. day⁻¹*	*0.001 - 1.000*	0.168
Slow groundwater carbon loss coeff. (sgw)	*coeff. day⁻¹*	*0.001 - 1.000*	0.002
Initial conditions - carbon pools			
Deep saturated zone	gC m⁻²	*0.0 - 28.5*	25.6
Saturated zone	gC m⁻²	*0.0 - 1.2*	0.4
Unsaturated zone	gC m⁻²	*0.0 - 1.2*	1.2
DOC-producing soils that are not wetlands	gC m⁻²	*0.0 - 2.9*	0.0
Wetlands	gC m⁻²	*0.0 - 1.5*	0.0

6.4.2 Magnitude and variability of forecast input data

The weather forecast input data for the study catchment (i.e., daily forecasted total precipitation and mean air temperature), the modelled forcing hydrology (daily catchment discharge, surface runoff and baseflow), and the DOC observations used for data assimilation to generate both Workflow A and Workflow B forecasts all showed variability across the meteorological seasons that reflected the typical patterns at this temperate site (Fig. 6.4; Table 6.3).

6.4.2.1 Weather forecast product

Daily forecasted mean air temperatures were highest during the summer (mean of 14.0 °C, median of 13.8 °C and 95th percentile of 18.0 °C) and lowest during the winter (mean of 6.3 °C, median of 6.5 °C and 95th percentile of 9.6 °C), but had the highest variability during the spring and autumn (standard deviation of 2.4 °C and 2.6 °C respectively, versus a standard deviation of 2.2 °C for the summer and winter) (Fig. 6.4a; Table 6.3).

The daily forecasted precipitation inputs were highest during the autumn (mean of 4.3 mm, median of 2.5 mm and 95th percentile of 14.1 mm), values which were relatively similar to those of the winter (mean of 3.4 mm, median of 1.9 mm and 95th percentile of 11.7), while the precipitation was lower during the spring (mean of 2.8 mm, median of 1.4 mm and 95th percentile of 10.8 mm) and the summer (mean of 2.6 mm, median of 1.0 mm and 95th percentile of 11.7 mm) (Fig. 6.4b). Autumn was the season for which the highest daily total rainfall was forecast, followed by the winter, spring and summer (the driest season) (see Table 6.3). Moreover, the variability in daily precipitation was highest during the autumn and lowest during the spring (standard deviation of 5.2 mm and 3.9 mm respectively), while the precipitation forecast in the summer and winter showed a similar variability (standard deviation of 4.3 mm and 4.2 mm respectively).

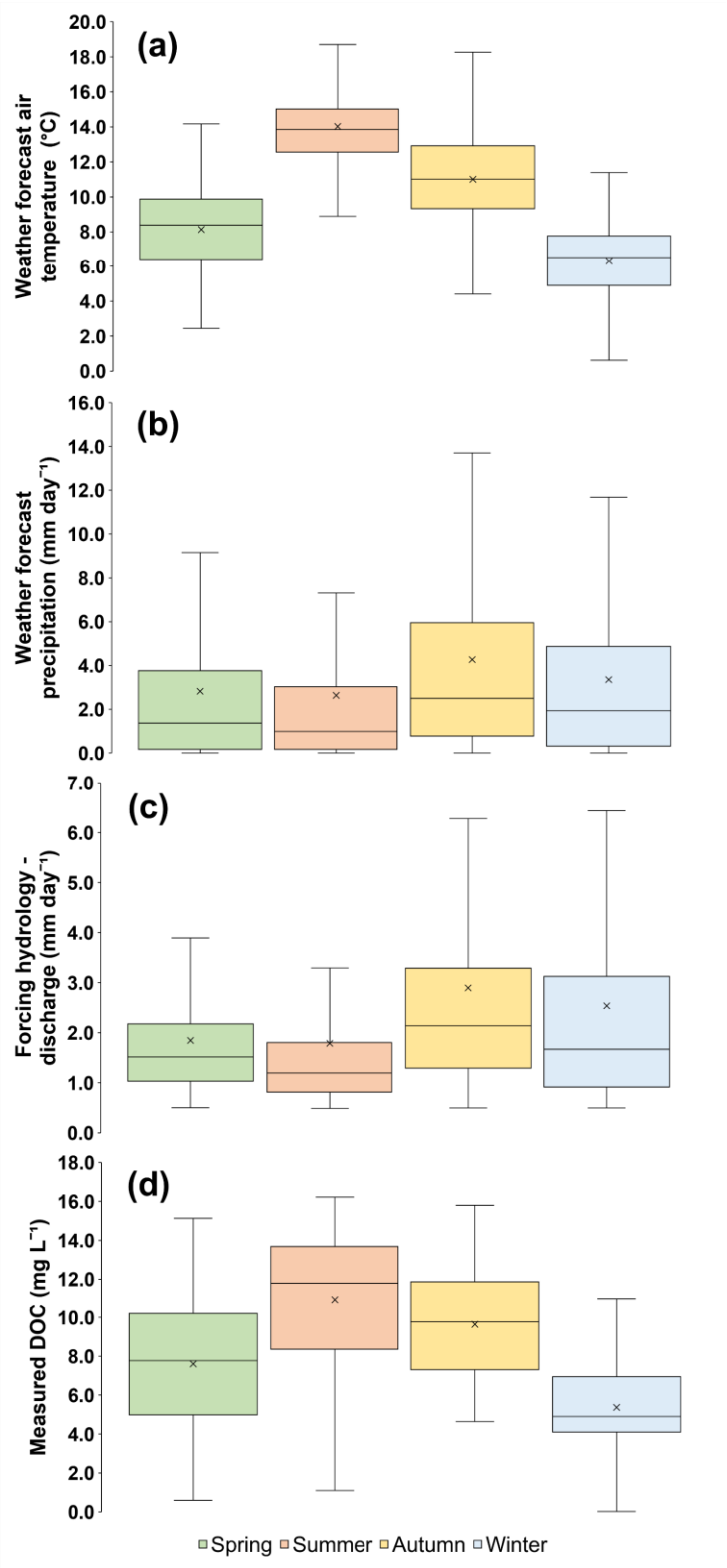


Figure 6.4 Boxplot distributions of the weather forecast product input data for GWLF-DOC (i.e., daily forecasted catchment precipitation and mean air temperature; n = 774 690 respectively) (a and b), modelled daily catchment discharge (n = 774 690) (c) and DOC observations used for data assimilation (n = 716) (d) over the meteorological seasons in the forecasting period (1st March 2021 – 1st March 2023).

Table 6.3 Magnitude and variability across seasons of all driver data used to generate DOC concentration forecasts using both Workflow A and Workflow B.

Season	Spring	Summer	Autumn	Winter
Weather forecast product - air temperature				
Daily air temperature range (°C)	2.4 - 14.2	8.6 - 21.6	4.4 - 18.5	0.1 - 11.4
Mean daily air temperature (°C)	8.1	14.0	11.0	6.3
Median daily air temperature (°C)	8.4	13.8	11.0	6.5
95th percentile daily air temperature (°C)	11.8	18.0	14.9	9.6
Standard deviation (°C day^{-1})	2.4	2.2	2.6	2.2
Weather forecast product - precipitation				
Daily precipitation range (mm day^{-1})	0.0 - 39.7	0.0 - 44.7	0.0 - 52.4	0.0 - 37.5
Mean daily precipitation (mm day^{-1})	2.8	2.6	4.3	3.4
Median daily precipitation (mm day^{-1})	1.4	1.0	2.5	1.9
95th percentile daily precipitation (mm day^{-1})	10.8	11.7	14.1	11.7
Standard deviation (mm day^{-1})	3.9	4.3	5.2	4.2
Mean monthly precipitation (mm $month^{-1}$)	86.1	80.6	128.1	100.5
Mean precipitation (mm $season^{-1}$)	258.3	241.7	384.2	301.4
Forcing hydrology - river discharge				
Mean daily discharge (mm day^{-1})	1.8	1.8	2.9	2.5
Median daily discharge (mm day^{-1})	1.5	1.2	2.1	1.7
95th percentile daily discharge (mm day^{-1})	4.4	5.5	7.9	7.8
Standard deviation (mm day^{-1})	1.4	2.1	2.9	2.6
Forcing hydrology - surface runoff				
Mean daily surface runoff (mm day^{-1})	0.8	0.7	1.5	1.2
Mean daily contribution to river discharge (%)	35%	46%	50%	53%
Forcing hydrology - baseflow				
Mean daily baseflow (mm day^{-1})	0.2	0.2	0.7	0.5
Mean daily contribution to river discharge (%)	65%	54%	50%	47%
Measured DOC				
DOC concentration range (mg L^{-1})	0.6 - 15.1	1.1 - 16.2	4.6 - 15.8	0.1 -11.0
Mean DOC concentration (mg L^{-1})	7.6	10.9	9.6	5.4
Median DOC concentration (mg L^{-1})	7.8	11.8	9.8	4.9
95th DOC concentration (mg L^{-1})	12.9	15.2	14.1	9.0
Standard deviation (mg L^{-1} day^{-1})	3.6	3.4	2.8	2.1

The weather ensemble forecast product showed some differences when compared to historical climate observations from the local meteorological station. The RMSE, NSE and r^2 for observed and forecast daily catchment mean air temperature (°C) ranged from 1.48 to 2.49 °C, from 0.87 to 0.53, and from 0.95 to 0.65 over the forecast horizon, respectively (Fig. 6.5). In the case of total precipitation, the fit was not as good, with RMSE, NSE and r^2 values that ranged from 6.09 to 8.10 mm day^{-1}, from 0.21 to -0.14 and from 0.22 to 0.00, respectively (Fig. 6.5).

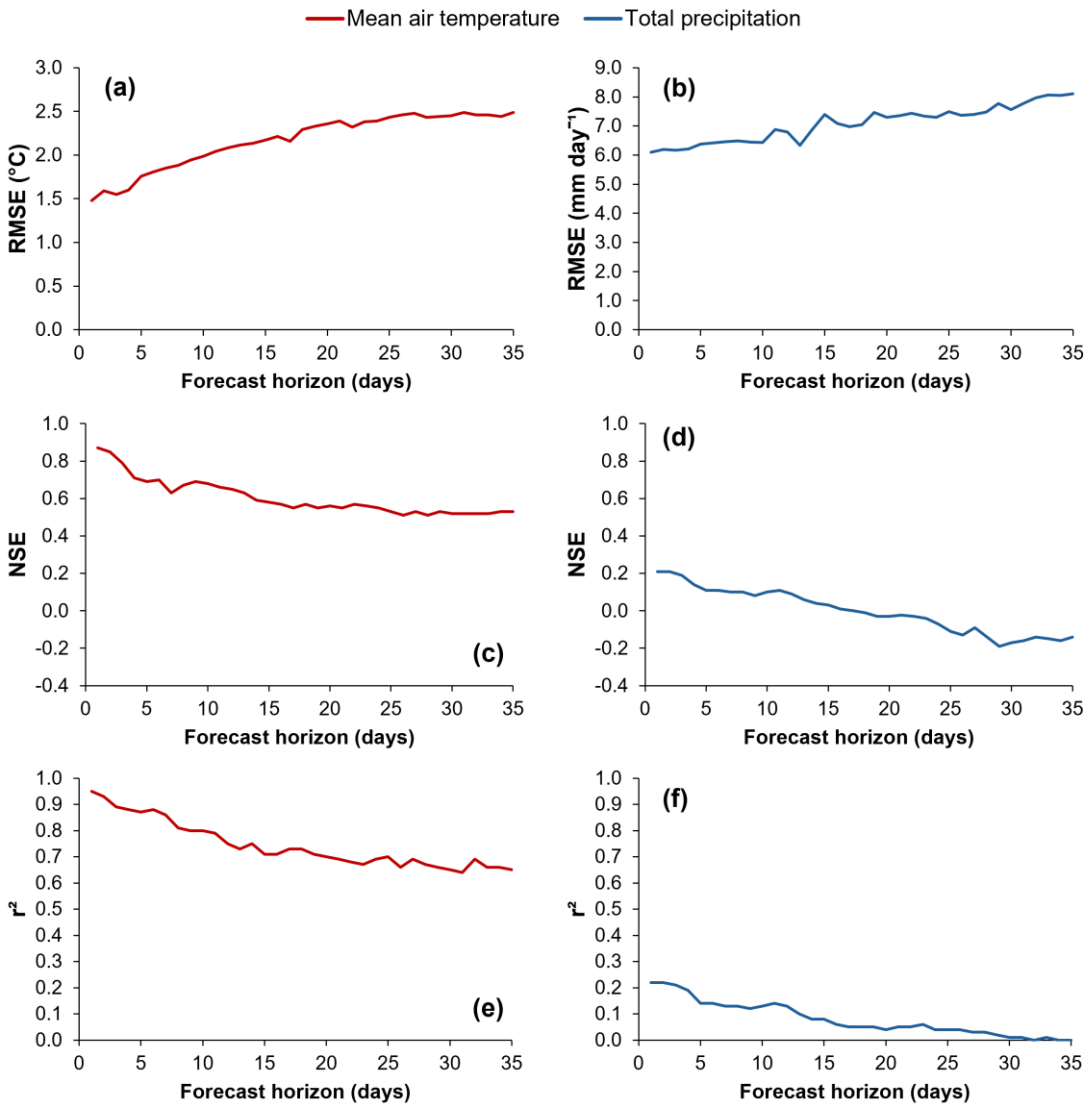


Figure 6.5 RMSE, NSE and r^2 values between the ensemble mean of the weather forecast product (NOAA GEFS) grid-cell for the Glenamong catchment and climate observations from a local meteorological station along the forecast horizon in the entire forecasting period (n = 24 990).

6.4.2.2 Forcing hydrology

The magnitude of the modelled daily catchment discharge used to drive the DOC module in the forecasting was highest during the autumn (mean of 2.9 mm day^{-1}, median of 2.1 mm day^{-1} and 95th percentile of 7.9 mm day^{-1}) followed by the winter (mean of 2.5 mm day^{-1}, median of 1.7 mm day^{-1} and 95th percentile of 7.8 mm day^{-1}), while it was much lower during the spring (mean of 1.8 mm day^{-1}, median of 1.5 mm day^{-1} and 95th percentile of 4.4 mm day^{-1}) and summer (mean of 1.8 mm day^{-1}, median of 1.2 mm day^{-1} and 95th percentile of 5.5 mm day^{-1}) (Fig. 6.4c; Table 6.3). The variability in daily catchment discharge was greatest for the autumn and the winter (standard deviation of 2.9 and 2.6 mm day^{-1} respectively). In contrast, catchment discharge was much less variable during the summer but particularly during the spring (standard deviation of 2.1 and 1.4 mm day^{-1} respectively). Modelled baseflow and surface runoff contributed to the total catchment discharge in different proportions throughout the annual cycle, with compensating percentage values (see Table 6.3). Daily mean baseflow contributions were maximum in the spring, followed by the summer, autumn and winter, and ranged from 65% to 47%. These contributions contrasted with the daily mean surface runoff contributions, which ranged from 35% in the spring to 53% in the winter.

6.4.2.3 DOC observations

The magnitudes of the observed daily DOC concentrations used for data assimilation in the forecasting peaked in the summer (mean of 10.9 mg L^{-1}, median of 11.8 mg L^{-1} and 95th percentile of 15.2 mg L^{-1}), followed by the autumn (mean of 9.6 mg L^{-1}, median of 9.8 mg L^{-1} and 95th percentile of 14.1 mg L^{-1}), spring (mean of 7.6 mg L^{-1}, median of 7.8 mg L^{-1} and 95th percentile of 12.9 mg L^{-1}) and were lowest in the winter (mean of 5.4 mg L^{-1}, median of 4.9 mg L^{-1} and 95th percentile of 9.0 mg L^{-1}) (Fig. 6.4d). It is to note, however, that the highest variability in daily DOC concentration was for the spring (standard deviation of 3.6) followed by the summer, autumn and winter (standard deviation of 3.4, 2.8 and 2.1 respectively) (Table 6.3).

6.4.3 DOC concentration forecasts

The DOC concentration forecasts for the two workflow methods and for Site Persistence for different forecast horizons (1-, 2-, 3-,7-, 14-, 21-, 28- and 35-days ahead) across the forecasting period are displayed in Figs. 6.6 – 6.8. These are plotted with the observed DOC concentrations used for evaluation. There was increased divergence between the forecast and observed DOC concentrations as the forecast horizon extended. It should be noted that observed DOC concentrations that were used for evaluation in one forecast then became available for use as observed data in data assimilation as the start day for the forecasting window progressed.

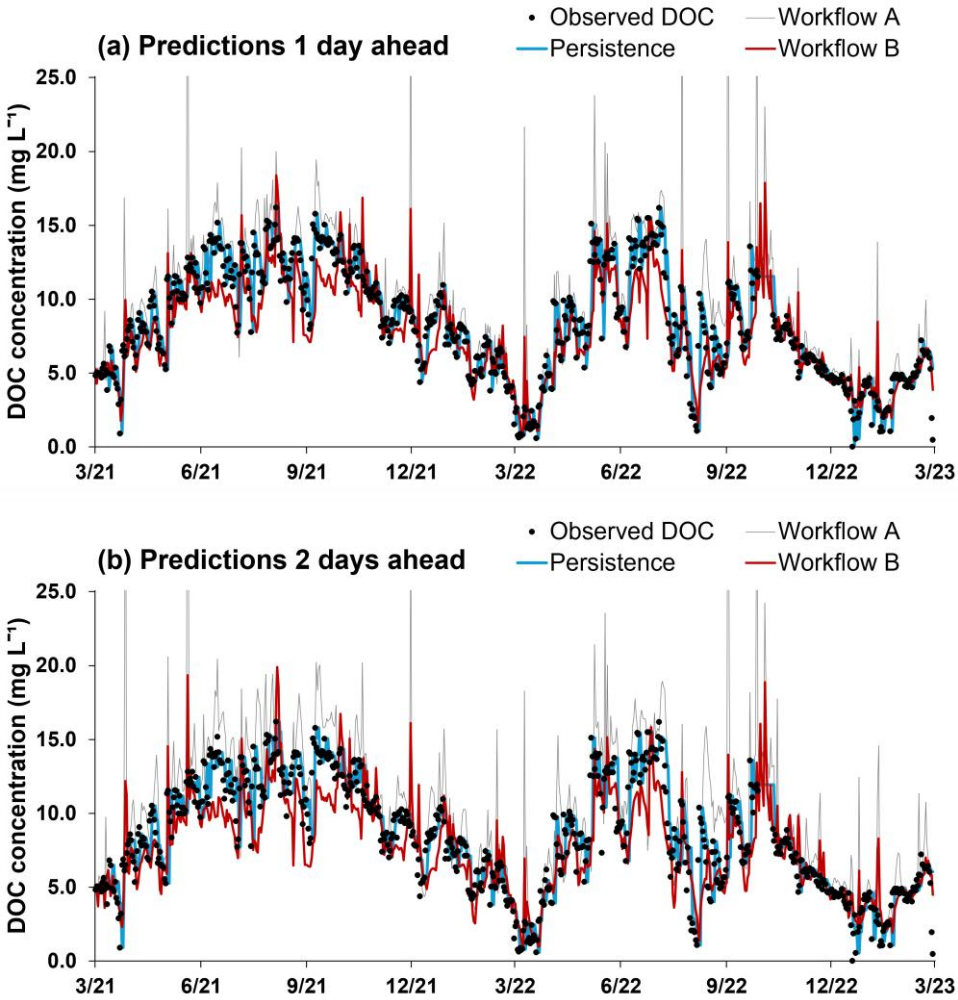


Figure 6.6 DOC concentration forecasts for the two process-based workflows (Workflow A and Workflow B) and for Site Persistence for 1- and 2-days ahead (forecast horizon) throughout the entire forecasting period plotted against the observed DOC concentrations used for evaluation.

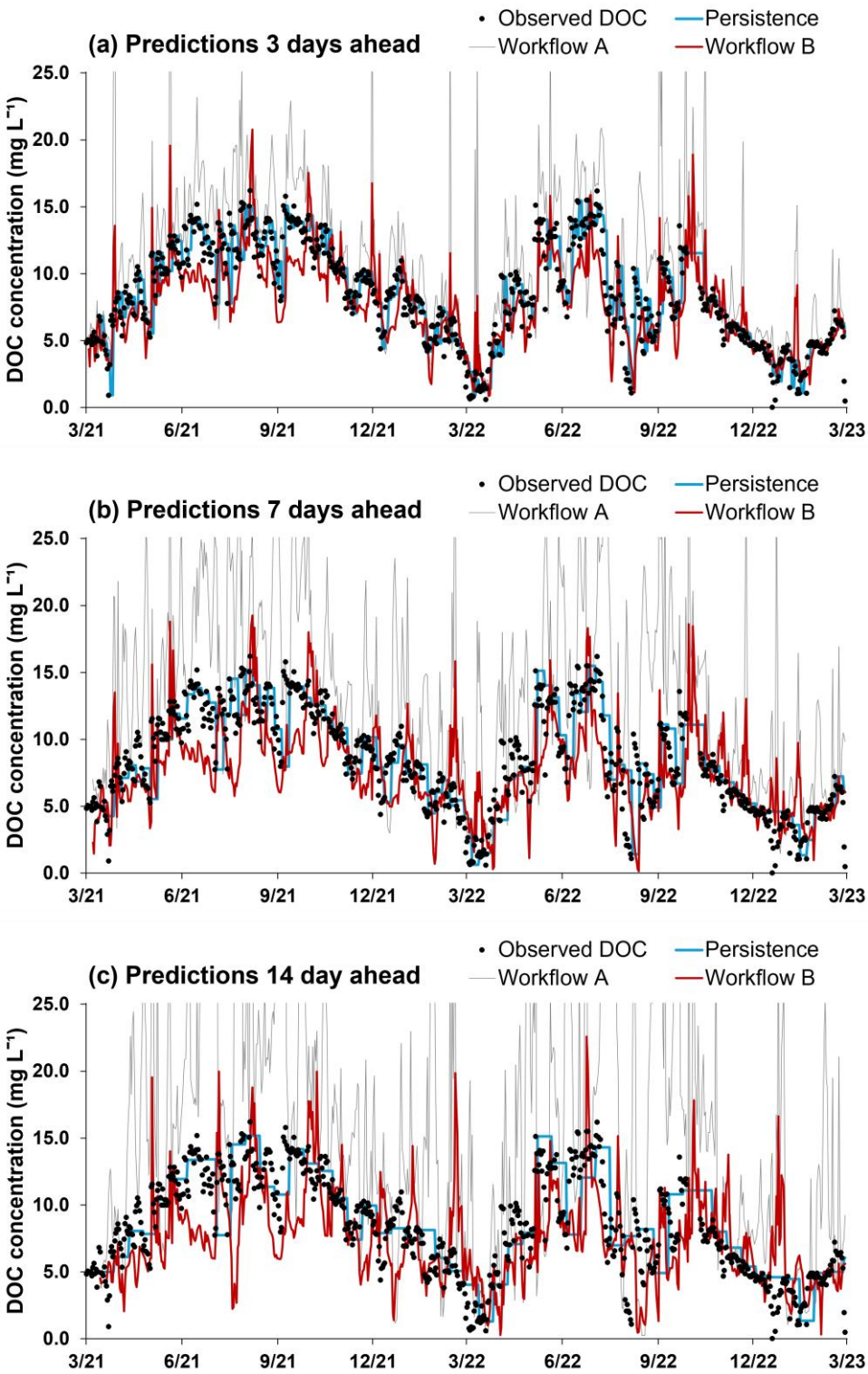


Figure 6.7 DOC concentration forecasts for the two process-based workflows (Workflow A and Workflow B) and for Site Persistence for 3-, 7- and 14-days ahead (forecast horizon) throughout the entire forecasting period plotted against the observed DOC concentrations used for evaluation.

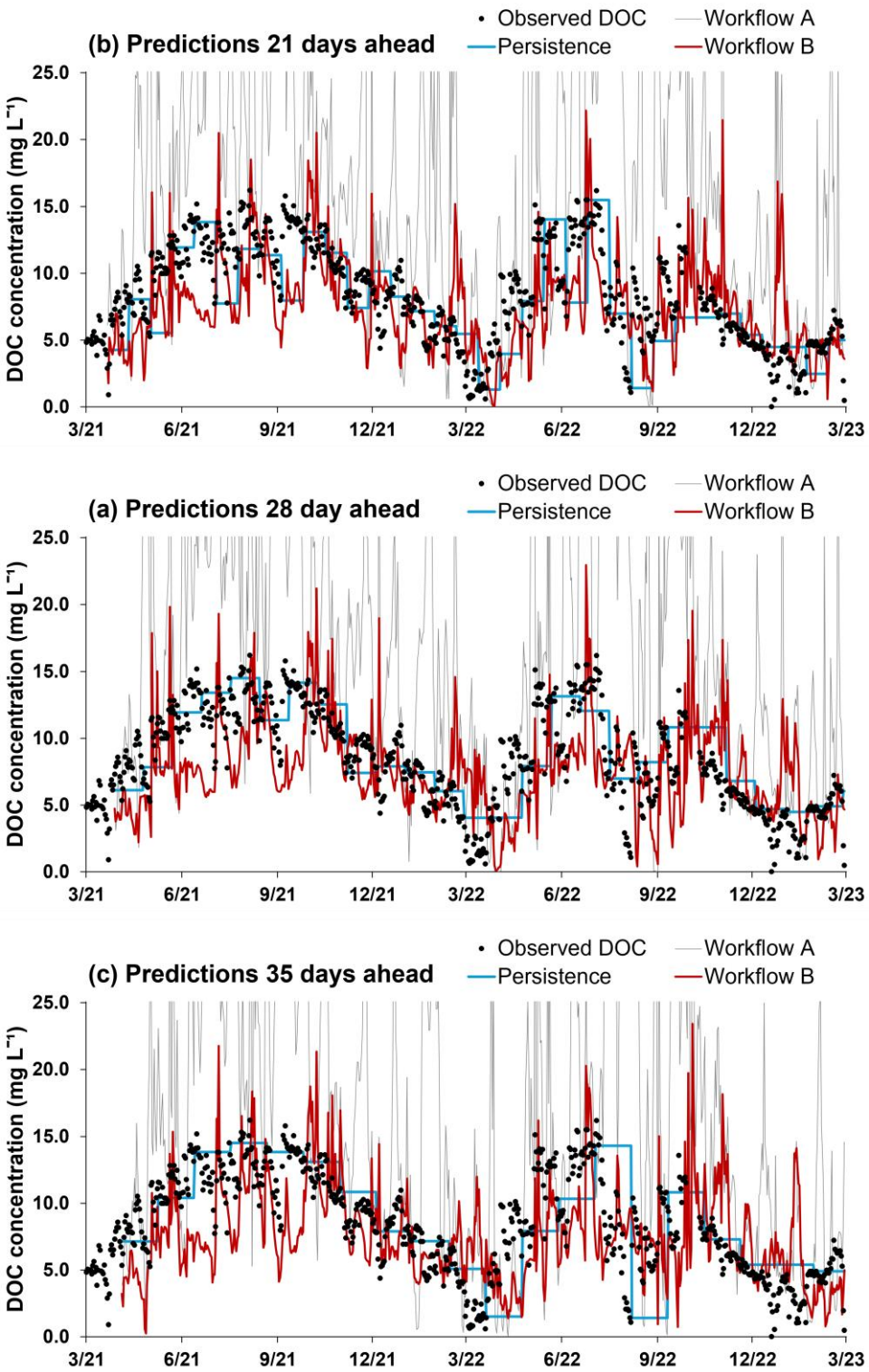


Figure 6.8 DOC concentration forecasts for the two process-based workflows (Workflow A and Workflow B) and for Site Persistence for 3-, 7- and 14-days ahead (forecast horizon) throughout the entire forecasting period plotted against the observed DOC concentrations used for evaluation.

6.4.3.1 Model optimisation during data assimilation

The calibration of the initial conditions for the five catchment carbon pools during the data assimilation phase of the forecasts produced differing values depending on the method, with Workflow B typically showing larger variability than Workflow A (Fig. 6.9a).

In Workflow A, the calibrated values for two of the three subsurface reservoirs (the deep saturated zone and unsaturated zone) were smaller than for Workflow B. In contrast, the calibrated values for the saturated zone carbon pool were larger for Workflow A but varied less than for Workflow B. In the case of the remaining two carbon reservoirs (i.e., the catchment surface area carbon pools), these showed a larger variability for Workflow B than for Workflow A.

The calibration of the DOC model parameters during the data assimilation period in Workflow A typically showed large variability in optimised values, ranges that included the values used in Workflow B for 8 out of the 9 DOC model parameters (Fig. 6.9b). The Workflow B value of the surface flow cap (a parameter that regulates DOC washout in surface runoff in overland flow conditions) was slightly outside of the range of calibrated values in Workflow A. Its variability range obtained in Workflow A, together with the variability of the slow groundwater carbon loss coefficient (a parameter that regulates DOC output through slow groundwater flow from the deep saturated zone), was much lower than was found for other DOC model parameters. It is of note, however, that the values used in Workflow B were close to the upper or lower limits of the variability ranges of Workflow A i.e., they were not similar to the average values of the model parameters calibrated in Workflow A.

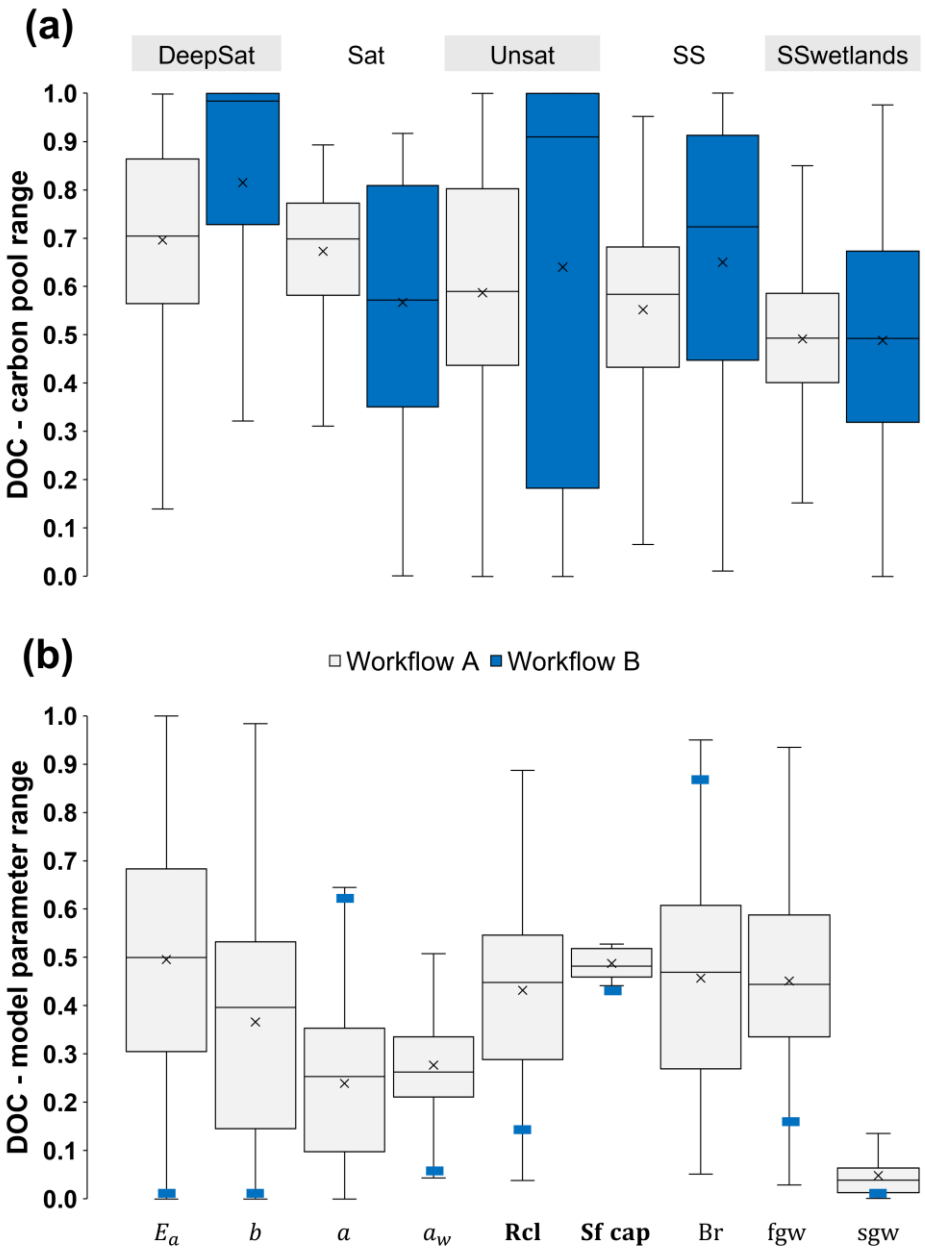


Figure 6.9 Average calibrated values for the initial conditions (i.e., carbon pools) (a) and DOC model parameters (b) of GWLF-DOC for DOC concentration forecasts using Workflow A and Workflow B (1st March 2021 – 1st March 2023) (n = 731 respectively). To facilitate comparison, ranges have been normalised (0.00 – 1.00). Carbon pools (a): deep saturated zone (DeepSat), saturated zone (Sat), unsaturated zone (Unsat), DOC producing surface areas excluding wetlands (SS) and wetlands (SSwetlands). DOC model parameters (b): activation energy (Ea), aerobic decomp. rate (b), anaerobic decomp. rate (a), anaerobic decomp. rate wetlands (aw), surface carbon loss coeff. (Rcl), surface flow cap (Sf cap), baseflow ratio (Br), fast groundwater carbon loss coeff. (fgw) and slow groundwater carbon loss coeff. (sgw).

6.4.3.2 Forecast performance

Forecast performance differed depending on the method (Workflow A, Workflow B and Site Persistence), forecast horizon (1- to 35-days ahead) and meteorological season (Figs. 6.10 – 6.11; Appendix C contains the full lists of performance values). However, all three approaches showed a typical decrease in performance as the forecast horizon became longer, with RMSE values increasing, and both NSE and r^2 values decreasing. Workflow A, in particular, displayed steep decreases in forecast performance over the horizon, especially for the metrics RMSE and NSE which declined from 1.69 (1-day ahead; winter) to 24.26 mg L^{-1} (19-days ahead; summer) and from 0.41 (1-day ahead; winter) to -47.71 (19-days ahead; summer), respectively. Generally, the DOC concentration forecasts of Workflow A did not perform well and were continuously outperformed in different proportions by the forecasts of Workflow B and Site Persistence. These differences were also reflected in the tercile plots displaying predictive skill based on r^2 (Fig. 6.12), with forecasts of both Workflow B and Site Persistence that explained the dispersion of the observed DOC concentrations much better along the forecast horizon and over the annual cycle.

In spring, the predictions of Workflow B (1.77 to 4.56 mg L^{-1} RMSE, 0.75 to -0.56 NSE and 0.77 to 0.07 r^2) and Persistence (2.18 to 5.40 mg L^{-1} RMSE, 0.65 to -1.13 NSE and 0.68 to 0.01 r^2) performed well and much better than Workflow A (3.85 to 13.67 mg L^{-1} RMSE, -0.18 to -13.27 NSE and 0.49 to 0.06 r^2), with Workflow B being best on the first 21 of 35 forecast horizon days (RMSE < 3.60 mg L^{-1}, NSE > 0.02, r^2 > 0.37) but particularly over the first 3 days (RMSE < 2.26 mg L^{-1}, NSE > 0.59, r^2 > 0.64) (Fig. 6.10a and 6.10e; Fig. 6.11a). In the summer, forecast performance was similar to that obtained in the spring, with good metrics for Workflow B (2.59 to 4.33 mg L^{-1} RMSE, 0.45 to -0.55 NSE and 0.62 to 0.13 r^2) and Persistence (2.22 to 5.56 mg L^{-1} RMSE, 0.63 to -1.31 NSE and 0.66 to 0.01 r^2), especially in shorter horizons e.g., 3-days. For this season, however, Persistence typically had a better performance as measured by RMSE and

NSE but alternated on best performance with Workflow B for r² (Fig. 6.10b and 6.10f; Fig. 6.11b).

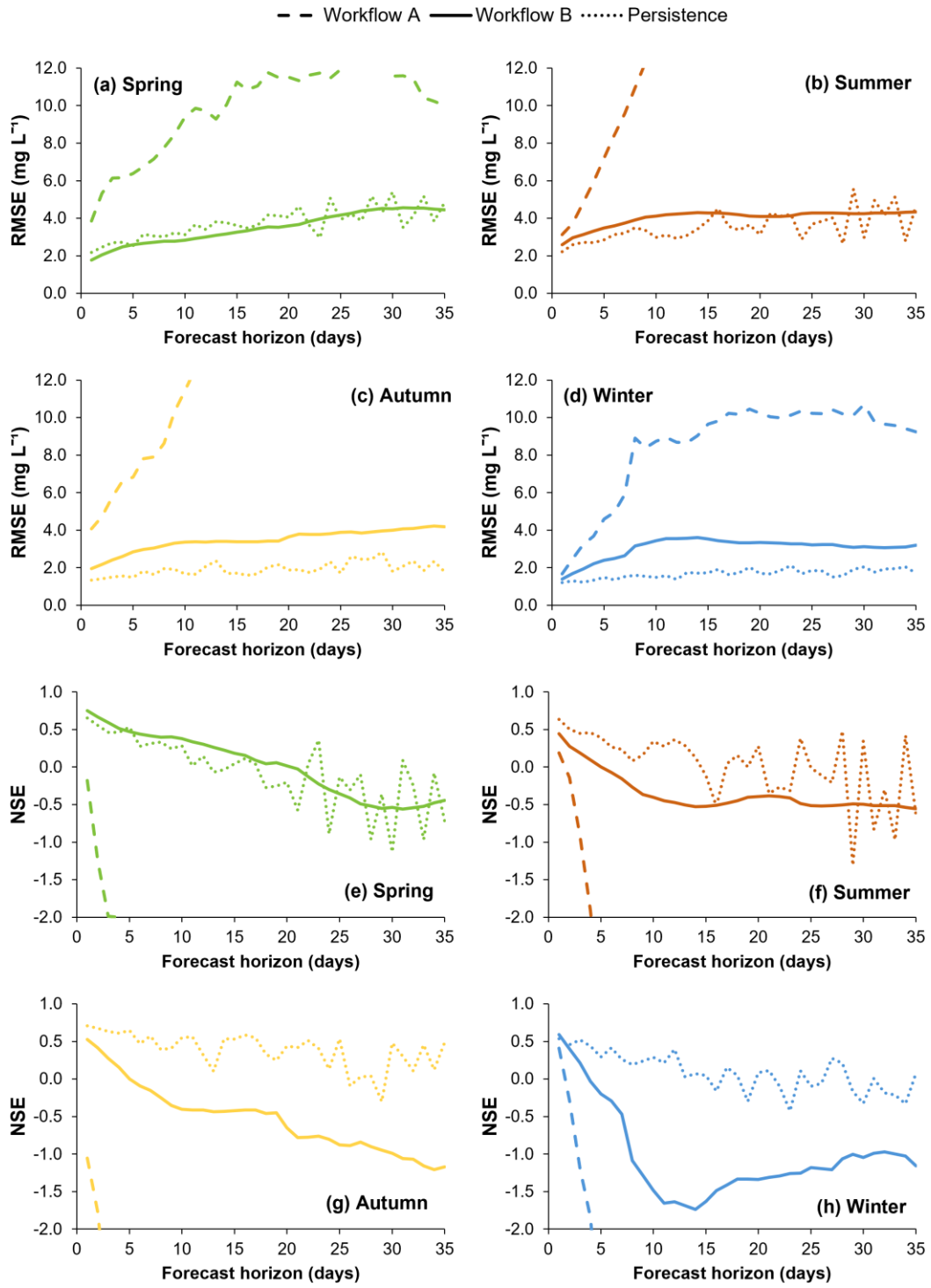


Figure 6.10 Root mean squared error (RMSE) and Nash-Sutcliffe coefficient (NSE) performance of Workflow A, Workflow B and Site Persistence for DOC concentration forecasts along the forecast horizon across seasons in the forecasting period.

A pronounced decrease in forecast performance was found for both workflows in the autumn and winter, relative to the performances obtained in the spring and summer, especially for the NSE and r^2 metrics (Fig. 6.10a – 6.10h; Fig. 6.11a – 6.11d). The forecasts of Workflow A were generally not good either in autumn (4.07 to 18.70 mg L^{-1} RMSE, 1.05 to -42.44 NSE and 0.40 to 0.08 r^2) or winter (1.68 to 10.69 mg L^{-1} RMSE, 0.41 to -22.99 NSE and 0.64 to 0.01 r^2). The forecasts of Workflow B, however, performed relatively well in the first 4 days of the horizon in the autumn (RMSE < 2.61 mg L^{-1}, NSE > 0.15, r^2 > 0.35) and in the first 3 days for winter forecasts (RMSE < 1.93 mg L^{-1}, NSE > 0.21, r^2 > 0.35). Site Persistence, in contrast, displayed a good performance both of these seasons, outperforming Workflow A and Workflow B consistently for all three metrics (except for r^2 and NSE 1-day ahead, for which Workflow A and Workflow B outperformed Persistence). The performance of Persistence ranged from 1.34 to 2.84 mg L-1 RMSE, 0.71 to -0.30 NSE and 0.73 to 0.33 r^2 in the autumn, and from 1.21 to 2.11 mg L-1 RMSE, 0.54 to -0.43 NSE and 0.59 to 0.18 r^2 in the winter.

6.4.3.3 Forecast uncertainty

The uncertainty in forecasts of both Workflow A and Workflow B typically increased as the forecast horizon became longer in all four meteorological seasons (Fig. 6.11e – 6.11h). Workflow A, in particular, displayed large uncertainties that ranged from 0.9 mg L^{-1} (1-day ahead; winter) to 8.5 mg L^{-1} (28-days ahead; summer). In contrast, the uncertainty in the predictions of Workflow B was much smaller ranging from 0.4 mg L^{-1} (1-day ahead; winter) to 1.6 mg L^{-1} (35-days ahead; autumn) and was characterised by small increases over the forecast horizon in all four seasons. Workflow A and Workflow B forecasts captured a similar number of observed DOC concentrations within their respective forecast confidence intervals for different forecast horizon days (Table 6.4). Although the number of observations that were captured by the forecasts increased as the confidence intervals increased, both Workflow A and Workflow B

forecasts were consistently overconfident i.e., they captured a relatively small number of observations within their respective forecast confidence intervals.

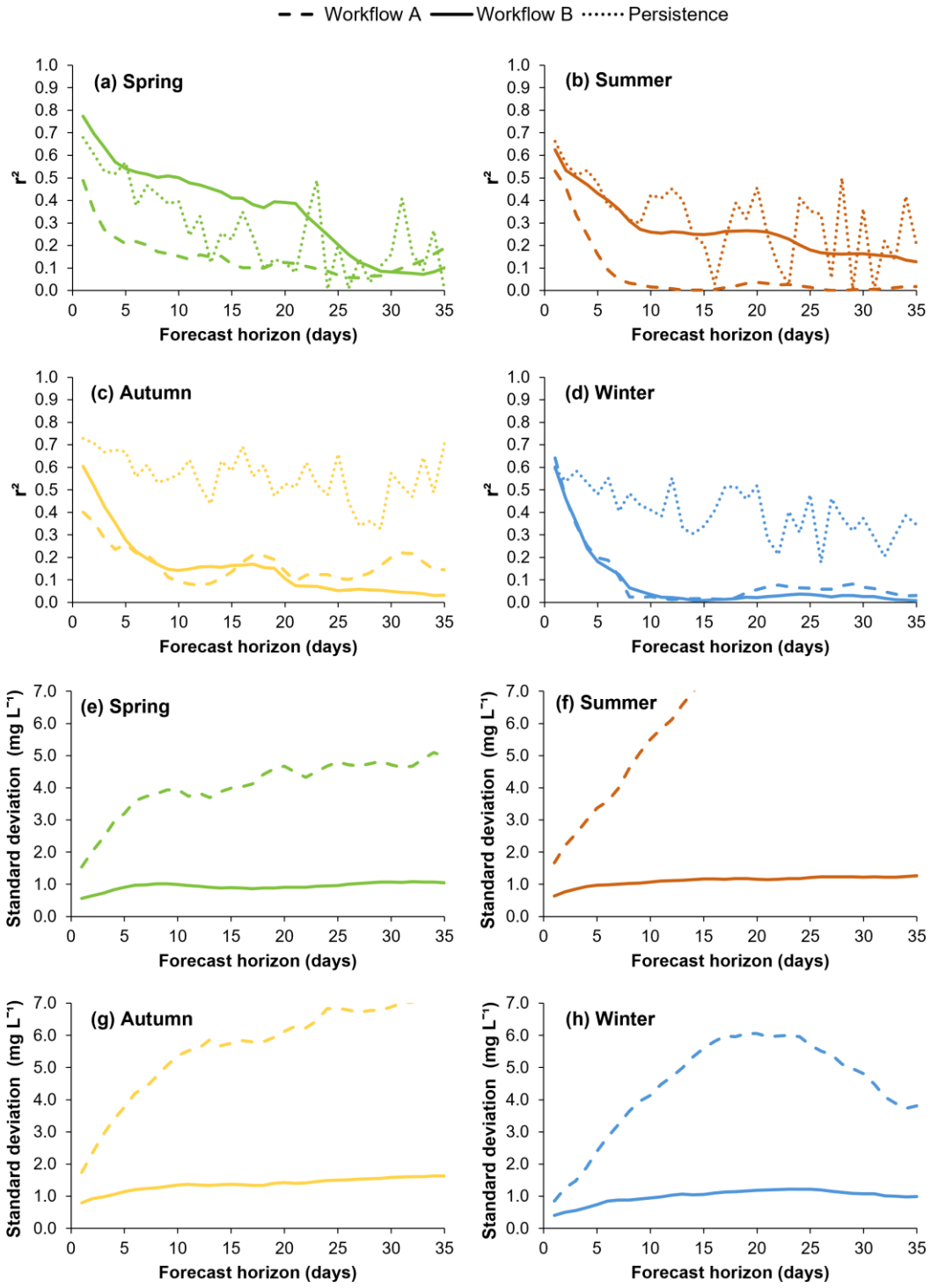


Figure 6.11 Coefficient of determination (r^2) performance and quantified forecast uncertainty (standard deviation) of Workflow A, Workflow B and Site Persistence for DOC concentration forecasts along the forecast horizon across seasons in the forecasting period.

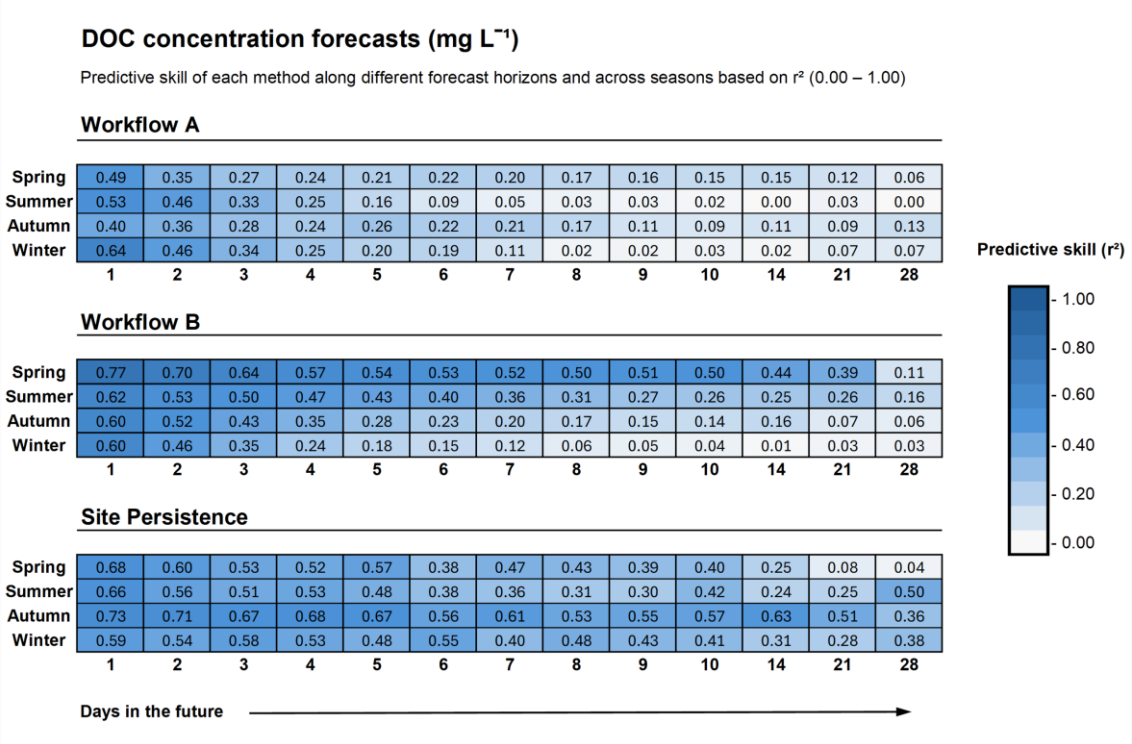


Figure 6.12 DOC concentration forecast skill visualization by means of tercile plots for each method (Workflow A, Workflow B and Site Persistence) along different forecast horizons and across seasons. Forecast skill is indicated based on the r² performance scale (0.00 – 1.00).

Table 6.4 Magnitude and variability across seasons of all driver data used to generate DOC concentration forecasts using both Workflow A and Workflow B.

Workflow A

Forecast confidence interval	Forecast horizon day					
	1	7	14	21	28	35
10th	*4%*	*5%*	*4%*	*3%*	*4%*	*3%*
25th	*11%*	*10%*	*8%*	*7%*	*9%*	*9%*
50th	*23%*	*23%*	*20%*	*18%*	*18%*	*21%*
75th	*37%*	*37%*	*36%*	*33%*	*33%*	*35%*
90th	*51%*	*51%*	*52%*	*50%*	*52%*	*53%*
95th	*58%*	*60%*	*60%*	*61%*	*62%*	*65%*

Workflow B

Forecast confidence interval	Forecast horizon day					
	1	7	14	21	28	35
10th	*2%*	*3%*	*2%*	*2%*	*2%*	*3%*
25th	*7%*	*6%*	*6%*	*6%*	*6%*	*7%*
50th	*15%*	*13%*	*14%*	*14%*	*13%*	*14%*
75th	*24%*	*24%*	*23%*	*22%*	*23%*	*24%*
90th	*38%*	*37%*	*38%*	*34%*	*35%*	*37%*
95th	*45%*	*47%*	*44%*	*41%*	*43%*	*44%*

6.5 Discussion

The value of research studies on ecological forecasting extends beyond the communication and use of future predictions to include the iterative refinement of forecasting frameworks through lessons learned during their development (Lofton et al., 2023). This study represents a successful proof-of-concept for predicting DOC concentration in river source water and contributes to ongoing efforts to advance the versatility of applications that predict short-term changes in water quality (see Carey et al., 2022; Lofton et al., 2023; Dietze et al., 2024). It shows that it is possible to generate riverine DOC concentration forecasts 35-days ahead, predictions for which their performance was assessed across seasons using different goodness-of-fit measures (RMSE, NSE and r^2). Each of these metrics has the potential to be individually associated with different features of success in the forecasting (Krause et al., 2005; Deng et al., 2022). Furthermore, the response of a process-based model parameterisation (here GWLF-DOC) to a set of forcing data was explored under two different forecasting configurations. This assessment was required as an initial step to better understand the use of process-based models in short-term forecasting applications (Cuddington et al., 2013), especially in a context where these tools are traditionally employed for long-term predictions.

While there was large variability in the results for forecast performance, the results showed that Workflow B could be an effective approach to anticipate DOC concentration in river water in short horizons, particularly during periods of high variability that could challenge water treatment. For instance, in spring (the season when observed DOC concentrations in the study river were most variable), Workflow B forecasts were the most accurate, showing relatively good performance up to 10-days ahead. Across other seasons, these forecasts showed relatively good performance in all metrics up to 3-days ahead. It was notable, however, that Site Persistence was much better in longer horizons, particularly in autumn and winter.

In the case of Workflow A, despite performing relatively well 1-day ahead as might be expected, its capacity to predict DOC concentrations over longer horizons was poor compared to Workflow B and Site Persistence. A contributing factor to this was that the calibrated values for DOC model parameters in Workflow A showed wide variation during the data assimilation period. When calibrating a large number of target variables, the optimisation process likely prioritised specific parameters (Wang et al., 2016; Loos et al., 2020a) potentially to reduce computational time in solving the payoff function (Dietze et al., 2013; Niu et al., 2014; Yassin et al., 2021), regardless of its impacts on future predictions. For instance, model parameters such as activation energy (E_a) and aerobic decomposition rate (b), two key controllers of soil organic carbon production in GWLF-DOC (Naden et al., 2010), varied widely over their entire calibration range in Workflow A. The selection of contrasting values for these parameters in the workflow could have resulted in relatively extreme responses in DOC production for future predictions (Paíz et al., 2025). These would have been a function of projected changes in soil temperatures (induced by mean air temperature forecasts) and water availability (induced by both modelled catchment hydrology and precipitation forecasts). Consequently, the wide range in simulated DOC concentrations forecast using Workflow A may have resulted from underestimations and/or overestimations of DOC production and therefore of DOC washout dynamics. This is supported by the fact that not only some parameters related to DOC production but also some related to DOC washout have shown sensitivity for this site during model simulations (Paíz et al., 2025). Small variations in calibrating values, therefore, may have contributed to the often high DOC concentrations forecasted in Workflow A, especially in longer horizons (see Figs. 6.6 – 6.8), which resulted in poor forecast performance and large uncertainties.

For Workflow B, the calibration of initial conditions showed less variability than for Workflow A, which translated into a more gradual response to the forcing data as the forecast time progressed. Using a fixed set of calibrated DOC model parameters and

adjusting only the carbon pools during data assimilation enabled Workflow B forecasts to predict DOC concentrations much better. This aligns with some recent research (e.g., Wang et al., 2016; Mohammed et al., 2022), where the use of previously calibrated values and/or very restrictive ranges for model parameters has been highlighted as a strategy, especially when the number of target variables to calibrate is large (Yassin et al., 2021). It is of note, however, that using a pre-calibrated set of model parameters in the forecasting for this study required a long-term observational dataset, which may not be always available in other sites. Nevertheless, efforts should aim to provide the best possible representation of model parameters within the modelling workflow (Höge et al., 2018; Schürz et al., 2019b; Marshall et al., 2021) rather than relying on relatively large calibration ranges. This would be particularly important when employing a DOC process-based model such as GWLF-DOC or INCA-C, for which their parameters can show sensitivity and impact key processes for simulating DOC concentration (Futter et al., 2011; O'Driscoll et al., 2018c; J. Xu et al., 2020; Paíz et al., 2025).

A notable aspect of the study was that both Workflow A and Workflow B showed a pronounced decrease in forecast performance in autumn and winter relative to Site Persistence and to their respective performance in spring and summer. A distinctive characteristic of the autumn and winter for this site was the elevated regime in river discharge and precipitation (see Fig. 6.4 and Table 6.3). It is possible that the model could not replicate discharge dynamics accurately and its impacts on simulating DOC in those two seasons. This was likely because the weather forecast ensemble product showed, differently than for mean air temperature, some discrepancy in precipitation inputs for this site relative to historical climate observations. For instance, peaks in daily rainfall could not be well represented in the forecast data, indicated by NSE and r^2 metrics (see Fig. A2) (Krause et al., 2005). This should be considered when forecasting DOC concentration in times of elevated river discharge with high contributions of surface runoff in response to precipitation inputs (see Table 6.3). To overcome this issue, a

catchment-scale downscaling method could be employed to represent more accurately precipitation inputs for the study site (Kay et al., 2023; Legrand et al., 2024). Multiple factors influence precipitation levels in settings like the Glenamong catchment including local and regional climate, ocean proximity, topographic gradient and size (Doyle et al., 2019; Kay et al., 2023). Hydrological modelling for such settings, therefore, should be aimed to better capture river discharge dynamics in wet i.e., high-rainfall seasons such as autumn and winter. This would be important for forecasting DOC concentration using a DOC model that is forced by hydrology (Wei et al., 2024), as is the case for GWLF-DOC but also for other widely employed DOC models (e.g., RHESSys and INCA-C) (Son et al., 2019; J. Xu et al., 2020).

Furthermore, both Workflow A and Workflow B captured a relatively small number of observations within their forecast confidence intervals, indicating a tendency towards overconfident predictions. One contributing factor to this could be structural limitations of GWLF-DOC in replicating short-term fluctuations in DOC concentration. GWLF-DOC simulates DOC dynamics based on lumped parameterised relationships governing hydrological and biogeochemical processes (Naden et al., 2010). However, the temporal resolution at which these processes operate may not fully capture the daily-frequency variability observed in DOC concentrations at the studied river (Jennings et al., 2020). Rapid changes in DOC levels, particularly those driven by episodic hydrological events, may not have been then well captured by the forecasts, which would have led to the underestimations of uncertainty. Another contributing factor could be associated with the data assimilation. The KF, although designed to correct model estimates based on observations, relies on the underlying model structure to propagate uncertainty (Evensen, 2009; Loos et al., 2020a). If the model on occasions did not fully reflect short-term DOC responses, then the KF may have been constrained in adjusting uncertainty estimates accordingly (Loos et al., 2020a), further contributing to the observed overconfidence. In the use of a model such as GWLF-DOC, exploring alternative

variations of the KF, different data assimilation frequencies, and/or other data assimilation methods could improve both forecasting accuracy and uncertainty estimations (Loos et al., 2020a; Li et al., 2021; Wander et al., 2024).

6.5.1 Implications for water management

The DOC concentration forecasts generated in this study could provide valuable information to water management applications under specific conditions. The use of the process-based forecasts that were indicated with good performance (e.g., Workflow B forecasts 3-days ahead across seasons and 10-days ahead in spring) although represent only a portion of the predictions along the entire forecast horizon in this study (i.e., 35-days ahead), have the potential to enhance water treatment operations. For instance, sub-daily and daily-scale treatment activities such as coagulation, flocculation, carbon adsorption, degradation (e.g., electrochemical oxidation) and filtration can benefit from source water DOC concentration forecasts 1-day to 1-week ahead (Köhler et al., 2016; DeMont et al., 2021; Siddique et al., 2022b; Piai et al., 2024). Disinfection of raw water with chlorine-based methods, in particular, could be better adjusted in advance for improved water supply along with a potential reduction in DBP levels (Aguilar-Alarcón et al., 2024; Pedregal-Montes et al., 2024; Valenti-Quiroga et al., 2024).

Moreover, the benefits of using such an approach could go beyond managers using the final modelling outputs i.e., the ensemble-based DOC concentration forecasts and their quantified uncertainty (Cuddington et al., 2013; Lofton et al., 2023). Managers could also obtain information on modelled variables that could be relevant for them and how such processes respond to the forcing data. For instance, modelled processes such as catchment soil water deficits, flood events, low water tables and droughts could be indicative of extreme events that could affect both DOC raw water quality (Blaurock et al., 2021; Wu and Yao, 2022; Wu et al., 2023a, 2023b) and drinking water supply (Warner and Saros, 2019; Fenner et al., 2021). Anticipating changes in such dynamics would, therefore, enable a proactive rather than reactive management at the river

catchment-scale as well. It is also to note that Site Persistence could be a method to anticipate DOC concentrations in times and forecast horizons for which other methods do not yield satisfactory results. Although this approach would not offer the benefits of process-based methods such as representing other processes within the modelled system, it can be explored as a relatively straightforward alternative that could be of use for management.

Lastly, it is important to highlight that the quantification of uncertainty for the process-based forecasts in this study is an important component of ensemble-based iterative forecasting (Dietze et al., 2018; Lewis et al., 2022a), that may improve the usability of the predictions by stakeholders (Carey et al., 2022). The uncertainty quantified for the DOC concentration forecasts in different horizons and across seasons in this study, therefore, should be evaluated when analysing the future predictions. This would be particularly relevant in the context of decision-making and resource allocation in management applications (Carey et al., 2022; Lofton et al., 2023) that deal with DOC water quality.

6.6 Conclusions

This study explored the short-term forecasting of DOC concentration in river water by evaluating two process-based workflows to generate daily ensemble-based predictions of DOC concentration 35 days ahead. The advantages of using a process-based approach for forecasting DOC were highlighted, as well as several issues that were encountered along the workflows that had implications on forecast accuracy and uncertainty. Importantly, some forecasts generated under specific conditions (across method, forecast horizon and season) showed reasonably good predictive skill and therefore, represent an example that could benefit operational water management applications. It is proposed that the insights of this study guide future efforts in short-term process-based forecasting development for DOC water quality, especially in the context where more tools for anticipating changes in water systems are needed.

Chapter 7

Synthesis

A substantial increase in predictive capacity is required to anticipate and address widespread ecosystem changes and their services in the face of climate and biodiversity crises (Bodner et al., 2021; Dietze et al., 2024). In a time of accelerating change, relying exclusively on historical references or long-term trends is not sufficient (Carey et al., 2022; Lewis et al., 2022a). Moving forward requires new approaches to research, management and decision-making. Implementing frameworks that benefit from emerging forecasting techniques and software modelling is crucial for anticipating ecological change at the scale and speed needed by society (Dietze et al., 2018; Lewis et al., 2022a; Lofton et al., 2023). Long-term forecasting frameworks can provide scenario-based projections to be used in planning, mitigation protocols and policy making (Nissan et al., 2019), while a short-term approach can focus on anticipating change in more operational timeframes (Cuddington et al., 2013; Bodner et al., 2021). Both approaches, however, are important and can contribute to developing more adaptive water management strategies (Dietze, 2017a; Bradford et al., 2020a; Bodner et al., 2021).

Two key areas for which ecological forecasting has huge potential to enhance resource allocation are drinking water supply and freshwater biodiversity conservation. While

these two areas are wide and comprised of many sectors, they have specific components for which anticipating changes in the dynamics of river and lake water systems requires a substantial increase in methods. The work described in this thesis addresses this aspect, by developing forecasting frameworks in three different case studies (chapters 4, 5 and 6, respectively) for real world applications that address a present-day management issue. Both long-term (Chapter 4) and short-term (Chapter 5 and Chapter 6) approaches were adopted, and each case study represents a successful example of how modelling tools can drive ecological forecasting applications. This work, therefore, not only demonstrates the value of quantifying changes in water systems but also of anticipating such changes to assist decision-making for improved environmental intervention, more efficient water use and a safer supply.

7.1 Forecasting frameworks

In Chapter 4, a forecasting framework to generate long-term scenario-based future predictions of river discharge and DOC dynamics was presented. The framework was applied to two contrasting catchments: one in Sweden and one in Ireland. These catchments represent systems in countries where drinking water is affected by increases in DOC (O'Driscoll et al., 2018b; Kritzberg et al., 2020). Future changes in river discharge and DOC dynamics including the likelihood of extreme events were assessed under three Shared Socioeconomic Pathways (i.e., different futures of climatic conditions, socio-economic development and adaptation to climate change): SSP126, SSP370 and SSP585. Importantly, the framework incorporated model parameter uncertainty in the model simulations, an aspect often omitted in climate change impact assessments. Moreover, the contributions of both future climate data and model parameterisation to the total uncertainty in future projections were quantified.

In Chapter 5, a lake model was applied to Lough Feeagh (Co. Mayo, Ireland) and used within an emerging freshwater quality short-term forecasting system: the Forecasting Lake and Reservoir Ecosystems system (FLARE) (Thomas et al., 2020). This study

centred on forecasting lake water temperature, and how to use that as a tool to predict the ecological dynamics of Atlantic salmon *(Salmo salar)* and European eel *(Anguilla anguilla)* between freshwater and the sea. The relevance of water temperature for predicting fish movements stemmed from previous research, which indicated that water temperature is a strong controller of the timing of fish migrations (although there are other controlling factors that operate simultaneously). The predictions for both lake water temperature and fish migrations were generated on a daily-basis and extended up to 34 days into the future, and were assessed robustly in terms of accuracy and uncertainty. The cyberinfrastructure of the framework and its scalability to other settings where fish species can face risk were also key elements of this study.

Components of both Chapter 4 (the catchment model) and Chapter 5 (the forecasting short-term approach) were used in Chapter 6 to explore the short-term forecasting of DOC concentration. Predictions of DOC concentration in a daily temporal scale (each daily forecast extending up to 35 days into the future) were generated using two different workflows for the Glenamong River (Co. Mayo, Ireland). The difference between the two workflows was the calibration and data assimilation strategy used in the forecasting. Importantly, the magnitude and variability of the ensemble of forcing data including short-term meteorological forecasts were assessed to gain insights into how each of the two workflows for DOC concentration responded. The predictive skill of each forecasting workflow was assessed across the typical meteorological seasons, as these are key periods for both the variability and management of DOC.

7.2 Future research

The forecasting frameworks developed in this thesis although were structured robustly and described extensively, have a number of research gaps that can be addressed in the future for further development and improved predictive capacity. In general, actions are indicated to enhance specific components of the frameworks and explore related issues that were found relevant in each of the case studies, respectively.

In Chapter 4, although the work accounted largely for model parameter uncertainty, further exploration of such uncertainty and model parameter sensitivity could benefit both hydrological and DOC modelling aspects. A more comprehensive assessment could be achieved by incorporating all behavioural parameter sets to quantify the GLUE uncertainty bounds, rather than limiting the analysis to the top 100 parameter sets (see Section 4.3.4) (Beven, 2009). This, although would demand more computational power, could capture even more accurately the impacts of model parameterisation in both the model calibration and future projections (Beven and Binley, 1992, 2014). Additionally, employing alternative random sampling strategies in the model parameter space could provide further insights into sensitivity responses (see Section 4.3.4). These strategies could involve variations of the current method employed i.e., the Monte Carlo method or alternative techniques (e.g., variance-based methods) (Beven, 2009; Gallagher et al., 2009) that could be assessed using a performance metric beyond NSE (Pianosi et al., 2016).

Moreover, the long-term projections were driven solely by GWLF, but incorporating an ensemble of models can improve robustness (Olsson et al., 2024). However, this would require a comprehensive understanding of each of the models to use. The use of different models or the use of a particular model in different settings could yield different results and thus predictive skill (Krause et al., 2005; Naden et al., 2010; Qi et al., 2017; J. Xu et al., 2020; Lindqvist, 2022). Furthermore, the ISIMIP3b GCM ensemble of future climate data used in Chapter 4 was only one of many datasets that are available for the modelling community to use climate change impact assessments. Exploring alternative sources and GCMs could contribute to a reduction in the uncertainty contributions from future climate data (Hattermann et al., 2018; Kundzewicz et al., 2018; Murphy et al., 2023). In line with this, only two sources of uncertainty were quantified in this study (future climate input data and model parameterisation). Other sources, such as of model initial conditions and model process representation, could be included in the analysis to

assess their influence on future projections (Hattermann et al., 2018; Lofton et al., 2022; Wu et al., 2022).

In Chapter 5, different lake models could be tested within FLARE or within other short-term forecasting approaches for water temperature (Mesman et al., 2020; Ayala et al., 2023; Olsson et al., 2024) and thus for predicting fish migrations. Variations in data assimilation techniques could also be explored such as different data assimilation periods or algorithms, as they have been shown to have implications on prediction skill and uncertainty (Beven and Freer, 2001; Loos et al., 2020b; Wander et al., 2024). Moreover, the high-frequency water temperature monitoring data could be used in different configurations to drive the forecasting, instead of computing a single value i.e., using the lake water temperature average. For instance, using only surface water temperatures within the framework could yield different predictive capacities for fish migrations, as forecasting accuracy for water temperature can vary depending on lake depth (Thomas et al., 2020, 2023b). Furthermore, a partitioning of uncertainty, similar to that performed in Chapter 4, could help identify key areas for improvement (Thomas et al., 2020; Lofton et al., 2022; Wander et al., 2024). Moreover, assessing the accuracy of the weather forecast data used to drive the water temperature forecasting, as well as evaluating multiple sources of weather forecast data, could enhance the predictive capacity (Dietze, 2017b) for both water temperature and fish migrations.

Many potential improvements to the framework in Chapter 6 align with those for previous chapters. Future workflows for short-term forecasting DOC concentrations in river water could benefit from exploring the use of alternative meteorological forecast data sources (Dietze, 2017b). Additionally, employing a catchment-scale downscaling method for the forecast gridded meteorological dataset could improve local climate spatial and temporal representation and therefore both the hydrological and DOC modelling (Kay et al., 2023; Legrand et al., 2024). Multiple factors influence precipitation levels in settings like the Glenamong catchment including local and regional climate, ocean proximity,

topographic gradient and size (Doyle et al., 2019; Kay et al., 2023). Because of these factors, the weather forecast ensemble product used in this study showed, differently than for mean air temperature, some discrepancy in precipitation inputs relative to historical climate observations. For instance, peaks in daily rainfall were not well represented in the forecast data, indicated by NSE and r2 metrics, an aspect that could have negative implications on accuracy and representation along further modelling steps. To overcome this issue, a catchment-scale downscaling method (e.g., quantile mapping, weather typing, linear and generalised linear regression) could be employed to represent precipitation inputs more accurately for the study site (Kay et al., 2023; Legrand et al., 2024) or a scaling method (e.g., quantile-based techniques) could be applied to either forecast precipitation inputs (before running the model) or river discharge (applied dynamically to data before feeding the hydrological data to the DOC module).

Moreover, As in Chapter 4 and Chapter 5, testing an ensemble of models within this framework could enhance predictive skill (Olsson et al., 2024). Other modelling approaches, such as machine learning, statistical models, or hybrid techniques, could also be explored, given their growing application in short-term ecological forecasting (Feigl et al., 2021; Deng et al., 2022; Kim and Ahn, 2022; Dietze et al., 2024). Machine learning models, for example, have emerged as potential tools for modelling complex environmental variables, including those related to hydrology and water quality. Generally, this is due to their capacity to handle high-dimensional data and capture complex relationships that are not often represented in process-based models. In the case of using GWLF-DOC for forecasting DOC, it is important to acknowledge that the model simplifies many DOC-related processes (Naden et al., 2010; Paíz et al., 2025), which may influence both prediction accuracy and uncertainty estimation, especially in a short-term approach. Furthermore, data assimilation experiments, as discussed in Chapter 5, could be incorporated. Exploring variations of the Kalman Filter, different

assimilation frequencies, and alternative data assimilation methods could refine accuracy and uncertainty in the DOC concentration predictions (Loos et al., 2020a; Li et al., 2021; Wander et al., 2024).

Moreover, limitations related to using a relatively small ensemble of hydrological parameter sets (represented by the GLUE uncertainty bounds in Chapter 4) or/and a single optimised hydrological parameter set (in Chapter 6) would have implications on the representation of the hydrological dynamics both spatially and temporally, which would impact the DOC modelling. One key limitation in hydrological modelling was the reliance on a constant precipitation correction factor across both historical simulations and future projections. While such a correction may improve model calibration under current climate conditions, it assumes that biases in precipitation data remain stable over time. This assumption overlooks the possibility that systematic errors in climate model outputs or in observational datasets may vary across different temporal and spatial scales, particularly under future climate scenarios (Kay et al., 2023; Pulka et al., 2024). Consequently, a fixed correction factor may lead to under- or over-estimation of hydrological variables such as surface runoff, baseflow and river discharge when applied to non-stationary climatic conditions. This simplification may also impact seasonal or event-based discrepancies in precipitation inputs, which are important for accurately simulating extreme events or water availability and, therefore, for simulating DOC dynamics. Therefore, using a temporally dynamic or scenario-specific correction approach may provide a more robust representation of precipitation uncertainty in both hindcasting and forecasting contexts.

7.3 Personal development

Throughout this thesis, I have been able to develop my research skills further, particularly those related to understanding and applying models and forecasting techniques for water systems. This has allowed me to grow and adapt in a world subjected to rapid technological advances, which we, as scientists, have to cope with.

The way I do science has evolved over the last years, beyond addressing research gaps to evaluating how my work can be applied in real-world management situations. Each of the three case studies presented in this thesis has been a unique experience, requiring me to overcome particular challenges and undergo different learning curves.

It is important for me to acknowledge that the work in this thesis would not have been possible without the power of collaboration and networking. Researchers and professionals from different institutions participated in this work through a range of different activities (e.g., data collection, data curation, software development, supervision, etc.), all of which were essential in producing the final product. This enabled my research to be more feasible, applicable, robust and of greater quality.

The work presented in this thesis reflects a key phase in my development as a researcher and has equipped me to address the challenges in water resources management more effectively.

7.4 Concluding statements

The compilation of case studies in this thesis represents a step forward in modelling and forecasting changes in water systems and contributes to growing efforts to increase the availability of methods to support critical management needs. This work also highlights the value of modelling tools, emerging forecasting techniques, collaboration and networking to develop and deliver innovative forecasting solutions. The frameworks applied in each case study are tools proposed to be used, explored and adapted based on a human-centred design to supply context-dependent management needs. The findings of this thesis and the recommendations for further work, therefore, have the potential to assist in the mitigation of further environmental degradation and in building a future that is more climate-resilient and safer for people.

References

Abbaspour, K.C., Rouholahnejad, E., Vaghefi, S., Srinivasan, R., Yang, H., Kløve, B., 2015. A continental-scale hydrology and water quality model for Europe: Calibration and uncertainty of a high-resolution large-scale SWAT model. J. Hydrol. 524, 733–752. https://doi.org/10.1016/j.jhydrol.2015.03.027

Abbass, K., Qasim, M.Z., Song, H., Murshed, M., Mahmood, H., Younis, I., 2022. A review of the global climate change impacts, adaptation, and sustainable mitigation measures. Environ. Sci. Pollut. Res. 29, 42539–42559. https://doi.org/10.1007/s11356-022-19718-6

Absalan, F., Hatam, F., Prévost, M., Barbeau, B., Bichai, F., 2024. Climate change and future water demand: Implications for chlorine and trihalomethanes management in water distribution systems. J. Environ. Manage. 355, 120470. https://doi.org/10.1016/j.jenvman.2024.120470

Adler, T., Underwood, K.L., Rizzo, D.M., Harpold, A., Sterle, G., Li, L., Wen, H., Stinson, L., Bristol, C., Stewart, B., Lini, A., Perdrial, N., Perdrial, J.N., 2021. Drivers of Dissolved Organic Carbon Mobilization From Forested Headwater Catchments: A Multi Scaled Approach. Front. Water 3.

Aguilar-Alarcón, P., Gros, M., Farré, M.J., 2024. Non-targeted (ultra-)high-resolution mass spectrometry of dissolved organic matter to predict the formation of disinfection byproducts. Trends Environ. Anal. Chem. 42, e00231. https://doi.org/10.1016/j.teac.2024.e00231

Åkesson, A., Curtsdotter, A., Eklöf, A., Ebenman, B., Norberg, J., Barabás, G., 2021. The importance of species interactions in eco-evolutionary community dynamics under climate change. Nat. Commun. 12, 4759. https://doi.org/10.1038/s41467-021-24977-x

Allen, R., 2005. PENMAN–MONTEITH EQUATION, in: Hillel, D. (Ed.), Encyclopedia of Soils in the Environment. Elsevier, Oxford, pp. 180–188. https://doi.org/10.1016/B0-12-348530-4/00399-4

Anderson, B., Borgonovo, E., Galeotti, M., Roson, R., 2014. Uncertainty in Climate Change Modeling: Can Global Sensitivity Analysis Be of Help? Risk Anal. 34, 271–293. https://doi.org/10.1111/risa.12117

Anderson, L.E., DeMont, I., Dunnington, D.D., Bjorndahl, P., Redden, D.J., Brophy, M.J., Gagnon, G.A., 2023. A review of long-term change in surface water natural organic matter concentration in the northern hemisphere and the implications for drinking water treatment. Sci. Total Environ. 858, 159699. https://doi.org/10.1016/j.scitotenv.2022.159699

Andersson, A., 2021. Uncharted Waters : Non-target analysis of disinfection by-products in drinking water, Linköping Studies in Arts and Sciences. Linköping University Electronic Press, Linköping. https://doi.org/10.3384/diss.diva-173312

Armstrong, J.S., Trevarthen, J.A., 1999. Forecasting for Environmental Decision Making, in: Dale, V.H., English, M.R. (Eds.), Tools to Aid Environmental Decision Making. Springer New York, New York, NY, pp. 192–230. https://doi.org/10.1007/978-1-4612-1418-2_7

Arnold, J.G., Allen, P.M., Muttiah, R., Bernhardt, G., 1995. Automated Base Flow Separation and Recession Analysis Techniques. Groundwater 33, 1010–1018. https://doi.org/10.1111/j.1745-6584.1995.tb00046.x

Arsenault, J., Talbot, J., Moore, T.R., Knorr, K.-H., Teickner, H., Lapierre, J.-F., 2024. Patterns and drivers of organic matter decomposition in peatland open-water pools. https://doi.org/10.5194/egusphere-2024-271

Arvola, L., George, G., Livingstone, D.M., Järvinen, M., Blenckner, T., Dokulil, M.T., Jennings, E., Aonghusa, C.N., Nõges, P., Nõges, T., Weyhenmeyer, G.A., 2010. The Impact of the Changing Climate on the Thermal Characteristics of Lakes, in: George, G. (Ed.), The Impact of Climate Change on European Lakes. Springer Netherlands, Dordrecht, pp. 85–101. https://doi.org/10.1007/978-90-481-2945-4_6

Ayala, A.I., Mesman, J.P., Jones, I.D., De Eyto, E., Jennings, E., Goyette, S., Pierson, D.C., 2023. Climate Change Impacts on Surface Heat Fluxes in a Deep Monomictic Lake. J. Geophys. Res. Atmospheres 128, e2022JD038355. https://doi.org/10.1029/2022JD038355

Ayala, A.I., Moras, S., Pierson, D.C., 2020. Simulations of future changes in thermal structure of Lake Erken: proof of concept for ISIMIP2b lake sector local simulation strategy. Hydrol. Earth Syst. Sci. 24, 3311–3330. https://doi.org/10.5194/hess-24-3311-2020

Baker, N.J., Boubée, J., Lokman, P.M., Bolland, J.D., 2020. Evaluating the impact of hydropower on downstream migrating anguillid eels: Catchment-wide and fine-scale approaches to identify cost-effective solutions. Sci. Total Environ. 748, 141111. https://doi.org/10.1016/j.scitotenv.2020.141111

Baldursson, F.M., 1991. A Stochastic Fisheries Problem with Seasonal Migrations, in: Arnason, R., Bjørndal, T. (Eds.), Essays on the Economics of Migratory Fish Stocks, Studies in Contemporary Economics. Springer, Berlin, Heidelberg, pp. 69–82. https://doi.org/10.1007/978-3-642-84565-9_6

Barbarossa, V., Schmitt, R.J.P., Huijbregts, M.A.J., Zarfl, C., King, H., Schipper, A.M., 2020. Impacts of current and future large dams on the geographic range connectivity of freshwater fish worldwide. Proc. Natl. Acad. Sci. 117, 3648–3655. https://doi.org/10.1073/pnas.1912776117

Bärlund, I., Kirkkala, T., Malve, O., Kämäri, J., 2007. Assessing SWAT model performance in the evaluation of management actions for the implementation of the Water Framework Directive in a Finnish catchment. Environ. Model. Softw. 22, 719–724. https://doi.org/10.1016/j.envsoft.2005.12.030

Basu, A.S., Gill, L.W., Pilla, F., Basu, B., 2022. Assessment of Variations in Runoff Due to Landcover Changes Using the SWAT Model in an Urban River in Dublin, Ireland. Sustainability 14, 534. https://doi.org/10.3390/su14010534

Battin, J., Wiley, M.W., Ruckelshaus, M.H., Palmer, R.N., Korb, E., Bartz, K.K., Imaki, H., 2007. Projected impacts of climate change on salmon habitat restoration. Proc. Natl. Acad. Sci. 104, 6720–6725. https://doi.org/10.1073/pnas.0701685104

Bauer, P., Thorpe, A.J., Brunet, G., 2015. The quiet revolution of numerical weather prediction. Nature 525, 47–55.

Bell, V.A., Naden, P.S., Tipping, E., Davies, H.N., Carnell, E., Davies, J.A.C., Dore, A.J., Dragosits, U., Lapworth, D.J., Muhammed, S.E., Quinton, J.N., Stuart, M., Tomlinson, S., Wang, L., Whitmore, A.P., Wu, L., 2021. Long term simulations of macronutrients (C, N and P) in UK freshwaters. Sci. Total Environ. 776, 145813. https://doi.org/10.1016/j.scitotenv.2021.145813

Benson, N.U., Akintokun, O.A., Adedapo, A.E., 2017. Disinfection Byproducts in Drinking Water and Evaluation of Potential Health Risks of Long-Term Exposure in Nigeria. J. Environ. Public Health 2017, 1–10. https://doi.org/10.1155/2017/7535797

Bento, V.A., Russo, A., Dutra, E., Ribeiro, A.F.S., Gouveia, C.M., Trigo, R.M., 2022. Persistence versus dynamical seasonal forecasts of cereal crop yields. Sci. Rep. 12, 7422. https://doi.org/10.1038/s41598-022-11228-2

Beven, K., 2012. Rainfall-runoff modelling: the primer, 2. ed. ed. Wiley-Blackwell, Chichester.

Beven, K., Binley, A., 2014. GLUE: 20 years on. Hydrol. Process. 28, 5897–5918. https://doi.org/10.1002/hyp.10082

Beven, K., Binley, A., 1992. The future of distributed models: Model calibration and uncertainty prediction. Hydrol. Process. 6, 279–298. https://doi.org/10.1002/hyp.3360060305

Beven, K., Freer, J., 2001. Equifinality, data assimilation, and uncertainty estimation in mechanistic modelling of complex environmental systems using the GLUE methodology. J. Hydrol. 249, 11–29. https://doi.org/10.1016/S0022-1694(01)00421-8

Beven, K.J., 2009. Environmental modelling : an uncertain future? : an introduction to techniques for uncertainty estimation in environmental prediction / Keith Beven. Routledge, London ;

Blaurock, K., Beudert, B., Gilfedder, B.S., Fleckenstein, J.H., Peiffer, S., Hopp, L., 2021. Low hydrological connectivity after summer drought inhibits DOC export in a forested headwater catchment. Hydrol. Earth Syst. Sci. 25, 5133–5151. https://doi.org/10.5194/hess-25-5133-2021

Bodner, K., Rauen Firkowski, C., Bennett, J.R., Brookson, C., Dietze, M., Green, S., Hughes, J., Kerr, J., Kunegel-Lion, M., Leroux, S.J., McIntire, E., Molnár, P.K., Simpkins, C., Tekwa, E., Watts, A., Fortin, M., 2021. Bridging the divide between ecological forecasts and environmental decision making. Ecosphere 12. https://doi.org/10.1002/ecs2.3869

Bolstad, G.H., Karlsson, S., Hagen, I.J., Fiske, P., Urdal, K., Sægrov, H., Florø-Larsen, B., Sollien, V.P., Østborg, G., Diserud, O.H., Jensen, A.J., Hindar, K., 2021. Introgression from farmed escapees affects the full life cycle of wild Atlantic salmon. Sci. Adv. 7, eabj3397. https://doi.org/10.1126/sciadv.abj3397

Bonacina, L., Fasano, F., Mezzanotte, V., Fornaroli, R., 2023. Effects of water temperature on freshwater macroinvertebrates: a systematic review. Biol. Rev. 98, 191–221. https://doi.org/10.1111/brv.12903

Boretti, A., Rosa, L., 2019. Reassessing the projections of the World Water Development Report. Npj Clean Water 2, 1–6. https://doi.org/10.1038/s41545-019-0039-9

Bornstein, Y., Dayan, B., Cahn, A., Wells, S., Housh, M., 2022. Environmental Decision Support Systems as a Service: Demonstration on CE-QUAL-W2 Model. Water 14, 885. https://doi.org/10.3390/w14060885

Bosen, J.F., 1960. A FORMULA FOR APPROXIMATION OF THE SATURATION VAPOR PRESSURE OVER WATER.

Boughton, W., 1989. A review of the USDA SCS curve number method. Soil Res. 27, 511–523.

Boulange, J., Yoshida, T., Nishina, K., Okada, M., Hanasaki, N., 2023. Delivering the latest global water resource simulation results to the public. Clim. Serv. 30, 100386. https://doi.org/10.1016/j.cliser.2023.100386

Bradarić, M., Kranstauber, B., Bouten, W., Shamoun-Baranes, J., 2024. Forecasting nocturnal bird migration for dynamic aeroconservation: The value of short-term datasets. J. Appl. Ecol. 61, 1147–1158. https://doi.org/10.1111/1365-2664.14651

Bradford, J.B., Betancourt, J.L., Butterfield, B.J., Munson, S.M., Wood, T.E., 2018. Anticipatory natural resource science and management for a changing future. Front. Ecol. Environ. 16, 295–303. https://doi.org/10.1002/fee.1806

Bradford, J.B., Weltzin, J., McCormick, M.L., Baron, J., Bowen, Z., Bristol, S., Carlisle, D., Crimmins, T., Cross, P.C., DeVivo, J., Dietze, M., Freeman, M., Goldberg, J., Hooten, M., Hsu, L., Jenni, K., Keisman, J.L., Kennen, J., Lee, K., Lesmes, D.P., Loftin, K., Miller, B.W., Murdoch, P.S., Newman, J., Prentice, K.L., Rangwala, I., Read, J., Sieracki, J., Sofaer, H., Thur, S., Toevs, G., Werner, F., White, C.L., White, T., Wiltermuth, M.T., 2020a. Ecological forecasting—21st century science for 21st century management (Report No. 2020–1073), Open-File Report. Reston, VA. https://doi.org/10.3133/ofr20201073

Bradford, J.B., Weltzin, J.F., Wiltermuth, M., 2020b. Ecological Forecasting - 21st Century Science for 21st Century Management (Open-File Report), Open-File Report.

Brentan, B.M., Luvizotto Jr., E., Herrera, M., Izquierdo, J., Pérez-García, R., 2017. Hybrid regression model for near real-time urban water demand forecasting. J. Comput. Appl. Math. 309, 532–541. https://doi.org/10.1016/j.cam.2016.02.009

Bröcker, J., 2012. Evaluating raw ensembles with the continuous ranked probability score. Q. J. R. Meteorol. Soc. 138, 1611–1617. https://doi.org/10.1002/qj.1891

Bröcker, J., Smith, L.A., 2007. Increasing the Reliability of Reliability Diagrams. Weather Forecast. 22, 651–661. https://doi.org/10.1175/WAF993.1

Brown, J.N., Hochman, Z., Holzworth, D., Horan, H., 2018. Seasonal climate forecasts provide more definitive and accurate crop yield predictions. Agric. For. Meteorol. 260–261, 247–254. https://doi.org/10.1016/j.agrformet.2018.06.001

Bruce, L.C., Frassl, M.A., Arhonditsis, G.B., Gal, G., Hamilton, D.P., Hanson, P.C., Hetherington, A.L., Melack, J.M., Read, J.S., Rinke, K., Rigosi, A., Trolle, D., Winslow, L., Adrian, R., Ayala, A.I., Bocaniov, S.A., Boehrer, B., Boon, C., Brookes, J.D., Bueche, T., Busch, B.D., Copetti, D., Cortés, A., De Eyto, E., Elliott, J.A., Gallina, N., Gilboa, Y., Guyennon, N., Huang, L., Kerimoglu, O., Lenters, J.D., MacIntyre, S., Makler-Pick, V., McBride, C.G., Moreira, S., Özkundakci, D., Pilotti, M., Rueda, F.J., Rusak, J.A., Samal, N.R., Schmid, M., Shatwell, T., Snorthheim, C., Soulignac, F., Valerio, G., Van Der Linden, L., Vetter, M., Vinçon-Leite, B., Wang, J., Weber, M., Wickramaratne, C., Woolway, R.I., Yao, H., Hipsey, M.R., 2018. A multi-lake comparative analysis of the General Lake Model (GLM): Stress-testing across a global observatory network. Environ. Model. Softw. 102, 274–291. https://doi.org/10.1016/j.envsoft.2017.11.016

Burchard, H., Bolding, K., Kühn, W., Meister, A., Neumann, T., Umlauf, L., 2006. Description of a flexible and extendable physical–biogeochemical model system for the water column. J. Mar. Syst., Workshop on Future Directions in Modelling Physical-Biological Interactions (WKFDPBI) 61, 180–211. https://doi.org/10.1016/j.jmarsys.2005.04.011

Burchard, H., Bolding, K., Villarreal, M.R., 1999. GOTM, a general ocean turbulence model: theory, implementation and test cases. Space Applications Institute.

Busico, G., Colombani, N., Fronzi, D., Pellegrini, M., Tazioli, A., Mastrocicco, M., 2020. Evaluating SWAT model performance, considering different soils data input, to quantify

actual and future runoff susceptibility in a highly urbanized basin. J. Environ. Manage. 266, 110625. https://doi.org/10.1016/j.jenvman.2020.110625

Büttner, G., Kosztra, B., Soukup, T., Sousa, A., Langanke, T., 2017. CLC2018 Technical Guidelines.

Byrne, C.J., Poole, R., Rogan, G., Dillane, M., Whelan, K.F., 2003. Temporal and environmental influences on the variation in Atlantic salmon smolt migration in the Burrishoole system 1970–2000. J. Fish Biol. 63, 1552–1564. https://doi.org/10.1111/j.1095-8649.2003.00266.x

Cai, Y., Wang, H., Zhang, T., Zhou, Y., Dong, A., Huang, R., Zeng, Q., Yuan, H., 2023. Seasonal variation regulate the endogenous phosphorus release in sediments of Shijiuhu Lake via water-level fluctuation. Environ. Res. 238, 117247. https://doi.org/10.1016/j.envres.2023.117247

Carey, C.C., Woelmer, W.M., Lofton, M.E., Figueiredo, R.J., Bookout, B.J., Corrigan, R.S., Daneshmand, V., Hounshell, A.G., Howard, D.W., Lewis, A.S.L., McClure, R.P., Wander, H.L., Ward, N.K., Thomas, R.Q., 2022. Advancing lake and reservoir water quality management with near-term, iterative ecological forecasting. Inland Waters 12, 107–120. https://doi.org/10.1080/20442041.2020.1816421

Carstensen, M.V., Molina-Navarro, E., Hashemi, F., Kronvang, B., Bieger, K., 2023. Modelling the impact of the Nordic Bioeconomy Pathways and climate change on water quantity and quality in a Danish River Basin. CATENA 222, 106795. https://doi.org/10.1016/j.catena.2022.106795

Carter, L.J., Wright, R.M., Thomas, R.E., Reeds, J., Murphy, L.A., Collier, S.J., Evans, O., Baktoft, H., Bolland, J.D., 2023. Timing is everything; operational changes at a pumping station with a gravity sluice to provide safe downstream passage for silver European eels and deliver considerable financial savings. J. Environ. Manage. 347, 119143. https://doi.org/10.1016/j.jenvman.2023.119143

Chamberlain, S., Tupper, B., Fernández Bejarano, S.J., Mendelssohn, R., 2024. General purpose R client for “ERDDAP” servers. Includes functions to search for “datasets”, get summary information on “datasets”, and fetch “datasets”, in either “csv” or “netCDF” format.

Chawanda, C.J., Nkwasa, A., Thiery, W., van Griensven, A., 2024. Combined impacts of climate and land-use change on future water resources in Africa. Hydrol. Earth Syst. Sci. 28, 117–138. https://doi.org/10.5194/hess-28-117-2024

Chen, X., Lee, R.M., Dwivedi, D., Son, K., Fang, Y., Zhang, X., Graham, E., Stegen, J., Fisher, J.B., Moulton, D., Scheibe, T.D., 2021. Integrating field observations and process-based modeling to predict watershed water quality under environmental perturbations. J. Hydrol. 602, 125762. https://doi.org/10.1016/j.jhydrol.2020.125762

Chen, Y., Marek, G.W., Marek, T.H., Moorhead, J.E., Heflin, K.R., Brauer, D.K., Gowda, P.H., Srinivasan, R., 2019. Simulating the impacts of climate change on hydrology and crop production in the Northern High Plains of Texas using an improved SWAT model. Agric. Water Manag. 221, 13–24. https://doi.org/10.1016/j.agwat.2019.04.021

Clark, J.M., Ashley, D., Wagner, M., Chapman, P.J., Lane, S.N., Evans, C.D., Heathwaite, A.L., 2009. Increased temperature sensitivity of net DOC production from ombrotrophic peat due to water table draw-down. Glob. Change Biol. 15, 794–807. https://doi.org/10.1111/j.1365-2486.2008.01683.x

Clark, J.M., Bottrell, S.H., Evans, C.D., Monteith, D.T., Bartlett, R., Rose, R., Newton, R.J., Chapman, P.J., 2010. The importance of the relationship between scale and process in understanding long-term DOC dynamics. Sci. Total Environ. 408, 2768–2775. https://doi.org/10.1016/j.scitotenv.2010.02.046

Costa, C.M. da S.B., Leite, I.R., Almeida, A.K., de Almeida, I.K., 2021. Choosing an appropriate water quality model—a review. Environ. Monit. Assess. 193, 38. https://doi.org/10.1007/s10661-020-08786-1

Couture, R.-M., Moe, S.J., Lin, Y., Kaste, Ø., Haande, S., Lyche Solheim, A., 2018. Simulating water quality and ecological status of Lake Vansjø, Norway, under land-use and climate change by linking process-oriented models with a Bayesian network. Sci. Total Environ. 621, 713–724. https://doi.org/10.1016/j.scitotenv.2017.11.303

Creed, I.F., Bergström, A.-K., Trick, C.G., Grimm, N.B., Hessen, D.O., Karlsson, J., Kidd, K.A., Kritzberg, E., McKnight, D.M., Freeman, E.C., Senar, O.E., Andersson, A., Ask, J., Berggren, M., Cherif, M., Giesler, R., Hotchkiss, E.R., Kortelainen, P., Palta, M.M., Vrede, T., Weyhenmeyer, G.A., 2018. Global change-driven effects on dissolved organic matter composition: Implications for food webs of northern lakes. Glob. Change Biol. 24, 3692–3714. https://doi.org/10.1111/gcb.14129

Crippa, N., Grillakis, M.G., Tsilimigkras, A., Yang, G., Giuliani, M., Koutroulis, A.G., 2023. Seasonal forecast-informed reservoir operation. Potential benefits for a water-stressed Mediterranean basin. Clim. Serv. 32, 100406. https://doi.org/10.1016/j.cliser.2023.100406

Cuddington, K., Fortin, M.-J., Gerber, L.R., Hastings, A., Liebhold, A., O'Connor, M., Ray, C., 2013. Process-based models are required to manage ecological systems in a changing world. Ecosphere 4, art20. https://doi.org/10.1890/ES12-00178.1

Cui, T., Sreekanth, J., Pickett, T., Rassam, D., Gilfedder, M., Barrett, D., 2021. Impact of model parameterization on predictive uncertainty of regional groundwater models in the context of environmental impact assessment. Environ. Impact Assess. Rev. 90, 106620. https://doi.org/10.1016/j.eiar.2021.106620

Dai, Y., Lang, Y., Wang, T., Han, X., Wang, L., Zhong, J., 2021. Modelling the sources and transport of ammonium nitrogen with the SPARROW model: A case study in a karst basin. J. Hydrol. 592, 125763. https://doi.org/10.1016/j.jhydrol.2020.125763

Dambrine, C., Lambert, P., Elliott, S., Boavida-Portugal, J., Mateus, C.S., O'Leary, C., Pauwels, I., Poole, R., Roche, W., Van den Bergh, E., Vanoverbeke, J., Chust, G., Lassalle, G., 2023. Connecting population functionality with distribution model predictions to support freshwater and marine management of diadromous fish species. Biol. Conserv. 287, 110324. https://doi.org/10.1016/j.biocon.2023.110324

Daniel, E.B., 2011. Watershed Modeling and its Applications: A State-of-the-Art Review. Open Hydrol. J. 5, 26–50. https://doi.org/10.2174/1874378101105010026

Daraei, H., Awad, J., Bertone, E., Stewart, R.A., Chow, C.W.K., Duan, J., Creamer, J., Van Leeuwen, J., 2023. DOC signal-based alum dose control for drinking water treatment plants. J. Water Process Eng. 54, 103934. https://doi.org/10.1016/j.jwpe.2023.103934

Davidson, E.A., Janssens, I.A., 2006. Temperature sensitivity of soil carbon decomposition and feedbacks to climate change. Nature 440, 165–173. https://doi.org/10.1038/nature04514

de Eyto, E., Doyle, B., King, N., Kilbane, T., Finlay, R., Sibigtroth, L., Graham, C., Poole, R., Ryder, E., Dillane, M., Jennings, E., 2020. Characterisation of salmonid food webs in the rivers and lakes of an Irish peatland ecosystem. Biol. Environ. Proc. R. Ir. Acad. 120B, 1–17. https://doi.org/10.1353/bae.2020.0013

de Eyto, E., Jennings, E., Ryder, E., Sparber, K., Dillane, M., Dalton, C., Poole, R., 2016. Response of a humic lake ecosystem to an extreme precipitation event: physical, chemical, and biological implications. Inland Waters 6, 483–498. https://doi.org/10.1080/IW-6.4.875

de Eyto, E., Kelly, S., Rogan, G., French, A., Cooney, J., Murphy, M., Nixon, P., Hughes, P., Sweeney, D., McGinnity, P., Dillane, M., Poole, R., 2022. Decadal Trends in the Migration Phenology of Diadromous Fishes Native to the Burrishoole Catchment, Ireland. Front. Ecol. Evol. 10, 915854. https://doi.org/10.3389/fevo.2022.915854

De Hertog, S.J., Orlov, A., Havermann, F., Guo, S., Manola, I., Pongratz, J., Lejeune, Q., Schleussner, C.-F., Menke, I., Humpenöder, F., Popp, A., Lawrence, P., Hurtt, G.C., Chini, L., Vanderkelen, I., Davin, E.L., Reerink, T., Seneviratne, S.I., Verbeeck, H., Thiery, W., 2025. Limited Effect of Future Land-Use Changes on Human Heat Stress and Labor Capacity. Earths Future 13, e2024EF005021. https://doi.org/10.1029/2024EF005021

de Wit, H.A., Mulder, J., Hindar, A., Hole, L., 2007. Long-Term Increase in Dissolved Organic Carbon in Streamwaters in Norway Is Response to Reduced Acid Deposition. Environ. Sci. Technol. 41, 7706–7713. https://doi.org/10.1021/es070557f

DeMont, I., Stoddart, A.K., Gagnon, G.A., 2021. Assessing strategies to improve the efficacy and efficiency of direct filtration plants facing changes in source water quality from anthropogenic and climatic pressures. J. Water Process Eng. 39, 101689. https://doi.org/10.1016/j.jwpe.2020.101689

Deng, B., Liu, P., Chin, R.J., Kumar, P., Jiang, C., Xiang, Y., Liu, Y., Lai, S.H., Luo, H., 2022. Hybrid metaheuristic machine learning approach for water level prediction: A case study in Dongting Lake. Front. Earth Sci. 10. https://doi.org/10.3389/feart.2022.928052

Diana, M., Felipe-Sotelo, M., Bond, T., 2019. Disinfection byproducts potentially responsible for the association between chlorinated drinking water and bladder cancer: A review. Water Res. 162, 492–504. https://doi.org/10.1016/j.watres.2019.07.014

Dias, B.S., Frisk, M.G., Jordaan, A., 2019. Opening the tap: Increased riverine connectivity strengthens marine food web pathways. PLOS ONE 14, e0217008. https://doi.org/10.1371/journal.pone.0217008

Dietze, M., Lynch, H., 2019. Forecasting a bright future for ecology. Front. Ecol. Environ. 17, 3–3. https://doi.org/10.1002/fee.1994

Dietze, M., White, E.P., Abeyta, A., Boettiger, C., Bueno Watts, N., Carey, C.C., Chaplin-Kramer, R., Emanuel, R.E., Ernest, S.K.M., Figueiredo, R.J., Gerst, M.D., Johnson, L.R., Kenney, M.A., McLachlan, J.S., Paschalidis, I.C., Peters, J.A., Rollinson, C.R., Simonis, J., Sullivan-Wiley, K., Thomas, R.Q., Wardle, G.M., Willson, A.M., Zwart, J., 2024. Near-term ecological forecasting for climate change action. Nat. Clim. Change 14, 1236–1244. https://doi.org/10.1038/s41558-024-02182-0

Dietze, M.C., 2017a. Ecological Forecasting. Princeton University Press. https://doi.org/10.2307/j.ctvc7796h

Dietze, M.C., 2017b. Prediction in ecology: a first-principles framework. Ecol. Appl. 27, 2048–2060. https://doi.org/10.1002/eap.1589

Dietze, M.C., Fox, A., Beck-Johnson, L.M., Betancourt, J.L., Hooten, M.B., Jarnevich, C.S., Keitt, T.H., Kenney, M.A., Laney, C.M., Larsen, L.G., Loescher, H.W., Lunch, C.K., Pijanowski, B.C., Randerson, J.T., Read, E.K., Tredennick, A.T., Vargas, R., Weathers, K.C., White, E.P., 2018. Iterative near-term ecological forecasting: Needs, opportunities, and challenges. Proc. Natl. Acad. Sci. 115, 1424–1432. https://doi.org/10.1073/pnas.1710231115

Dietze, M.C., Lebauer, D.S., Kooper, R., 2013. On improving the communication between models and data. Plant Cell Environ. 36, 1575–1585. https://doi.org/10.1111/pce.12043

Diffenbaugh, N.S., 2020. Verification of extreme event attribution: Using out-of-sample observations to assess changes in probabilities of unprecedented events. Sci. Adv. 6, eaay2368. https://doi.org/10.1126/sciadv.aay2368

Doak, D.F., Estes, J.A., Halpern, B.S., Jacob, U., Lindberg, D.R., Lovvorn, J., Monson, D.H., Tinker, M.T., Williams, T.M., Wootton, J.T., Carroll, I., Emmerson, M., Micheli, F., Novak, M., 2008. UNDERSTANDING AND PREDICTING ECOLOGICAL DYNAMICS: ARE MAJOR SURPRISES INEVITABLE. Ecology 89, 952–961. https://doi.org/10.1890/07-0965.1

Dong, H., Zhang, S., Lin, J., Zhu, B., 2021. Responses of soil microbial biomass carbon and dissolved organic carbon to drying-rewetting cycles: A *meta*-analysis. CATENA 207, 105610. https://doi.org/10.1016/j.catena.2021.105610

Doyle, B.C., de Eyto, E., Dillane, M., Poole, R., McCarthy, V., Ryder, E., Jennings, E., 2019. Synchrony in catchment stream colour levels is driven by both local and regional climate. Biogeosciences 16, 1053–1071. https://doi.org/10.5194/bg-16-1053-2019

Doyle, B.C., De Eyto, E., McCarthy, V., Dillane, M., Jennings, E., 2023. The organic carbon budget of an oligotrophic temperate peatland lake. Limnol. Oceanogr. 68, 544–556. https://doi.org/10.1002/lno.12292

Doyle, B.C., de Eyto, E., McCarthy, V., Dillane, M., Poole, R., Jennings, E., 2021a. Late summer peak in p CO_2 corresponds with catchment export of DOC in a temperate, humic lake. Inland Waters 11, 234–249. https://doi.org/10.1080/20442041.2021.1893098

Doyle, B.C., de Eyto, E., McCarthy, V., Dillane, M., Poole, R., Jennings, E., 2021b. Late summer peak in p CO_2 corresponds with catchment export of DOC in a temperate, humic lake. Inland Waters 11, 234–249. https://doi.org/10.1080/20442041.2021.1893098

Du, J., Deng, G., 2022. How Should a Numerical Weather Prediction Be Used: Full Field or Anomaly? A Conceptual Demonstration with a Lorenz Model. Atmosphere 13, 1487. https://doi.org/10.3390/atmos13091487

Du, X., Zhang, X., Mukundan, R., Hoang, L., Owens, E.M., 2019. Integrating terrestrial and aquatic processes toward watershed scale modeling of dissolved organic carbon fluxes. Environ. Pollut. 249, 125–135. https://doi.org/10.1016/j.envpol.2019.03.014

Duan, W.L., He, B., Takara, K., Luo, P.P., Nover, D., Hu, M.C., 2015. Modeling suspended sediment sources and transport in the Ishikari River basin, Japan, using SPARROW. Hydrol. Earth Syst. Sci. 19, 1293–1306. https://doi.org/10.5194/hess-19-1293-2015

Durif, C.M.F., Elie, P., 2008. Predicting downstream migration of silver eels in a large river catchment based on commercial fishery data. Fish. Manag. Ecol. 15, 127–137. https://doi.org/10.1111/j.1365-2400.2008.00593.x

Einola, E., 2013. Present and future fluxes of nitrogen, phosphorus and carbon from catchments to lakes in a boreal landscape [WWW Document]. URL https://helda.helsinki.fi/items/dc588164-5870-4759-824c-ed610b4ed26b (accessed 2.27.24).

EPA, 2013. EPA Drinking Water Guidance on Disinfection By-Products. Advice Note No. 4. Version 2. Disinfection By-Products in Drinking Water (No. ISBN 978-1-84095-444-9), 2.

Ervinia, A., Huang, J., Zhang, Z., 2020. Nitrogen sources, processes, and associated impacts of climate and land-use changes in a coastal China watershed: Insights from the INCA-N model. Mar. Pollut. Bull. 159, 111502. https://doi.org/10.1016/j.marpolbul.2020.111502

Esper, J., Torbenson, M., Büntgen, U., 2024. 2023 summer warmth unparalleled over the past 2,000 years. Nature 631, 94–97. https://doi.org/10.1038/s41586-024-07512-y

Evans, C.D., Chapman, P.J., Clark, J.M., Monteith, D.T., Cresser, M.S., 2006. Alternative explanations for rising dissolved organic carbon export from organic soils. Glob. Change Biol. 12, 2044–2053. https://doi.org/10.1111/j.1365-2486.2006.01241.x

Evans, C.D., Monteith, D.T., Cooper, D.M., 2005. Long-term increases in surface water dissolved organic carbon: Observations, possible causes and environmental impacts. Environ. Pollut., Recovery from acidificationin the UK: Evidence from 15 years of acid waters monitoring 137, 55–71. https://doi.org/10.1016/j.envpol.2004.12.031

Evensen, G., 2009. Data Assimilation: The Ensemble Kalman Filter. Springer, Berlin, Heidelberg. https://doi.org/10.1007/978-3-642-03711-5

Exbrayat, J.-F., Viney, N.R., Seibert, J., Wrede, S., Frede, H.-G., Breuer, L., 2010. Ensemble modelling of nitrogen fluxes: data fusion for a Swedish meso-scale catchment. Hydrol. Earth Syst. Sci. 14, 2383–2397. https://doi.org/10.5194/hess-14-2383-2010

Fang, X., Zhang, J., Chen, Y., Xu, X., 2008. QUAL2K Model Used in the Water Quality Assessment of Qiantang River, China. Water Environ. Res. 80, 2125–2133.

Farkas, C., Shore, M., Engebretsen, A., Skarbøvik, E., 2023. Suspended sediment response to Nordic bioeconomy and climate change scenarios in a first-order agricultural catchment. CATENA 222, 106794. https://doi.org/10.1016/j.catena.2022.106794

Feigl, M., Lebiedzinski, K., Herrnegger, M., Schulz, K., 2021. Machine-learning methods for stream water temperature prediction. Hydrol. Earth Syst. Sci. 25, 2951–2977. https://doi.org/10.5194/hess-25-2951-2021

Fenner, N., Meadham, J., Jones, T., Hayes, F., Freeman, C., 2021. Effects of Climate Change on Peatland Reservoirs: A DOC Perspective. Glob. Biogeochem. Cycles 35, e2021GB006992. https://doi.org/10.1029/2021GB006992

Fer, I., Gardella, A.K., Shiklomanov, A.N., Campbell, E.E., Cowdery, E.M., De Kauwe, M.G., Desai, A., Duveneck, M.J., Fisher, J.B., Haynes, K.D., Hoffman, F.M., Johnston, M.R., Kooper, R., LeBauer, D.S., Mantooth, J., Parton, W.J., Poulter, B., Quaife, T., Raiho, A., Schaefer, K., Serbin, S.P., Simkins, J., Wilcox, K.R., Viskari, T., Dietze, M.C., 2021. Beyond ecosystem modeling: A roadmap to community cyberinfrastructure for ecological data-model integration. Glob. Change Biol. 27, 13–26. https://doi.org/10.1111/gcb.15409

Finstad, A.G., Andersen, T., Larsen, S., Tominaga, K., Blumentrath, S., de Wit, H.A., Tømmervik, H., Hessen, D.O., 2016. From greening to browning: Catchment vegetation development and reduced S-deposition promote organic carbon load on decadal time scales in Nordic lakes. Sci. Rep. 6, 31944. https://doi.org/10.1038/srep31944

Foley, M.M., Martone, R.G., Fox, M.D., Kappel, C.V., Mease, L.A., Erickson, A.L., Halpern, B.S., Selkoe, K.A., Taylor, P., Scarborough, C., 2015. Using Ecological Thresholds to Inform Resource Management: Current Options and Future Possibilities. Front. Mar. Sci. 2. https://doi.org/10.3389/fmars.2015.00095

Francesconi, W., Srinivasan, R., Pérez-Miñana, E., Willcock, S.P., Quintero, M., 2016. Using the Soil and Water Assessment Tool (SWAT) to model ecosystem services: A systematic review. J. Hydrol. 535, 625–636. https://doi.org/10.1016/j.jhydrol.2016.01.034

Franklin, H.M., Doederer, K., Neale, P.A., Hayton, J.B., Fisher, P., Maxwell, P., Carroll, A.R., Burford, M.A., Leusch, F.D.L., 2021a. Terrestrial dissolved organic matter source affects disinfection by-product formation during water treatment and subsequent toxicity. Environ. Pollut. 283, 117232. https://doi.org/10.1016/j.envpol.2021.117232

Franklin, H.M., Doederer, K., Neale, P.A., Hayton, J.B., Fisher, P., Maxwell, P., Carroll, A.R., Burford, M.A., Leusch, F.D.L., 2021b. Terrestrial dissolved organic matter source affects disinfection by-product formation during water treatment and subsequent toxicity. Environ. Pollut. 283, 117232. https://doi.org/10.1016/j.envpol.2021.117232

Franklin, P.A., Bašić, T., Davison, P.I., Dunkley, K., Ellis, J., Gangal, M., González-Ferreras, A.M., Gutmann Roberts, C., Hunt, G., Joyce, D., Klöcker, C.A., Mawer, R., Rittweg, T., Stoilova, V., Gutowsky, L.F.G., 2024. Aquatic connectivity: challenges and solutions in a changing climate. J. Fish Biol. n/a. https://doi.org/10.1111/jfb.15727

Fry, Apps Deanna, Gronewold Andrew D., 2020. Operational Seasonal Water Supply and Water Level Forecasting for the Laurentian Great Lakes. J. Water Resour. Plan. Manag. 146, 04020072. https://doi.org/10.1061/(ASCE)WR.1943-5452.0001214

Fu, B., Horsburgh, J.S., Jakeman, A.J., Gualtieri, C., Arnold, T., Marshall, L., Green, T.R., Quinn, N.W.T., Volk, M., Hunt, R.J., Vezzaro, L., Croke, B.F.W., Jakeman, J.D., Snow, V., Rashleigh, B., 2020. Modeling Water Quality in Watersheds: From Here to the Next Generation. Water Resour. Res. 56. https://doi.org/10.1029/2020WR027721

Fu, B., Merritt, W.S., Croke, B.F.W., Weber, T.R., Jakeman, A.J., 2019. A review of catchment-scale water quality and erosion models and a synthesis of future prospects. Environ. Model. Softw. 114, 75–97. https://doi.org/10.1016/j.envsoft.2018.12.008

Futter, M.N., Butterfield, D., Cosby, B.J., Dillon, P.J., Wade, A.J., Whitehead, P.G., 2007. Modeling the mechanisms that control in-stream dissolved organic carbon dynamics in upland and forested catchments. Water Resour. Res. 43. https://doi.org/10.1029/2006WR004960

Futter, M.N., Löfgren, S., Köhler, S.J., Lundin, L., Moldan, F., Bringmark, L., 2011. Simulating Dissolved Organic Carbon Dynamics at the Swedish Integrated Monitoring Sites with the Integrated Catchments Model for Carbon, INCA-C. AMBIO 40, 906–919. https://doi.org/10.1007/s13280-011-0203-z

Gal, G., Hipsey, M.R., Parparov, A., Wagner, U., Makler, V., Zohary, T., 2009. Implementation of ecological modeling as an effective management and investigation tool: Lake Kinneret as a case study. Ecol. Model. 220, 1697–1718. https://doi.org/10.1016/j.ecolmodel.2009.04.010

Gallagher, K., Charvin, K., Nielsen, S., Sambridge, M., Stephenson, J., 2009. Markov chain Monte Carlo (MCMC) sampling methods to determine optimal models, model resolution and model choice for Earth Science problems. Mar. Pet. Geol., Thematic Set on Basin Modeling Perspectives 26, 525–535. https://doi.org/10.1016/j.marpetgeo.2009.01.003

Gao, L., Li, D., 2014. A review of hydrological/water-quality models. Front. Agric. Sci. Eng. 1, 267. https://doi.org/10.15302/J-FASE-2014041

Gargan, P.G., Stafford, T., Økland, F., Thorstad, E.B., 2015. Survival of wild Atlantic salmon (*Salmo salar*) after catch and release angling in three Irish rivers. Fish. Res. 161, 252–260. https://doi.org/10.1016/j.fishres.2014.08.005

Garmo, Ø.A., Skjelkvåle, B.L., de Wit, H.A., Colombo, L., Curtis, C., Fölster, J., Hoffmann, A., Hruška, J., Høgåsen, T., Jeffries, D.S., Keller, W.B., Krám, P., Majer, V., Monteith, D.T., Paterson, A.M., Rogora, M., Rzychon, D., Steingruber, S., Stoddard, J.L., Vuorenmaa, J., Worsztynowicz, A., 2014. Trends in Surface Water Chemistry in Acidified Areas in Europe and North America from 1990 to 2008. Water. Air. Soil Pollut. 225, 1880. https://doi.org/10.1007/s11270-014-1880-6

Gassman, M. R. Reyes, C. H. Green, J. G. Arnold, 2007. The Soil and Water Assessment Tool: Historical Development, Applications, and Future Research Directions. Trans. ASABE 50, 1211–1250. https://doi.org/10.13031/2013.23637

Gaudard, A., Råman Vinnå, L., Bärenbold, F., Schmid, M., Bouffard, D., 2019. Toward an open access to high-frequency lake modeling and statistics data for scientists and practitioners – the case of Swiss lakes using Simstrat v2.1. Geosci. Model Dev. 12, 3955–3974. https://doi.org/10.5194/gmd-12-3955-2019

Gende, S.M., Edwards, R.T., Willson, M.F., Wipfli, M.S., 2002. Pacific Salmon in Aquatic and Terrestrial Ecosystems: Pacific salmon subsidize freshwater and terrestrial ecosystems through several pathways, which generates unique management and conservation issues but also provides valuable research opportunities. BioScience 52, 917–928. https://doi.org/10.1641/0006-3568(2002)052[0917:PSIAAT]2.0.CO;2

George, G., Järvinen, M., Nõges, T., Blenckner, T., Moore, K., 2010. The Impact of the Changing Climate on the Supply and Recycling of Nitrate, in: George, G. (Ed.), The Impact of Climate Change on European Lakes. Springer Netherlands, Dordrecht, pp. 161–178. https://doi.org/10.1007/978-90-481-2945-4_10

Georgescu, P.-L., Moldovanu, S., Iticescu, C., Calmuc, M., Calmuc, V., Topa, C., Moraru, L., 2023. Assessing and forecasting water quality in the Danube River by using neural network approaches. Sci. Total Environ. 879, 162998. https://doi.org/10.1016/j.scitotenv.2023.162998

Gilca, A.F., Teodosiu, C., Fiore, S., Musteret, C.P., 2020. Emerging disinfection byproducts: A review on their occurrence and control in drinking water treatment processes. Chemosphere 259, 127476. https://doi.org/10.1016/j.chemosphere.2020.127476

Glock, K., Tritthart, M., Habersack, H., Hauer, C., 2019. Comparison of Hydrodynamics Simulated by 1D, 2D and 3D Models Focusing on Bed Shear Stresses. Water 11. https://doi.org/10.3390/w11020226

Gonsior, M., Schmitt-Kopplin, P., Stavklint, H., Richardson, S.D., Hertkorn, N., Bastviken, D., 2014. Changes in Dissolved Organic Matter during the Treatment Processes of a Drinking Water Plant in Sweden and Formation of Previously Unknown Disinfection Byproducts. Environ. Sci. Technol. 48, 12714–12722. https://doi.org/10.1021/es504349p

Goudsmit, G.-H., Burchard, H., Peeters, F., Wüest, A., 2002. Application of k-ϵ turbulence models to enclosed basins: The role of internal seiches. J. Geophys. Res. Oceans 107, 23-1-23–13. https://doi.org/10.1029/2001JC000954

Graneli, W., 2012. Brownification of Lakes, in: Bengtsson, L., Herschy, R.W., Fairbridge, R.W. (Eds.), Encyclopedia of Lakes and Reservoirs. Springer Netherlands, Dordrecht, pp. 117–119. https://doi.org/10.1007/978-1-4020-4410-6_256

Gumpinger, C., Höfler, S., Berg, K., Pichler-Scheder, C., 2010. Water Temperature as an Applicable Parameter with a High Indicative Value for the General Condition of a River-Ecosystem, Drawing on the Example of the River Trattnach in Upper Austria. Transylv Rev Syst Ecol Res 10 2010 Wetl. Divers. Transylv. Rev. Syst. Ecol. Res., 1–14.

Haith, D.A., Shoemaker, L.L., 1987. GENERALIZED WATERSHED LOADING FUNCTIONS FOR STREAM FLOW NUTRIENTS1. JAWRA J. Am. Water Resour. Assoc. 23, 471–478. https://doi.org/10.1111/j.1752-1688.1987.tb00825.x

Hamill, T.M., Whitaker, J.S., Shlyaeva, A., Bates, G., Fredrick, S., Pegion, P., Sinsky, E., Zhu, Y., Tallapragada, V., Guan, H., Zhou, X., Woollen, J., 2022. The Reanalysis for the Global Ensemble Forecast System, Version 12. Mon. Weather Rev. 150, 59–79. https://doi.org/10.1175/MWR-D-21-0023.1

Hamon, W.R., 1961. Estimating Potential Evapotranspiration. J. Hydraul. Div. 87, 107–120. https://doi.org/10.1061/JYCEAJ.0000599

Harenda, K.M., Lamentowicz, M., Samson, M., Chojnicki, B.H., 2018. The Role of Peatlands and Their Carbon Storage Function in the Context of Climate Change, in: Zielinski, T.,

Sagan, I., Surosz, W. (Eds.), Interdisciplinary Approaches for Sustainable Development Goals, GeoPlanet: Earth and Planetary Sciences. Springer International Publishing, Cham, pp. 169–187. https://doi.org/10.1007/978-3-319-71788-3_12

Harringmeyer, O.S., Woolfolk, M.L., Hoekstra, H.E., 2021. Fishing for the genetic basis of migratory behavior. Cell 184, 303–305. https://doi.org/10.1016/j.cell.2020.12.037

Harris, J.H., Kingsford, R.T., Peirson, W., Baumgartner, L.J., 2016. Mitigating the effects of barriers to freshwater fish migrations: the Australian experience. Mar. Freshw. Res. 68, 614–628. https://doi.org/10.1071/MF15284

Hattermann, F.F., Vetter, T., Breuer, L., Su, B., Daggupati, P., Donnelly, C., Fekete, B., Flörke, F., Gosling, S.N., Hoffmann, P., Liersch, S., Masaki, Y., Motovilov, Y., Müller, C., Samaniego, L., Stacke, T., Wada, Y., Yang, T., Krysnaova, V., 2018. Sources of uncertainty in hydrological climate impact assessment: a cross-scale study. Environ. Res. Lett. 13, 015006. https://doi.org/10.1088/1748-9326/aa9938

He, S., Chen, K., Liu, Z., Deng, L., 2023. Exploring the impacts of climate change and human activities on future runoff variations at the seasonal scale. J. Hydrol. 619, 129382. https://doi.org/10.1016/j.jhydrol.2023.129382

Her, Y., Yoo, S.-H., Cho, J., Hwang, S., Jeong, J., Seong, C., 2019a. Uncertainty in hydrological analysis of climate change: multi-parameter vs. multi-GCM ensemble predictions. Sci. Rep. 9, 4974. https://doi.org/10.1038/s41598-019-41334-7

Her, Y., Yoo, S.-H., Cho, J., Hwang, S., Jeong, J., Seong, C., 2019b. Uncertainty in hydrological analysis of climate change: multi-parameter vs. multi-GCM ensemble predictions. Sci. Rep. 9, 4974. https://doi.org/10.1038/s41598-019-41334-7

Hipsey, M.R., Bruce, L.C., Boon, C., Busch, B., Carey, C.C., Hamilton, D.P., Hanson, P.C., Read, J.S., de Sousa, E., Weber, M., Winslow, L.A., 2019. A General Lake Model (GLM 3.0) for linking with high-frequency sensor data from the Global Lake Ecological Observatory Network (GLEON). Geosci. Model Dev. 12, 473–523. https://doi.org/10.5194/gmd-12-473-2019

Hipsey, M.R., Bruce, L.C., Boon, C., Busch, B., Carey, C.C., Hamilton, D.P., Hanson, P.C., Read, J.S., De Sousa, E., Weber, M., Winslow, L.A., 2017. A General Lake Model (GLM 2.4) for linking with high-frequency sensor data from the Global Lake Ecological Observatory Network (GLEON) (preprint). Hydrology. https://doi.org/10.5194/gmd-2017-257

Hipsey, M.R., Bruce, L.C., Hamilton, D.P., 2014. GLM Manual v2 [WWW Document]. URL https://swan.science.uwa.edu.au/downloads/AED_GLM_v2_0b0_20141025.pdf (accessed 2.5.25).

Hipsey, M.R., Bruce, L.C., Hamilton, D.P., 2013. AED Manual v4 [WWW Document]. URL https://aed.see.uwa.edu.au/research/models/aed/Download/AED_ScienceManual_v4_draft.pdf (accessed 2.5.25).

Hobday, A.J., Spillman, C.M., Paige Eveson, J., Hartog, J.R., 2016. Seasonal forecasting for decision support in marine fisheries and aquaculture. Fish. Oceanogr. 25, 45–56. https://doi.org/10.1111/fog.12083

Höge, M., Wöhling, T., Nowak, W., 2018. A Primer for Model Selection: The Decisive Role of Model Complexity. Water Resour. Res. 54, 1688–1715. https://doi.org/10.1002/2017WR021902

Hollaway, M.J., Beven, K.J., Benskin, C.McW.H., Collins, A.L., Evans, R., Falloon, P.D., Forber, K.J., Hiscock, K.M., Kahana, R., Macleod, C.J.A., Ockenden, M.C., Villamizar, M.L., Wearing, C., Withers, P.J.A., Zhou, J.G., Barber, N.J., Haygarth, P.M., 2018. The challenges of modelling phosphorus in a headwater catchment: Applying a ‘limits of

acceptability' uncertainty framework to a water quality model. J. Hydrol. 558, 607–624. https://doi.org/10.1016/j.jhydrol.2018.01.063

Holman, I.P., Brown, C., Carter, T.R., Harrison, P.A., Rounsevell, M., 2019. Improving the representation of adaptation in climate change impact models. Reg. Environ. Change 19, 711–721. https://doi.org/10.1007/s10113-018-1328-4

Horppila, J., Pippingsköld, E., Estlander, S., 2022. Effects of water colour on the pigment content of a floating-leaved macrophyte—Implications of lake brownification. Aquat. Bot. 181, 103540. https://doi.org/10.1016/j.aquabot.2022.103540

Hutton, R.J.B., 2019. Minding the weather: how forecasters think. Ergonomics 62, 128–129. https://doi.org/10.1080/00140139.2018.1507523

Imberger, J., Patterson, J.C., 1981. A DYNAMIC RESERVOIR SIMULATION MODEL - DYRESM: 5. Elsevier, pp. 310–361. https://doi.org/10.1016/B978-0-12-258152-6.50014-2

IPCC, Calvin, K., Dasgupta, D., Krinner, G., Mukherji, A., Thorne, P.W., Trisos, C., Romero, J., Aldunce, P., Barrett, K., Blanco, G., Cheung, W.W.L., Connors, S., Denton, F., Diongue-Niang, A., Dodman, D., Garschagen, M., Geden, O., Hayward, B., Jones, C., Jotzo, F., Krug, T., Lasco, R., Lee, Y.-Y., Masson-Delmotte, V., Meinshausen, M., Mintenbeck, K., Mokssit, A., Otto, F.E.L., Pathak, M., Pirani, A., Poloczanska, E., Pörtner, H.-O., Revi, A., Roberts, D.C., Roy, J., Ruane, A.C., Skea, J., Shukla, P.R., Slade, R., Slangen, A., Sokona, Y., Sörensson, A.A., Tignor, M., Van Vuuren, D., Wei, Y.-M., Winkler, H., Zhai, P., Zommers, Z., Hourcade, J.-C., Johnson, F.X., Pachauri, S., Simpson, N.P., Singh, C., Thomas, A., Totin, E., Arias, P., Bustamante, M., Elgizouli, I., Flato, G., Howden, M., Méndez-Vallejo, C., Pereira, J.J., Pichs-Madruga, R., Rose, S.K., Saheb, Y., Sánchez Rodríguez, R., Ürge-Vorsatz, D., Xiao, C., Yassaa, N., Alegría, A., Armour, K., Bednar-Friedl, B., Blok, K., Cissé, G., Dentener, F., Eriksen, S., Fischer, E., Garner, G., Guivarch, C., Haasnoot, M., Hansen, G., Hauser, M., Hawkins, E., Hermans, T., Kopp, R., Leprince-Ringuet, N., Lewis, J., Ley, D., Ludden, C., Niamir, L., Nicholls, Z., Some, S., Szopa, S., Trewin, B., Van Der Wijst, K.-I., Winter, G., Witting, M., Birt, A., Ha, M., Romero, J., Kim, J., Haites, E.F., Jung, Y., Stavins, R., Birt, A., Ha, M., Orendain, D.J.A., Ignon, L., Park, S., Park, Y., Reisinger, A., Cammaramo, D., Fischlin, A., Fuglestvedt, J.S., Hansen, G., Ludden, C., Masson-Delmotte, V., Matthews, J.B.R., Mintenbeck, K., Pirani, A., Poloczanska, E., Leprince-Ringuet, N., Péan, C., 2023. IPCC, 2023: Climate Change 2023: Synthesis Report. Contribution of Working Groups I, II and III to the Sixth Assessment Report of the Intergovernmental Panel on Climate Change [Core Writing Team, H. Lee and J. Romero (eds.)]. IPCC, Geneva, Switzerland. Intergovernmental Panel on Climate Change (IPCC). https://doi.org/10.59327/IPCC/AR6-9789291691647

Jaafar, H.H., Ahmad, F.A., El Beyrouthy, N., 2019. GCN250, new global gridded curve numbers for hydrologic modeling and design. Sci. Data 6, 145. https://doi.org/10.1038/s41597-019-0155-x

Jackson-Blake, L.A., Wade, A.J., Futter, M.N., Butterfield, D., Couture, R.-M., Cox, B.A., Crossman, J., Ekholm, P., Halliday, S.J., Jin, L., Lawrence, D.S.L., Lepistö, A., Lin, Y., Rankinen, K., Whitehead, P.G., 2016. The INtegrated CAtchment model of phosphorus dynamics (INCA-P): Description and demonstration of new model structure and equations. Environ. Model. Softw. 83, 356–386. https://doi.org/10.1016/j.envsoft.2016.05.022

Jacox, M.G., Alexander, M.A., Siedlecki, S., Chen, K., Kwon, Y.-O., Brodie, S., Ortiz, I., Tommasi, D., Widlansky, M.J., Barrie, D., Capotondi, A., Cheng, W., Di Lorenzo, E., Edwards, C., Fiechter, J., Fratantoni, P., Hazen, E.L., Hermann, A.J., Kumar, A., Miller, A.J., Pirhalla, D., Pozo Buil, M., Ray, S., Sheridan, S.C., Subramanian, A., Thompson, P., Thorne, L., Annamalai, H., Aydin, K., Bograd, S.J., Griffis, R.B., Kearney, K., Kim,

H., Mariotti, A., Merrifield, M., Rykaczewski, R., 2020. Seasonal-to-interannual prediction of North American coastal marine ecosystems: Forecast methods, mechanisms of predictability, and priority developments. Prog. Oceanogr. 183, 102307. https://doi.org/10.1016/j.pocean.2020.102307

Jain, Sharad Kumar, Mani, P., Jain, Sanjay K., Prakash, P., Singh, V.P., Tullos, D., Kumar, S., Agarwal, S.P., Dimri, A.P., 2018. A Brief review of flood forecasting techniques and their applications. Int. J. River Basin Manag. 16, 329–344. https://doi.org/10.1080/15715124.2017.1411920

Jennings, E., Allott, N., Pierson, D.C., Schneiderman, E.M., Lenihan, D., Samuelsson, P., Taylor, D., 2009. Impacts of climate change on phosphorus loading from a grassland catchment: Implications for future management. Water Res. 43, 4316–4326. https://doi.org/10.1016/j.watres.2009.06.032

Jennings, E., de Eyto, E., Dillane, M., Mellander, P.-E., Regan, F., Wilkes, R., O'Neill, M., Briciu-Burghina, C., Antunes, P., Jordan, P., Arnscheidt, J., Linnane, S., McCarthy, V., McElarney, Y., hUallacháin, D.Ó., Rolston, A., Wynne, C., 2022. Using High Frequency In-Situ Monitoring to Gain New Insights into Irish Aquatic Systems. Biol. Environ. Proc. R. Ir. Acad. 122B, 201–221. https://doi.org/10.1353/bae.2022.0014

Jennings, E., de Eyto, E., Moore, T., Dillane, M., Ryder, E., Allott, N., Nic Aonghusa, C., Rouen, M., Poole, R., Pierson, D.C., 2020. From Highs to Lows: Changes in Dissolved Organic Carbon in a Peatland Catchment and Lake Following Extreme Flow Events. Water 12. https://doi.org/10.3390/w12102843

Jennings, E., Järvinen, M., Allott, N., Arvola, L., Moore, K., Naden, P., Aonghusa, C.N., Nõges, T., Weyhenmeyer, G.A., 2010a. Impacts of Climate on the Flux of Dissolved Organic Carbon from Catchments, in: George, G. (Ed.), The Impact of Climate Change on European Lakes. Springer Netherlands, Dordrecht, pp. 199–220. https://doi.org/10.1007/978-90-481-2945-4_12

Jennings, E., Järvinen, M., Allott, N., Arvola, L., Moore, K., Naden, P., Aonghusa, C.N., Nõges, T., Weyhenmeyer, G.A., 2010b. Impacts of Climate on the Flux of Dissolved Organic Carbon from Catchments, in: George, G. (Ed.), The Impact of Climate Change on European Lakes. Springer Netherlands, Dordrecht, pp. 199–220. https://doi.org/10.1007/978-90-481-2945-4_12

Jian, L., Xiaosheng, Q., Ming, C., 2016. Evaluating Chlorophyll- *a* Changes During Algal Bloom in Three Gorges Reservoir Using an Extended WASP Model. MATEC Web Conf. 47, 05005. https://doi.org/10.1051/matecconf/20164705005

Jin, T., Cai, S., Jiang, D., Liu, J., 2019. A data-driven model for real-time water quality prediction and early warning by an integration method. Environ. Sci. Pollut. Res. 26, 30374–30385. https://doi.org/10.1007/s11356-019-06049-2

Jin, T., Zhang, X., Wang, T., Liang, J., Ma, W., Xie, J., 2024. Spatiotemporal impacts of climate change and human activities on blue and green water resources in northwest river basins of China. Ecol. Indic. 160, 111823. https://doi.org/10.1016/j.ecolind.2024.111823

Johnes, P.J., Evershed, R.P., Jones, D.L., Maberly, S.C., 2023. Exploring the nature, origins and ecological significance of dissolved organic matter in freshwaters: state of the science and new directions. Biogeochemistry 164, 1–12. https://doi.org/10.1007/s10533-023-01040-z

Jonsson, B., Jonsson, N., 2009. A review of the likely effects of climate change on anadromous Atlantic salmon Salmo salar and brown trout Salmo trutta, with particular reference to water temperature and flow. J. Fish Biol. 75, 2381–2447. https://doi.org/10.1111/j.1095-8649.2009.02380.x

Jutebring Sterte, E., Lidman, F., Sjöberg, Y., Ploum, S.W., Laudon, H., 2022. Groundwater travel times predict DOC in streams and riparian soils across a heterogeneous boreal landscape. Sci. Total Environ. 849, 157398. https://doi.org/10.1016/j.scitotenv.2022.157398

Kannel, P.R., Kanel, S.R., Lee, S., Lee, Y.-S., Gan, T.Y., 2011. A Review of Public Domain Water Quality Models for Simulating Dissolved Oxygen in Rivers and Streams. Environ. Model. Assess. 16, 183–204. https://doi.org/10.1007/s10666-010-9235-1

Karhu, K., Fritze, H., Tuomi, M., Vanhala, P., Spetz, P., Kitunen, V., Liski, J., 2010. Temperature sensitivity of organic matter decomposition in two boreal forest soil profiles. Soil Biol. Biochem. 42, 72–82. https://doi.org/10.1016/j.soilbio.2009.10.002

Katopodis, C., Williams, J.G., 2012. The development of fish passage research in a historical context. Ecol. Eng., Ecohydraulic Approaches for Restoring Habitat Connectivity and Suitability 48, 8–18. https://doi.org/10.1016/j.ecoleng.2011.07.004

Kay, A.L., Rudd, A.C., Coulson, J., 2023. Spatial downscaling of precipitation for hydrological modelling: Assessing a simple method and its application under climate change in Britain. Hydrol. Process. 37, e14823. https://doi.org/10.1002/hyp.14823

Khodabandeh, F., Dehghani Darmian, M., Azhdary Moghaddam, M., Hashemi Monfared, S.A., 2021. Reservoir quality management with CE-QUAL-W2/ANN surrogate model and PSO algorithm (case study: Pishin Dam, Iran). Arab. J. Geosci. 14, 401. https://doi.org/10.1007/s12517-021-06735-x

Kiani, M., Ylivainio, K., 2024. Methods for testing short- and long-term phosphorus fertilizing efficiency of products with varying solubility. Sci. Total Environ. 922, 170965. https://doi.org/10.1016/j.scitotenv.2024.170965

Kikon, A., Deka, P.C., 2022. Artificial intelligence application in drought assessment, monitoring and forecasting: a review. Stoch. Environ. Res. Risk Assess. 36, 1197–1214. https://doi.org/10.1007/s00477-021-02129-3

Kim, K.-M., Ahn, J.-H., 2022. Machine learning predictions of chlorophyll-a in the Han river basin, Korea. J. Environ. Manage. 318, 115636. https://doi.org/10.1016/j.jenvman.2022.115636

King, K., Burgess, M., Schultz, E.T., Knighton, J., 2023. Forecasting hydrologic controls on juvenile anadromous fish out-migration with process-based modeling and machine learning. J. Environ. Manage. 344, 118420. https://doi.org/10.1016/j.jenvman.2023.118420

Klante, C., Hägg, K., Larson, M., 2022. Understanding short-term organic matter fluctuations to optimize drinking water treatment. Water Pract. Technol. 17, 2141–2159. https://doi.org/10.2166/wpt.2022.121

Klante, C., Larson, M., Persson, K.M., 2021. Brownification in Lake Bolmen, Sweden, and its relationship to natural and human-induced changes. J. Hydrol. Reg. Stud. 36, 100863. https://doi.org/10.1016/j.ejrh.2021.100863

Klimek, B., Chodak, M., Jaźwa, M., Azarbad, H., Niklińska, M., 2020. Soil physicochemical and microbial drivers of temperature sensitivity of soil organic matter decomposition under boreal forests. Pedosphere 30, 528–534. https://doi.org/10.1016/S1002-0160(17)60400-4

Knott, J., Mueller, M., Pander, J., Geist, J., 2023. Downstream fish passage at small-scale hydropower plants: Turbine or bypass? Front. Environ. Sci. 11, 1168473. https://doi.org/10.3389/fenvs.2023.1168473

Kobler, U.G., Schmid, M., 2019. Ensemble modelling of ice cover for a reservoir affected by pumped-storage operation and climate change. Hydrol. Process. 33, 2676–2690. https://doi.org/10.1002/hyp.13519

Köhler, S.J., Lavonen, E., Keucken, A., Schmitt-Kopplin, P., Spanjer, T., Persson, K., 2016. Upgrading coagulation with hollow-fibre nanofiltration for improved organic matter removal during surface water treatment. Water Res. 89, 232–240. https://doi.org/10.1016/j.watres.2015.11.048

Kouadio, C.A., Kouassi, K.L., Diedhiou, A., Obahoundje, S., Amoussou, E., Kamagate, B., Paturel, J., Coulibaly, T.J.H., Coulibaly, H.S.J.P., Didi, R.S., Savane, I., 2022. Assessing the Hydropower Potential Using Hydrological Models and Geospatial Tools in the White Bandama Watershed (Côte d'Ivoire, West Africa). Front. Water 4, 844934. https://doi.org/10.3389/frwa.2022.844934

Krause, P., Boyle, D.P., Bäse, F., 2005. Comparison of different efficiency criteria for hydrological model assessment. Adv. Geosci. 5, 89–97. https://doi.org/10.5194/adgeo-5-89-2005

Kritzberg, E.S., Hasselquist, E.M., Škerlep, M., Löfgren, S., Olsson, O., Stadmark, J., Valinia, S., Hansson, L.-A., Laudon, H., 2020. Browning of freshwaters: Consequences to ecosystem services, underlying drivers, and potential mitigation measures. Ambio 49, 375–390. https://doi.org/10.1007/s13280-019-01227-5

Kumari, M., Gupta, S.K., 2022. Cumulative human health risk analysis of trihalomethanes exposure in drinking water systems. J. Environ. Manage. 321, 115949. https://doi.org/10.1016/j.jenvman.2022.115949

Kundzewicz, Z.W., Krysanova, V., Benestad, R.E., Hov, Ø., Piniewski, M., Otto, I.M., 2018. Uncertainty in climate change impacts on water resources. Environ. Sci. Policy 79, 1–8. https://doi.org/10.1016/j.envsci.2017.10.008

La Fuente, S., Jennings, E., Lenters, J.D., Verburg, P., Tan, Z., Perroud, M., Janssen, A.B.G., Woolway, R.I., 2024. Ensemble modeling of global lake evaporation under climate change. J. Hydrol. 631, 130647. https://doi.org/10.1016/j.jhydrol.2024.130647

Lange, S., Büchner, M., 2021. ISIMIP3b bias-adjusted atmospheric climate input data (v1.1). https://doi.org/10.48364/ISIMIP.842396.1

Lapierre, J.-F., Guillemette, F., Berggren, M., del Giorgio, P.A., 2013. Increases in terrestrially derived carbon stimulate organic carbon processing and CO2 emissions in boreal aquatic ecosystems. Nat. Commun. 4, 2972. https://doi.org/10.1038/ncomms3972

Lavonen, E.E., Kothawala, D.N., Tranvik, L.J., Gonsior, M., Schmitt-Kopplin, P., Köhler, S.J., 2015. Tracking changes in the optical properties and molecular composition of dissolved organic matter during drinking water production. Water Res. 85, 286–294. https://doi.org/10.1016/j.watres.2015.08.024

Ledesma, J.L.J., Köhler, S.J., Futter, M.N., 2012. Long-term dynamics of dissolved organic carbon: Implications for drinking water supply. Sci. Total Environ. 432, 1–11. https://doi.org/10.1016/j.scitotenv.2012.05.071

Legrand, C., Hingray, B., Wilhelm, B., Ménégoz, M., 2024. Assessing downscaling methods to simulate hydrologically relevant weather scenarios from a global atmospheric reanalysis: case study of the upper Rhône River (1902–2009). Hydrol. Earth Syst. Sci. 28, 2139–2166. https://doi.org/10.5194/hess-28-2139-2024

Legrand, M., Briand, C., Buisson, L., Besse, T., Artur, G., Azam, D., Baisez, A., Barracou, D., Bourré, N., Carry, L., Caudal, A.-L., Corre, J., Croguennec, E., Der Mikaélian, S., Josset, Q., Le Gurun, L., Schaeffer, F., Toussaint, R., Laffaille, P., 2021. Diadromous fish modified timing of upstream migration over the last 30 years in France. Freshw. Biol. 66, 286–302. https://doi.org/10.1111/fwb.13638

Lewis, A.S.L., Rollinson, C.R., Allyn, A.J., Ashander, J., Brodie, S., Brookson, C.B., Collins, E., Dietze, M.C., Gallinat, A.S., Juvigny-Khenafou, N., Koren, G., McGlinn, D.J., Moustahfid, H., Peters, J.A., Record, N.R., Robbins, C.J., Tonkin, J., Wardle, G.M., 2022a. The power of forecasts to advance ecological theory. Methods Ecol. Evol. 2041–210X.13955. https://doi.org/10.1111/2041-210X.13955

Lewis, A.S.L., Woelmer, W.M., Wander, H.L., Howard, D.W., Smith, J.W., McClure, R.P., Lofton, M.E., Hammond, N.W., Corrigan, R.S., Thomas, R.Q., Carey, C.C., 2022b. Increased adoption of best practices in ecological forecasting enables comparisons of forecastability. Ecol. Appl. 32, e2500. https://doi.org/10.1002/eap.2500

Lewy, P., Nielsen, A., 2003. Modelling stochastic fish stock dynamics using Markov Chain Monte Carlo. ICES J. Mar. Sci. 60, 743–752. https://doi.org/10.1016/S1054-3139(03)00080-8

LHOMME, J.-P., 1997. A THEORETICAL BASIS FOR THE PRIESTLEY-TAYLOR COEFFICIENT. Bound.-Layer Meteorol. 82, 179–191. https://doi.org/10.1023/A:1000281114105

Li, N., Kinzelbach, W., Li, H., Li, W., Chen, F., 2021. Improving parameter and state estimation of a hydrological model with the ensemble square root filter. Adv. Water Resour. 147, 103813. https://doi.org/10.1016/j.advwatres.2020.103813

Li, X.-F., Mitch, W.A., 2018. Drinking Water Disinfection Byproducts (DBPs) and Human Health Effects: Multidisciplinary Challenges and Opportunities. Environ. Sci. Technol. 52, 1681–1689. https://doi.org/10.1021/acs.est.7b05440

Lin, H.-Y., 2017. Conserving migratory species under human impacts and climate change (PhD Thesis). The University of Queensland. https://doi.org/10.14264/uql.2017.750

Lindenschmidt, K.-E., Carr, M.K., Sadeghian, A., Morales-Marin, L., 2019. CE-QUAL-W2 model of dam outflow elevation impact on temperature, dissolved oxygen and nutrients in a reservoir. Sci. Data 6, 312. https://doi.org/10.1038/s41597-019-0316-y

Lindqvist, K., 2022. Modelling the Effects of Climate Change on Future DOC Export to Lake Mälaren Using a Generalized Watershed Loading Functions (GWLF) Model. Uppsala University, Sweden.

Liu, H., Cheng, W., Xiong, P., Li, H., Liu, Z., Ai, J., Yuan, D., Wan, F., Wan, Y., Zou, H., Shu, P., 2023. Temporal variation of plankton and zoobenthos communities in a freshwater reservoir: Structure feature, construction mechanism, associated symbiosis and environmental response. Ecol. Indic. 154, 110774. https://doi.org/10.1016/j.ecolind.2023.110774

Liu, Y., Ji, C., Wang, Y., Zhang, Y., Jiang, Z., Ma, Q., Hou, X., 2023. Effect of the quality of streamflow forecasts on the operation of cascade hydropower stations using stochastic optimization models. Energy 273, 127298. https://doi.org/10.1016/j.energy.2023.127298

Lofton, M.E., Brentrup, J.A., Beck, W.S., Zwart, J.A., Bhattacharya, R., Brighenti, L.S., Burnet, S.H., McCullough, I.M., Steele, B.G., Carey, C.C., Cottingham, K.L., Dietze, M.C., Ewing, H.A., Weathers, K.C., LaDeau, S.L., 2022. Using near-term forecasts and uncertainty partitioning to inform prediction of oligotrophic lake cyanobacterial density. Ecol. Appl. 32, e2590. https://doi.org/10.1002/eap.2590

Lofton, M.E., Howard, D.W., Thomas, R.Q., Carey, C.C., 2023. Progress and opportunities in advancing near-term forecasting of freshwater quality. Glob. Change Biol. 29, 1691–1714. https://doi.org/10.1111/gcb.16590

Long, A.P., Vaughan, L., Tray, E., Thomas, K., Maoiléidigh, N.Ó., Poole, R., Cotter, D., Doogan, A., Brophy, D., 2023. Recent marine growth declines in wild and ranched

Atlantic salmon *Salmo salar* from a western European catchment discovered using a 62-year time series. ICES J. Mar. Sci. 80, 1697–1709. https://doi.org/10.1093/icesjms/fsad101

Loos, S., Shin, C.M., Sumihar, J., Kim, K., Cho, J., Weerts, A.H., 2020a. Ensemble data assimilation methods for improving river water quality forecasting accuracy. Water Res. 171, 115343. https://doi.org/10.1016/j.watres.2019.115343

Loos, S., Shin, C.M., Sumihar, J., Kim, K., Cho, J., Weerts, A.H., 2020b. Ensemble data assimilation methods for improving river water quality forecasting accuracy. Water Res. 171, 115343. https://doi.org/10.1016/j.watres.2019.115343

Lowerre-Barbieri, S.K., Kays, R., Thorson, J.T., Wikelski, M., 2019. The ocean's movescape: fisheries management in the bio-logging decade (2018–2028). ICES J. Mar. Sci. 76, 477–488. https://doi.org/10.1093/icesjms/fsy211

Lundqvist, J., Andersson, A., Johannisson, A., Lavonen, E., Mandava, G., Kylin, H., Bastviken, D., Oskarsson, A., 2019. Innovative drinking water treatment techniques reduce the disinfection-induced oxidative stress and genotoxic activity. Water Res. 155, 182–192. https://doi.org/10.1016/j.watres.2019.02.052

Maberly, S.C., O'Donnell, R.A., Woolway, R.I., Cutler, M.E.J., Gong, M., Jones, I.D., Merchant, C.J., Miller, C.A., Politi, E., Scott, E.M., Thackeray, S.J., Tyler, A.N., 2020. Global lake thermal regions shift under climate change. Nat. Commun. 11, 1232. https://doi.org/10.1038/s41467-020-15108-z

Malhi, Y., Franklin, J., Seddon, N., Solan, M., Turner, M.G., Field, C.B., Knowlton, N., 2020. Climate change and ecosystems: threats, opportunities and solutions. Philos. Trans. R. Soc. B Biol. Sci. 375, 20190104. https://doi.org/10.1098/rstb.2019.0104

Mamani Larico, A.J., Zúñiga Medina, S.A., 2019. Application of WASP model for assessment of water quality for eutrophication control for a reservoir in the Peruvian Andes. Lakes Reserv. Sci. Policy Manag. Sustain. Use 24, 37–47. https://doi.org/10.1111/lre.12256

Marine Institute, 2017. Data Catalogue: Bathymetric Survey of Lough Feeagh, Co. Mayo. [WWW Document]. URL https://data.marine.ie/geonetwork/srv/eng/catalog.search#/metadata/ie.marine.data:dataset.1226 (accessed 6.7.24).

Marshall, A.M., Link, T.E., Flerchinger, G.N., Lucash, M.S., 2021. Importance of Parameter and Climate Data Uncertainty for Future Changes in Boreal Hydrology. Water Resour. Res. 57, e2021WR029911. https://doi.org/10.1029/2021WR029911

Maskey, S., 2022. Chapter 1 - Introduction, in: Maskey, S. (Ed.), Catchment Hydrological Modelling. Elsevier, pp. 1–16. https://doi.org/10.1016/B978-0-12-818337-3.00001-5

Matonse, A.H., Pierson, D.C., Frei, A., Zion, M.S., Anandhi, A., Schneiderman, E., Wright, B., 2013. Investigating the impact of climate change on New York City's primary water supply. Clim. Change 116, 437–456. https://doi.org/10.1007/s10584-012-0515-4

Mercado-Bettín, D., Clayer, F., Shikhani, M., Moore, T.N., Frías, M.D., Jackson-Blake, L., Sample, J., Iturbide, M., Herrera, S., French, A.S., Norling, M.D., Rinke, K., Marcé, R., 2021. Forecasting water temperature in lakes and reservoirs using seasonal climate prediction. Water Res. 201, 117286. https://doi.org/10.1016/j.watres.2021.117286

Mesman, J.P., Ayala, A.I., Adrian, R., De Eyto, E., Frassl, M.A., Goyette, S., Kasparian, J., Perroud, M., Stelzer, J.A.A., Pierson, D.C., Ibelings, B.W., 2020. Performance of one-dimensional hydrodynamic lake models during short-term extreme weather events. Environ. Model. Softw. 133, 104852. https://doi.org/10.1016/j.envsoft.2020.104852

Meyer-Jacob, C., Michelutti, N., Paterson, A.M., Cumming, B.F., Keller, W. (Bill), Smol, J.P., 2019. The browning and re-browning of lakes: Divergent lake-water organic carbon

trends linked to acid deposition and climate change. Sci. Rep. 9, 16676. https://doi.org/10.1038/s41598-019-52912-0

Milner, N.J., Solomon, D.J., Smith, G.W., 2012. The role of river flow in the migration of adult Atlantic salmon, Salmo salar, through estuaries and rivers. Fish. Manag. Ecol. 19, 537–547. https://doi.org/10.1111/fme.12011

Mironov, D., Heise, E., Kourzeneva, E., Ritter, B., Schneider, N., Terzhevik, A., 2010. Implementation of the lake parameterisation saheme FLake into the numerical weather prediction model COSMO. Boreal Environ. Res. 15.

Mironov, D.V., 2005. Parameterization of lakes in numerical weather prediction. Part 1: Description of a lake model. Ger. Weather Serv. Offenb. Am Main Ger.

Mishra, S., Ghosh, A., Rai, K., Jaiswal, B., Yadav, D.S., Agrawal, M., Agrawal, S.B., 2021. 6 - Dimensions of climate change and its consequences on ecosystem functioning, in: Singh, S., Singh, P., Rangabhashiyam, S., Srivastava, K.K. (Eds.), Global Climate Change. Elsevier, pp. 109–149. https://doi.org/10.1016/B978-0-12-822928-6.00003-4

Mitchell, G., McDonald, A.T., 1992. Discolouration of water by peat following induced drought and rainfall simulation. Water Res. 26, 321–326. https://doi.org/10.1016/0043-1354(92)90029-4

Mohammed, H., Michel Tornyeviadzi, H., Seidu, R., 2022. Emulating process-based water quality modelling in water source reservoirs using machine learning. J. Hydrol. 609, 127675. https://doi.org/10.1016/j.jhydrol.2022.127675

Moore, K., 2007. Climate Change Impacts on the Catchment Contribution to Lake Water Quantity and Quality.

Moore, K., Jennings, E., Allott, N., May, L., Järvinen, M., Arvola, L., Tamm, T., Järvet, A., Nõges, T., Pierson, D., Schneiderman, E., 2010. Modelling the Effects of Climate Change on the Supply of Inorganic Nitrogen, in: George, G. (Ed.), The Impact of Climate Change on European Lakes. Springer Netherlands, Dordrecht, pp. 179–197. https://doi.org/10.1007/978-90-481-2945-4_11

Moore, T.N., 2020. Predicting in-lake responses to short and long-term changes using lake physical models.

Moore, T.N., Mesman, J.P., Ladwig, R., Feldbauer, J., Olsson, F., Pilla, R.M., Shatwell, T., Venkiteswaran, J.J., Delany, A.D., Dugan, H., Rose, K.C., Read, J.S., 2021. LakeEnsemblR: An R package that facilitates ensemble modelling of lakes. Environ. Model. Softw. 143, 105101. https://doi.org/10.1016/j.envsoft.2021.105101

Moras, S., Ayala, A.I., Pierson, D.C., 2019. Historical modelling of changes in Lake Erken thermal conditions. Hydrol. Earth Syst. Sci. 23, 5001–5016. https://doi.org/10.5194/hess-23-5001-2019

Mozafari, B., Bruen, M., Donohue, S., Renou-Wilson, F., O'Loughlin, F., 2023. Peatland dynamics: A review of process-based models and approaches. Sci. Total Environ. 877, 162890. https://doi.org/10.1016/j.scitotenv.2023.162890

Murphy, A.H., 1992. Climatology, Persistence, and Their Linear Combination as Standards of Reference in Skill Scores. Weather Forecast. 7, 692–698. https://doi.org/10.1175/1520-0434(1992)007<0692:CPATLC>2.0.CO;2

Murphy, C., Kettle, A., Meresa, H., Golian, S., Bruen, M., O'Loughlin, F., Mellander, P.-E., 2023. Climate Change Impacts on Irish River Flows: High Resolution Scenarios and Comparison with CORDEX and CMIP6 Ensembles. Water Resour. Manag. 37, 1841–1858. https://doi.org/10.1007/s11269-023-03458-4

Musyoka, F.K., Strauss, P., Zhao, G., Srinivasan, R., Klik, A., 2021. Multi-Step Calibration Approach for SWAT Model Using Soil Moisture and Crop Yields in a Small Agricultural Catchment. Water 13, 2238. https://doi.org/10.3390/w13162238

Naden, P.S., Allott, N., Arvola, L., Järvinen, M., Jennings, E., Moore, K., Nic Aonghusa, C., Pierson, D., Schneiderman, E., 2010. Modelling the Impacts of Climate Change on Dissolved Organic Carbon, in: George, G. (Ed.), The Impact of Climate Change on European Lakes. Springer Netherlands, Dordrecht, pp. 221–252. https://doi.org/10.1007/978-90-481-2945-4_13

Nafees Ahmad, H.M., Sinclair, A., Jamieson, R., Madani, A., Hebb, D., Havard, P., Yiridoe, E.K., 2011. Modeling Sediment and Nitrogen Export from a Rural Watershed in Eastern Canada Using the Soil and Water Assessment Tool. J. Environ. Qual. 40, 1182–1194. https://doi.org/10.2134/jeq2010.0530

Nasr, A., Bruen, M., Jordan, P., Moles, R., Kiely, G., Byrne, P., 2007. A comparison of SWAT, HSPF and SHETRAN/GOPC for modelling phosphorus export from three catchments in Ireland. Water Res. 41, 1065–1073. https://doi.org/10.1016/j.watres.2006.11.026

Niraula, R., Kalin, L., Srivastava, P., Anderson, C.J., 2013. Identifying critical source areas of nonpoint source pollution with SWAT and GWLF. Ecol. Model. 268, 123–133. https://doi.org/10.1016/j.ecolmodel.2013.08.007

Nissan, H., Goddard, L., De Perez, E.C., Furlow, J., Baethgen, W., Thomson, M.C., Mason, S.J., 2019. On the use and misuse of climate change projections in international development. WIREs Clim. Change 10, e579. https://doi.org/10.1002/wcc.579

Niu, S., Luo, Y., Dietze, M.C., Keenan, T.F., Shi, Z., Li, J., Iii, F.S.C., 2014. The role of data assimilation in predictive ecology. Ecosphere 5, art65. https://doi.org/10.1890/ES13-00273.1

Noori, R., Yeh, H.-D., Ashrafi, K., Rezazadeh, N., Bateni, S.M., Karbassi, A., Kachoosangi, F.T., Moazami, S., 2015. A reduced-order based CE-QUAL-W2 model for simulation of nitrate concentration in dam reservoirs. J. Hydrol. 530, 645–656. https://doi.org/10.1016/j.jhydrol.2015.10.022

Norman, J., Wright, R.M., Don, A., Bolland, J.D., 2023. Understanding the temporal dynamics of a lowland river fish community at a hazardous intake and floodgate to inform safe operation. J. Environ. Manage. 336, 117716. https://doi.org/10.1016/j.jenvman.2023.117716

Nyqvist, D., Nilsson, P.A., Alenäs, I., Elghagen, J., Hebrand, M., Karlsson, S., Kläppe, S., Calles, O., 2017. Upstream and downstream passage of migrating adult Atlantic salmon: Remedial measures improve passage performance at a hydropower dam. Ecol. Eng. 102, 331–343. https://doi.org/10.1016/j.ecoleng.2017.02.055

Obin, N., Tao, H., Ge, F., Liu, X., 2021. Research on Water Quality Simulation and Water Environmental Capacity in Lushui River Based on WASP Model. Water 13, 2819. https://doi.org/10.3390/w13202819

O'Driscoll, C., Ledesma, J.L.J., Coll, J., Murnane, J.G., Nolan, P., Mockler, E.M., Futter, M.N., Xiao, L.W., 2018a. Minimal climate change impacts on natural organic matter forecasted for a potable water supply in Ireland. Sci. Total Environ. 630, 869–877. https://doi.org/10.1016/j.scitotenv.2018.02.248

O'Driscoll, C., Sheahan, J., Renou-Wilson, F., Croot, P., Pilla, F., Misstear, B., Xiao, L., 2018b. National scale assessment of total trihalomethanes in Irish drinking water. J. Environ. Manage. 212, 131–141. https://doi.org/10.1016/j.jenvman.2018.01.070

O'Driscoll, C., Sheahan, J., Renou-Wilson, F., Croot, P., Pilla, F., Misstear, B., Xiao, L., 2018c. National scale assessment of total trihalomethanes in Irish drinking water. J. Environ. Manage. 212, 131–141. https://doi.org/10.1016/j.jenvman.2018.01.070

Oke, K.B., Cunningham, C.J., Westley, P.A.H., Baskett, M.L., Carlson, S.M., Clark, J., Hendry, A.P., Karatayev, V.A., Kendall, N.W., Kibele, J., Kindsvater, H.K., Kobayashi, K.M., Lewis, B., Munch, S., Reynolds, J.D., Vick, G.K., Palkovacs, E.P., 2020. Recent declines in salmon body size impact ecosystems and fisheries. Nat. Commun. 11, 4155. https://doi.org/10.1038/s41467-020-17726-z

Oke, K.B., Hendry, A.P., 2019. Genetic insights into the past, present, and future of a keystone species. Proc. Natl. Acad. Sci. 116, 344–346. https://doi.org/10.1073/pnas.1819789116

Okiria, E., Okazawa, H., Noda, K., Kobayashi, Y., Suzuki, S., Yamazaki, Y., 2022. A Comparative Evaluation of Lumped and Semi-Distributed Conceptual Hydrological Models: Does Model Complexity Enhance Hydrograph Prediction? Hydrology 9, 89. https://doi.org/10.3390/hydrology9050089

Olsson, F., Moore, T.N., Carey, C.C., Breef-Pilz, A., Thomas, R.Q., 2024. A Multi-Model Ensemble of Baseline and Process-Based Models Improves the Predictive Skill of Near-Term Lake Forecasts. Water Resour. Res. 60, e2023WR035901. https://doi.org/10.1029/2023WR035901

Osborne, J.W., Overbay, A., 2004. The power of outliers. https://doi.org/10.7275/QF69-7K43

Ouellet, V., Collins, M.J., Kocik, J.F., Saunders, R., Sheehan, T.F., Ogburn, M.B., Trinko Lake, T., 2022. The diadromous watersheds-ocean continuum: Managing diadromous fish as a community for ecosystem resilience. Front. Ecol. Evol. 10, 1007599. https://doi.org/10.3389/fevo.2022.1007599

Oulehle, F., Hruška, J., 2009. Rising trends of dissolved organic matter in drinking-water reservoirs as a result of recovery from acidification in the Ore Mts., Czech Republic. Environ. Pollut., Persistent Organic Pollutants in Mountainous Areas 157, 3433–3439. https://doi.org/10.1016/j.envpol.2009.06.020

Paíz, R., Pierson, D.C., Lindqvist, K., Naden, P.S., de Eyto, E., Dillane, M., McCarthy, V., Linnane, S., Jennings, E., 2025. Accounting for model parameter uncertainty provides more robust projections of dissolved organic carbon dynamics to aid drinking water management. Water Res. 123238. https://doi.org/10.1016/j.watres.2025.123238

Paniconi, C., Putti, M., 2015. Physically based modeling in catchment hydrology at 50: Survey and outlook. Water Resour. Res. 51, 7090–7129. https://doi.org/10.1002/2015WR017780

Payne, M.R., Hobday, A.J., MacKenzie, B.R., Tommasi, D., Dempsey, D.P., Fässler, S.M.M., Haynie, A.C., Ji, R., Liu, G., Lynch, P.D., Matei, D., Miesner, A.K., Mills, K.E., Strand, K.O., Villarino, E., 2017. Lessons from the First Generation of Marine Ecological Forecast Products. Front. Mar. Sci. 4. https://doi.org/10.3389/fmars.2017.00289

Pedregal-Montes, A., Jennings, E., Kothawala, D., Jones, K., Sjöstedt, J., Langenheder, S., Marcé, R., Farré, M.J., 2024. Disinfection by-product formation potential in response to variability in dissolved organic matter and nutrient inputs: Insights from a mesocosm study. Water Res. 258, 121791. https://doi.org/10.1016/j.watres.2024.121791

Peñas, F.J., Álvarez-Cabria, M., Sáinz-Bariáin, M., Mata-Campo, M.P., Pérez-Haase, A., Ventura, M., Polo-Gómez, M.J., Alonso, C., Granados, I., Morellón, M., Pérez-Martínez, C., Rubio-Romero, Á., Carrillo, P., Zamora-Muñoz, C., Valladolid-Martín, M., Camarero, L., Gacia, E., Puig, M., Buchaca, T., Barquín, J., 2023. An evaluation of freshwater monitoring programs in ILTER nodes and mountain national parks: identifying key variables to monitor global change effects. Biodivers. Conserv. 32, 65–94. https://doi.org/10.1007/s10531-022-02466-x

Perretti, C.T., Munch, S.B., Sugihara, G., 2013. Model-free forecasting outperforms the correct mechanistic model for simulated and experimental data. Proc. Natl. Acad. Sci. 110, 5253–5257. https://doi.org/10.1073/pnas.1216076110

Pettersson, K., George, G., Nõges, P., Nõges, T., Blenckner, T., 2010. The Impact of the Changing Climate on the Supply and Re-Cycling of Phosphorus, in: George, G. (Ed.), The Impact of Climate Change on European Lakes. Springer Netherlands, Dordrecht, pp. 121–137. https://doi.org/10.1007/978-90-481-2945-4_8

Piai, L., Mei, S., van Gijn, K., Langenhoff, A., 2024. Effects of organic matter in drinking water and wastewater on micropollutant adsorption to activated carbon. Int. J. Environ. Sci. Technol. 21, 2547–2558. https://doi.org/10.1007/s13762-023-05132-z

Pianosi, F., Beven, K., Freer, J., Hall, J.W., Rougier, J., Stephenson, D.B., Wagener, T., 2016. Sensitivity analysis of environmental models: A systematic review with practical workflow. Environ. Model. Softw. 79, 214–232. https://doi.org/10.1016/j.envsoft.2016.02.008

Piccolroaz, S., Zhu, S., Ladwig, R., Carrea, L., Oliver, S., Piotrowski, A.P., Ptak, M., Shinohara, R., Sojka, M., Woolway, R.I., Zhu, D.Z., 2024. Lake Water Temperature Modeling in an Era of Climate Change: Data Sources, Models, and Future Prospects. Rev. Geophys. 62, e2023RG000816. https://doi.org/10.1029/2023RG000816

Pierson, D., Arvola, L., Allott, N., Järvinen, M., Jennings, E., May, L., Moore, K., Schneiderman, E., 2010. Modeling the Effects of Climate Change on the Supply of Phosphate-Phosphorus, in: George, G. (Ed.), The Impact of Climate Change on European Lakes. Springer Netherlands, Dordrecht, pp. 139–159. https://doi.org/10.1007/978-90-481-2945-4_9

Piper, A.T., Rosewarne, P.J., Wright, R.M., Kemp, P.S., 2020. Using 'trap and transport' to facilitate seaward migration of landlocked European eel (*Anguilla anguilla*) from lakes and reservoirs. Fish. Res. 228, 105567. https://doi.org/10.1016/j.fishres.2020.105567

Piper, A.T., Wright, R.M., Walker, A.M., Kemp, P.S., 2013. Escapement, route choice, barrier passage and entrainment of seaward migrating European eel, *Anguilla anguilla*, within a highly regulated lowland river. Ecol. Eng. 57, 88–96. https://doi.org/10.1016/j.ecoleng.2013.04.030

Ploum, S., Laudon, H., Peralta Tapia, A., Kuglerová, L., 2020. Are dissolved organic carbon concentrations in riparian groundwater linked to hydrological pathways in the boreal forest? Hydrol. Earth Syst. Sci. 24, 1709–1720. https://doi.org/10.5194/hess-24-1709-2020

Poole, W.R., Diserud, O.H., Thorstad, E.B., Durif, C.M., Dolan, C., Sandlund, O.T., Bergesen, K., Rogan, G., Kelly, S., Vøllestad, L.A., 2018. Long-term variation in numbers and biomass of silver eels being produced in two European river systems. ICES J. Mar. Sci. 75, 1627–1637. https://doi.org/10.1093/icesjms/fsy053

Preston, S.D., Alexander, R.B., Wolock, D.M., 2011. Sparrow Modeling to Understand Water-Quality Conditions in Major Regions of the United States: A Featured Collection Introduction1: SPARROW Modeling to Understand Water-Quality Conditions in Major Regions of the United States: A Featured Collection Introduction. JAWRA J. Am. Water Resour. Assoc. 47, 887–890. https://doi.org/10.1111/j.1752-1688.2011.00585.x

Prijac, A., Gandois, L., Taillardat, P., Bourgault, M.-A., Riahi, K., Ponçot, A., Tremblay, A., Garneau, M., 2023. Hydrological connectivity controls dissolved organic carbon exports in a peatland-dominated boreal catchment stream. Hydrol. Earth Syst. Sci. 27, 3935–3955. https://doi.org/10.5194/hess-27-3935-2023

Priya, A.K., M, M., Rajamanickam, S., Sivarethinamohan, S., Gaddam, M.K.R., Velusamy, P., R, G., Ravindiran, G., Gurugubelli, T.R., Muniasamy, S.K., 2023. Impact of climate

change and anthropogenic activities on aquatic ecosystem – A review. Environ. Res. 238, 117233. https://doi.org/10.1016/j.envres.2023.117233

Pulka, T., Herrnegger, M., Ehrendorfer, C., Lücking, S., Avanzi, F., Formayer, H., Schulz, K., Koch, F., 2024. Evaluating precipitation corrections to enhance high-alpine hydrological modeling. J. Hydrol. 645, 132202. https://doi.org/10.1016/j.jhydrol.2024.132202

Qi, J., Li, S., Li, Q., Xing, Z., Bourque, C.P.-A., Meng, F.-R., 2016. A new soil-temperature module for SWAT application in regions with seasonal snow cover. J. Hydrol. 538, 863–877. https://doi.org/10.1016/j.jhydrol.2016.05.003

Qi, J., Zhang, X., Yang, Q., Srinivasan, R., Arnold, J.G., Li, J., Waldholf, S.T., Cole, J., 2020. SWAT ungauged: Water quality modeling in the Upper Mississippi River Basin. J. Hydrol. 584, 124601. https://doi.org/10.1016/j.jhydrol.2020.124601

Qi, Z., Kang, G., Chu, C., Qiu, Y., Xu, Z., Wang, Y., 2017. Comparison of SWAT and GWLF Model Simulation Performance in Humid South and Semi-Arid North of China. Water 9, 567. https://doi.org/10.3390/w9080567

Qiu, R., Wang, Y., Rhoads, B., Wang, D., Qiu, W., Tao, Y., Wu, J., 2021. River water temperature forecasting using a deep learning method. J. Hydrol. 595, 126016. https://doi.org/10.1016/j.jhydrol.2021.126016

Raeisi, N., Moradi, S., Scholz, M., 2022. Surface Water Resources Assessment and Planning with the QUAL2KW Model: A Case Study of the Maroon and Jarahi Basin (Iran). Water 14. https://doi.org/10.3390/w14050705

Rankinen, K., Thouvenot-Korppoo, M., Lazar, A., Lawrence, D.S.L., Butterfield, D., Veijalainen, N., Huttunen, I., Lepistö, A., 2010. Application of catchment scale sediment delivery model INCA-Sed to four small study catchments in Finland. CATENA 83, 64–75. https://doi.org/10.1016/j.catena.2010.07.005

Recknagel, F., 2023. Cyberinfrastructure for sourcing and processing ecological data. Ecol. Inform. 75, 102039. https://doi.org/10.1016/j.ecoinf.2023.102039

Reed, T.E., De Eyto, E., O'Higgins, K., Gargan, P., Roche, W., White, J., O'Maoileidigh, N., Quinn, T.P., McGinnity, P., 2017. Availability of holding habitat in lakes and rivers affects the incidence of spring (premature) upriver migration by Atlantic salmon. Can. J. Fish. Aquat. Sci. 74, 668–679. https://doi.org/10.1139/cjfas-2016-0191

Riley, W.D., Maxwell, D.L., Ives, M.J., Bendall, B., 2012. Some observations on the impact of temperature and low flow on the onset of downstream movement of wild Atlantic salmon, Salmo salar L., smolts. Smolt 2009 Proc. 8th Int. Workshop Smoltification 362–363, 216–223. https://doi.org/10.1016/j.aquaculture.2011.04.042

Rinaldo, A., de Eyto, E., Reed, T., Gjelland, K.Ø., McGinnity, P., 2024. Global warming is projected to lead to increased freshwater growth potential and changes in pace of life in Atlantic salmon Salmo salar. J. Fish Biol. 104, 647–661. https://doi.org/10.1111/jfb.15603

Ripple, W.J., Wolf, C., Gregg, J.W., Rockström, J., Newsome, T.M., Law, B.E., Marques, L., Lenton, T.M., Xu, C., Huq, S., Simons, L., King, S.D.A., 2023. The 2023 state of the climate report: Entering uncharted territory. BioScience 73, 841–850. https://doi.org/10.1093/biosci/biad080

Ritson, J.P., Graham, N.J.D., Templeton, M.R., Clark, J.M., Gough, R., Freeman, C., 2014. The impact of climate change on the treatability of dissolved organic matter (DOM) in upland water supplies: A UK perspective. Sci. Total Environ. 473–474, 714–730. https://doi.org/10.1016/j.scitotenv.2013.12.095

Riyadh, A., Peleato, N.M., 2024. Natural Organic Matter Character in Drinking Water Distribution Systems: A Review of Impacts on Water Quality and Characterization Techniques. Water 16, 446. https://doi.org/10.3390/w16030446

Roberts, K.E., Stepanuk, J.E.F., Kim, H., Thorne, L.H., Chong-Montenegro, C., Nye, J.A., 2023. Developing a subseasonal ecological forecast to reduce fisheries bycatch in the Northeast U.S. Prog. Oceanogr. 213, 103021. https://doi.org/10.1016/j.pocean.2023.103021

Rodríguez-Cardona, B.M., Wymore, A.S., Argerich, A., Barnes, R.T., Bernal, S., Brookshire, E.N.J., Coble, A.A., Dodds, W.K., Fazekas, H.M., Helton, A.M., Johnes, P.J., Johnson, S.L., Jones, J.B., Kaushal, S.S., Kortelainen, P., López-Lloreda, C., Spencer, R.G.M., McDowell, W.H., 2022. Shifting stoichiometry: Long-term trends in stream-dissolved organic matter reveal altered C:N ratios due to history of atmospheric acid deposition. Glob. Change Biol. 28, 98–114. https://doi.org/10.1111/gcb.15965

Rolston, A., Linnane, S., 2020. Drinking Water Source Protection for Surface Water Abstractions: An Overview of the Group Water Scheme Sector in the Republic of Ireland. Water 12, 2437. https://doi.org/10.3390/w12092437

Rousso, B.Z., Bertone, E., Stewart, R., Hamilton, D.P., 2020. A systematic literature review of forecasting and predictive models for cyanobacteria blooms in freshwater lakes. Water Res. 182, 115959. https://doi.org/10.1016/j.watres.2020.115959

Ruokonen, T.J., Suuronen, P., Pulkkinen, H., Erkinaro, J., 2022. Release mortality of wild Atlantic salmon in coastal pontoon-trap fishery in the northern Baltic Sea. Fish. Res. 252, 106336. https://doi.org/10.1016/j.fishres.2022.106336

Ryder, E., de Eyto, E., Dillane, M., Poole, R., Jennings, E., 2014. Identifying the role of environmental drivers in organic carbon export from a forested peat catchment. Sci. Total Environ. 490, 28–36. https://doi.org/10.1016/j.scitotenv.2014.04.091

Sachse, R., Petzoldt, T., Blumstock, M., Moreira, S., Pätzig, M., Rücker, J., Janse, J.H., Mooij, W.M., Hilt, S., 2014. Extending one-dimensional models for deep lakes to simulate the impact of submerged macrophytes on water quality. Environ. Model. Softw. 61, 410–423. https://doi.org/10.1016/j.envsoft.2014.05.023

Saeed, A., Alsini, A., Amin, D., 2024. Water quality multivariate forecasting using deep learning in a West Australian estuary. Environ. Model. Softw. 171, 105884. https://doi.org/10.1016/j.envsoft.2023.105884

Saloranta, T.M., Andersen, T., 2007. MyLake—A multi-year lake simulation model code suitable for uncertainty and sensitivity analysis simulations. Ecol. Model., Uncertainty in Ecological Models 207, 45–60. https://doi.org/10.1016/j.ecolmodel.2007.03.018

Sánchez-Pinillos, M., Dakos, V., Kéfi, S., 2024. Ecological dynamic regimes: A key concept for assessing ecological resilience. Biol. Conserv. 289, 110409. https://doi.org/10.1016/j.biocon.2023.110409

SanClements, M.D., Oelsner, G.P., McKnight, D.M., Stoddard, J.L., Nelson, S.J., 2012. New Insights into the Source of Decadal Increases of Dissolved Organic Matter in Acid-Sensitive Lakes of the Northeastern United States. Environ. Sci. Technol. 46, 3212–3219. https://doi.org/10.1021/es204321x

Sandlund, O.T., Diserud, O.H., Poole, R., Bergesen, K., Dillane, M., Rogan, G., Durif, C., Thorstad, E.B., Vøllestad, L.A., 2017. Timing and pattern of annual silver eel migration in two European watersheds are determined by similar cues. Ecol. Evol. 7, 5956–5966. https://doi.org/10.1002/ece3.3099

Schaeffer, B.A., Reynolds, N., Ferriby, H., Salls, W., Smith, D., Johnston, J.M., Myer, M., 2024. Forecasting freshwater cyanobacterial harmful algal blooms for Sentinel-3 satellite

resolved U.S. lakes and reservoirs. J. Environ. Manage. 349, 119518. https://doi.org/10.1016/j.jenvman.2023.119518

Schneiderman, E., Järvinen, M., Jennings, E., May, L., Moore, K., Naden, P.S., Pierson, D., 2010. Modeling the Effects of Climate Change on Catchment Hydrology with the GWLF Model, in: George, G. (Ed.), The Impact of Climate Change on European Lakes. Springer Netherlands, Dordrecht, pp. 33–50. https://doi.org/10.1007/978-90-481-2945-4_3

Schneiderman, E.M., Pierson, D.C., Lounsbury, D.G., Zion, M.S., 2002. Modeling of hydrochemistry of the cannonsville watershed with Generalized Watershed Loading Functions (GWLF). JAWRA J. Am. Water Resour. Assoc. 38, 1323–1347. https://doi.org/10.1111/j.1752-1688.2002.tb04350.x

Schürz, C., Hollosi, B., Matulla, C., Pressl, A., Ertl, T., Schulz, K., Mehdi, B., 2019a. A comprehensive sensitivity and uncertainty analysis for discharge and nitrate-nitrogen loads involving multiple discrete model inputs under future changing conditions. Hydrol. Earth Syst. Sci. 23, 1211–1244. https://doi.org/10.5194/hess-23-1211-2019

Schürz, C., Hollosi, B., Matulla, C., Pressl, A., Ertl, T., Schulz, K., Mehdi, B., 2019b. A comprehensive sensitivity and uncertainty analysis for discharge and nitrate-nitrogen loads involving multiple discrete model inputs under future changing conditions. Hydrol. Earth Syst. Sci. 23, 1211–1244. https://doi.org/10.5194/hess-23-1211-2019

Schwarz, G.E., Hoos, A.B., Alexander, R.B., Smith, R.A., 2006. The SPARROW Surface Water-Quality Model: Theory, Application and User Documentation--Part 1. U.S. Geological Survey Techniques and Methods.

Schwarz, G.E., Shih, J.S., Alexander, R.B., Smith, R.A., 2010. The SPARROW Surface Water-Quality Model: Theory, Application and User Documentation--Part 1.

Seebacher, F., Post, E., 2015. Climate change impacts on animal migration. Clim. Change Responses 2, 5. https://doi.org/10.1186/s40665-015-0013-9

Seifert-Dähnn, I., Furuseth, I.S., Vondolia, G.K., Gal, G., de Eyto, E., Jennings, E., Pierson, D., 2021. Costs and benefits of automated high-frequency environmental monitoring – The case of lake water management. J. Environ. Manage. 285, 112108. https://doi.org/10.1016/j.jenvman.2021.112108

Shabani, A., Zhang, X., Chu, X., Zheng, H., 2021. Automatic Calibration for CE-QUAL-W2 Model Using Improved Global-Best Harmony Search Algorithm. Water 13, 2308. https://doi.org/10.3390/w13162308

Siabi, E.K., Awafo, E.A., Kabo-bah, A.T., Derkyi, N.S.A., Akpoti, K., Mortey, E.M., Yazdanie, M., 2023. Assessment of Shared Socioeconomic Pathway (SSP) climate scenarios and its impacts on the Greater Accra region. Urban Clim. 49, 101432. https://doi.org/10.1016/j.uclim.2023.101432

Siddique, M.S., Xiong, X., Yang, H., Maqbool, T., Graham, N., Yu, W., 2022a. Dynamic variations in DOM and DBPs formation potential during surface water treatment by ozonation-nanofiltration: Using spectroscopic indices approach. Chem. Eng. J. 427, 132010. https://doi.org/10.1016/j.cej.2021.132010

Siddique, M.S., Xiong, X., Yang, H., Maqbool, T., Graham, N., Yu, W., 2022b. Dynamic variations in DOM and DBPs formation potential during surface water treatment by ozonation-nanofiltration: Using spectroscopic indices approach. Chem. Eng. J. 427, 132010. https://doi.org/10.1016/j.cej.2021.132010

Silvola, J., Alm, J., Ahlholm, U., Nykanen, H., Martikainen, P.J., 1996. CO2 Fluxes from Peat in Boreal Mires under Varying Temperature and Moisture Conditions. J. Ecol. 84, 219–228. https://doi.org/10.2307/2261357

Singer, A., Johst, K., Banitz, T., Fowler, M.S., Groeneveld, J., Gutiérrez, A.G., Hartig, F., Krug, R.M., Liess, M., Matlack, G., Meyer, K.M., Pe'er, G., Radchuk, V., Voinopol-Sassu, A.-J., Travis, J.M.J., 2016. Community dynamics under environmental change: How can next generation mechanistic models improve projections of species distributions? Ecol. Model., Next generation ecological modelling, concepts, and theory: structural realism, emergence, and predictions 326, 63–74. https://doi.org/10.1016/j.ecolmodel.2015.11.007

Slingsby, J.A., Wilson, A.M., Maitner, B., Moncrieff, G.R., 2023. Regional ecological forecasting across scales: A manifesto for a biodiversity hotspot. Methods Ecol. Evol. 14, 757–770. https://doi.org/10.1111/2041-210X.14046

Smedberg, E., Mörth, C.-M., Swaney, D.P., Humborg, C., 2006. Modeling hydrology and silicon-carbon interactions in taiga and tundra biomes from a landscape perspective: Implications for global warming feedbacks. Glob. Biogeochem. Cycles 20. https://doi.org/10.1029/2005GB002567

Smith, R.A., Schwarz, G.E., Alexander, R.B., 1997. Regional interpretation of water-quality monitoring data. Water Resour. Res. 33, 2781–2798. https://doi.org/10.1029/97WR02171

Sohn, J., Kim, H.-S., 2002. Modeling of chlorination disinfection by-products (DBPs) formation at the full-scale study. KSCE J. Civ. Eng. 6, 89–100. https://doi.org/10.1007/BF02829039

Son, K., Lin, L., Band, L., Owens, E.M., 2019. Modelling the interaction of climate, forest ecosystem, and hydrology to estimate catchment dissolved organic carbon export. Hydrol. Process. 33, 1448–1464. https://doi.org/10.1002/hyp.13412

Song, C., Omalley, A., Roy, S.G., Barber, B.L., Zydlewski, J., Mo, W., 2019. Managing dams for energy and fish tradeoffs: What does a win-win solution take? Sci. Total Environ. 669, 833–843. https://doi.org/10.1016/j.scitotenv.2019.03.042

Sparks, M.M., Falke, J.A., Quinn, T.P., Adkison, M.D., Schindler, D.E., Bartz, K., Young, D., Westley, P.A.H., 2019. Influences of spawning timing, water temperature, and climatic warming on early life history phenology in western Alaska sockeye salmon. Can. J. Fish. Aquat. Sci. 76, 123–135. https://doi.org/10.1139/cjfas-2017-0468

Srivastav, A.L., Patel, N., Chaudhary, V.K., 2020. Disinfection by-products in drinking water: Occurrence, toxicity and abatement. Environ. Pollut. 267, 115474. https://doi.org/10.1016/j.envpol.2020.115474

Staudinger, M.D., Lynch, A.J., Gaichas, S.K., Fox, M.G., Gibson-Reinemer, D., Langan, J.A., Teffer, A.K., Thackeray, S.J., Winfield, I.J., 2021. How Does Climate Change Affect Emergent Properties of Aquatic Ecosystems? Fisheries 46, 423–441. https://doi.org/10.1002/fsh.10606

Steffensen, S.M., Thiem, J.D., Stamplecoskie, K.M., Binder, T.R., Hatry, C., Langlois-Anderson, N., Cooke, S.J., 2013. Biological effectiveness of an inexpensive nature-like fishway for passage of warmwater fish in a small Ontario stream. Ecol. Freshw. Fish 22, 374–383. https://doi.org/10.1111/eff.12032

Stepanenko, V.M., Martynov, A., Jöhnk, K.D., Subin, Z.M., Perroud, M., Fang, X., Beyrich, F., Mironov, D., Goyette, S., 2013. A one-dimensional model intercomparison study of thermal regime of a shallow, turbid midlatitude lake. Geosci. Model Dev. 6, 1337–1352. https://doi.org/10.5194/gmd-6-1337-2013

St-Hilaire, A., Caissie, D., Bergeron, N.E., Ouarda, T.B.M.J., Boyer, C., 2021. Chapter 3 - Climate change and extreme river temperature, in: Fares, A. (Ed.), Climate Change and Extreme Events. Elsevier, pp. 25–37. https://doi.org/10.1016/B978-0-12-822700-8.00011-1

Sykes, G.E., Johnson, C.J., Shrimpton, J.M., 2009. Temperature and Flow Effects on Migration Timing of Chinook Salmon Smolts. Trans. Am. Fish. Soc. 138, 1252–1265. https://doi.org/10.1577/T08-180.1

Taillardat, M., Fougères, A.-L., Naveau, P., de Fondeville, R., 2023. Evaluating probabilistic forecasts of extremes using continuous ranked probability score distributions. Int. J. Forecast. 39, 1448–1459. https://doi.org/10.1016/j.ijforecast.2022.07.003

Tamario, C., Sunde, J., Petersson, E., Tibblin, P., Forsman, A., 2019. Ecological and Evolutionary Consequences of Environmental Change and Management Actions for Migrating Fish. Front. Ecol. Evol. 7, 271. https://doi.org/10.3389/fevo.2019.00271

Tan, M.L., Gassman, P.W., Yang, X., Haywood, J., 2020. A review of SWAT applications, performance and future needs for simulation of hydro-climatic extremes. Adv. Water Resour. 143, 103662. https://doi.org/10.1016/j.advwatres.2020.103662

Teichert, N., Benitez, J.-P., Dierckx, A., Tétard, S., de Oliveira, E., Trancart, T., Feunteun, E., Ovidio, M., 2020a. Development of an accurate model to predict the phenology of Atlantic salmon smolt spring migration. Aquat. Conserv. Mar. Freshw. Ecosyst. 30, 1552–1565. https://doi.org/10.1002/aqc.3382

Teichert, N., Tétard, S., Trancart, T., de Oliveira, E., Acou, A., Carpentier, A., Bourillon, B., Feunteun, E., 2020b. Towards transferability in fish migration models: A generic operational tool for predicting silver eel migration in rivers. Sci. Total Environ. 739, 140069. https://doi.org/10.1016/j.scitotenv.2020.140069

Teweldebrhan, A.T., Burkhart, J.F., Schuler, T.V., 2018. Parameter uncertainty analysis for an operational hydrological model using residual-based and limits of acceptability approaches. Hydrol. Earth Syst. Sci. 22, 5021–5039. https://doi.org/10.5194/hess-22-5021-2018

Thiery, W., Martynov, A., Darchambeau, F., Descy, J.-P., Plisnier, P.-D., Sushama, L., van Lipzig, N.P.M., 2014a. Understanding the performance of the FLake model over two African Great Lakes. Geosci. Model Dev. 7, 317–337. https://doi.org/10.5194/gmd-7-317-2014

Thiery, W., Stepanenko, V.M., Fang, X., Jöhnk, K.D., Li, Z., Martynov, A., Perroud, M., Subin, Z.M., Darchambeau, F., Mironov, D., Lipzig, N.P.M.V., 2014b. LakeMIP Kivu: evaluating the representation of a large, deep tropical lake by a set of one-dimensional lake models. Tellus Dyn. Meteorol. Oceanogr. 66. https://doi.org/10.3402/tellusa.v66.21390

Thomas, R.Q., Figueiredo, R.J., Daneshmand, V., Bookout, B.J., Puckett, L.K., Carey, C.C., 2020. A Near-Term Iterative Forecasting System Successfully Predicts Reservoir Hydrodynamics and Partitions Uncertainty in Real Time. Water Resour. Res. 56, e2019WR026138. https://doi.org/10.1029/2019WR026138

Thomas, R.Q., McClure, R.P., Moore, T.N., Woelmer, W.M., Boettiger, C., Figueiredo, R.J., Hensley, R.T., Carey, C.C., 2023a. Near-term forecasts of NEON lakes reveal gradients of environmental predictability across the US. Front. Ecol. Environ. n/a. https://doi.org/10.1002/fee.2623

Thomas, R.Q., McClure, R.P., Moore, T.N., Woelmer, W.M., Boettiger, C., Figueiredo, R.J., Hensley, R.T., Carey, C.C., 2023b. Near-term forecasts of NEON lakes reveal gradients of environmental predictability across the US. Front. Ecol. Environ. 21, 220–226. https://doi.org/10.1002/fee.2623

Tickner, D., Opperman, J.J., Abell, R., Acreman, M., Arthington, A.H., Bunn, S.E., Cooke, S.J., Dalton, J., Darwall, W., Edwards, G., Harrison, I., Hughes, K., Jones, T., Leclère, D., Lynch, A.J., Leonard, P., McClain, M.E., Muruven, D., Olden, J.D., Ormerod, S.J., Robinson, J., Tharme, R.E., Thieme, M., Tockner, K., Wright, M., Young, L., 2020.

Bending the Curve of Global Freshwater Biodiversity Loss: An Emergency Recovery Plan. BioScience 70, 330–342. https://doi.org/10.1093/biosci/biaa002

Trancart, T., Carpentier, A., Acou, A., Charrier, F., Mazel, V., Danet, V., Feunteun, É., 2020. When “safe” dams kill: Analyzing combination of impacts of overflow dams on the migration of silver eels. Ecol. Eng. 145, 105741. https://doi.org/10.1016/j.ecoleng.2020.105741

Troin, M., Arsenault, R., Wood, A.W., Brissette, F., Martel, J.-L., 2021. Generating Ensemble Streamflow Forecasts: A Review of Methods and Approaches Over the Past 40 Years. Water Resour. Res. 57, e2020WR028392. https://doi.org/10.1029/2020WR028392

Tulloch, A.I.T., Hagger, V., Greenville, A.C., 2020. Ecological forecasts to inform near-term management of threats to biodiversity. Glob. Change Biol. 26, 5816–5828. https://doi.org/10.1111/gcb.15272

Umlauf, L., Burchard, H., Bolding, K., 2005. GOTM sourcecode and test case documentation. Devel Version-Pre 4.

US EPA, 1987. The enhanced stream water quality models (QUAL2E and QUAL2E - UNCAS).

Valenti-Quiroga, M., Farré, M.J., Roccaro, P., 2024. Upgrading water treatment trains to comply with the disinfection by-products standards introduced by the Directive (EU) 2020/2184. Curr. Opin. Environ. Sci. Health 39, 100547. https://doi.org/10.1016/j.coesh.2024.100547

Valiente, A.G., Juanes, F., Garcia-Vazquez, E., 2011. Increasing Regional Temperatures Associated with Delays in Atlantic Salmon Sea-Run Timing at the Southern Edge of the European Distribution. Trans. Am. Fish. Soc. 140, 367–373. https://doi.org/10.1080/00028487.2011.557018

van der Wiel, K., Bintanja, R., 2021. Contribution of climatic changes in mean and variability to monthly temperature and precipitation extremes. Commun. Earth Environ. 2, 1–11. https://doi.org/10.1038/s43247-020-00077-4

van Vliet, M.T.H., Flörke, M., Wada, Y., 2017. Quality matters for water scarcity. Nat. Geosci. 10, 800–802. https://doi.org/10.1038/ngeo3047

van Vliet, M.T.H., Thorslund, J., Strokal, M., Hofstra, N., Flörke, M., Ehalt Macedo, H., Nkwasa, A., Tang, T., Kaushal, S.S., Kumar, R., van Griensven, A., Bouwman, L., Mosley, L.M., 2023. Global river water quality under climate change and hydroclimatic extremes. Nat. Rev. Earth Environ. 4, 687–702. https://doi.org/10.1038/s43017-023-00472-3

Vautard, R., Beekmann, M., Menut, L., 2000. Applications of adjoint modelling in atmospheric chemistry: sensitivity and inverse modelling. Environ. Model. Softw., Air pollution modelling and simulation 15, 703–709. https://doi.org/10.1016/S1364-8152(00)00058-X

Villanueva, C.M., Evlampidou, I., Ibrahim, F., Donat-Vargas, C., Valentin, A., Tugulea, A.-M., Echigo, S., Jovanovic, D., Lebedev, A.T., Lemus-Pérez, M., Rodriguez-Susa, M., Luzati, A., de Cássia dos Santos Nery, T., Pastén, P.A., Quiñones, M., Regli, S., Weisman, R., Dong, S., Ha, M., Phattarapattamawong, S., Manasfi, T., Musah, S.-I.E., Eng, A., Janák, K., Rush, S.C., Reckhow, D., Krasner, S.W., Vineis, P., Richardson, S.D., Kogevinas, M., 2023. Global assessment of chemical quality of drinking water: The case of trihalomethanes. Water Res. 230, 119568. https://doi.org/10.1016/j.watres.2023.119568

Vladic, T., Petersson, E., 2016. Evolutionary biology of the Atlantic salmon. CRC Press, Taylor & Francis Group Boca Raton, Boca Raton.

Wagener, T., Reinecke, R., Pianosi, F., 2022. On the evaluation of climate change impact models. WIREs Clim. Change 13, e772. https://doi.org/10.1002/wcc.772

Wander, H.L., Thomas, R.Q., Moore, T.N., Lofton, M.E., Breef-Pilz, A., Carey, C., 2023. Data assimilation experiments inform monitoring needs for near-term ecological forecasts in a eutrophic reservoir (preprint). Preprints. https://doi.org/10.22541/essoar.168500255.59108131/v1

Wander, H.L., Thomas, R.Q., Moore, T.N., Lofton, M.E., Breef-Pilz, A., Carey, C.C., 2024. Data assimilation experiments inform monitoring needs for near-term ecological forecasts in a eutrophic reservoir. Ecosphere 15, e4752. https://doi.org/10.1002/ecs2.4752

Wang, X., Jia, J., Su, T., Zhao, Z., Xu, J., Wang, L., 2018. A Fusion Water Quality Soft-Sensing Method Based on WASP Model and Its Application in Water Eutrophication Evaluation. J. Chem. 2018, 1–14. https://doi.org/10.1155/2018/9616841

Wang, X., Jiang, D., Lang, X., 2017. Future extreme climate changes linked to global warming intensity. Sci. Bull. 62, 1673–1680. https://doi.org/10.1016/j.scib.2017.11.004

Wang, X., Zhang, J., Babovic, V., 2016. Improving real-time forecasting of water quality indicators with combination of process-based models and data assimilation technique. Ecol. Indic. 66, 428–439. https://doi.org/10.1016/j.ecolind.2016.02.016

Wang, Y., Zhu, G., Engel, B., 2019. Health risk assessment of trihalomethanes in water treatment plants in Jiangsu Province, China. Ecotoxicol. Environ. Saf. 170, 346–354. https://doi.org/10.1016/j.ecoenv.2018.12.004

Warner, K.A., Saros, J.E., 2019. Variable responses of dissolved organic carbon to precipitation events in boreal drinking water lakes. Water Res. 156, 315–326. https://doi.org/10.1016/j.watres.2019.03.036

Watling, J.I., Brandt, L.A., Bucklin, D.N., Fujisaki, I., Mazzotti, F.J., Romañach, S.S., Speroterra, C., 2015. Performance metrics and variance partitioning reveal sources of uncertainty in species distribution models. Ecol. Model. 309–310, 48–59. https://doi.org/10.1016/j.ecolmodel.2015.03.017

Weaver, D.M., Coghlan, S.M., Zydlewski, J., 2018. Effects of sea lamprey substrate modification and carcass nutrients on macroinvertebrate assemblages in a small Atlantic coastal stream. J. Freshw. Ecol. 33, 19–30. https://doi.org/10.1080/02705060.2017.1417168

Wei, X., Hayes, D.J., Butman, D.E., Qi, J., Ricciuto, D.M., Yang, X., 2024. Modeling exports of dissolved organic carbon from landscapes: a review of challenges and opportunities. Environ. Res. Lett. 19, 053001. https://doi.org/10.1088/1748-9326/ad3cf8

Weiskopf, S.R., Rubenstein, M.A., Crozier, L.G., Gaichas, S., Griffis, R., Halofsky, J.E., Hyde, K.J.W., Morelli, T.L., Morisette, J.T., Muñoz, R.C., Pershing, A.J., Peterson, D.L., Poudel, R., Staudinger, M.D., Sutton-Grier, A.E., Thompson, L., Vose, J., Weltzin, J.F., Whyte, K.P., 2020. Climate change effects on biodiversity, ecosystems, ecosystem services, and natural resource management in the United States. Sci. Total Environ. 733, 137782. https://doi.org/10.1016/j.scitotenv.2020.137782

Welch, H., Hazen, E.L., Bograd, S.J., Jacox, M.G., Brodie, S., Robinson, D., Scales, K.L., Dewitt, L., Lewison, R., 2019. Practical considerations for operationalizing dynamic management tools. J. Appl. Ecol. 56, 459–469. https://doi.org/10.1111/1365-2664.13281

Whitehead, Leckie, H., Rankinen, K., Butterfield, D., Futter, M.N., Bussi, G., 2016. An INCA model for pathogens in rivers and catchments: Model structure, sensitivity analysis and application to the River Thames catchment, UK. Sci. Total Environ. 572, 1601–1610. https://doi.org/10.1016/j.scitotenv.2016.01.128

Whitehead, Mimouni, Z., Butterfield, D., Bussi, G., Hossain, M.A., Peters, R., Shawal, S., Holdship, P., Rampley, C.P.N., Jin, L., Ager, D., 2021. A New Multibranch Model for Metals in River Systems: Impacts and Control of Tannery Wastes in Bangladesh. Sustainability 13, 3556. https://doi.org/10.3390/su13063556

Whitehead, P.G., Wilson, E.J., Butterfield, D., 1998. A semi-distributed Integrated Nitrogen model for multiple source assessment in Catchments (INCA): Part I — model structure and process equations. Sci. Total Environ. 210–211, 547–558. https://doi.org/10.1016/S0048-9697(98)00037-0

WHO, G., 2011. Guidelines for drinking-water quality. World Health Organ. 216, 303–304.

Wickberg, A., Lidström, S., Lagerkvist, A., Meyer, T., Wormbs, N., Gärdebo, J., Sörlin, S., Höhler, S., 2024. The mediated planet: Datafication and the environmental SDGs. Environ. Sci. Policy 153, 103673. https://doi.org/10.1016/j.envsci.2024.103673

Wilks, D.S., 2019. Statistical methods in the atmospheric sciences: an introduction, 4th ed. ed. Elsevier, Amsterdam.

Williamson, J., Evans, C., Spears, B., Pickard, A., Chapman, P.J., Feuchtmayr, H., Leith, F., Waldron, S., Monteith, D., 2023. Reviews and syntheses: Understanding the impacts of peatland catchment management on dissolved organic matter concentration and treatability. Biogeosciences 20, 3751–3766. https://doi.org/10.5194/bg-20-3751-2023

Winterdahl, M., Temnerud, J., Futter, M.N., Löfgren, S., Moldan, F., Bishop, K., 2011. Riparian Zone Influence on Stream Water Dissolved Organic Carbon Concentrations at the Swedish Integrated Monitoring Sites. AMBIO 40, 920–930. https://doi.org/10.1007/s13280-011-0199-4

Wit, H.A. de, Stoddard, J.L., Monteith, D.T., Sample, J.E., Austnes, K., Couture, S., Fölster, J., Higgins, S.N., Houle, D., Hruška, J., Krám, P., Kopáček, J., Paterson, A.M., Valinia, S., Dam, H.V., Vuorenmaa, J., Evans, C.D., 2021. Cleaner air reveals growing influence of climate on dissolved organic carbon trends in northern headwaters. Environ. Res. Lett. 16, 104009. https://doi.org/10.1088/1748-9326/ac2526

Woelmer, W.M., Thomas, R.Q., Lofton, M.E., McClure, R.P., Wander, H.L., Carey, C.C., 2022. Near-term phytoplankton forecasts reveal the effects of model time step and forecast horizon on predictability. Ecol. Appl. 32, e2642. https://doi.org/10.1002/eap.2642

Woelmer, W.M., Thomas, R.Q., Olsson, F., Steele, B.G., Weathers, K.C., Carey, C.C., 2024. Process-Based Forecasts of Lake Water Temperature and Dissolved Oxygen Outperform Null Models, with Variability Over Time and Depth. https://doi.org/10.2139/ssrn.4699835

Wool, T., Ambrose, R.B., Martin, J.L., Comer, A., 2020. WASP 8: The Next Generation in the 50-year Evolution of USEPA's Water Quality Model. Water 12, 1398. https://doi.org/10.3390/w12051398

Woolway, R.I., Kraemer, B.M., Lenters, J.D., Merchant, C.J., O'Reilly, C.M., Sharma, S., 2020. Global lake responses to climate change. Nat. Rev. Earth Environ. 1, 388–403. https://doi.org/10.1038/s43017-020-0067-5

Woolway, R.I., Maberly, S.C., Jones, I.D., Feuchtmayr, H., 2014. A novel method for estimating the onset of thermal stratification in lakes from surface water measurements. Water Resour. Res. 50, 5131–5140. https://doi.org/10.1002/2013WR014975

Worrall, F., Burt, T., Adamson, J., 2004. Can climate change explain increases in DOC flux from upland peat catchments? Sci. Total Environ. 326, 95–112. https://doi.org/10.1016/j.scitotenv.2003.11.022

Wu, J., Yao, H., 2024. Enhanced Role of Streamflow Processes in the Evolutionary Trends of Dissolved Organic Carbon. Environ. Sci. Technol. 58, 4772–4780. https://doi.org/10.1021/acs.est.3c09508

Wu, J., Yao, H., 2022. Simulating dissolved organic carbon during dryness/wetness periods based on hydrological characteristics under multiple timescales. J. Hydrol. 614, 128534. https://doi.org/10.1016/j.jhydrol.2022.128534

Wu, J., Yao, H., Chen, Xiaohong, Chen, Xingwei, 2023a. Dynamics of dissolved organic carbon during drought and flood events: A phase-by-stages perspective. Sci. Total Environ. 871, 162158. https://doi.org/10.1016/j.scitotenv.2023.162158

Wu, J., Yao, H., Wang, G., Chen, X., Yuan, X., Zhou, Y., Zhang, D., 2023b. Dynamics of DOC concentration and flux in different propagation stages of hydrological drought: Patterns and drivers. J. Hydrol. 617, 128939. https://doi.org/10.1016/j.jhydrol.2022.128939

Wu, Y., Miao, C., Fan, X., Gou, J., Zhang, Q., Zheng, H., 2022. Quantifying the Uncertainty Sources of Future Climate Projections and Narrowing Uncertainties With Bias Correction Techniques. Earths Future 10, e2022EF002963. https://doi.org/10.1029/2022EF002963

Xiao, R., Deng, Y., Xu, Z., Chu, W., 2024. Disinfection Byproducts and Their Precursors in Drinking Water Sources: Origins, Influencing Factors, and Environmental Insights. Engineering 36, 36–50. https://doi.org/10.1016/j.eng.2023.08.017

Xu, J., Morris, P.J., Liu, J., Holden, J., 2018. Hotspots of peatland-derived potable water use identified by global analysis. Nat. Sustain. 1, 246–253. https://doi.org/10.1038/s41893-018-0064-6

Xu, J., Morris, P.J., Liu, J., Ledesma, J.L.J., Holden, J., 2020. Increased Dissolved Organic Carbon Concentrations in Peat-Fed UK Water Supplies Under Future Climate and Sulfate Deposition Scenarios. Water Resour. Res. 56, e2019WR025592. https://doi.org/10.1029/2019WR025592

Xu, Z., Yang, Z., Cai, X., Yin, X., Cai, Y., 2020. Modeling Framework for Reservoir Capacity Planning Accounting for Fish Migration. J. Water Resour. Plan. Manag. 146, 04020006. https://doi.org/10.1061/(ASCE)WR.1943-5452.0001170

Yang, D., 2019. Making reference solar forecasts with climatology, persistence, and their optimal convex combination. Sol. Energy 193, 981–985. https://doi.org/10.1016/j.solener.2019.10.006

Yang, Q., Zhang, X., 2016. Improving SWAT for simulating water and carbon fluxes of forest ecosystems. Sci. Total Environ. 569–570, 1478–1488. https://doi.org/10.1016/j.scitotenv.2016.06.238

Yassin, M., Asfaw, A., Speight, V., Shucksmith, J.D., 2021. Evaluation of Data-Driven and Process-Based Real-Time Flow Forecasting Techniques for Informing Operation of Surface Water Abstraction. J. Water Resour. Plan. Manag. 147, 04021037. https://doi.org/10.1061/(ASCE)WR.1943-5452.0001397

Yin, H., Yin, P., Yang, Z., 2023. Seasonal sediment phosphorus release across sediment-water interface and its potential role in supporting algal blooms in a large shallow eutrophic Lake (Lake Taihu, China). Sci. Total Environ. 896, 165252. https://doi.org/10.1016/j.scitotenv.2023.165252

Yuan, L., Sinshaw, T., Forshay, K.J., 2020. Review of Watershed-Scale Water Quality and Nonpoint Source Pollution Models. Geosciences 10. https://doi.org/10.3390/geosciences10010025

Zachow, M., Nóia Júnior, R. de S., Asseng, S., 2023. Seasonal climate models for national wheat yield forecasts in Brazil. Agric. For. Meteorol. 342, 109753. https://doi.org/10.1016/j.agrformet.2023.109753

Zafer Defne, Frederick J. Spitz, Vincent DePaul, Tim A. Wool, 2017. Toward a Comprehensive Water-Quality Modeling of Barnegat Bay: Development of ROMS to WASP Coupler. J. Coast. Res. 78, 34–45. https://doi.org/10.2112/SI78-004.1

Zhong, J., Cai, W., 2015. Differential evolution with sensitivity analysis and the Powell's method for crowd model calibration. J. Comput. Sci., Computational Science at the Gates of Nature 9, 26–32. https://doi.org/10.1016/j.jocs.2015.04.013

Zhu, S., Zhang, Z., Liu, X., 2017. Enhanced Two Dimensional Hydrodynamic and Water Quality Model (CE-QUAL-W2) for Simulating Mercury Transport and Cycling in Water Bodies. Water 9, 643. https://doi.org/10.3390/w9090643

Zwart, J.A., Oliver, S.K., Watkins, W.D., Sadler, J.M., Appling, A.P., Corson-Dosch, H.R., Jia, X., Kumar, V., Read, J.S., 2023. Near-term forecasts of stream temperature using deep learning and data assimilation in support of management decisions. JAWRA J. Am. Water Resour. Assoc. 59, 317–337. https://doi.org/10.1111/1752-1688.13093

Zydlewski, G.B., Haro, A., McCormick, S.D., 2005. Evidence for cumulative temperature as an initiating and terminating factor in downstream migratory behavior of Atlantic salmon (*Salmo salar*) smolts. Can. J. Fish. Aquat. Sci. 62, 68–78. https://doi.org/10.1139/f04-179

Zydlewski, G.B., Stich, D.S., McCormick, S.D., 2014. Photoperiod control of downstream movements of Atlantic salmon *Salmo salar* smolts. J. Fish Biol. 85, 1023–1041. https://doi.org/10.1111/jfb.12509

Appendix A

Appendix A contains future climate projections for the meteorological inputs used in the catchment modelling framework of Chapter 4. These projections were derived from the 5-member GCM ensemble provided by the open-access Inter-Sectoral Impact Model Intercomparison Project (0.5° ISIMIP 3b simulation round; data.isimip.org) (Lange and Büchner, 2021). Below are presented annual grid-cell daily bias-corrected values of future precipitation and mean air temperature for each study catchment during the baseline period (1985 – 2014) and during P1 (2050 – 2059) and P2 (2090 – 2099) under three Shared Socioeconomic Pathways (SSP): SSP126, SSP370 and SSP585.

Table A.1 Vattholma - annual precipitation values for each ISIMIP3b ensemble member during the baseline period (1985 – 2014).

Vattholma: precipitation (mm / year)

Baseline period (1985 - 2014)

	GCM 1	**GCM 2**	**GCM 3**	**GCM 4**	**GCM 5**
Year	*GFDL-ESM4*	*IPSL-CM6A-LR*	*MPI-ESM1-2-HR*	*MRI-ESM2-0*	*UKESM1-0-LL*
1985	595	706	578	761	727
1986	866	786	610	555	715
1987	623	638	660	739	650
1988	761	703	828	812	779
1989	657	767	695	814	524
1990	758	624	643	620	849
1991	688	763	534	631	697
1992	709	755	657	866	554
1993	719	821	766	650	752
1994	581	745	686	792	620
1995	764	753	599	710	525
1996	902	669	745	684	625
1997	846	807	706	614	708
1998	640	655	693	714	592
1999	809	687	593	582	644
2000	881	599	795	756	664
2001	571	714	772	788	907
2002	694	669	716	752	796
2003	586	546	629	820	994
2004	522	910	761	950	861
2005	645	705	489	638	832
2006	766	639	705	695	707
2007	756	659	711	789	893
2008	940	863	713	619	686
2009	819	618	903	687	580
2010	685	938	697	795	710
2011	759	720	803	812	666
2012	591	704	685	720	552
2013	765	765	731	536	676
2014	590	767	744	628	758
GCM Average	716	723	695	718	708
Standard deviation	108	88	86	96	116
Period average	**712**				
Standard deviation	**100**				

Table A.2 Vattholma – annual mean air temperature values for each ISIMIP3b ensemble member during the baseline period (1985 – 2014).

Vattholma: mean air temperature (°C)

Baseline period (1985 - 2014)

	GCM 1	**GCM 2**	**GCM 3**	**GCM 4**	**GCM 5**
Year	*GFDL-ESM4*	*IPSL-CM6A-LR*	*MPI-ESM1-2-HR*	*MRI-ESM2-0*	*UKESM1-0-LL*
1985	6.6	5.6	5.5	5.8	4.3
1986	3.9	6.9	6.1	4.7	7.2
1987	6.6	6.5	5.5	6.0	5.9
1988	5.5	5.2	4.8	4.8	5.9
1989	7.7	7.6	6.4	6.1	7.1
1990	7.3	5.7	7.1	5.2	7.0
1991	6.0	4.5	6.9	5.1	8.9
1992	5.2	6.0	5.2	4.3	6.5
1993	5.3	6.0	5.7	7.2	7.3
1994	4.8	6.4	4.2	4.6	7.3
1995	6.0	6.5	4.6	5.2	6.5
1996	5.4	7.2	6.2	6.9	6.5
1997	6.0	6.3	5.4	5.3	5.6
1998	7.6	5.2	4.9	8.5	4.9
1999	7.1	6.0	5.3	6.1	4.9
2000	6.0	3.7	6.0	6.1	7.3
2001	7.7	4.5	6.0	6.2	3.9
2002	5.0	5.6	5.1	6.8	5.4
2003	4.3	7.3	6.6	7.0	7.3
2004	6.9	6.6	7.9	5.5	5.9
2005	7.1	6.8	7.8	6.1	7.5
2006	6.9	7.1	6.0	7.0	2.9
2007	6.1	7.8	7.0	5.9	6.3
2008	7.2	6.4	7.7	6.9	4.7
2009	6.5	7.1	6.9	6.5	5.4
2010	4.8	6.0	6.2	5.9	7.3
2011	7.4	6.4	6.4	6.2	8.8
2012	5.9	7.1	7.9	7.1	8.4
2013	8.2	6.5	6.1	8.3	6.9
2014	6.0	7.7	7.9	8.7	7.3
GCM Average	6.2	6.3	6.2	6.2	6.4
Standard deviation	1.1	1.0	1.0	1.1	1.4
Period average	**6.3**				
Standard deviation	**1.1**				

Table A.3 Vattholma – SSP126, SSP370 and SSP585 scenarios. Future annual precipitation values for each ISIMIP3b ensemble member during P1 (2050 – 2060).

Vattholma: precipitation (mm / year)

SSP126 - P1 (2050-2060)

	GCM 1	**GCM 2**	**GCM 3**	**GCM 4**	**GCM 5**
Year	*GFDL-ESM4*	*IPSL-CM6A-LR*	*MPI-ESM1-2-HR*	*MRI-ESM2-0*	*UKESM1-0-LL*
2050	650	720	644	568	635
2051	699	1107	729	675	766
2052	1038	606	611	758	636
2053	892	914	761	637	785
2054	869	704	605	666	716
2055	596	607	555	771	954
2056	796	676	788	717	805
2057	706	626	734	728	659
2058	600	728	712	773	818
2059	741	836	658	622	901
GCM Average	759	752	680	692	768
Standard deviation	134	151	72	66	103
Period average	**730**				
Standard deviation	**116**				

Vattholma: precipitation (mm / year)

SSP370 - P1 (2050-2060)

	GCM 1	**GCM 2**	**GCM 3**	**GCM 4**	**GCM 5**
Year	*GFDL-ESM4*	*IPSL-CM6A-LR*	*MPI-ESM1-2-HR*	*MRI-ESM2-0*	*UKESM1-0-LL*
2050	737	610	624	734	669
2051	859	840	698	817	1070
2052	746	570	773	655	651
2053	716	734	752	884	757
2054	827	633	821	743	775
2055	711	882	782	822	781
2056	525	663	988	960	831
2057	824	829	777	899	1024
2058	950	861	996	746	757
2059	799	738	897	648	714
GCM Average	770	736	811	791	803
Standard deviation	107	107	113	99	132
Period average	**782**				
Standard deviation	**116**				

Vattholma: precipitation (mm / year)

SSP585 - P1 (2050-2060)

	GCM 1	**GCM 2**	**GCM 3**	**GCM 4**	**GCM 5**
Year	*GFDL-ESM4*	*IPSL-CM6A-LR*	*MPI-ESM1-2-HR*	*MRI-ESM2-0*	*UKESM1-0-LL*
2050	630	615	881	672	723
2051	689	706	779	621	777
2052	698	841	691	707	808
2053	784	739	550	774	699
2054	927	812	806	836	735
2055	788	1076	598	933	865
2056	951	920	655	805	836
2057	887	798	544	635	826
2058	670	698	697	747	883
2059	644	720	892	813	807
GCM Average	767	792	709	754	796
Standard deviation	114	125	121	93	58
Period average	**764**				
Standard deviation	**109**				

Table A.4 Vattholma – SSP126, SSP370 and SSP585 scenarios. Future annual mean air temperature values for each ISIMIP3b ensemble member during P1 (2050 – 2060).

Vattholma: mean air temperature (°C)

SSP126 - P1 (2050-2060)

	GCM 1	**GCM 2**	**GCM 3**	**GCM 4**	**GCM 5**
Year	*GFDL-ESM4*	*IPSL-CM6A-LR*	*MPI-ESM1-2-HR*	*MRI-ESM2-0*	*UKESM1-0-LL*
2050	6.9	10.0	8.4	7.2	9.7
2051	6.0	8.5	8.2	7.3	9.9
2052	8.3	7.5	7.2	6.5	9.9
2053	7.3	9.7	6.6	7.5	8.5
2054	8.2	9.4	9.0	7.9	7.6
2055	9.0	8.9	8.1	7.8	9.9
2056	8.4	7.3	8.0	8.2	9.1
2057	7.6	8.9	8.2	7.6	10.2
2058	7.7	8.4	9.2	8.0	9.6
2059	9.4	8.2	8.8	9.0	9.9
GCM Average	7.9	8.7	8.2	7.7	9.4
Standard deviation	1.0	0.9	0.7	0.6	0.8
Period average	**8.4**				
Standard deviation	**1.0**				

Vattholma: mean air temperature (°C)

SSP370 - P1 (2050-2060)

	GCM 1	**GCM 2**	**GCM 3**	**GCM 4**	**GCM 5**
Year	*GFDL-ESM4*	*IPSL-CM6A-LR*	*MPI-ESM1-2-HR*	*MRI-ESM2-0*	*UKESM1-0-LL*
2050	7.8	7.6	10.3	9.7	10.5
2051	8.3	8.9	8.0	7.8	10.6
2052	8.3	8.7	9.2	7.5	10.3
2053	8.4	8.5	9.7	7.9	8.8
2054	7.8	11.1	9.4	8.2	11.7
2055	9.4	9.2	10.1	7.1	12.3
2056	9.2	9.4	7.2	7.6	12.4
2057	9.5	8.8	8.0	8.5	10.4
2058	9.0	8.2	8.6	7.6	10.2
2059	8.9	8.6	9.2	8.7	11.1
GCM Average	8.7	8.9	9.0	8.1	10.8
Standard deviation	0.6	0.9	1.0	0.7	1.0
Period average	**9.1**				
Standard deviation	**1.3**				

Vattholma: mean air temperature (°C)

SSP585 - P1 (2050-2060)

	GCM 1	**GCM 2**	**GCM 3**	**GCM 4**	**GCM 5**
Year	*GFDL-ESM4*	*IPSL-CM6A-LR*	*MPI-ESM1-2-HR*	*MRI-ESM2-0*	*UKESM1-0-LL*
2050	8.4	10.4	7.9	9.5	12.1
2051	8.9	9.0	7.6	9.1	11.0
2052	9.6	10.1	7.1	7.5	10.0
2053	8.6	9.9	9.5	8.6	11.6
2054	8.7	10.1	8.7	9.1	11.9
2055	8.9	9.9	7.6	9.2	10.1
2056	8.7	9.9	7.3	8.1	10.8
2057	9.8	10.1	10.2	8.5	12.1
2058	8.2	9.9	8.8	7.9	10.9
2059	9.2	7.4	5.5	9.9	11.7
GCM Average	8.9	9.7	8.0	8.7	11.2
Standard deviation	0.5	0.8	1.3	0.7	0.7
Period average	**9.3**				
Standard deviation	**1.4**				

Table A.5 Vattholma – SSP126, SSP370 and SSP585 scenarios. Future annual precipitation values for each ISIMIP3b ensemble member during P2 (2090 – 2100).

Vattholma: precipitation (mm / year)

SSP126 - P2 (2090-2100)

	GCM 1	**GCM 2**	**GCM 3**	**GCM 4**	**GCM 5**
Year	*GFDL-ESM4*	*IPSL-CM6A-LR*	*MPI-ESM1-2-HR*	*MRI-ESM2-0*	*UKESM1-0-LL*
2090	612	749	766	761	971
2091	776	854	882	561	604
2092	771	461	1095	854	627
2093	808	723	703	709	630
2094	593	873	711	653	722
2095	723	1117	585	931	719
2096	741	911	821	912	933
2097	709	1097	593	662	646
2098	855	615	718	743	863
2099	748	982	739	663	688
GCM Average	734	838	761	745	740
Standard deviation	77	196	140	115	127
Period average	**764**				
Standard deviation	**142**				

Vattholma: precipitation (mm / year)

SSP370 - P2 (2090-2100)

	GCM 1	**GCM 2**	**GCM 3**	**GCM 4**	**GCM 5**
Year	*GFDL-ESM4*	*IPSL-CM6A-LR*	*MPI-ESM1-2-HR*	*MRI-ESM2-0*	*UKESM1-0-LL*
2090	818	713	733	636	770
2091	783	771	864	798	1188
2092	559	965	568	652	928
2093	824	705	878	950	663
2094	723	822	571	866	732
2095	842	875	715	843	968
2096	825	794	999	1100	1061
2097	775	713	1005	886	733
2098	831	782	903	941	698
2099	1050	914	735	687	830
GCM Average	803	805	797	836	857
Standard deviation	115	84	150	140	165
Period average	**820**				
Standard deviation	**136**				

Vattholma: precipitation (mm / year)

SSP585 - P2 (2090-2100)

	GCM 1	**GCM 2**	**GCM 3**	**GCM 4**	**GCM 5**
Year	*GFDL-ESM4*	*IPSL-CM6A-LR*	*MPI-ESM1-2-HR*	*MRI-ESM2-0*	*UKESM1-0-LL*
2090	742	1131	904	777	921
2091	833	965	702	874	719
2092	921	958	704	637	943
2093	812	705	668	695	918
2094	858	1154	674	1082	744
2095	850	623	1033	816	967
2096	782	538	472	657	902
2097	778	992	743	706	787
2098	680	907	677	675	685
2099	976	918	778	809	784
GCM Average	823	889	736	773	837
Standard deviation	81	195	142	127	98
Period average	**812**				
Standard deviation	**145**				

Table A.6 Vattholma – SSP126, SSP370 and SSP585 scenarios. Future annual mean air temperature values for each ISIMIP3b ensemble member during P2 (2090 – 2100).

Vattholma: mean air temperature (°C)

SSP126 - P2 (2090-2100)

	GCM 1	**GCM 2**	**GCM 3**	**GCM 4**	**GCM 5**
Year	*GFDL-ESM4*	*IPSL-CM6A-LR*	*MPI-ESM1-2-HR*	*MRI-ESM2-0*	*UKESM1-0-LL*
2090	7.6	10.1	7.2	4.7	10.6
2091	7.2	8.2	6.3	5.8	9.9
2092	7.9	8.1	6.9	6.9	8.9
2093	7.4	9.2	7.3	4.8	9.4
2094	8.6	7.3	8.2	5.6	11.6
2095	7.3	7.4	8.5	6.3	11.0
2096	8.0	7.9	7.1	6.3	9.7
2097	7.1	8.4	6.9	7.3	10.6
2098	5.4	9.7	7.3	6.1	8.9
2099	5.8	8.9	8.2	6.0	9.9
GCM Average	7.2	8.5	7.4	6.0	10.0
Standard deviation	0.9	0.9	0.7	0.8	0.8
Period average	**7.8**				
Standard deviation	**1.6**				

Vattholma: mean air temperature (°C)

SSP370 - P2 (2090-2100)

	GCM 1	**GCM 2**	**GCM 3**	**GCM 4**	**GCM 5**
Year	*GFDL-ESM4*	*IPSL-CM6A-LR*	*MPI-ESM1-2-HR*	*MRI-ESM2-0*	*UKESM1-0-LL*
2090	10.3	11.3	10.0	9.4	13.7
2091	9.0	12.7	9.8	9.1	13.7
2092	10.4	12.9	10.3	7.9	13.7
2093	10.7	11.7	10.2	8.3	14.7
2094	9.5	12.4	11.0	9.1	15.5
2095	9.5	12.5	10.4	9.3	15.9
2096	10.3	13.1	10.9	8.8	13.5
2097	10.0	12.9	9.8	9.1	15.3
2098	10.5	13.8	10.7	7.8	15.5
2099	9.7	12.1	11.0	8.3	15.7
GCM Average	10.0	12.5	10.4	8.7	14.7
Standard deviation	0.5	0.7	0.5	0.6	0.9
Period average	**11.3**				
Standard deviation	**2.2**				

Vattholma: mean air temperature (°C)

SSP585 - P2 (2090-2100)

	GCM 1	**GCM 2**	**GCM 3**	**GCM 4**	**GCM 5**
Year	*GFDL-ESM4*	*IPSL-CM6A-LR*	*MPI-ESM1-2-HR*	*MRI-ESM2-0*	*UKESM1-0-LL*
2090	11.3	13.5	11.0	9.3	15.0
2091	10.2	13.1	10.7	10.7	15.3
2092	11.2	13.5	9.7	9.3	16.2
2093	11.4	14.9	11.9	9.5	15.6
2094	10.1	12.8	11.3	9.4	17.3
2095	10.9	14.7	10.8	8.1	14.8
2096	9.9	14.5	12.2	8.5	15.8
2097	10.8	14.4	11.7	10.7	15.8
2098	11.0	14.6	11.4	9.8	17.6
2099	11.3	13.9	11.3	9.5	16.4
GCM Average	10.8	14.0	11.2	9.5	16.0
Standard deviation	0.5	0.7	0.7	0.8	0.9
Period average	**12.3**				
Standard deviation	**2.5**				

Table A.7 Glenamong - annual precipitation values for each ISIMIP3b ensemble member during the baseline period (1985 – 2014).

Glenamong: precipitation (mm / year)

Baseline period (1985 - 2014)

	GCM 1	**GCM 2**	**GCM 3**	**GCM 4**	**GCM 5**
Year	*GFDL-ESM4*	*IPSL-CM6A-LR*	*MPI-ESM1-2-HR*	*MRI-ESM2-0*	*UKESM1-0-LL*
1985	1644	1746	1491	1658	1718
1986	1659	1718	1717	1517	2245
1987	1688	1867	1636	1311	1790
1988	1856	1614	2058	1378	1872
1989	1820	1659	1658	1814	1536
1990	1626	1617	1395	1821	1500
1991	1892	1751	1821	1420	1892
1992	1439	1648	1611	1804	1652
1993	1738	1873	1597	1903	1660
1994	1674	1816	1553	1700	1723
1995	1740	1602	1561	1645	1802
1996	2163	1571	1844	1669	1915
1997	2156	1536	1635	1402	1599
1998	1776	1743	1608	1967	1659
1999	1548	1692	1662	1271	2080
2000	1847	1512	1871	1720	1746
2001	1766	1656	1840	1490	2043
2002	1404	1702	1691	1539	1819
2003	1757	1669	1876	1791	1798
2004	1548	1627	1936	1775	1635
2005	1471	1726	2011	1813	1734
2006	1652	1770	1944	1809	1489
2007	1553	1715	1885	1730	1672
2008	1541	1855	1536	1721	1464
2009	1654	1540	1782	1717	1848
2010	1983	1618	1395	1583	1910
2011	1741	1653	1626	1892	1796
2012	1773	1729	1477	1712	1569
2013	1745	1849	1794	1794	1628
2014	1552	1877	1704	2201	1564
GCM Average	1714	1698	1707	1686	1745
Standard deviation	179	102	173	201	179
Period average	**1710**				
Standard deviation	**171**				

Table A.8 Glenamong – annual mean air temperature values for each ISIMIP3b ensemble member during the baseline period (1985 – 2014).

Glenamong: mean air temperature (°C)

Baseline period (1985 - 2014)

	GCM 1	**GCM 2**	**GCM 3**	**GCM 4**	**GCM 5**
Year	*GFDL-ESM4*	*IPSL-CM6A-LR*	*MPI-ESM1-2-HR*	*MRI-ESM2-0*	*UKESM1-0-LL*
1985	9.2	8.1	9.4	8.6	8.1
1986	8.5	9.0	9.5	9.3	8.4
1987	9.9	8.4	9.9	9.4	8.0
1988	9.1	8.7	9.1	8.5	8.7
1989	8.9	9.1	9.4	9.7	9.6
1990	9.1	9.1	9.7	8.8	9.4
1991	8.8	9.5	9.0	9.1	8.8
1992	8.5	9.5	8.8	8.5	8.7
1993	8.9	9.3	8.4	9.2	9.1
1994	8.9	9.0	9.2	8.9	9.8
1995	8.9	9.3	8.5	8.6	9.3
1996	9.3	10.0	9.0	8.7	9.2
1997	9.2	8.8	8.9	8.8	9.2
1998	9.4	8.2	8.6	9.1	9.3
1999	9.1	9.0	9.3	8.9	9.1
2000	9.0	9.9	8.9	9.3	9.6
2001	9.4	9.4	8.8	8.8	9.5
2002	8.8	9.2	8.9	8.7	9.7
2003	8.3	9.4	9.3	9.3	10.2
2004	9.4	9.1	8.5	8.6	9.6
2005	9.1	9.5	9.0	9.8	9.7
2006	9.5	9.8	8.4	9.7	8.8
2007	9.5	9.6	9.2	9.1	9.6
2008	9.4	9.8	8.9	9.3	9.7
2009	9.0	9.4	8.9	9.7	9.0
2010	9.8	9.6	9.7	8.9	9.6
2011	9.4	9.1	9.8	9.2	9.2
2012	9.0	9.7	9.6	9.4	10.2
2013	10.2	8.9	8.8	9.8	9.8
2014	9.7	9.4	9.6	9.6	9.9
GCM Average	9.2	9.2	9.1	9.1	9.3
Standard deviation	0.4	0.5	0.4	0.4	0.6
Period average	**9.2**				
Standard deviation	**0.5**				

Table A.9 Glenamong – SSP126, SSP370 and SSP585 scenarios. Future annual precipitation values for each ISIMIP3b ensemble member during P1 (2050 – 2060).

Glenamong: precipitation (mm / year)

SSP126 - P1 (2050-2060)

	GCM 1	**GCM 2**	**GCM 3**	**GCM 4**	**GCM 5**
Year	*GFDL-ESM4*	*IPSL-CM6A-LR*	*MPI-ESM1-2-HR*	*MRI-ESM2-0*	*UKESM1-0-LL*
2050	1707	1841	1495	1530	1603
2051	1516	1787	1588	1647	1451
2052	2153	1912	1685	1889	1857
2053	1795	1755	1921	1598	1728
2054	1884	1791	1596	1664	1364
2055	1608	1596	1617	1619	1819
2056	1780	1412	1704	1674	1908
2057	1842	1912	1818	1856	1902
2058	2082	1776	1742	1834	1663
2059	1489	1704	1633	1821	1842
GCM Average	1786	1749	1680	1713	1714
Standard deviation	208	143	117	119	181
Period average	**1728**				
Standard deviation	**162**				

Glenamong: precipitation (mm / year)

SSP370 - P1 (2050-2060)

	GCM 1	**GCM 2**	**GCM 3**	**GCM 4**	**GCM 5**
Year	*GFDL-ESM4*	*IPSL-CM6A-LR*	*MPI-ESM1-2-HR*	*MRI-ESM2-0*	*UKESM1-0-LL*
2050	1952	2015	1532	1723	1681
2051	1876	1728	1660	1388	1255
2052	1643	1333	2004	1568	1507
2053	1811	1631	1634	1679	2053
2054	1873	2038	1757	1998	1626
2055	1670	1488	1462	2012	1735
2056	1673	2074	1666	2028	1851
2057	1897	1890	1500	1766	1620
2058	1988	1696	1691	1697	2103
2059	1871	1935	1912	1700	1551
GCM Average	1825	1783	1682	1756	1698
Standard deviation	116	237	164	196	241
Period average	**1749**				
Standard deviation	**204**				

Glenamong: precipitation (mm / year)

SSP585 - P1 (2050-2060)

	GCM 1	**GCM 2**	**GCM 3**	**GCM 4**	**GCM 5**
Year	*GFDL-ESM4*	*IPSL-CM6A-LR*	*MPI-ESM1-2-HR*	*MRI-ESM2-0*	*UKESM1-0-LL*
2050	1464	1569	1671	1517	1746
2051	1856	1417	1521	1504	1632
2052	1686	1807	1738	1562	1601
2053	2180	1484	1973	1412	1514
2054	1622	1881	1876	1689	1934
2055	2320	1609	1429	1751	2001
2056	1807	1562	1371	1787	1884
2057	2146	1824	1847	1602	2003
2058	1425	2322	1862	1857	1823
2059	1852	1747	1858	1805	1481
GCM Average	1836	1722	1715	1649	1762
Standard deviation	287	248	198	142	186
Period average	**1737**				
Standard deviation	**227**				

Table A.10 Glenamong – SSP126, SSP370 and SSP585 scenarios. Future annual mean air temperature values for each ISIMIP3b ensemble member during P1 (2050 – 2060).

Glenamong: mean air temperature (°C)

SSP126 - P1 (2050-2060)

	GCM 1	**GCM 2**	**GCM 3**	**GCM 4**	**GCM 5**
Year	*GFDL-ESM4*	*IPSL-CM6A-LR*	*MPI-ESM1-2-HR*	*MRI-ESM2-0*	*UKESM1-0-LL*
2050	9.4	9.8	9.2	8.4	11.6
2051	9.4	10.5	9.2	8.8	10.3
2052	9.5	9.0	9.4	8.4	9.8
2053	9.3	9.9	9.1	9.0	10.2
2054	9.5	9.9	10.2	9.5	9.1
2055	9.7	10.6	9.9	8.7	10.2
2056	9.3	10.1	9.8	8.6	9.9
2057	9.4	10.8	9.0	8.9	10.6
2058	9.6	10.2	9.7	8.4	11.1
2059	9.9	10.1	8.9	8.8	10.7
GCM Average	9.5	10.1	9.4	8.8	10.3
Standard deviation	0.2	0.5	0.4	0.3	0.7
Period average	**9.6**				
Standard deviation	**0.7**				

Glenamong: mean air temperature (°C)

SSP370 - P1 (2050-2060)

	GCM 1	**GCM 2**	**GCM 3**	**GCM 4**	**GCM 5**
Year	*GFDL-ESM4*	*IPSL-CM6A-LR*	*MPI-ESM1-2-HR*	*MRI-ESM2-0*	*UKESM1-0-LL*
2050	10.0	10.3	10.1	9.5	10.5
2051	10.3	10.0	10.1	9.3	11.4
2052	10.3	10.9	10.5	9.3	11.0
2053	10.4	10.0	9.9	9.1	11.4
2054	10.5	11.2	10.2	9.3	11.2
2055	10.0	10.3	9.1	8.7	11.7
2056	10.4	9.5	9.6	9.2	11.5
2057	10.4	9.5	10.1	8.5	10.5
2058	10.7	9.1	10.2	10.0	10.9
2059	10.6	9.6	10.6	10.1	10.5
GCM Average	10.4	10.0	10.0	9.3	11.1
Standard deviation	0.2	0.6	0.4	0.5	0.4
Period average	**10.2**				
Standard deviation	**0.7**				

Glenamong: mean air temperature (°C)

SSP585 - P1 (2050-2060)

	GCM 1	**GCM 2**	**GCM 3**	**GCM 4**	**GCM 5**
Year	*GFDL-ESM4*	*IPSL-CM6A-LR*	*MPI-ESM1-2-HR*	*MRI-ESM2-0*	*UKESM1-0-LL*
2050	10.6	10.6	9.3	10.1	11.4
2051	9.8	10.7	10.0	9.7	11.2
2052	9.8	10.3	10.0	9.4	11.5
2053	10.0	11.0	9.5	10.7	11.8
2054	9.8	11.3	9.9	9.7	10.7
2055	9.9	11.5	10.0	9.1	11.5
2056	9.7	12.4	9.1	9.2	11.9
2057	9.9	10.9	10.5	9.9	10.1
2058	10.0	11.2	9.5	9.8	11.5
2059	10.7	10.5	7.8	9.7	11.2
GCM Average	10.0	11.0	9.6	9.7	11.3
Standard deviation	0.3	0.6	0.7	0.4	0.5
Period average	**10.3**				
Standard deviation	**0.9**				

Table A.11 Glenamong– SSP126, SSP370 and SSP585 scenarios. Future annual precipitation values for each ISIMIP3b ensemble member during P2 (2090 – 2100).

Glenamong: precipitation (mm / year)

SSP126 - P2 (2090-2100)

	GCM 1	**GCM 2**	**GCM 3**	**GCM 4**	**GCM 5**
Year	*GFDL-ESM4*	*IPSL-CM6A-LR*	*MPI-ESM1-2-HR*	*MRI-ESM2-0*	*UKESM1-0-LL*
2090	1687	1895	1588	1552	1941
2091	1820	2024	1520	1632	1392
2092	1883	1669	1886	1530	1556
2093	1730	1513	1766	1428	1656
2094	1682	1989	1676	1469	1748
2095	1840	1990	1809	1655	1907
2096	1788	1683	1542	1514	2045
2097	1631	1937	1664	1496	1533
2098	2183	1617	1871	1489	1899
2099	1884	1723	1623	1529	1667
GCM Average	1813	1804	1695	1529	1734
Standard deviation	149	174	125	66	199
Period average	**1715**				
Standard deviation	**182**				

Glenamong: precipitation (mm / year)

SSP370 - P2 (2090-2100)

	GCM 1	**GCM 2**	**GCM 3**	**GCM 4**	**GCM 5**
Year	*GFDL-ESM4*	*IPSL-CM6A-LR*	*MPI-ESM1-2-HR*	*MRI-ESM2-0*	*UKESM1-0-LL*
2090	1782	1668	1599	1730	1788
2091	1635	1788	1440	1663	1700
2092	2013	2034	1341	1631	1739
2093	1642	1910	1827	1856	1648
2094	1823	2182	1555	1927	1600
2095	1931	1941	1905	1798	1976
2096	1712	1939	1569	2171	1857
2097	1944	1556	1557	1548	1484
2098	1835	1577	1718	1506	2073
2099	1759	1878	1691	1859	1864
GCM Average	1808	1847	1620	1769	1773
Standard deviation	121	190	161	188	168
Period average	**1763**				
Standard deviation	**184**				

Glenamong: precipitation (mm / year)

SSP585 - P2 (2090-2100)

	GCM 1	**GCM 2**	**GCM 3**	**GCM 4**	**GCM 5**
Year	*GFDL-ESM4*	*IPSL-CM6A-LR*	*MPI-ESM1-2-HR*	*MRI-ESM2-0*	*UKESM1-0-LL*
2090	1960	2070	1744	1830	1500
2091	2186	2073	1722	1825	1514
2092	2185	1777	2256	1511	2083
2093	1977	1743	1951	1999	1908
2094	1769	1898	1546	1404	1355
2095	1728	1726	1952	1787	1810
2096	1937	1986	1840	1647	1449
2097	2107	1841	1644	1666	1947
2098	2022	2167	2044	2223	1870
2099	2065	2013	1867	1621	1534
GCM Average	1994	1929	1857	1751	1697
Standard deviation	148	147	196	226	240
Period average	**1846**				
Standard deviation	**224**				

Table A.12 Glenamong– SSP126, SSP370 and SSP585 scenarios. Future annual mean air temperature values for each ISIMIP3b ensemble member during P2 (2090 – 2100).

Glenamong: mean air temperature (°C)

SSP126 - P2 (2090-2100)

	GCM 1	**GCM 2**	**GCM 3**	**GCM 4**	**GCM 5**
Year	*GFDL-ESM4*	*IPSL-CM6A-LR*	*MPI-ESM1-2-HR*	*MRI-ESM2-0*	*UKESM1-0-LL*
2090	9.4	10.9	8.2	7.0	10.8
2091	9.3	9.8	8.6	7.8	11.3
2092	9.9	9.7	8.5	7.7	11.6
2093	9.1	10.2	9.6	7.8	11.0
2094	9.2	9.6	10.1	7.2	11.5
2095	9.1	9.7	9.2	6.8	10.6
2096	9.8	10.8	9.0	7.1	10.1
2097	9.6	10.2	9.4	7.3	11.1
2098	9.1	10.4	9.6	7.9	10.5
2099	8.6	9.1	9.6	8.6	10.5
GCM Average	9.3	10.0	9.2	7.5	10.9
Standard deviation	0.4	0.5	0.6	0.5	0.5
Period average	**9.4**				
Standard deviation	**1.2**				

Glenamong: mean air temperature (°C)

SSP370 - P2 (2090-2100)

	GCM 1	**GCM 2**	**GCM 3**	**GCM 4**	**GCM 5**
Year	*GFDL-ESM4*	*IPSL-CM6A-LR*	*MPI-ESM1-2-HR*	*MRI-ESM2-0*	*UKESM1-0-LL*
2090	10.7	12.7	10.4	9.8	13.2
2091	10.5	12.4	11.0	9.2	13.5
2092	11.6	12.5	10.2	9.4	13.8
2093	11.4	12.6	10.2	8.9	13.5
2094	11.6	11.9	10.6	9.5	14.6
2095	10.7	12.5	10.8	9.4	14.0
2096	11.0	12.8	9.8	8.7	13.0
2097	11.2	12.5	9.8	9.4	13.8
2098	11.0	13.5	10.5	9.1	14.0
2099	10.4	12.4	11.0	10.2	14.2
GCM Average	11.0	12.6	10.4	9.4	13.8
Standard deviation	0.4	0.4	0.4	0.4	0.4
Period average	**11.4**				
Standard deviation	**1.6**				

Glenamong: mean air temperature (°C)

SSP585 - P2 (2090-2100)

	GCM 1	**GCM 2**	**GCM 3**	**GCM 4**	**GCM 5**
Year	*GFDL-ESM4*	*IPSL-CM6A-LR*	*MPI-ESM1-2-HR*	*MRI-ESM2-0*	*UKESM1-0-LL*
2090	11.2	12.6	11.1	10.5	15.0
2091	10.3	13.5	11.1	10.9	14.9
2092	10.9	13.7	10.6	10.9	14.7
2093	11.5	13.7	11.0	9.1	13.1
2094	12.2	13.2	10.8	9.2	15.4
2095	11.3	14.9	10.1	9.8	14.6
2096	10.7	14.7	11.1	10.1	14.7
2097	11.7	13.7	11.0	10.8	15.2
2098	11.5	14.0	11.3	10.7	15.8
2099	11.3	14.0	11.6	10.2	14.6
GCM Average	11.3	13.8	10.9	10.2	14.8
Standard deviation	0.5	0.6	0.4	0.6	0.7
Period average	**12.2**				
Standard deviation	**1.9**				

Appendix B

Appendix B contains information on the configuration files of GLM and FLARE for Lough Feeagh in western Ireland, including GitHub repository links, as part of the modelling and forecasting framework developed in Chapter 5.

General Lake Model (GLM) configuration details for Lough Feeagh.

GLM parameters for Lough Feeagh were set to the default values (Hipsey et al., 2019) except for six parameters that are commonly calibrated in other FLARE applications (Thomas et al., 2023b; Wander et al., 2024). Specifically, calibration was for the mean temperature for each of the four sediment zones (*sed_temp_mean)* located at heights of *5, 15, 30* and *47* m (bottom to top), the light extinction coefficient (*Kw*), and the longwave scaling factor (*lw_factor*). The GLM configuration file (*glm3.nml*), including initial conditions and calibration ranges, can be found in the following GitHub repository: FLARE_GLM_configuration_repository.

FLARE configuration details for water temperature forecasting in Lough Feeagh.

A range of 36 depths to generate depth-specific water temperature forecasts were defined, with an increasing resolution towards the lake water surface. These depths included all 13 monitoring depths. The number of FLARE forecast ensemble members was set to 248 to avoid erroneous data correlations that can arise when using smaller ensembles (Wander et al., 2024) (so that each of the 31 weather forecast ensemble members was used 8 times to drive the lake model). The normal distribution standard

deviations for each calibrating parameter was defined based on previous studies (Thomas et al., 2023b; Wander et al., 2024) (1.00 °C for the *sed_temp_mean* of all four sediment zones and 0.02 for both the *Kw* and the *lw_factor*), for water temperature observations (0.10 °C) and for the process noise (1.35 °C).

All six parameters (*sed_temp_mean 1, 2, 3* and *4; Kw* and *lw_factor)* were initially calibrated during a GLM spin-up from 1st October to 1st November 2020, a period on which data assimilation occurred but forecasts were not produced. This allowed a spin-up of the lake model before the start of the forecasting period (1st Nov 2020). For each forecast generation, all calibrating parameters and water temperature values were continuously updated via data assimilation when observations were available. All FLARE configuration files used in this study can be found in the following GitHub repository: FLARE configuration repository.

Extraction of *in-situ* water temperature monitoring data in Lough Feeagh.

Real-time access to lake water temperature data was obtained via ERDDAP, by accessing their server using the rerddap - *General Purpose Client for "ERDDAP" Servers* - R package (Chamberlain et al., 2024). GitHub Repository. Water temperature observations Lough Feeagh: water temperature data extraction repository.

FLARE workflow for Lough Feeagh.

Execution of FLARE, performed in a cloud-based server using a Docker container image as host, equipped with the R environment. GitHub Repository. FLARE for Lake Feeagh: FLARE workflow repository.

Appendix C

Appendix C contains the full list of individual performance values along the entire forecast horizon (1-day ahead to 35-days ahead) based on RMSE, NSE and r^2 for the DOC concentration forecasts of Workflow A, Workflow B and Site Persistence, and the quantified forecast uncertainty (indicated by the standard deviation) for the DOC concentration forecasts of Workflow A and Workflow B as part of the work undertaken in Chapter 6.

Table C.1 Forecast skill along the forecast horizon and across seasons for the DOC concentration forecasts of Workflow A, Workflow B and Site Persistence indicated by the root mean squared error (RMSE).

DOC concentration forecast performance

RMSE (mg L^{-1}) *(Workflow A ; Workflow B ; Persistence)*

Forecast horizon (days)	Spring	Summer	Autumn	Winter
1	3.85 ; 1.77 ; 2.18	3.13 ; 2.59 ; 2.22	4.07 ; 1.95 ; 1.34	1.68 ; 1.39 ; 1.21
2	5.32 ; 2.05 ; 2.46	3.72 ; 2.95 ; 2.58	4.73 ; 2.17 ; 1.42	2.48 ; 1.69 ; 1.31
3	6.14 ; 2.26 ; 2.7	4.81 ; 3.13 ; 2.72	5.78 ; 2.42 ; 1.51	3.23 ; 1.93 ; 1.23
4	6.16 ; 2.48 ; 2.71	5.94 ; 3.31 ; 2.69	6.62 ; 2.61 ; 1.55	3.68 ; 2.22 ; 1.33
5	6.38 ; 2.59 ; 2.53	7.2 ; 3.47 ; 2.86	6.83 ; 2.84 ; 1.48	4.6 ; 2.39 ; 1.49
6	6.75 ; 2.67 ; 3.14	8.41 ; 3.6 ; 3.13	7.8 ; 2.96 ; 1.81	4.94 ; 2.48 ; 1.36
7	7.16 ; 2.73 ; 3.06	9.57 ; 3.73 ; 3.21	7.9 ; 3.05 ; 1.63	5.89 ; 2.64 ; 1.52
8	7.75 ; 2.77 ; 3.02	10.96 ; 3.91 ; 3.51	8.63 ; 3.17 ; 1.94	8.9 ; 3.15 ; 1.59
9	8.46 ; 2.77 ; 3.21	12.31 ; 4.06 ; 3.36	10.31 ; 3.3 ; 1.92	8.38 ; 3.3 ; 1.55
10	9.39 ; 2.83 ; 3.12	13.82 ; 4.12 ; 2.97	11.44 ; 3.36 ; 1.67	8.74 ; 3.44 ; 1.49
11	9.87 ; 2.93 ; 3.67	15.53 ; 4.18 ; 3.11	12.63 ; 3.37 ; 1.65	8.95 ; 3.55 ; 1.57
12	9.72 ; 3 ; 3.41	17.16 ; 4.22 ; 2.92	14.15 ; 3.37 ; 2.05	8.67 ; 3.54 ; 1.38
13	9.29 ; 3.08 ; 3.81	18.51 ; 4.27 ; 3.1	15.17 ; 3.4 ; 2.36	8.67 ; 3.58 ; 1.74
14	10.04 ; 3.17 ; 3.76	20.24 ; 4.3 ; 3.42	15.45 ; 3.4 ; 1.7	9.04 ; 3.61 ; 1.71
15	11.26 ; 3.26 ; 3.61	21.89 ; 4.29 ; 3.86	15.52 ; 3.38 ; 1.71	9.66 ; 3.54 ; 1.73
16	10.84 ; 3.32 ; 3.47	23.23 ; 4.27 ; 4.52	15.01 ; 3.38 ; 1.6	9.82 ; 3.44 ; 1.91
17	11.05 ; 3.45 ; 3.62	24.11 ; 4.23 ; 3.58	14.15 ; 3.37 ; 1.67	10.23 ; 3.39 ; 1.63
18	11.75 ; 3.54 ; 4.17	24.17 ; 4.19 ; 3.36	13.61 ; 3.43 ; 2.04	10.17 ; 3.33 ; 1.73
19	11.5 ; 3.52 ; 4.13	24.26 ; 4.12 ; 3.66	13.5 ; 3.42 ; 2.16	10.45 ; 3.33 ; 2.02
20	11.51 ; 3.6 ; 4.05	24.01 ; 4.1 ; 3.12	14.5 ; 3.64 ; 1.87	10.22 ; 3.34 ; 1.7
21	11.34 ; 3.67 ; 4.63	23.57 ; 4.09 ; 4.26	15.62 ; 3.79 ; 1.9	10.03 ; 3.32 ; 1.67
22	11.63 ; 3.84 ; 3.62	22.94 ; 4.1 ; 4.12	15.11 ; 3.78 ; 1.74	9.99 ; 3.3 ; 1.86
23	11.74 ; 3.97 ; 2.95	23.59 ; 4.13 ; 4.2	15.91 ; 3.77 ; 1.92	10.13 ; 3.28 ; 2.11
24	11.45 ; 4.08 ; 5.08	23.41 ; 4.24 ; 2.87	16.95 ; 3.81 ; 2.32	10.36 ; 3.28 ; 1.67
25	11.92 ; 4.17 ; 3.93	22.53 ; 4.27 ; 3.68	17.93 ; 3.89 ; 1.7	10.23 ; 3.22 ; 1.85
26	12.76 ; 4.27 ; 4.22	22.49 ; 4.29 ; 3.86	18.58 ; 3.9 ; 2.61	10.2 ; 3.23 ; 1.83
27	13.21 ; 4.4 ; 3.87	23.24 ; 4.28 ; 4.03	18.34 ; 3.85 ; 2.46	10.41 ; 3.24 ; 1.51
28	13.65 ; 4.45 ; 5.17	23.56 ; 4.27 ; 2.64	17.7 ; 3.91 ; 2.44	10.2 ; 3.13 ; 1.57
29	13.67 ; 4.51 ; 4.31	23.42 ; 4.24 ; 5.56	16.85 ; 3.96 ; 2.84	10.13 ; 3.09 ; 1.91
30	11.56 ; 4.51 ; 5.4	23.78 ; 4.25 ; 2.96	16.37 ; 4 ; 1.8	10.69 ; 3.12 ; 2.04
31	11.58 ; 4.56 ; 3.53	24.11 ; 4.28 ; 4.95	16.53 ; 4.07 ; 2.08	9.78 ; 3.08 ; 1.77
32	11.45 ; 4.54 ; 4.12	23.7 ; 4.28 ; 4.17	16.66 ; 4.08 ; 2.35	9.65 ; 3.06 ; 1.93
33	10.43 ; 4.53 ; 5.18	23.42 ; 4.28 ; 5.14	17.55 ; 4.17 ; 1.84	9.57 ; 3.08 ; 1.95
34	10.24 ; 4.48 ; 3.84	22.89 ; 4.31 ; 2.79	18.45 ; 4.21 ; 2.34	9.41 ; 3.11 ; 2.04
35	10 ; 4.44 ; 4.84	23.02 ; 4.33 ; 4.68	18.7 ; 4.18 ; 1.79	9.24 ; 3.2 ; 1.7

Table C.2 Forecast skill along the forecast horizon and across seasons for the DOC concentration forecasts of Workflow A, Workflow B and Site Persistence indicated by the by the Nash-Sutcliffe coefficient (NSE).

DOC concentration forecast performance

NSE *(Workflow A ; Workflow B ; Persistence)*

Forecast horizon (days)	Spring	Summer	Autumn	Winter
1	-0.18 ; 0.75 ; 0.65	0.19 ; 0.45 ; 0.63	-1.05 ; 0.53 ; 0.71	0.41 ; 0.59 ; 0.54
2	-1.25 ; 0.67 ; 0.56	-0.14 ; 0.28 ; 0.5	-1.78 ; 0.41 ; 0.68	-0.29 ; 0.4 ; 0.46
3	-1.99 ; 0.59 ; 0.46	-0.92 ; 0.19 ; 0.45	-3.14 ; 0.27 ; 0.63	-1.19 ; 0.21 ; 0.52
4	-2 ; 0.52 ; 0.46	-1.92 ; 0.09 ; 0.46	-4.45 ; 0.15 ; 0.61	-1.85 ; -0.03 ; 0.44
5	-2.21 ; 0.47 ; 0.53	-3.29 ; 0 ; 0.39	-4.79 ; 0 ; 0.65	-3.44 ; -0.2 ; 0.29
6	-2.58 ; 0.44 ; 0.28	-4.85 ; -0.07 ; 0.27	-6.56 ; -0.09 ; 0.47	-4.13 ; -0.29 ; 0.41
7	-3.03 ; 0.42 ; 0.32	-6.58 ; -0.15 ; 0.23	-6.74 ; -0.15 ; 0.57	-6.28 ; -0.47 ; 0.26
8	-3.7 ; 0.4 ; 0.33	-8.94 ; -0.27 ; 0.08	-8.25 ; -0.25 ; 0.39	-15.65 ; -1.09 ; 0.19
9	-4.58 ; 0.4 ; 0.24	-11.54 ; -0.36 ; 0.16	-12.21 ; -0.35 ; 0.41	-13.75 ; -1.28 ; 0.24
10	-5.87 ; 0.38 ; 0.28	-14.81 ; -0.4 ; 0.34	-15.25 ; -0.4 ; 0.55	-15.05 ; -1.48 ; 0.29
11	-6.55 ; 0.34 ; 0.01	-18.97 ; -0.45 ; 0.28	-18.79 ; -0.41 ; 0.56	-15.83 ; -1.65 ; 0.21
12	-6.34 ; 0.3 ; 0.15	-23.38 ; -0.47 ; 0.36	-23.85 ; -0.41 ; 0.32	-14.81 ; -1.64 ; 0.39
13	-5.68 ; 0.26 ; -0.07	-27.35 ; -0.51 ; 0.29	-27.58 ; -0.44 ; 0.11	-14.79 ; -1.69 ; 0.03
14	-6.77 ; 0.23 ; -0.04	-32.91 ; -0.53 ; 0.13	-28.64 ; -0.43 ; 0.54	-16.15 ; -1.74 ; 0.07
15	-8.72 ; 0.18 ; 0.04	-38.67 ; -0.52 ; -0.11	-28.92 ; -0.42 ; 0.53	-18.59 ; -1.63 ; 0.05
16	-8 ; 0.15 ; 0.12	-43.68 ; -0.51 ; -0.52	-26.97 ; -0.42 ; 0.59	-19.26 ; -1.49 ; -0.16
17	-8.32 ; 0.09 ; 0.04	-47.11 ; -0.48 ; 0.04	-23.86 ; -0.41 ; 0.55	-21.01 ; -1.41 ; 0.16
18	-9.52 ; 0.04 ; -0.27	-47.35 ; -0.45 ; 0.16	-21.99 ; -0.46 ; 0.33	-20.72 ; -1.33 ; 0.05
19	-9.04 ; 0.06 ; -0.25	-47.71 ; -0.4 ; 0	-21.64 ; -0.45 ; 0.25	-21.95 ; -1.33 ; -0.3
20	-9.07 ; 0.02 ; -0.2	-46.71 ; -0.39 ; 0.27	-25.1 ; -0.65 ; 0.44	-20.95 ; -1.34 ; 0.08
21	-8.77 ; -0.02 ; -0.57	-44.98 ; -0.38 ; -0.35	-29.28 ; -0.78 ; 0.42	-20.15 ; -1.31 ; 0.11
22	-9.34 ; -0.13 ; 0.04	-42.54 ; -0.39 ; -0.27	-27.35 ; -0.77 ; 0.51	-19.96 ; -1.29 ; -0.1
23	-9.74 ; -0.22 ; 0.36	-45.05 ; -0.41 ; -0.32	-30.43 ; -0.76 ; 0.41	-20.55 ; -1.26 ; -0.43
24	-9.26 ; -0.3 ; -0.89	-44.36 ; -0.49 ; 0.38	-34.69 ; -0.8 ; 0.13	-21.56 ; -1.26 ; 0.11
25	-10.07 ; -0.35 ; -0.13	-41 ; -0.51 ; -0.01	-38.91 ; -0.88 ; 0.53	-20.99 ; -1.18 ; -0.1
26	-11.6 ; -0.41 ; -0.3	-40.87 ; -0.52 ; -0.11	-41.85 ; -0.89 ; -0.09	-20.86 ; -1.19 ; -0.06
27	-12.44 ; -0.49 ; -0.1	-43.68 ; -0.52 ; -0.21	-40.74 ; -0.84 ; 0.03	-21.78 ; -1.21 ; 0.28
28	-13.27 ; -0.52 ; -0.96	-44.94 ; -0.51 ; 0.48	-37.89 ; -0.9 ; 0.04	-20.84 ; -1.06 ; 0.21
29	-13.23 ; -0.55 ; -0.36	-44.38 ; -0.49 ; -1.31	-34.23 ; -0.95 ; -0.3	-20.57 ; -1 ; -0.16
30	-9.11 ; -0.54 ; -1.13	-45.8 ; -0.5 ; 0.35	-32.26 ; -0.99 ; 0.48	-22.99 ; -1.05 ; -0.33
31	-9.09 ; -0.56 ; 0.09	-47.11 ; -0.51 ; -0.83	-32.92 ; -1.06 ; 0.3	-19.1 ; -0.99 ; 0.01
32	-8.79 ; -0.54 ; -0.24	-45.5 ; -0.51 ; -0.3	-33.45 ; -1.07 ; 0.11	-18.57 ; -0.97 ; -0.18
33	-7.07 ; -0.52 ; -0.97	-44.41 ; -0.51 ; -0.97	-37.23 ; -1.16 ; 0.46	-18.24 ; -1 ; -0.21
34	-6.73 ; -0.48 ; -0.08	-42.36 ; -0.54 ; 0.42	-41.26 ; -1.21 ; 0.12	-17.59 ; -1.03 ; -0.33
35	-6.33 ; -0.45 ; -0.71	-42.87 ; -0.55 ; -0.63	-42.44 ; -1.17 ; 0.48	-16.95 ; -1.16 ; 0.08

Table C.3 Forecast skill along the forecast horizon and across seasons for the DOC concentration forecasts of Workflow A, Workflow B and Site Persistence indicated by the coefficient of determination (r^2).

DOC concentration forecast performance

r^2 *(Workflow A ; Workflow B ; Persistence)*

Forecast horizon (days)	Spring	Summer	Autumn	Winter
1	0.49 ; 0.77 ; 0.68	0.53 ; 0.62 ; 0.66	0.4 ; 0.6 ; 0.73	0.64 ; 0.6 ; 0.59
2	0.35 ; 0.7 ; 0.6	0.46 ; 0.53 ; 0.56	0.36 ; 0.52 ; 0.71	0.46 ; 0.46 ; 0.54
3	0.27 ; 0.64 ; 0.53	0.33 ; 0.5 ; 0.51	0.28 ; 0.43 ; 0.67	0.34 ; 0.35 ; 0.58
4	0.24 ; 0.57 ; 0.52	0.25 ; 0.47 ; 0.53	0.24 ; 0.35 ; 0.68	0.25 ; 0.24 ; 0.53
5	0.21 ; 0.54 ; 0.57	0.16 ; 0.43 ; 0.48	0.26 ; 0.28 ; 0.67	0.2 ; 0.18 ; 0.48
6	0.22 ; 0.53 ; 0.38	0.09 ; 0.4 ; 0.38	0.22 ; 0.23 ; 0.56	0.19 ; 0.15 ; 0.55
7	0.2 ; 0.52 ; 0.47	0.05 ; 0.36 ; 0.36	0.21 ; 0.2 ; 0.61	0.11 ; 0.12 ; 0.4
8	0.17 ; 0.5 ; 0.43	0.03 ; 0.31 ; 0.31	0.17 ; 0.17 ; 0.53	0.02 ; 0.06 ; 0.48
9	0.16 ; 0.51 ; 0.39	0.03 ; 0.27 ; 0.3	0.11 ; 0.15 ; 0.55	0.02 ; 0.05 ; 0.43
10	0.15 ; 0.5 ; 0.4	0.02 ; 0.26 ; 0.42	0.09 ; 0.14 ; 0.57	0.03 ; 0.04 ; 0.41
11	0.14 ; 0.48 ; 0.24	0.01 ; 0.26 ; 0.41	0.08 ; 0.15 ; 0.63	0.02 ; 0.02 ; 0.38
12	0.16 ; 0.47 ; 0.33	0.01 ; 0.26 ; 0.45	0.08 ; 0.16 ; 0.52	0.01 ; 0.02 ; 0.55
13	0.15 ; 0.45 ; 0.12	0 ; 0.26 ; 0.4	0.09 ; 0.16 ; 0.44	0.02 ; 0.02 ; 0.33
14	0.15 ; 0.44 ; 0.25	0 ; 0.25 ; 0.24	0.11 ; 0.16 ; 0.63	0.02 ; 0.01 ; 0.31
15	0.12 ; 0.41 ; 0.23	0 ; 0.25 ; 0.21	0.14 ; 0.16 ; 0.58	0.02 ; 0.01 ; 0.34
16	0.1 ; 0.41 ; 0.35	0 ; 0.25 ; 0.03	0.18 ; 0.17 ; 0.69	0.01 ; 0.01 ; 0.41
17	0.1 ; 0.38 ; 0.24	0.01 ; 0.26 ; 0.22	0.21 ; 0.17 ; 0.56	0.01 ; 0.01 ; 0.51
18	0.1 ; 0.37 ; 0.1	0.02 ; 0.26 ; 0.39	0.21 ; 0.15 ; 0.61	0.02 ; 0.02 ; 0.51
19	0.12 ; 0.39 ; 0.14	0.03 ; 0.27 ; 0.32	0.19 ; 0.15 ; 0.47	0.04 ; 0.02 ; 0.46
20	0.12 ; 0.39 ; 0.12	0.04 ; 0.26 ; 0.46	0.14 ; 0.11 ; 0.53	0.06 ; 0.02 ; 0.52
21	0.12 ; 0.39 ; 0.08	0.03 ; 0.26 ; 0.25	0.09 ; 0.07 ; 0.51	0.07 ; 0.03 ; 0.28
22	0.11 ; 0.33 ; 0.31	0.03 ; 0.24 ; 0.1	0.12 ; 0.07 ; 0.62	0.08 ; 0.03 ; 0.21
23	0.1 ; 0.29 ; 0.49	0.03 ; 0.23 ; 0.02	0.12 ; 0.07 ; 0.52	0.07 ; 0.03 ; 0.4
24	0.09 ; 0.25 ; 0.01	0.02 ; 0.2 ; 0.41	0.12 ; 0.06 ; 0.48	0.06 ; 0.04 ; 0.31
25	0.07 ; 0.2 ; 0.21	0.01 ; 0.18 ; 0.35	0.11 ; 0.05 ; 0.66	0.06 ; 0.04 ; 0.48
26	0.06 ; 0.16 ; 0.01	0.01 ; 0.17 ; 0.34	0.1 ; 0.05 ; 0.44	0.06 ; 0.03 ; 0.18
27	0.06 ; 0.13 ; 0.14	0 ; 0.16 ; 0.05	0.11 ; 0.06 ; 0.34	0.06 ; 0.03 ; 0.46
28	0.06 ; 0.11 ; 0.04	0 ; 0.16 ; 0.5	0.13 ; 0.06 ; 0.36	0.07 ; 0.03 ; 0.38
29	0.06 ; 0.09 ; 0.11	0 ; 0.16 ; 0.01	0.16 ; 0.05 ; 0.33	0.08 ; 0.03 ; 0.32
30	0.08 ; 0.08 ; 0.16	0 ; 0.16 ; 0.36	0.2 ; 0.05 ; 0.57	0.07 ; 0.03 ; 0.37
31	0.1 ; 0.08 ; 0.41	0 ; 0.16 ; 0	0.22 ; 0.04 ; 0.52	0.06 ; 0.03 ; 0.29
32	0.11 ; 0.08 ; 0.16	0.01 ; 0.15 ; 0.22	0.22 ; 0.04 ; 0.47	0.05 ; 0.02 ; 0.2
33	0.13 ; 0.07 ; 0.09	0.01 ; 0.15 ; 0.13	0.18 ; 0.04 ; 0.65	0.04 ; 0.01 ; 0.3
34	0.16 ; 0.08 ; 0.27	0.02 ; 0.14 ; 0.42	0.15 ; 0.03 ; 0.49	0.03 ; 0.01 ; 0.39
35	0.19 ; 0.1 ; 0	0.02 ; 0.13 ; 0.2	0.14 ; 0.03 ; 0.7	0.03 ; 0.01 ; 0.35

Table C.4 Estimated forecast uncertainty (quantified using the standard deviation of the forecast ensemble) along the forecast horizon and across seasons for the DOC concentration forecasts of Workflow A and Workflow B.

DOC concentration forecast uncertainty				
Standard deviation *(Workflow A ; Workflow B)*				
Forecast horizon (days)	**Spring**	**Summer**	**Autumn**	**Winter**
1	1.54 ; 0.56	1.67 ; 0.64	1.74 ; 0.79	0.85 ; 0.41
2	2.03 ; 0.65	2.2 ; 0.76	2.34 ; 0.93	1.25 ; 0.5
3	2.43 ; 0.72	2.56 ; 0.85	2.91 ; 0.98	1.48 ; 0.56
4	2.93 ; 0.83	2.97 ; 0.93	3.39 ; 1.05	1.88 ; 0.64
5	3.19 ; 0.91	3.37 ; 0.97	3.77 ; 1.14	2.41 ; 0.74
6	3.6 ; 0.97	3.57 ; 0.99	4.2 ; 1.21	2.83 ; 0.85
7	3.73 ; 0.98	3.97 ; 1.01	4.4 ; 1.24	3.23 ; 0.89
8	3.82 ; 1.02	4.59 ; 1.02	4.72 ; 1.26	3.63 ; 0.88
9	3.93 ; 1.02	5.07 ; 1.03	5.07 ; 1.3	3.95 ; 0.91
10	3.95 ; 0.99	5.5 ; 1.07	5.36 ; 1.35	4.14 ; 0.95
11	3.73 ; 0.96	5.82 ; 1.1	5.52 ; 1.37	4.47 ; 0.98
12	3.84 ; 0.94	6.12 ; 1.11	5.6 ; 1.35	4.72 ; 1.03
13	3.69 ; 0.9	6.57 ; 1.13	5.87 ; 1.34	4.98 ; 1.07
14	3.88 ; 0.88	6.98 ; 1.14	5.68 ; 1.36	5.32 ; 1.04
15	3.99 ; 0.9	7.35 ; 1.17	5.75 ; 1.37	5.6 ; 1.06
16	4.03 ; 0.89	7.68 ; 1.17	5.84 ; 1.36	5.8 ; 1.1
17	4.11 ; 0.86	7.94 ; 1.16	5.79 ; 1.33	5.98 ; 1.13
18	4.41 ; 0.89	8.07 ; 1.17	5.8 ; 1.34	5.96 ; 1.14
19	4.59 ; 0.88	8.21 ; 1.18	5.94 ; 1.4	6.06 ; 1.17
20	4.67 ; 0.91	8.29 ; 1.16	6.12 ; 1.43	6.06 ; 1.18
21	4.48 ; 0.91	8.15 ; 1.15	6.28 ; 1.4	5.96 ; 1.2
22	4.32 ; 0.9	8.23 ; 1.16	6.23 ; 1.41	5.98 ; 1.21
23	4.5 ; 0.94	8.3 ; 1.18	6.45 ; 1.46	6 ; 1.22
24	4.68 ; 0.95	8.18 ; 1.18	6.82 ; 1.49	5.96 ; 1.22
25	4.8 ; 0.96	8.16 ; 1.21	6.85 ; 1.5	5.7 ; 1.21
26	4.71 ; 1.01	8.3 ; 1.23	6.78 ; 1.51	5.51 ; 1.2
27	4.69 ; 1.03	8.33 ; 1.23	6.71 ; 1.53	5.39 ; 1.15
28	4.74 ; 1.05	8.43 ; 1.24	6.77 ; 1.54	5.11 ; 1.12
29	4.82 ; 1.07	8.38 ; 1.23	6.79 ; 1.56	4.96 ; 1.09
30	4.72 ; 1.06	8.15 ; 1.22	6.88 ; 1.58	4.81 ; 1.08
31	4.63 ; 1.06	8.02 ; 1.23	7.01 ; 1.6	4.48 ; 1.08
32	4.67 ; 1.08	7.87 ; 1.22	7.03 ; 1.61	4.08 ; 1.01
33	4.89 ; 1.07	7.68 ; 1.22	7.2 ; 1.61	3.88 ; 1
34	5.09 ; 1.06	7.75 ; 1.25	7.27 ; 1.63	3.74 ; 0.98
35	4.97 ; 1.05	7.87 ; 1.26	7.11 ; 1.63	3.82 ; 0.99

Appendix D

Appendix D contains the following research papers:

Paíz, R., Pierson, D.C., Lindqvist, K., Naden, P.S., de Eyto, E., Dillane, M., McCarthy, V., Linnane, S., Jennings, E., 2025. *Accounting for model parameter uncertainty provides more robust projections of dissolved organic carbon dynamics to aid drinking water management*. Water Res. 123238. https://doi.org/10.1016/j.watres.2025.123238. This research paper was a result of the work undertaken in Chapter 4 of this thesis.

Paíz, R., Thomas, Q., Carey, C., de Eyto, E., Delany, A.D., Poole, R., Nixon, P., Dillane, M., McCarthy, V., Linnane, S., Jennings, E., *Near-term lake water temperature forecasts can be used to anticipate the dynamics of freshwater species.* Ecosphere 16(7): e70335. https://doi.org/10.1002/ecs2.70335. This research paper was a result of the work undertaken in Chapter 5 of this thesis.

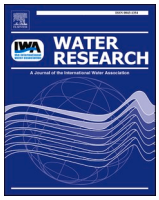
Water Research 276 (2025) 123238



Contents lists available at ScienceDirect

Water Research

journal homepage: www.elsevier.com/locate/watres





Accounting for model parameter uncertainty provides more robust projections of dissolved organic carbon dynamics to aid drinking water management

Ricardo Paíz [a,*], Donald C. Pierson [b], Klara Lindqvist [c,d], Pamela S. Naden [e], Elvira de Eyto [f], Mary Dillane [f], Valerie McCarthy [g], Suzanne Linnane [a], Eleanor Jennings [a]

[a] Centre for Freshwater and Environmental Studies, Dundalk Institute of Technology, A91 K584 Dundalk, Co. Louth, Ireland
[b] Department of Ecology and Genetics – Limnology, Uppsala University, 752 36 Uppsala, Sweden
[c] Department of Earth Sciences, Uppsala University, 752 36 Uppsala, Sweden
[d] Swedish Meteorological and Hydrological Institute, 601 76 Norrköping, Sweden
[e] UK Centre for Ecology and Hydrology, Crowmarsh Gifford, Wallingford, Oxfordshire OX10 8BB, UK
[f] Fisheries & Ecosystem Advisory Services, Marine Institute, F28 PF65 Newport, Co. Mayo, Ireland
[g] School of History and Geography, Dublin City University, D09 YT18 9, Dublin, Ireland

ARTICLE INFO

Keywords:
Hydrological modelling
Water quality modelling
DOC
Climate change
Uncertainty analysis
GWLF

ABSTRACT

Changes in climate and human behaviour impact catchment hydrology and the export of nutrients including dissolved organic carbon (DOC), with consequences for drinking water supply. In this study, we projected future river discharge and DOC dynamics under three Shared Socioeconomic Pathways (i.e., different futures of climatic conditions, socio-economic development and adaptation to climate change) and quantified change relative to a baseline for two contrasting catchments: one in Sweden and one in Ireland. For this, we used the Generalised Watershed Loading Functions Model (GWLF) with an integrated DOC module (GWLF-DOC) and drove it with data from an ensemble of global climate models, taking into account variability derived from multiple model parameter sets. We assessed the relative contribution of each of these two factors (climate input data and model parameterisation) to the total uncertainty in predictions. Projections for river discharge differed between the two sites in magnitude, variability and direction of change depending on the future scenario and time period. In contrast, DOC was always projected to show increases in concentration throughout the annual cycle and over time, with the highest levels by the end of the century, for scenarios with greater warming and low mitigation efforts. Future climate data provided the dominant source of uncertainty in all of our projections. However, the DOC model parameters, which respond to temperature and soil moisture conditions, became more influential in scenarios of higher climatic variability. Our approach highlights the benefits of incorporating often ignored parameter uncertainty in climate change impact assessments for both interpreting outputs and communicating results to water managers.

1. Introduction

Terrestrially sourced dissolved organic matter (DOM) entering freshwaters has many impacts on aquatic ecology (Rodríguez-Cardona et al., 2022) and on water use and supply (Johnes et al., 2023). High concentrations are associated with water browning (Kritzberg et al., 2020), a condition that affects both ecosystem function (Evans et al., 2005) and drinking water quality (Riyadh and Peleato, 2024). Concentrations of DOM (operationally quantified using dissolved organic carbon (DOC)) must be reduced during drinking water treatment prior to any chlorination (Köhler et al., 2016; Piai et al., 2024), as it is a precursor to the formation of disinfection by-products (DBPs) (Srivastav et al., 2020; Franklin et al., 2021). The presence of DBPs in drinking water, although unintended, remains a critical safety issue due to the adverse effects of DBPs such as trihalomethanes (THMs) on human health (Diana et al., 2019; Kumari and Gupta, 2022). The formation of these contaminants has raised concern in many regions (Villanueva et al., 2023), especially those where DOC drains from terrestrial soil

* Corresponding author.
E-mail address: ricardo.marroquinpaiz@dkit.ie (R. Paíz).

https://doi.org/10.1016/j.watres.2025.123238
Received 2 December 2024; Received in revised form 28 January 2025; Accepted 31 January 2025
Available online 1 February 2025
0043-1354/© 2025 The Author(s). Published by Elsevier Ltd. This is an open access article under the CC BY license (http://creativecommons.org/licenses/by/4.0/).

stores that are rich in organic carbon (e.g., from peatlands and other organic soils) (Xu et al., 2020; Fenner et al., 2021).

The production and transport of DOC in catchments result from interactions between landscape, land use and climate, including atmospheric deposition factors (Jennings et al., 2010; Adler et al., 2021). Temperature, water availability and acid deposition (e.g., sulphur deposition) influence physicochemical and biological mechanisms that regulate soil decomposition and hence DOC production, while hydrological processes control its transport (Evans et al., 2006; Clark et al., 2009; Wit et al., 2021). All of these factors have been reported as drivers of long-term DOC increases in recent decades across the northern hemisphere, although the importance of any factor can vary from site to site (Evans et al., 2005; de Wit et al., 2007; Oulehle and Hruška, 2009; SanClements et al., 2012; Anderson et al., 2023). However, with acid deposition gradually levelling off (Garmo et al., 2014; Wit et al., 2021), the interactions between the other climatic factors and catchment hydrology will likely be more relevant in future DOC dynamics (Clark et al., 2010; Anderson et al., 2023; Wu and Yao, 2024).

Increasingly variable temperature and precipitation patterns, including those related to global warming (Wang et al., 2017; van der Wiel and Bintanja, 2021), can induce important changes in the magnitude and seasonality of DOC export. For instance, dry periods (e.g., hotter, drier summers), wet periods (e.g., wetter winters), prolonged dry conditions, drought-rewetting cycles, lower water tables, and flooding, can all lead to higher variability in catchment DOC concentrations and fluxes (Blaurock et al., 2021; Dong et al., 2021; Wu and Yao, 2022; Wu et al., 2023a, 2023b) that can, in turn, result in higher DBP levels following treatment (Warner and Saros, 2019; Fenner et al., 2021). Increased variability in source water DOC levels can also make water treatment more difficult to manage (Köhler et al., 2016; Piai et al., 2024). It is important, therefore, to quantify the response of both catchment hydrology and DOC dynamics to future climatic conditions. By determining this, drinking water managers may better anticipate future DOC levels, assess risk for supplies, and prepare basin and/or treatment scale mitigation actions accordingly (Ritson et al., 2014; Xu et al., 2020; Klante et al., 2022).

Catchment modelling exercises allow us to quantify change between past and future water quantity and quality, including DOC concentrations and flux. However, all modelling is associated with differing degrees of uncertainty, that are related to a range of sources (Hattermann et al., 2018; Her et al., 2019a). While uncertainty related to projecting future climate (by using ensembles of global climate models [GCMs]) and to human behaviour (by use of multiple scenarios for population behaviour) are now generally incorporated into climate change impact assessments (Kundzewicz et al., 2018; Schürz et al., 2019), other sources are generally not. These include variability related to climate bias correction methods, model structure and model parameterisation i.e., the model state variables, governing equations and parameter selection. Model parameterisation, in particular, can be a complex source of uncertainty since differing sets of parameters can produce equally good simulations of key model variables during calibration (i.e., model parameter equifinality) (Beven and Binley, 1992, 2014), but produce differing results in future scenarios. This uncertainty has been quantified in some studies of changes in DOC dynamics (e.g., O'Driscoll et al., 2018a; Xu et al., 2020), but to date, has not been incorporated into climate change impact simulations. Moreover, the relative contribution of both GCM uncertainty and parameter uncertainty to these future projections has not been explored. Accounting for such uncertainty in future projections will produce more robust outputs (Her et al., 2019a; Marshall et al., 2021), and therefore provide more appropriate information to assist decision making at a catchment management level (Teweldebrhan et al., 2018; Cui et al., 2021).

In this study, we used a previously described DOC model (Naden et al., 2010) that is coupled with the Generalised Watershed Loading Functions Model (GWLF) (Schneiderman et al., 2010) to calibrate and simulate future discharge, DOC concentration and DOC flux under climate change scenarios in one Irish and one Swedish catchment. These sites were selected as they are contrasting in size, climate and hydrology, with high organic soils, and represent systems in countries where drinking water is affected by increases in DOC (O'Driscoll et al., 2018b; Kritzberg et al., 2020), leading to issues in treatment and supply. After years of continuous THM exceedances in several supplies, Ireland has recently been ruled against by the Court of Justice of the European Union (25 January 2024; Case C-481/22) for failure to fulfil obligations on the quality of water intended for human consumption. Similarly, the formation of DBPs has been a persistent problem in Sweden, affecting many drinking water schemes (Kritzberg et al., 2020) including the supply to its capital Stockholm (Köhler et al., 2016).

Within this context, we aimed to: (1) quantify the future change in catchment discharge, DOC concentration and DOC flux between a historical baseline and three future scenarios; (2) determine the periods in the annual cycle when any future changes will be most relevant; and (3) quantify the relative contribution from future climate conditions and model parametrisation to the total uncertainty in these predictions. We capture and summarise the modelling outputs in a way that would be usable by catchment and source water managers. Lastly, we discuss how these results could assist the drinking water sector.

2. Materials and methods

2.1. Study sites

The Glenamong and Vattholma catchments are located in western Ireland (53° 57′ N, 9° 35′ W) and southeastern Sweden (60° 10′ N, 17° 50′ E), respectively (Fig. 1). Both catchments export relatively large quantities of carbon from terrestrial stores to downstream lakes (Ryder et al., 2014; Doyle et al., 2021; Lindqvist, 2022), reflecting their peatland and forest dominated land covers (Coordination of Information on the Environment—CORINE—classification) (Büttner et al., 2017) (Table 1). The Glenamong River is one of the two main inflows to Lough Feeagh and Vattholma flows into Lake Mälaren, the drinking water source for two million people, including the city of Stockholm. While the Glenamong and Feeagh are not used as a source of potable water, they are intensively monitored sites that are representative of similar rivers and small lakes used as drinking water supplies in the region.

The study sites have contrasting characteristics. The Glenamong is small (18 km^2) and unpopulated, characterised by a relatively high variability in daily river discharge due to high precipitation levels and a steep landscape (Doyle et al., 2019; Jennings et al., 2020). Vattholma, in contrast, hosts several communities in a much larger area (261 km^2) and features more gradual variations in daily discharge reflecting a much flatter terrain, longer river network, lower precipitation levels and cooler air temperatures. Vattholma is also drier than Glenamong, only registering measurable rainfall on 37 % of days within a calendar year versus 84 % at the Irish site. While the average DOC concentration recorded at Vattholma is over twice that of the Glenamong, the annual DOC flux on an areal basis is four times lower for the Swedish site due to its much larger basin area (Fig. 1; Table 1).

2.1.1. Data availability

Observed climate data for Vattholma were obtained from the European Climate Assessment & Dataset E-OBS repository (0.1°grid, www.ecad.eu). Daily discharge data at the river outlet (1980–2022) were obtained from the Swedish Meteorological and Hydrological Institute monitoring services (www.smhi.se). Monthly measurements of total organic carbon (TOC) (mg TOC L^{-1}) concentrations at the outlet (1991–2022) were obtained from the Swedish Agricultural University monitoring services (www.slu.se) and were used as a direct proxy for DOC (mg DOC L^{-1}) in line with previous studies for this and other Swedish catchments (e.g., Ledesma et al., 2012; Lindqvist, 2022); TOC = 0.95 DOC + 1.4, $r^2 = 0.93$, $n = 47$. In Glenamong, climate observations from local meteorological stations and daily river discharge data (2013

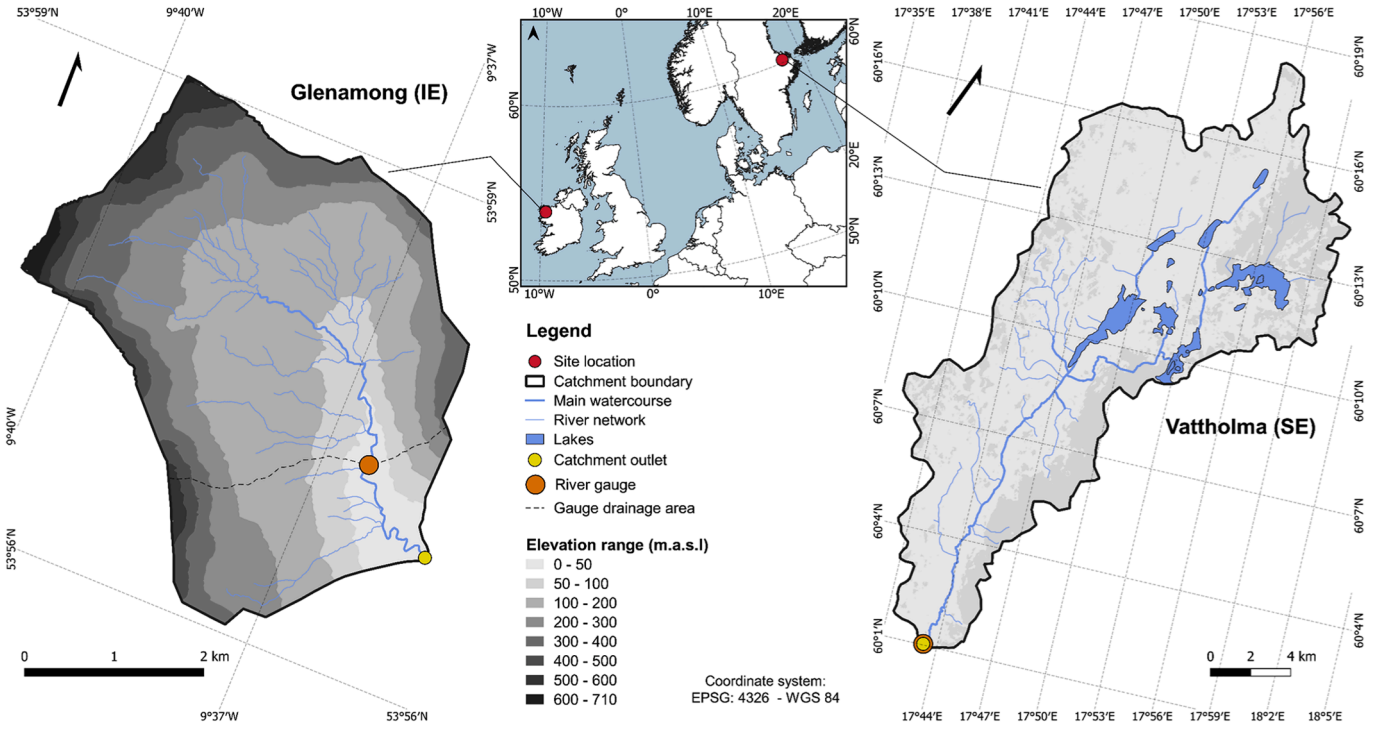


Fig. 1. Location of the study catchments including river network and topographic elevation.

Table 1
Main characteristics of the study catchments. Units for altitude are meters above sea level (m.a.s.l.).

Catchment	Glenamong (IE)	Vattholma (SE)
Area (km^2)	18	261
Altitude range (m.a.s.l.)	8–710	5–83
Main soil type	Blanket peat	Silty clay
Land cover		
Peatland	69 %	5 %
Agriculture	0 %	17 %
Grassland	4 %	15 %
Urban	0 %	2 %
Forest	26 %	58 %
Watercourse	1 %	3 %
Climate and hydrology	*2013–2023*	*1980–2022*
Mean air temperature (°C)	10.8	6.0
Annual precipitation range (mm yr^{-1})	1660–2570	460–875
Mean annual precipitation (mm yr^{-1})	2050	610
Main watercourse length (km)	4.8	39.1
Median river discharge (m^3 s^{-1})	0.4	1.1
Mean river discharge (m^3 s^{-1})	0.8	1.7
Q5 river discharge (m^3 s^{-1})	2.8	5.3
DOC	*2016–2023*	*1992–2022*
DOC concentration range (mg L^{-1})	2.8–18.0	8.2–36.9
Mean DOC concentration (mg L^{-1})	8.7	19.6
Mean annual DOC flux (tC km^{-2} yr^{-1})	16.2	4.0
Mean monthly DOC flux (tC km^{-2} month^{-1})	1.4	0.3

to 2023) were obtained from the Marine Institute monitoring services (https://www.marine.ie). Weekly water colour measurements (expressed as mg PtCo L^{-1}) were also available (2016–2023), based on absorption measurements performed with a HACH Dr 2000 spectrophotometer at 455 nm (wavelength accuracy of ±2 nm) on water filtered through Whatman GF/C filters (1.2 µm pore size). These were used as a proxy for DOC (Doyle et al., 2019), converted via a linear regression relationship with DOC laboratory measurements (samples filtered through 0.45 µm pore size); DOC = 0.067 water colour + 2.69, r^2 = 0.88, n = 551. Observed daily DOC fluxes (kg C km^{-2} day^{-1}) for both sites were computed as the product of DOC concentrations and mean daily measured discharge and normalised to the watershed area.

2.2. The model

The Generalised Watershed Loading Functions Model (GWLF) is a lumped parameter hydrological and water quality model introduced by Haith and Shoemaker (1987). It simulates water balance, water partition among the different flow pathways, sediment loading and nutrient export in a daily time step. The model input requirements include daily time series of precipitation and air temperature as well as land cover, land use, and soil characterisation. In this study, we used the GWLF version developed by the New York City Department of Environmental Protection (NYC DEP) (Schneiderman et al., 2002) that was further developed (Naden et al., 2010; Schneiderman et al., 2010) to include a process-based module for DOC. This model has been previously applied to several catchments to quantify changes in DOC export, including in the Lough Feeagh and Mälaren catchments (Naden et al., 2010; Lindqvist, 2022). Three changes were made to the model configuration in the current study, with the aim of improving DOC simulation capacity and better reflect DOC dynamics. These changes did not increase model complexity and do not require additional input data. Below, we describe key features of the base model and the changes we have implemented.

2.2.1. Hydrology module

GWLF simulates discharge from both surface runoff and from subsurface baseflow based on interactions between climate and the catchment land cover characteristics. Surface runoff is calculated using the USDA SCS curve number method (Boughton, 1989), and varies as a function of land uses and soil characteristics. In the current study, curve numbers associated with watershed CORINE land use areas were extracted from the GCN 250 dataset (Jaafar et al., 2019) and a value was calculated for each land cover area based as an area-weighted mean. Baseflow is calculated as a lumped contribution from the entire watershed as both slow- and fast-moving groundwater flows (see Schneiderman et al., 2010) from three subsurface lumped reservoirs (i.e., averaged over the whole catchment): (1) the unsaturated zone (subjected to evapotranspiration), (2) a saturated zone (not subjected to

evapotranspiration), and (3) a deep saturated zone with sustained low flow discharge. Evapotranspiration is calculated within the model using the Hamon temperature index equation as default (Hamon, 1961). The original hydrology model included seven adjustable parameters to regulate the different hydrological states: (1) *precipitation correction factor*, (2) *melt coefficient*, (3) *runoff curve number adjustment*, (4) *soil water capacity*, (5) *recess coefficient*, (6) *slow recess coefficient* and (7) *baseflow capacity* (Schneiderman et al., 2010). We incorporated one additional parameter: (8) a *river channel flow coefficient* (change 1). The latter partitions surface runoff into two separate pathways: a *direct runoff* pathway and a *river channel stored discharge* pathway. With this, we aimed to represent better the timing of water flow and DOC in basins of large size and/or regulated river networks, in which water (and the DOC contained therein) is stored in the channel at times exceeding the daily time step. This stored water was subjected to evapotranspiration. A description of the model parameters for hydrology and a conceptual diagram depicting change 1 in the model structure can be found in Supp. Mat. A1.

2.2.2. DOC module

GWLF follows a two-phase process for simulating DOC concentrations at the catchment outlet: (1) DOC production and (2) DOC washout. DOC production is regulated by two processes: temperature-dependent decomposition (D_T) and moisture-dependent decomposition (D_S) of soil organic matter. In the model described by Naden et al. (2010), three adjustable parameters controlled production: (1) *activation energy* (E_a) and (2) *anaerobic decomposition rate* (a) controlled D_T, while (3) the *aerobic decomposition rate* (b) controlled D_S. Here, we assigned an independent D_T for surface land covers we defined as wetland areas (e.g., peatlands, inland marshes) for which a new separate (4) *anaerobic decomposition rate* (a_w) only was used (change 2). The aim was to account for the difference in DOC production between areas that would be subject to continual fluctuations in water level and areas which would remain water-logged, and therefore not be subjected to the same decomposition rates (Mozafari et al., 2023; Arsenault et al., 2024). Furthermore, the calculation of D_S is based on simulated soil water storage which is a basin lumped variable and which would not be representative of the conditions in water-logged areas. A description of the parameters for DOC production and a conceptual diagram depicting change 2 in the model structure can be found in Supp. Mat. A2.

The DOC produced in the original model was stored in a single carbon catchment pool and made available for washout via all runoff and groundwater flows, regulated by three parameters (Naden et al., 2010). Here, instead of using a single pool, we defined pools that mirrored the main hydrological stores (i.e., the surface soils of the catchment, the unsaturated zone, and the deeper saturated zones), and accounting for the available carbon resulting from wetlands production as well. With this change, we aimed to track more closely how the different hydrological states drive DOC production and transport in the model. Four main pools were defined as lumped carbon reservoirs (change 3): (1) DOC produced by surface wetland-like areas, (2) DOC produced by DOC-producing surface areas that are not wetlands (see Naden et al., 2010), (3) DOC produced in the catchment unsaturated zone, and (4) DOC produced in the catchment saturated zones. Consistent with the model hydrology, DOC from surface pools 1 and 2 is available for washout via runoff flows (*direct runoff* and *channel stored discharge*), while DOC from pools 3 and 4 is available for washout via baseflow (slow- and fast- moving groundwater flows). As a result, the number of parameters to regulate the DOC transport increased from three to five: (1) *surface carbon loss coefficient,* (2) *surface flow cap,* (3) *baseflow ratio,* (4) *fast groundwater flow carbon loss coefficient* and (5) *slow groundwater flow carbon loss coefficient* (see Supp. Mat. A3 for more details). Streamflow DOC concentrations and fluxes were calculated as in the original model, from the sum of all DOC contributions (kg C day^{-1}) and using the total discharge (m^3 day^{-1}) (Naden et al., 2010).

2.3. Model calibration

For calibration of the hydrology, the measured discharge datasets were divided into two periods. The first was used for calibration and the second for validation: Vattholma (1980–2011, 2012–2022) and Glenamong (2013–2018, 2019–2023). For DOC, due to lower data availability, a single period was used for calibration only: Vattholma (1992–2022) and Glenamong (2016–2023). Model performance was evaluated based on the Nash-Sutcliffe coefficient (NSE) and the coefficient of determination (r^2) (Krause et al., 2005) between daily measured and simulated discharge, DOC concentration and DOC flux.

We adopted multistep script-based calibrations to adjust the model parameters. In line with Schneiderman et al. (2010) and Naden et al. (2010), on each calibration step, target functions were defined and the Powell search-optimisation method (Zhong and Cai, 2015) within VENSIM software (Ventana Systems Inc.) was used to calibrate parameters between pre-determined ranges. The range limits were set based on previous modelling studies and relevant literature (e.g., Evans et al., 2006; Karhu et al., 2010; Naden et al., 2010; Klimek et al., 2020; Lindqvist, 2022). The target functions for hydrology included checks for daily water balance and payoffs between simulated and measured discharge, runoff and baseflow (measured runoff and baseflow based on the Arnold et al. (1995) hydrograph separation method; see Schneiderman et al., 2010). For DOC, a payoff between daily measured and simulated DOC concentration was used as the target function on each step. Model spin-up periods of four and two years were used for Vattholma and Glenamong, respectively. Details on the range for each parameter, optimisation target functions, and a summary description of the calibration scripts can be found in Supp. Mat. A4.

2.4. Model uncertainty and sensitivity

We employed the Generalised Likelihood Uncertainty Estimation (GLUE) method (Beven and Binley, 1992, 2014) to quantify model parameter uncertainty. GLUE allows the exploration of parameter uncertainty by sampling from the parameter space and evaluating model performance against observed data. First, a Monte Carlo simulation round (30,000 model runs) was performed for each catchment, varying the parameters within calibration ranges. Second, an NSE threshold of 0.60 was defined for hydrology (simulated vs measured discharge) and of 0.30 for DOC (simulated vs measured DOC concentration) respectively, as a likelihood measure to constrain parameter variability space (i.e., to further constrain the parameter ranges so that more simulations with an acceptable NSE value above the selected thresholds are output) (Pianosi et al., 2016). A second simulation round (30,000 runs) was then performed using these constrained ranges. From all parameter sets above the likelihood measure thresholds (i.e., behavioural parameter sets), the 100 best-performing sets were used to compute 5 % to 95 % range GLUE uncertainty bounds (Beven, 2009). Model equifinality (i.e., how sensitive the model is to different parameter sets that produce acceptable simulations of observed behaviour) (Beven and Freer, 2001) was assessed individually for hydrology and DOC, relative to the selected likelihood measure (i.e., the NSE metric) and using all behavioural parameter sets.

2.5. Future projections

Future climate projections for the meteorological input variables were derived from the 5-member GCM ensemble provided by the open-access Inter-Sectoral Impact Model Intercomparison Project (0.5° ISIMIP 3b simulation round; data.isimip.org) (Lange and Büchner, 2021). Grid-cell daily values of future precipitation and mean air temperature from 2021 to 2100 were extracted for each study catchment for three Shared Socioeconomic Pathways (SSP): SSP126, SSP370 and SSP585. These represent three different futures of greenhouse gas (GHG) emission levels, societal development, and adaptation to climate change

(IPCC, 2023). Ranging from a more to a less optimistic scenario, SSP126 reflects rapid efforts to mitigate GHG emissions while promoting environmental and economic sustainability, SSP370 adopts intermediate efforts for both adaptation and mitigation, and SSP585 assumes increasing trends in fossil-fuelled development i.e., a high level of human-induced global warming. In addition, a 30-year baseline period from 1985 to 2014 was defined, for which daily input data for each catchment were extracted from the historical period of the same ISIMIP3b GCMs. All ISIMIP3b data have been subject to robust statistical downscaling and bias adjustment (see Supp. Mat. A5 for more details).

2.5.1. Data processing and analysis

For each scenario simulation (baseline, SSP126, SSP370 and SSP585), one meteorological dataset for each GCM was used to drive GWLF-DOC for each of the 100 top behavioural parameter sets (see Section 2.4) so that the uncertainty associated with the different GCMs and that associated with model parameters were estimated. A daily, monthly, and annual ensemble mean of the resulting 500 simulations for each scenario (5 GCMs x 100 behavioural parameter sets) was calculated for each SSP scenario. The model outputs for the SSPs were collated for two decadal periods: 2050–2059 (P1) and 2090–2099 (P2), which were used to compare against outputs for the baseline period. Furthermore, we computed future anomalies at the annual scale (Du and Deng, 2022) from 2030 to 2100 for discharge and DOC concentration between each future scenario and the baseline. The uncertainty in the predictions was calculated as the standard deviation of the ensemble. We also displayed the likelihood that each scenario would exceed 95th percentile baseline levels for DOC concentration and flux (as metrics of current extreme conditions) in future meteorological seasons. Seasonal analyses were based on the typical three-month periods relevant for management: spring (March to May), summer (June to August), autumn (September to November) and winter (December to February). Lastly, the relative contribution of (1) future climate input data and (2) model parameterisation to the total uncertainty in predictions was assessed based on a variance partitioning procedure (Watling et al., 2015; Lofton et al., 2022). For this, the model was run with all five GCMs but using only the calibrated set of model parameters (see Section 2.3). Then, it was run using all 100 best-performing model parameter sets with each GCM dataset. A normalised difference of the variances in the simulation results was then computed to estimate individual relative uncertainty contributions (Lofton et al., 2022). The same calculations were followed for each of the two catchments.

3. Results

3.1. Model performance and uncertainty

The results from the optimisation procedure for catchment hydrology indicated a good fit at both sites. The NSE values for average monthly and daily discharge based on the best optimised simulation ranged from 0.73 to 0.79 for Vattholma, and from 0.60 to 0.78 for Glenamong (Figs. 2 and B1). Similarly, r^2 values ranged from 0.76 to 0.80 for Vattholma, and from 0.60 to 0.78 for Glenamong (Figs. 2 and B1). For DOC, the metrics for the best optimised simulation were higher for DOC fluxes than for DOC concentrations at both sites. For Vattholma, the NSE and r^2 values for the daily DOC flux were 0.73 and 0.74 respectively, while those for daily DOC concentration were 0.39 and 0.39 (Fig. 3a and c). For Glenamong, the NSE and r^2 values for daily DOC flux were 0.60 and 0.62, while those for daily DOC concentration were 0.45 and 0.47 respectively (Fig. 3b and d). Simulated DOC flux for each study site reflected site-specific dynamics and intra-annual variations (Fig. B2a and b). Baseflow was a major contributor to both discharge

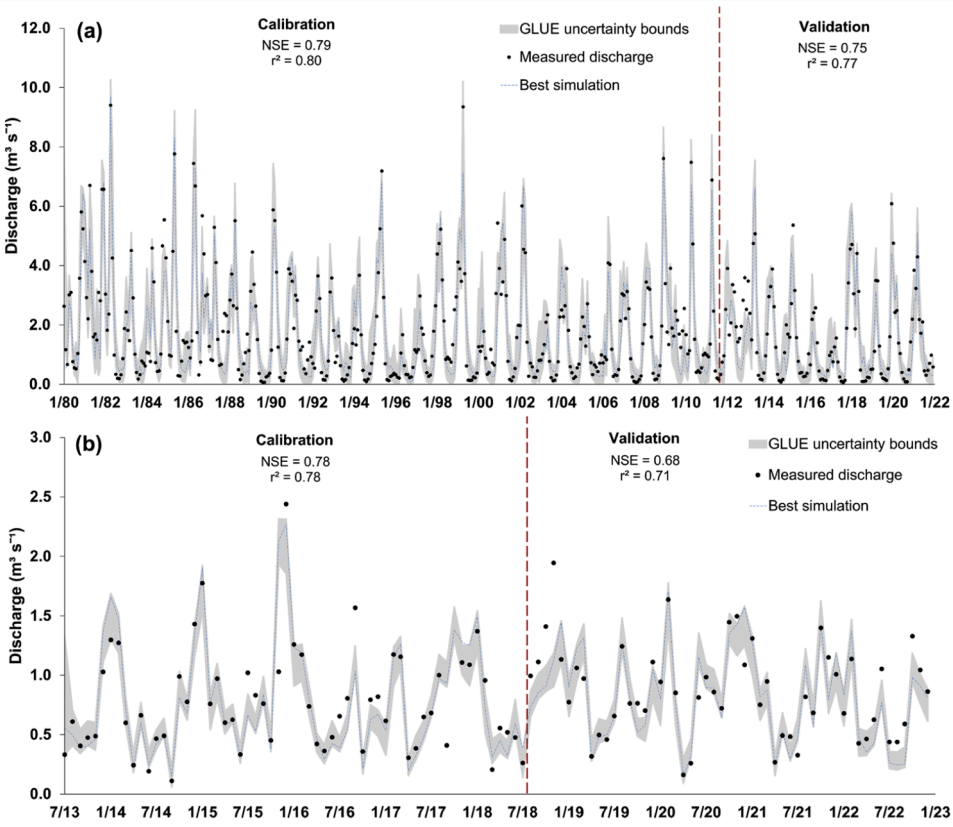


Fig. 2. Observed and simulated monthly river discharge for Vattholma (a) and Glenamong (b) catchments during model calibration and validation. NSE and r^2 values are indicated for the calibrated parameter set (best optimised simulation). The grey area denotes the 5–95 % range GLUE uncertainty bounds for river discharge based on the 100 best-performing parameter sets.

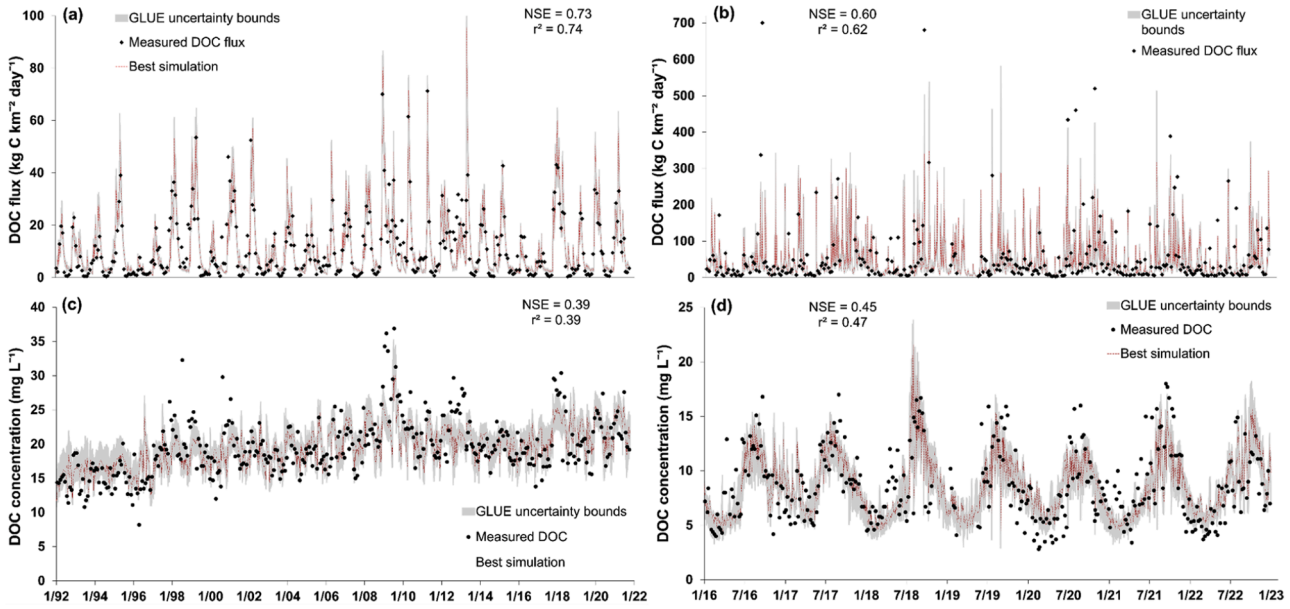


Fig. 3. Observed and simulated daily DOC flux and DOC concentrations for Vattholma (a and c) and Glenamong (b and d) catchments during model calibration. NSE and r^2 values are indicated for the calibrated parameter set (best optimised simulation). The grey area denotes the 5–95 % range GLUE uncertainty bounds for DOC flux and DOC concentrations based on the 100 best-performing parameter sets.

(Fig. B2c–f) and carbon export in Vattholma, while there was a more balanced ratio between baseflow and surface runoff for Glenamong.

The set of calibrated model parameters obtained for the best optimisation run reflected the differences between the study sites (Table B1). Except for the precipitation correction factor and soil water capacity, the optimised values for the hydrological parameters were generally higher for Glenamong than for Vattholma, particularly the river channel flow coefficient. For DOC production, the optimisation resulted in a higher activation energy (E_a = 6.4) and aerobic decomposition rate (b = 7.4) for Vattholma, indicating a greater sensitivity to changes in soil temperature and moisture levels at this site than for Glenamong (E_a = 3.0 and b = 1.0). In contrast, the values for both anaerobic decomposition rates were an order of magnitude greater at the Glenamong, reflecting the importance of saturation of the deep Irish peat soils. In terms of DOC transport, the optimised values for the Glenamong reflected a larger contribution of surface runoff at that site, with higher values for the runoff carbon loss coefficient and surface flow cap than for Vattholma. Subsurface carbon transport through fast groundwater flow was favoured over slow groundwater flow at both sites, with both optimisations also indicating relatively low groundwater carbon loss coefficients.

The GLUE uncertainty bounds captured a similar level of variation in measured discharge and DOC concentration to that captured by the optimisation process, but allowed for a range of parameter values rather than a single optimised set (Table B1). For discharge, 73 % and 60 % of the measured monthly observations and 65 % and 50 % of the daily observations were captured by the uncertainty bounds for Vattholma (Figs. 2 and B1) and Glenamong (Figs. 2 and B1) respectively, while the values for DOC concentration were 45 % and 38 % (Fig. 3c and d). Furthermore, sensitivity plots showed that the DOC model was typically more sensitive to parameter variation than the hydrology model (Figs. B3–B6). Discharge was sensitive to the value of the precipitation correction factor for both sites, and insensitive to the value used for baseflow capacity and soil water capacity (i.e., acceptable model performance occurred over the entire parameter range). Parameters related to flow attenuation (recess coefficient, slow recess coefficient and melt coefficient) were sensitive only at Vattholma. In contrast, parameters more related to catchment surface water retention (runoff curve number adjustment and river channel flow coefficient) were more sensitive for Glenamong. Parameters related to DOC production were sensitive for both catchments except for activation energy at Vattholma, where a wide range of values produced an equally good fit. Similarly, parameters related to DOC transport were sensitive at both sites, although the surface flow cap displayed less sensitivity (i.e., acceptable performance over a large extent of its parameter range).

3.2. Future climate impacts

The GCM ensemble for all three future SSP scenarios projected changes in climatic conditions for each site relative to their baseline periods (Table 2; Fig. 4a–d) (Tables B2–B13 show conditions projected by each GCM ensemble member). Large air temperature increases were projected for Vattholma, ranging from +1.5 °C (+24 %; SSP126) to +6.0 °C (+95 %; SSP585) across the scenarios. However, SSP126, the scenario that incorporates some mitigation effects, was the only scenario for which temperature first increased in P1 (2050–2059) (+2.1 °C; +33 %) and then decreased in P2 (2090–2099) (+1.5 °C; +24 %). For the Glenamong, there was only a slight increase in air temperature for projections based on SSP126 in both P1 (+0.4 °C; +4 %) and P2 (+0.2 °C; +2 %). In contrast, the ensemble mean for SSP370 and SSP585 indicated much warmer conditions during both P1 (up to +12 %) and P2 (up to +33 %). Under SSP585, it was of note that, although similar annual air temperatures were projected for both sites in the final decade of the century (Vattholma: 12.3 °C; Glenamong: 12.2 °C), this represented a more extreme increase at the Swedish site (+6.0 °C; +95 %) than at the Irish site (+3.0 °C; +33 %).

Annual precipitation was also projected to increase in Vattholma under all scenarios during both P1 and P2 (Table 2). However, the increases were, in relative terms, less extreme than those for temperature. They ranged by up to +10 % in P1 and +15 % in P2. The largest increase in that latter period was actually projected for SSP370 (+108 mm yr^{-1}). Smaller relative increases in annual precipitation were projected for

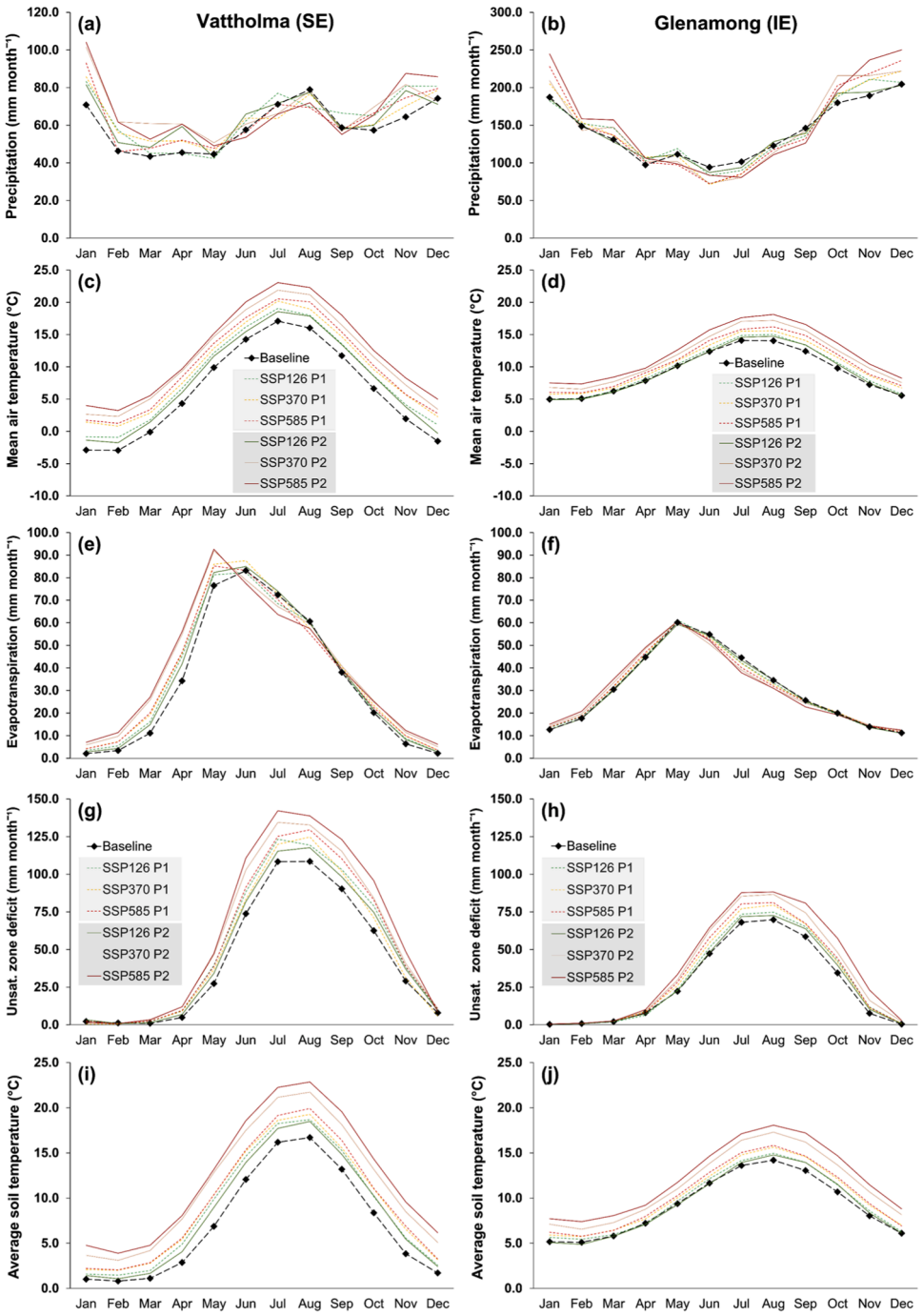


Fig. 4. ISIMIP3b GCM-ensemble average monthly precipitation (a and b), ISIMIP3b GCM-ensemble mean air temperature (c and d), average modelled monthly actual evapotranspiration (e and f), average modelled unsaturated zone deficit (g and h) and average modelled soil temperature (i and j) for the baseline period and for the SSP126, SS370 and SSP585 scenarios during P1 and P2. Note the different scaling in panels a and b. Vattholma: a, c, e, g, i; Glenamong: b, d, f, h, j.

Glenamong, up to +2 % in P1 and +8 % in P2. In fact, for Glenamong, where annual precipitation was already over twice that at Vattholma for the baseline period (1710 mm yr^{-1} versus 712 mm yr^{-1}, respectively), all projections were similar to the baseline with the exception for SSP585 in P2 (+136 mm yr^{-1}). There was, however, a pronounced seasonal shift in precipitation at the Irish site, with generally drier conditions than the baseline period between April and September, and wetter conditions between October and March (Fig. 4a and b). At Vattholma, future precipitation was clearly elevated in the autumn and winter from October to March, but the direction of change projected by the different CGMs varied in other months. The variability in future climate, indicated by the standard deviation, increased by the end of the century at both sites and was highest under SSP585 (Table 2).

The future changes in evapotranspiration reflected the changes in both air temperature and precipitation (Fig. 4e and f). In general, higher monthly actual evapotranspiration was projected from October to May at both sites, followed by decreases from June to September, although the changes were greater at Vattholma.

Table 2
ISIMIP3b GCM ensemble-mean future annual precipitation and mean air temperature values for the historical period (baseline) and for the SSP126, SSP370 and SSP585 scenarios during P1 (2050–2060) and P2 (2090–2100), for each study catchment. The standard deviation is indicated in parentheses.

	Vattholma (SE)		Glenamong (IE)	
Period	Mean air temperature (°C)	Precipitation (mm yr^{-1})	Mean air temperature (°C)	Precipitation (mm yr^{-1})
Baseline (1985–2014)	6.3 (±1.1)	712 (±100)	9.2 (±0.5)	1710 (±171)
SSP 126				
P1 (2050–2059)	8.4 (±1.0)	730 (±116)	9.6 (±0.7)	1728 (±162)
P2 (2090–2099)	7.8 (±1.6)	764 (±142)	9.4 (±1.2)	1715 (±182)
SSP 370				
P1 (2050–2059)	9.1 (±1.3)	782 (±116)	10.2 (±0.7)	1749 (±204)
P2 (2090–2099)	11.3 (±2.2)	820 (±136)	11.4 (±1.6)	1763 (±184)
SSP 585				
P1 (2050–2059)	9.3 (±1.4)	764 (±109)	10.3 (±0.9)	1737 (±227)
P2 (2090–2099)	12.3 (±2.5)	812 (±145)	12.2 (±1.9)	1846 (±224)

3.3. Future change in discharge

There were pronounced changes in seasonal discharge patterns, especially for Vattholma during the first six calendar months (Fig. 5a). Most noticeable was that, except for SSP126 in P1, the peak month for discharge shifted to earlier in the year, with increased discharge from January to March particularly in P2 (+63 %; SSP585). These increases were followed by decreases in discharge from April to June under all three scenarios, with the lowest levels in P2 as well (up to −38 %; SSP585). There was a slight upward shift in daily discharge magnitudes for SSP126 during the last decade of the century, while values for SSP370 and SSP585 were similar to those during P1 but with more variability (Fig. 5b). In the Glenamong, the projections indicated that discharge would be relatively unchanged under SSP126 (Fig. 5d). In contrast to the Swedish site, it was projected to decrease from April to September followed by increased levels from October to March under SSP370 and SSP585. The decreases were greatest for July in P1 (up to −25 %; SSP370) and the largest increases in discharge were for January in P2 (up to +30 %; SSP585). There was little change in the magnitude of discharge at the daily timescale for the Glenamong in both P1 and P2 under all three scenarios, although SSP585 had a greater range of values (Fig. 5e).

Ensemble mean annual discharge anomalies for Vattholma sometimes contrasted between future scenarios, but were all similar in magnitude: up to ±1.1 $m^3\ s^{-1}$ under SSP126, up to ±1.3 $m^3\ s^{-1}$ under SSP370, and up to ±1.1 $m^3\ s^{-1}$ under SSP585 relative to a baseline average of 2.4 $m^3\ s^{-1}$ (Fig. 5c). For Glenamong, discharge anomalies were lower in magnitude than for the Swedish site but greatest for SSP585 (up to ±0.2 $m^3\ s^{-1}$) than for SSP126 and SSP370 (up to ±0.1 $m^3\ s^{-1}$) relative to a baseline average of 0.6 $m^3\ s^{-1}$ (Fig. 5f). At each of the study sites, all three future projections displayed a similar uncertainty range throughout the simulation, which slightly increased towards the end of the century (Fig. 5c and f).

3.4. Future change in DOC concentrations and flux

The variables that drive carbon decomposition in the model also showed large changes in the future, with increases projected in soil temperatures (reflecting higher air temperature), and a drier soil matrix in summer (reflecting both increases in evapotranspiration and lower precipitation in summer) (Fig. 4g–j). Conditions that would be expected to increase decomposition and ultimately stream DOC concentration.

The simulations indicated that DOC concentrations would increase for Vattholma throughout the calendar year under all three SSPs (Fig. 6a). In P1, these increases ranged from +4 mg L^{-1} (SSP370) to +6 mg L^{-1} (SSP585) (baseline average of 13.7 mg L^{-1}). In P2, even larger increases were projected, particularly for SSP370 and SSP585, exceeding baseline levels by up to +9 mg L^{-1}. However, it is of note that the increases projected for SSP126 were lower in P2 (up to +3 mg L^{-1}) than those for all scenarios in P1. A clear general upward shift in the magnitude and minimum DOC concentration was indicated for all three scenarios (Fig. 6b). Again, the levels projected using SSP126 were closer to the baseline by the end of the century. DOC variability was also projected to increase, especially in P2 under SSP370 and SSP585. Ensemble mean annual DOC concentration anomalies for Vattholma were always positive, that is they were always higher than the historical baseline, in the order of ≃ +3, +4 and +5 mg L^{-1} for SSP126, SSP370 and SSP585, respectively (Fig. 6c). The anomalies continued to increase until the end of the century under both SSP370 and SSP585, while those for SSP126 decreased after 2060. The output for SSP126 also had the lowest uncertainty range, while that for SSP585 was the largest, particularly during P2, projecting futures with extremely high annual DOC concentrations of up to +13 mg L^{-1} above the baseline mean.

DOC concentrations were also projected to increase for Glenamong in all months under all three SSPs (Fig. 6d). The lowest increases were for SSP126, and were similar in P1 and in P2 (≃ +1 mg L^{-1}) (baseline average of 9.2 mg L^{-1}). The concentrations projected under SSP370 and SSP585 were larger, particularly from July to November in P2, exceeding baseline levels by ≃ +4 mg L^{-1}. A small upward shift in the magnitudes and variability of DOC concentrations relative to the baseline was projected in P1 under all three scenarios (Fig. 6e). In P2, the magnitude and variability increased more under SSP370 and SSP585 but, as with Vattholma, decreased under SSP126. Ensemble mean annual DOC concentration anomalies were also consistently positive for Glenamong in the order of ≃ +0.6, +1.0 and +1.3 mg L^{-1} for SSP126, SSP370 and SSP585, respectively (Fig. 6f). The anomalies increased over time under SSP370 and SSP585, while SSP126 anomalies decreased after 2070. Uncertainty increased with time under all three scenarios, with SSP126 displaying the narrowest range. SSP585 projections were the most uncertain, with anomalies of up to +5 mg L^{-1} over the last decade.

The probabilities of exceeding the 95th percentile baseline DOC concentration level (a metric of current extreme conditions) were much higher for Vattholma during each season than for Glenamong under all three future climate scenarios (Fig. 7). In line with other results, extreme DOC concentrations for Vattholma were lowest for SSP126 than for the other two scenarios, and therefore the probabilities of exceeding the historical 95th percentile threshold concentration of 15 mg L^{-1} were also lower across seasons (Fig. 7a). In particular, increases in the likelihood of occurrence for extreme concentrations were projected for all seasons under SSP370 and SSP585, while spring and winter were the most affected under SSP126. For Glenamong, in contrast, the probability of exceeding the baseline 95th percentile DOC concentration threshold of 13 mg L^{-1} were zero during the spring and winter under all three scenarios (Fig. 7b). However, there was an increased probability for exceeding this threshold in the summer and even higher probability of exceedance for the autumn under all three scenarios but higher under SSP370 and SSP585.

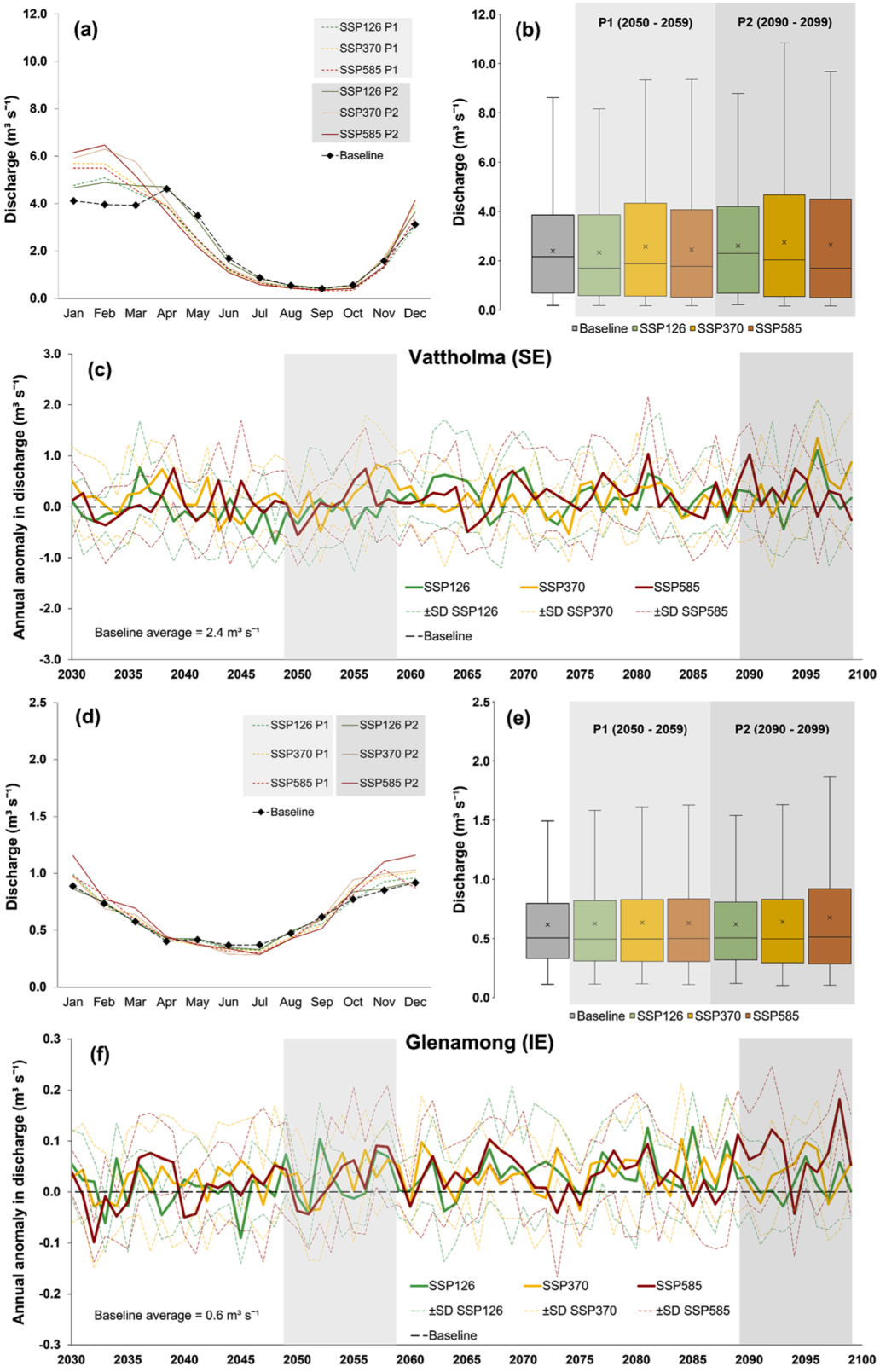


Fig. 5. Average calendar month discharge (a and d); boxplot distributions of average daily discharge for the baseline period, and for the SSP126, SS370 and SSP585 scenarios during P1 and P2 (b and e); annual anomalies for discharge under SSP126, SS370 and SSP585 scenarios from 2030 to 2100 (c and f). Uncertainty in the discharge anomaly panels is indicated by the standard deviation (±SD) and delimited by SSP126, SS370 and SSP585 legend colour dotted lines respectively. Vattholma: a, b, c; Glenamong: d, e, f.

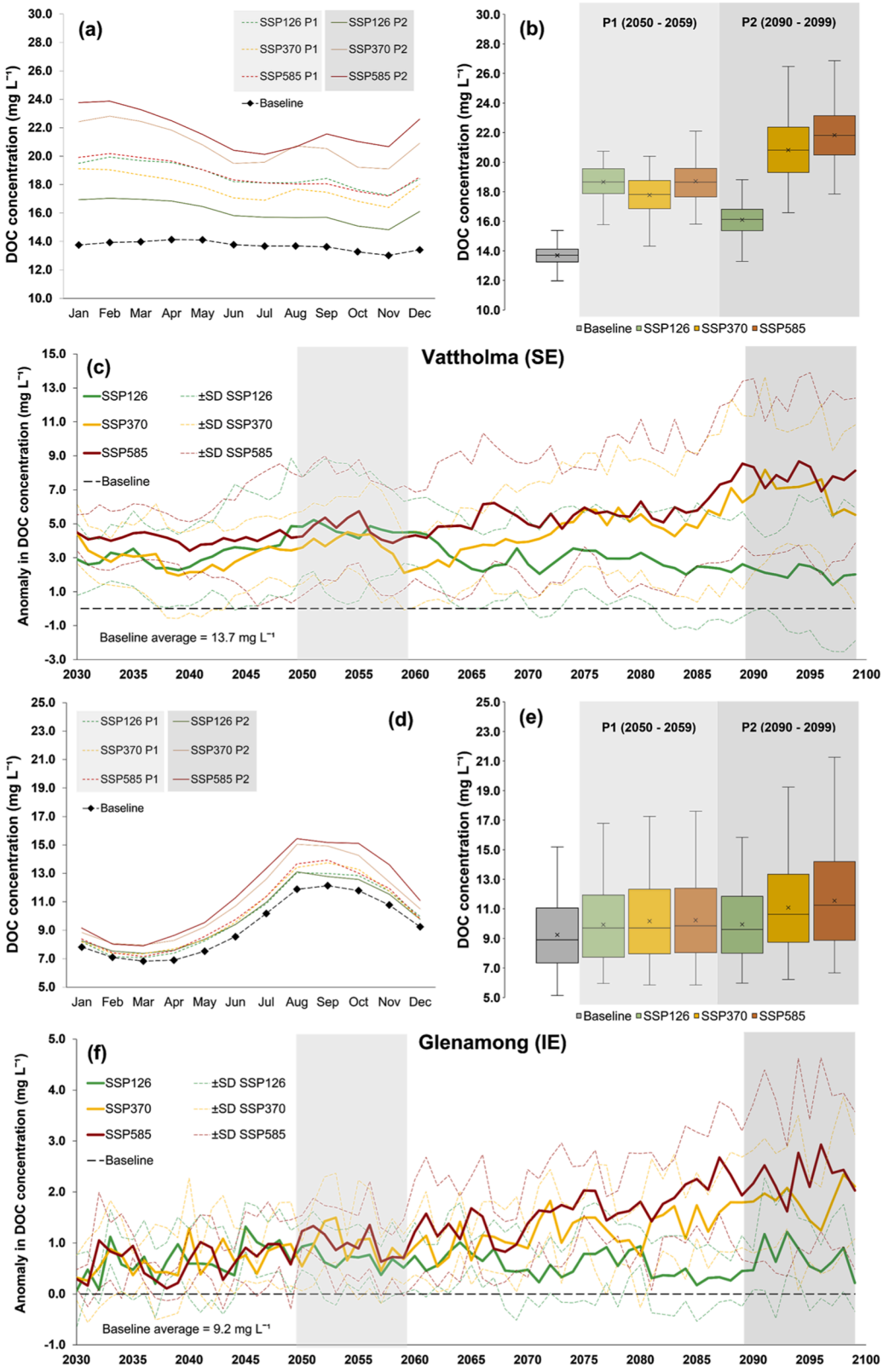


Fig. 6. Average calendar month DOC concentration (a and d); boxplot distributions of average daily DOC concentrations for the baseline period, and for the SSP126, SS370 and SSP585 scenarios during P1 and P2 (b and e); annual anomalies for DOC concentration under SSP126, SS370 and SSP585 scenarios from 2030 to 2100 (c and f). Uncertainty in the DOC concentration anomaly panels is indicated by the standard deviation (±SD) and delimited by SSP126, SS370 and SSP585 legend colour dotted lines respectively. Vattholma: a, b, c; Glenamong: d, e, f.

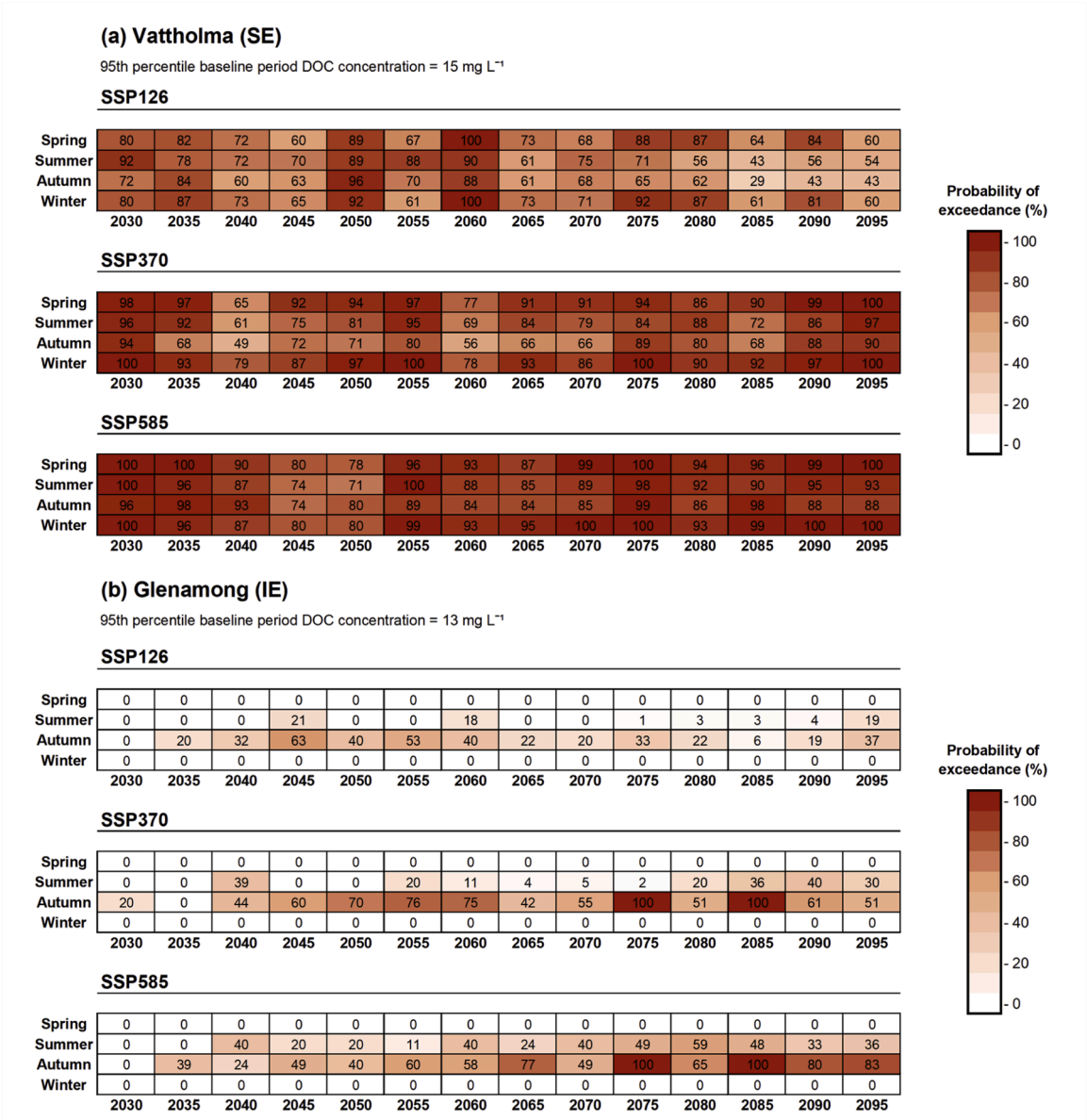


Fig. 7. Tercile plots displaying the probability of exceeding the 95th percentile baseline DOC concentration (mg L^{-1}) for each typical meteorological season (spring, summer, autumn and winter) in the future (every 5 years) under SSP126, SSP370 and SSP585 scenarios for Vattholma (a) and Glenamong (b). The shading of each square represents the probability of exceedance based on the categorised colour bar legend. The ensemble size was comprised of 500 members for each scenario.

Furthermore, extreme DOC concentrations for Vattholma were projected to be accompanied by an increasing likeliness of extreme DOC flux in spring and winter under all three scenarios, while the summer and autumn were not affected (Fig. B7a). For Glenamong, the likelihood of occurrence for extreme DOC flux was virtually zero across seasons under all three SSPs (Fig. B7b).

3.5. *Uncertainty partitioning*

In all projections for both river discharge and DOC concentration, the uncertainty (indicated by the standard deviation) typically increased with time and the relative contribution of the future climate driving data (i.e., for the five GCMs) to total uncertainty was generally much larger than the contribution of model parameterisation (i.e., for the 100 behavioural parameter sets) (Figs. 8 and B8). Variation between GCMs made the greatest contributions (up to 85 %) to total uncertainty for all discharge simulations, although the hydrological model parameters accounted for a greater percentage of variation in simulation for Vattholma than for Glenamong (Fig. B8). For DOC concentrations, future climate data were also the most important source of uncertainty, but of note were the higher contributions from the DOC model parameters for the Swedish site (Fig. 8). These were relatively large, particularly under SSP370 and SSP585, and at times contributed up to 50 %. In contrast, the DOC model parameters contributed much less to the uncertainty in DOC projections for the Glenamong, especially under SSP585.

4. Discussion

Implementing adaptive management in response to the impacts of global warming is becoming more and more critical as records of climatic extremes continue to be exceeded (Ripple et al., 2023; Esper et al., 2024). These changes are having profound impacts on water quantity and quality (van Vliet et al., 2023), including on the DOC concentration in drinking source waters and therefore potentially on the formation of DBPs (Absalan et al., 2024). In order to respond and adapt, water

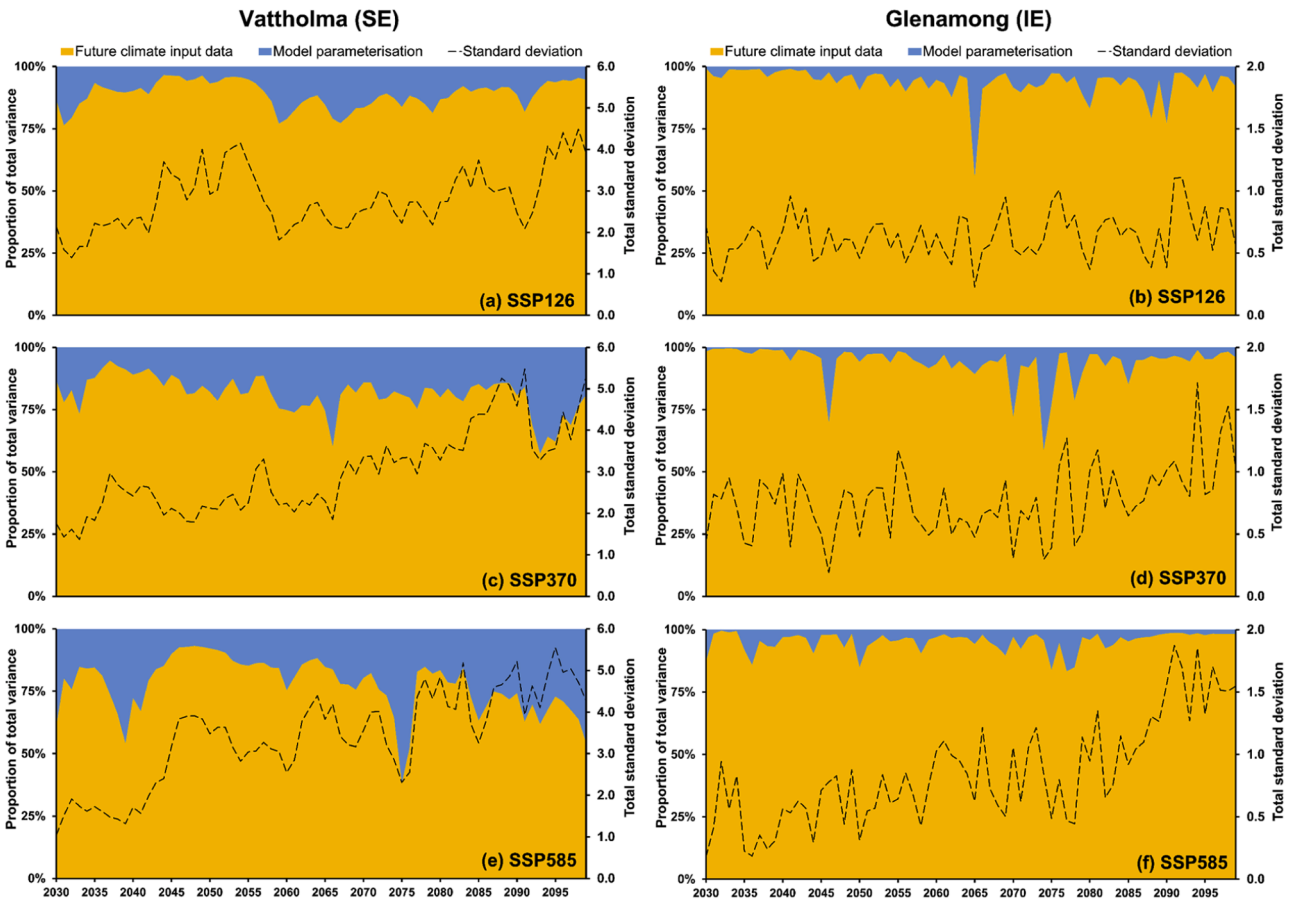


Fig. 8. Relative contribution of (1) future climate input data and (2) model parameterisation as individual sources of uncertainty to the total uncertainty in future projections of DOC concentration under SSP126, SSP370 and SSP585 scenarios for Vattholma (a, c, and e) and Glenamong (b, d and f).

managers require robust estimates of future change from the modelling community. Our projections for two contrasting catchments, in regions were DBP formation is already an issue, show that DOC concentrations are projected to show large increases, with the highest levels related to scenarios where mitigation is not addressed. They also highlight the importance of incorporating model parameter uncertainty into the future projections, a source of uncertainty that is often omitted. This is especially important for model parameters such as those related to carbon decomposition and transport in organic soils, that will respond directly to variations in temperature and water availability.

Our results relative to many recent studies (e.g., Futter et al., 2011; Son et al., 2019; Xu et al., 2020) have a similarly good or better model performance, especially for modelling DOC concentration. The future changes quantified for river discharge and DOC concentration in this study also lie in a similar order of magnitude to those projected in other research for these sites (e.g., Naden et al., 2010; Lindqvist, 2022). That is, discharge projections indicate both decreasing and increasing levels under different scenarios depending on the time scale, season and context. In terms of DOC, the overall picture is for an increase in concentration and flux with different magnitudes depending on the study site and scenario. It is important to be aware, however, that these results should not be compared directly to the work of others without acknowledging the differences in modelling approach. These include changes in model structure, driver data type (e.g., stationary projections compared to transient GCM-driven projections), future scenario conditions, and the examination here of effects related to model parameterisation.

Although accounting for model parameterisation can result in simulations with larger uncertainty (Schürz et al., 2019), this is generally outweighed by producing a more accurate range of variability for the modelled variables (Her et al., 2019b; Marshall et al., 2021). Furthermore, by partitioning the total uncertainty of the predictions, we have quantified the impacts of this parameterisation on long-term projections for river discharge and DOC concentration (Figs. 8 and B8). While the GCM ensemble was the dominant source of uncertainty, a finding in line with many other climate change impact assessments (Hattermann et al., 2018; Kundzewicz et al., 2018), the variability in DOC model parameterisation was also important for some of our simulations. This was the case for the Vattholma catchment in Sweden under all three SSPs. An important contributing factor to this was that the behavioural ranges of key soil decomposition parameters (i.e., activation energy (E_a) and aerobic decomposition rate (b)) were higher in magnitude for this site than for the Irish site. This led to the parameters showing larger responses to increasing temperatures and changes in soil moisture levels in the Swedish catchment, and in turn to larger uncertainty contributions, particularly under SSP370 and SSP585. This also led to such large increases projected for DOC concentration at that site under these two scenarios (see Fig. 6a), as the response of these parameters likely translated to a higher amount of DOC produced in the soil matrix and, therefore, to a higher DOC export.

Determining the relative importance of model parameterisation versus future climate inputs can inform efforts to reduce total uncertainty in such projections. In GCM-driven projections for water resources, improving the quality of climate data, increasing GCM ensemble size, and better spatial and temporal input resolution are often indicated as the most effective steps (Hattermann et al., 2018; Kundzewicz et al., 2018; Her et al., 2019b). However, when model parameter uncertainty plays an important role, improving catchment model structure and parameter representation for both hydrology and water quality should also be evaluated (Schürz et al., 2019; Marshall et al.,

2021). Using as an example the model structure of GWLF-DOC, these actions could be focused on the parameters that showed the greatest sensitivity (see Section 3.1).

Moreover, although other potential sources of uncertainty were not included (e.g., methods for bias correction, use of an ensemble of catchment models, land use change projections, and input data downscaling), this study represents a step forward in catchment DOC water quality modelling. By incorporating model parameter uncertainty, all of our results including those representing the likelihood of extreme DOC concentration and DOC flux account, to a large extent, for model equifinality. This key aspect is required for a better interpretation of the results (Naden et al., 2010), especially of DOC model outputs that were produced using a model structure forced by hydrology (Wei et al., 2024). It is to note, however, that GWLF-DOC does not replicate other factors that influence DOC dynamics such as those related to biochemistry in soils (e.g., pH response and microbial populations) or in-stream processes. Nevertheless, we consider it captured the fundamental processes related to temperature and water availability variations in the soil that drive DOC dynamics at the catchment scale.

4.1. Implications for water management

Our simulations quantify the DOC concentration envelope within which water managers at similar sites may need to operate in the future. Such results could be used to evaluate scenario-based management for preserving source water quality and supply. It was clear, however, that the SSP126 scenario represented the best trajectory in terms of future change, not only for climate but also for DOC source waters. Higher and more variable concentrations, and the likelihood of extremes, were much smaller under this scenario, especially over the long term. Moreover, a process-based modelling approach such as that described can provide insights into how climate and other key catchment dynamics influence DOC concentrations at the outlet. This allows the identification of site-specific measures to reduce DOC thereby safeguard drinking water in the context of DBPs both by catchment management or improved water treatment.

Catchment-scale measures could include improved soil management, riparian buffers, land use regulations, soil treatment, drain-blocking in peatlands, and preservation of organic soils (Ritson et al., 2014; Kritzberg et al., 2020; Anderson et al., 2023). These could be implemented in a targeted way for a specific hydrological zone or land cover (Xu et al., 2018; Williamson et al., 2023). At the treatment scale, understanding the magnitude of future increases could allow planning for mitigation measures, for example, improved DOM removal during pretreatment (Anderson et al., 2023) and enhanced disinfection during treatment and post-treatment (Xiao et al., 2024). Both catchment and treatment scale measures could be applied for a particular time of the year, for a management period (e.g., 5 years), or implemented gradually over the years (Anderson et al., 2023; Williamson et al., 2023). They can also be conducted while closely monitoring key variables at the water source intake (e.g., meteorology, discharge, DOC) and intensified accordingly during periods of rising DOM, such as a particular season, flow regime, or event (e.g., a drought) (Warner and Saros, 2019; Srivastav et al., 2020; Xiao et al., 2024).

At our Swedish site Vattholma, the elevated river discharge and DOC loading projected in the winter and spring may pose additional challenges, along with increased DOC concentrations. Higher amounts of carbon export would have implications downstream for Lake Mälaren that further complicate current water treatment (Köhler et al., 2016) and DBP reduction (Andersson, 2021) during these seasons. Moreover, our results indicated that groundwater flow pathways play a critical role in DOC export for this site. This finding has also been highlighted for other Swedish sites in other modelling studies (Naden et al., 2010; Jutebring Sterte et al., 2022). Therefore, extra attention could be paid to measures that consider the saturated sub-surface zone, its impacts on baseflow and the transport of DOC in the porous media including sorption-related processes (Ploum et al., 2020).

The Glenamong (Ireland) represents catchments that face a challenge directly associated with the sensitivity of a peatland-dominated land cover to climate-induced DOC release (Jennings et al., 2010; Mozafari et al., 2023). Here, the largest increases in DOC concentration, combined with a lower discharge, were indicated for the summer and autumn especially under warmer, drier scenarios. Both surface runoff and baseflow were equally important for DOC export in this catchment, emphasizing the role of the peaty topsoil not only for organic carbon decomposition (Arsenault et al., 2024) but also for transport (Prijac et al., 2023). Moreover, maximum DOC concentrations (indicated by increases and extreme events) would have a pronounced seasonality, peaking in the autumn (Fig. 7). This volatility, in particular, could represent an important challenge for water treatment (Klante et al., 2022; Riyadh and Peleato, 2024) that, along with other climate-induced impacts on catchment dynamics (Jennings et al., 2009), can further complicate Irish water supply in complying with European Union regulations, especially in the context of DPBs (O'Driscoll et al., 2018b). Management steps should, therefore, evaluate not only reducing the potential DOC increases over monthly to annual time scales but also account for high levels of temporal variability associated with extreme events (Jennings et al., 2020).

5. Conclusions

Our study has highlighted the dominant impacts of future climate variability on the uncertainty in future projections of catchment discharge and DOC dynamics. However, it also showed how model parameterisation can be an important source of uncertainty in climate change impact assessments. Importantly, DOC concentrations for our study sites were projected to increase in all simulated futures, sometimes to levels that can largely exceed the historical reference. It is of note, however, that the smallest increases and variability were estimated under SSP126, especially by the end of the century. This suggests, with regard to catchment DOC export and potentially for drinking water supply, that it might be worth adopting more long-term sustainability actions aligned with that scenario (e.g., efforts for climate adaptation, infrastructure development, and a reduction in GHG emissions). We propose that the use of our site-specific findings can assist in developing mitigation protocols and strategies that can lead to a more adaptive catchment and water treatment management.

CRediT authorship contribution statement

Ricardo Paíz: Writing – review & editing, Writing – original draft, Visualization, Software, Methodology, Formal analysis, Data curation, Conceptualization. **Donald C. Pierson:** Writing – review & editing, Validation, Supervision, Software, Resources, Methodology, Formal analysis, Conceptualization. **Klara Lindqvist:** Software, Methodology, Data curation. **Pamela S. Naden:** Writing – review & editing, Software. **Elvira de Eyto:** Writing – review & editing, Resources, Investigation, Data curation. **Mary Dillane:** Resources, Investigation, Data curation. **Valerie McCarthy:** Writing – review & editing, Supervision. **Suzanne Linnane:** Writing – review & editing, Supervision. **Eleanor Jennings:** Writing – review & editing, Validation, Supervision, Software, Resources, Project administration, Methodology, Funding acquisition, Formal analysis, Data curation, Conceptualization.

Declaration of competing interest

The authors declare that they have no known competing financial interests or personal relationships that could have appeared to influence the work reported in this paper.

Acknowledgements

This research has been funded by the inventWater Innovative Training Network (ITN) (Inventive forecasting tools for adapting water quality management to a new climate) through the European Union's Horizon 2020 research and innovation programme, under the Marie Sklodowska-Curie grant agreement no. 956623. Special thanks to the Marine Institute, the Swedish Meteorological and Hydrological Institute (SMHI), and the Swedish Agricultural University (SLU) for their efforts in data monitoring and collection

Supplementary materials

Supplementary material associated with this article can be found, in the online version, at doi:10.1016/j.watres.2025.123238.

Data availability

Data will be made available on request.

References

Absalan, F., Hatam, F., Prévost, M., Barbeau, B., Bichai, F., 2024. Climate change and future water demand: implications for chlorine and trihalomethanes management in water distribution systems. J. Environ. Manag. 355, 120470. https://doi.org/10.1016/j.jenvman.2024.120470.

Adler, T., Underwood, K.L., Rizzo, D.M., Harpold, A., Sterle, G., Li, L., Wen, H., Stinson, L., Bristol, C., Stewart, B., Lini, A., Perdrial, N., Perdrial, J.N., 2021. Drivers of dissolved organic carbon mobilization from forested headwater catchments: a multi scaled approach. Front. Water 3, 578608. https://doi.org/10.3389/frwa.2021.578608.

Anderson, L.E., DeMont, I., Dunnington, D.D., Bjorndahl, P., Redden, D.J., Brophy, M.J., Gagnon, G.A., 2023. A review of long-term change in surface water natural organic matter concentration in the northern hemisphere and the implications for drinking water treatment. Sci. Total Environ. 858, 159699. https://doi.org/10.1016/j.scitotenv.2022.159699.

Andersson, A., 2021. Uncharted Waters: non-target analysis of disinfection by-products in drinking water. Linköping Studies in Arts and Sciences. Linköping University Electronic Press, Linköping. https://doi.org/10.3384/diss.diva-173312.

Arnold, J.G., Allen, P.M., Muttiah, R., Bernhardt, G., 1995. Automated base flow separation and recession analysis techniques. Groundwater 33, 1010–1018. https://doi.org/10.1111/j.1745-6584.1995.tb00046.x.

Arsenault, J., Talbot, J., Moore, T.R., Knorr, K.-H., Teickner, H., Lapierre, J.-F., 2024. Patterns and drivers of organic matter decomposition in peatland open-water pools. https://doi.org/10.5194/egusphere-2024-271.

Büttner, G., Kosztra, B., Soukup, T., Sousa, A., Langanke, T., 2017. CLC2018 Technical guidelines.

Beven, K., Binley, A., 1992. The future of distributed models: model calibration and uncertainty prediction. Hydrol. Process. 6, 279–298. https://doi.org/10.1002/hyp.3360060305.

Beven, K., Binley, A., 2014. GLUE: 20 years on. Hydrol. Process. 28, 5897–5918. https://doi.org/10.1002/hyp.10082.

Beven, K., Freer, J., 2001. Equifinality, data assimilation, and uncertainty estimation in mechanistic modelling of complex environmental systems using the GLUE methodology. J. Hydrol. 249, 11–29. https://doi.org/10.1016/S0022-1694(01)00421-8.

Beven, K.J., 2009. Environmental Modelling: An Uncertain Future?: An Introduction to Techniques for Uncertainty Estimation in Environmental Prediction /Keith Beven. Routledge, London.

Blaurock, K., Beudert, B., Gilfedder, B.S., Fleckenstein, J.H., Peiffer, S., Hopp, L., 2021. Low hydrological connectivity after summer drought inhibits DOC export in a forested headwater catchment. Hydrol. Earth Syst. Sci. 25, 5133–5151. https://doi.org/10.5194/hess-25-5133-2021.

Boughton, W., 1989. A review of the USDA SCS curve number method. Soil Res. 27, 511–523.

Clark, J.M., Ashley, D., Wagner, M., Chapman, P.J., Lane, S.N., Evans, C.D., Heathwaite, A.L., 2009. Increased temperature sensitivity of net DOC production from ombrotrophic peat due to water table draw-down. Glob. Change Biol. 15, 794–807. https://doi.org/10.1111/j.1365-2486.2008.01683.x.

Clark, J.M., Bottrell, S.H., Evans, C.D., Monteith, D.T., Bartlett, R., Rose, R., Newton, R. J., Chapman, P.J., 2010. The importance of the relationship between scale and process in understanding long-term DOC dynamics. Sci. Total Environ. 408, 2768–2775. https://doi.org/10.1016/j.scitotenv.2010.02.046.

Cui, T., Sreekanth, J., Pickett, T., Rassam, D., Gilfedder, M., Barrett, D., 2021. Impact of model parameterization on predictive uncertainty of regional groundwater models in the context of environmental impact assessment. Environ. Impact Assess. Rev. 90, 106620. https://doi.org/10.1016/j.eiar.2021.106620.

de Wit, H.A., Mulder, J., Hindar, A., Hole, L., 2007. Long-term increase in dissolved organic carbon in streamwaters in Norway is response to reduced acid deposition. Environ. Sci. Technol. 41, 7706–7713. https://doi.org/10.1021/es070557f.

Diana, M., Felipe-Sotelo, M., Bond, T., 2019. Disinfection byproducts potentially responsible for the association between chlorinated drinking water and bladder cancer: a review. Water Res. 162, 492–504. https://doi.org/10.1016/j.watres.2019.07.014.

Dong, H., Zhang, S., Lin, J., Zhu, B., 2021. Responses of soil microbial biomass carbon and dissolved organic carbon to drying-rewetting cycles: a *meta*-analysis. CATENA 207, 105610. https://doi.org/10.1016/j.catena.2021.105610.

Doyle, B.C., de Eyto, E., Dillane, M., Poole, R., McCarthy, V., Ryder, E., Jennings, E., 2019. Synchrony in catchment stream colour levels is driven by both local and regional climate. Biogeosciences 16, 1053–1071. https://doi.org/10.5194/bg-16-1053-2019.

Doyle, B.C., de Eyto, E., McCarthy, V., Dillane, M., Poole, R., Jennings, E., 2021. Late summer peak in pCO_2 corresponds with catchment export of DOC in a temperate, humic lake. Inland Waters 11, 234–249. https://doi.org/10.1080/20442041.2021.1893098.

Du, J., Deng, G., 2022. How should a numerical weather prediction Be used: full field or anomaly? A conceptual demonstration with a Lorenz model. Atmosphere 13, 1487. https://doi.org/10.3390/atmos13091487.

Esper, J., Torbenson, M., Büntgen, U., 2024. 2023 summer warmth unparalleled over the past 2000 years. Nature 631, 94–97. https://doi.org/10.1038/s41586-024-07512-y.

Evans, C.D., Monteith, D.T., Cooper, D.M., 2005. Long-term increases in surface water dissolved organic carbon: observations, possible causes and environmental impacts. Environ. Pollut. 137, 55–71. https://doi.org/10.1016/j.envpol.2004.12.031. Recovery from acidificationin the UK: Evidence from 15 years of acid waters monitoring.

Evans, C.D., Chapman, P.J., Clark, J.M., Monteith, D.T., Cresser, M.S., 2006. Alternative explanations for rising dissolved organic carbon export from organic soils. Glob. Change Biol. 12, 2044–2053. https://doi.org/10.1111/j.1365-2486.2006.01241.x.

Fenner, N., Meadham, J., Jones, T., Hayes, F., Freeman, C., 2021. Effects of climate change on Peatland reservoirs: a DOC perspective. Glob. Biogeochem. Cycles 35. https://doi.org/10.1029/2021GB006992 e2021GB006992.

Franklin, H.M., Doederer, K., Neale, P.A., Hayton, J.B., Fisher, P., Maxwell, P., Carroll, A. R., Burford, M.A., Leusch, F.D.L., 2021. Terrestrial dissolved organic matter source affects disinfection by-product formation during water treatment and subsequent toxicity. Environ. Pollut. 283, 117232. https://doi.org/10.1016/j.envpol.2021.117232.

Futter, M.N., Löfgren, S., Köhler, S.J., Lundin, L., Moldan, F., Bringmark, L., 2011. Simulating dissolved organic carbon dynamics at the Swedish Integrated Monitoring sites with the integrated catchments model for carbon, INCA-C. Ambio 40, 906–919. https://doi.org/10.1007/s13280-011-0203-z.

Garmo, Ø.A., Skjelkvåle, B.L., de Wit, H.A., Colombo, L., Curtis, C., Fölster, J., Hoffmann, A., Hruška, J., Høgåsen, T., Jeffries, D.S., Keller, W.B., Krám, P., Majer, V., Monteith, D.T., Paterson, A.M., Rogora, M., Rzychon, D., Steingruber, S., Stoddard, J.L., Vuorenmaa, J., Worsztynowicz, A., 2014. Trends in surface water chemistry in acidified areas in Europe and North America from 1990 to 2008. Water, Air, Soil Pollut. 225, 1880. https://doi.org/10.1007/s11270-014-1880-6.

Haith, D.A., Shoemaker, L.L., 1987. Generalized watershed loading functions for stream flow Nutrients1. JAWRA J. Am. Water Resour. Assoc. 23, 471–478. https://doi.org/10.1111/j.1752-1688.1987.tb00825.x.

Hamon, W.R., 1961. Estimating potential evapotranspiration. J. Hydraul. Div. 87, 107–120. https://doi.org/10.1061/JYCEAJ.0000599.

Hattermann, F.F., Vetter, T., Breuer, L., Su, B., Daggupati, P., Donnelly, C., Fekete, B., Flörke, F., Gosling, S.N., Hoffmann, P., Liersch, S., Masaki, Y., Motovilov, Y., Müller, C., Samaniego, L., Stacke, T., Wada, Y., Yang, T., Krysnaova, V., 2018. Sources of uncertainty in hydrological climate impact assessment: a cross-scale study. Environ. Res. Lett. 13, 015006. https://doi.org/10.1088/1748-9326/aa9938.

Her, Y., Yoo, S.-H., Cho, J., Hwang, S., Jeong, J., Seong, C., 2019a. Uncertainty in hydrological analysis of climate change: multi-parameter vs. multi-GCM ensemble predictions. Sci. Rep. 9, 4974. https://doi.org/10.1038/s41598-019-41334-7.

Her, Y., Yoo, S.-H., Cho, J., Hwang, S., Jeong, J., Seong, C., 2019b. Uncertainty in hydrological analysis of climate change: multi-parameter vs. multi-GCM ensemble predictions. Sci. Rep. 9, 4974. https://doi.org/10.1038/s41598-019-41334-7.

IPCC, Calvin, K., Dasgupta, D., Krinner, G., Mukherji, A., Thorne, P.W., Trisos, C., Romero, J., Aldunce, P., Barrett, K., Blanco, G., Cheung, W.W.L., Connors, S., Denton, F., Diongue-Niang, A., Dodman, D., Garschagen, M., Geden, O., Hayward, B., Jones, C., Jotzo, F., Krug, T., Lasco, R., Lee, Y.-Y., Masson-Delmotte, V., Meinshausen, M., Mintenbeck, K., Mokssit, A., Otto, F.E.L., Pathak, M., Pirani, A., Poloczanska, E., Pörtner, H.-O., Revi, A., Roberts, D.C., Roy, J., Ruane, A.C., Skea, J., Shukla, P.R., Slade, R., Slangen, A., Sokona, Y., Sörensson, A.A., Tignor, M., Van Vuuren, D., Wei, Y.-M., Winkler, H., Zhai, P., Zommers, Z., Hourcade, J.-C., Johnson, F.X., Pachauri, S., Simpson, N.P., Singh, C., Thomas, A., Totin, E., Arias, P., Bustamante, M., Elgizouli, I., Flato, G., Howden, M., Méndez-Vallejo, C., Pereira, J. J., Pichs-Madruga, R., Rose, S.K., Saheb, Y., Sánchez Rodríguez, R., Ürge-Vorsatz, D., Xiao, C., Yassaa, N., Alegría, A., Armour, K., Bednar-Friedl, B., Blok, K., Cissé, G., Dentener, F., Eriksen, S., Fischer, E., Garner, G., Guivarch, C., Haasnoot, M., Hansen, G., Hauser, M., Hawkins, E., Hermans, T., Kopp, R., Leprince-Ringuet, N., Lewis, J., Ley, D., Ludden, C., Niamir, L., Nicholls, Z., Some, S., Szopa, S., Trewin, B., Van Der Wijst, K.-I., Winter, G., Witting, M., Birt, A., Ha, M., Romero, J., Kim, J., Haites, E.F., Jung, Y., Stavins, R., Birt, A., Ha, M., Orendain, D.J.A., Ignon, L., Park, S., Park, Y., Reisinger, A., Cammaramo, D., Fischlin, A., Fuglestvedt, J.S., Hansen, G., Ludden, C., Masson-Delmotte, V., Matthews, J.B.R., Mintenbeck, K., Pirani, A., Poloczanska, E., Leprince-Ringuet, N., Péan, C., Core Writing Team, 2023. IPCC, 2023: climate change 2023: synthesis report. In: Lee, H., Romero, J. (Eds.),

Contribution of Working Groups I, II and III to the Sixth Assessment Report of the Intergovernmental Panel on Climate Change. IPCC, Geneva, Switzerland. https://doi.org/10.59327/IPCC/AR6-9789291691647. Intergovernmental Panel on Climate Change (IPCC).

Jaafar, H.H., Ahmad, F.A., El Beyrouthy, N., 2019. GCN250, new global gridded curve numbers for hydrologic modeling and design. Sci. Data 6, 145. https://doi.org/10.1038/s41597-019-0155-x.

Jennings, E., Allott, N., Pierson, D.C., Schneiderman, E.M., Lenihan, D., Samuelsson, P., Taylor, D., 2009. Impacts of climate change on phosphorus loading from a grassland catchment: implications for future management. Water Res. 43, 4316–4326. https://doi.org/10.1016/j.watres.2009.06.032.

Jennings, E., Järvinen, M., Allott, N., Arvola, L., Moore, K., Naden, P., Aonghusa, C.N., Nõges, T., Weyhenmeyer, G.A., 2010. Impacts of climate on the flux of dissolved organic carbon from catchments. In: George, G. (Ed.), The Impact of Climate Change on European Lakes. Springer, Netherlands, Dordrecht, pp. 199–220. https://doi.org/10.1007/978-90-481-2945-4_12.

Jennings, E., de Eyto, E., Moore, T., Dillane, M., Ryder, E., Allott, N., Nic Aonghusa, C., Rouen, M., Poole, R., Pierson, D.C., 2020. From highs to lows: changes in dissolved organic carbon in a peatland catchment and lake following extreme flow events. Water 12. https://doi.org/10.3390/w12102843.

Johnes, P.J., Evershed, R.P., Jones, D.L., Maberly, S.C., 2023. Exploring the nature, origins and ecological significance of dissolved organic matter in freshwaters: state of the science and new directions. Biogeochemistry 164, 1–12. https://doi.org/10.1007/s10533-023-01040-z.

Jutebring Sterte, E., Lidman, F., Sjöberg, Y., Ploum, S.W., Laudon, H., 2022. Groundwater travel times predict DOC in streams and riparian soils across a heterogeneous boreal landscape. Sci. Total Environ. 849, 157398. https://doi.org/10.1016/j.scitotenv.2022.157398.

Köhler, S.J., Lavonen, E., Keucken, A., Schmitt-Kopplin, P., Spanjer, T., Persson, K., 2016. Upgrading coagulation with hollow-fibre nanofiltration for improved organic matter removal during surface water treatment. Water Res. 89, 232–240. https://doi.org/10.1016/j.watres.2015.11.048.

Karhu, K., Fritze, H., Tuomi, M., Vanhala, P., Spetz, P., Kitunen, V., Liski, J., 2010. Temperature sensitivity of organic matter decomposition in two boreal forest soil profiles. Soil Biol. Biochem. 42, 72–82. https://doi.org/10.1016/j.soilbio.2009.10.002.

Klante, C., Hägg, K., Larson, M., 2022. Understanding short-term organic matter fluctuations to optimize drinking water treatment. Water Pract. Technol. 17, 2141–2159. https://doi.org/10.2166/wpt.2022.121.

Klimek, B., Chodak, M., Jaźwa, M., Azarbad, H., Niklińska, M., 2020. Soil physicochemical and microbial drivers of temperature sensitivity of soil organic matter decomposition under boreal forests. Pedosphere 30, 528–534. https://doi.org/10.1016/S1002-0160(17)60400-4.

Krause, P., Boyle, D.P., Bäse, F., 2005. Comparison of different efficiency criteria for hydrological model assessment. Adv. Geosci. 5, 89–97. https://doi.org/10.5194/adgeo-5-89-2005.

Kritzberg, E.S., Hasselquist, E.M., Škerlep, M., Löfgren, S., Olsson, O., Stadmark, J., Valinia, S., Hansson, L.-A., Laudon, H., 2020. Browning of freshwaters: consequences to ecosystem services, underlying drivers, and potential mitigation measures. Ambio 49, 375–390. https://doi.org/10.1007/s13280-019-01227-5.

Kumari, M., Gupta, S.K., 2022. Cumulative human health risk analysis of trihalomethanes exposure in drinking water systems. J. Environ. Manag. 321, 115949. https://doi.org/10.1016/j.jenvman.2022.115949.

Kundzewicz, Z.W., Krysanova, V., Benestad, R.E., Hov, Ø., Piniewski, M., Otto, I.M., 2018. Uncertainty in climate change impacts on water resources. Environ. Sci. Policy 79, 1–8. https://doi.org/10.1016/j.envsci.2017.10.008.

Lange, S., Büchner, M., 2021. ISIMIP3b bias-adjusted atmospheric climate input data (v1.1). https://doi.org/10.48364/ISIMIP.842396.1.

Ledesma, J.L.J., Köhler, S.J., Futter, M.N., 2012. Long-term dynamics of dissolved organic carbon: implications for drinking water supply. Sci. Total Environ. 432, 1–11. https://doi.org/10.1016/j.scitotenv.2012.05.071.

Lindqvist, K., 2022. Modelling the Effects of Climate Change on Future DOC Export to Lake Mälaren Using a Generalized Watershed Loading Functions (GWLF) Model. Uppsala University, Sweden.

Lofton, M.E., Brentrup, J.A., Beck, W.S., Zwart, J.A., Bhattacharya, R., Brighenti, L.S., Burnet, S.H., McCullough, I.M., Steele, B.G., Carey, C.C., Cottingham, K.L., Dietze, M.C., Ewing, H.A., Weathers, K.C., LaDeau, S.L., 2022. Using near-term forecasts and uncertainty partitioning to inform prediction of oligotrophic lake cyanobacterial density. Ecol. Appl. 32, e2590. https://doi.org/10.1002/eap.2590.

Marshall, A.M., Link, T.E., Flerchinger, G.N., Lucash, M.S., 2021. Importance of parameter and climate data uncertainty for future changes in boreal hydrology. Water Resour. Res. 57. https://doi.org/10.1029/2021WR029911 e2021WR029911.

Mozafari, B., Bruen, M., Donohue, S., Renou-Wilson, F., O'Loughlin, F., 2023. Peatland dynamics: a review of process-based models and approaches. Sci. Total Environ. 877, 162890. https://doi.org/10.1016/j.scitotenv.2023.162890.

Naden, P.S., Allott, N., Arvola, L., Järvinen, M., Jennings, E., Moore, K., Nic Aonghusa, C., Pierson, D., Schneiderman, E., 2010. Modelling the impacts of climate change on dissolved organic carbon. In: George, G. (Ed.), The Impact of Climate Change on European Lakes. Springer, Netherlands, Dordrecht, pp. 221–252. https://doi.org/10.1007/978-90-481-2945-4_13.

O'Driscoll, C., Ledesma, J.L.J., Coll, J., Murnane, J.G., Nolan, P., Mockler, E.M., Futter, M.N., Xiao, L.W., 2018a. Minimal climate change impacts on natural organic matter forecasted for a potable water supply in Ireland. Sci. Total Environ. 630, 869–877. https://doi.org/10.1016/j.scitotenv.2018.02.248.

O'Driscoll, C., Sheahan, J., Renou-Wilson, F., Croot, P., Pilla, F., Misstear, B., Xiao, L., 2018b. National scale assessment of total trihalomethanes in Irish drinking water. J. Environ. Manag. 212, 131–141. https://doi.org/10.1016/j.jenvman.2018.01.070.

Oulehle, F., Hruška, J., 2009. Rising trends of dissolved organic matter in drinking-water reservoirs as a result of recovery from acidification in the Ore Mts., Czech Republic. Environ. Pollut. 157, 3433–3439. https://doi.org/10.1016/j.envpol.2009.06.020. Persistent Organic Pollutants in Mountainous Areas.

Piai, L., Mei, S., van Gijn, K., Langenhoff, A., 2024. Effects of organic matter in drinking water and wastewater on micropollutant adsorption to activated carbon. Int. J. Environ. Sci. Technol. 21, 2547–2558. https://doi.org/10.1007/s13762-023-05132-z.

Pianosi, F., Beven, K., Freer, J., Hall, J.W., Rougier, J., Stephenson, D.B., Wagener, T., 2016. Sensitivity analysis of environmental models: a systematic review with practical workflow. Environ. Model. Softw. 79, 214–232. https://doi.org/10.1016/j.envsoft.2016.02.008.

Ploum, S., Laudon, H., Peralta Tapia, A., Kuglerová, L., 2020. Are dissolved organic carbon concentrations in riparian groundwater linked to hydrological pathways in the boreal forest? Hydrol. Earth Syst. Sci. 24, 1709–1720. https://doi.org/10.5194/hess-24-1709-2020.

Prijac, A., Gandois, L., Taillardat, P., Bourgault, M.-A., Riahi, K., Ponçot, A., Tremblay, A., Garneau, M., 2023. Hydrological connectivity controls dissolved organic carbon exports in a peatland-dominated boreal catchment stream. Hydrol. Earth Syst. Sci. 27, 3935–3955. https://doi.org/10.5194/hess-27-3935-2023.

Ripple, W.J., Wolf, C., Gregg, J.W., Rockström, J., Newsome, T.M., Law, B.E., Marques, L., Lenton, T.M., Xu, C., Huq, S., Simons, L., King, S.D.A., 2023. The 2023 state of the climate report: entering uncharted territory. Bioscience 73, 841–850. https://doi.org/10.1093/biosci/biad080.

Ritson, J.P., Graham, N.J.D., Templeton, M.R., Clark, J.M., Gough, R., Freeman, C., 2014. The impact of climate change on the treatability of dissolved organic matter (DOM) in upland water supplies: a UK perspective. Sci. Total Environ. 473-474, 714–730. https://doi.org/10.1016/j.scitotenv.2013.12.095.

Riyadh, A., Peleato, N.M., 2024. Natural organic matter character in drinking water distribution systems: a review of impacts on water quality and characterization techniques. Water 16, 446. https://doi.org/10.3390/w16030446.

Rodríguez-Cardona, B.M., Wymore, A.S., Argerich, A., Barnes, R.T., Bernal, S., Brookshire, E.N.J., Coble, A.A., Dodds, W.K., Fazekas, H.M., Helton, A.M., Johnes, P. J., Johnson, S.L., Jones, J.B., Kaushal, S.S., Kortelainen, P., López-Lloreda, C., Spencer, R.G.M., McDowell, W.H., 2022. Shifting stoichiometry: long-term trends in stream-dissolved organic matter reveal altered C:N ratios due to history of atmospheric acid deposition. Glob. Change Biol. 28, 98–114. https://doi.org/10.1111/gcb.15965.

Ryder, E., de Eyto, E., Dillane, M., Poole, R., Jennings, E., 2014. Identifying the role of environmental drivers in organic carbon export from a forested peat catchment. Sci. Total Environ. 490, 28–36. https://doi.org/10.1016/j.scitotenv.2014.04.091.

SanClements, M.D., Oelsner, G.P., McKnight, D.M., Stoddard, J.L., Nelson, S.J., 2012. New insights into the source of decadal increases of dissolved organic matter in acid-sensitive lakes of the northeastern United States. Environ. Sci. Technol. 46, 3212–3219. https://doi.org/10.1021/es204321x.

Schürz, C., Hollosi, B., Matulla, C., Pressl, A., Ertl, T., Schulz, K., Mehdi, B., 2019. A comprehensive sensitivity and uncertainty analysis for discharge and nitrate-nitrogen loads involving multiple discrete model inputs under future changing conditions. Hydrol. Earth Syst. Sci. 23, 1211–1244. https://doi.org/10.5194/hess-23-1211-2019.

Schneiderman, E.M., Pierson, D.C., Lounsbury, D.G., Zion, M.S., 2002. Modeling of hydrochemistry of the cannonsville watershed with Generalized Watershed loading functions (GWLF). JAWRA J. Am. Water Resour. Assoc. 38, 1323–1347. https://doi.org/10.1111/j.1752-1688.2002.tb04350.x.

Schneiderman, E., Järvinen, M., Jennings, E., May, L., Moore, K., Naden, P.S., Pierson, D., 2010. Modeling the effects of climate change on catchment hydrology with the GWLF model. In: George, G. (Ed.), The Impact of Climate Change on European Lakes. Springer, Netherlands, Dordrecht, pp. 33–50. https://doi.org/10.1007/978-90-481-2945-4_3.

Son, K., Lin, L., Band, L., Owens, E.M., 2019. Modelling the interaction of climate, forest ecosystem, and hydrology to estimate catchment dissolved organic carbon export. Hydrol. Process. 33, 1448–1464. https://doi.org/10.1002/hyp.13412.

Srivastav, A.L., Patel, N., Chaudhary, V.K., 2020. Disinfection by-products in drinking water: occurrence, toxicity and abatement. Environ. Pollut. 267, 115474. https://doi.org/10.1016/j.envpol.2020.115474.

Teweldebrhan, A.T., Burkhart, J.F., Schuler, T.V., 2018. Parameter uncertainty analysis for an operational hydrological model using residual-based and limits of acceptability approaches. Hydrol. Earth Syst. Sci. 22, 5021–5039. https://doi.org/10.5194/hess-22-5021-2018.

van der Wiel, K., Bintanja, R., 2021. Contribution of climatic changes in mean and variability to monthly temperature and precipitation extremes. Commun. Earth Environ. 2, 1–11. https://doi.org/10.1038/s43247-020-00077-4.

van Vliet, M.T.H., Thorslund, J., Strokal, M., Hofstra, N., Flörke, M., Ehalt Macedo, H., Nkwasa, A., Tang, T., Kaushal, S.S., Kumar, R., van Griensven, A., Bouwman, L., Mosley, L.M., 2023. Global river water quality under climate change and hydroclimatic extremes. Nat. Rev. Earth Environ. 4, 687–702. https://doi.org/10.1038/s43017-023-00472-3.

Villanueva, C.M., Evlampidou, I., Ibrahim, F., Donat-Vargas, C., Valentin, A., Tugulea, A.-M., Echigo, S., Jovanovic, D., Lebedev, A.T., Lemus-Pérez, M., Rodriguez-Susa, M., Luzati, A., de Cássia dos Santos Nery, T., Pastén, P.A., Quiñones, M., Regli, S., Weisman, R., Dong, S., Ha, M., Phattarapattamawong, S., Manasfi, T., Musah, S.-I.E., Eng, A., Janák, K., Rush, S.C., Reckhow, D., Krasner, S. W., Vineis, P., Richardson, S.D., Kogevinas, M., 2023. Global assessment of chemical

quality of drinking water: the case of trihalomethanes. Water Res. 230, 119568. https://doi.org/10.1016/j.watres.2023.119568.
Wang, X., Jiang, D., Lang, X., 2017. Future extreme climate changes linked to global warming intensity. Sci. Bull. 62, 1673–1680. https://doi.org/10.1016/j.scib.2017.11.004.
Warner, K.A., Saros, J.E., 2019. Variable responses of dissolved organic carbon to precipitation events in boreal drinking water lakes. Water Res. 156, 315–326. https://doi.org/10.1016/j.watres.2019.03.036.
Watling, J.I., Brandt, L.A., Bucklin, D.N., Fujisaki, I., Mazzotti, F.J., Romañach, S.S., Speroterra, C., 2015. Performance metrics and variance partitioning reveal sources of uncertainty in species distribution models. Ecol. Model. 309-310, 48–59. https://doi.org/10.1016/j.ecolmodel.2015.03.017.
Wei, X., Hayes, D.J., Butman, D.E., Qi, J., Ricciuto, D.M., Yang, X., 2024. Modeling exports of dissolved organic carbon from landscapes: a review of challenges and opportunities. Environ. Res. Lett. 19, 053001. https://doi.org/10.1088/1748-9326/ad3cf8.
Williamson, J., Evans, C., Spears, B., Pickard, A., Chapman, P.J., Feuchtmayr, H., Leith, F., Waldron, S., Monteith, D., 2023. Reviews and syntheses: understanding the impacts of peatland catchment management on dissolved organic matter concentration and treatability. Biogeosciences 20, 3751–3766. https://doi.org/10.5194/bg-20-3751-2023.
Wit, H.A.de, Stoddard, J.L., Monteith, D.T., Sample, J.E., Austnes, K., Couture, S., Fölster, J., Higgins, S.N., Houle, D., Hruška, J., Krám, P., Kopáček, J., Paterson, A.M., Valinia, S., Dam, H.V., Vuorenmaa, J., Evans, C.D., 2021. Cleaner air reveals growing influence of climate on dissolved organic carbon trends in northern headwaters. Environ. Res. Lett. 16, 104009. https://doi.org/10.1088/1748-9326/ac2526.
Wu, J., Yao, H., 2022. Simulating dissolved organic carbon during dryness/wetness periods based on hydrological characteristics under multiple timescales. J. Hydrol. 614, 128534. https://doi.org/10.1016/j.jhydrol.2022.128534.
Wu, J., Yao, H., 2024. Enhanced role of streamflow processes in the evolutionary trends of dissolved organic carbon. Environ. Sci. Technol. 58, 4772–4780. https://doi.org/10.1021/acs.est.3c09508.
Wu, J., Yao, H., Chen, X., Chen, X., 2023a. Dynamics of dissolved organic carbon during drought and flood events: a phase-by-stages perspective. Sci. Total Environ. 871, 162158. https://doi.org/10.1016/j.scitotenv.2023.162158.
Wu, J., Yao, H., Wang, G., Chen, X., Yuan, X., Zhou, Y., Zhang, D., 2023b. Dynamics of DOC concentration and flux in different propagation stages of hydrological drought: patterns and drivers. J. Hydrol. 617, 128939. https://doi.org/10.1016/j.jhydrol.2022.128939.
Xiao, R., Deng, Y., Xu, Z., Chu, W., 2024. Disinfection byproducts and their precursors in drinking water sources: origins, influencing factors, and environmental insights. Engineering 36, 36–50. https://doi.org/10.1016/j.eng.2023.08.017.
Xu, J., Morris, P.J., Liu, J., Holden, J., 2018. Hotspots of peatland-derived potable water use identified by global analysis. Nat. Sustain. 1, 246–253. https://doi.org/10.1038/s41893-018-0064-6.
Xu, J., Morris, P.J., Liu, J., Ledesma, J.L.J., Holden, J., 2020. Increased dissolved organic carbon concentrations in peat-fed UK water supplies under future climate and sulfate deposition scenarios. Water Resour. Res. 56. https://doi.org/10.1029/2019WR025592 e2019WR025592.
Zhong, J., Cai, W., 2015. Differential evolution with sensitivity analysis and the Powell's method for crowd model calibration. J. Comput. Sci., Comput. Sci. Gates Nat. 9, 26–32. https://doi.org/10.1016/j.jocs.2015.04.013.

Check for updates

Received: 25 September 2024 | Revised: 8 May 2025 | Accepted: 21 May 2025

DOI: 10.1002/ecs2.70335

ECOSPHERE
AN ESA OPEN ACCESS JOURNAL

ARTICLE

Freshwater Ecology

Near-term lake water temperature forecasts can be used to anticipate the ecological dynamics of freshwater species

Ricardo Paíz[1] | **R. Quinn Thomas**[2,3,4] | **Cayelan C. Carey**[2,4] | **Elvira de Eyto**[5] | **Ian D. Jones**[6] | **Austin D. Delany**[2,4] | **Russell Poole**[5] | **Pat Nixon**[5] | **Mary Dillane**[5] | **Valerie McCarthy**[7] | **Suzanne Linnane**[1] | **Eleanor Jennings**[1]

[1]Centre for Freshwater and Environmental Studies, Dundalk Institute of Technology, Louth, Ireland

[2]Department of Biological Sciences, Virginia Tech, Blacksburg, Virginia, USA

[3]Department of Forest Resources and Environmental Conservation, Virginia Tech, Blacksburg, Virginia, USA

[4]Center for Ecosystem Forecasting, Virginia Tech, Blacksburg, Virginia, USA

[5]Fisheries & Ecosystem Advisory Services, Marine Institute, Mayo, Ireland

[6]Biological and Environmental Sciences, University of Stirling, Stirling, UK

[7]School of History and Geography, Dublin City University, Dublin, Ireland

Correspondence
Ricardo Paíz
Email: ricardo.marroquinpaiz@dkit.ie

Funding information
Division of Emerging Frontiers and Multidisciplinary Activities, Grant/Award Number: EF-2318861; Office of Advanced Cyberinfrastructure, Grant/Award Number: OAC-2209866; Directorate for Biological Sciences, Grant/Award Number: DBI-1933016; HORIZON EUROPE Marie Sklodowska-Curie Actions, Grant/Award Number: 956623

Handling Editor: Andrew L. Rypel

Abstract

Near-term ecological forecasting can be used to improve operational resource management in freshwater ecosystems. Here, we developed a framework that uses water temperature forecasting as a tool to predict the migrations of Atlantic salmon (*Salmo salar*) and European eel (*Anguilla anguilla*) between freshwater and the sea. We used historical observations of lake water temperature and fish migrations from an internationally important long-term monitoring site (the Burrishoole catchment, Ireland) to generate daily probabilistic predictions (0%–100%) of when relatively large numbers of fish migrate. For this, we produced daily lake water temperature forecasts that extended up to 34 days into the future using Forecasting Lake and Reservoir Ecosystems (FLARE), an open-source ensemble-based forecasting system. We used this system to forecast lake water temperature conditions associated with percentile-based fish migrations. Two metrics, P66 and P95, were used to indicate days with migrations in excess of 66% and 95%, respectively, of the historical daily fish counts. The results were first validated against water temperature observations, with an overall root mean squared error (RMSE) of 0.97°C. Our forecasts outperformed two other possible water temperature forecasting approaches, using site climatology (1.36°C) and site persistence (1.19°C). The predictions for fish migrations performed better for the P66 metric than for the more extreme P95 metric based on the continuous ranked probability score (CRPS), and the best results were obtained for the salmon downstream migration. This forecasting approach with quantified uncertainty levels has the potential to assist decision making, especially in the face of increased risks for these species. We conclude by discussing the scalability of the framework to other settings as a tool aimed at supporting management practices in real time.

This is an open access article under the terms of the Creative Commons Attribution License, which permits use, distribution and reproduction in any medium, provided the original work is properly cited.
© 2025 The Author(s). *Ecosphere* published by Wiley Periodicals LLC on behalf of The Ecological Society of America.

KEYWORDS
diadromous fish, ecological forecasting, lake modeling, probabilistic prediction, water management

INTRODUCTION

The biota of freshwater ecosystems is responding to an increasing range of human and climatic pressures (Priya et al., 2023), resulting in changes in behavior and ecology (Mishra et al., 2021; Staudinger et al., 2021). Such changes represent a challenge for environmental management because they are often unforeseen and straightforward mitigation or conservation measures cannot always be applied (Abbass et al., 2022; IPCC et al., 2023). Basing management actions on past conditions is becoming less reliable (Diffenbaugh, 2020; Nissan et al., 2019), especially as ecosystem dynamics become more variable, leaving managers with limited time to react (Foley et al., 2015). However, anticipating some of these alterations in ecosystem function is becoming possible through the application of near-term ecological forecasting systems (Bradford et al., 2020; Dietze et al., 2018). These types of systems generate forecasts (i.e., predictions of future environmental conditions with quantified uncertainty; Lewis et al., 2022) in operational time frames (e.g., monthly, weekly, daily, or sub-daily) and generally integrate data into workflows in near real time (i.e., as new data are collected through the use of automated sensors, wireless data transfer, and cyberinfrastructure), allowing for quick iterative generation of information (Carey et al., 2022).

Recent deployments of near-term ecological forecasting systems for predicting specific environmental variables, including water temperature, have successfully supported water management in a range of applications (e.g., drinking water supply, hydropower, and agriculture) (Kim & Ahn, 2022; Lofton et al., 2023; Saeed et al., 2024; Zwart et al., 2023). Water temperature is a key controller of many processes in the freshwater environment (Bonacina et al., 2023; Maberly et al., 2020) and one of the most monitored parameters in lakes and reservoirs worldwide (Peñas et al., 2023; Piccolroaz et al., 2024). This makes it a useful parameter for forecasting change in aquatic systems (Gumpinger et al., 2010; St-Hilaire et al., 2021). For example, water column mixing (turnover), the occurrence of algal blooms, and the sediment nutrient release in lakes/reservoirs are often associated with water temperature changes (Cai et al., 2023; Liu et al., 2023; Yin et al., 2023) and hence have been the focus of near-term forecasting in aquatic systems (e.g., Rousso et al., 2020; Schaeffer et al., 2024; Thomas et al., 2020). To date, however, there has been less focus on forecasting the dynamics of other, equally important, components of freshwater ecology, such as the biology of fishes (Slingsby et al., 2023).

Fishes are an important component of freshwater ecosystems globally (Tamario et al., 2019), and migratory species are of intrinsic social, cultural, and economic value to many societies (Gende et al., 2002; Oke et al., 2020). The life cycle timing (phenology) of fish migrating from freshwaters to the sea and vice versa (i.e., diadromous fish) has a direct impact on aquatic food webs (Dias et al., 2019; Ouellet et al., 2022), nutrient cycling (Oke & Hendry, 2019; Weaver et al., 2018), aquaculture (Ouellet et al., 2022; Vladic & Petersson, 2016), and hydropower (Carter et al., 2023; Knott et al., 2023). In general, diadromous fish migrations are driven by a combination of environmental factors, including temperature, flow conditions, photoperiod, and moonlight exposure (Lin, 2017; Sparks et al., 2019; Valiente et al., 2011). In particular, water temperature influences the metabolism and other physiological processes of fish directly (Seebacher & Post, 2015), resulting in pronounced effects on the timing and extent of migrations (Riley et al., 2012; Zydlewski et al., 2014). It, therefore, has potential as an explanatory variable on which to build a near-term migration forecast, especially in the face of an increasingly variable climate, which can induce shifts in the phenology of (but not limited to) diadromous fish (Legrand et al., 2021; Lowerre-Barbieri et al., 2019; Rinaldo et al., 2024).

Previous work on predicting or hindcasting diadromous fish migrations (e.g., Battin et al., 2007; Durif & Elie, 2008; Hobday et al., 2016; Jacox et al., 2020; Sykes et al., 2009; Teichert, Benitez, et al., 2020) has centered on recreating catchment flow conditions in specific settings with modeling approaches (e.g., statistical, process-based), often using long-term climate projections and incorporating multiple variables besides water temperature. However, most of those predictions are measured on a seasonal to annual scale, while management applications and conservation measures for these species could benefit from near-term forecasts (Roberts et al., 2023; Welch et al., 2019), which could be deployed using a lower number of variables (King et al., 2023; Teichert, Tétard, et al., 2020). Such an approach could be particularly applicable in sites with limited monitoring and/or in settings where fish migrations could be significantly impacted by human activities (e.g., dam and turbine operations) (Barbarossa et al., 2020; Carter et al., 2023).

21508925, 2025, 7, Downloaded from https://esajournals.onlinelibrary.wiley.com/doi/10.1002/ecs2.70335 by Ricardo Paíz - Dublin City University , Wiley Online Library on [11/08/2025]. See the Terms and Conditions (https://onlinelibrary.wiley.com/terms-and-conditions) on Wiley Online Library for rules of use; OA articles are governed by the applicable Creative Commons License

Here, we present a near-real-time framework that uses water temperature as a determinant of diadromous fish migrations. A daily automated ensemble-based forecasting system was developed to provide probabilistic predictions of fish migrations. This system was applied to Lough Feeagh (Burrishoole catchment, western Ireland), a site with long-term observation datasets of water temperature and daily diadromous fish migrations. Historical data (January 2004 to November 2020) were used to determine the lake temperature conditions associated with percentile-based migration regimes of two diadromous species: Atlantic salmon (*Salmo salar*) and European eel (*Anguilla anguilla*). We then combined the ensemble lake temperature forecasts and the percentile-based migration conditions to generate daily probabilistic predictions of future migrations, and we evaluated the prediction skill against the most recent fish monitoring records (November 2020 to November 2023).

Our study aimed to address the gap in near-real time forecasting of daily fish migrations by building a forecast for fish migration using a single explanatory variable that is both readily available in near real time and relatively straightforward to model (i.e., water temperature). We assessed this approach by first evaluating the water temperature forecasting system performance at our study site and second by quantifying forecast performance for the probabilistic predictions of the different fish migrations. We discuss the implications of the results within a freshwater resource management context. We highlight the potential benefits and limitations of the forecasting framework for real-world operational applications and how it might be a scalable tool in those settings.

METHODS

The framework of this study consisted of three main phases graphically presented in Figure 1, which also outlines the study site monitoring arrangement.

Study site

Lough Feeagh is a monomictic lake located in the Burrishoole catchment in western Ireland (53°56′ N, 9°35′ W). It is the largest water body (~3.95 km^2) in a system of lakes interconnected by river networks that discharge into the Atlantic Ocean (Figure 2). It holds a volume of ~6.0 × 10^7 m^3, with mean and maximum depths of 14.5 and 46.8 m, respectively. The Black and the Glenamong rivers are its primary inflows, and the Salmon Leap and the Mill Race water channels are its outflows. The climate in the area is temperate oceanic, with an average annual rainfall of 1700 mm year^{-1} and mean air temperature of 11°C (2004–2023).

Atlantic salmon (*S. salar*) and European eel (*A. anguilla*) fish species are endemic to the Burrishoole catchment and are key constituents of its aquatic food web (de Eyto et al., 2020). The migrations of these species to and from freshwater and the ocean are well documented (e.g., Byrne et al., 2003; de Eyto et al., 2022; Poole et al., 2018; Reed et al., 2017; Sandlund et al., 2017). In brief, salmon spawn in the Burrishoole catchment in winter, and juveniles spend a little over two years in freshwater. They migrate to the Atlantic Ocean as smolts in late spring, and after spending one winter at sea, they return to freshwater in the summer as mature adults to spawn. Current evidence supports the view that European eel spawn as a single spawning stock in the Atlantic Ocean in the area of the Sargasso Sea (Als et al., 2011). Juveniles arrive off the Irish coast in autumn and enter estuaries from November to February. As temperatures rise, many commence active migration into freshwaters as elvers. Once in freshwater, elvers grow into yellow eel, which is the life stage in which they spend most of their life (7–58 years in the west of Ireland). Eels mature only once when they undergo a process known as silvering before returning to the Atlantic Ocean to spawn, after which they die.

Water temperature monitoring

As part of an Automatic Water Quality Monitoring System (AWQMS) deployed in Feeagh, the water temperature has been measured at 13 different depths (0.9, 2.5, 5, 8, 11, 14, 16, 18, 20, 22, 27, 32, and 42 m) at a high frequency (2-min intervals) since 2004. The surface water temperature (0.9 m) is measured via a Hach Environmental Hydrolab Data Sonde X5 with an accuracy of ±0.1°C (UK OTT Hydrometry Ltd.; https://www.otthydromet.com), while the other 12 depths are measured via platinum resistance thermometers with an accuracy of ±0.2°C (UK Labfacility Ltd. PT100 1/10DIN 4 wire sensor; http://labfacility.com), enabling a complete vertical profile reading. The sensors are cleaned monthly, and the multiparameter probe is calibrated once per month (de Eyto et al., 2016).

Water temperature data from the AWQMS that had undergone appropriate quality assurance/quality control (QA/QC) were obtained from the Marine Institute monitoring web services (http://marine.ie). Data from 2004 to 2023 were used in this study, together with the volumetric percentage of lake water corresponding to each depth (Marine Institute, 2017). Lake thermal stratification in Feeagh was defined as the difference

21508925, 2025, 7, Downloaded from https://esajournals.onlinelibrary.wiley.com/doi/10.1002/ecs2.70335 by Ricardo Pérz - Dublin City University , Wiley Online Library on [11/08/2025]. See the Terms and Conditions (https://onlinelibrary.wiley.com/terms-and-conditions) on Wiley Online Library for rules of use; OA articles are governed by the applicable Creative Commons License

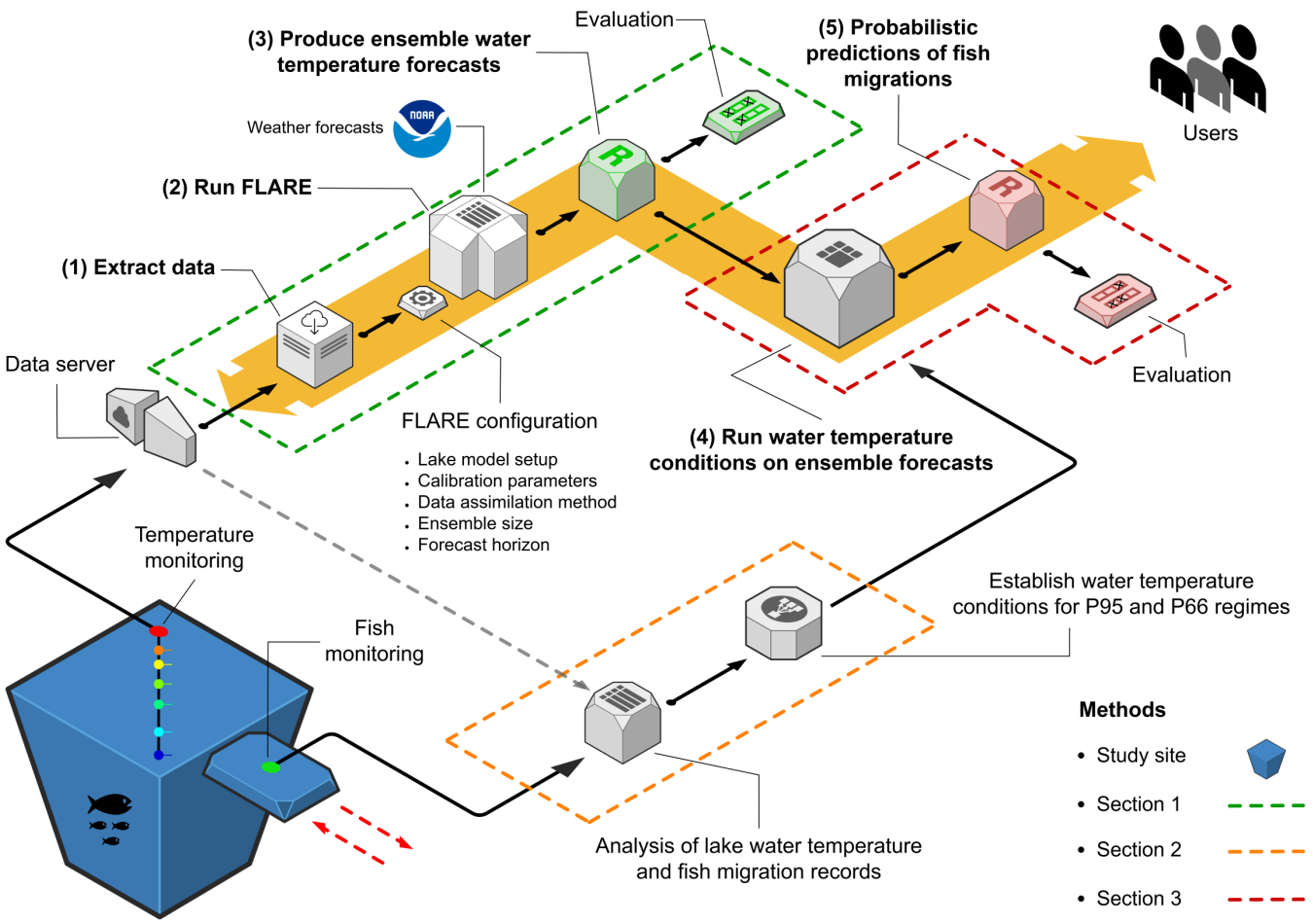


FIGURE 1 Flow diagram of the forecasting framework structure. The framework contains three main phases indicated by dashed lines (see key). The automated components of the framework are indicated by five iterative steps denoted in boldface alongside a continuous solid yellow arrow. Illustration credit: Ricardo Paíz. FLARE, Forecasting Lake and Reservoir Ecosystems.

of >1°C between the surface (0.9 m) and bottom (42 m) lake temperatures (Woolway et al., 2020).

Fish monitoring

Three fish migration datasets from 2004 to 2023 (matching the water temperature monitoring data period) were used in this study: (1) daily downstream (juvenile smolt) and (2) daily upstream movements (adults) of Atlantic salmon; and (3) daily downstream movements of maturing adult European "silver" eel.

All fish moving into and out of the catchment were counted at two sites, the Salmon Leap and the Mill Race, the two water channels connecting freshwater Feeagh with the downstream brackish lagoon, Lough Furnace, which leads directly to the Atlantic Ocean through Clew Bay (Figure 2). The daily counts were performed manually using permanent whole river upstream and downstream fish traps and are part of long-term monitoring efforts that record the transition of fish migrations between the freshwater and marine domains (de Eyto et al., 2022; Long et al., 2023). The fish traps follow a Wolf type trap design employing horizontal grids with 10-mm gaps on a 1:10 inclination (Poole et al., 2018; Wolf, 1951). Trapping at the catchment involves a fish fence and wolf trap on the Mill Race outflow installed in 1958 and a full flow controlled Wolf trap on the Salmon Leap outflow installed in 1970 (see Poole et al., 2018 for more details).

Water temperature forecasting

We deployed the Forecasting Lake And Reservoir Ecosystems system (FLARE) to generate daily water temperature forecasts in Feeagh for three years (1 November 2020 to 1 November 2023; 1095 days). FLARE is an open-source system for lake and reservoir water quality forecasting aimed at supporting management (Carey

21508925, 2025, 7, Downloaded from https://esajournals.onlinelibrary.wiley.com/doi/10.1002/ecs2.70335 by Ricardo Paíz - Dublin City University , Wiley Online Library on [11/08/2025]. See the Terms and Conditions (https://onlinelibrary.wiley.com/terms-and-conditions) on Wiley Online Library for rules of use; OA articles are governed by the applicable Creative Commons License

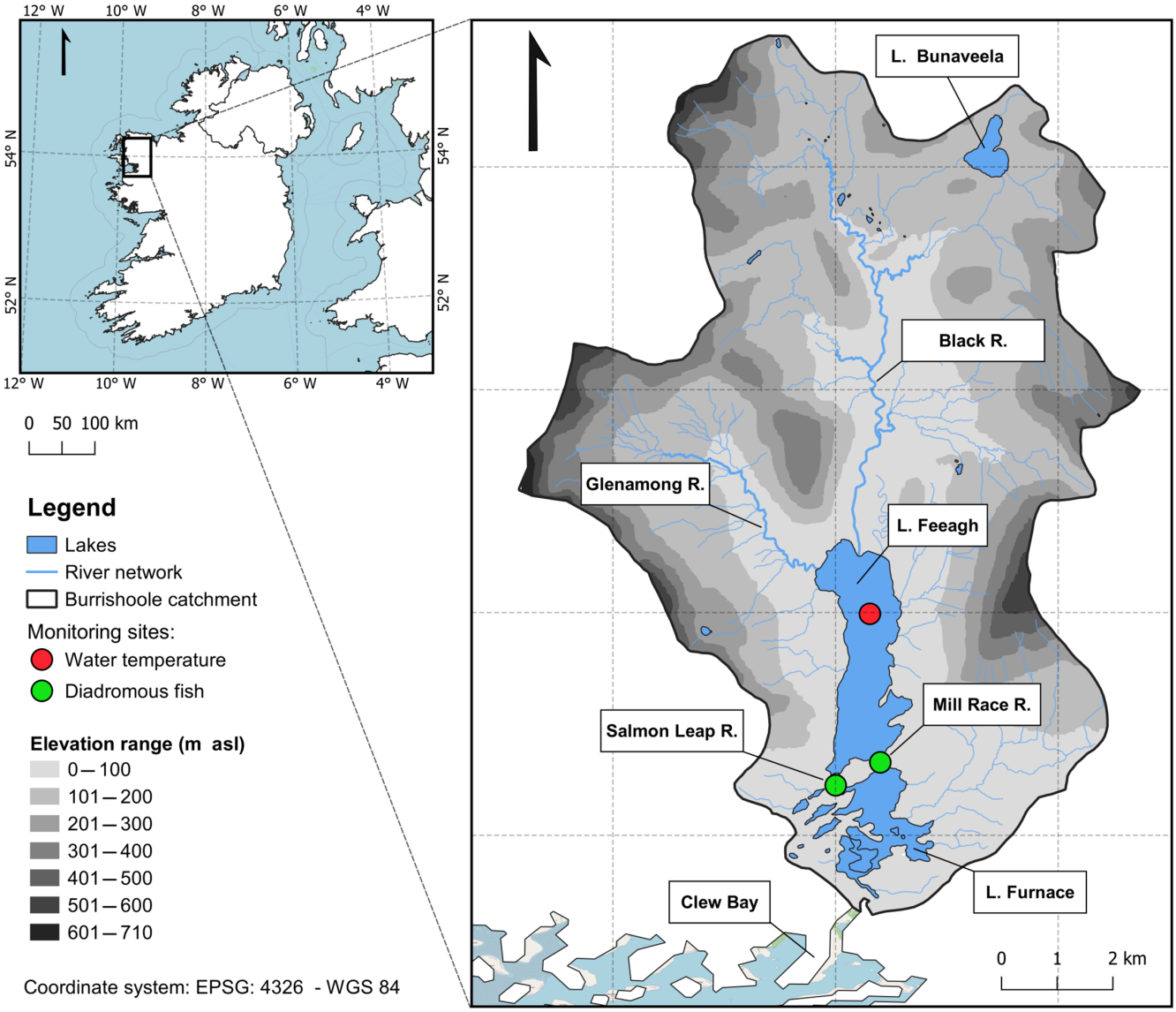


FIGURE 2 Location of Lough Feeagh and the Burrishoole catchment in western Ireland, including main water bodies and topographic elevation in meters above sea level (m asl). The monitoring sites for water temperature and fish are indicated by red and green dots, respectively.

et al., 2022; Thomas et al., 2020). By integrating real-time monitoring, hydrodynamic modeling with data assimilation, and an ensemble-based forecasting algorithm, FLARE provides daily water quality forecasts for multiple lake/reservoir depths with a forecast horizon of up to 35 days with quantified uncertainty (Thomas et al., 2020, 2023; Wander et al., 2024). To date, several FLARE-based forecasting systems have been deployed to provide predictions of different water quality variables, for example, water temperature, dissolved oxygen, and chlorophyll *a* (Carey et al., 2022; Thomas et al., 2023; Wander et al., 2024; Woelmer et al., 2022, 2024).

FLARE uses the General Lake Model (GLM) (Hipsey et al., 2019), a widely used one-dimensional (1-D) model, as the process model to generate predictions for each ensemble member. GLM has been previously applied to Feeagh in non-forecasting studies (Bruce et al., 2018; Mesman et al., 2020). We used the 31-member National Oceanic and Atmospheric Administration Global Ensemble Forecasting System (NOAA GEFS) (https://www.ncei.noaa.gov) (Hamill et al., 2022) output for the grid cell that contains Feeagh as the forcing weather forecast ensemble. FLARE quantifies uncertainty by adding random noise to each FLARE ensemble member (process uncertainty), assigning one of the 31 members of the weather forecast ensemble to each FLARE ensemble member (driver uncertainty) and having different parameter values for each FLARE ensemble member (see Wander et al., 2024, for more details). FLARE uses data

21508925, 2025, 7, Downloaded from https://esajournals.onlinelibrary.wiley.com/doi/10.1002/ecs2.70335 by Ricardo Paiz - Dublin City University , Wiley Online Library on [11/08/2025]. See the Terms and Conditions (https://onlinelibrary.wiley.com/terms-and-conditions) on Wiley Online Library for rules of use; OA articles are governed by the applicable Creative Commons License

assimilation (specifically the Ensemble Kalman Filter with state augmentation) to calibrate the parameter values and set the spread of the ensemble when each forecast was initiated (day 0 of the forecast).

Configuration

FLARE was configured based on previous applications of the system (Thomas et al., 2020, 2023; Wander et al., 2024). First, we configured GLM for Feeagh with the bathymetry used in previous model applications at the site (Mesman et al., 2020). Second, we configured FLARE-specific settings for water temperature forecasting. The number of FLARE forecast ensemble members was set to 248 to avoid erroneous data correlations that can arise when using smaller ensembles (Wander et al., 2024); so that each of the 31 weather forecast ensemble members was used eight times to drive the lake model, with each having slightly different process noise, parameters, and initial conditions (following Thomas et al., 2020). Details on the GLM configuration and FLARE water temperature forecasting configuration for Feeagh can be found in Appendix S1.

Infrastructure

To make FLARE functional in real time at Feeagh, we developed an infrastructure that runs in the cloud and interconnects the framework system with the extraction of field observations to generate forecasts (see Figure 1).

For each day that a forecast is generated, first, we extracted the most recent water temperature monitoring data from a local data server using an R script (see Appendix S1). This script was automatically run in a public GitHub repository via a scheduled GitHub Action (.yml file). These data were collated into daily mean water temperature values for each monitoring sensor and stored in a single target file in the same repository. This target file was updated every time the action ran. The FLARE workflow was then run in the same repository using an R script with the "FLAREr" R package via a scheduled GitHub Action (.yml file). The target file with the new observations was acquired within the workflow before a forecast generation, allowing FLARE to perform data assimilation as specified in the configuration. The resulting water temperature forecasts were collated by several filters, including depth, ensemble member, date, and forecast horizon, and were allocated into columnar storage data format files (.parquet) (see Appendix S1).

Evaluation

We evaluated the performance of the lake water temperature forecasts against observations based on root mean square error (RMSE; see Appendix S1). RMSE is commonly used to assess the accuracy of water temperature predictions in many forecasting applications (Feigl et al., 2021; Qiu et al., 2021), including other FLARE deployments (Thomas et al., 2023; Wander et al., 2024). The evaluation was carried out for the volume-averaged lake water temperature calculated using the 13 monitoring depths (hereafter referred to as average lake water temperature) and for each monitored depth. RMSE values were computed for all 1–34 forecast horizon days over the entire forecasting period (excluding the time from 1 January to 9 May 2021 when no observations were available). The results were averaged for each forecast horizon day and for FLARE (overall performance calculated by aggregating all FLARE forecasts produced, i.e., all average lake water temperature forecasts and all individual depth forecasts).

We compared the performance of FLARE to (1) site persistence and (2) site climatology. Predictions based on both persistence and climatology have been widely used in environmental science as they are relatively easy to generate (Murphy, 1992) and provide an important baseline that enables the performance of new forecasting systems to be contextualized (Bento et al., 2022; Brown et al., 2018; Thomas et al., 2020; Yang, 2019; Zachow et al., 2023). Persistence predictions were based on the assumption that future water temperature conditions will be the same as the recent past (Wilks, 2019), that is, they would vary depending on the forecast horizon. For example, a persistence forecast set with a 16-day forecast horizon and produced on date d will use the observed water temperature on date $d-1$ as a prediction, extending that value over the next 16 days. Climatology predictions were based on long-term average conditions of lake water temperature so that the historical average of a specific day in a year is indicative of the water temperature for the same day in the future. A climatology forecast produced for 18 March 2021 will, for example, be equal to the average water temperature of Feeagh on that same day (18 March) in the historical records (2004–2020).

Lastly, we generated a reliability diagram to evaluate how well the uncertainty was characterized for the water temperature forecasts (Thomas et al., 2020; Zwart et al., 2023) by quantifying proportions of observations within different confidence intervals (CIs) (10th, 25th, 50th, 75th, and 90th) for different forecast horizons (1, 7, 14, 21, 28, and 34 days ahead). An ideally calibrated forecasting system would have 10% observations

21508925, 2025, 7, Downloaded from https://esajournals.onlinelibrary.wiley.com/doi/10.1002/ecs2.70335 by Ricardo Paíz - Dublin City University , Wiley Online Library on [11/08/2025]. See the Terms and Conditions (https://onlinelibrary.wiley.com/terms-and-conditions) on Wiley Online Library for rules of use; OA articles are governed by the applicable Creative Commons License

within the 10% forecast CI (the range containing the middle 10% of the ensemble distribution), 25% observations in the 25% forecast CI (the range containing the middle 25% values of the ensemble distribution), etc. If the percentage of observations within its given CI is higher or lower, the forecasting would be considered underconfident or overconfident, respectively (Bröcker & Smith, 2007).

Historical analysis: Fish migrations and water temperature

To relate the fish migrations with lake water temperature, we consulted research on which water temperatures have been linked to diadromous fish migrations. This indicated that (1) ambient water temperatures and (2) cumulative water temperature values have a strong role in triggering the timing and extent of diadromous migrations (e.g., Riley et al., 2012; Sparks et al., 2019; Sykes et al., 2009; Zydlewski et al., 2005, 2014). Therefore, we used both temperature metrics as hydrologic controls of daily fish runs of Atlantic salmon and European eel migrations. Note that daily fish runs refer to fish migrations occurring in a day.

Cumulative lake water temperature is a function of the start date chosen and is calculated by integrating the daily average temperatures over time during an annual cycle, starting from 0°C. In contrast to related metrics such as degree days and growing degree days, cumulative water temperature simply accumulates daily temperature magnitudes, rather than considering differences from a baseline value (which can be a specific threshold or 0°C) or between daily values. Zydlewski et al. (2005, 2014) defined the start of cumulative temperatures on 1st January. By contrast, Riley et al. (2012) defined the start using two dates, 21 December (winter solstice) and 15 February, and found a better correlation for the latter date which was attributed to the proximity of their migrations to that time (15 March). Similarly, Sykes et al. (2009) defined the start on 9 March and found a strong correlation with salmon smolt migrations (which started in April). Here, we defined 1 March as the start of the cumulative temperatures for Feeagh, as this date indicates the beginning of spring in Ireland, the season when temperatures start to rise and when salmonids start to manifest strong migratory behavior (de Eyto et al., 2022).

Daily observed values of average lake water temperature in degrees Celsius and average lake cumulative temperature in degrees Celsius-days were computed for Feeagh. These were compared with datasets for all three diadromous fish migrations, matching daily fish counts from January 2004 to November 2020. Then, two sub-datasets were created by extracting values based on two daily fish count percentiles, respectively: 95th (P95) and 66th (P66). These metrics were selected to represent two different regimes for the number of fish going through the traps each day for each species. P66 and P95, therefore, indicate days when daily counts are in excess of 66% and 95%, respectively, of the historical daily fish count records. With these two metrics, we aimed to identify two distinct regimes where the number of fish migrating was likely to be high (P66) and very high (P95; indicative of extreme events). Both P66 and P95 indicate meaningful regimes of migration intensities with implications for applied management that could require important resources to ensure safe fish passage.

On each of these sub-datasets, we performed a symmetric outlier reduction (5% trim) on the driver data (i.e., the lake water temperatures and cumulative lake water temperatures) to focus on the central tendency of the migrations (Benhadi-Marín, 2018; Osborne & Overbay, 2004; Xu, Mazur, et al., 2020). Then, for each sub-dataset, we extracted the minimum and maximum values of the two water temperature metrics, respectively. As a result, we obtained (1) a range of daily lake water temperatures and (2) a range of daily lake cumulative water temperatures for each fish migration regime. These ranges were then used as the start and end points for the specific lake water temperature conditions necessary for the different fish migrations to occur, notwithstanding that we recognize that other controlling factors, including photoperiod, moon phase and water flow, also play a role (Byrne et al., 2003; Sandlund et al., 2017).

Probabilistic forecasting of fish migrations

Using both the lake water temperature forecasts produced and the lake water temperature ranges established, we generated daily probabilistic predictions for each fish migration regime for the period 1 November 2020 to 1 November 2023. For the generation of each fish migration prediction, we used the nowcasted lake average water temperature instead of using temperature observations from individual sensors. We used this approach for simplicity and also to support future scaling to other lake ecosystems.

First, we calculated a daily value for forecasted lake cumulative water temperatures from the daily forecasted lake water temperatures (both collated by forecast horizon, 1–34 days ahead; and ensemble member, 1–248). Then, to generate the probabilistic predictions for a specific fish migration regime (e.g., P66 salmon downstream), we assessed when both water temperature conditions were met. For each day, the percentage of the 248 ensemble members that (1) fell within the maximum–minimum

21508925, 2025, 7, Downloaded from https://esajournals.onlinelibrary.wiley.com/doi/10.1002/ecs2.70335 by Ricardo Pérz - Dublin City University , Wiley Online Library on [11/08/2025]. See the Terms and Conditions (https://onlinelibrary.wiley.com/terms-and-conditions) on Wiley Online Library for rules of use; OA articles are governed by the applicable Creative Commons License

range for the lake water temperature condition and (2) also fell within the maximum–minimum range for the cumulative lake water temperature condition represented the daily probability of that fish migration regime occurring. Consequently, we were able to obtain daily probabilistic predictions, in the order of 0%–100%, for each forecast horizon (i.e., 1- to 34-day-ahead probabilistic predictions per fish migration regime). Our modeling approach, therefore, predicts fish migrations based solely on lake water temperature variation. Similar to other models (e.g., Sykes et al., 2009; Teichert, Tétard, et al., 2020), our forecasting framework does not account for any fish stock number in the catchment before and after a model prediction. An illustrative example of a daily output of the forecasting framework showing an average lake water temperature forecast, an average cumulative lake water temperature forecast, and probabilistic predictions for the P66 and P95 regimes of the Atlantic Salmon downstream migration are presented in Figure 3.

Evaluation

We evaluated the performance of the probabilistic predictions for the fish migrations against the most recent fish monitoring data based on the continuous ranked probability score (CRPS). CRPS measures both the precision and accuracy of our probabilistic forecasts by comparing them to observations (Bröcker, 2012; Taillardat et al., 2023). A lower CRPS value indicates a higher performing forecast with a smaller error margin (see Appendix S1 for more details). The evaluation was carried out for all 1–34 forecast horizon days over the entire forecasting period (November 2020 to November 2023), and the results were averaged for each forecast horizon day. Only the observed daily fish runs equal to or exceeding historical P66 and P95 runs were used for the P66 and P95 regime CRPS evaluations, respectively, and represented percentage values of 100% against the probabilistic predictions (the rest were treated as 0%).

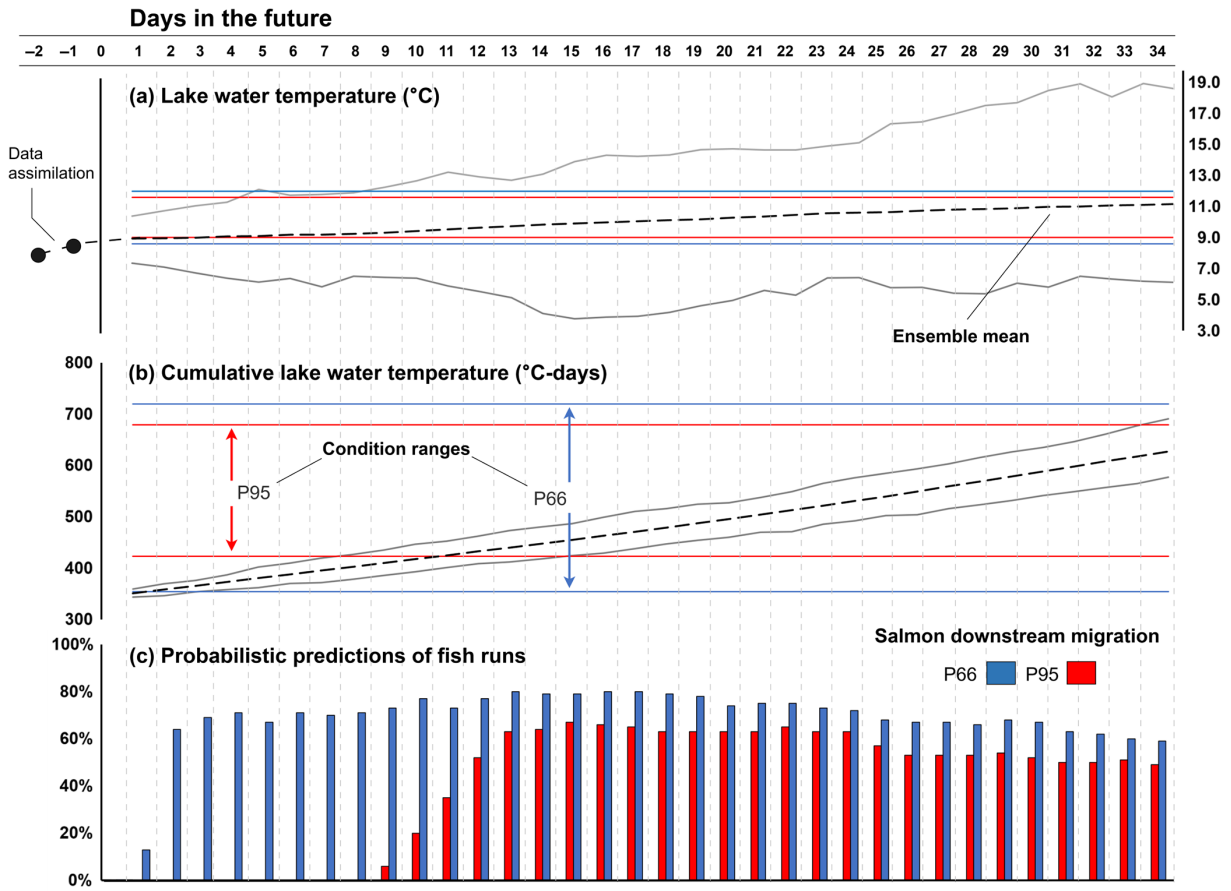


FIGURE 3 Illustrative example of a daily output of the forecasting framework containing (a) an average lake water temperature forecast, (b) an average cumulative lake water temperature forecast, and (c) probabilistic predictions of the P66 and P95 regimes for the Atlantic salmon downstream migration. The red and blue bands in panels (a) and (b) indicate the lake water temperature conditions necessary for the P66 and P95 regimes to occur, respectively. The two black dots in panel (a) represent measured water temperature observations used for data assimilation. The continuous gray lines around the ensemble mean (dotted black line) in panels (a) and (b) denote the 95% CI uncertainty of the temperature forecasts. Illustration credit: Ricardo Paíz.

21508925, 2025, 7, Downloaded from https://esajournals.onlinelibrary.wiley.com/doi/10.1002/ecs2.70335 by Ricardo Paíz - Dublin City University , Wiley Online Library on [11/08/2025]. See the Terms and Conditions (https://onlinelibrary.wiley.com/terms-and-conditions) on Wiley Online Library for rules of use; OA articles are governed by the applicable Creative Commons License

RESULTS

Water temperature observations

The observed average lake temperatures in Feeagh exhibited relatively stable dynamics during both the historical period (January 2004 to November 2020) and the forecasting period (November 2020 to November 2023), ranging from 3.5 to 16.5°C (average of 10.7°C) (Figure 4). Peak temperatures and thermal stratification were observed typically from April to September (spring and summer). Conversely, mixed lake conditions presenting the lowest water temperatures prevailed from October to March (autumn and winter) (see Appendix S2: Figure S1 for water temperature measurements at each monitoring depth). Throughout the forecasting period, the lake exhibited thermal stratification 44% of the time (486/1095 days) and mixed conditions 56% of the time (609/1095 days).

Water temperature forecasts

The overall RMSE performance for all forecasts produced using FLARE (for all 13 individual depths and the average lake water temperature aggregated across all 1- to 34-day-ahead horizons) over the three-year forecasting period was 0.94°C. The climatology and persistence forecasts performed worse than FLARE, with overall values of 1.36 and 1.19°C RMSE, respectively.

For the surface temperature only, the RMSE values of the FLARE temperature forecasts consistently increased as the forecast horizon became longer (indicating a

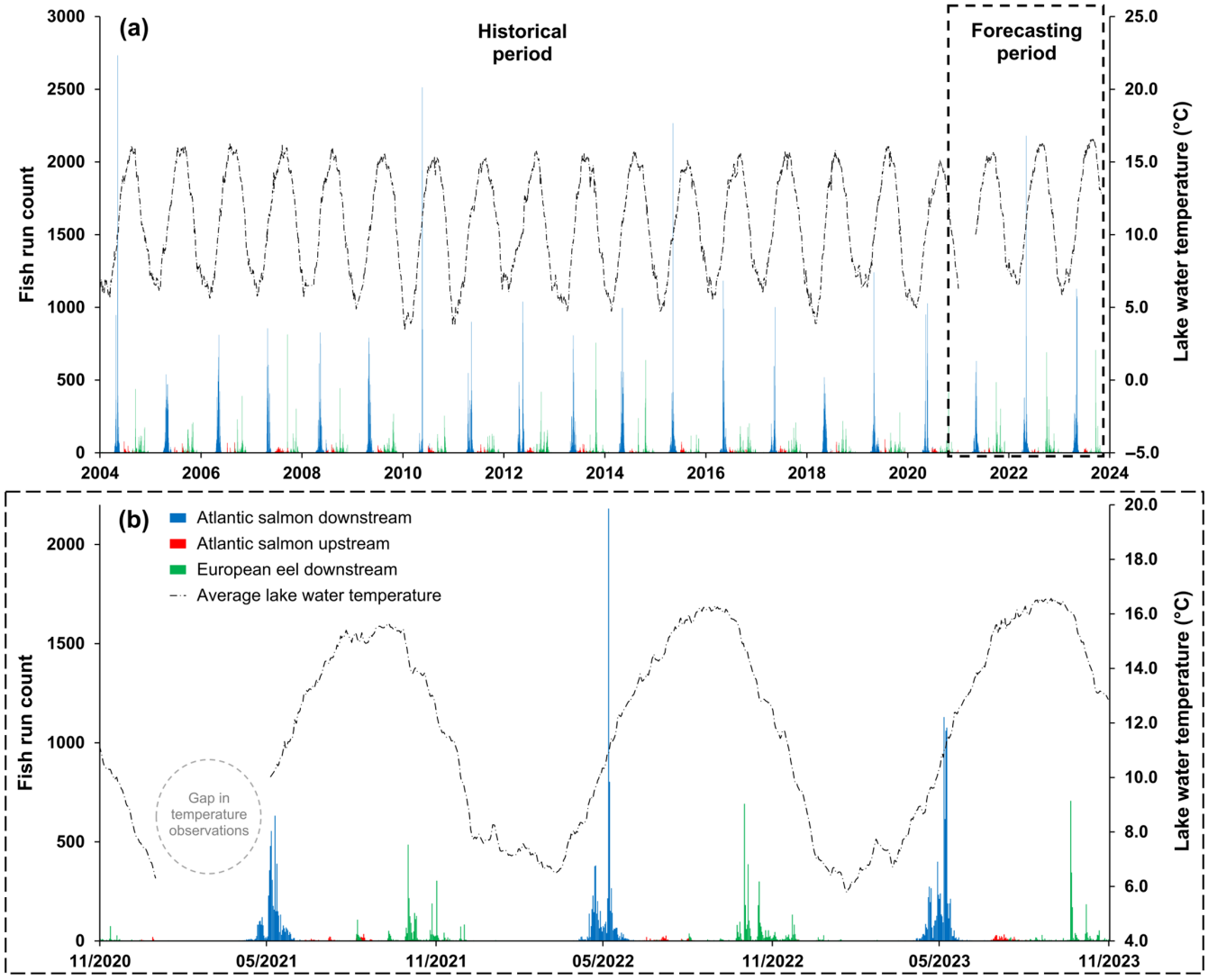


FIGURE 4 Measured average water temperature observations in Lough Feeagh and daily fish counts of Atlantic salmon downstream, Atlantic salmon upstream, and European eel downstream migrations in the Burrishoole catchment. The observed data within the forecasting period (black dashed box) in (a) is highlighted in greater detail in (b).

21508925, 2025, 7, Downloaded from https://esajournals.onlinelibrary.wiley.com/doi/10.1002/ecs2.70335 by Ricardo Paiz - Dublin City University , Wiley Online Library on [11/08/2025]. See the Terms and Conditions (https://onlinelibrary.wiley.com/terms-and-conditions) on Wiley Online Library for rules of use; OA articles are governed by the applicable Creative Commons License

decrease in performance), from 0.30 to 1.58°C (Figure 5a). Climatology surface temperature forecasts, with an RMSE of 1.41°C, were outperformed by FLARE on the first 28 of 34 forecast horizon days. Persistence forecasts for the surface temperature ranged from 0.34 to 1.96°C and were consistently outperformed by FLARE on all forecast horizon days. The average lake water temperature forecasts using FLARE performed slightly better than the surface temperature forecasts, with RMSE values ranging from 0.20 to 1.34°C (Figure 5b). Climatology average lake water temperature forecasts, with an RMSE of 1.10°C, were outperformed by FLARE on the first 21 of 34 forecast horizon days. Persistence forecasts for the average lake water temperature ranged from 0.20 to 1.59°C and performed similarly to FLARE on the first 21 forecast horizon days, but then, they were outperformed by FLARE on days 21–34. Typically, FLARE predictions produced during lake mixed conditions were more accurate than those produced during stratified conditions (Figure 5).

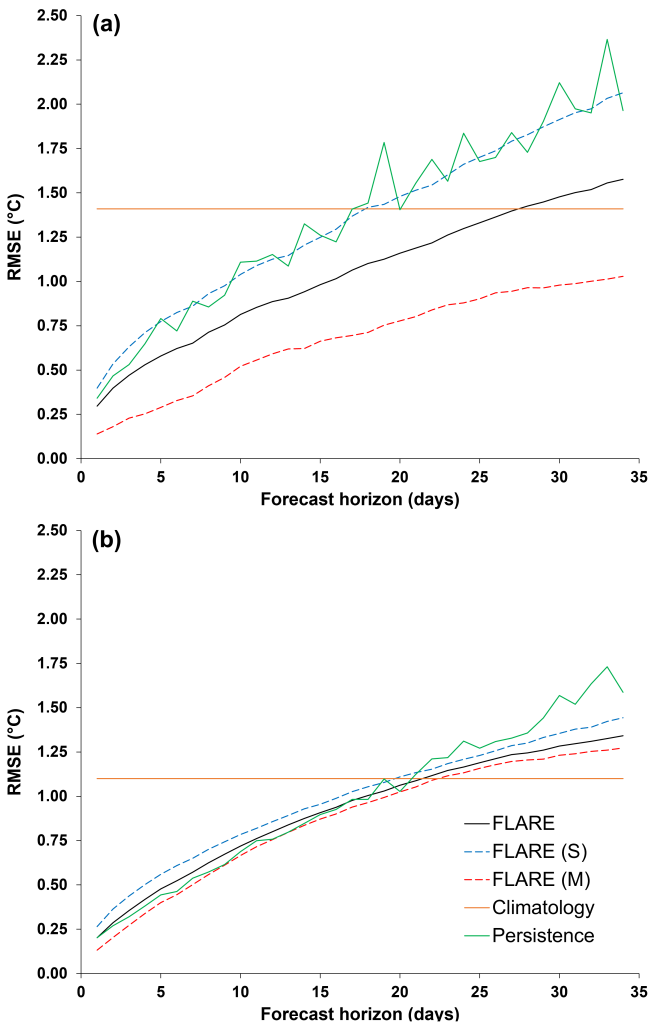


FIGURE 5 Root mean square error (RMSE) of the (a) surface lake water temperature (0.9 m) and (b) average lake water temperature forecasts produced over the entire forecasting period. Forecasting Lake and Reservoir Ecosystems (FLARE) (S) and FLARE (M) represent FLARE RMSE values for forecasts produced under stratified and mixed lake conditions, respectively. Climatology and persistence indicate RMSE performance for forecasts produced using their respective approaches.

Moreover, forecast uncertainty was well characterized by FLARE for all forecasts produced in Feeagh (forecasts for average lake water temperature and each monitoring depth). Relatively small variations in confidence from an ideal forecast were observed, although these varied depending on the forecast horizon length (Figure 6). On short to intermediate forecast horizons (<21 days ahead), FLARE predictions were mostly underconfident by up to 16%. In longer forecast horizons (>28 days ahead), the uncertainty estimates fluctuated from more confidence (up to −9%) to less confidence (up to 6%).

Fish migration dynamics

The fish migrations during the historical period (January 2004 to November 2020) exhibited a day-sensitive phenological behavior with substantial differences in magnitudes and regime timings (Figure 4; Table 1). On average, 90 juvenile smolt Atlantic salmon moved downstream per day during fish runs (median of 14), with a maximum count of 2733 observed in a single day (7 May 2004). The P66 and P95 numbers of salmon migrating downstream were 39 and 431 fish, respectively. Salmon began to go downstream around April, coinciding with rising lake water temperatures (Figure 4). Their migratory behavior decreased in mid-May and generally ceased after June. The maximum count of adult salmon migrating upstream was 92 individuals (18 July 2019), with an average of 7 fish (median of 3). The P66 and P95 for the daily upstream migration of salmon were 6 and 27 fish. The counts were more sporadic than daily counts of downstream migrating salmon. Salmon started to migrate upstream in June, sometimes overlapping with the end of the downstream migration movements. The fish runs of salmon going upstream decreased usually around October, but some counts extended till December.

In contrast to Atlantic salmon, the core of European eel migrations took place when there was a decreasing trend in lake water temperatures (Figure 4). The daily average for the number of adult eel migrating was 18 individuals (median of 5). The maximum count was 813 (17 September 2007). The P66 and P95 daily downstream migrations were 9 and 80 eels, respectively. Downstream migrations of eel were recorded all year round. However, the highest numbers (in the order of the P95) were recorded between

21508925, 2025, 7, Downloaded from https://esajournals.onlinelibrary.wiley.com/doi/10.1002/ecs2.70335 by Ricardo Paíz - Dublin City University , Wiley Online Library on [11/08/2025]. See the Terms and Conditions (https://onlinelibrary.wiley.com/terms-and-conditions) on Wiley Online Library for rules of use; OA articles are governed by the applicable Creative Commons License

August and November. The P66 and P95 metrics established for all three fish migrations were representative of all annual cycles of the 17 years of the historical period of this study (Appendix S2: Figure S2).

Water temperature conditions for fish migrations

In general, all six fish migration regimes (P66 and P95 for all three migrations) required the lake water temperatures to be temperate to warm (8.8–15.9°C), with the ranges for the P95 regimes generally being narrower than those for the P66 regimes (Table 2). The widest ranges were for eel downstream, reflecting the longer period over which that migration occurred. The salmon upstream migration coincided with the warmest lake water temperatures. By contrast, colder temperatures were associated with the two downstream migrations, with lower range limits in the order of 9.0°C (Table 2). These low temperatures aligned with the onset and end of winter, when eel migration terminated and salmon downstream migration started, respectively.

The cumulative lake water temperature conditions differed for the three different fish migrations. The salmon downstream migration occurred over small and well-constrained ranges of cumulative lake water temperatures for both regimes. By contrast, much larger and broader ranges of cumulative lake water temperatures were associated with the salmon upstream and eel downstream migrations (Table 2).

Probabilistic predictions of fish migrations

Using predictions of Atlantic salmon downstream migration for 2021 as an example, the P95 regime predictions generally extended before and after the observed P95 fish runs; however, the observed P66 fish runs were well captured by the forecasts (Figure 7; Appendix S2: Figures S3–S8). Predictions for shorter horizons displayed relatively large fluctuations in value before and after observed fish run counts reflecting that not only the general block of migrations could be captured but also a degree of day-to-day variations. For instance, European eel predictions for short horizons (<8 days ahead) displayed much lower probabilities prior to observed events than during events (Appendix S2: Figures S7–S8). Another clear difference among the probabilistic predictions for the different forecast horizons was the order of percentage magnitude, which decreased on average with the horizon (Appendix S2: Figure S9).

In general, the P66 regime probabilistic predictions for all three fish migrations performed better, with lower CRPS values, than those for the P95 regimes (Figure 8).

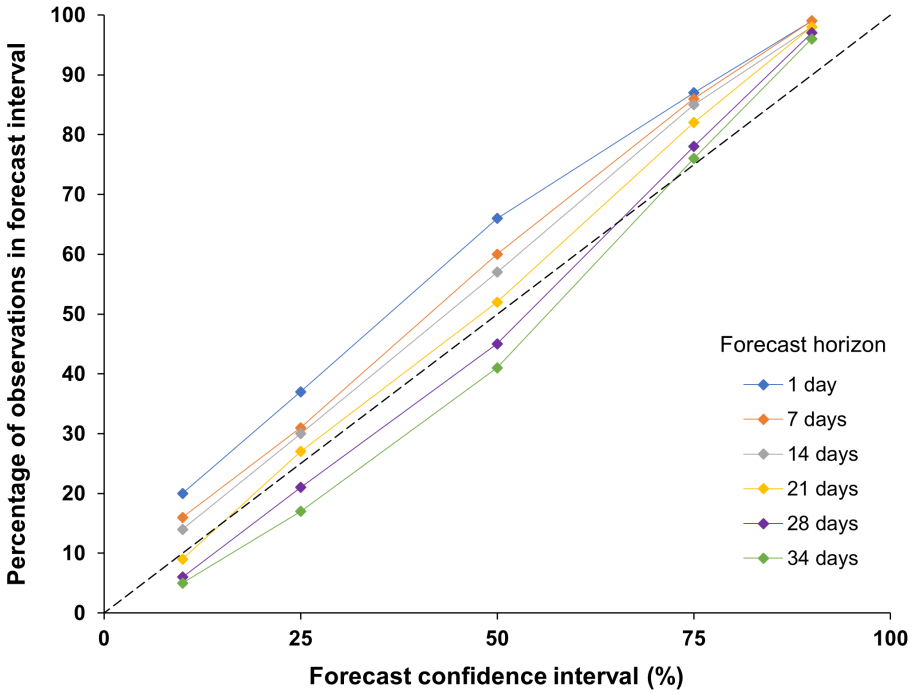


FIGURE 6 Reliability diagram for all lake water temperature forecasts produced by Forecasting Lake and Reservoir Ecosystems over the entire forecasting period. The percentage of lake water temperature observations within different forecast CIs is indicated for different forecast horizons. The continuous black dotted line represents ideal forecast confidence calibration (i.e., a forecasting system that perfectly characterizes uncertainty; 1:1 relationship between forecast CI and the percentage of observations within it).

21508925, 2025, 7, Downloaded from https://esajournals.onlinelibrary.wiley.com/doi/10.1002/ecs2.70335 by Ricardo Paiz - Dublin City University , Wiley Online Library on [11/08/2025]. See the Terms and Conditions (https://onlinelibrary.wiley.com/terms-and-conditions) on Wiley Online Library for rules of use; OA articles are governed by the applicable Creative Commons License

The predictions for the salmon downstream migration performed best, starting at a CRPS of 5% followed by a generally linear trend (Figure 8a). However, the score was still under 11% at the end of the forecast. The upstream migration for salmon had the widest range of CRPS values, increasing from 9% to 18% over the forecast. The P66 predictions for eel performed more stably, with CRPS starting at 8% but then remaining at about 12% from 5 days ahead. By contrast, the performance of the P95 regime predictions across the forecast horizon was not as good. Higher CRPS values were obtained of up to 31% (Figure 8b). The predictions for eel were the best in this regime, with a narrow CRPS range of values from 13% to 16%. The CRPS values for the two salmon migrations increased steeply in very short horizons (<5 days ahead) and then continuously decreased.

DISCUSSION

Accurate ecological forecasts and associated uncertainty have the potential to aid management in an increasingly uncertain world, including decisions on the allocation of resources for fish monitoring programs. Our study shows that the FLARE system accurately replicated lake temperature dynamics in our study lake, which we used to produce reasonable probabilistic predictions for three fish migrations up to 34 days into the future, with the best results being for the P66 regime of Atlantic salmon downstream migration (Figure 7; Appendix S2: Figure S3). Enhancing decision making in freshwater management with such forecasts has the potential to yield not only environmental but also economic benefits as it can allow more appropriate allocation of human and economic resources (Baker et al., 2020; Franklin et al., 2024; Xu, Yang, et al., 2020). A forecast of fish migration with associated probability produced today for the subsequent 7- to 10-day period, for example, could allow an operator to plan resource allocation in advance. This could be particularly relevant for lakes and reservoirs that provide different services (e.g., navigation, drinking water supply, flood control, hydropower, aquaculture), where more informed daily or sub-daily scale operations could enhance the protection of diadromous fish (Carter et al., 2023; Harris et al., 2016; Norman et al., 2023).

Although our example was for a catchment with a relatively low degree of human intervention, the approach is transferable to catchments where daily management of fish migrations is considered crucial to their survival (Bolstad et al., 2021; Ouellet et al., 2022). With informed fish migration regime forecasts, various mitigation measures can be evaluated for improved conservation of diadromous fish. Forecasts for relatively short horizons (e.g., <14 days ahead) could enhance daily-scale actions, such as the operation of fish bypass structures in drinking water reservoirs (Piper et al., 2013; Song et al., 2019), scheduling of dam releasing in flood control (Katopodis & Williams, 2012; Trancart et al., 2020), and periodic pumping and turbine shutdowns in hydropower (Carter et al., 2023; Nyqvist et al., 2017), all of which could enable safer passages for fish. Forecasts for longer horizons (e.g., >14 days ahead) could be more relevant for (but not limited to) the control of nature-like fishways (Steffensen et al., 2013), planning of fishing timing in aquaculture (Gargan et al., 2015; Harringmeyer et al., 2021), and routine operation of fish traps/racks in monitoring and research (Piper et al., 2020; Ruokonen et al., 2022). In addition, having future predictions of fish moving in and/or out of the systems could enable the estimation of fish counts in situations and periods where direct counting is not feasible due to restrictions on environmental factors (e.g., flow conditions) and other limitations (e.g., staff, funds).

While many studies have simulated diadromous fish migrations, there are few that have developed true forecasts with quantified uncertainty, especially on a daily time scale. By using lake water temperature as a core variable, our study expands the available pool of near-term ecological forecasting tools for predicting fish migrations (e.g., King et al., 2023; Teichert, Tétard, et al., 2020; two previous frameworks that were developed using river

TABLE 1 Average, median, maximum, P66, and P95 regime fish run counts for the Atlantic salmon downstream, Atlantic salmon upstream, and European eel downstream migrations in the Burrishoole catchment during the historical period of this study, January 2004 to November 2020 ($n = 6150$).

	Atlantic salmon		European eel,
Metric	Downstream	Upstream	downstream
Average fish run count	90	7	18
Median fish run count	14	3	5
Maximum fish run count	2733	92	813
P66 fish run count	39	6	9
P66 time frame	April to July	June to December	January to December
P95 fish run count	431	27	80
P95 time frame	April to May	June to September	August to November

Note: The P66 and P95 time frames indicate the earliest and latest months in a year when the P66 and P95 fish runs have been counted, respectively.

21508925, 2025, 7, Downloaded from https://esajournals.onlinelibrary.wiley.com/doi/10.1002/ecs2.70335 by Ricardo Paíz - Dublin City University , Wiley Online Library on [11/08/2025]. See the Terms and Conditions (https://onlinelibrary.wiley.com/terms-and-conditions) on Wiley Online Library for rules of use; OA articles are governed by the applicable Creative Commons License

TABLE 2 Lake water temperature conditions established for the different regimes (P95 and P66) of the Atlantic salmon downstream, Atlantic salmon upstream, and European eel downstream migrations in Lough Feeagh, Burrishoole catchment.

	Atlantic salmon					
	Downstream		Upstream		European eel, downstream	
Metric	P95	P66	P95	P66	P95	P66
Lake water temperature (°C)	9.2–11.8	8.8–12.2	13.4–15.9	12.8–15.8	10.0–15.3	8.9–15.6
Cumulative lake water temperature (°C-days)	423–679	354–720	1078–2122	1053–2475	2151–3132	1746–3247

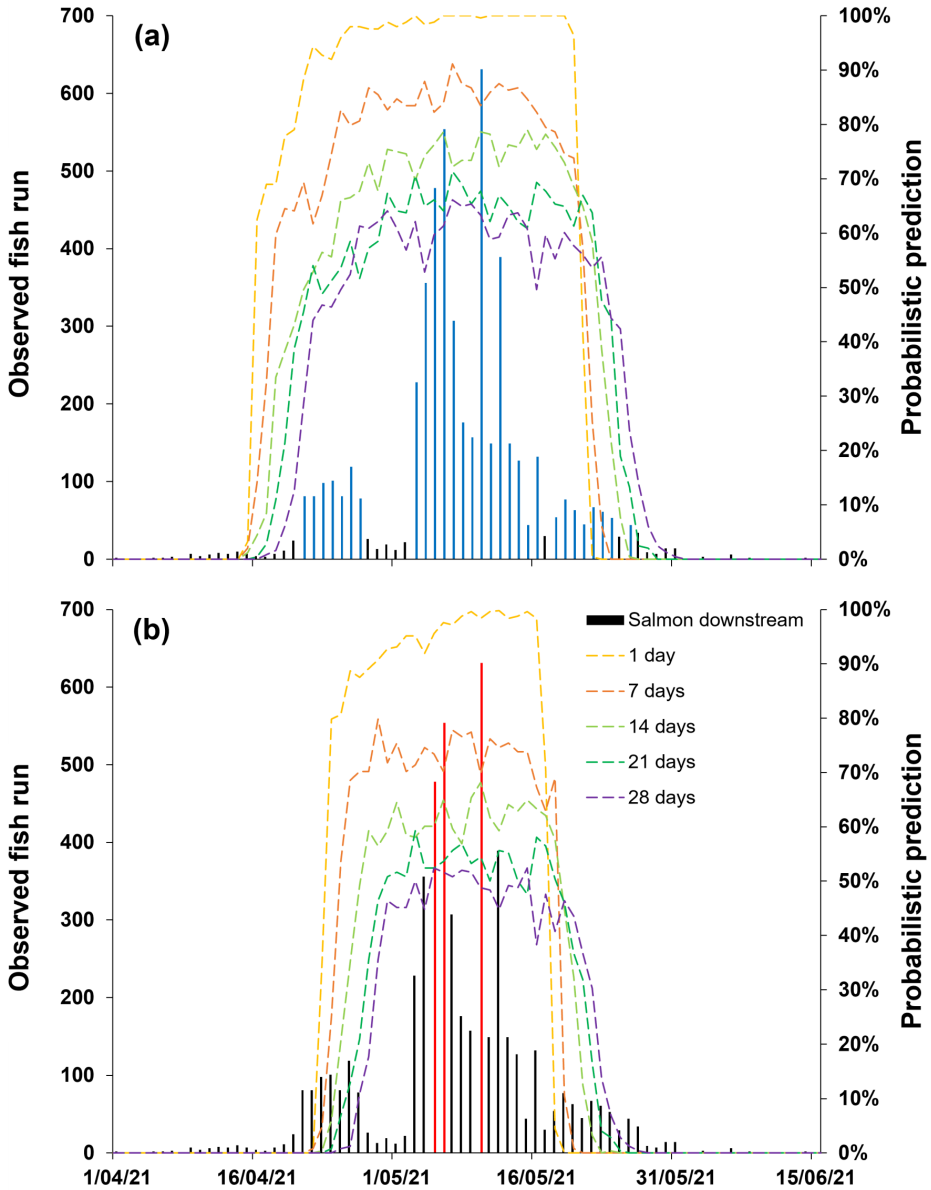


FIGURE 7 Daily probabilistic predictions of Atlantic salmon downstream migration for different forecast horizons (1, 7, 14, 21, and 28 days ahead) against observed fish runs during 2021: (a) the P66 regime predictions and (b) the P95 regime predictions. The observed fish run counts equal to or exceeding historical P66 and P95 fish run counts are highlighted in blue and red, respectively.

21508925, 2025, 7, Downloaded from https://esajournals.onlinelibrary.wiley.com/doi/10.1002/ecs2.70335 by Ricardo Paiz - Dublin City University , Wiley Online Library on [11/08/2025]. See the Terms and Conditions (https://onlinelibrary.wiley.com/terms-and-conditions) on Wiley Online Library for rules of use; OA articles are governed by the applicable Creative Commons License

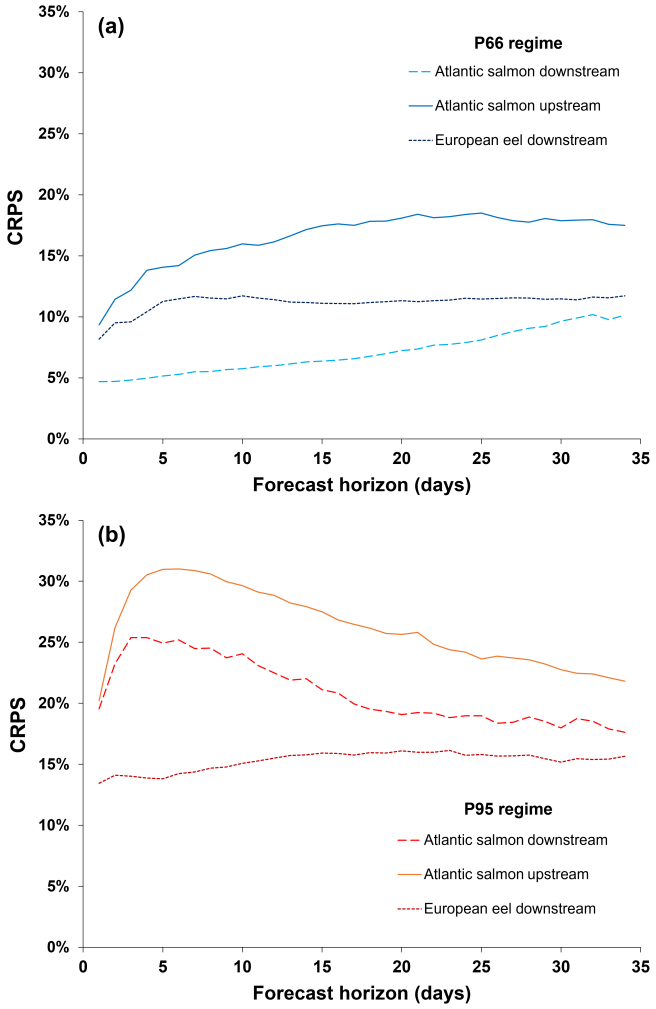


FIGURE 8 Continuous ranked probability score (CRPS) of the (a) P66 and (b) P95 probabilistic predictions of Atlantic salmon downstream, Atlantic salmon upstream, and European eel downstream migrations produced over the entire forecasting period.

hydrologic connectivity data). Importantly, our forecasting framework is flexible. It can be adapted with site-specific information to anticipate local fish migration regimes and therefore inform decisions as to when mitigation measures should be applied. An optimal approach to implement and adapt it would be with a human-centered design to supply context-dependent management needs (Carey et al., 2022; Lofton et al., 2023). Mitigation measures for migrating fish will differ between sites depending on many factors, for example, management concerns, ecological status, infrastructure, financial options, socioeconomic conditions, and regulatory frameworks (Tamario et al., 2019). Although we forecast two regimes in this study, P66 and P95, other tailored solutions could be explored as appropriate. Such a modeling framework could also allow scenario testing to be undertaken for the upcoming management period. For example, trade-offs between the requirements of different stakeholders and sectors could be evaluated, aiming to achieve sustainability in management practices and production systems (Franklin et al., 2024).

Uncertainty in the predictions

Including uncertainty in forecasts and communicating that uncertainty to stakeholders is a critical aspect of successful ecological forecasting (Dietze et al., 2018; Lewis et al., 2022). Our forecasts will have uncertainty related to both aspects of the workflow: water temperature and fish migration. In general, the water temperature forecasts performed very well at our study site (with a low RMSE), although uncertainty estimates tended to be slightly underconfident, especially in shorter horizons (Figure 6). This is likely due to overfitting observations during data assimilation, a factor that is relatively common in model-based forecasting frameworks (Wander et al., 2024; Zwart et al., 2023). Water temperature forecast uncertainty also increased for longer time horizons (Figure 3), again a common feature of ecological forecasting. A partitioning of uncertainty could be used in future work to quantify the relative contribution of different sources to total uncertainty so that key areas for improvement could be identified (Wander et al., 2024). Previous studies have reported that the ability of FLARE to reproduce water temperatures (i.e., model process) and the error related to the meteorological driver data contributed most to total uncertainty, especially in longer horizons (Thomas et al., 2020). The results presented here performed similarly to other deployments of FLARE for surface water temperature forecasting (Thomas et al., 2020, 2023; Wander et al., 2024), which is reassuring, as this was the first application of FLARE for forecasting volume-averaged lake water temperature and cumulative water temperature.

The uncertainty associated with our water temperature forecasts will feed into the fish migration forecasts, while additional uncertainty will be related to how well water temperature acts as a control of fish movements. Although water temperature is a key driver of diadromous fish migrations, we recognize that it is only one of a suite of variables that act together (Sandlund et al., 2017; Tamario et al., 2019; Teichert, Benitez, et al., 2020). The degree to which a change in water temperatures will trigger fish run events is difficult to quantify even under completely controlled conditions (Sparks et al., 2019) because of its intrinsic interactions with other triggering variables (Zydlewski et al., 2014) and because of the complexity of fish life histories, especially for migratory species. Despite these complexities, our framework was still able to (1) represent historical fish migrations through the use of the P66 and P95 metrics, as these accounted for events in all 17 years of migration

21508925, 2025, 7, Downloaded from https://esajournals.onlinelibrary.wiley.com/doi/10.1002/ecs2.70335 by Ricardo Paíz - Dublin City University , Wiley Online Library on [11/08/2025]. See the Terms and Conditions (https://onlinelibrary.wiley.com/terms-and-conditions) on Wiley Online Library for rules of use; OA articles are governed by the applicable Creative Commons License

data (Appendix S2: Figure S2), and (2) hindcast migration extent and timing relatively well, especially for the P66 regime. We do note that the temporal distribution of the probabilistic predictions for all three migrations was somewhat restricted by the cumulative lake water temperature condition. However, relying solely on ambient lake water temperature as a condition would have been problematic. Predictions for the salmon downstream migration, for example, would then have extended not only from April to July for this site but also included November to January, a period with no observed fish runs. The use of a combination of both lake water temperature metrics as conditions to trigger the diadromous fish migrations was therefore more prudent.

The probabilistic predictions for all three fish migrations based on P66 regimes performed best, again with a decrease in performance for longer forecast horizons. By contrast, a different pattern was observed for the more extreme P95 regimes, where the performance of the salmon migration predictions increased for longer horizons. While this may appear counterintuitive, the improved CRPS performance at longer horizons reflects a reduction in overestimation, as the magnitude of the predictions decreased with the forecast horizon. This occurred because the P95 daily probabilistic predictions tended to overextend around P95 fish run observations throughout the forecasting period (see Figure 7; Appendix S2: Figures S3–S8), and higher probabilities are penalized more on days with no observed P95 fish run than lower probabilities in the CRPS metric. The absolute magnitude difference between 0% (no observed P95 fish run) and 55% (longer horizon daily probability) is smaller than with 82% (shorter horizon daily probability), for example, favoring the CRPS metric.

There were also differences in performance across our selected migrations, with a lower performance for the salmon upstream migration, especially for the P95 regimes. This may have reflected stochasticity in fish migration dynamics (Baldursson, 1991; Lewy & Nielsen, 2003). For instance, during the forecasting period, a limited number of salmon upstream runs (five in total) fell within the range of the historical P95 runs. Consequently, there was a clear overestimation of our P95 for salmon migrating upstream. For example, P95 events were predicted from June to September 2022 when no P95 upstream runs were observed (Appendix S2: Figure S6). It is likely that runs with very large numbers migrating upstream are more controlled by factors other than temperature (e.g., increased water flow enabling catchment upstream accessibility) (Milner et al., 2012). Moreover, adult salmon going upstream will have experienced marine temperatures before migrating (Jonsson & Jonsson, 2009). This may induce different phenotypical responses than in fish undertaking downstream migration, which will have been regulated by temperatures in the freshwater environment.

Scalability and further development

Our framework provides an initial step that can be built on not only at our study site but also potentially at other sites. It has several advantages that increase its potential to be scalable to other settings. First, a large number of lakes and reservoirs globally already monitor water temperature with a range of different methods (e.g., point measurements, profilers, thermistor chains) (Piccolroaz et al., 2024). This includes sites that are important for diadromous fish (Ouellet et al., 2022; Tickner et al., 2020) and where available data for fish runs could provide points of reference for testing the framework (Nyqvist et al., 2017; Piper et al., 2020; Teichert, Benitez, et al., 2020; Teichert, Tétard, et al., 2020). Furthermore, data-poor sites could implement the necessary water temperature monitoring relatively easily, as temperature is one of the initial and least resource-consuming parameters included in monitoring programs (Peñas et al., 2023). A critical point in other settings would be to investigate site-specific temperature conditions for fish migration at other sites. Indeed, by undertaking a comparison with other lakes with fish migration data, it could be possible to identify general conditions so that the approach could be applied even in locations which do not monitor fish counts but have water temperature monitoring.

A second aspect that facilitates the application of the framework at other sites is its use of cyberinfrastructure. Having the framework set up in the cloud provides additional flexibility and utility, especially as more advanced modeling techniques and forecasting approaches emerge. For instance, other lake water temperature models than GLM could be tested within FLARE (Olsson et al., 2024), or other weather forecast products could be used as driver data. Having the framework online also allows remote management and troubleshooting which may lead to lower maintenance efforts than on more traditional systems (Fer et al., 2021; Recknagel, 2023). Additionally, the forecasting framework can operate iteratively and automatically. The production of forecasts does not require manually triggered actions unless wanted, rather it can work with scheduled actions in online repositories. This feature is particularly relevant because, once the system is set up and its accuracy assessed, its automation can facilitate the dissemination of both water temperature and, in our framework example, fish migration forecasts to operators and managers. This also enables forecasts to be easily reproduced, archived, and used in the future for research and to facilitate collaboration (Carey et al., 2022; Lofton et al., 2023).

21508925, 2025, 7, Downloaded from https://esajournals.onlinelibrary.wiley.com/doi/10.1002/ecs2.70335 by Ricardo Paiz - Dublin City University , Wiley Online Library on [11/08/2025]. See the Terms and Conditions (https://onlinelibrary.wiley.com/terms-and-conditions) on Wiley Online Library for rules of use; OA articles are governed by the applicable Creative Commons License

CONCLUSIONS

This study provides an investigative example of near-term (daily-scale) ecological forecasting of freshwater species (here, Atlantic salmon and European eel) using water temperature as an environmental driver. Our example showed that daily lake water temperature forecasts could be translated into fish migration predictions extending up to 34 days ahead. While such predictions and their associated uncertainty would need to be put in context for local users, we propose that a similar approach could assist ecological forecasting and management applications at other sites, where understanding the dynamics of fish migration has management implications. It, therefore, has the potential to contribute to adaptation in freshwater management in a time of increasing global change.

ACKNOWLEDGMENTS

This research has been funded by the inventWater Innovative Training Network (ITN) (Inventive forecasting tools for adapting water quality management to a new climate) through the European Union's Horizon 2020 research and innovation program, under the Marie Sklodowska-Curie grant agreement no. 956623, and the US National Science Foundation (DBI-1933016, OAC-2209866, EF-2318861). Special thanks to the Marine Institute staff for their support in data monitoring and collection. Thanks to Don C. Pierson for his support and feedback.

CONFLICT OF INTEREST STATEMENT

The authors declare no conflicts of interest.

DATA AVAILABILITY STATEMENT

Data and code (Paíz, 2024a, 2024b) are available on Zenodo: https://doi.org/10.5281/zenodo.15364329 and https://doi.org/10.5281/zenodo.13627954, respectively.

ORCID

Ricardo Paíz https://orcid.org/0009-0001-4507-0139
R. Quinn Thomas https://orcid.org/0000-0003-1282-7825
Cayelan C. Carey https://orcid.org/0000-0001-8835-4476

REFERENCES

Abbass, K., M. Z. Qasim, H. Song, M. Murshed, H. Mahmood, and I. Younis. 2022. "A Review of the Global Climate Change Impacts, Adaptation, and Sustainable Mitigation Measures." *Environmental Science and Pollution Research* 29: 42539–59. https://doi.org/10.1007/s11356-022-19718-6.

Als, T. D., M. M. Hansen, G. E. Maes, M. Castonguay, L. Riemann, K. Aarestrup, P. Munk, H. Sparholt, R. Hanel, and L. Bernatchez. 2011. "All Roads Lead to Home: Panmixia of European Eel in the Sargasso Sea." *Molecular Ecology* 20: 1333–46. https://doi.org/10.1111/j.1365-294X.2011.05011.x.

Baker, N. J., J. Boubée, P. M. Lokman, and J. D. Bolland. 2020. "Evaluating the Impact of Hydropower on Downstream Migrating Anguillid Eels: Catchment-Wide and Fine-Scale Approaches to Identify Cost-Effective Solutions." *Sci. Total Environ.* 748: 141111. https://doi.org/10.1016/j.scitotenv.2020.141111.

Baldursson, F. M. 1991. "A Stochastic Fisheries Problem with Seasonal Migrations." In *Essays on the Economics of Migratory Fish Stocks, Studies in Contemporary Economics*, edited by R. Arnason and T. Bjørndal, 69–82. Berlin, Heidelberg: Springer. https://doi.org/10.1007/978-3-642-84565-9_6.

Barbarossa, V., R. J. P. Schmitt, M. A. J. Huijbregts, C. Zarfl, H. King, and A. M. Schipper. 2020. "Impacts of Current and Future Large Dams on the Geographic Range Connectivity of Freshwater Fish Worldwide." *Proceedings of the National Academy of Sciences of the United States of America* 117: 3648–55. https://doi.org/10.1073/pnas.1912776117.

Battin, J., M. W. Wiley, M. H. Ruckelshaus, R. N. Palmer, E. Korb, K. K. Bartz, and H. Imaki. 2007. "Projected Impacts of Climate Change on Salmon Habitat Restoration." *Proceedings of the National Academy of Sciences of the United States of America* 104: 6720–25. https://doi.org/10.1073/pnas.0701685104.

Benhadi-Marín, J. 2018. "A Conceptual Framework to Deal with Outliers in Ecology." *Biodiversity and Conservation* 27: 3295–3300. https://doi.org/10.1007/s10531-018-1602-2.

Bento, V. A., A. Russo, E. Dutra, A. F. S. Ribeiro, C. M. Gouveia, and R. M. Trigo. 2022. "Persistence Versus Dynamical Seasonal Forecasts of Cereal Crop Yields." *Scientific Reports* 12: 7422. https://doi.org/10.1038/s41598-022-11228-2.

Bolstad, G. H., S. Karlsson, I. J. Hagen, P. Fiske, K. Urdal, H. Sægrov, B. Florø-Larsen, et al. 2021. "Introgression from Farmed Escapees Affects the Full Life Cycle of Wild Atlantic Salmon." *Science Advances* 7: eabj3397. https://doi.org/10.1126/sciadv.abj3397.

Bonacina, L., F. Fasano, V. Mezzanotte, and R. Fornaroli. 2023. "Effects of Water Temperature on Freshwater Macroinvertebrates: A Systematic Review." *Biological Reviews* 98: 191–221. https://doi.org/10.1111/brv.12903.

Bradford, J. B., J. F. Weltzin, and M. Wiltermuth. 2020. "Ecological Forecasting – 21st Century Science for 21st Century Management (Open-File Report)."

Bröcker, J. 2012. "Evaluating Raw Ensembles with the Continuous Ranked Probability Score." *Quarterly Journal of the Royal Meteorological Society* 138: 1611–17. https://doi.org/10.1002/qj.1891.

Bröcker, J., and L. A. Smith. 2007. "Increasing the Reliability of Reliability Diagrams." *Weather and Forecasting* 22: 651–661. https://doi.org/10.1175/WAF993.1.

Brown, J. N., Z. Hochman, D. Holzworth, and H. Horan. 2018. "Seasonal Climate Forecasts Provide more Definitive and Accurate Crop Yield Predictions." *Agricultural and Forest Meteorology* 260–261: 247–254. https://doi.org/10.1016/j.agrformet.2018.06.001.

Bruce, L. C., M. A. Frassl, G. B. Arhonditsis, G. Gal, D. P. Hamilton, P. C. Hanson, A. L. Hetherington, et al. 2018. "A Multi-Lake Comparative Analysis of the General Lake Model (GLM): Stress-Testing across a Global Observatory Network."

21508925, 2025, 7, Downloaded from https://esajournals.onlinelibrary.wiley.com/doi/10.1002/ecs2.70335 by Ricardo Paíz - Dublin City University , Wiley Online Library on [11/08/2025]. See the Terms and Conditions (https://onlinelibrary.wiley.com/terms-and-conditions) on Wiley Online Library for rules of use; OA articles are governed by the applicable Creative Commons License

Environmental Modelling & Software 102: 274–291. https://doi.org/10.1016/j.envsoft.2017.11.016.

Byrne, C. J., R. Poole, G. Rogan, M. Dillane, and K. F. Whelan. 2003. "Temporal and Environmental Influences on the Variation in Atlantic Salmon Smolt Migration in the Burrishoole System 1970–2000." *Journal of Fish Biology* 63: 1552–64. https://doi.org/10.1111/j.1095-8649.2003.00266.x.

Cai, Y., H. Wang, T. Zhang, Y. Zhou, A. Dong, R. Huang, Q. Zeng, and H. Yuan. 2023. "Seasonal Variation Regulate the Endogenous Phosphorus Release in Sediments of Shijiuhu Lake Via Water-Level Fluctuation." *Environmental Research* 238: 117247. https://doi.org/10.1016/j.envres.2023.117247.

Carey, C. C., W. M. Woelmer, M. E. Lofton, R. J. Figueiredo, B. J. Bookout, R. S. Corrigan, V. Daneshmand, et al. 2022. "Advancing Lake and Reservoir Water Quality Management with near-Term, Iterative Ecological Forecasting." *Inland Waters* 12: 107–120. https://doi.org/10.1080/20442041.2020.1816421.

Carter, L. J., R. M. Wright, R. E. Thomas, J. Reeds, L. A. Murphy, S. J. Collier, O. Evans, H. Baktoft, and J. D. Bolland. 2023. "Timing Is Everything; Operational Changes at a Pumping Station with a Gravity Sluice to Provide Safe Downstream Passage for Silver European Eels and Deliver Considerable Financial Savings." *Journal of Environmental Management* 347: 119143. https://doi.org/10.1016/j.jenvman.2023.119143.

de Eyto, E., B. Doyle, N. King, T. Kilbane, R. Finlay, L. Sibigtroth, C. Graham, et al. 2020. "Characterisation of Salmonid Food Webs in the Rivers and Lakes of an Irish Peatland Ecosystem." *Biology and Environment; Proceedings of the Royal Irish Academy* 120: 1–17. https://doi.org/10.1353/bae.2020.0013.

de Eyto, E., E. Jennings, E. Ryder, K. Sparber, M. Dillane, C. Dalton, and R. Poole. 2016. "Response of a Humic Lake Ecosystem to an Extreme Precipitation Event: Physical, Chemical, and Biological Implications." *Inland Waters* 6: 483–498. https://doi.org/10.1080/IW-6.4.875.

de Eyto, E., S. Kelly, G. Rogan, A. French, J. Cooney, M. Murphy, P. Nixon, et al. 2022. "Decadal Trends in the Migration Phenology of Diadromous Fishes Native to the Burrishoole Catchment, Ireland." *Frontiers in Ecology and Evolution* 10: 915854. https://doi.org/10.3389/fevo.2022.915854.

Dias, B. S., M. G. Frisk, and A. Jordaan. 2019. "Opening the Tap: Increased Riverine Connectivity Strengthens Marine Food Web Pathways." *PLoS One* 14: e0217008. https://doi.org/10.1371/journal.pone.0217008.

Dietze, M. C., A. Fox, L. M. Beck-Johnson, J. L. Betancourt, M. B. Hooten, C. S. Jarnevich, T. H. Keitt, et al. 2018. "Iterative near-Term Ecological Forecasting: Needs, Opportunities, and Challenges." *Proceedings of the National Academy of Sciences of the United States of America* 115: 1424–32. https://doi.org/10.1073/pnas.1710231115.

Diffenbaugh, N. S. 2020. "Verification of Extreme Event Attribution: Using Out-Of-Sample Observations to Assess Changes in Probabilities of Unprecedented Events." *Science Advances* 6: eaay2368. https://doi.org/10.1126/sciadv.aay2368.

Durif, C. M. F., and P. Elie. 2008. "Predicting Downstream Migration of Silver Eels in a Large River Catchment Based on Commercial Fishery Data." *Fisheries Management and Ecology* 15: 127–137. https://doi.org/10.1111/j.1365-2400.2008.00593.x.

Feigl, M., K. Lebiedzinski, M. Herrnegger, and K. Schulz. 2021. "Machine-Learning Methods for Stream Water Temperature Prediction." *Hydrology and Earth System Sciences* 25: 2951–77. https://doi.org/10.5194/hess-25-2951-2021.

Fer, I., A. K. Gardella, A. N. Shiklomanov, E. E. Campbell, E. M. Cowdery, M. G. De Kauwe, A. Desai, et al. 2021. "Beyond Ecosystem Modeling: A Roadmap to Community Cyberinfrastructure for Ecological Data-Model Integration." *Global Change Biology* 27: 13–26. https://doi.org/10.1111/gcb.15409.

Foley, M. M., R. G. Martone, M. D. Fox, C. V. Kappel, L. A. Mease, A. L. Erickson, B. S. Halpern, K. A. Selkoe, P. Taylor, and C. Scarborough. 2015. "Using Ecological Thresholds to Inform Resource Management: Current Options and Future Possibilities." *Frontiers in Marine Science* 2: 2–9. https://doi.org/10.3389/fmars.2015.00095.

Franklin, P. A., T. Bašić, P. I. Davison, K. Dunkley, J. Ellis, M. Gangal, A. M. González-Ferreras, et al. 2024. "Aquatic Connectivity: Challenges and Solutions in a Changing Climate." *Journal of Fish Biology* 105: 392–411. https://doi.org/10.1111/jfb.15727.

Gargan, P. G., T. Stafford, F. Økland, and E. B. Thorstad. 2015. "Survival of Wild Atlantic Salmon (*Salmo salar*) after Catch and Release Angling in Three Irish Rivers." *Fisheries Research* 161: 252–260. https://doi.org/10.1016/j.fishres.2014.08.005.

Gende, S. M., R. T. Edwards, M. F. Willson, and M. S. Wipfli. 2002. "Pacific Salmon in Aquatic and Terrestrial Ecosystems: Pacific Salmon Subsidize Freshwater and Terrestrial Ecosystems through Several Pathways, which Generates Unique Management and Conservation Issues but Also Provides Valuable Research Opportunities." *BioScience* 52: 917–928. https://doi.org/10.1641/0006-3568(2002)052[0917:PSIAAT]2.0.CO;2.

Gumpinger, C., S. Höfler, K. Berg, and C. Pichler-Scheder. 2010. "Water Temperature as an Applicable Parameter with a High Indicative Value for the General Condition of a River-Ecosystem, Drawing on the Example of the River Trattnach in Upper Austria." *Transylvanian Review of Systematical and Ecological Research* 10: 1–14.

Hamill, T. M., J. S. Whitaker, A. Shlyaeva, G. Bates, S. Fredrick, P. Pegion, E. Sinsky, et al. 2022. "The Reanalysis for the Global Ensemble Forecast System, Version 12." *Monthly Weather Review* 150: 59–79. https://doi.org/10.1175/MWR-D-21-0023.1.

Harringmeyer, O. S., M. L. Woolfolk, and H. E. Hoekstra. 2021. "Fishing for the Genetic Basis of Migratory Behavior." *Cell* 184: 303–5. https://doi.org/10.1016/j.cell.2020.12.037.

Harris, J. H., R. T. Kingsford, W. Peirson, and L. J. Baumgartner. 2016. "Mitigating the Effects of Barriers to Freshwater Fish Migrations: The Australian Experience." *Marine and Freshwater Research* 68: 614–628. https://doi.org/10.1071/MF15284.

Hipsey, M. R., L. C. Bruce, C. Boon, B. Busch, C. C. Carey, D. P. Hamilton, P. C. Hanson, et al. 2019. "A General Lake Model (GLM 3.0) for Linking with High-Frequency Sensor Data from the Global Lake Ecological Observatory Network (GLEON)." *Geoscientific Model Development* 12: 473–523. https://doi.org/10.5194/gmd-12-473-2019.

Hobday, A. J., C. M. Spillman, J. Paige Eveson, and J. R. Hartog. 2016. "Seasonal Forecasting for Decision Support in Marine

21508925, 2025, 7, Downloaded from https://esajournals.onlinelibrary.wiley.com/doi/10.1002/ecs2.70335 by Ricardo Pérz - Dublin City University , Wiley Online Library on [11/08/2025]. See the Terms and Conditions (https://onlinelibrary.wiley.com/terms-and-conditions) on Wiley Online Library for rules of use; OA articles are governed by the applicable Creative Commons License

Fisheries and Aquaculture." *Fisheries Oceanography* 25: 45–56. https://doi.org/10.1111/fog.12083.

IPCC, K. Calvin, D. Dasgupta, G. Krinner, A. Mukherji, P. W. Thorne, C. Trisos, et al. 2023. "Climate Change 2023: Synthesis Report." In *Contribution of Working Groups I, II and III to the Sixth Assessment Report of the Intergovernmental Panel on Climate Change*, edited by Core Writing Team, H. Lee, and J. Romero. Geneva: IPCC. https://doi.org/10.59327/IPCC/AR6-9789291691647.

Jacox, M. G., M. A. Alexander, S. Siedlecki, K. Chen, Y.-O. Kwon, S. Brodie, I. Ortiz, et al. 2020. "Seasonal-to-Interannual Prediction of North American Coastal Marine Ecosystems: Forecast Methods, Mechanisms of Predictability, and Priority Developments." *Progress in Oceanography* 183: 102307. https://doi.org/10.1016/j.pocean.2020.102307.

Jonsson, B., and N. Jonsson. 2009. "A Review of the Likely Effects of Climate Change on Anadromous Atlantic Salmon *Salmo salar* and Brown Trout *Salmo trutta*, with Particular Reference to Water Temperature and Flow." *Journal of Fish Biology* 75: 2381–2447. https://doi.org/10.1111/j.1095-8649.2009.02380.x.

Katopodis, C., and J. G. Williams. 2012. "The Development of Fish Passage Research in a Historical Context." *Ecological Engineering* 48: 8–18. https://doi.org/10.1016/j.ecoleng.2011.07.004.

Kim, K.-M., and J.-H. Ahn. 2022. "Machine Learning Predictions of Chlorophyll-a in the Han River Basin, Korea." *Journal of Environmental Management* 318: 115636. https://doi.org/10.1016/j.jenvman.2022.115636.

King, K., M. Burgess, E. T. Schultz, and J. Knighton. 2023. "Forecasting Hydrologic Controls on Juvenile Anadromous Fish Out-Migration with Process-Based Modeling and Machine Learning." *Journal of Environmental Management* 344: 118420. https://doi.org/10.1016/j.jenvman.2023.118420.

Knott, J., M. Mueller, J. Pander, and J. Geist. 2023. "Downstream Fish Passage at Small-Scale Hydropower Plants: Turbine or Bypass?" *Frontiers in Environmental Science* 11: 1168473. https://doi.org/10.3389/fenvs.2023.1168473.

Legrand, M., C. Briand, L. Buisson, T. Besse, G. Artur, D. Azam, A. Baisez, et al. 2021. "Diadromous Fish Modified Timing of Upstream Migration over the Last 30 Years in France." *Freshwater Biology* 66: 286–302. https://doi.org/10.1111/fwb.13638.

Lewis, A. S. L., C. R. Rollinson, A. J. Allyn, J. Ashander, S. Brodie, C. B. Brookson, E. Collins, et al. 2022. "The Power of Forecasts to Advance Ecological Theory." *Methods in Ecology and Evolution* 14: 746–756. https://doi.org/10.1111/2041-210X.13955.

Lewy, P., and A. Nielsen. 2003. "Modelling Stochastic Fish Stock Dynamics Using Markov Chain Monte Carlo." *ICES Journal of Marine Science* 60: 743–752. https://doi.org/10.1016/S1054-3139(03)00080-8.

Lin, H.-Y. 2017. "Conserving Migratory Species under Human Impacts and Climate Change." PhD thesis, The University of Queensland. https://doi.org/10.14264/uql.2017.750.

Liu, H., W. Cheng, P. Xiong, H. Li, Z. Liu, J. Ai, D. Yuan, et al. 2023. "Temporal Variation of Plankton and Zoobenthos Communities in a Freshwater Reservoir: Structure Feature, Construction Mechanism, Associated Symbiosis and Environmental Response." *Ecological Indicators* 154: 110774. https://doi.org/10.1016/j.ecolind.2023.110774.

Lofton, M. E., D. W. Howard, R. Q. Thomas, and C. C. Carey. 2023. "Progress and Opportunities in Advancing Near-Term Forecasting of Freshwater Quality." *Global Change Biology* 29: 1691–1714. https://doi.org/10.1111/gcb.16590.

Long, A. P., L. Vaughan, E. Tray, K. Thomas, N. Ó. Maoiléidigh, R. Poole, D. Cotter, A. Doogan, and D. Brophy. 2023. "Recent Marine Growth Declines in Wild and Ranched Atlantic Salmon *Salmo salar* from a Western European Catchment Discovered Using a 62-Year Time Series." *ICES Journal of Marine Science* 80: 1697–1709. https://doi.org/10.1093/icesjms/fsad101.

Lowerre-Barbieri, S. K., R. Kays, J. T. Thorson, and M. Wikelski. 2019. "The Ocean's Movescape: Fisheries Management in the Bio-Logging Decade (2018–2028)." *ICES Journal of Marine Science* 76: 477–488. https://doi.org/10.1093/icesjms/fsy211.

Maberly, S. C., R. A. O'Donnell, R. I. Woolway, M. E. J. Cutler, M. Gong, I. D. Jones, C. J. Merchant, et al. 2020. "Global Lake Thermal Regions Shift under Climate Change." *Nature Communications* 11: 1232. https://doi.org/10.1038/s41467-020-15108-z.

Marine Institute. 2017. "Data Catalogue: Bathymetric Survey of Lough Feeagh, Co. Mayo." https://data.marine.ie/geonetwork/srv/eng/catalog.search#/metadata/ie.marine.data:dataset.1226.

Mesman, J. P., A. I. Ayala, R. Adrian, E. De Eyto, M. A. Frassl, S. Goyette, J. Kasparian, et al. 2020. "Performance of One-Dimensional Hydrodynamic Lake Models during Short-Term Extreme Weather Events." *Environmental Modelling & Software* 133: 104852. https://doi.org/10.1016/j.envsoft.2020.104852.

Milner, N. J., D. J. Solomon, and G. W. Smith. 2012. "The Role of River Flow in the Migration of Adult Atlantic Salmon, *Salmo salar*, through Estuaries and Rivers." *Fisheries Management and Ecology* 19: 537–547. https://doi.org/10.1111/fme.12011.

Mishra, S., A. Ghosh, K. Rai, B. Jaiswal, D. S. Yadav, M. Agrawal, and S. B. Agrawal. 2021. "6 – Dimensions of Climate Change and Its Consequences on Ecosystem Functioning." In *Global Climate Change*, edited by S. Singh, P. Singh, S. Rangabhashiyam, and K. K. Srivastava, 109–149. Elsevier. https://doi.org/10.1016/B978-0-12-822928-6.00003-4.

Murphy, A. H. 1992. "Climatology, Persistence, and Their Linear Combination as Standards of Reference in Skill Scores." *Weather and Forecasting* 7: 692–98. https://doi.org/10.1175/1520-0434(1992)007<0692:CPATLC>2.0.CO;2.

Nissan, H., L. Goddard, E. C. De Perez, J. Furlow, W. Baethgen, M. C. Thomson, and S. J. Mason. 2019. "On the Use and Misuse of Climate Change Projections in International Development." *WIREs Climate Change* 10: e579. https://doi.org/10.1002/wcc.579.

Norman, J., R. M. Wright, A. Don, and J. D. Bolland. 2023. "Understanding the Temporal Dynamics of a Lowland River Fish Community at a Hazardous Intake and Floodgate to Inform Safe Operation." *Journal of Environmental Management* 336: 117716. https://doi.org/10.1016/j.jenvman.2023.117716.

Nyqvist, D., P. A. Nilsson, I. Alenäs, J. Elghagen, M. Hebrand, S. Karlsson, S. Kläppe, and O. Calles. 2017. "Upstream and Downstream Passage of Migrating Adult Atlantic Salmon: Remedial Measures Improve Passage Performance at a Hydropower Dam." *Ecological Engineering* 102: 331–343. https://doi.org/10.1016/j.ecoleng.2017.02.055.

21508925, 2025, 7, Downloaded from https://esajournals.onlinelibrary.wiley.com/doi/10.1002/ecs2.70335 by Ricardo Paíz - Dublin City University , Wiley Online Library on [11/08/2025]. See the Terms and Conditions (https://onlinelibrary.wiley.com/terms-and-conditions) on Wiley Online Library for rules of use; OA articles are governed by the applicable Creative Commons License

Oke, K. B., C. J. Cunningham, P. A. H. Westley, M. L. Baskett, S. M. Carlson, J. Clark, A. P. Hendry, et al. 2020. "Recent Declines in Salmon Body Size Impact Ecosystems and Fisheries." *Nature Communications* 11: 4155. https://doi.org/10.1038/s41467-020-17726-z.

Oke, K. B., and A. P. Hendry. 2019. "Genetic Insights into the Past, Present, and Future of a Keystone Species." *Proceedings of the National Academy of Sciences of the United States of America* 116: 344–46. https://doi.org/10.1073/pnas.1819789116.

Olsson, F., T. N. Moore, C. C. Carey, A. Breef-Pilz, and R. Q. Thomas. 2024. "A Multi-Model Ensemble of Baseline and Process-Based Models Improves the Predictive Skill of Near-Term Lake Forecasts." *Water Resources Research* 60: e2023WR035901. https://doi.org/10.1029/2023WR035901.

Osborne, J. W., and A. Overbay. 2004. "The Power of Outliers." https://doi.org/10.7275/QF69-7K43.

Ouellet, V., M. J. Collins, J. F. Kocik, R. Saunders, T. F. Sheehan, M. B. Ogburn, and T. Trinko Lake. 2022. "The Diadromous Watersheds-Ocean Continuum: Managing Diadromous Fish as a Community for Ecosystem Resilience." *Frontiers in Ecology and Evolution* 10: 1007599. https://doi.org/10.3389/fevo.2022.1007599.

Paíz, R. 2024a. "Data for Manuscript – Near-Term Lake Water Temperature Forecasts Can be Used to Anticipate the Ecological Dynamics of Freshwater Species." Zenodo. https://doi.org/10.5281/zenodo.15364329.

Paíz, R. 2024b. "Code for Manuscript – Near-Term Lake Water Temperature Forecasts Can be Used to Anticipate the Ecological Dynamics of Freshwater Species." Zenodo. https://doi.org/10.5281/zenodo.13627954.

Peñas, F. J., M. Álvarez-Cabria, M. Sáinz-Bariáin, M. P. Mata-Campo, A. Pérez-Haase, M. Ventura, M. J. Polo-Gómez, et al. 2023. "An Evaluation of Freshwater Monitoring Programs in ILTER Nodes and Mountain National Parks: Identifying Key Variables to Monitor Global Change Effects." *Biodiversity and Conservation* 32: 65–94. https://doi.org/10.1007/s10531-022-02466-x.

Piccolroaz, S., S. Zhu, R. Ladwig, L. Carrea, S. Oliver, A. P. Piotrowski, M. Ptak, et al. 2024. "Lake Water Temperature Modeling in an Era of Climate Change: Data Sources, Models, and Future Prospects." *Reviews of Geophysics* 62: e2023RG000816. https://doi.org/10.1029/2023RG000816.

Piper, A. T., P. J. Rosewarne, R. M. Wright, and P. S. Kemp. 2020. "Using 'Trap and Transport' to Facilitate Seaward Migration of Landlocked European Eel (*Anguilla anguilla*) from Lakes and Reservoirs." *Fisheries Research* 228: 105567. https://doi.org/10.1016/j.fishres.2020.105567.

Piper, A. T., R. M. Wright, A. M. Walker, and P. S. Kemp. 2013. "Escapement, Route Choice, Barrier Passage and Entrainment of Seaward Migrating European Eel, *Anguilla anguilla*, within a Highly Regulated Lowland River." *Ecological Engineering* 57: 88–96. https://doi.org/10.1016/j.ecoleng.2013.04.030.

Poole, W. R., O. H. Diserud, E. B. Thorstad, C. M. Durif, C. Dolan, O. T. Sandlund, K. Bergesen, G. Rogan, S. Kelly, and L. A. Vøllestad. 2018. "Long-Term Variation in Numbers and Biomass of Silver Eels Being Produced in Two European River Systems." *ICES Journal of Marine Science* 75: 1627–37. https://doi.org/10.1093/icesjms/fsy053.

Priya, A. K., M. Muruganandam, S. Rajamanickam, S. Sivarethinamohan, M. K. R. Gaddam, P. Velusamy, G. Ravindiran, T. R. Gurugubelli, and S. K. Muniasamy. 2023. "Impact of Climate Change and Anthropogenic Activities on Aquatic Ecosystem – A Review." *Environmental Research* 238: 117233. https://doi.org/10.1016/j.envres.2023.117233.

Qiu, R., Y. Wang, B. Rhoads, D. Wang, W. Qiu, Y. Tao, and J. Wu. 2021. "River Water Temperature Forecasting Using a Deep Learning Method." *Journal of Hydrology* 595: 126016. https://doi.org/10.1016/j.jhydrol.2021.126016.

Recknagel, F. 2023. "Cyberinfrastructure for Sourcing and Processing Ecological Data." *Ecological Informatics* 75: 102039. https://doi.org/10.1016/j.ecoinf.2023.102039.

Reed, T. E., E. De Eyto, K. O'Higgins, P. Gargan, W. Roche, J. White, N. O'Maoileidigh, T. P. Quinn, and P. McGinnity. 2017. "Availability of Holding Habitat in Lakes and Rivers Affects the Incidence of Spring (Premature) Upriver Migration by Atlantic Salmon." *Canadian Journal of Fisheries and Aquatic Sciences* 74: 668–679. https://doi.org/10.1139/cjfas-2016-0191.

Riley, W. D., D. L. Maxwell, M. J. Ives, and B. Bendall. 2012. "Some Observations on the Impact of Temperature and Low Flow on the Onset of Downstream Movement of Wild Atlantic Salmon, *Salmo salar* L., Smolts." *Aquaculture* 362: 216–223. https://doi.org/10.1016/j.aquaculture.2011.04.042.

Rinaldo, A., E. de Eyto, T. Reed, K. Ø. Gjelland, and P. McGinnity. 2024. "Global Warming Is Projected to Lead to Increased Freshwater Growth Potential and Changes in Pace of Life in Atlantic Salmon *Salmo salar*." *Journal of Fish Biology* 104: 647–661. https://doi.org/10.1111/jfb.15603.

Roberts, K. E., J. E. F. Stepanuk, H. Kim, L. H. Thorne, C. Chong-Montenegro, and J. A. Nye. 2023. "Developing a Subseasonal Ecological Forecast to Reduce Fisheries Bycatch in the Northeast U.S." *Progress in Oceanography* 213: 103021. https://doi.org/10.1016/j.pocean.2023.103021.

Rousso, B. Z., E. Bertone, R. Stewart, and D. P. Hamilton. 2020. "A Systematic Literature Review of Forecasting and Predictive Models for Cyanobacteria Blooms in Freshwater Lakes." *Water Research* 182: 115959. https://doi.org/10.1016/j.watres.2020.115959.

Ruokonen, T. J., P. Suuronen, H. Pulkkinen, and J. Erkinaro. 2022. "Release Mortality of Wild Atlantic Salmon in Coastal Pontoon-Trap Fishery in the Northern Baltic Sea." *Fisheries Research* 252: 106336. https://doi.org/10.1016/j.fishres.2022.106336.

Saeed, A., A. Alsini, and D. Amin. 2024. "Water Quality Multivariate Forecasting Using Deep Learning in a West Australian Estuary." *Environmental Modelling & Software* 171: 105884. https://doi.org/10.1016/j.envsoft.2023.105884.

Sandlund, O. T., O. H. Diserud, R. Poole, K. Bergesen, M. Dillane, G. Rogan, C. Durif, E. B. Thorstad, and L. A. Vøllestad. 2017. "Timing and Pattern of Annual Silver Eel Migration in Two European Watersheds Are Determined by Similar Cues." *Ecology and Evolution* 7: 5956–66. https://doi.org/10.1002/ece3.3099.

Schaeffer, B. A., N. Reynolds, H. Ferriby, W. Salls, D. Smith, J. M. Johnston, and M. Myer. 2024. "Forecasting Freshwater Cyanobacterial Harmful Algal Blooms for Sentinel-3 Satellite Resolved U.S. Lakes and Reservoirs." *Journal of Environmental Management* 349: 119518. https://doi.org/10.1016/j.jenvman.2023.119518.

21508925, 2025, 7, Downloaded from https://esajournals.onlinelibrary.wiley.com/doi/10.1002/ecs2.70335 by Ricardo Paíz - Dublin City University , Wiley Online Library on [11/08/2025]. See the Terms and Conditions (https://onlinelibrary.wiley.com/terms-and-conditions) on Wiley Online Library for rules of use; OA articles are governed by the applicable Creative Commons License

Seebacher, F., and E. Post. 2015. "Climate Change Impacts on Animal Migration." *Climate Change Responses* 2: 5. https://doi.org/10.1186/s40665-015-0013-9.

Slingsby, J. A., A. M. Wilson, B. Maitner, and G. R. Moncrieff. 2023. "Regional Ecological Forecasting across Scales: A Manifesto for a Biodiversity Hotspot." *Methods in Ecology and Evolution* 14: 757–770. https://doi.org/10.1111/2041-210X.14046.

Song, C., A. Omalley, S. G. Roy, B. L. Barber, J. Zydlewski, and W. Mo. 2019. "Managing Dams for Energy and Fish Tradeoffs: What Does a Win-Win Solution Take?" *Science of the Total Environment* 669: 833–843. https://doi.org/10.1016/j.scitotenv.2019.03.042.

Sparks, M. M., J. A. Falke, T. P. Quinn, M. D. Adkison, D. E. Schindler, K. Bartz, D. Young, and P. A. H. Westley. 2019. "Influences of Spawning Timing, Water Temperature, and Climatic Warming on Early Life History Phenology in Western Alaska Sockeye Salmon." *Canadian Journal of Fisheries and Aquatic Sciences* 76: 123–135. https://doi.org/10.1139/cjfas-2017-0468.

Staudinger, M. D., A. J. Lynch, S. K. Gaichas, M. G. Fox, D. Gibson-Reinemer, J. A. Langan, A. K. Teffer, S. J. Thackeray, and I. J. Winfield. 2021. "How Does Climate Change Affect Emergent Properties of Aquatic Ecosystems?" *Fisheries* 46: 423–441. https://doi.org/10.1002/fsh.10606.

Steffensen, S. M., J. D. Thiem, K. M. Stamplecoskie, T. R. Binder, C. Hatry, N. Langlois-Anderson, and S. J. Cooke. 2013. "Biological Effectiveness of an Inexpensive Nature-Like Fishway for Passage of Warmwater Fish in a Small Ontario Stream." *Ecology of Freshwater Fish* 22: 374–383. https://doi.org/10.1111/eff.12032.

St-Hilaire, A., D. Caissie, N. E. Bergeron, T. B. M. J. Ouarda, and C. Boyer. 2021. "Chapter 3 – Climate Change and Extreme River Temperature." In *Climate Change and Extreme Events*, edited by A. Fares, 25–37. Elsevier. https://doi.org/10.1016/B978-0-12-822700-8.00011-1.

Sykes, G. E., C. J. Johnson, and J. M. Shrimpton. 2009. "Temperature and Flow Effects on Migration Timing of Chinook Salmon Smolts." *Transactions of the American Fisheries Society* 138: 1252–65. https://doi.org/10.1577/T08-180.1.

Taillardat, M., A.-L. Fougères, P. Naveau, and R. de Fondeville. 2023. "Evaluating Probabilistic Forecasts of Extremes Using Continuous Ranked Probability Score Distributions." *International Journal of Forecasting* 39: 1448–59. https://doi.org/10.1016/j.ijforecast.2022.07.003.

Tamario, C., J. Sunde, E. Petersson, P. Tibblin, and A. Forsman. 2019. "Ecological and Evolutionary Consequences of Environmental Change and Management Actions for Migrating Fish." *Frontiers in Ecology and Evolution* 7: 271. https://doi.org/10.3389/fevo.2019.00271.

Teichert, N., J.-P. Benitez, A. Dierckx, S. Tétard, E. de Oliveira, T. Trancart, E. Feunteun, and M. Ovidio. 2020. "Development of an Accurate Model to Predict the Phenology of Atlantic Salmon Smolt Spring Migration." *Aquatic Conservation: Marine and Freshwater Ecosystems* 30: 1552–65. https://doi.org/10.1002/aqc.3382.

Teichert, N., S. Tétard, T. Trancart, E. de Oliveira, A. Acou, A. Carpentier, B. Bourillon, and E. Feunteun. 2020. "Towards Transferability in Fish Migration Models: A Generic Operational Tool for Predicting Silver Eel Migration in Rivers." *Sci. Total Environ.* 739: 140069. https://doi.org/10.1016/j.scitotenv.2020.140069.

Thomas, R. Q., R. J. Figueiredo, V. Daneshmand, B. J. Bookout, L. K. Puckett, and C. C. Carey. 2020. "A Near-Term Iterative Forecasting System Successfully Predicts Reservoir Hydrodynamics and Partitions Uncertainty in Real Time." *Water Resources Research* 56: e2019WR026138. https://doi.org/10.1029/2019WR026138.

Thomas, R. Q., R. P. McClure, T. N. Moore, W. M. Woelmer, C. Boettiger, R. J. Figueiredo, R. T. Hensley, and C. C. Carey. 2023. "Near-Term Forecasts of NEON Lakes Reveal Gradients of Environmental Predictability across the US." *Frontiers in Ecology and the Environment* 21: 220–26. https://doi.org/10.1002/fee.2623.

Tickner, D., J. J. Opperman, R. Abell, M. Acreman, A. H. Arthington, S. E. Bunn, S. J. Cooke, et al. 2020. "Bending the Curve of Global Freshwater Biodiversity Loss: An Emergency Recovery Plan." *BioScience* 70: 330–342. https://doi.org/10.1093/biosci/biaa002.

Trancart, T., A. Carpentier, A. Acou, F. Charrier, V. Mazel, V. Danet, and É. Feunteun. 2020. "When "Safe" Dams Kill: Analyzing Combination of Impacts of Overflow Dams on the Migration of Silver Eels." *Ecological Engineering* 145: 105741. https://doi.org/10.1016/j.ecoleng.2020.105741.

Valiente, A. G., F. Juanes, and E. Garcia-Vazquez. 2011. "Increasing Regional Temperatures Associated with Delays in Atlantic Salmon Sea-Run Timing at the Southern Edge of the European Distribution." *Transactions of the American Fisheries Society* 140: 367–373. https://doi.org/10.1080/00028487.2011.557018.

Vladic, T., and E. Petersson. 2016. *Evolutionary Biology of the Atlantic Salmon*. Boca Raton, FL: CRC Press, Taylor & Francis Group.

Wander, H. L., R. Q. Thomas, T. N. Moore, M. E. Lofton, A. Breef-Pilz, and C. C. Carey. 2024. "Data Assimilation Experiments Inform Monitoring Needs for Near-Term Ecological Forecasts in a Eutrophic Reservoir." *Ecosphere* 15: e4752. https://doi.org/10.1002/ecs2.4752.

Weaver, D. M., S. M. Coghlan, and J. Zydlewski. 2018. "Effects of Sea Lamprey Substrate Modification and Carcass Nutrients on Macroinvertebrate Assemblages in a Small Atlantic Coastal Stream." *Journal of Freshwater Ecology* 33: 19–30. https://doi.org/10.1080/02705060.2017.1417168.

Welch, H., E. L. Hazen, S. J. Bograd, M. G. Jacox, S. Brodie, D. Robinson, K. L. Scales, L. Dewitt, and R. Lewison. 2019. "Practical Considerations for Operationalizing Dynamic Management Tools." *Journal of Applied Ecology* 56: 459–469. https://doi.org/10.1111/1365-2664.13281.

Wilks, D. S. 2019. *Statistical Methods in the Atmospheric Sciences: An Introduction*, 4th ed. Amsterdam: Elsevier.

Woelmer, W. M., R. Q. Thomas, M. E. Lofton, R. P. McClure, H. L. Wander, and C. C. Carey. 2022. "Near-Term Phytoplankton Forecasts Reveal the Effects of Model Time Step and Forecast Horizon on Predictability." *Ecological Applications* 32: e2642. https://doi.org/10.1002/eap.2642.

Woelmer, W. M., R. Q. Thomas, F. Olsson, B. G. Steele, K. C. Weathers, and C. C. Carey. 2024. "Process-Based Forecasts of Lake Water Temperature and Dissolved Oxygen Outperform Null Models, with Variability Over Time and Depth." https://doi.org/10.2139/ssrn.4699835.

21508925, 2025, 7, Downloaded from https://esajournals.onlinelibrary.wiley.com/doi/10.1002/ecs2.70335 by Ricardo Paíz - Dublin City University , Wiley Online Library on [11/08/2025]. See the Terms and Conditions (https://onlinelibrary.wiley.com/terms-and-conditions) on Wiley Online Library for rules of use; OA articles are governed by the applicable Creative Commons License

Wolf, P. 1951. "A Trap for the Capture of Fish and Other Organisms Moving Downstream." *Transactions of the American Fisheries Society* 80: 41–45. https://doi.org/10.1577/1548-8659(1950)80[41:ATFTCO]2.0.CO;2.

Woolway, R. I., B. M. Kraemer, J. D. Lenters, C. J. Merchant, C. M. O'Reilly, and S. Sharma. 2020. "Global Lake Responses to Climate Change." *Nature Reviews Earth & Environment* 1: 388–403. https://doi.org/10.1038/s43017-020-0067-5.

Xu, L., M. Mazur, X. Chen, and Y. Chen. 2020. "Improving the Robustness of Fisheries Stock Assessment Models to Outliers in Input Data." *Fisheries Research* 230: 105641. https://doi.org/10.1016/j.fishres.2020.105641.

Xu, Z., Z. Yang, X. Cai, X. Yin, and Y. Cai. 2020. "Modeling Framework for Reservoir Capacity Planning Accounting for Fish Migration." *Journal of Water Resources Planning and Management* 146: 04020006. https://doi.org/10.1061/(ASCE)WR.1943-5452.0001170.

Yang, D. 2019. "Making Reference Solar Forecasts with Climatology, Persistence, and Their Optimal Convex Combination." *Solar Energy* 193: 981–85. https://doi.org/10.1016/j.solener.2019.10.006.

Yin, H., P. Yin, and Z. Yang. 2023. "Seasonal Sediment Phosphorus Release across Sediment-Water Interface and Its Potential Role in Supporting Algal Blooms in a Large Shallow Eutrophic Lake (Lake Taihu, China)." *Science of the Total Environment* 896: 165252. https://doi.org/10.1016/j.scitotenv.2023.165252.

Zachow, M., R. D. S. Nóia Júnior, and S. Asseng. 2023. "Seasonal Climate Models for National Wheat Yield Forecasts in Brazil." *Agricultural and Forest Meteorology* 342: 109753. https://doi.org/10.1016/j.agrformet.2023.109753.

Zwart, J. A., S. K. Oliver, W. D. Watkins, J. M. Sadler, A. P. Appling, H. R. Corson-Dosch, X. Jia, V. Kumar, and J. S. Read. 2023. "Near-Term Forecasts of Stream Temperature Using Deep Learning and Data Assimilation in Support of Management Decisions." *JAWRA Journal of the American Water Resources Association* 59: 317–337. https://doi.org/10.1111/1752-1688.13093.

Zydlewski, G. B., A. Haro, and S. D. McCormick. 2005. "Evidence for Cumulative Temperature as an Initiating and Terminating Factor in Downstream Migratory Behavior of Atlantic Salmon (*Salmo salar*) Smolts." *Canadian Journal of Fisheries and Aquatic Sciences* 62: 68–78. https://doi.org/10.1139/f04-179.

Zydlewski, G. B., D. S. Stich, and S. D. McCormick. 2014. "Photoperiod Control of Downstream Movements of Atlantic Salmon *Salmo salar* Smolts." *Journal of Fish Biology* 85: 1023–41. https://doi.org/10.1111/jfb.12509.

SUPPORTING INFORMATION

Additional supporting information can be found online in the Supporting Information section at the end of this article.

How to cite this article: Paíz, Ricardo, R. Quinn Thomas, Cayelan C. Carey, Elvira de Eyto, Ian D. Jones, Austin D. Delany, Russell Poole, et al. 2025. "Near-Term Lake Water Temperature Forecasts Can Be Used to Anticipate the Ecological Dynamics of Freshwater Species." *Ecosphere* 16(7): e70335. https://doi.org/10.1002/ecs2.70335

21508925, 2025, 7, Downloaded from https://esajournals.onlinelibrary.wiley.com/doi/10.1002/ecs2.70335 by Ricardo Paíz - Dublin City University , Wiley Online Library on [11/08/2025]. See the Terms and Conditions (https://onlinelibrary.wiley.com/terms-and-conditions) on Wiley Online Library for rules of use; OA articles are governed by the applicable Creative Commons License